

AD

USAAVLABS TECHNICAL REPORT 67-26

**INVESTIGATION OF A VARIABLE AREA SCROLL FOR POWER TRANSFER
IN TIP TURBINE LIFT FAN SYSTEMS**

By

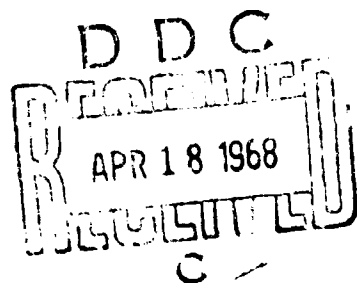
E. G. Smith

November 1967

**U. S. ARMY AVIATION MATERIEL LABORATORIES
FORT EUSTIS, VIRGINIA**

**CONTRACT DA 44-177-AMC-220(T)
GENERAL ELECTRIC COMPANY
CINCINNATI, OHIO**

*This document has been approved
for public release and sale; its
distribution is unlimited.*



Disclaimers

The findings in this report are not to be construed as an official Department of the Army position unless so designated by other authorized documents.

When Government drawings, specifications, or other data are used for any purpose other than in connection with a definitely related Government procurement operation, the United States Government thereby incurs no responsibility nor any obligation whatsoever; and the fact that the Government may have formulated, furnished, or in any way supplied the said drawings, specifications, or other data is not to be regarded by implication or otherwise as in any manner licensing the holder or any other person or corporation, or conveying any rights or permission, to manufacture, use, or sell any patented invention that may in any way be related thereto.

Trade names cited in this report do not constitute an official endorsement or approval of the use of such commercial hardware or software.

Disposition Instructions

Destroy this report when no longer needed. Do not return it to originator.

ACCESSION FOR	
CPSTI	WHITE SECTION <input checked="" type="checkbox"/>
DDC	DDFF SECTION <input type="checkbox"/>
UNANNOUNCED	<input type="checkbox"/>
JUSTIFICATION	
BY	
DISTRIBUTION AVAILABILITY CODES	
DIST.	AVAIL. CODE OR SPECIAL



DEPARTMENT OF THE ARMY
U. S. ARMY AVIATION MATERIEL LABORATORIES
FORT EUSTIS, VIRGINIA 23604

This report has been reviewed by the U.S. Army Aviation Materiel Laboratories and is considered to be technically sound.

Included in this report are (1) the variable area scroll effort performed under Contract DA 44-177-AMC-220(T) and (2) related LF2 fan rotor investigations conducted under the Air Force Contributing Engineering Program.

This program has established the mechanical feasibility of a variable area scroll for power transfer in a tip turbine lift fan system. Operational feasibility of the LF2/VAS system for power transfer would be dependent upon aircraft configuration and V/STOL control criteria.

Results from this program would have been more complete if J85-GE-13 gas generators had been available for testing. This problem, coupled with a scroll area limitation due to unacceptable tip turbine bucket stresses, greatly reduced the test range. However, it is considered that the test data obtained were adequate and suitable for extrapolation.

Project 1F131201D161
Contract DA 44-177-AMC-220(T)
USAAVLABS Technical Report 67-26
November 1967

INVESTIGATIONS OF A VARIABLE AREA SCROLL FOR POWER TRANSFER
IN TIP TURBINE LIFT FAN SYSTEMS

by

E.G. Smith

Prepared by

General Electric Company
Flight Propulsion Division
Advanced Technology and Demonstrator Programs Department
Lift Fan Systems Operation
Cincinnati, Ohio

for

U.S. ARMY AVIATION MATERIEL LABORATORIES
FORT EUSTIS, VIRGINIA

This document has been approved
for public release and sale; its
distribution is unlimited.

SUMMARY

A program was conducted to demonstrate the performance of the variable area scroll power transfer system using full scale lift fan hardware and system analog simulation. The demonstrator lift fan system utilizes the lightweight LF2 rotor system. The analog simulation was performed to predict and verify test results and to extend predicted performance to ranges of operation outside the limits of the demonstration tests.

The variable area scroll power transfer system was demonstrated to be an acceptable method of providing aircraft control. Response rates of 0.31 second for roll control and 0.10 second for height control were demonstrated. Insertion of an anticipatory device, called the jazzier, can improve fan response for roll control to about one-half the original level without overshoot.

Performance of the lightweight LF2 rotor system, with the variable area scroll, exceeded performance objectives as established by previous X353-5B experience.

FOREWORD

This report describes the results of a program for the design, demonstration, and evaluation of a variable area scroll concept applicable to lightweight tip turbine lift fan systems. The variable area scroll concept utilizes a variable area turbine nozzle to provide thrust modulation for aircraft control. The lightweight fan was the LF2 system, a design improvement over the existing X353-5 lift fans that powered the XV-5A aircraft.

The program was initiated in June 1964, with first demonstration tests in August 1966; the program was completed in December 1966. Simultaneous with the design and demonstration phases, an analog simulation program was conducted. The analog program provided numerous inputs during the early design phases. The analog simulation also provided a method of predicting system performance outside the range of the demonstration program.

The program was conducted by the Flight Propulsion Division of the General Electric Company, Cincinnati, Ohio. Component design and manufacture and conduct of the test programs were under the direction of General Electric personnel. The demonstration tests and analog simulation were performed in the facilities of the General Electric Company. The variable area scroll was designed and manufactured under United States Army Contract DA 44-177-AMC-220(T). The lightweight LF2 lift fan rotor assembly was provided by the United States Air Force Contributing Engineering Program. The demonstration test program was conducted to obtain both lift fan system performance using the LF2 rotor and variable area scroll control system performance.

This report summarizes the design and manufacture of the variable area scroll; the results of the demonstration tests, both LF2 and variable area scroll performance; and the results of the analog simulation program.

The efforts of many people contributed to the successful accomplishment of the program reported herein. Acknowledgement is hereby given to L.J. Volk for the analog simulation program, to E.J. Ferko for the design and design description of the variable area scroll, to T.L. Oller for test data processing, to G.C. Alford for analysis of rotating components, and to D.V. Robinett for conduct of the test and performance analysis.

CONTENTS

	<u>Page</u>
SUMMARY	iii
FOREWORD	v
LIST OF ILLUSTRATIONS	ix
LIST OF TABLES	xxxi
LIST OF SYMBOLS	xxxv
INTRODUCTION	1
VARIABLE AREA SCROLL CONCEPTS	3
POWER TRANSFER FOR ROLL CONTROL	4
FAN AREA FOR HEIGHT CONTROL	4
CORE ENGINES FOR HEIGHT CONTROL	4
LIFT FAN DYNAMIC PERFORMANCE	5
THE JAZZER SYSTEM	6
FAN RESPONSE WITH SINUSOIDAL INPUTS	7
VARIABLE AREA SCROLL DESIGN, MANUFACTURE, AND ASSEMBLY	9
BACKGROUND	9
PROGRAM OBJECTIVES	9
MATERIAL DESIGN LIMITS	10
SCROLL DESIGN, MANUFACTURE, AND ASSEMBLY	10
VARIABLE AREA MECHANISM AND ACTUATOR SYSTEM	13
WEIGHT	26
RECOMMENDATIONS	26
DESCRIPTION OF TEST EQUIPMENT	28
FAN ASSEMBLY	28
TEST FACILITY	28
VAS CONTROL SYSTEM	29
EXPERIMENTAL PROCEDURE	31
INSTRUMENTATION	31
DATA ACQUISITION	32
DATA REDUCTION PROCEDURES	34
TEST PROCEDURES	37
DEMONSTRATION TEST RESULTS	43
CORE ENGINE PERFORMANCE	43
STEADY-STATE AERODYNAMIC PERFORMANCE	45
DYNAMIC PERFORMANCE	49
AERODYNAMIC TEMPERATURE AND PRESSURE DISTRIBUTIONS	55

	<u>Page</u>
STATIC STRUCTURAL COMPONENT PERFORMANCE	56
ROTATING STRUCTURAL COMPONENT PERFORMANCE	58
ANALYSIS AND DISCUSSION OF TEST RESULTS	64
EFFECTS OF FAN CONFIGURATION ON PERFORMANCE	64
VARIABLE AREA SCROLL EFFECTIVE AREA	66
LOSSES OF DIVERTER VALVE AND CROSS DUCT	67
EXTENSION OF PERFORMANCE TO THE J85/J4 LEVEL	68
FAN PERFORMANCE WITH EXIT LOUVERS	69
COMPARISON OF X353-5B AND LF2 FAN PERFORMANCE	69
FAN TIME CONSTANTS BASED ON SINUSOIDAL INPUT TEST RESULTS	71
THE EFFECTS OF THE JAZZER ON FAN RESPONSE	72
COMPARISON OF FAN TIME CONSTANTS FOR STEP AND SINUSOIDAL TYPES OF INPUTS	72
FAN RESPONSE USING ENGINE THROTTLES FOR HEIGHT CONTROL	73
CORRECTION OF FAN THRUST RESPONSE CHARACTERISTICS FOR LOAD CELL RESPONSE	73
DISCUSSION OF ROTOR BLADE STRESSES	74
DISCUSSION OF TURBINE BUCKET STRESSES	75
DISCUSSION OF TORQUE BAND STRESSES	77
DISCUSSION OF ROTATING COMPONENT TEMPERATURES	78
TURBINE BUCKET RESPONSE CHARACTERISTICS	79
HARMONIC ANALYSIS OF TURBINE EXCITING FORCES	80
THE J85/LF2 ANALOG COMPUTER SIMULATION	82
THE ANALOG FACILITY	83
THE SYSTEM SIMULATION	83
THE J85/J4 CORE ENGINE SIMULATION	83
THE DUCT SIMULATION	85
THE LIFT FAN SIMULATION	85
ANALOG FAN AREA DEFINED	87
STEADY-STATE FAN PERFORMANCE	87
EFFECT OF ACTUATOR SLEW RATE	87
FAN RESPONSE TO AREA STEP CHANGE WITHOUT A JAZZER	88
FAN RESPONSE TO STEP CHANGES WITH A JAZZER	88
FAN STEADY-STATE FREQUENCY RESPONSE	89
FAN FOR HEIGHT CONTROL	91
ENGINES FOR HEIGHT CONTROL	91
COMPARISON OF GAS POWER TRANSFER AND THRUST SPOILING CONTROL SYSTEMS	93
CONCLUSIONS	94
BIBLIOGRAPHY	96
APPENDIX - DATA REDUCTION PROCEDURE	97
DISTRIBUTION	587

ILLUSTRATIONS

<u>Figure</u>		<u>Page</u>
1	Comparison of Lift Losses for Full Roll Control	125
2	V/STOL Aircraft Control Efficiency Comparison	125
3	Power Transfer for Roll Control	126
4	Variable Area for Height Control	126
5	Electrical and Mechanical Jazzer Systems	127
6	Typical Response Characteristics for a Step Input Showing Effects of Jazzer	128
7	Typical Attenuation and Phase Angle Characteristics of a Single Time Constant System	129
8	Decibel Conversion Chart	130
9	Typical Attenuation and Phase Angle Characteristics for a Jazzer With a Magnification Factor, m , of 1.0	131
10	0.2-Percent Yield Strength for Materials Used in Variable Area Scroll Assembly	132
11	Stress Range Diagram for Materials Used in Variable Area Scroll Assembly	132
12	Scroll (Drawing 4013007-008, Sheet 1)	133
13	Scroll (Drawing 4013007-008, Sheet 2)	139
14	Physical Fixed and Variable Scroll Turbine Area	145
15	Nozzle Diaphragm During Manufacturing	146
16	Nozzle Diaphragm During Manufacturing	147
17	Scroll Mechanism and Front Frame Flange	148
18	Enlarging the Scroll Arms for Assembly	149
19	Comparison of Performance of the Two Methods of Nozzle Area Control	150
20	Variable Area Scroll Actuation	151
21	Flat Splitter Vanes for Scroll	152

<u>Figure</u>		<u>Page</u>
22	Biconvex Splitter Vanes for Scroll	152
23	Scroll Nozzle Physical Area Distribution	153
24	Splitter Vane - Aft (Drawing 4013007-640)	155
25	Splitter Vane - Forward (Drawing 4013007-639)	157
26	Scroll and Splitter Vane Assembly (Drawing 4013007-641)	159
27	Flat Splitter Vane Throat Ratio	161
28	Biconvex Splitter Vane Throat Ratio	162
29	Splitter Vane Assembled in Scroll	163
30	Flat Splitter Vane Section Properties	164
31	Biconvex Splitter Vane Section Properties	165
32	Biconvex Splitter at End of Scroll Arm	166
33	Rework of Flat Splitter Vane Camber	166
34	Aft Lever (Drawing 4013007-084)	167
35	Aft Bellcrank (Drawing 4013007-075)	169
36	Aft Tie Bar (Drawing 4013007-086)	171
37	Roller Bearing (Drawing 4013007-040)	173
38	Front Frame Gussets Modified for Cam Tracks	175
39	Forward Bellcrank Moment Arm, Flat Splitter Vanes . . .	176
40	Aft Bellcrank Moment Arm, Biconvex Splitter Vanes . .	177
41	Cam Track - Forward (Drawing 4013007-116)	178
42	Cam Track - Center (Drawing 4013007-117)	179
43	Cam Track - Aft (Drawing 4013007-115)	181
44	Flat Splitter Vane Rotation Sequence	183
45	Biconvex Splitter Vane Rotation Sequence	184
46	Aft Cam Track Bracket (Drawing 4013007-284)	185

<u>Figure</u>		<u>Page</u>
47	Forward Cam Track Bracket (Drawing 4013007-033)	187
48	Cam Tracks Disassembled From Scroll	189
49	Cam Tracks Assembled to Scroll	190
50	Forward Link (Drawing 4013007-098)	191
51	Aft Link (Drawing 4013007-094)	193
52	Forward and Aft Links	195
53	Serrated Connector (Drawing 4013007-239)	197
54	Serrated Connector Assembled to Aft Link	199
55	Link Support Assembly (Drawing 4013007-101)	201
56	Link Support Bracket (Drawing 4013007-102)	203
57	Link Support Assembly	204
58	Test Actuator (Drawing 4013016-178)	207
59	Actuator and Drive Links	209
60	Actuator Bracket Assembly (Drawing 4013007-228)	210
61	Actuator Bracket (Drawing 4013007-223)	211
62	LF2 Fan Assembly (Drawing 4013007-300)	213
63	Variable Area Scroll Assembly (Drawing 4013007-450, Sheet 1)	217
64	Variable Area Scroll Assembly (Drawing 4013007-450, Sheet 2)	221
65	Photograph of LF2 Rotor Assembly	223
66	Top View of Variable Area Scroll Assembly	224
67	Bottom View of Variable Area Scroll Assembly	225
68	Photograph of LF2/VAS Assembly Installed in Test Facility	226
69	Hydraulic System Block Diagram	227

<u>Figure</u>		<u>Page</u>
70	Control System Block Diagram	228
71	Photograph of Overboard Dump Valve System	229
72	Core Engine Inlet Instrumentation - Station 2.0	230
73	Core Engine Turbine Discharge Instrumentation - Station 5.1	231
74	Core Engine Tailpipe Instrumentation - Station 6.0	232
75	Overboard Dump Ducting Instrumentation - Station 5.6	233
76	Scroll Duct Static Pressure Instrumentation	234
77	Fan Inlet Screen Instrumentation - Station 10.0	235
78	Fan Inlet Instrumentation - Station 10.2	236
79	Fan Bullethead Pressure Instrumentation	237
80	Rotor Discharge Pressure Instrumentation - Station 10.6	238
81	Seal Temperature Instrumentation Location	239
82	Front Frame Main Strut Temperature Instrumentation	240
83	Front Frame and Actuation Structure Temperature Instrumentation	241
84	Variable Area Scroll Actuator Temperatures	242
85	Scroll Actuator Bracket Instrumentation	243
86	Fan Bearing Temperature Instrumentation	244
87	Torque Band and Tip Tang Instrumentation	245
88	Turbine Bucket Instrumentation Location	246
89	Rear Frame Strain Gage Instrumentation	247
90	Fan Blade Strain Gage Locations	248
91	Lift Fan Test Facility Control Room, East Wall	249
92	Lift Fan Test Facility Control Room, South Wall	250

<u>Figure</u>		<u>Page</u>
93	Graphical Representation of Two Definitions of Time Constant	251
94	Cruise Mode Compressor Inlet Airflow for Engine 1, YJ85-GE-5, S/N 230105	252
95	Cruise Mode Fuel Flow for Engine 1, YJ85-GE-5, S/N 230105	253
96	Cruise Mode Turbine Discharge Pressure for Engine 1, YJ85-GE-5, S/N 230105	254
97	Calibration of Indicated EGT on Digital Recorder on Engine 1, YJ85-GE-5, S/N 230105	255
98	Cruise Mode Tailpipe Temperature for Engine 1, YJ85-GE-5, S/N 230105	256
99	Cruise Mode Turbine Discharge Ideal Gas Horsepower for Engine 1, YJ85-GE-5, S/N 230105	257
100	Cruise Mode Thrust for Engine 1, YJ85-GE-5, S/N 230105	258
101	Correlation of Average Tailpipe Temperature With Fuel-Air Ratio for Engine 1, YJ85-GE-5, S/N 230105	259
102	Calibration of Indicated EGT on Panel Meter for Engine 1, YJ85-GE-5, S/N 230105	260
103	Cruise Mode Compressor Inlet Airflow for Engine 2, J85-GE-5, S/N 231233	261
104	Cruise Mode Fuel Flow for Engine 2, J85-GE-5, S/N 231233	262
105	Cruise Mode Turbine Discharge Pressure for Engine 2, J85-GE-5, S/N 231233	263
106	Calibration of Indicated EGT on Digital Recorder on Engine 2, J85-GE-5, S/N 231233	264
107	Cruise Mode Tailpipe Temperature for Engine 2, J85-GE-5, S/N 231233	265
108	Cruise Mode Turbine Discharge Ideal Gas Horsepower for Engine 2, J85-GE-5, S/N 231233	266

<u>Figure</u>		<u>Page</u>
109	Cruise Mode Thrust for Engine 2, J85-GE-5, S/N 231233	267
110	Correlation of Average Tailpipe Temperature With Fuel- Air Ratio for Engine 2, J85-GE-5, S/N 231233	268
111	Calibration of Indicated EGT on Panel Meter for Engine 2, J85-GE-5, S/N 231233	269
112	Effect of Bullethead Configuration on Engine Inlet Dynamic Head	270
113	Lift Versus Fan Speed, Run 7, Stator Stiffener Rings Out, $\delta_S = 110$ Percent	271
114	Speed Versus Horsepower, Run 7, Stator Stiffener Rings Out, $\delta_S = 110$ Percent	272
115	Lift Versus Horsepower, Run 7, Stator Stiffener Rings Out, $\delta_S = 110$ Percent	273
116	Lift Versus Fan Speed, Run 9, Stator Stiffener Rings In, $\delta_S = 110$ Percent	274
117	Speed Versus Horsepower, Run 9, Stator Stiffener Rings In, $\delta_S = 110$ Percent	275
118	Lift Versus Horsepower, Run 9, Stator Stiffener Rings In, $\delta_S = 110$ Percent	276
119	Lift Versus Fan Speed, Run 17, $\delta_S = 80$ Percent, Before and After Bleed Nozzle Correction	277
120	Fan Speed Versus Available Fan Horsepower, Run 17, $\delta_S = 80$ Percent	278
121	Lift Versus Available Fan Horsepower, Run 17, $\delta_S = 80$ Percent	279
122	Lift Versus Fan Speed, Run 17, $\delta_S = 80$ Percent, Slip Ring Cavity Covered	280
123	Fan Speed Versus Available Fan Horsepower, Run 17, $\delta_S = 80$ Percent, Slip Ring Cavity Covered	281
124	Lift Versus Available Fan Horsepower, Run 17, $\delta_S = 80$ Percent, Slip Ring Cavity Covered	282

<u>Figure</u>		<u>Page</u>
125	Lift Versus Fan Speed, Run 17, $\delta_S = 80$ Percent, Covered Space Around Blade Tip Tangs	283
126	Fan Speed Versus Available Fan Horsepower, Run 17, $\delta_S = 80$ Percent, Covered Space Around Blade Tip Tangs .	284
127	Lift Versus Available Fan Horsepower, Run 17, $\delta_S = 80$ Percent, Covered Space Around Blade Tip Tangs .	285
128	Lift Versus Fan Speed, Run 18, $\delta_S = 80$ Percent, 3 to 6 O'clock Inlet Vane Quadrant Raised	286
129	Fan Speed Versus Available Fan Horsepower, Run 18, $\delta_S = 80$ Percent, 3 to 6 O'clock Inlet Vane Quadrant Raised	287
130	Lift Versus Available Fan Horsepower, Run 18, $\delta_S = 80$ Percent, 3 to 6 O'clock Inlet Vane Quadrant Raised	288
131	Lift Versus Fan Speed, Run 18, Exit Louvers Removed . .	289
132	Fan Speed Versus Available Fan Horsepower, Run 18, Exit Louvers Removed	290
133	Lift Versus Available Fan Horsepower, Run 18, Exit Louver Removed	291
134	Lift Versus Fan Speed, Run 18, Inlet Vane Out	292
135	Fan Speed Versus Available Fan Horsepower, Run 18, Inlet Vane Out	293
136	Lift Versus Available Fan Horsepower, Run 18, Inlet Vane Out	294
137	Lift Versus Fan Speed, Run 19, Improved Forward Air Seal	295
138	Fan Speed Versus Available Fan Horsepower, Run 19, Improved Forward Air Seal	296
139	Lift Versus Available Fan Horsepower, Run 19, Improved Forward Air Seal	297
140	Lift Versus Fan Speed, Run 19, Stator Stiffener Rings Out	298

<u>Figure</u>		<u>Page</u>
141	Fan Speed Versus Available Fan Horsepower, Run 19, Stator Stiffener Rings Out	299
142	Lift Versus Available Fan Horsepower, Run 19, Stator Stiffener Rings Out	300
143	Lift Versus Fan Speed, Runs 10 and 11, Variable ϵ_S From -8 to 110 Percent	301
144	Fan Speed Versus Available Fan Horsepower, Runs 10 and 11, Variable δ_S From -8 to 110 Percent	302
145	Lift Versus Available Fan Horsepower, Runs 10 and 11, Variable δ_S From -8 to 110 Percent	303
146	Lift Versus Fan Speed, Runs 12 and 14, Variable δ_S . .	304
147	Fan Speed Versus Available Fan Horsepower, Runs 12 and 14, Variable δ_S	305
148	Lift Versus Available Fan Horsepower, Runs 12 and 14, Variable δ_S	306
149	Lift Versus Fan Speed, Runs 15 and 16, Variable δ_S From 0 to 80 Percent, $\beta_V = 0$ Degrees	307
150	Fan Speed Versus Available Fan Horsepower, Runs 15 and 16, Variable δ_S From 0 to 80 Percent, $\beta_V = 0$ Degrees	308
151	Lift Versus Available Fan Horsepower, Runs 15 and 16, Variable δ_S From 0 to 80 Percent, $\beta_V = 0$ Degrees. .	309
152	Thrust Versus Available Fan Horsepower, Run 15, Variable ϵ_S , $\beta_V = 0$ Degrees	310
153	Fan Speed Versus Available Fan Horsepower, Run 17, δ_S Variable From 0 to 80 Percent, $\beta_V = -7$ Degrees . . .	311
154	Lift Versus Available Fan Horsepower, Run 17, δ_S Variable From 0 to 80 Percent, $\beta_V = -7$ Degrees	312
155	Thrust Versus Available Fan Horsepower, Run 17, δ_S Variable From 0 to 80 Percent, $\beta_V = -7$ Degrees	313
156	Fan Speed Versus Available Fan Horsepower, Run 12, $\delta_S = 76$ Percent, $\beta_V = 10$ Degrees	314

<u>Figure</u>		<u>Page</u>
157	Lift Versus Available Fan Horsepower, Run 12, $\delta_S = 76$ Percent, $\beta_V = 10$ Degrees	315
158	Thrust Versus Available Fan Horsepower, Run 12, $\delta_S = 76$ Percent, $\beta_V = 10$ Degrees	316
159	Fan Speed Versus Available Fan Horsepower, Run 16, δ_S Variable From 0 to 80 Percent, $\beta_V = 20.5$ Degrees . .	317
160	Lift Versus Available Fan Horsepower, Run 16, δ_S Variable From 0 to 80 Percent, $\beta_V = 20.5$ Degrees . .	318
161	Thrust Versus Available Fan Horsepower, Run 16, δ_S Variable From 0 to 80 Percent, $\beta_V = 20.5$ Degrees . .	319
162	Fan Speed Versus Available Fan Horsepower, Run 12, $\delta_S = 76$ Percent, $\beta_V = 30$ Degrees	320
163	Lift Versus Available Fan Horsepower, Run 12, $\delta_S = 76$ Percent, $\beta_V = 30$ Degrees	321
164	Thrust Versus Available Fan Horsepower, Run 12, $\delta_S = 76$ Percent, $\beta_V = 30$ Degrees	322
165	Fan Speed Versus Available Fan Horsepower, Run 16, δ_S Variable From 0 to 80 Percent, $\beta_V = 37$ Degrees . . .	323
166	Lift Versus Available Fan Horsepower, Run 16, δ_S Variable From 0 to 80 Percent, $\beta_V = 37$ Degrees	324
167	Thrust Versus Available Fan Horsepower, Run 16, δ_S Variable From 0 to 80 Percent, $\beta_V = 37$ Degrees	325
168	Variation of Scroll Actuator Position and Dump Valve Actuator Position as Required to Maintain Constant Core Engine Operation	326
169	Scroll Actuator and Dump Valve Position Variation With Percent of Scroll Actuator Stroke	327
170	Engine Horsepower Delivered to Fan as a Function of Scroll Position for Initial Rigging	328
171	Engine Horsepower Delivered to Fan as a Function of Scroll Position for Final Rigging	329
172	Effects of Scroll Area on Engine 1 Performance for Initial Rigging	330

<u>Figure</u>		<u>Page</u>
173	Effects of Scroll Area on Engine 1 Performance for Initial Rigging	331
174	Effects of Scroll Area on Engine 2 Performance for Initial Rigging	332
175	Effects of Scroll Area on Engine 2 Performance for Initial Rigging	333
176	Effects of Scroll Area on Engine 1 Performance for Final Rigging	334
177	Effects of Scroll Area on Engine 1 Performance for Final Rigging	335
178	Effects of Scroll Area on Engine 2 Performance for Final Rigging	336
179	Effects of Scroll Area on Engine 2 Performance for Final Rigging	337
180	Variation of Scroll Flow Function With Scroll Actuator Position	338
181	Variation of Scroll Loss Coefficient With Scroll Actuator Position	339
182	Variation of Scroll Loss Coefficient With Scroll Flow Function	340
183	Variation of Scroll Effective Area With Scroll Actuator Position	341
184	Variation of Overboard Dump System Losses With Flow Function	342
185	Variation of Dump Valve Effective Area With Position	343
186	Scroll Actuator Forces Versus Actuator Position	344
187	Response of the Vertical Lift Load Cells to a Step Input	345
188	Typical Response Characteristics for a Sinusoidal Input of 80 ± 20 Percent, $N_e = 95$ Percent	347
189	Frequency Response Characteristics Based on Fan Speed, $N_{Fc} = 1780$ rpm, $\delta_S = 20 \pm 20$ Percent	349

<u>Figure</u>		<u>Page</u>
190	Frequency Response Characteristics Based on Fan Speed, $N_{Fc} = 1940$ rpm, $\delta_S = 50 \pm 20$ Percent	350
191	Frequency Response Characteristics Based on Fan Speed, $N_{Fc} = 1940$ rpm, $\delta_S = 50 \pm 50$ Percent	351
192	Frequency Response Characteristics Based on Fan Speed, $N_{Fc} = 2050$ rpm, $\delta_S = 70 \pm 10$ Percent	352
193	Frequency Response Characteristics Based on Fan Speed, $N_{Fc} = 2050$ rpm, $\delta_S = 70 \pm 20$ Percent	353
194	Frequency Response Characteristics Based on Fan Speed, $N_{Fc} = 2050$ rpm, $\delta_S = 70 \pm 30$ Percent	354
195	Frequency Response Characteristics Based on Fan Speed, $N_{Fc} = 2090$ rpm, $\delta_S = 80 \pm 20$ Percent	355
196	Frequency Response Characteristics Based on Fan Speed, $N_{Fc} = 2000$ rpm, $\delta_S = 20 \pm 20$ Percent	356
197	Frequency Response Characteristics Based on Fan Speed, $N_{Fc} = 2220$ rpm, $\delta_S = 50 \pm 20$ Percent	357
198	Frequency Response Characteristics Based on Fan Speed, $N_{Fc} = 2220$ rpm, $\delta_S = 50 \pm 50$ Percent	358
199	Frequency Response Characteristics Based on Fan Speed, $N_{Fc} = 2330$ rpm, $\delta_S = 70 \pm 10$ Percent	359
200	Frequency Response Characteristics Based on Fan Speed, $N_{Fc} = 2330$ rpm, $\delta_S = 70 \pm 20$ Percent	360
201	Frequency Response Characteristics Based on Fan Speed, $N_{Fc} = 2330$ rpm, $\delta_S = 70 \pm 30$ Percent	361
202	Frequency Response Characteristics Based on Fan Speed, $N_{Fc} = 2370$ rpm, $\delta_S = 80 \pm 20$ Percent	362
203	Typical Response Characteristics, With Jazzer m of 1.0, for a Sinusoidal Input of 50 ± 10 Percent, $N_c = 100$ Percent	363
204	Frequency Response Characteristics of the Jazzer, $\tau_J = 0.31$, $m = 1$, $\delta_S = 50 \pm 10$ Percent	365
205	Frequency Response Characteristics With Jazzer, Based on Fan Speed, $N_{Fc} = 2220$ rpm, $m = 1$, $\delta_S = 50 \pm 10$ Percent	366

<u>Figure</u>		<u>Page</u>
206	Frequency Response Characteristics With Jazzer, Based on Thrust, $N_{Fc} = 2220$ rpm, $m = 1$, $\delta_S = 50 \pm 10$ Percent	367
207	Frequency Response Characteristics of the Jazzer, $\tau_J = 0.31$, $m = 1$, $\delta_S = 50 \pm 20$ Percent	368
208	Frequency Response Characteristics With Jazzer, Based on Fan Speed, $N_{Fc} = 2220$ rpm, $m = 1$, $\delta_S = 50 \pm 20$ Percent	369
209	Frequency Response Characteristics With Jazzer, Based on Thrust, $N_{Fc} = 2220$ rpm, $m = 1$, $\delta_S = 50 \pm 20$ Percent	370
210	Frequency Response Characteristics of the Jazzer, $\tau_J = 0.15$, $m = 3$, $\delta_S = 50 \pm 10$ Percent	371
211	Frequency Response Characteristics With Jazzer, Based on Fan Speed, $N_{Fc} = 2220$ rpm, $m = 3$, $\delta_S = 50 \pm 10$ Percent	372
212	Frequency Response Characteristics With Jazzer, Based on Thrust, $N_{Fc} = 2220$ rpm, $m = 3$, $\delta_S = 50 \pm 10$ Percent	373
213	Typical Response Characteristic for a Step Input of ± 20 Percent, $N_e = 100$ Percent	375
214	Typical Response Characteristics for a Step Input, With Jazzer m of 3.0, of ± 20 Percent, $N_e = 100$ Percent	377
215	Fan Time Constants During Step Inputs Based on 63 Percent of Change During Transient, $N_e = 95$ Percent	379
216	Fan Time Constants During Step Inputs Based on 63 Percent of Change During Transient, $N_e = 100$ Percent	380
217	Fan Time Constants During Step Inputs Based on Initial Slope of Transient, $N_e = 100$ Percent	381
218	Effects of Jazzer Setting on Actuator Overshoot Levels, $\delta_S = 50 \pm 10$ Percent	382
219	Typical Response Characteristics for a Step Input of 15 Percent Using Area for Height Control, $N_e = 100$ Percent	383

<u>Figure</u>		<u>Page</u>
220	Fan Time Constants During Step Inputs Using Fan Area for Height Control	385
221	Typical Response Characteristics for a Step Input of Engine Throttle	387
222	Variation of Fan Speed Time Constant With Size of Speed Change Using Engines for Altitude Control, $\delta_S = 0$ Percent and $\delta_S = 20$ Percent	389
223	Variation of Fan Speed Time Constant With Size of Speed Change Using Engines for Altitude Control, $\delta_S = 40$ Percent and $\delta_S = 60$ Percent	390
224	Variation of Fan Speed Time Constant With Size of Speed Change Using Engines for Altitude Control, $\delta_S = 80$ Percent	391
225	Typical Fan Inlet Screen Temperature Distribution . . .	392
226	Fan Inlet Screen Temperature Distribution With High Reingestion Region	393
227	Fan Flow Coefficient and Pressure Coefficient Characteristics, Run 7, Stator Stiffener Rings Out, $\delta_S = 100$ Percent	394
228	Fan Flow Coefficient and Pressure Coefficient Characteristics, Run 9, Stator Stiffener Rings In, $\delta_S = 100$ Percent	395
229	Fan Flow Coefficient and Pressure Coefficient Characteristics, Run 11, Stator Stiffener Rings In, $\delta_S = 0$ Percent	396
230	Fan Flow Coefficient and Pressure Coefficient Characteristics, Run 12, $\beta_V = 37$ Degrees, $\delta_S = 76$ Percent	397
231	Fan Flow Coefficient and Discharge Pressure Coefficient Characteristics, Run 17, Slip Ring Cavity Covered, $\delta_S = 80$ Percent	398
232	Fan Flow Coefficient and Pressure Coefficient Characteristics, Run 18, 3 to 6 O'clock Inlet Vane Quadrant Raised, $\delta_S = 80$ Percent	399

<u>Figure</u>		<u>Page</u>
233	Fan Flow Coefficient and Pressure Coefficient Characteristics, Run 18, Exit Louvers Removed $\delta_S = 80$ Percent	400
234	Fan Flow Coefficient and Pressure Coefficient Characteristics, Run 18, Inlet Vane Out, $\delta_S = 80$ Percent	401
235	Fan Flow Coefficient and Pressure Coefficient Characteristics, Run 19, Improved Forward Air Seal, $\delta_S = 80$ Percent	402
236	Fan Flow Coefficient and Pressure Coefficient Characteristics, Run 19, Stator Stiffener Rings Out, $\delta_S = 80$ Percent	403
237	Typical Core Engine Inlet Temperature Distribution . .	404
238	Typical Engine 2 Inlet Pressure Profile, $P_a = 14.467$ psia, $N_{ec2} = 99.2$ Percent	405
239	Typical Engine 1 Turbine Discharge Pressure Profile . .	406
240	Typical Engine 2 Turbine Discharge Pressure Profile . .	407
241	Tailpipe Temperature Profile of Engine 1, YJ85-GE-5, S/N 230105, $N_e = 97.5$ Percent, $A_g = 117.8$ Square Inches	408
242	Tailpipe Temperature Profile of Engine 2, J85-GE-5, S/N 231233, $N_e = 100.4$ Percent, $A_g = 111.8$ Square Inches	409
243	Temperature Distribution Measured in Dump System Supplied by Engine 1	410
244	Temperature Distribution Measured in Dump System Supplied by Engine 2	411
245	Pressure Distribution Measured in Dump System Supplied by Engine 1	412
246	Pressure Distribution Measured in Dump System Supplied by Engine 2	413
247	Observed Vibration Characteristics of Engine 1	414
248	Observed Vibration Characteristics of Engine 2	415

<u>Figure</u>		<u>Page</u>
249	Observed Fan Vibration Characteristics	416
250	Comparison of Fan Bullethead Axial Vibration Measurements	417
251	Scroll Actuation Slide Bracket Temperature	418
252	Scroll Actuator Body Temperature.	418
253	Front Frame Flange Temperature	419
254	Front Frame Tube Temperature	419
255	LF2 Front Frame Strut Temperature, Run 7	420
256	Overall Blade Stress Level Versus Fan Speed for Blade Gage 1, $\delta_S = 100$ Percent	421
257	Overall Blade Stress Level Versus Fan Speed for Blade Gage 3, $\delta_S = 100$ Percent	422
258	Overall Blade Stress Level Versus Fan Speed for Blade Gage 4, $\delta_S = 100$ Percent	423
259	Overall Blade Stress Level Versus Fan Speed for Blade Gage 4, $\delta_S = 80$ Percent	424
260	Overall Blade Stress Level Versus Fan Speed for Blade Gage 4, $\delta_S = 60$ Percent	425
261	Overall Blade Stress Level Versus Fan Speed for Blade Gage 4, $\delta_S = 40$ Percent	426
262	Overall Blade Stress Level Versus Fan Speed for Blade Gage 4, $\delta_S = 20$ Percent	427
263	Overall Blade Stress Level Versus Fan Speed for Blade Gage 4, $\delta_S = 0$ Percent	428
264	Peak Blade Stress at 1610 rpm Versus Scroll Actuator Position for Blade Gage 4. Blade First Flexural Frequency With 12-Per-Revolution Excitation	429
265	Peak Blade Stress at 1850 rpm Versus Scroll Actuator Position for Blade Gage 4. Blade Second Flexural Frequency With 16-Per-Revolution Excitation	430

<u>Figure</u>		<u>Page</u>
266	Peak Blade Stress at 1960 rpm Versus Scroll Actuator Position for Blade Gage 1. Wheel 30 Mode Critical Speed	431
267	Peak Blade Stress Level in First Flexural and Second Flexural Modes Versus Exit Louver Vector Angle for Blade Gage 4	432
268	Overall Blade Stress Level Versus Fan Speed to Show Effect of Removing the Inlet Vane	433
269	Campbell Diagram of LF2 Blade	434
270	Turbine Bucket Overall Stress Level Versus Fan Speed From Run 7 LF2/VAS Test and From LF2 Demonstrator Test	435
271	Turbine Bucket Overall Stress Level Versus Fan Speed for 100-Percent Open Scroll Area and for Reduced Scroll Area at 95-Percent Engine Speed	436
272	Turbine Bucket Overall Stress Level Versus Fan Speed at 100-Percent Open Scroll Area and at Reduced Scroll Areas for 95-Percent Engine Speed	437
273	Turbine Bucket Overall Stress Level Versus Fan Speed for 100-Percent Open and 0-Percent Open Scroll Areas With Intermediate Areas for 100-Percent Engine Speed. .	438
274	Turbine Bucket Overall Stress Level Versus Fan Speed for 100-Percent Open Scroll Area	439
275	Turbine Bucket Overall Stress Level Versus Fan Speed for 90-Percent Open Scroll Area	440
276	Turbine Bucket Overall Stress Level Versus Fan Speed for 50-Percent Open Scroll Area	441
277	Turbine Bucket Predominant Vibratory Frequency Versus Fan Speed	442
278	Turbine Bucket Gage 7 Spectrum Analysis, 1900 and 2100 rpm	443
279	Turbine Bucket Gage 7 Spectrum Analysis, 2200 and 2325 rpm	444
280	Turbine Bucket Gage 7 Spectrum Analysis, 2325 and 2440 rpm	445

<u>Figure</u>		<u>Page</u>
281	Turbine Bucket One-Per-Revolution Stress Levels, Gage 7	446
282	Ratio of Turbine Bucket One-Per-Revolution Stress Component at Reduced Scroll Areas to the One-Per- Revolution Stress Level at 100-Percent Open Area . . .	447
283	Turbine Bucket Overall Stress Level Versus Scroll Actuator Position and Ratio of Percent Change in Stress to Percent Change in Scroll Area Versus Fan Speed Squared	448
284	Effect of Scroll Area on Turbine Bucket Stress Wave Form, Gage 7	449
285	Torque Band Overall Stress Level Versus Fan Speed for 80-Percent Open Scroll Area	450
286	Torque Band Overall Stress Level Versus Scroll Actuator Position for Constant Fan Speed	451
287	Torque Band Overall Stress Level Versus Scroll Effective Area	452
288	Rotor Stress Transient Response, Scroll Actuator Sine Wave Input, $\delta_s = 50 \pm 20$ Percent	453
289	Time History of Rotor Component Temperatures	454
290	Rotor Component Temperatures Versus Scroll Actuator Position for Constant Engine Power	455
291	Rotor Component Temperature Versus Core Engine Exhaust Gas Temperature	456
292	Time History of Bearing Temperatures	457
293	Ball Bearing and Roller Bearing Temperature Versus Fan Speed	458
294	Effect of Scroll Area Variation on Tunnel Gas Temperature	459
295	Effect of Exhaust Gas Temperatures on Tunnel Gas Temperature	460
296	Circumferential Distribution of Tunnel Gas Temperature for Two Scroll Area Settings	461

<u>Figure</u>		<u>Page</u>
297	Fan Circular Vane Orientation	462
298	Comparison of Fan Turbine Nozzle Effective and Physical Areas for Scroll 1	463
299	Comparison of Fan Turbine Nozzle Effective and Physical Areas for Scroll 2	464
300	Variation of Fan Scroll Total Effective and Physical Area With Actuator Stroke	465
301	Ducting System Losses Versus Flow Function	466
302	Typical J85/J4 Performance, Airflow and Exhaust Gas Temperature	467
303	Typical J85/J4 Performance, Fuel Flow and Flow Function	468
304	Typical J85/J4 Performance, Turbine Discharge Pressure and Horsepower	469
305	Variation of Lift With Fan Speed Used in Analysis, Scroll Arc Constant at 168 Degrees	470
306	Variation of Fan Speed With Available Horsepower Used in Analysis	471
307	Estimated Variation of Fan Lift With Admission Arc at a Constant Fan Speed	472
308	Effects of Scroll Arc on Fan Horsepower Absorption Characteristics	473
309	Comparison of Scroll Actuator Position and Scroll Arc Size	474
310	Fan Scroll Flow Function as a Function of Scroll Arc and Actuator Position	475
311	Percentage of J85/J4 Engine Flow Supplied to Fan as a Function of Scroll Arc and Actuator Position . . .	476
312	Estimated Available Gas Horsepower to Fan as a Function of Active Arc Size	477
313	Estimated Fan Speed Variation With Scroll Arc or Actuator Position for the Fan Driven by J85/J4 Engines	478

<u>Figure</u>		<u>Page</u>
314	Estimated Fan Lift Variation With Scroll Arc or Actuator Position for the Fan Driven by J85/J4 Engines	479
315	Fan Speed Versus Indicated Louver Angle and Scroll Actuator Position at Constant Core Engine Horsepower .	480
316	Lift Variation With Louver Angle and Scroll Actuator Position for Constant Core Engine Horsepower	481
317	Horizontal Thrust Variation With Louver Angle and Scroll Actuator Position for Constant Core Engine Horsepower	482
318	Actual Turning Angle Versus Indicated Louver Angle . .	483
319	Comparison of X353-5B and LF2 Fan Test Results	484
320	Comparison of Fan Speed Versus Available Fan Horsepower With Characteristic From First LF2 Test Configuration .	485
321	Frequency to Time Constant Conversion Chart	486
322	Effects of Scroll Position and Size of Scroll Position Change on Fan Time Constant, $N_e = 95$ Percent	487
323	Effects of Scroll Position and Size of Scroll Position Change on Fan Time Constants, $N_e = 100$ Percent	488
324	Effects of Jazzer on Fan Time Constants With Steady State Sinusoidal Inputs, $N_e = 100$ Percent	489
325	Theoretical Response Characteristics of a Fan With a Jazzer Magnification Factor of 1.0	490
326	Theoretical Response Characteristics of a Fan With a Jazzer Magnification Factor of 3.0	491
327	Comparison of Time Constants Measured for Sine Wave and Step Input Types of Commands	492
328	Effects of Jazzer on Fan Time Constant	493
329	Limits of Amplitude and Frequency for Sinusoidal Inputs as Established by Actuator Slew Rates	494
330	Effects of Actuator Slew Rate on Time Required to Achieve Command Level During Step Inputs	495

<u>Figure</u>		<u>Page</u>
331	Effects of Actuator Slew Rate and Size of Step Command on Actuator Overshoot With Jazzer	496
332	Effects of Scroll Area Setting and Size of Fan Speed Changes on Time Constant when Using Engines for Altitude Control	497
333	Steady State Frequency Response Characteristics of the Vertical Lift System Based on a Time Constant of 0.47 Second	498
334	Comparison of Fan Response Based on Fan Speed and Corrected Lift Data, $\tau_J = 0.31$, $m = 1.0$, $\delta_S = 50 \pm 20$ Percent	499
335	Comparison of Fan Response Based on Fan Speed and Corrected Lift Data, $\tau_J = 0.31$, $m = 1.0$, $\delta_S = 50 \pm 10$ Percent	500
336	Comparison of Fan Response Based on Fan Speed and Corrected Lift Data, $\tau_J = 0.15$, $m = 3.0$, $\delta_S = 50 \pm 10$ Percent	501
337	Frequency Response Characteristics of the LF2 Turbine Bucket	502
338	Harmonic Breakdown of Exciting Forces in the LF2/VAS System at Full-Open Scroll Conditions	503
339	General Electric Evendale Analog Computer Laboratory	504
340	System Analog Block Diagram	505
341	Engine Analog Block Diagram	506
342	Engine Analog Wiring Diagram	507
343	J85/J4 Gas Generator Temperature Factor ($\partial T_{51} / \partial P_{51}$) Versus Engine Speed	509
344	J85/J4 Gas Generator Unbalanced Power Factor ($\partial Q_e / \partial P_{51}$) Versus Engine Speed	510
345	Duct Analog Block Diagram	511
346	Duct Analog Wiring Diagram	513

<u>Figure</u>		<u>Page</u>
347	LF2 Lift Fan Scroll Total Pressure Loss Versus Scroll Flow Function	515
348	Fan Analog Block Diagram	516
349	Fan Number 1 Analog Wiring Diagram - Sheet 1	517
350	Fan Number 1 Analog Wiring Diagram - Sheet 2	519
351	Fan Number 2 Analog Wiring Diagram - Sheet 1	521
352	Fan Number 2 Analog Wiring Diagram - Sheet 2	523
353	Fan Area Control Wiring Diagram	525
354	Tip Turbine Map - Flow Function Versus Corrected Speed and Turbine Pressure Ratio	527
355	LF2 Tip Turbine Map - Energy Function Versus Corrected Speed and Turbine Pressure Ratio	529
356	Tip Turbine Map Operating Line	530
357	Tip Turbine Arc of Admission and Flow Related to Analog Fan Area	531
358	Test Hardware Actuator Stroke Related to Analog Fan Area	532
359	Fan Steady-State Speed Versus Analog Fan Area	533
360	Fan Steady-State Lift Versus Analog Fan Area	534
361	Fan Steady State Lift Versus Speed	535
362	Analog Results - Effect of Actuator Slew Rate on Fan Time Constants for Step Changes in Fan Area	536
363	Typical Analog Recorder Trace of Fan Response to a Step Change in Fan Area Without a Jazzer	537
364	Analog Results - Fan Speed Time Constants for Positive Step Changes in Fan Area Without a Jazzer	538
365	Analog Results - Fan Speed Time Constants for Negative Step Changes in Fan Area Without a Jazzer	539
366	Analog Results - Summary of Fan Speed Time Constants for Step Changes in Fan Area Without a Jazzer	540

<u>Figure</u>		<u>Page</u>
367	Comparison of Analog and Hardware Test Results - Fan Speed Time Constants for Positive Step Changes in Fan Area Without a Jazzer	541
368	Comparison of Analog and Hardware Test Results for Fan Speed Time Constants for Negative Step Changes in Fan Area Without a Jazzer	542
369	Analog Results - Fan Thrust Time Constants for Positive Step Changes in Fan Area Without a Jazzer . .	543
370	Analog Results - Fan Thrust Time Constants for Negative Step Changes in Fan Area Without a Jazzer . .	544
371	Analog Results - Summary of Fan Thrust Time Constants for Step Changes in Fan Area Without a Jazzer	545
372	Analog Results - Fan Thrust Time Constants Versus Initial Speed, for Step Changes in Fan Area Without a Jazzer	546
373	Typical Analog Recorder Trace of Fan Response to a Step Change in Fan Area With a Jazzer	547
374	Analog Results - Fan Time Constants for a 5-Percent Step Change in Fan Area With a Jazzer	549
375	Analog Results - Fan Time Constants for a 10-Percent Step Change in Fan Area With a Jazzer	550
376	Steady State Frequency Response - Comparison of Analog and Test Results for Test Actuator Stroke of 50 ± 20 Percent Without a Jazzer	551
377	Steady State Frequency Response - Comparison of Analog and Test Results for Test Actuator Stroke of 50 ± 50 Percent Without a Jazzer	552
378	Steady State Frequency Response - Comparison of Analog and Test Results for Test Actuator Stroke of 70 ± 10 Percent Without a Jazzer	553
379	Steady State Frequency Response - Comparison of Analog and Test Results for Test Actuator Stroke of 70 ± 20 Percent Without a Jazzer	554
380	Steady State Frequency Response - Comparison of Analog and Test Results for Test Actuator Stroke of 70 ± 30 Percent Without a Jazzer	555

<u>Figure</u>		<u>Page</u>
381	Steady State Frequency Response - Analog Results for 100 \pm 5 Percent Area Without a Jazzer	556
382	Steady State Frequency Response - Analog Results for 100 \pm 10 Percent Area Without a Jazzer	557
383	Steady State Frequency Response - Analog Results for 100 \pm 20 Percent Area Without a Jazzer	558
384	Steady State Frequency Response - Comparison of Analog and Test Results for Fan Test Actuator Stroke 50 \pm 10 Percent With Jazzer Magnification Factor of 1	559
385	Steady State Frequency Response - Comparison of Analog and Test Results for an Actuator Stroke of 50 \pm 20 Percent With a Jazzer Magnification Factor of 1	560
386	Steady State Frequency Response - Comparison of Analog and Test Results for Test Actuator Stroke 50 \pm 10 Percent With Jazzer Magnification Factor of 3	561
387	Steady State Frequency Response - Analog Results for 100 \pm 5 Percent Area With a Jazzer Magnification Factor of 1	562
388	Steady State Frequency Response - Analog Results for 100 \pm 5 Percent Area With a Jazzer Magnification Factor of 2	563
389	Steady State Frequency Response - Analog Results for 100 \pm 50 Percent Area With a Jazzer Magnification Factor of 3	564
390	Steady State Frequency Response - Analog Results for 100 \pm 5 Percent Area With a Jazzer Magnification Factor of 4	565
391	Steady State Frequency Response - Analog Fan Area Response for 100 \pm 5 Percent Area With a Jazzer Magnification Factor of 1	566
392	Steady State Frequency Response - Analog Results for 100 \pm 10 Percent Area Wit a Jazzer Magnification Factor of 1	567
393	Steady State Frequency Response - Analog Results for 100 \pm 10 Percent Area With a Jazzer Magnification Factor of 3	568

<u>Figure</u>		<u>Page</u>
394	Analog Results - Summary of Fan Time Constants for Steady State Frequency Response With a Jazzer	569
395	Analog Results - Summary of Effects of Jazzer on Fan Response for Roll Control	570
396	Typical Analog Recorder Trace of Fan and Engine Response to Step Changes in Fan Area Using Fans for Height Control	571
397	Analog Results - Fan Speed and Thrust Versus Fan Analog Area, Using Fans for Height Control	573
398	Analog Results - Engine Speed and Exhaust Temperature Versus Fan Analog Area, Using Fans for Height Control	574
399	Analog Results - Fan Speed and Thrust Time Constants for Step Changes in Fan Area From the Design Point, Using Fans for Height Control	575
400	Analog Results - Fan Speed and Thrust Time Constants for Step Changes in Fan Area to the Design Point, Using Fans for Height Control	576
401	Analog Results - Effects of Jazzer Washout Rate on Fan Time Constants for Step Changes in Fan Area Using Fans for Height Control	577
402	Typical Analog Recorder Trace of Fan and Engine Response to Step Changes in Engine Speed Using Engines for Height Control	578
403	Analog Results - Engine and Fan Time Constants for Step Changes in Engine Speed, Using Engines for Height Control	579
404	Engine 2 Airflow Calibration	580
405	Lift Contribution of Bleed Nozzles Versus Core Engine Speed, Run 17, $\delta_S = 80$ Percent	581
406	Bleed Nozzle Thrust Contribution Versus Core Engine Speed, Run 17, $\delta_S = 80$ Percent	582
407	J85/LF2 Lift Versus Flow	583
408	J85/LF2 Gas Power Transfer Performance	584

<u>Figure</u>		<u>Page</u>
409	Comparison of Gas Power Transfer and Thrust Spoiling - Lift Loss Versus Desired Control Force	585
410	Comparison of Dynamic Response for Gas Power Transfer and Thrust Spoiling	586

TABLES

<u>Table</u>		<u>Page</u>
I	Material Properties for Components Used in Variable Area Scroll	104
II	Variable Area Scroll Mechanism and Actuation Component Weights	105
III	List of Test Instrumentation	106
IV	Summary of Test Runs	111
V	Stress Ratios for Gage Locations	117
VI	Effects of Test Configuration on Lift Measured at a Fan Speed of 2300 rpm	118
VII	Comparisons of Lift Increments at 2300 rpm	119
VIII	Summary of Blade Stress Resonant Points - LF2/VAS ($\delta_S = 100\%$) ($\beta_V = 0^\circ$)	120
IX	LF2 and X353-5B Vectoring Characteristics at Constant Input Gas Horsepower	121
X	Steady State J85/J4 Core Engine Performance Data	122
XI	Analog Engine Cycle Parameters	123
XII	Analog Fan Design Point Data	124

SYMBOLS

A	area
c_p	specific heat
C	a constant
EGT	exhaust gas temperature
f	frequency
f_a	fuel-air ratio
F	horizontal thrust
F_T	turbine thrust
FHP	fan horsepower
g	gravitational constant
h	enthalpy
HP	horsepower
J	a constant, $\sqrt{-1}$
J	polar moment of inertia
L	vertical lift
L_T	fan total thrust
m	jazzer magnification factor
M	Mach number
N	fan speed
P	pressure
q	velocity head, $P_t - P_s$
Q	unbalanced torque
R	gas constant
s	Laplacian operator, d/dt

t	time
T	temperature
W	gas flow
W_f	fuel flow
α	attenuation
β	louver air turning angle
β_v	louver orientation angle
γ_1, γ_2	engine internal cycle parameter
γ	ratio of specific heats
δ	pressure correction to standard or position of a component
δ_s	scroll actuator position
Δ	incremental change
ζ	damping coefficient
θ	temperature correction to standard
ξ_1	engine internal cycle parameter
ρ	density
τ	time constant
ϕ	phase shift or flow function
ϕ_1, ϕ_2	engine internal cycle parameters
Φ	flow coefficient
Ψ	pressure coefficient
Ψ_1, Ψ_2	engine internal cycle parameters
ω	angular frequency
$\bar{\omega}$	loss coefficient

SUBSCRIPTS

0	at louver angle of zero degrees or at natural frequency
1	system 1
2	system 2 or engine compressor inlet
3	engine compressor discharge station
5.1 or 51	engine turbine discharge station
5.2 or 52	diverter valve discharge station
5.3 or 53	scroll inlet station
5.4 or 54	scroll nozzle discharge station
5.5 or 55	turbine bucket discharge station
5.8 or 58	fan turbine discharge station
10	fan rotor inlet station
10.6	fan rotor discharge station
11.0	fan discharge station
a	ambient or free stream
c	corrected to standard conditions
D	dump
e	effective or engine
f	fan or based on thrust
J	jazzer
N	based on fan speed
s	static
S	scroll
t	total
T	fan turbine or fan tip

INTRODUCTION

The XV-5A flight research aircraft has successfully demonstrated the capabilities of the lift fan propulsion system in V/STOL flight. Aircraft control is obtained during vertical and transition flight by a fast response, thrust spoiling, exit louver system. Although relatively simple, the louver spoiling system is inadequate for heavier aircraft because it requires that part of the lift be spoiled and held in reserve to supply the aircraft control forces.

Investigations of the control and propulsion system requirements of future V/STOL aircraft designs have shown that a power transfer type of control system is very attractive when compared to both the thrust spoiling concept and separate control devices. The next logical step in the evaluation of improved lift fan systems was the actual demonstration of the power transfer method of lift modulation.

With this goal in mind, the task was undertaken to design and manufacture a variable area scroll capable of producing the required power transfer. The demonstration testing of the system would include the second generation of lift fan rotors, the LF2. The LF2 rotor level of polar moment of inertia is required to permit demonstration with the control response rates compatible with the aircraft requirements. Fan and scroll assembly sized for XV-5A installation was an established requirement for the demonstration system.

With these requirements established, the demonstrator vehicle, called the LF2/VAS, consisted of the following major components:

- o The partial admission variable area scroll
- o The lightweight LF2 rotor
- o The lightweight LF2 front frame
- o Existing XV-5A type cross ducts and diverter valves
- o Existing X353-5A lift fan rear frame and louver systems
- o Two J85 core engines as gas producers
- o An overboard dump system to simulate the opposite hand fan installation

The demonstration tests were performed in the lift fan test facility of General Electric in Evendale, Ohio. The test program was established to demonstrate the control effectiveness of the variable area scroll system, the dynamic response of the control system, and the mechanical performance of the variable area scroll and LF2 rotor system.

The demonstration test program was begun on August 26, 1966, and completed on October 31, 1966. The test program encompassed over 15 hours of fan operation, mostly at 95 percent and above power levels, and 200 steady state performance conditions were measured. In addition to the steady state performance, numerous transient tests were conducted to obtain control effectiveness using power transfer for roll control, using fan area for height

control, and using engine power for height control.

A second program, performed in parallel with the demonstration program, was an analog simulation of the power transfer lift fan system. The demonstrator fan was limited in scroll size capability and consequently in power modulation range. This limit was dictated by the restrictions of envelope established by use of the existing fan frames. Total fan turbine active arc was restricted to 168 degrees, while desired power transfer system may require greater than 200 degrees of arc.

The analog simulation provided a means of predicting power transfer system performance in scroll designs employing higher admission arcs. Analytical methods were used to establish the basic inputs for the analog simulation. The full-scale demonstrator fan was tested, and performance, steady state and dynamic, was measured. The analog was compared to demonstrated performance and then used to demonstrate the larger control levels.

This report summarizes all phases of this test program, beginning with the design of the variable area scroll and ending with the completion of the analog simulation. Aerodynamic and mechanical performance of both the variable area scroll and LF2 rotor system is presented. The results of the analog program are presented, compared with demonstrated performance, and used to predict dynamic fan performance over a large range of power levels.

VARIABLE AREA SCROLL CONCEPTS

The concept of lift fan gas power transfer is simple. It is a means to shift the center of propulsive lift relative to an aircraft's center of gravity or maneuvering axis. It assumes that an aircraft will have two or more lift or lift/cruise fans with their individual lift centers displaced from the aircraft center of gravity. Thus, if it is possible to modulate fan lifts relative to each other, forces and moments can be generated to maneuver an aircraft or to trim unbalances.

Lift modulation can be accomplished by spoiling, as demonstrated in the XV-5A. This is an entirely practical system for low inertia aircraft of 5,000 to 10,000 pounds gross weight, but it imposes an unacceptable lift penalty as aircraft gross weight is scaled up for a given configuration. Figure 1 illustrates this effect for simple aircraft of the XV-5A type. The curves shown are for a specific fan-airframe relationship and are not universally applicable to all aircraft configurations. However, the message is clear: large aircraft require more efficient means of lift modulation than spoiling. The increasing difficulty of V/STOL aircraft control as a function of gross weight is due simply to a divergence of the available control moment and the inertia which must be accelerated. If "L" is an aircraft dimensional scale factor, then

Gross weight is proportional to L^3 .

Available fan control moment is proportional to L^4 .

Aircraft polar moment of inertia is proportional to L^5 .

The variation in the required control performance versus aircraft gross weight has been subjected to endless argument. As it now stands, the control efficiency or weight-plus-performance penalty must improve with increasing gross weight. For lift and lift/cruise fan powered V/STOL aircraft, this tends to define three categories of control concepts:

1. Lift spoiling applied to fans
2. Gas power transfer applied to fans
3. Separate control devices

Figure 2 illustrates a typical relationship of these categories. Large V/STOL assault transports will not incorporate lift spoiling type controls. The choice between gas power transfer and separate control devices is not clear. Airframe contractor CX6 studies show a division of preference. Generally, those who used both lift and lift/cruise fans preferred gas power transfer.

Two methods of power transfer using the tip turbine concept have been identified. The two methods are the variable area scroll and energy modulation. This report is concerned with the demonstration of the variable area scroll method, and a detailed description of the concept follows.

POWER TRANSFER FOR ROLL CONTROL

Power transfer for roll control in pneumatic-driven fans may be accomplished by shifting gas flow from one fan to another. To change the flow delivered requires a power turbine inlet area change. To increase the power in a fan, the turbine inlet area must be increased while another fan turbine area is decreased an equivalent amount, thus shifting the flow from one fan to another while maintaining a constant core engine discharge total area, gas temperature, and pressure. The system is shown in Figure 3 in the normal balanced condition and a condition representing roll power transfer.

The area variation is accomplished by incorporating small splitter vanes between the turbine nozzle partitions. These splitters are ganged through a linkage which will actuate these splitters in small groups making gradual increases or decreases in admission arc. This approach minimizes throttling losses and provides a nearly linear and ideal thrust change with flow. The fan turbine thus operates with varying degrees of turbine admission arc. Thrust performance in this system ideally would vary as the two thirds power of the ratio of turbine gas flows. Deviations from this ideal occur because of changes in ducting pressure losses, additional partial admission power losses in the scroll inactive arc, and changes in turbine efficiency and scroll leakage.

FAN AREA FOR HEIGHT CONTROL

Height control using fan area may be accomplished by shifting the core engine operating conditions. To change the engine operating point, the core engine discharge effective area must be changed. This change in area may be produced by changes of the fan turbine inlet area. In contrast to the case of roll control, height control is obtained by increasing or decreasing the area on two equivalent fan turbines simultaneously and an equal amount. As the core engine area increases, the total available energy decreases as determined by the core engine performance cycle. Decreases in area increase the total energy with a limit established at the maximum exhaust gas temperature or pressure of the engine. The system is shown in Figure 4 in the balanced condition and a representative decreased lift condition.

Thrust performance of the two fan systems will vary as the two-thirds power of the total energy being supplied of the core engine. The total energy variation is a direct function of the fan total turbine inlet area.

CORE ENGINES FOR HEIGHT CONTROL

A second method of height control that has proved effective in some research VTOL aircraft is manipulation of the core engine power level by the engine throttle system. In this case, the total fan turbine area is held fixed and total system thrust is varied simply by changing the core engine speed.

LIFT FAN DYNAMIC PERFORMANCE

A measure of the responsiveness of a lift fan power transfer system to input commands can be analytically determined by calculating the time constant for plus or minus an infinitesimal speed change about the design point. This technique is useful in comparing the response of different system configurations.

The time constant is, by definition, the time required for the fan to traverse an incremental change in speed at a uniform acceleration equal to the initial value:

$$\tau = \lim_{\Delta N \rightarrow 0} \frac{\Delta N}{(dN/dt)}$$

where

τ = time constant, seconds

ΔN = incremental speed change

dN/dt = fan rotor acceleration

This time constant for tip turbine fans can be found by solution of the differential equation:

$$T_T - T_F = (2\pi/60) J_0 (dN/dt)$$

where

T_T = turbine torque, ft-lbs

T_F = fan torque, ft-lbs

J_0 = fan rotor polar moment of inertia, slug-ft²

N = fan speed, rpm

d/dt = derivative with respect to time

Representing the turbine torque as a linear function of speed, and fan torque from the fan laws as a function of the square of the speed, and taking the limit, the following expression for fan time constant is obtained:

$$\tau = (2\pi/60) J_0 N_{DP} / T_{DP} (k + 1)$$

where

k = ratio of the locked rotor turbine torque to the design point turbine torque

N_{DP} = fan design point speed, rpm

T_{DP} = fan design point torque, ft-lbs

The predicted lift fan rotor speed time constant for the LF2/VAS system was calculated to be 0.31 second at 100-percent fan speed, 2750 revolutions per minute.

THE JAZZER SYSTEM

Improvements in responsiveness of a fan system may be obtained by including a device commonly referred to as a jazzer. The jazzer is a simple anticipatory device inserted into the fan control system. The device can be either mechanical or electrical. A mechanical device may be preferred over the electrical system for reliability. However, during this test program an electrical device was used because of its simplicity to changing operation constants.

The mechanical jazzer system and an equivalent electrical circuit are shown in Figure 5. The electrical circuit is a simple resistance-capacitance network. The mechanical jazzer is a simple spring dashpot device.

The response of a jazzer system is of the following form for a step type of input.

$$\frac{\text{Output}}{\text{Input}} = 1 + me \left(\exp - \frac{t}{\tau_J} \right)$$

This relationship represents a function that is equal to unity plus a magnification factor, m , at time equals zero, and is washed out exponentially to unity as time increases. Thus, the jazzer system initially magnifies a control input command to overcome fan inertia and quicken fan response. It then exponentially washes out this overshoot to the steady-state input level. Figure 6 shows a typical jazzer response characteristic and its effects on fan system responses.

The upper figure shows a step input of unity occurring at time equal zero. The next figure shows the input command as modified by the jazzer. The initial level at zero time instantaneously achieves a level of one plus the magnification factor and exponentially decays to unity in about three time constants. The third figure shows the variation of the scroll actuator and consequently the area as a function of time. The initial ramp at zero time is due to actuator slew rate and the maximum level does not quite achieve the command level before the exponential washout occurs. The lower curve shows the fan system relative response. The effects of the jazzer increase the fan response or reduce the time to achieve the commanded level of output.

FAN RESPONSE WITH SINUSOIDAL INPUTS

In the analysis of a dynamic system such as the tip turbine variable area scroll system, performance under conditions of steady sine wave input commands is of significant interest. For conditions of steady sinusoidal inputs, it is quite easy to determine both the attenuation and phase shift at a particular input frequency level. The attenuation is defined as the ratio of the output level for a given sinusoidal input command to the steady-state level for the same input. The phase angle is defined as the phase shift of the sinusoidal output relative to the input. By using the attenuation and phase angle characteristics, comparison of test results and calculated results is quite easy; for example, the test results of the actual LF2/VAS fan system can be compared to the analog simulation results. The following discussion presents some useful information concerning the behavior of the attenuation and phase angle relationship for a typical dynamic system.

A common form for writing the equation of a single-order system as a function of frequency, ω , is as follows:

$$\frac{O}{I} = \frac{\text{Output}}{\text{Input}} = \frac{1}{1 + j\omega\tau}$$

Solving for the magnitude of this expression, the equation then becomes

$$\frac{O}{I} = \frac{1}{[1 + (\omega\tau)^2]^{1/2}}$$

The phase angle also becomes

$$\phi = -\text{Arctan } (\omega\tau)$$

This phase angle and attenuation characteristics are shown in Figure 7. The ratio of output to input levels are connected into units of decibels to facilitate representation of the variation with frequency. Figure 8 shows a conversion chart relating output-input ratio and attenuation in decibels.

One interesting characteristic of this type of presentation is the shape of the asymptotes for both the high and low frequency regions:

$$\text{for } \omega\tau < 1 \quad \frac{O}{I} \approx 1$$

$$\text{for } \omega\tau > 1 \quad \frac{O}{I} \approx \frac{1}{\omega\tau}$$

In terms of decibels, the high frequency region has a slope of -20 decibels per decade and intersects the zero decibel line at the value of $\omega\tau$ equal to unity. Also at this frequency point, the phase angle is 45 degrees.

These relationships will prove to be very useful in the analysis of the test results obtained during this program.

A similar discussion of the jazzer circuit is possible. The jazzer system for steady-state sinusoidal inputs is represented by the following equation:

$$\frac{O}{I} = \frac{\text{Output}}{\text{Input}} = \frac{1+j\omega(1+m)\tau_J}{1+j\omega\tau_J}$$

The jazzer is therefore a two-time-constant system. One time constant is τ_J and the other is $(1+m)\tau_J$. Using a similar method as above, it is possible to derive the phase shift and attenuation diagrams for this equation. The resulting characteristic for a typical jazzer system is shown in Figure 9.

VARIABLE AREA SCROLL DESIGN, MANUFACTURE, AND ASSEMBLY

BACKGROUND

Initial program statement of work called for:

1. Scroll design including analytical studies and model/bench tests to assure optimum configurations.
2. Manufacture of one flight-weight, flight-quality variable area scroll suitable for assembly and test with LF2 rotor and front frame components.
3. Scroll sized to fit existing XV-5A wing contour and handle 110 percent of GE J85/J4 engine flow.

Preliminary design studies defined a 200-degree admission arc scroll with plus or minus 25-percent area change about the nominal 90-percent J85/J4 flow, which was the basis of the LF2 rotor design, as the best configuration to meet program objectives. The scroll selected would be sized to handle 112.5-percent J85/J4 flow to meet the maximum power condition and would employ variable vanes mounted in the scroll nozzle to facilitate flow modulation.

During the course of detailed designs, it became increasingly evident that an optimum scroll configuration with minimum pressure losses could not be sized for engine flow requirements and packaged within the XV-5A wing contour. As the scroll arms approached the XV-5A wing spars, the change in area and contour required to fit the scroll in the wing resulted in high power setting Mach numbers of 0.47 compared to Mach 0.38 for the optimum design. Change in Mach number would result in an additional 3.7-percent pressure loss. No estimate was made of additional losses due to contour modification.

The studies on scroll design were concluded with the recommendation that the requirement of 110-percent J85/J4 gas flow be eliminated. The demonstration of power transfer, by means of a variable area scroll, would be demonstrated by the following design objectives.

PROGRAM OBJECTIVES

1. Design and build a 168-degree-arc flight-weight, flight-quality scroll. This scroll would fit the XV-5A wing contour and cause no compromise in optimum scroll area or contour.
2. Demonstration would be based on Mach numbers and pressure losses typical of the optimum configuration.
3. Variable area scroll performance could be compared directly with fixed area scrolls.

4. The scroll could be manufactured from existing tools. Front frame design modification would be significantly reduced by eliminating the changes required to go through or over the scroll to reach primary fan mounting points.
5. Scroll materials, including actuation system, would be based on possible demonstration with J85/J4.
6. Scroll material thickness would be established as typical for flight type parts without requiring irreparable changes to XV-5A scroll tools, and would be capable of sufficient life to complete program demonstration objectives.
7. Flow modulation changes on 168-degree scroll would be sufficient to permit demonstration of flight type LF2 system and provide an accurate basis for parameters used in computer program defining LF2 and advanced variable area scroll systems.

MATERIAL DESIGN LIMITS

Material design limits for components in the scroll area control system were governed by the following criteria:

1. 80 percent of the stress rupture strength at 1350°F for 300 hours.
2. 0.2-percent offset yield strength, reduced by three deviation factors.
3. Stress range diagram, modified Goodman diagram, for components subjected to alternating loads.
4. All materials selected on the basis of properties at 1350°F and availability.

Material properties were obtained from General Electric Material Handbooks, Volume I. The design philosophy was guided by General Electric Design Practices Manual, Section 14C201.

Figures 10 and 11 and Table I list the material properties used for component design.

SCROLL DESIGN, MANUFACTURE, AND ASSEMBLY

A full-scale scroll similar to that used in the General Electric X353-5B lift fan was manufactured for this program. The major differences between this scroll and the X353-5B scroll were:

1. The nozzle partition length was reduced to match the LF2 rotor geometry.

2. Bosses for mounting the variable area control mechanism were incorporated into the scroll structure.
3. The area trim feature of the X353-5B fan system would be incorporated into the area control system.

Manufacturing of the scroll began in May 1965, and the assembly of the lift fan system was completed in June 1966.

Mechanical Design

The X353-5B scroll design has proven to be structurally reliable, as evidenced by its cumulative flight time in the XV-5A aircraft; consequently, no changes were made which affected the structural design intent. Details for the mechanical design of the X353-5A* scroll can be found in Reference 2.

Provisions for mounting the mechanism to the scroll were made by brazing cylindrical bosses into the inner band hat section which supports the nozzle partitions. The bosses were tapped after brazing for 10-32 size bolts. The close spacing of the nozzle partitions and bosses on the aft scroll arm made it necessary to utilize a solid inner band hat section to maintain the structural integrity of that component.

The detail drawings of the scroll can be found in Figures 12 and 13.

Aerodynamic Design

Scroll design (including nozzle partition contours, spacing, flow, and area distribution) is identical to that of the X353-5B scroll. The nozzle height was reduced to match the LF2 rotor geometry.

The objective nozzle area was 48.9 square inches per side of scroll. Figure 14 shows the breakdown of the nozzle area as measured for the actual test scroll. Nominal fan Mach number is 0.30.

Manufacturing

The vendor selected for the scroll manufacture was Solar Aircraft Corporation in San Diego, California.

The scroll manufacturing tooling was part of the X353-5B program. Modifications to the tooling were kept to a minimum so that the tooling could be returned to its original form. A duplicate scroll mock-up model, reflecting the new nozzle exit contour, was procured.

*The X353-5A scroll differs from the X353-5B scroll in that it has a single inlet rather than dual inlets and it is made from L-605 material rather than Hastelloy X material.

Figures 15 and 16 show a portion of the nozzle diaphragm, struts, and hat section prior to welding the shell to this structure.

Prior to brazing the nozzle partitions into the torque tube, Hastelloy X shims had to be inserted in the oversized gaps. During eloxing of the partition contour into the torque tube, insufficient trimming and excessive movement of the electrode had increased the size of the contour cut-out. Since the integrity of a brazed joint is affected by the gap between adjacent parts, it was necessary to decrease the gap to an acceptable size. The braze alloy used was J8103.

A second braze cycle was required to fill the voids of the first braze cycle. Voids and cracks remaining from the second cycle were repaired by using a gold-nickel torch braze process rather than by going through a third complete cycle*.

Assembly

During the assembly of the scroll to the LF2 front frame, measurements taken to the end of the scroll arms indicated the radius to be 0.190 inch under minimum. The smaller radius made the assembly of the slip seals, honeycomb seals, and operation of the mechanism virtually impossible (Figure 17). It was necessary to spread the scroll arms apart to allow assembly of the fan and scroll system.

A hydraulic ram was placed between the ends of the scroll arm (Figure 18). To distribute the load on the scroll arms, a box structure containing Cerrobend** was built around the ends of the scroll arm. Incremental deflections were made until the scroll arms had been permanently enlarged 0.220 inch radially.

A gold-nickel torch braze process was used to repair the cracks incurred in the braze as a result of bending the scroll. An inspection after repair brazing indicated that the scroll arms had pulled inward 0.109 inch. The scroll was again enlarged. This time the scroll structure was cut at two places near the scroll inlet stiffeners (see Figure 66) to reduce the forces required to expand the arms. A slow rate of braze repair resulted in negligible shrinkage, even though there were twice as many braze cracks (36) incurred during the second bending.

*It is desirable to minimize the time at high braze temperatures to prevent boron from penetrating the grain boundaries of the nickel and thus reducing the ductility of the parent material.

**Cerrobend is the trade name for a low-melting temperature alloy that is the product of the Cerro de Pasco Copper Company, New York, New York.

VARIABLE AREA MECHANISM AND ACTUATOR SYSTEM

Two configurations for varying the scroll nozzle area were evaluated in terms of aerodynamic performance. One configuration consisted of splitter vanes installed between pairs of nozzle partitions, and the second configuration consisted of partial rotation of the nozzle partition itself. The results of this evaluation are shown in Figure 19. The addition of variable geometry in the nozzle diaphragm, and its attendant leakage, inherently results in a decrease in gas horsepower available to the fan turbine. The variable nozzle partition concept compares favorably with the splitter vane concept in terms of aerodynamic performance during nominal operation; however, at the extreme operating positions, the performance of the variable nozzle partition deteriorates rapidly. The increased performance loss is basically the off-design performance of the turbine bucket geometry. Additional losses can be expected due to the off-design operating conditions of the nozzle. It can thus be concluded that over the flow range studied for aircraft roll control, the splitter vane is superior to the variable nozzle partition concept.

The variable area scroll* mechanism and actuation system consists primarily of splitter vanes, bellcranks, cam followers, cam tracks, drive links, serrated connectors, an actuator support, and a test actuator (see Figure 20). Except for the third mount of the actuator bracket, the mechanism and actuation system is mounted to the scroll inner hat section and thus does not increase the fan envelope. It is designed to operate at J85/J4 core engine exhaust temperatures. A single, test-type hydraulic actuator would be used to drive the scroll area system.

The variation of scroll nozzle area is accomplished by partial rotation of splitter vanes which are located between sets of nozzle partitions. The splitter vanes (banked together to form six groups in each scroll arm) are rotated by cam followers, indirectly attached to the vane by a bellcrank. Each cam follower is guided by a face cam machined in a bar. The spacing of the face cams results in an overlap in the closing and opening of the splitter vane banks, in order to obtain a short actuation stroke consistent with a fast response system.

The actuation links are supported by sets of rollers and wheels mounted to a bracket. A serrated connector, which can be used on an area trim device, is used to connect the bars containing the face cams to the links.

The VAS mechanism and actuator system was designed for the 168-degree scroll, and it can easily be adapted for use with larger admission arcs.

*Throughout the discussion, the variable area scroll system will be referred to as the VAS.

Splitter Vane Design

The discharge area of the scroll is varied by opening and closing splitter vanes located in the turbine nozzle diaphragm. The splitter vanes installed between pairs of nozzle partitions, rotate through an angle of 55 degrees between the full open and full closed positions (see Figures 21 and 22). Since the nozzle partition contours at the ends of each scroll arm are different, the splitter vane contours are also different.

The initial design objective of the 200-degree-arc scroll was to provide plus or minus 25-percent turbine area variation, using 90 percent of J85/J4 exhaust flow as the nominal flow condition. However, when the program was redirected toward using a 168-degree scroll, the nominal condition was reduced to 65 percent of J85/J4 exhaust gas flow with the variable admission arc for the 168-degree scroll remaining the same as for the 200-degree scroll. Thus, the quantity of splitter vanes was determined to be 24 bi-convex vanes and 12 flat vanes. Figure 23 shows the distribution of the nozzle area for the 168-degree scroll.

The splitter vanes at the ends of the scroll arms are the first to close when the actuator is retracted, and those near the center of the scroll are the first to open when the actuator is extended.

The detail drawings of the splitter vanes are given in Figures 24 and 25, the drawing of the vane and scroll assembly is given in Figure 26.

The aerodynamic design intent for the splitter vane contour was to create a converging passage between the splitter vane surfaces and the nozzle partitions. When the vanes are in the open position, the minimum flow area occurs at the trailing edge of the nozzle partition. As the splitter vane begins to rotate toward the closed position, the throat location is changed to the leading and trailing edges of the splitter vane, see Figures 27 and 28. It is to be noted that the splitter vane can rotate approximately 5 degrees before the minimum flow area occurs at the vane. This rotation is advantageous because it compensates for aerodynamic losses which would occur because of manufacturing tolerances and assembly clearances.

The size and location of the splitter vane are the result of several conditions. Aerodynamically, it was desirable to locate the vane as far upstream between the nozzle partitions as is feasible. This results in minimum vane profile losses because the flow velocity is also at a minimum. However, the upstream location is limited because the leading edge of the splitter vane must not protrude above the nozzle partition leading edge. Since it was desirable to minimize the aerodynamic moment on the splitter vane, the pivot axis was chosen at the midchord of the vane. The chord length was then dictated by geometry, and the thickness of the vane was governed by the allowable stress.

Each splitter vane is supported on its sides at the midchord. The mounting

design was dictated primarily by assembly considerations, see Figure 29.

The outer support consists of a shaft which is welded to the vane blank. A spherical head is machined on the shaft to prevent binding in the event that the vane axis and bushing axis are not aligned. The bushing does not rotate because of a tongue-in-groove arrangement with the scroll housing.

The inner support for the splitter vane consists of bolting three parts together; namely, the vane, a torque plug, and a lever. The torque plug and lever are separable parts for assembly purposes. The flange on the torque plug prevents the sides of the splitter vane from rubbing the scroll. In the event of excessive wear, the torque plug can be exchanged for a new part.

The splitter vane assembly is Hastelloy X material. This material was chosen because the scroll is Hastelloy Y and it was desirable to maintain the same coefficient of thermal expansion.

The bushing and torque plug are L-605 material. This material was also chosen because of its high temperature oxidation resistance and wear resistance. By using a cobalt base material, L-605, sliding against a nickel base material, Hastelloy X, the possibility of fretting and consequent seizing is minimized.

Anti-sieze compounds were not applied to the bearing surfaces because of their limited life at J85-13 exhaust temperatures. Also, it was advantageous to operate the bearing in the unlubricated condition, since it would provide quantitative information as to the useful life of the dry bearing.

Stresses in the splitter vane were calculated by assuming the vane to be simply supported and loaded by a uniform pressure differential of 22 psi. Figures 30 and 31 summarize the section properties in the splitter vanes. The maximum bending stress in the splitter vane occurs at the transition of the shaft into the vane and is 32,800 psi.

The structural design of the mechanism is sized by the splitter vane aerodynamic moment. A conservative approach was used to determine this moment; that is, it was assumed that one-half the vane was subjected to a pressure differential of 22 psi. Since the vane is nearly aerodynamically balanced, this moment represents an extreme condition.

A friction coefficient of 0.60 was used on splitter vane journals throughout the analysis. The friction loads were then combined with the air loads to obtain the total external loads on the vanes. For the biconvex splitter vanes the moment required to rotate a vane was 9.1 inch-pounds and for the flat splitter vanes the moment was 15.2 inch-pounds.

Splitter Vane Assembly and Manufacturing

The flat splitter vanes can be easily installed or removed from the discharge side of the scroll. However, the biconvex splitter vanes are more difficult to install or remove and require disassembly from the inlet side of the nozzle box.

The last biconvex splitter vane at the end of the scroll arm was impossible to remove. The scroll shell above this vane tapers toward the scroll end mount and thus prevents removal of this particular vane, see Figure 32.

The flat splitter vanes were manufactured with the aerodynamic camber inverted. All 12 vanes were reworked to correct the camber, Figure 33. Aerodynamic losses of inverted installation and subsequent rework are considered to be negligible.

It was found that the splitter vanes would not close completely when they were assembled to the levers. The vanes were removed from the scroll and reworked to obtain clearance with the scroll. Several of the splitter vanes also had to be welded using Hastelloy X weld filler because of excessive notches in the support shaft.

After the above rework was completed, another problem occurred when the lever and splitter vane were bolted together. The torque plug was binding in the scroll. It was concluded that the axis of the bolted assembly did not coincide with the axis of the nut bushing and scroll. By increasing the diameter of the nut bushing and scroll to obtain 0.010-inch radial clearance, the binding was relieved.

Bellcranks and Levers Design

Each splitter vane is rotated by either a lever or a bellcrank, depending on its location in the assembly. The lever, torque plug, and splitter vane are clamped together with a 0.190-32 bolt and, therefore, rotate as an assembly. A sheet metal tie bar connects one or more levers to a bellcrank to form a three-bar linkage.

The bellcrank is rotated by a force exerted on the roller bearing attached to it. The roller bearing is used as a cam follower in conjunction with the cam track.

The detail drawings of the levers, bellcranks, tie bar, and roller bearings are shown in Figures 34 through 37. The forward and aft levers and bellcranks are nearly identical except for being opposite-hand parts.

To package the mechanism between the scroll and existing front frame, it was necessary to minimize the size of the lever, bellcrank, and cam track. The finalized design required modifying only the gussets on the hot side torque tube (see Figure 38). However, less than desirable clearance between stationary and moving parts had to be maintained to accomplish this. The minimum clearances were 0.025 inch between the lever and nut bushing and

0.046 inch between the roller bearing nut and the nozzle partition cover plate.

Since a locknut could not be used to retain the roller bearing, it was necessary to employ an interference fit between the roller bearing shaft and bellcrank hole. A locknut could not be used because:

1. There was no method whereby the miniature roller bearing could be held while torquing the locknut.
2. The commercial locknuts were dimensionally higher than desirable.
3. René 41 material was desired.

A straight knurl on the roller bearing shaft was used as a secondary retaining feature and to reduce the assembly stresses resulting from the interference fit.

The tongue-in-slot connection of the lever and bellcrank to the torque plug was by necessity rather than by choice. The small size of the stub shaft makes serrations expensive and therefore undesirable in a one-of-a-kind vehicle. Also, the tongue-in-slot design results in lower bearing stresses at the connection.

Careful consideration was given to the design of the face cam to minimize peak loads on the bellcrank. The final design for the cam produced the optimum bellcrank moment arm and short control stroke for the mechanism. Figures 39 and 40 show the effective moment arm for the forward and aft bellcranks. The friction coefficient of the roller bearing and face cam increases or decreases the moment arm, as these figures indicate. Since the actual roller bearing friction coefficient will be less than 0.10, the 0.20 friction coefficient used for bellcranks and lever analysis is conservative. Limited bench testing of the roller bearing indicated that it will operate satisfactorily for the temperature and loads anticipated. The detailed results of these tests are presented in Appendix II.

The geometry and quantities of the levers and bellcranks lend themselves to precision castings. Because of the long lead time required for castings, it was necessary to change the material from cast René 41 to Inconel X bar stock. The original selection of René 41 material was based primarily on the anticipated J85/J4 core engine temperatures.

The maximum stress in the bellcrank occurs on the tab which supports the roller bearing and is 35,600 pounds per square inch tension. Although this stress approaches the endurance limit of the material, it will be satisfactory because of the conservative assumptions used for the calculations.

A slot for mating with the "tongue" on the tongue plug was machined in the levers and bellcranks as part of the assembly sequence because it was

anticipated that the splitter vane closure angles would vary from part to part. The closure angle was measured by setting the scroll nozzle diaphragm on a surface plate and measuring the angle with an optical inclinometer. An additional 2 degrees was added to the measured angle when machining the slot in the levers and bellcranks to prevent overtravel of the splitter vane.

The aft levers and bellcranks rotated freely prior to assembling the tie bar to them; after the tie bar was assembled, the subassemblies tended to bind. The reason for the binding was the vertical misalignment in the levers resulting from the magnification of a slight misfit between the lever and torque plug. The misfit was corrected and resulted in relieving the binding in nearly all subassemblies.

The bolt which connects the lever, torque plug, and splitter vane is lockwired to the lever by an 0.016-inch-diameter wire. The bolt for the bellcrank is lockwired to the roller bearing nut.

Cam Track Assemblies

The cam track assembly is analogous to part of an actuator ring used for core engine compressor stators. However, it is different in that it drives only one bank of vanes at a time and that it is part of a fast response system. The cam track assemblies are connected to a set of links to make up a 180-degree actuation ring.

Two cam track assemblies are utilized to rotate the splitter vanes. Each assembly consists of three sectors, or "tracks", which are riveted in series. Two face cams are machined in each sector.

Both cam track assemblies are supported by six equally spaced slide brackets. Approximately 0.050-inch clearance is maintained between the track and the bracket to prevent binding.

A serrated connector, which is used to connect the cam track assembly to the other drive links, provides for a means for trimming the scroll nozzle areas in the adjacent sides of the scroll.

The detail drawings of the forward and aft cam tracks are given in Figures 41 through 43.

The size of the cam track cross section was governed primarily by the available space between the scroll and front frame tube. This space is a minimum at the ends of the scroll arms when the scroll is cold; as the scroll expands, this space increases until it is uniform around the scroll periphery.

The minimum wall thickness of the cam track was limited to 0.048 inch. This thickness was sufficient to prevent elastic instability. It was also felt that reducing the thickness would limit the manufacturing method to

eloxing since machining of thin-walled parts is undesirable and difficult. The wall thickness tolerance was then stacked so that a minimum clearance of 0.016 inch would exist between the cam faces and the roller bearing.

The actuation stroke of the mechanism for 168 degrees scroll was limited to approximately 4.90 inches. This limitation is set by the geometry of the scroll corner seals. Using this limitation as a base point, the design and spacing of the face cams in the cam tracks could be evaluated. Figures 44 and 45 show the final design characteristics of the cam spacing effects. This spacing results in rotating one bellcrank and its associated levers until their splitter vanes are nearly closed before the next bank starts to rotate. Successive opening and closing of splitter vanes result in a nearly linear nozzle area variation. Actuation of the cam tracks causes the splitter vane banks at the ends of each scroll arm to close first, and inversely, those towards or near the center of the scroll to open first.

The cam contours and spacing of the contours are the same for all the face cams in a subassembly; however, each subassembly had a different contour and contour spacing. The design intent of the cam contour in each subassembly was to maintain a constant moment arm, or a minimum of 0.40 inch on the bellcranks; see Figures 39 and 40. To maintain the lightweight design feature, several of the face cam grooves were made longer than necessary. This was felt to be the simplest method of reducing weight.

The cam track sectors are connected by a clevis configuration. An 0.250-inch-diameter Inconel rivet, with a countersunk head, is used principally as a shear member. The formed head of the rivet is flush so that the cam tracks can slide between the brackets. A minimum of 0.050 inch clearance was maintained between the male and female ears of the clevis to prevent bending stresses in the ears and tension loads in the rivet. This type of loading can occur when there is a thermal lag or thermal differential between the scroll and cam tracks.

Because the clevis connection does not provide restraint against in-plane torque loads, a tongue-in-slot feature was incorporated as part of the connection. Again to prevent bending stresses, a minimum clearance of 0.040 inch was maintained between adjacent parts. This type of loading can occur when the scroll deflects axially.

Each cam track assembly is supported by six equally spaced brackets. By positioning the bracket next to a bellcrank, it was possible to minimize the bending loads on the cam tracks. A minimum clearance of 0.050 inch was maintained between the cam track and the bracket to aid in preventing binding.

The cam track assemblies are connected to the actuation links by serrated connectors. A "post" on the connector is inserted into a dovetail slot in the cam track. Adequate clearance is designed into the mating parts to prevent bending stresses. By rigging the connector, when the actuator is extended, a predetermined clearance between the roller bearing and the end

of the face cam can be obtained.

The cam tracks are made from L-605 material. This material was selected because of its wear resistance at 1300°F and its oxidation resistance. Since the cam tracks will be sliding on René 41 (a nickel base material), it was felt that L-605 (a cobalt base material) would offer the best material compatibility. The utilization of the higher strength material was felt to be unnecessary since the tensile stresses were within the allowable limits of L-605 material and also because elastic stability was the predominant design limitation.

The maximum tensile stress occurs at the clevis of the center cam track and is 9,900 psi. A stress concentration factor of 2.6 was used to determine the alternating stress. Combined steady state and alternating stresses are within the limits of the stress-range diagram.

Cam Track Support Brackets

Each cam track assembly is supported by six equally spaced brackets. The brackets also serve the function of retaining the splitter vane nut bushings adjacent to them. Shear bolts, 0.190-32, are used to attach the brackets to the scroll.

The detailed drawings of the forward and aft brackets are given in Figures 46 and 47; Figures 48 and 49 show the aft brackets assembled to the scroll.

The geometry of the bracket was dictated by maintaining clearance with the adjacent bellcrank and lever at the extreme positions of their travel. Because the spacing of the nozzle partitions is different in each scroll arm, it was necessary to design a forward bracket and an aft bracket.

The limited space for the mechanism made it necessary to utilize the sides of the bracket for retaining the splitter vane nut bushings. The sides of the bracket are designed to align with one of the faces on the hex nut portion of the bushing. Each aft bracket retains three nut bushings and each forward bracket retains two nut bushings.

There are six brackets used to support each cam track assembly. Each bracket is positioned adjacent to a bellcrank and consequently provides the vertical reaction required to support the cam tracks. To prevent binding, a minimum clearance of 0.050 inch was maintained between the sides of the bracket and cam track.

The brackets are bolted to bosses in the scroll hat section using 0.190-32 bolts. Three bolts are used to support the forward bracket; two bolts and a tongue-in-slot connection are used to support the aft brackets. To compensate for differential thermal expansion and thermal lag between the scroll and the brackets, one of the bolt holes is slotted and the bolt in that hole has reduced torque. The bolts are lockwired together at assembly.

After the cam tracks have been installed into the brackets, a "T" retainer is assembled to the bracket using a 0.190-32 shear bolt. The bolt is then lockwired to the bracket.

The maximum bending stress occurs in the aft bracket and is 30,500 psi. The combined steady state stress and alternating stresses are within the limits of the Goodman diagram.

The brackets are made from cast René 41 material. This material was chosen because of its wear resistance, strength, and castability. Wear resistance was the prime consideration because the cam tracks slide on the bracket during operation. The geometry and quantity of the brackets make them suitable for precision castings.

Forward and Aft Links

The forward and aft links drive the cam track assemblies by means of a linear actuator attached to the aft link. A system of wheels and rollers, mounted to a bracket on the scroll, supports the links and reacts the loads induced in the links. The links are connected by a clevis. A serrated connector is used to connect each link to its respective cam track.

The detail drawings of the forward and aft link are given in Figures 50 and 51. Figure 52 is a photograph of the separate parts.

The initial design of the cam track drive assembly was to be composed of a system of levers, and the actuator for the system was to be located between the scroll inlets and inside the aircraft fuselage. However, a layout study revealed that there could be possible interference with adjacent aircraft components (pitch fan diverter valves and crossover ducts).

The design effort was redirected toward placing the actuator between the front frame bellmouth and scroll. When it was determined that there would be adequate space for the actuator, it was necessary to evolve a drive system. Because of the limited space between the front frame torque tube and scroll, the geometry and size of the system were dictated rather than designed by choice.

To minimize friction loads and wear, the links were designed to operate on a system of wheels and rollers. Because of the limited space, a lipped channel was considered to be the best geometry for the link sliding surfaces. A 0.016-inch gap was maintained between the surfaces of the link and the periphery of the wheels and rollers to prevent possible seizing.

Although the links could have been made as a single part, it was considered to be advantageous to make them as separate parts for several reasons. First, it was advantageous from a manufacturing viewpoint because of the size consideration. Second, the length of the part would make it susceptible to large bending moments. Third, differential thermal expansion

and thermal lag would tend to induce loads and stresses in the link and scroll. Fourth, it would be nearly impossible to include an area trim feature in the design.

The actuator is connected to the aft link by a clevis arrangement. Because the actuator load had a radial component (relative to the fan centerline), it was necessary to provide a reaction to this load. Analysis indicated that the magnitude of the load was sufficiently small to allow a roller-in-retainer design to be used.

The maximum predicted stress in the aft link is 12,500 psi and occurs in the weld which connects the clevis to the web. Several gussets are used in this region to distribute the load.

The maximum predicted stress in the forward link is 10,100 psi and occurs at the midspan of the link.

The aft link is made from L-605 material. This material was chosen primarily because of its wear resistance at 1300°F.

The forward link is made from Hastelloy X material. This material was chosen because of availability and also because it is much easier to machine than L-605. Wear resistance is not as important in the forward link because of the relatively small loads.

Serrated Connector

The function of the serrated connectors is to connect the forward and aft cam track assemblies to the actuator links. They also provide a simple means of adjusting the cam tracks for trimming the nozzle area of the core engines.

The drawing of the serrated connector assembly is given in Figure 53; Figure 54 shows the connector assembled to the aft link.

The design intent for the serrated connector was to incorporate an area trim feature in the design of the cam track-link connector. This area trim feature was to be such that only minor fan disassembly would be required. Because the LF2 front frame does not support the bellmouth, the problem was simplified; however, the design would have to be altered if the bellmouth were attached to the front frame.

The connector assembly consists of two parts, a serrated plate and a serrated block with a dovetail. Serrations were used to provide a reliable method of transmitting the shear load from the block to the plate.

To minimize bending loads and stresses in the cam tracks and links, the serrated connector dovetail floats in the dovetail slot on the cam track. Relative movement of the cam track to the link cannot exceed 0.008 inch, but the rotation between the parts can exceed 3 degrees. These values

were considered to be necessary and acceptable to the operation of the mechanism.

Each serrated connector assembly is attached to the actuation link by two 0.190-32 bolts. The holes in the serrated plate are toleranced for minimum clearance with the bolts, since shear is the predominant load. Limited clearance between the connector and the scroll nozzle partitions made it necessary to use gang channels rather than individual locknuts.

The serrated connector assembly is made from Inconel X material.

The maximum stress in the serrated connector occurs at the fillet radius of the dovetail and is calculated to be 22,800 psi.

Link Support Assembly

As its name implies, this assembly is used to support the forward actuation link. The assembly consists of a wheel and a set of roller bearings attached to a bracket. The bracket is bolted to the scroll hat section. The drawings of the assembly are given in Figures 55 and 56; a photograph of the assembly is shown in Figure 57.

The design intent for the link support assembly was to provide a radial reaction on the forward drive link, thus reducing the bending stresses in the link and eliminating a bending stress in the serrated connector and cam track. The radial reaction occurs on the roller bearings assembled to the bracket. These bearings are the same as those used as cam followers on the splitter vane bellcranks.

The wheel which supports the weight of the forward link turns freely on a bushing. The bushing is press fitted into the bracket and is retained by a rivet.

The bracket is made from Hastelloy X material.

The maximum predicted stress in the bracket is 19,300 psi and occurs at the roller bearing mounting hole.

Actuator

The actuator selected for the VAS actuation system demonstration was a linear, nonflight type, hydraulic actuator. It was designed to have an extended length of 17.5 inches and a stroke of 5.0 inches. It must operate in a 1200°F environment and must have a slew rate of 0.40 second or less.

The drawing and engineering specifications for the actuator are shown in Figure 58; Figure 59 shows the actuator assembled to the scroll.

An attempt was made in the early design state to utilize an actuator which was already available. However, because of both mechanical and size cri-

teria, it was necessary to design an actuator which would specifically meet the requirements of the VAS system.

It was necessary to fix the length of the actuator at 17.5 inches extended. This length was arrived at by the requirement for a 5.0-inch stroke and to permit it to fit between the front frame bellmouth and scroll and at the same time not extend past the 3 o'clock strut on the front frame. The cross-sectional size was then dictated, concurrently, by the load requirement and available space.

The stroke of the actuator can be changed by adjusting the jam nut at the rod end of the actuator. It is necessary to change the stroke when adjustments for area trim in the serrated connector have been made.

Since the space available for the actuator was at a minimum, it was impossible to provide insulation to that section of the scroll. Provisions were designed in the actuator for cooling flow through the actuator body and rod end seals.

The 1500-pound load requirement for the actuator was arrived at by doubling the maximum aerodynamic, inertia, and friction loads. The aerodynamic load constitutes the major portion of the resistive load, and it was arrived at by conservative assumptions. Consequently, the actual load margin is greater than 5 to 1.

An electrical position indicator is contained within the actuator body. This device supplies the feedback signal for the control circuit of the system. A standard military electrical connector is attached to the head end of the actuator.

The VAS system is designed as a fast response system. Since the operation of a power transfer system depends also on the response of the actuator it was necessary to design the actuator for a slew rate of 0.40 second.

The attachment points of the actuator contain spherical bearings. This is necessary to circumvent misalignment and to allow the actuator to rotate at its hinge points during operation.

Actuator Bracket Assembly

The functions of the bracket assembly are to support the actuator, to react to the actuator load, and to support the aft link. The bracket itself is a triangular shaped sheet metal structure with an actuator support clevis at the upper corner; it is mounted to the scroll with two bolts and a pin. Assembled to the bracket are sets of rollers and wheels which support the links.

The drawings of the components in the bracket assembly, the bracket, and the assembly are shown in Figures 60 and 61.

Since the bracket assembly reacts the entire actuator load, it was necessary to give careful attention to the load points and load paths in the bracket. The limited clearance between the front frame and scroll made this fact even more pronounced. By correlating the design of the aft link and the bracket assembly, it was possible to balance the load internally. Except for the actuator thrust and the weight of the components, no other loads are induced in the scroll structure.

Sets of wheels and roller bearings attached to the bracket are utilized to support the aft link, to minimize friction loads, and to reduce wear. The roller bearings in the bracket assembly are the same as those used for cam followers in the splitter vane bellcrank. Since there are two bearings mounted to each block, it was necessary to provide a pivot axis on the block so that the loads would be equal to each bearing.

The bushing which acts as a shaft for the wheel is assembled to the bracket by an interference fit between the diameter. To maintain rolling action, the inside radius of the wheel was designed so that the friction moment at the inside was always less than the friction moment at the periphery of the wheel.

A clevis welded to the bracket at the upper corner supports the actuator. Stiffeners are welded from the clevis to the web to distribute the actuator load, to prevent buckling, and to increase the structural moment of inertia.

The bracket is mounted to the scroll by two 0.250-28 bolts and a shear pin. To provide for thermal differential expansion, all the bolt holes in the bracket are slotted. A bushing is used in conjunction with the bolts to reduce the bearing stress and to provide a retaining shoulder. During assembly, the bolts have reduced torque to allow for thermal expansion and deflection of the bracket relative to the scroll.

The actuator load is reacted by a shear pin in the scroll. To compensate for misalignment of any of the holes, the hole for the shear pin was slotted vertically. Sufficient bearing area was obtained by making the sides of the shear pin flat.

Behind the actuator support clevis is a fourth mount for the bracket. This mount provides a reaction against the out-of-plane component of the actuator load. By slotting the holes and making the secondary clevis wide, the bracket can expand and deflect in all other directions.

A rectangular bar and two doublers are welded to the base of the bracket. They were needed to provide adequate torsional stiffness to the bracket because the loads of the wheels are eccentric to the bracket centroidal line. As mentioned previously, the mounting bolts are assembled with reduced torque because it is likely that they would provide rotational restraint which would be greater than that of the torsion bar.

The bracket is made from Inconel X material.

WEIGHT

The weight of the area control system for the scroll, including the non flight-type actuator, is 28.11 pounds. Table II represents the weight distribution of the various components in the complete system. The components weight is subtotaled to indicate the weight contribution of each major subassembly.

RECOMMENDATIONS

Several minor changes are recommended in order to improve the integrity of the components, to facilitate assembly, and to improve performance of the system. These recommendations are based primarily on manufacturing and assembly difficulties which were encountered in this program.

Scroll

1. Specify the allowable weld buildup in the areas where the scroll struts protrude through the torque tube. The lack of clearance between the outer band seal rod and the weld buildup made assembly of the seal sectors difficult and, consequently, time-consuming.
2. Change the hat section which supports the actuator bracket shear pin to a solid bar in the vicinity of the shear pin boss. It was necessary to add shims between the bracket and the scroll during assembly; consequently, the bending moment in the shear pin and its boss was tripled. By making the hat section solid, the scroll structure is better able to react a bending moment.
3. Increase the diameter of the splitter vane support rod. The integrity of several of the rods in this assembly was marginal as a result of excessive benching; consequently, they had to be repaired. A larger rod and conscientious quality control inspection would minimize this problem.
4. Enforce the splitter vane benching requirements. Almost none of the vanes would close properly when bolted to the torque plug; consequently, they had to be removed and reworked. A design engineer and/or quality control engineer should approve the benching before the scroll shell is welded to the nozzle diaphragm.
5. Relocate the pivot axis 0.100 inch toward the splitter vane trailing edge so that the air load will tend to keep it closed when it is in the closed position. As it is presently designed, the splitter vane is nearly balanced and, subsequently, could flutter. Changing the pivot axis could reduce the tendency to

flutter and would also provide a more positive sealing effect.

Mechanism

1. Eliminate the need for rivets on the middle levers in the aft lever and bellcrank subassembly. This would require a longer (approximately 0.12 inch) stub shaft on these particular levers to prevent the tie bar from disengaging; however, it would eliminate binding in the subassembly.
2. Add a 0.030-inch-diameter lockwire hole to the aft and forward bellcranks. Presently, the bolt is lockwired to the roller bearing nut and it is not as reliable as it could be.
3. Reduce the diameter of the stub shaft on the levers and bellcranks by 0.015 inch. This would reduce protrusions resulting from the torque plug diameter's not being concentric.
4. Change the design of the actuator bracket so that the "wheels" can be coupled directly by a torsion bar. The present design incorporates a torsion bar also, but there are several stress risers between the wheels and the torsion bar.

DESCRIPTION OF TEST EQUIPMENT

FAN ASSEMBLY

The test vehicle used during this program was a lift fan assembly consisting of the variable area scroll and the LF2 lift fan system. The assembly drawing of the LF2 fan system is shown in Figure 62, and the variable area scroll assembly is shown in Figures 63 and 64. This complete assembly is commonly referred to as the LF2/VAS fan assembly. The complete assembly consisted of four major subassemblies; namely, a modified X353-5A rear frame, a modified LF2 front frame, an LF2 rotor assembly, and the variable area scroll assembly.

The X353-5A rear frame is one of the components designed for the original X353 lift fan assembly, a model of which was used to power the XV-5A aircraft. The details of the design of this component are given in Reference 5. The rear frame component, other than providing a supporting structure of the fan system, includes the fan and fan turbine exit stators and provides the supporting structure for the fan exit louver system.

The LF2 front frame is the major supporting component of the fan system. It provides a method of supporting the rotor assembly and the fan scroll. A complete design summary of this component is given in Reference 9. The LF2 front frame represents advanced technology in frame design through the use of different materials selected on a basis of load-temperature application. The LF2 frame as designed does not include an integral bellmouth. The bellmouth for this test was a stainless steel component supported from the wing structure.

The LF2 rotor assembly is also a lightweight component that represents a design improvement over the existing X353-5 rotor system. The component makes use of lightweight titanium fan blades and rotor discs. A lightweight turbine design is also used in this component. Except for mechanical design changes, the LF2 rotor assembly was designed to be aerodynamically similar to the X353-5B fan system. A photograph of the complete LF2 rotor assembly is given in Figure 65. The mechanical performance of the LF2 rotor assembly during a previous test is given in Reference 1.

The variable area scroll assembly is the major component modification in the test vehicle from the X353-5 type of system. The design of the scroll has previously been given in detail. A photograph of the completed scroll assembly is shown in Figures 66 and 67.

TEST FACILITY

The test vehicle was installed in the Lift Fan Test Facility located at General Electric in Evendale, Ohio. This facility was previously used during flightworthiness testing of the X353-5B propulsion system. The facility is described in detail in Reference 4.

In this facility, the test fan assembly is installed in a wing type of installation. The gas producers used to drive the lift fan are two J85 engines. The engine exhaust gas is ducted to the fan assembly through two diverter valves and cross duct systems, similar to the XV-5A aircraft type of installation. The lift fan is installed in the right wing location, and overboard dump through exhaust nozzles is provided to handle the remainder of the core engine gas flow not being delivered to the test fan. Methods used in setting this overboard dump flow will be discussed later during description of the test procedures and test results.

In order to test the variable area scroll, a method of varying the overboard dump system in synchronism with the variable area scroll was required. This system was designed and built specifically for these tests and is described later.

Figure 68 shows photographs of the LF2/VAS fan assembly installed in the test facility. The upper photograph shows a top view of the fan installed in the wing. This photograph was taken during facility buildup prior to installation of the fairings between the bellmouth assembly and the wing upper surface. The lower photograph shows a view of the lower side of the fan installation. The exit louver assembly and the lower parts of the scroll and cross ducts are visible. The two pipes pointing downward are exhaust nozzles that were provided to bleed part of the core engine flow, as will be described in detail later.

VAS CONTROL SYSTEM

When a variable area scroll system is installed in an aircraft, at least two fans will be used. In this test, only one fan system was available. The other fan was simulated by an overboard dump that allowed for area control in unison with the test fan.

Block diagrams of the hydraulic and electrical control systems are shown in Figures 69 and 70. As shown in Figure 69, hydraulic fluid (at 2000 to 3000 pounds per square inch pressure) is supplied by a pump and two accumulators. The linear actuator of the variable area scroll is controlled by an electrically operated servo valve. Actuation of the dump valves is accomplished in a similar manner using a rotary actuator to operate the butterfly dump valves. A third part of the hydraulic system provides for operation of the two engine diverter valves. Control valves and actuators select the diverter valve position corresponding to fan or direct jet thrust modes of operation.

The block diagram of the system used to supply the electrical control input to the dump valve and scroll servo valves is shown in Figure 70. In this system a three-position function switch is provided. This switch permits selection of the following three types of input commands for the control system:

- o A variable frequency sine wave input with control of both the

average level and the amplitude of the sine wave.

- o An independent manual control of both the scroll and dump valve system.
- o A synchronized control of both the scroll and dump valve system, with the capability of producing step changes in the level of the input command.

The input command of the dump valve then passes through a phase change system that either provides for in-phase or out-of-phase operation relative to the scroll system. The purpose of the three types of input commands as well as the phase change system will be described in the presentation and discussion of the test results.

The input commands from this point follow similar flow paths through the block diagram. The commands next pass through a "jazzzer" network. This device is a simple phase lead network that was described previously. The next operation is a conversion of the input commands by means of a flexible analog system. The flexible analog is an electrical device that operates on the input commands and essentially converts the commands to an area level of the scroll and dump valve systems. The programs used for the flexible analog were selected during the conduct of the test program such that the sum of both the scroll and dump valve areas remained a constant value as the control input level was varied with the function selector switch in either position one or position three.

The output of the flexible analog then drives a servo amplifier that provides the electrical signal to the hydraulic valves as previously described. Position feedback is provided, as well as an adjustment of actuator maximum slew rate.

Photographs of the scroll actuator and associated mechanisms may be observed in Figures 66 and 67. Figure 71 shows a photograph of the overboard dump valve system. The two ducts extending from the facility are connected to the two engine cross duct discharge flanges in the location of the left wing fan. The two dump valves are located at the ends of these ducts. The spiral cooling columns are the shafts and bearings of the dump valves. An extension pipe is attached to both dump valves to straighten the flow before the overboard dump. The hydraulic actuator, accumulator, and servo valves are located below the left-hand dump valve in the photograph.

EXPERIMENTAL PROCEDURE

INSTRUMENTATION

The instrumentation for the LF2/VAS test is presented in Table III. Aerodynamic and mechanical instrumentation of both core engines and fan are included along with facility instrumentation for operational and safety purposes.

Core engine inlet aerodynamic instrumentation is shown in Figure 72. Two 5-element boundary layer total pressure rakes were installed on engine 2. These were used to determine the flow calibration of the bellmouth. Core engine inlet flow measurements during fan running were determined from the above calibration using static pressure elements A and C on engine 1 and B and D on engine 2.

Figure 73 illustrates core engine turbine discharge instrumentation. Both engines used YJ85-5 EGT harnesses. The elements $P_{t5.1c}$ and $P_{s5.1c}$ were installed for the purpose of observing dynamic response during fan transient investigations. These elements installed in core engine 1 were recorded on Sanborn recorders during all the fan testing.

One core engine tailpipe was instrumented with eight 4-element temperature rakes for the purpose of calibrating the exhaust gas temperature (EGT) harnesses; see Figure 74. The harness calibrations are done in the jet mode. The same instrumented tailpipe is used for the calibration of each core engine EGT harness.

The ducting system of each engine contains an overboard dump leg which is instrumented as shown in Figure 75. The three total pressure rakes are oriented 90 degrees apart and the top centerline of each duct was chosen in an attempt to locate the total pressure rakes symmetrically in relation to the flow. From the measured total pressure, static pressure and total temperature, the gas flow rate through these ducts is calculated.

Static pressure taps are located in the two scroll ends as illustrated in Figure 76. As the scroll is closed, these pressure elements become representative of scroll nozzle inlet total pressure.

Fan inlet temperature thermocouples are located on the screen as shown in Figure 77. There are 12 elements spaced to represent equal flow areas of the screen. The four inlet static pressure rakes, Figure 78, were used to measure fan airflow. A series of wall static pressures along the bullet-nose as shown in Figure 79 was also monitored.

Rotor discharge total pressures were measured in each quadrant of the fan and were located as shown in Figure 80. Upper and lower surface hub statics are also indicated in the figure and were recorded throughout the fan testing.

Seal temperature instrumentation, Figure 81, was installed before run 15 and remained in place throughout the subsequent 10 hours of fan testing.

Mechanical and structural temperatures monitored throughout the test are presented in Figures 82 through 88. Thermocouples were installed on the fan front frame, Figure 82, on the variable area scroll mechanism, Figure 83, on the variable area scroll actuator, Figure 84, on the scroll actuator bracket, Figure 85, and on the front frame shaft in line with the ball bearing race, Figure 86. Rotating thermocouples were installed on the torque band and blade tip tang, Figure 87, and on the fan turbine bucket, Figure 88.

Steady-state strain gage instrumentation was installed on the scroll actuator support bracket, Figure 85, but was not used throughout the test. The required actuation force was relatively small and the drift in these gages was excessive compared to the total range to be measured. As a consequence, hydraulic gages were used in place of these strain gages for the measurement of actuation forces.

Rear frame strain gages, Figure 89, were necessary mainly for the required fan running without stator stiffener rings installed. Torque band gages, Figure 87, fan blade gages, Figure 90, and turbine bucket gages, Figure 88, were the rotating gages monitored and recorded throughout the test.

DATA ACQUISITION

The control room is located adjacent to the lift fan test facility and houses data recording equipment and operating personnel. Figures 91 and 92 show the inside of the control room and the arrangement of the data recording systems used for the LF2 variable area scroll test.

All steady-state performance parameters, including aerodynamic pressures and temperatures, fan and core engine speeds, horizontal and vertical load cell readings, scroll and dump valve positions, and fan vibrations, were recorded on the digital data system shown in Figure 91. The digital system automatically scans and records all of these parameters on punch tape and on a printed listing. The punch tape is a convenient data recording used for input to other computer programs, while the printed listing is a duplicate record available for reference purposes.

Pressure transducers are used in conjunction with the digital system for recording pressures. For purposes of this test, 12 transducers were used, each containing provision for 12 pressure connections. One port was vented to atmosphere for reference purposes, leaving 11 ports per transducer, or a total of 132 ports, available for recording pressures. Six transducers were calibrated for recording pressure ranges from ambient to 25 pounds/square inch above ambient, and the other six were calibrated for recording pressures within 5 pounds/square inch of ambient.

Two 8-channel Sanborn recorders were used to make continuous time record-

ings of selected parameters for measuring transient response characteristics. Parameters included on Sanborn recorders were as follows:

Core Engine 1 Speed, N_{e1}
 Core Engine 2 Speed, N_{e2}
 Core Engine 1 EGT, EGT_1
 Core Engine 2 EGT, EGT_2
 Engine 1 Fuel Flow, W_{F1}
 Engine 2 Fuel Flow, W_{F2}
 Engine 2 Throttle Setting, TA_2
 Turbine Discharge Total Pressure, $P_{t5.11}$
 Turbine Discharge Static Pressure, $P_{s5.11}$
 Fan Bullethead Axial Vibrations
 Scroll Actuator Position, δ_S
 Dump Valve Actuator Position, δ_D
 Fan Speed, N_F
 Total Load Cell Lift, L
 Scroll Actuator Input Signal

All structural temperatures were recorded on two Speed-O-Max recorders. The items included were as follows:

Speed-O-Max 1

Fan Front Frame (Tube 1 o'clock)	TFF1
Fan Front Frame (Flange 1 o'clock)	TFF2
Fan Front Frame (Tube 3:30 o'clock)	TFF3
Fan Front Frame (Flange 3:30 o'clock)	TFF4
Fan Front Frame (Tube 5 o'clock)	TFF5
Fan Front Frame (Flange 5 o'clock)	TFF6
Fan Front Frame (Structural 12 o'clock)	TFF7

Fan Front Frame (Structural 6 o'clock)	TFF8
Fan Scroll Actuator (Bracket 1 o'clock)	TSA1
Fan Scroll Actuator (Bracket 5 o'clock)	TSA2
Fan Scroll Actuator (Actuator)	TSA3
Fan Scroll Actuator (Actuator)	TSA4
Engine 1 Lube Tank	TLT-1
Engine 2 Lube Tank	TLT-2
Hydraulic Tank	THT

Speed-O-Max 2

Fan Ball Bearing (3 Channels)	TLF1
Fan Roller Bearing (3 Channels)	TUF1
Fan Rotating, Tip Tang (3 Channels)	TFR1
Fan Rotating, Torque Band (4 Channels)	TFR2
Fan Rotating, Turbine Bucket (3 Channels)	TFR3
Fan Rear Frame Seal (2 Channels)	TS1
Fan Rear Frame Seal (2 Channels)	TS2
Fan Rear Frame Seal (2 Channels)	TS3
Scroll Actuator Bracket (1 Channel)	TSB1

The stress monitor system is shown in Figure 92. It includes scopes for visually monitoring stress levels during the test as well as a tape recorder for recording the data for future analysis.

Readout and/or control devices for all facility, operational, and safety instrumentation are located on panels near the engine operator's station; see Figure 92. Manual recording of this data on test run log sheets was performed for each reading.

DATA REDUCTION PROCEDURES

Reduction of the performance test data into useable engineering units and parameters was accomplished using high-speed electronic computing machines. Two separate data reduction procedures or methods were employed. One method provided for a quick look at the data and performed the simple operation of

converting all data to engineering units using the appropriate calibration constants of the recording systems. This method utilized a time-sharing computer system. The system uses a teletype transmitter-receiver station installed at the test facility. The station is coupled through telephone lines to a number of large electronic computers. The teletype station accepted the punched tape output of the digital recording system, converted the digital data, and provided a listing of all parameters as well as some more important average performance indicators. This computation technique provided a method of monitoring test progress and operation of the instrumentation systems.

A second and more complex program was used to perform all the detailed performance calculations. This calculation program was written explicitly for this test and utilized the General Electric computational facilities at Evendale. The detailed procedures and calculation methods incorporated into this program are given in the Appendix. The output of the program provided the basic performance data presented and discussed in this report.

In addition to the electronic data processing methods, manual data reduction was required for analysis of the transient performance of the system under conditions of both sine wave and step inputs. The reduction procedures used were as follows.

For tests where the input command to the fan system was of a sine wave type, the input command to the fan was held constant and only the frequency of the command was varied. Since at a frequency of 0.07 and below the fan response is within a few percent of the steady-state response, the speed and lift change at this condition was assigned a level of one. The speed and lift levels at the progressively higher frequencies were then ratioed to this base level. This gave the relative response as a function of command input frequency. The resulting amplitude ratio was then converted to units of decibels for presentation of the data. A conversion chart between amplitude ratio and decibels is given in Figure 8.

The phase angle of the fan output, either fan speed or thrust, was obtained by comparing the time lag of the output and input command at the mean or average levels of each cycle of sinusoidal input. Knowing the frequency of the input command, the time for one cycle, and consequently the phase angle in degrees, was obtained. The resulting attenuation ratio and phase angle were then presented as a function of the input frequency to show the measured test results.

For tests where a step change of the input command was used, the performance will be presented as a time constant. Step inputs of scroll area, either in or out of phase, and step inputs of engine throttle will be presented in this form. To obtain the time constant, the levels of output, fan speed or thrust, were obtained for the conditions both before and after the transient. Knowing these levels and assuming that the fan system is a single-order response system, the time constant is defined as the time required to achieve 63 percent of the total change during the transient.

A second method that should yield the same time constant for a single-order system makes use of the initial slope of the transient at the instant when the step input is made. Extrapolation of the initial slope of the curve to the final level of the output yield a time interval equal to one time constant as described above. Nonlinearities and second-order effects produce differences of time constants obtained by these two methods. A comparison of the significance of these two methods of measuring time constants is depicted in Figure 93 for a typical ideal first-order transient system.

During conduct of the tests, strain gages are used to monitor vibratory stresses at critical points on the rotor components. Observation of the stress signals on oscilloscopes provides knowledge of stress conditions during the test. Simultaneously, the stress signals were recorded on magnetic tape for future analysis. The magnetic tape record was reduced to a more useable form using the facilities of the Automatic Data Reduction Center at General Electric Company in Evendale. This facility provides several methods for aiding the analysis of vibratory stress data. Among the methods used in the analysis of LF2/VAS stress data were:

Overall Level Playback

This provides a chart trace of maximum peak-to-peak amplitude of vibratory stress as a function of time. The fan speed signal is provided in parallel with the stress signal.

Spectrum Analysis

The spectrum analysis provides a stress amplitude versus frequency from the stress signal for a specified time period. By this method, the amplitude of each component making up the complex wave form can be determined.

Mode Analysis

The peak-to-peak amplitude of each of the primary vibratory modes is plotted as a function of time. Band-pass filters are chosen to selectively filter the stress signal and record that part of the signal within a specified frequency range.

Wave Form

The shape of the stress signal wave form can be obtained for study of the stress variation during one or more revolutions of the rotor.

Rotor mechanical data were obtained in a similar manner during the LF2 Demonstration Test in 1964, Reference 1. The test data from the LF2/VAS

testing will be compared to the previous data when it is helpful in explaining the results.

TEST PROCEDURES

Throughout the test program, any particular test may be classified as one of the following types.

- o Core engine calibration
- o Fan performance with variable speed
- o Fan performance with variable louver position
- o Fan performance with variable scroll position
- o Variable area scroll calibration
- o Steady-state sinusoidal control system response
- o Control response with step inputs of area
- o Control response with step inputs of core engine power

The following procedure will describe the general test procedures used to accomplish each type of test program. Prior to each test, normal facility inspections and checks were performed to insure satisfactory condition of the test hardware.

Core Engine Calibration Run

The core engine calibration runs were intended to produce basic engine performance during operation in the turbojet mode. During these types of runs, typical variables that were tested included engine exhaust nozzle area and inlet bulletnose configuration. The test procedures were as follows:

1. Air motor engine on air impingement starter to a minimum of 14-percent speed.
2. Turn on ignition and advance the throttle to the idle position.
3. Observe normal starting cycle and idle speed.
4. Accelerate the engine to the desired power setting or engine speed.
5. Record two complete scans of the digital instrumentation and record all safety instrumentation.
6. Repeat the above procedures at each desired power setting not exceeding the engine maximum speed rating of 101 percent or

the maximum exhaust gas temperature rating of 685 degrees centigrade for the J85 engine and 665 degrees centigrade for the YJ85 engine.

7. After completion of the desired test program, set the core engine speed at 70 percent and cool down for 2 minutes.

8. Shut down the engines and observe normal engine coast down.

Fan Performance With Variable Speed

Fan performance runs with variable speed were typical tests used to observe effects of the numerous test variables on system performance. Typical variables were stator stiffener rings, scroll area setting, influence of exit louvers, and effects of fan inlet circular vane. The test procedures were as follows:

1. Adjust test configuration to desired values of exit louver angle and scroll area.
2. Start both engines using normal procedures.
3. Accelerate the engines to 70 percent speed and observe normal operation.
4. Operate the diverter valves from the cruise position, turbojet mode, to the lift position, fan mode, and observe fan speed run-up.
5. While observing safety instrumentation, increase core engine power setting to desired speed level on either the fan or core engine.
6. Take two complete scans of the digital instrumentation and proceed to the next desired test point.
7. After completion of the desired test program, set the core engine speed to 70 percent and operate the diverter valves to cruise.
8. Allow the engine to cool down for 2 minutes at 70 percent speed and shut down.

Fan Performance With Variable Louver Position

This type of test was used to determine the performance of the fan system under conditions of variable fan exit louver angle conditions.

1. Set the configuration to the desired test condition.

2. Start the core engines and divert to the fan mode as in the previous procedures.
3. Accelerate the core engines to the desired power level.
4. Take two complete scans of the digital instrumentation.
5. Maintaining constant core engine power, reset the exit louver angle to the next set of test conditions and record data.
6. Repeat the above procedures until the test is completed and shut down the core engine as previously described.

Fan Performance With Variable Scroll Position

This type of test was intended to yield steady-state control characteristics of the fan by varying scroll area. The test procedures are similar to those previously described except that the scroll area is varied. Synchronized movement of the dump valve is maintained.

Variable Area Scroll Calibration

This test program was run to obtain the desired relationship of the scroll actuator and dump valve actuator as required to maintain constant core engine operating conditions. The following procedures apply to engine power settings of 100 and 95 percent.

1. Set the scroll area to the maximum open position and the exit louvers to zero degrees.
2. Start up the engines and divert to the fan mode of operation.
3. Accelerate the engines to the desired power setting of 100 or 95 percent and slowly adjust the dump valve position until rated exhaust gas temperature is obtained on engine 1. Observe that engine 2 is near rated temperature.
4. Take two complete scans of the digital instrumentation.
5. Slowly open the dump valve until the exhaust gas temperature on engine 1 drops by 30 degrees centigrade.
6. Slowly close the scroll actuator until the exhaust gas temperature for engine 1 is again at rated conditions. The above procedure has now resulted in a change of scroll area with engine 1 returned to the initial operating conditions. Engine 2 should remain at near rated exhaust gas temperature.
7. Take two complete scans of the digital instrumentation.

8. Repeat the above procedures until further motion of the scroll actuator is not possible. At this condition with the scroll actuator full closed, slowly close down the dump valve until rated exhaust gas temperature is achieved.
9. Take two complete digital data scans.
10. Shut down the core engine as previously described.

Steady State Sinusoidal Control System Response

This type of test applies to that part of the test program when response of the fan system to sine wave input commands was measured. Prior to the conduct of these tests, programming of the flexible analog system as previously described was completed; the scroll and dump valve actuation systems were operated at power-off conditions using sine wave input commands; and the jazzer settings were calibrated to give the desired time constants and magnification. The following procedures were then used to conduct the test.

1. Set nominal scroll actuator position and jazzer settings as required for the test.
2. Start up the core engines, accelerate, and divert to the fan mode of operation.
3. Accelerate to the desired core engine power setting of 95 or 100 percent.
4. Adjust the sine wave generator to 0.05 or 0.07 cycles per second and set the level and amplitude controls to the desired value; for example, a level of 80 percent and an amplitude of plus or minus 10 percent.
5. Set the Sanborn recording system at 5 millimeter per second.
6. After one to two cycles of the input command are completed, increase the signal generator frequency to the next level.
7. Again observe one or two cycles of control input and repeat the above procedure throughout the complete frequency range. The signal generator is set up so that when frequency is changed, the amplitude and level values will remain constant.
8. After the frequency sweep is completed, proceed with the next frequency sweep or shut down as previously described.

Control Response With Step Inputs

The procedures described below apply to that part of the test program where control system response to step input commands was obtained. This case applies to either the roll control mode, out of phase, or the height control mode, in phase. It also applies to tests either with jazzer or without jazzer.

1. Set nominal scroll actuator position, louver angle, phase switch, and jazzer settings prior to starting the core engines.
2. Start the engines and divert to the fan mode.
3. Accelerate the core engine to the desired power and stabilize.
4. Set the manual control to the desired initial level of scroll actuator position. Verify that phase switch and jazzer settings are at the required level.
5. Set the step level control to the desired final value after stepping.
6. Set the Sanborn recorder speed to 25 millimeters per second and operate the step switch. After the transient is completed, return the step switch to the initial position.
7. Repeat the above procedure for each step size and initial level desired and shut down the core engine.

Control Response With Step Inputs of Core Engine Power

The following procedures apply to the tests intended to show the response characteristics when the core engines are used for height control. The detailed procedures are as follows:

1. Set the desired level of scroll actuator position.
2. Start the core engines and divert to the fan mode of operation.
3. Accelerate the core engines to the desired power level, for example, 98 percent.
4. Set the Sanborn speed to 25 millimeters per second and rapidly advance the two engine throttles to maximum as determined by engine high-speed setting in fuel control.
5. Observe transient response. Once transient is complete, rapidly retard the throttles to the initial position and observe the transient response.

6. Complete the above tests for all desired levels of initial core engine power and scroll actuator position and shut down according to normal procedures.

DEMONSTRATION TEST RESULTS

This section of the report will present the test results obtained during the demonstration of the LF2/VAS fan system. A summary of the test runs is given in Table IV along with remarks concerning the purpose of each series of tests and significant configuration changes.

The data will be separated into five categories as listed below:

Core engine performance

Steady state, including fan system performance, scroll and dump valve performance, and system programming

Dynamic performance

Performance and operation of the static structural components, primarily the variable area scroll

Performance and operation of the rotating structural components, the rotor and bearings

CORE ENGINE PERFORMANCE

The fan system was driven by the discharge flow from two J85 engines operating in a dry turbojet configuration. Engine 1, the left-hand engine, was a YJ85-GE-5 engine, serial number 230105. Engine 2, the right-hand engine, was a J85-GE-5A engine, serial number 213233. The "YJ" type engine is a prototype of the "J" type; the main difference in performance and operation is the maximum exhaust gas temperature rating. The "YJ" is limited to a maximum temperature of 665 degrees centigrade, and the "J" is limited to 685 degrees centigrade.

In the test configuration, engine 1 delivers flow to the forward scroll section of the fan. Engine 2 delivers flow to the rear scroll section. The fan configuration rotated clockwise, aft looking forward, such that flow from engine 1 was the first to impinge on the fan turbine buckets during rotation of the fan.

The basic performance of the two core engines was obtained for the engines operating as conventional turbojets. The core engine flow is discharged through the diverter valve and a short convergent nozzle. Nozzle area variation was obtained by inserting tabs in the throat. The maximum nozzle area without trim tabs was 120.8 square inches. The results of this part of the test program are presented in Figures 94 through 111. All performance presents corrected engine parameters versus corrected core engine speed. The data are presented for a range of nozzle areas between 117.8 and 120.8 square inches for engine 1 and between 111.8 and 117.8 square inches for engine 2.

Normal variations of airflow, fuel flow, turbine discharge pressure, and exhaust gas temperature for engine 1 are shown in Figures 94 through 96 and in Figure 98. Figure 97 presents a comparison of indicated harness exhaust gas temperature and the tailpipe temperature based on the average of the 32 tailpipe thermocouples. This characteristic for engine 1 shows that the harness indication is about 30 degrees Rankine higher than the average. The average tailpipe temperature is used as true measured temperature. A similar comparison of temperature indicated on the engine control panel meter with the average tailpipe temperature is given in Figure 102. This figure also shows an error of about 40 degrees Rankine.

Figure 101 presents the average tailpipe temperature as a function of combustor fuel to air ratio. Comparison of the actual test data with representative predicted performance shows excellent agreement. This result verifies that the average tailpipe temperature as measured is a true exhaust gas temperature measurement.

Variations of corrected measured thrust and calculated gas horsepower with both speed and nozzle area are shown in Figures 99 and 100. At a rated exhaust gas temperature of 1690 degrees Rankine or 665 degrees centigrade, the turbine discharge horsepower for engine 1 is about 5000. The predicted horsepower level at these conditions is about 5450. This comparison indicates the deficiency of performance experienced in this engine and consequently its inability to drive the test fan to high rotational speeds.

Similar performance data for engine 2 are shown in Figures 103 through 112. Errors in indicated harness temperature of between 20 and 50 degrees Fahrenheit were observed. Measured levels of gas horsepower at rated exhaust gas temperature were about 5300 horsepower as compared to a predicted level of 5700 for a status J85 engine. Similar to engine 1, this engine also exhibited a considerable deficiency in the available horsepower level.

Figure 112 presents the variation of engine measured velocity heads in the inlet bellmouth for engine 2 with a long cylindrical bulletnose and with the standard short engine bulletnose. With the long bulletnose installed, the measurement plane for determining engine airflow is a constant annular section. This configuration provides an accurate measure of engine inlet flow based on the annulus area and a known flow coefficient. For the case of the short bulletnose configuration, considerable flow distortion exists in the measurement plane, so an erroneous velocity head used in calculating airflow exists. However, using the long bulletnose as a standard, a correction factor can be obtained for the short bulletnose case. This correction factor was obtained and used in the airflow calculations as described in the Appendix. This type of correction factor is required because the long bulletnose configuration could not be installed on the "YJ" engine. The engine bulletnose attachment is not compatible with the long bulletnose configuration.

STEADY-STATE AERODYNAMIC PERFORMANCE

Fan System Performance

Steady-state fan aerodynamic performance is presented at three different types of characteristics:

total fan lift versus fan speed

fan speed versus available horsepower

total fan lift versus available horsepower

The first characteristic is a direct comparison of fan performance that is affected only negligibly by the fan turbine performance. The second and third types of characteristics are representative of the complete system efficiency, including both the fan and the fan turbine effects. The available horsepower used in the presentation is simply the percentage of the total core engine horsepower being directed into the fan turbine system.

These characteristics are presented in Figures 113 through 167 and include a number of configuration and test variables. The configurations comparable to previously tested LF2 and X353-5B fans are represented by runs 7 and 9 for maximum open scroll area, equivalent to a scroll actuator position, δ_s , of 110 percent. Comparison of run 7 and run 9 performance shown in Figures 113 through 118 will also indicate the effect of adding stator stiffener rings.

Figures 119 through 121 show run 17 performance indicating the lift correction for bleed nozzles and representing the base performance level at a scroll actuator position of 80 percent. High turbine bucket stress levels established the 80 percent limit. Effects of scroll actuator position on turbine bucket stress levels are described in detail in the section on discussion of turbine bucket stresses.

A sequence of configuration changes was investigated at 80-percent scroll actuator position to determine incremental fan performance changes. The first change was to cover the slip ring cavity in the rear frame dishpan, and the resulting performance is presented in Figures 122 through 124. Figures 125 through 127 represent performance with slip ring cavity covered and with space around blade tip tangs covered. The tape used to cover the tip tangs did not remain in place as well as expected and was removed after the run. The cover on the slip ring cavity remained in place for all succeeding configurations.

For the next run, the 3 to 6 o'clock inlet vane quadrant was raised 0.5 inch and rotated 4 degrees open; see Figures 128 through 130. The configuration was the same as above; the exit louvers removed, the stator stiffener rings were installed, and the slip ring cavity was covered.

The performance of this configuration at 80-percent scroll actuator position and at maximum engine power with variable scroll actuator position is presented in Figures 131 through 133. The change due to removal of the inlet vane is indicated in Figures 134 through 136. Removal of the inlet vane resulted in very poor fan performance and high blade vibratory stresses, limiting maximum fan speed obtained to approximately 1750 revolutions per minute. The inlet vane was again installed before proceeding with further testing. It was still in the raised position but not rotated 4 degrees open as before. Figures 137 through 142 show the performance of the two succeeding configurations with the improved forward air seal and with stator stiffener rings removed. Fan characteristics for both constant scroll area, δ_s of 80 percent, and variable scroll area at maximum engine power were investigated.

Figures 143 through 167 represent fan performance characteristics with variable area scroll. The initial calibration of scroll position versus dump valve position was determined from runs 10 and 11, Figures 143 through 145. These data were generated by manually positioning the scroll actuator and then positioning the dump system for rated engine exhaust gas temperature. The specific program derived from this data will be discussed later in this section of the report. During the variable area scroll transient investigations with sinusoidal input, data points were taken at the base setting before each transient and are presented in Figures 146 through 148.

Due to a failure of a dump valve position potentiometer, the variable area system had to be reprogrammed. Figures 149 through 151 show the fan characteristics with variable area at two engine power settings after reprogramming was accomplished.

Fan performance with variable exit louver angle and variable scroll actuator position is described in Figures 149 through 167. Horizontal thrust versus available horsepower characteristics are also included.

Programming of Scroll and Dump Valve System

During the early phases of the test program, a series of specific tests was conducted to determine the relative positions of the scroll actuator and dump valves as required to maintain constant engine operating conditions. The test procedures have already been presented. During the first attempt to run these tests, when the scroll actuator was closed to about 70 to 80 percent of the stroke, it became apparent that the overboard dump system could not handle all of the overboard flow. This problem was primarily the result of the poor performance exhibited by the two core engines. Both engines required excessive discharge area to maintain rated exhaust gas temperature. This excess area must be accounted for by the dump valve system and, therefore, must be added to the discharge area deficiency. The solution to this problem was to install bleed nozzles on the legs of the cross ducts normally supplying flow to the pitch fan in the XV-5A installation. The area of the bleed nozzles selected for the

remainder of the running was 18.7 square inches for engine 1 and 12.7 square inches for engine 2.

The tests were then performed with the bleed nozzles installed, and the results are shown in Figure 168 for engine power settings of 100- and 95-percent speed. The actual test data and data corrected for the small inconsistencies in setting the same exhaust gas temperature are shown on the figure. Both engine power settings exhibit similar characteristics, and the higher power setting shows the need of a more open dump valve setting. This difference is the result of selecting a base exhaust gas temperature higher than the normal operating conditions of the engines at the 95-percent power level. The 100-percent curve was therefore used to establish the analog program requirements. These data also established the range of scroll and dump valve operation. The scroll actuator range was from 0.4 to 4.15 inches. This represents a scroll actuator stroke of 3.75 inches for 100-percent scroll actuator position. The range of dump valve operation ranges was between 21 and 38 degrees from the full-open position.

A second problem occurred in the dump valve system after test run 14. During checkout between test runs, it was observed that the position and feedback potentiometer for the overboard dump valve had failed. A new potentiometer was installed and the system recalibrated. Because of inaccuracies in setting the position potentiometer and programming the analog circuits, two different dump valve to scroll actuator programs existed. These are shown in Figures 169. The figure shows the definition of scroll actuator position as a percent of stroke in terms of true actuator position, or inches from full retracted. For the program applicable for runs 9 through 14, the dump valve was more closed than for a similar condition after run 14.

The performance of the engine systems when subjected to the above described programs is shown in Figures 170 through 179. Figures 170 and 171 show the percentage of core engine flow supplied to the test fan as a function of scroll actuator position. For the final rigging condition, a smaller percentage of the total engine flow is delivered to the fan system at a given scroll position. This is the result of the dump valve being more open for the second test setup.

Typical variations of the significant engine performance parameters with scroll position are shown in Figures 172 through 175 for the initial rigging setup, and in Figures 176 through 179 for the final system rigging. It is apparent from the figures that the final rigging yielded more consistent engine operation throughout the complete range of scroll actuator position. Variation of engine 2 operating conditions is apparent. This condition existed because engine 1 was selected as the master engine, being a YJ engine with a severe exhaust gas temperature limit, and engine 2 was allowed to drift around the operating point, since it was a J-type engine with a much higher temperature limit.

Variable Area Scroll Losses and Effective Area

The effective area of the variable area scroll turbine nozzles can be obtained quite easily for choked flow conditions by using the calculated values of scroll gas flow, temperature, and total pressure. This calculated parameter, commonly referred to as flow function, is shown in Figure 180 for the two halves of the scroll. This flow function is based on the turbine discharge pressure rather than the scroll total pressure. In order to convert this parameter to effective area terms, the scroll total pressure was measured using static pressure taps located in the extreme ends of the scrolls as shown in Figure 76.

This pressure probe will indicate scroll duct total pressure when the outer ends of the scroll nozzles are closed down. This occurs at or at less than 80 percent of actuator stroke. The level of this pressure, presented as a loss coefficient, is shown in Figure 181. The data show that the scroll losses are constant for a range of scroll actuator positions from full closed to about 80 percent. Above 80 percent, the loss coefficient appears to increase rapidly. This increase is not a loss but a result of the pressure probe indicating static rather than total pressure. It can therefore be concluded from this result that the scroll loss coefficient for this configuration is constant throughout the complete range from full open to full closed.

Figure 182 presents the variation of these same coefficients with scroll flow function. Again at high scroll openings, the pressure coefficient is high because of erroneous indications of the pressure sensor.

Assuming that the scroll loss coefficients are constant at the value shown in Figures 181 and 182, and using the flow function shown in Figure 180, an effective area of the scroll can be calculated. The results of this calculation are shown in Figure 183. The effective areas of both halves of the scroll are presented as a function of scroll actuator position.

Overboard Dump System Losses and Effective Area

The overboard dump system in this installation simulates the other wing fan system by using extension ducts and controllable butterfly valve systems. Therefore, similar losses and area variations as presented for the scroll system are of interest.

Variation of the loss coefficient in the overboard duct system with flow function is shown in Figure 184. The loss coefficient is based on total measurements in the overboard bleed duct system just upstream of the butterfly or dump valves. An additional curve is shown representing the estimated friction losses in the straight pipe section of the bleed duct system. The significance of this estimate will be discussed in future analysis of the test data.

Figure 185 presents the variation of dump valve effective area with dump valve position. The area for the valves of both engine 1 and engine 2 are shown. Since dump valve 1 is the master valve, and its position is the only one measured, the differences in level of the two valves may be because of slight differences in setting of the valve doors relative to one another.

Scroll Actuator Forces

Early in the program it became apparent that the forces required to actuate the scroll mechanism were very low and could not be measured using the strain gage installed on the actuator bracket (Figure 85). In place of this measurement, the pressure difference across the scroll actuator piston was measured. The hydraulic pressure gages were located outside the control room near the fan and were photographed by a movie camera during an acceleration of the fan and an excursion of the scroll actuator at maximum power levels.

Using these pressure measurements and the actuator piston areas, rod end and back-side end, the actuator force was obtained and is shown in Figure 186. The data in the upper figure are shown for the condition when the actuator is being moved slowly at a nearly constant rate. The lower figure shows the force that existed when the actuator was stationary or static.

The data show the following types of forces:

- o During motion, the force of the mechanism opposes the motion. This may be actuator as well as mechanism friction. The difference between the moving and static force is about 200 pounds.
- o In the static condition there is a reversal of force at the full-closed position. With the actuator extended, as the motion is towards the retracted condition, the static force tends to extend the actuator. With the actuator retracted, as the motion is towards the extended position, the force tends to retract the actuator. This tends to indicate some type of hysteresis in the vane aerodynamic forces. The reasons for these forces are not known, but in all cases the forces did not exceed 200 pounds.

DYNAMIC PERFORMANCE

The results of that phase of the test program directed towards obtaining the dynamic performance characteristics of the LF2/VAS system are presented in the following section. The system was tested at conditions representative of the three types of control modulation as previously described in detail:

fan variable area for roll control

fan variable area for height control

variable engine power for height control

The dynamic response of the system was determined by observing the response of both fan speed and total thrust to a particular type of input command. In order to provide these types of dynamic measurements, the response rates of the instrumentation system may be significant. In order to record a response rate of a system with a time constant of about 0.3 to 0.6, as is the case of the LF2/VAS system, a recording system with a time constant of less than one-tenth of the system is necessary. Therefore, a time constant of less than 0.03 second is required for the particular measuring system. The Sanborn recording system has a very low time constant of about 0.002 second. The fan speed signal is obtained by converting the output of the fan speed pickup, 60 cycles per revolution, to a direct current level. The time constant of this system was checked and found to be less than the Sanborn recorder used for presenting the parameters.

The performance of the thrust measuring system presents another situation. The load cell system is a hydraulic circuit with the force readout on a Bourdon tube gage. In parallel with this gage, a pressure transducer was installed and used to drive the Sanborn recorder. A check of the response rate of this load cell system to a step input of about 150 pounds, showed the characteristics given in Figure 187. These data yield a time constant of about 0.47 second for both of the major load cells. This time constant is definitely too long for measuring transient variations of thrust. This long time constant is probably caused by the volumetric displacement of the Bourdon tube gages.

This long time constant for the lift measuring is not acceptable for determining the dynamic performance of the system. However, later in the analysis, a correction for this effect will be applied to the thrust data. The following discussion of test results will therefore be primarily concerned with fan speed measurements. Thrust measurements were reduced for the tests with jazzier only.

Roll Control Response With Sinusoidal Input

Demonstration of the response of the fan system was obtained by exciting the scroll actuator with a sinusoidal input. The tests were performed at average scroll actuator positions between 20 and 80 percent. Effects of sinusoidal amplitude were obtained at average scroll actuator position of 50 and 10 percent. These tests were performed at core engine power settings of 95 and 100 percent. The test results are presented in Figures 189 through 202 in the form of phase shift-attenuation diagrams.

Figure 188 shows a typical Sanborn record as taken during the testing. This record shows the variation of the sinusoidal input command with time. The scroll and dump valve positions are recorded and follow the input command. The scroll actuator is in phase and the dump valve out of phase with the input. This in-phase/out-of-phase condition is required for roll control so that constant engine operating conditions are maintained. The fan speed and thrust levels as shown exhibit a phase lag and attenuation indicative of the fan response characteristics.

Figures 189 through 195 represent the data obtained at engine power setting of 95 percent. Figures 196 through 202 are for a 100-percent power level. Each performance characteristic shows an increase in phase lag and attenuation as the impressed frequency is increased. The 20-decibel-per-decade asymptote, as previously described, is also shown as a dashed line. The intersection of this asymptote with the zero decibel line occurs at frequencies of around 0.3 to 0.4 cycle per second. A discussion of this frequency intercept and the associated time constants will follow in the analysis of test results beginning at page 71.

Roll Control Response With Jazzer and Sinusoidal Inputs

A certain part of the program was performed to demonstrate the frequency response characteristic of the fan when a jazzer system was inserted in the input channels. The jazzer configuration was set such that the expression $(m + 1) \tau_J$ is a constant equal to 0.62. The reason for assuming this equality will be discussed later in the analysis section.

Using this equality for m equal to 1, the jazzer time constant was 0.31; for m equal to 3, τ_J was equal to 0.155. For these two values of jazzer setting, the steady-state frequency response of the jazzer systems can be written as follows:

$$\frac{\text{Output}}{\text{Input}} = \frac{1 + j\omega (m + 1) \tau_J}{1 + j\omega \tau_J}$$

$$\text{for } m = 1, \tau_J = 0.31$$

$$\frac{\text{Output}}{\text{Input}} = \frac{1 + j\omega (0.62)}{1 + j\omega (0.31)}$$

$$\text{for } m = 3, \tau_J = 0.155$$

$$\frac{\text{Output}}{\text{Input}} = \frac{1 + j\omega (0.62)}{1 + j\omega (0.15)}$$

Then the asymptotes of the response characteristics are as follows:

for small values of ω

$$\frac{\text{Output}}{\text{Input}} = 1.0$$

for large values of ω

$$\frac{\text{Output}}{\text{Input}} = (m + 1)$$

The results of this series of tests are presented in Figures 203 through 212. Figure 203 presents a typical Sanborn recording taken during the test. The input command is shown to be at a constant level and a constant amplitude; only the frequency of the command is changing. The jazzer output level remains constant, but as frequency is increased, the amplitude increases. The level approaches a two-to-one ratio at the high frequency range of input. This is representative of a jazzer setting of m equal to 1 or $m + 1$ equal to 2, as described above. The response of the fan speed and thrust to these commands shows the characteristic phase lag and attenuation levels as the impressed frequency is increased.

The resulting attenuation and phase shift of the jazzer output, of fan speed, and of total lift were obtained from this type of Sanborn record. The results were then presented as a function of impressed frequency as shown in Figures 204 through 212. For each test configuration, three separate characteristics are shown. The first curve of each series presents the response characteristics of the jazzer system. The measured response of the jazzer is shown and compared to the theoretical response characteristic. Agreement of the actual jazzer and the desired performance is very good.

The second curve of each series shows the fan response based on the fan speed measurements. These characteristics present the attenuation and phase shift based on the reference levels of the input command, not the jazzer output. For the tests with jazzer, the thrust response of the fan system is also shown. A phase shift and an attenuation much larger than obtained using fan speed are apparent. Part of this difference is probably due to the long time constant and consequently poor response of the thrust measuring system. This effect will be discussed later in the analysis sections.

Roll Control Response to Step Inputs

Transient performance of a system may be obtained by providing sinusoidal input commands or by inserting step changes of input levels and observing the response rates. These results for sinusoidal inputs have been presented. This section will present the test results for the step type of

input command, both with and without the jazzer system. The test results are shown in Figures 213 through 218.

Figures 213 and 214 show typical Sanborn records obtained during the tests with step inputs. Figure 213 is a test condition without the jazzer. The input command record shows a step input 20 percent towards the open position. The response of the scroll and dump valve actuators to this command shows out-of-phase operation. At the instant of the step command, both the dump and scroll actuators undergo maximum slew rates to achieve the new commanded position. The fan speed and thrust records show the transient response of the fan during the interval following the step input.

Figure 214 shows a similar test condition with the jazzer in the system. The jazzer output shows a typical response as expected for a jazzer m of one. At the initial instant after the step input command, the jazzer output level reaches two times the command and then goes through an exponential washout in about 1.5 seconds. The response of the scroll and dump valve systems follows the jazzer input command; the difference in response is caused by the slew rate limit of the actuator systems. The transient of fan speed and thrust occurs immediately after the step input command, with rates of change much more rapid than shown for the case without the jazzer in Figure 213.

The test results obtained during step inputs of roll control are shown in Figures 215 through 217. The transient performance is presented as the variation of fan time constant based on fan speed and as a function of initial scroll position, size of step command, jazzer m setting, and core engine power level.

Figure 215 shows the measured time constants at a core engine power level of 95 percent. The lower curve of Figure 216 is similar performance at a core engine power level of 100 percent. Both of these sets of data were for the case without the jazzer. The two upper curves in Figure 216 show the effects of jazzer at a power setting of 100 percent.

Figure 217 shows the results of the same tests as shown in Figure 216. The difference in the two figures is the method used to determine the time constants from the test data. As previously discussed, the time constant for a first-order transient system may be defined in two different ways. Figure 216 used the definition based on 63 percent of the change, while Figure 217 used the initial slope definition. There is a slight difference in the results shown, the data in Figure 217 showing a higher or longer time constant.

Figure 218 is presented to show the effects of actuator maximum slew rates on the overshoot levels of the jazzer system. The jazzer system commands an overshoot of both the scroll and dump valve actuators at the instant the step command is initiated. This overshoot level varies directly as the jazzer m setting. Because of slew rate limitations, the actuator never really achieves the commanded level as was previously shown in

Figure 6. The data shown in Figure 218 show this effect. It is apparent that there will be a reduced effectiveness of the jazzer for large values of magnification. The actual overshoot as demonstrated is considerably less than the level commanded by the jazzer. This condition will be discussed later in the analysis section of the report.

Height Control Using Fan Area

Tests were performed to determine the fan response during conditions simulating height control using fan area changes. The electronic systems of the actuator control system dictated that these tests were to be performed at a scroll area setting of 50 percent and larger. For height control, the dump and scroll actuators must operate in the in-phase mode. To accomplish this, a typical area change would be from 65-percent to 50-percent conditions; the total effective area of the dump and scroll systems will be larger than required for the core engines. Therefore, the engines will be operating at a reduced temperature and horsepower level. As the area is closed down to the 50-percent condition, the design area for the engines will exist and the engine exhaust gas temperature will return to the rated condition. Rated exhaust gas temperature conditions represent a higher horsepower level of the core engine and therefore an increased fan speed and lift.

A typical set of Sanborn records showing both the fan and engine performance for this type of control input is shown in Figure 219. The changes in core engine operating conditions due to the area change as well as the fan transient are presented.

Figure 220 presents a summary of the fan time constant representative of this type of control. The fan time constants are shown for two power settings of the core engine.

Height Control Using Engine Power

A second method of providing for height control makes use of modulation of lift by varying the power level of the core engine. During this program, numerous tests were performed to demonstrate this type of control. A typical Sanborn record of this type of transient is shown in Figure 221. The basic input command for this type of transient response is a step input of the engine throttle as shown on the records. Immediately following the step input of throttle, the engine begins to accelerate at the maximum rate as established by the fuel control of the engine, and achieves the final engine power levels as determined by throttle position. These engine transients are shown in the figure. Attendant with the engine power change, a change in fan speed occurs as shown. This change in fan speed then produces a change in lift simulating this type of height control. The transient performance is determined by the time constant of the fan speed change.

The preceding tests were performed for a range of fan speed changes and a series of scroll areas. The resulting time constants are shown in Figures 222 through 224. Transient fan speed changes between 2 and 10 percent are shown.

AERODYNAMIC TEMPERATURE AND PRESSURE DISTRIBUTIONS

The fan system temperature and pressure distributions are shown in Figures 225 through 236. Typical fan inlet screen temperature distribution is shown in Figure 225. Figure 226 shows the high reingestion region experienced during initial fan running when excessive diverter valve leakage was present.

Fan pressure distributions are presented in the form of flow coefficients and pressure coefficients in Figures 227 through 236. These are typical distributions presented for the highest speed point of each fan configuration tested. Fan inlet static pressures and fan bulletnose static pressures are presented as flow coefficients. The bulletnose statics were measured in only one axial plane and are shown in the quadrant designated rake D. Rotor discharge total pressures and hub or dishpan static pressures are presented as pressure coefficients. As noted earlier, hub statics were measured above and below the rear frame dishpan and the ones presented here for rake D are above the dishpan in the plane of the rotor discharge elements. The location of the inlet vane is easily identified by the discontinuity of the flow coefficient characteristic near the fan tip. For each configuration, an average flow and pressure coefficient characteristic is presented along with the indicated overall area weighted average values.

Temperature and pressure distributions for engine and dump system measuring stations are presented in Figures 237 through 246. Figure 237 indicates typical engine inlet temperature measurements with a variation of approximately 1 degree Fahrenheit. Engine inlet pressures are shown in Figure 238, giving average static pressure level along with the total pressure profile as determined from the two 5-element boundary layer rakes. The total variation in engine turbine discharge total pressures was 4 pounds per square inch for engine 1 (Figure 239) and 1 pound per square inch for engine 2 (Figure 240). Tailpipe temperature profile, shown in Figures 241 and 242, shows a total spread of 100 degrees Fahrenheit for engine 1 versus 140 degrees Fahrenheit for engine 2. However, engine 2 exhibits a much more uniform circumferential profile for a given immersion depth as indicated by constant rake element location. The temperature profiles of the dump system, Figures 243 and 244, and engine tailpipe are similar in that the circumferential profile for a given immersion depth is more uniform for the dump supplied by engine 2. The total variation in measured temperatures is approximately 25 degrees for both dump systems. The dump system pressure profiles shown in Figures 245 and 246 are similar and are reasonably uniform.

The observed vibration characteristics of the engine and the fan are pre-

sented in Figures 247 through 250. The maximum indicated vibration level was 2 mils for engine 1 and 0.7 mil for engine 2 (Figures 247 and 248). Figure 249 shows average fan vibration levels as recorded from the panel meters. Bullethead axial vibration levels were also recorded on the Sine-born charts, and the comparison (Figure 250), shows consistently higher levels than the panel-meter readings.

STATIC STRUCTURAL COMPONENT PERFORMANCE

The following discussion will present static component performance as observed during conduct of the test by monitoring critical component structural temperatures and by the results of post-test inspections.

Component Temperatures

During conduct of the test, the temperatures at certain critical locations in the static structural components were monitored and recorded on Speed-O-Max type temperature recorders. The location of these temperature sensors has previously been discussed in the instrumentation section of this report and are shown in Figures 82 through 85.

A typical set of time histories of these component temperatures is presented in Figures 251 through 255. The temperatures are shown for a typical performance run where the core engines were started, the diverter valves operated to the fan mode, and the fan accelerated to the maximum power setting of the engines. Data points were then taken at four fan speeds between maximum and 1900 revolutions per minute. The system was then shut down after about 25 minutes of operation. The timing of the significant events of the test is given at the top of Figure 251.

Maximum structural component temperatures observed during the run were as follows:

scroll actuation slide bracket -----	540°F
scroll actuator body temperature -----	220°F
front frame flange temperature -----	410°F
front frame tube temperature -----	380°F
front frame strut temperature -----	340°F

The temperatures as presented above are with a cooling air system. The cooling air system consisted of 12 air nozzles spaced around the active arc of the fan. These nozzles directed cooling air flow at the critical components of the front frame structure that were temperature limited. A total cooling flow rate of about 0.2 pounds per second was provided by this system. For a short time (about 10 minutes) during the first run (run 5), the system was operated with no cooling air. This cooling system

was required to maintain the front fan components within the established 400-degree-Fahrenheit limit. The VAS mechanism is not temperature limiting because materials used in design are capable of operating at engine exhaust gas temperature.

Post-Test Inspections

All post-test inspections except the one after run 16 failed to show any discrepancies of the static structural component. A description of the test events that occurred prior to shutdown after run 16 is as follows.

Test run 16 was intended to investigate the performance of the fan system with sinusoidal inputs in the roll control mode of operation with the jazzer. Tests were run at the following scroll position and jazzer settings at maximum core engine power.

<u>Scroll Settings</u>	<u>Jazzer "m"</u>
50 ± 10%	1
50 ± 10%	3
50 ± 20%	1

While running the last test sequence of 50 plus or minus 20 percent scroll area, at an impressed frequency level of about 1.5 cycles per second, the scroll actuator failed to respond to the commands from the control system. The system failed to respond four times when moving from the open position towards closed. The motion of the scroll actuator stopped abruptly at 60 to 70 percent of stroke.

The tests were immediately discontinued and an investigation of the malfunction was initiated immediately. After troubleshooting the electrical and hydraulic systems, it became obvious that the scroll actuator was being supplied a hydraulic pressure differential across the actuator piston of sufficient level (greater than 1500 pounds) to move the mechanism, but motion did not occur. An audible "klunk" of the variable area scroll mechanism was observed at the conditions when the actuator failed to respond to the commands and the high force was applied. These observations were made before the scroll mechanism had completely cooled down after the test.

After the system had completely cooled down, the conditions of the malfunction were no longer present. Since this malfunction occurred at a point in the test program after most of the dynamic response tests had been completed, it was decided to continue the test program using only manual control of the variable area scroll. The parts of the test program not completed were roll control with jazzer at 95-percent core engine speed and height control with jazzer.

Following completion of all desired testing, representing about 15 hours of fan operation, further investigations of the malfunction were initiated. The bellmouth quadrant between the 3 and 6 o'clock locations was removed to inspect the scroll actuator and variable area scroll mechanism. No noticeable indications of the malfunction were observed. The actuator and mechanism were operated throughout the complete range simulating the conditions of the malfunction, but no repeat of the conditions was observed. The teardown inspection was not continued past this point.

It is believed that the only component hang-up capable of completely stalling the actuator would be an interference between the actuator push rod and some static structure. Detailed visual inspection failed to show any area of impact damage. Subsequent cold, full-hydraulic-pressure cycling of the system did not reproduce the problem. Further scroll teardown inspection at this time would not contribute any data to the actuator stalling problem; hence it was not pursued. At this time there is apparently no explanation; and until it occurs again, it will be considered a minor problem.

ROTATING STRUCTURAL COMPONENT PERFORMANCE

The rotating structure consisted of the LF2 rotor, the fan and tip turbine, and the rotor bearing system. Performance of these components was monitored during the test by observing the response of strain gages and thermocouples installed at control points on the component. The location of each of these strain gages and thermocouples has been defined previously in the instrumentation section of this report. The following section presents some of the more significant results obtained from these measurements.

Fan Blade Stress Levels

The strain gage locations on the fan blades were chosen after considering the steady-state and vibratory stress distributions for the various modes of vibration. These distributions were established during design by utilizing computer techniques and were verified by bench testing of the components. Table V gives the stress ratios for the fan blade strain gages shown in Figure 90.

The blade stress data shown in Figures 256, 257, and 258 show the variation of overall stress level with fan speed for the gage 1, gage 3, and gage 4 locations respectively. The data are shown for the scroll area in the full-open position and the exit louvers in the neutral or zero-degree position.

Similar blade stress versus fan speed data for blade gage 4 are shown in Figures 259 through 263, where in each case the scroll area is held constant. In these figures, curves are shown for three exit louver settings: -7, 20, and 37 degrees.

In order to show the effect of scroll area on fan blade response, three

resonant points were selected. For the first flexural mode, Figure 264 shows the blade overall stress versus scroll actuator position with fan speed held constant at 1610 revolutions per minute. Figure 265 shows the effect on the second flexural mode with a constant fan speed of 1850 revolutions per minute. Similarly, the 3 θ response is shown in Figure 266 as a function of scroll actuator position with fan speed held constant at 1960 revolutions per minute.

Gage 4 data are used in Figure 267 to show the effect of louver vector angle on blade stress. In this figure the first flexural and second flexural modes are shown with data for constant fan speed of 1610 revolutions per minute and 1850 revolutions per minute.

Figure 268 shows overall stress level as a function of fan speed for gage 4 with the inlet turning vane removed. Data from test runs with the inlet vane installed are included for comparison. The effects of the inlet vane based on gage 2 data are also shown in the figure.

The predominant frequency of the blades vibratory stress is shown as a function of fan speed in Figure 269. Data from the LF2 demonstration test are included to define more completely the entire fan speed range. The shapes of the curves shown for the fundamental vibratory modes were derived from design analysis and bench test results.

Turbine Bucket Stress Levels

Turbine bucket stresses were monitored by strain gages located as shown in Figure 88. The primary gage for the first flexural mode of vibration was the type 7 gage, with a stress ratio of 1.0, and the secondary gage was the type 9 gage, with a stress ratio of 0.70. Early in the test runs, after test run 11, the type 7 gage became inoperative. Test data following run 11 are based on the type 9 strain gage.

Overall turbine bucket stress levels are shown as a function of fan speed for gage 7 in Figures 270 through 273. These figures present data from runs 7, 9, 10, and 11 respectively. Note that Figure 270 includes a curve of overall stress level versus fan speed obtained during the LF2 demonstrator test.

In Figures 271, 272, and 273, data are shown for various scroll actuator positions as well as for the 100-percent open position. The core engine power was held constant for the various scroll actuator settings as indicated by the J85 engine speed, N_e , given in each figure.

Turbine bucket stress data based on gage 9 are shown in Figures 274, 275, and 276, where scroll actuator position is constant at 100 percent, 90 percent, and 50 percent respectively.

The predominant frequency observed in most of the turbine bucket stress data corresponds to the first flexural mode as identified by component

bench tests. Predominant frequency is plotted as a function of fan speed in Figure 277. LF2 demonstrator test data are included for comparison.

The spectrum analysis results as presented in Figures 278, 279, and 280 show the many component frequencies which make up the complex stress cycling of the turbine bucket. These plots are made from stress data during a specified short time interval for which the fan speed is held constant. Two characteristics are brought out in the spectrum analysis plots: a relatively high amplitude of the signal corresponding to a frequency of one cycle per revolution, and a relatively high amplitude for particular frequencies in a band near the bucket's first flexural natural frequency, 980 cycles per second.

The one-per-revolution frequency is generated by the partial admission turbine effect of applying pneumatic load during a portion of the revolution within the scroll arc, and coasting under centrifugal loading during the remaining portion. The amplitude of this stress component is plotted as a function of fan speed squared in Figure 281 for the scroll actuator in the 100-percent open position. Similar data obtained during the LF2 demonstration tests in 1964 are also shown on the figure.

In order to show the effect of changing scroll admission arc on the one-per-revolution component of bucket stress, Figure 282 presents the ratio of the one area to the one-per-revolution stress level at 100-percent open area. Each data point represents a different fan speed, and each ratio is formed by using the one-per-revolution stress level obtained at that speed with 100-percent scroll actuator position. The expected variation of this stress ratio with scroll area is also shown on the figure and will be discussed in the analysis of the data.

The effect of changing scroll admission arc on overall turbine bucket stress level at constant fan speed is shown in Figure 283. The reduction in overall stress level obtained as the scroll admission arc is closed down is even more impressive when the increased one-per-revolution stress component shown in Figure 282 is considered. Note also that a given change in scroll area or actuator position causes a larger change in overall stress level at higher fan speeds than a similar area change would make at lower fan speeds. Figure 283 also shows this effect as a ratio of percent change in stress to percent change in area plotted versus fan speed squared.

The wave form of the turbine bucket stress signal changes as the scroll admission arc is changed. This change in amplitude and in proportion to active and inactive arcs is shown in Figure 284.

Torque Band Stress Levels

The torque band is subjected to a vibratory loading of one cycle per revolution due to the nature of its role in transmitting the excess input torque in the turbine active arc to the fan blades in the inactive region.

Since the magnitude of this loading will vary with admission arc, a strain gage, type 6, was located on the torque band as shown in Figure 87 to obtain data on this effect. For practical purposes, the only vibratory stresses observed on this gage was due to the torque loading.

The torque band stress data are presented in Figures 285, 286, and 287. In Figure 285 the overall stress level is shown as a function of fan speed for a constant scroll area of 80 percent.

The effect of varying scroll area at constant fan power is shown in Figure 286, where overall torque band stress is plotted versus scroll actuator position along lines of constant fan speed. Figure 287 shows overall torque band stress level versus scroll effective area for one constant fan speed.

Scroll Transient Effects on Stress

During the various scroll actuator transients (sine wave, step changes, and step changes with jagger), stress data did not show a significant effect due to the transients. While the overall stress levels varied as a function of fan speed and scroll area during the transient, the response was not discernibly different than would be obtained for steady-state operation at the same fan speed and scroll area. To demonstrate this type of operation, Figure 288 shows stress and fan speed variation for a sine wave input to the scroll actuator.

Rotor Temperature

Thermocouples were attached to certain rotor components in order to determine operating temperatures. These temperatures are used as test safety instrumentation, and they also provide data for confirmation of design calculations and assumptions. The LF2 rotor temperature data are presented in two groups. The first group consists of the data from the thermocouples on the turbine bucket, the blade tip tang, and the torque bands; while the second group is data from the ball bearing and roller bearing thermocouples.

Stationary thermocouples were installed as shown in Figure 81 to determine the turbine's operating temperature environment by measuring the temperature of the surrounding gas.

A typical temperature history for a test run is presented in Figure 289, where rotor component temperatures are plotted as a function of time. Important events are noted in the figure. This run included manual variation of scroll area by initially opening the dump valve followed by closing of the scroll area.

Varying scroll area while holding engine power constant did not significantly affect rotor component temperatures as indicated in Figure 290.

Figure 291 gives rotor component temperatures as a function of average exhaust gas temperature of the two core engines. Data are presented for two runs at constant scroll area settings: 100 percent open and 80 percent open.

Bearing temperature data are presented as a time history for a test run in Figure 292 and as a function of fan speed in Figure 293. As shown in the latter figure, several quite different trends can be obtained in the plot of bearing temperature versus fan speed. These trends seem to be a function of the sequence of operation during the test run. The two extreme cases are shown in the figure for both the ball bearing and roller bearing temperatures. The higher bearing temperatures were obtained on test runs which began with a relatively rapid acceleration to maximum power followed by reduction of fan speed in steps to obtain performance data. The lower bearing temperatures were obtained on test runs which began with an acceleration to a lower power setting followed by step increases in speed to obtain performance data. Arrowheads are used to indicate increasing run time in the figure.

One of the stationary thermocouples measuring gas temperature in the tunnel aft of the turbine was located in the active arc, while the other two were located in the inactive arc. Data were taken in one of two ways: fixed power and variable scroll area, or fixed scroll area and variable power. Data taken by the first method are presented in Figure 294, where turbine inlet gas total temperature, turbine bucket temperature, tip tang temperature, and the three tunnel gas temperatures are plotted versus percent scroll area. The same parameters are shown as a function of exhaust gas temperature in Figure 295 for data taken by the second method.

Figure 296 shows typical circumferential distributions of tunnel gas temperature. Data are given for two scroll area settings.

Post-Test Inspection

The following discussion presents the significant results of inspections performed on the rotor system after each test run.

After test run 5, inspection of the rotor revealed that foreign object damage had been sustained in the fan turbine. The location of the damage was random in nature, with 11 buckets involved. The most serious damage was a 0.2-inch tear in the bucket leading edge 1 inch from the bucket tip on bucket 3, carrier serial number 12. The remainder of the damage was minor in nature and the cause was not identified.

Operation was continued with frequent inspection of the damaged area. No further progression of the leading edge tear was noted.

After test run 14, cracks were found in two turbine buckets. These cracks in the bucket skin adjacent to the root braze filler were located at the leading edge of the bucket in carrier position 1 and at the trailing edge

of the bucket in carrier position 9.

The two buckets were removed before the test was continued. Because of their diametrically opposed location on the rotor, no balance correction was required. Operation was continued until the test plan was completed with no further incidents. Scroll area was limited to 80 percent where turbine bucket stress levels were lower in order to preclude additional failures.

The accumulated time up to the bucket failures was slightly more than 5 hours. After removal of the two buckets, 10 hours of additional running time were accumulated.

ANALYSIS AND DISCUSSION OF TEST RESULTS

This section presents some interesting comparisons of test results, results of further analysis, and significant trends shown in the test data. Some extrapolations of the test results for fan operation with the J85/J4 engine configuration are also included.

This section of analysis is concerned only with the test results. A section later in the report will be concerned with the results of the analog simulation studies. That section will present detailed comparisons of test and simulator results. Extension of fan performance to larger scroll sizes and operation with the J85/J4 engine will be presented.

EFFECTS OF FAN CONFIGURATION ON PERFORMANCE

During the test program, numerous changes of the fan configuration were made to determine possible changes in performance. These test results have been previously shown as variations of lift, fan speed, and available horsepower throughout the complete test range. A tabulation of this measured performance in terms of lift at a given fan speed of 2300 revolutions per minute is given in Table VI.

Comparison of these data shows the lift increments as given in Table VII. The lift increment due to installing the stator stiffener rings was obtained by comparing runs 7 and 9. An increment of 2.3-percent loss in lift was apparent. Comparison of runs 9 and 11 includes two configuration changes: installation of the bleed nozzles to permit dump valve programming, and operation at a scroll position of 70 percent rather than full open. This 70-percent scroll area existed because, in run 11, fan speed was varied using scroll setting rather than engine power level. The resulting lift increment is a 1.3-percent reduction in lift. A lift decrement of 1.8 percent was estimated to exist because the scroll is at 70 percent rather than 100 percent. Therefore, the effect of installing the bleed nozzles shows about a 1/2-percent difference in performance. This is negligible when considering the expected test accuracy.

The lift increment due to covering the hole in the frame dishpan around the slip ring cavity produced an increased lift of 0.4 percent. The existence of this hole in the dishpan would allow air to flow from the bottom side of the fan stators towards the cavity between the fan rotor and stators. There was always concern that this flow would appreciably influence fan performance in the hub region. These test results showed that this effect may be negligible.

Previous testing of lift fan configurations has shown that the orientation of the circular vane in the fan inlet can appreciably influence performance of the fan system. For this reason, it was measured prior to conducting this test program. The results of these measurements are summarized in Figure 297. The prime measurement for circular vane location is the angle of the vane chord line relative to the bellmouth radial line, as shown by

the schematic on the figure. The design value of this angle was selected at 67 degrees, based on previous X353-5 test results. The circular vane as installed in the LF2 was oriented at, or at less than, this angle in all quadrants except between the 90- and 180-degree position in the fan. Since an orientation angle less than design is more desirable than greater than design, it was decided that the 90- to 180-degree quadrant should be reoriented. This was accomplished by loosening, rotating, and raising the vane until the angle at the 135-degree position was at the design angle of 67 degrees.

The results of testing this configuration, with the one quadrant of the circular vane reoriented, showed a lift decrement of 3.1 percent even though a lift increase was anticipated. Why a lift decrement was observed is not understood. This reverse trend tends to indicate that additional investigations of the circular vane system are required to explore fully the effects on fan performance.

The fan exit louvers were removed in order to obtain their incremental performance effects on fan lift. The remaining fan systems were retained at the previous test configuration, especially the location of the fan inlet circular vane. Comparison of these results, run 18, shows that the total lift increase was 5.6 percent due to removing the exit louvers. The aerodynamic drag of the louver system was estimated to be about 2 to 3 percent of the total fan lift. The additional 3 to 4 percent lift increase observed during the test may be accounted for as an unthrottling of the fan when the louver blockage was removed. This unthrottling of the fan was also verified by the increase in power absorbed by the fan at a given fan speed, louvers on and off.

The next major configuration change at the conclusion of run 18 was to remove the inlet vane system completely. Testing of the fan in this configuration showed that a large decrease of fan performance was experienced; coupled with this, there was a large increase in rotor blade stress level, which is characteristic of poor aerodynamic performance.

Following these tests, the inlet vane was reinstalled as near as possible to the original orientation as given in Figure 297. At the same time, the fan forward air seal was built up with a silicone adhesive sealant such that there was almost zero seal clearance around the active arc of the fan. With the exit louvers still removed, the fan was run to investigate any possible performance improvement. Comparison of these test results, run 19 with run 17, shows a lift increment of 6.3-percent. However, run 17 is with the exit louvers on so an increment of 5.6 percent due to the louvers is included in the 6.3 percent. The net effect due to the improved forward air seal is about 0.7 percent.

The last configuration change was to remove the stator stiffener rings. Comparison of the cases of stiffener rings in and out for run 19 shows a lift increment of 0.6 percent. A similar configuration change was made during run 7. The lift increment for this case was 2.3 percent. The

difference in the lift increments for these two cases may be the result of exit louver interference effects. With the exit louvers installed on the fan, a 2.3-percent lift increment was observed. The lower lift increment was observed when the louvers were off. Apparently there is some type of interference losses associated with the combination of stiffener rings plus exit louvers that produced the larger changes in fan system lift.

So in summary, it is possible to conclude that the LF2 fan system at full-open scroll will develop 5560 pounds of lift at 2300 revolutions per minute. A potential lift increase of 22 pounds due to covering the slip-ring hole will increase this lift to 5582 pounds. This lift level will be used as the basis for extrapolated performance using J85/J4 engines to drive the fan. At this level of performance, the available horsepower required to drive the fan is 3090, and this will also serve as a basis in future analysis.

VARIABLE AREA SCROLL EFFECTIVE AREA

During the conduct of the test program, the effective area of the fan scrolls was determined using fan scroll airflow, engine discharge total temperature, and scroll total pressure. The variation of scroll area with actuator stroke has been presented in Figure 183. Figure 23 also shows the physical area of the fan turbine nozzles taken from inspection measurements.

Comparison of the effective and physical areas of the two parts of the scroll is shown in Figures 298 and 299. For fan scroll 1, that is, the forward scroll and the one having the biconvex nozzle partitions, the comparison is shown in Figure 298. At the full-closed or zero-percent scroll position, the physical and effective areas are in good agreement. As the scroll is opened, the increase in effective area is much less than that expected based on the physical area measurement. If these test measurements are accurate, this effect indicates a blockage of unknown origin in the turbine nozzles containing the splitter vanes.

A different condition is apparent for fan scroll 2. In this case, the difference in both the full-closed and full-open case is about 5 square inches of area, the effective area being less than the physical area. In this scroll section, the nozzle partitions are the flat type. A possible explanation of the flow conditions is as follows:

- o With all the variable nozzle partitions closed, the flow incidence on the open nozzles is at a very high negative angle.
- o With this high incidence, separation occurs and the effective area is reduced considerably.
- o In the full-open position, all nozzles are at near-normal flow incidence; but there is still a blockage effect as

observed for the biconvex nozzles, possibly due to the splitter vanes.

No matter how good an explanation is possible, there is also a doubt as to the accuracy of the methods used in determining the fan scroll flow. As described in the data reduction procedures, the fan flow is obtained by taking the difference of the total engine flow and all known over-board flows such as diverter valve leakage, bleed nozzles, and overboard dump. This could produce inaccuracies in the calculation of fan flow, but with the levels observed, it is difficult to imagine so large an inaccuracy in the measurements. The test results show this lack of area, and unless proven to be in error, the deficiency of flow effective area may indeed be real.

If this low effective area trend really exists, the effect on fan design would be an increase in scroll arc size to obtain a given power transfer capability. Similar tests of the X353 22 and previous LP2 tests did not show this trend; effective and physical areas were in close agreement with normal test accuracy. Detailed aerodynamic flow tests of the scroll position and area control devices may provide some knowledge as to possible aerodynamic design changes that would reduce the flow over deficiency.

The combined fan scroll area variation with actuator stroke is the sum of that for the two scrolls. This summation is given in Figure 300.

LOSSES OF DIVERTER VALVE AND CROSS DUCT

During this test, the scroll pressure was measured by wall static pressures, and the overboard dump system total pressure was measured by arrays of total pressure probes. The measured loss coefficients were presented in Figures 182 and 184. Using these data, the curves shown in Figure 301 summarizing the pressure losses of the four legs of the ducting were derived. The right-rear and right-forward duct loss coefficients are the measured data based on scroll pressure measurements. The left-rear and left-forward loss coefficients are those of the overboard dump system with the straight duct losses subtracted. The dashed part of the curves represents the extrapolation of the data, assuming the left-forward and right-rear ducts have similar loss coefficient variations with Mach number. The right-forward and left-rear ducts were also assumed to be similar. This assumption is based on the fact that both the cross duct system and the fan scrolls are similar configurations diagonally opposite each other. The scroll losses (left-hand system) represent the complete system losses, while the dump duct losses (right-hand system) represent all losses except for the extreme ends of the scroll arms.

Comparison of the loss levels, right to left and forward to rear, shows that both the left duct system and the forward ducts have higher losses.

This comparison agrees with expected trends observed in the XV-5A propulsion system, where the fan area required to obtain a given fan power level was an

indication of relative loss levels. Similar trends of high losses in the right and forward ducting systems were observed.

EXTENSION OF PERFORMANCE TO THE J85/J4 LEVEL

The core engines used to power the LF2/VAS configuration in this test were one each of J85 and YJ85 engines. The LF2/VAS was intended for use with an advanced engine, the J85/J4. This engine operates at a much higher exhaust gas temperature and consequently higher power level. Typical performance characteristics for this engine are shown in Figures 302 through 304.

In order to extrapolate the fan performance, a base level of performance was required. The lift base was 5580 pounds of lift at 2360 revolutions per minute (see Table VII). The fan speed level of 2410 revolutions per minute at a horsepower level of 3500 was also selected at the base (see Figure 117). Using these two base points and assuming ideal fan laws, the characteristics shown in Figures 305 and 306 were obtained. In Figure 305 it is assumed that fan lift varies directly with fan speed squared, and in Figure 306 it is assumed that fan speed varies as the cube root of the horsepower.

To correct fan performance for variable scroll arc operating conditions, the characteristics shown in Figures 307 and 308 are required. Figure 307 presents the lift multiplier to correct fan turbine thrust effects as a function of scroll arc. This multiplier was derived using standard performance calculation techniques and is not truly a test result. However, this trend was observed in the test results, as was the probable cause of the lift decrement with variable area scroll as shown in Figures 131 and 137.

The second set of characteristics required is the effects of scroll arc on the power-speed relationship of the fan system. This characteristic based on test results is shown in Figure 308. This curve shows the effects of scroll arc to be negligible and will be neglected in the future analysis.

The next step in the analysis was to determine what percentage of the core engine is supplied to the fan as a function of scroll arc or actuator position. The relationship between scroll admission arc and actuator position for the LF2/VAS is shown in Figure 309. The variation of flow function with scroll arc was then obtained by summing the results shown in Figure 180. Figure 310 presents this sum as a function of scroll arc and scroll actuator position. Making use of this flow function variation with scroll arc and an engine flow function of 51.2 as shown in Figure 303, the percentage of the core engine being delivered to the fan was obtained and is shown in Figure 311. Total available horsepower as a function of scroll arc is then the percentage in Figure 311 times the engine rated horsepower as shown in Figure 304. The results are presented in Figure 312, where the total available horsepower as a function of scroll arc and scroll actuator position is shown. This is the available horsepower required to determine the fan speed and fan lift using the performance as shown in Figures 305 through 308.

The resulting estimated fan performance for the LF2/VAS operating with J85/J4 engine is shown in Figures 313 and 314. The fan performance as demonstrated in this test is also shown for comparison.

FAN PERFORMANCE WITH EXIT LOUVERS

The variation of fan speed, lift, and thrust is presented as a function of scroll actuator position and exit louver angle in Figures 315 through 317. Actual turning angle, based on measured lift and thrust, is a constant 2 degrees more than the indicated louver angle as shown in Figure 318.

For the LF2 test, the exit louvers were ganged together so that all louvers were positioned at the same angle at all times. On the X353-5B fans, the louvers were more open both fore and aft of the center louvers, and the center louvers were used to measure indicated louver angle.

The LF2 and X353-5B louvers have the same airfoil shape, but the LF2 louvers are test hardware and are much stiffer, resulting in less deflection under air loading. A comparison of LF2 and X353-5B fan characteristics at constant turning angle and constant available gas horsepower is given in Table IX.

For turning angles as high as 22 degrees, both fans have very little overspeed, but the total thrust of the LF2 has already dropped 4 percent, indicating that it is already being throttled. As turning is increased, the LF2 overspeed becomes greater and total lift becomes smaller than those of the X353-5B. These characteristics indicate that the LF2 rotor is more sensitive than the X353-5B rotor to downstream throttling. This was further substantiated by the total lift improvement of 5.6 percent experienced by the removal of the exit louvers. From X353-5B testing, removal of exit louvers was found to produce only 1.5 to 2 percent improvement, typical of louver drag losses only.

COMPARISON OF X353-5B AND LF2 FAN PERFORMANCE

The LF2 fan buildup configuration for the variable area scroll test reported herein is referred to as LF2/VAS to distinguish it from the first buildup configuration for the LF2 demonstration test conducted in December 1964. As shown in Figure 319, the test results of the first LF2 indicated a lift deficiency of 9.5 percent at constant fan speed. The LF2/VAS fan test results, shown as the circled data points in Figure 319, are in very close agreement with the average X353-5B level. The improvement in LF2 performance must be attributed to buildup and installation changes. These changes were:

1. Stator stiffener rings removed.
2. Reduced axial spacing between rotor hub and rear frame dishpan.

3. New steel inlet vane with XV-5A contour and depth relative to rotor blade optimized.
4. XV-5A type scroll modified for smaller nozzle passage height of the LF2 buckets and incorporating the variable area feature.
5. Closer forward air seal clearances.
6. Rear frame center-body hole covered.

Several configuration changes were made and investigated during the LF2 variable area scroll test. The results are included in Table VII and provide the following indications concerning the performance due to buildup configuration:

1. Stator stiffener rings cause a 2.3-percent lift decrement at the same fan speed.
2. Reduced axial spacing provides a small improvement, as indicated by the effect of covering the slip ring hole in the rear frame dishpan.
3. The fan is very sensitive to inlet vane position, as indicated by the 3.1-percent decrement resulting from repositioning one quadrant of the inlet vane.
4. The variable area scroll should have no effect on fan lift-speed characteristic, with comparisons being made at maximum scroll area to eliminate any differences in fan turbine thrust due to scroll arc differences.
5. A relatively small lift increment (0.7 percent) is indicated for improved forward air seal. The actual amount of improvement from the first LF2 buildup is not known but is estimated to be relatively small compared to the total 9.3-percent increment.
6. Covering the slip ring hole in the fan rear frame showed small lift increase of 0.4 percent.
7. The fan exhibited throttling sensitivity greater than indicated by X353-5B experience. Increased throttling sensitivity coupled with any other configuration problem could cause larger than expected performance losses.

With the exception of the variable area scroll, all of the above items contributed to the fan performance improvement, with the largest incremental change being attributed to the closer attention given to correct inlet vane position.

A comparison of fan speed versus available fan horsepower with the comparable characteristic determined from the first LF2 test is shown in

Figure 320. These data indicate that the LF2/VAS fan requires approximately 16 percent less available fan horsepower to operate at the same fan speed. The configuration changes that may account for a small part of this improvement are the new fan turbine and the XV-5A type double-entry scroll incorporating the variable area modifications. The new turbine is aerodynamically the same and should cause no performance change. The scroll losses were expected to be lower by a small amount, but the factor that may have contributed most significantly was the improved scroll to turbine passage matching.

FAN TIME CONSTANTS BASED ON SINUSOIDAL INPUT TEST RESULTS

Comparison of fan response characteristics for both step inputs and sinusoidal inputs is possible because the sinusoidal response characteristics can be changed to an effective time constant once the intersection of the two asymptotes is known. This relationship of asymptotes has previously been discussed. The time constant is then related to the frequency at the intersection or so-called break in the attenuation diagram as given below:

$$\tau = \frac{1}{2\pi f_0}$$

This relationship of time constant and frequency is shown in Figure 321.

The data obtained during the sinusoidal test program were converted to time constants and are presented in Figures 322 and 323. Engine power settings of 95 and 100 percent are shown. The data are presented for two conditions: one for a constant amplitude of scroll area change as a function of nominal scroll actuator position, and the other for a constant nominal scroll actuator position as a function of the amplitude of the sinusoidal variation of scroll actuator position.

The data show that the nominal scroll setting has a negligible effect on the time constant, at least for the full range of the test VAS. This effect will be discussed in detail in the analog simulator results. The characteristics also show that the optimum time constant exists at a scroll area change of about plus or minus 20 percent. This characteristic is probably the result of test accuracy, since the analog simulation to be described later did not show this effect. The analog showed optimum time constant at infinitesimal scroll area changes.

A similar analysis of the tests with the jazzier can be performed, and the results are shown in Figure 324. In this case, the fan time constant is plotted against the jazzier m factor. The results show that with the jazzier the fan time constant can be reduced from about 0.38 to less than 0.10. However, to obtain this level of time constant, an overshoot of about 1 decibel was experienced at about 0.4-cycle-per-second impressed frequency.

THE EFFECTS OF THE JAZZER ON FAN RESPONSE

The effects of the jazzer on fan response to sinusoidal inputs can be derived theoretically once the basis for response characteristics for sinusoidal inputs is known. Figures 325 and 326 present the results of such an analysis. Previous analysis of the jazzer circuit shows that the attenuation of a fan with jazzer is the sum of the basic fan and jazzer attenuation, in decibels, at a particular impressed frequency. Similarly, the phase shift is the sum of the two phase shift angles. This relationship was used in defining the curve shown in Figures 325 and 326.

A typical fan response characteristic without the jazzer is shown as the solid lines in the figures. This characteristic is based on an assumed fan time constant of 0.45 second. Both phase shift and attenuation characteristics are shown. The jazzer response is also shown for the particular jazzer m and τ_j values used in the test. Combining the jazzer and fan response characteristics results in the curve as shown by the solid line. The dashed curves on the figure show the test results obtained for the same jazzer settings. Excellent agreement of the test results is shown.

COMPARISON OF FAN TIME CONSTANTS FOR STEP AND SINUSOIDAL TYPES OF INPUTS

Since the fan response was obtained for conditions of step inputs as well as sinusoidal inputs, a comparison of these two sets of test results is desirable. Such a comparison of fan response without jazzer is shown in Figure 327. The comparison with jazzer is shown in Figure 328. For both cases, the time constants with step inputs are of higher level than for similar conditions with sinusoidal inputs. This difference may be attributed partly to the effects of actuator slew rate on fan performance.

The curves in Figure 329 show the conditions when actuator slew rate affects performance with sinusoidal type of inputs. This figure shows the regions of frequency and amplitude that are not influenced by the slew rate limit. Three actuator slew rates are shown. Operation on the left side of the slew rate line is free of actuator slew rate effects, and to the right the actuator motion will be limited by the slew rate. For the VAS test program, the slew rate could be adjusted and was set at about 0.2 second.* Therefore, for scroll actuator sinusoidal inputs of plus or minus 20 percent, actuator slew rates are insignificant at impressed frequency below 4.0 cycles per second.

*Actuator design criteria set a maximum slew rate of 0.4 second at full design load. The slew rate for the test program was set at 0.2 second for the no-load condition. No measurable change in slew rate was observed for the operational load conditions.

However, for the case of step inputs, the actuator slew rate is always a contributing factor. At the instant that a step input is commanded, the actuator begins moving at the slew rate limit until the final commanded level is achieved. The time required to move from the initial to the final level is a function of slew rate, as shown in Figure 330. For slow slew rates and large step inputs, the time required to reach the command levels becomes very significant relative to the fan response rates. For example, with a 0.2-second slew rate and a step command of 20 percent, the time to slew is 0.04 second as compared to a fan time constant of about 0.4 second. It is apparent that the actuator slew rate can increase the fan time constants.

The effects of actuator slew rate with jazzer during step inputs are more pronounced. For the case with the jazzer, the input commands are modified to an overshoot level followed by an exponential washout effect as previously shown in Figure 6. The actuator slew rate significantly affects the level of overshoot, because part of the exponential washout occurs before the actuator actually reaches the command level. This effect then reduces the level of the jazzer overshoot significantly. These effects are shown in Figure 331.

This curve shows that for a step input of 10 percent, a jazzer m of 3.0, and a slew rate of 0.2 second, the overshoot level is about 85 percent. Therefore, for a jazzer m of 3.0, the overshoot will be about 2.6 rather than the desired level of 3.0. This effect contributes to the difference in fan with jazzer response for step and sinusoidal inputs as previously shown in Figure 328.

FAN RESPONSE USING ENGINE THROTTLES FOR HEIGHT CONTROL

Numerous tests were run to determine the fan response to step inputs of core engine power level. These results have previously been shown in Figures 221 through 224. An interesting correlation of these data is possible and is shown in Figure 332. The figure shows the effects of scroll area on fan response for small changes in fan speed. The increased scroll area improves the fan response considerably. Fan response also decreases as the size of the fan speed change increases. The upper curve in the figure shows that for a 10-percent change in fan speed, the time constant is about double the level for a very small speed change.

CORRECTION OF FAN THRUST RESPONSE CHARACTERISTICS FOR LOAD CELL RESPONSE

Prior to the test program, it was apparent that the response characteristics of the load cell system were not adequate for this test program. Because the system was designed primarily for steady-state response testing of the X353-5 fan system, it was not desirable to attempt to improve the response of the system. In lieu of this, the time constant of the thrust system was measured and found to be 0.47 second, as shown by the test results in Figure 187. Knowing this time constant, the response of the load cells to sinusoidal inputs shown in Figure 333 can be obtained.

This correction due to load cell response was then applied to the fan response characteristics based on thrust, shown in Figures 205, 208, and 211. The resulting corrected response characteristics are shown in Figures 334 through 336. The measured fan speed characteristics are also shown on the figures. The applied correction to the thrust data does tend to show the desired agreement, but is not accurate enough to evaluate system performance using the measured thrust response characteristics. Thrust performance during the analog simulation is much more accurate, and the data will be used for analysis rather than actual test results.

DISCUSSION OF ROTOR BLADE STRESSES

The blade stress data presented in Figures 256 through 263 are characterized by a series of stress peaks where the frequency of one of the blades fundamental modes is coincident with a relatively strong excitation source. If these peak stresses or resonant points are neglected, the trend shows a gradually increasing stress level as fan speed increases.

The resonant points are predicted during the fan design and are usually presented in a Campbell diagram such as Figure 269. From previous turbomachinery experience, it is known that excitation forces often exist at "n" cycles per revolution, where "n" is an integer usually related to the geometry of the hardware in the vicinity of the rotor. For the LF2 fan, the four front frame struts in front of the rotor probably cause the strongest disturbance in the air flowing through the fan blades. Thus, the most significant excitation should occur at a frequency of 4 cycles per revolution or multiples thereof; i.e., 4 per revolution, 8 per revolution, 12 per revolution, etc.

By correlation between the stress peaks and the Campbell diagram, the most significant resonant points can be determined. Table VIII summarizes these resonant points.

The level of the blades vibratory stress is directly related to the magnitude of the excitation source. The magnitude of the excitation force is largely determined by the relative velocity of the air to the fan blading, whether the excitation is the relatively strong "n"-per-revolution type or whether it is the weaker random airflow noise type. The increased relative velocity occurring at higher fan speeds causes the increase in blade stress activity noted in the data. The exit louver vector angle effect on blade stress in Figure 267, which indicates slightly lower blade stresses as the vector angle is increased, can be explained in terms of the change in relative air velocity. The throttling effect of the higher vector angles reduces the velocity of the airflow through the fan and results in a lower relative velocity for the blades at a given fan speed. This trend should continue until the throttling becomes severe enough to approach a fan stall condition. Operation near stall can cause blade flow separation and greatly increased nonsteady airflow excitation and can result in greatly increased blade stress levels.

The effects of scroll area variation on the fan blade stress response in its fundamental modes were not expected to be significant. The data for the first flexural mode in Figure 264 indicate little, if any, effect. The second flexural mode results of Figure 265 show conflicting trends at the different vector angles included in the figure. The data scatter obtained would indicate that the change in stress level is small.

The 3 θ mode response as observed on blade strain gage data is influenced somewhat by scroll area as shown in Figure 266. This mode of vibration forms a standing wave characterized by axial displacement of the wheel periphery in a sinusoidal pattern having six nodal points located on three equally spaced diameters. At the rotor's critical speed, approximately 1965 revolutions per minute, it is easily excited in this mode by circumferential pressure or flow distortions which can be in phase with all or a portion of the sinusoidal displacement. The partial admission turbine is a readily available source for such a distortion, and the variation of admission arc can affect the phase relationship of the distortion and the wheel's axial displacement, thereby affecting the magnitude of the response. On this basis, a small admission arc coincident with one-half cycle of the displacement might be expected to have higher response in the 3 θ mode, and the data of Figure 266 indicate such a trend. The off-design operation of the turbine which occurs at the smaller scroll areas causes an increased axial pressure difference across the turbine which may also tend to increase the wheel's response at small scroll area areas.

A test run was made with the inlet turning vane removed to evaluate the vane's effect on fan performance. This run was restricted at 2100 revolutions per minute fan speed because of high blade stresses. The curves of Figure 268 compare the blade stress data for runs with and without the inlet vanes. The greatly increased stress level observed when operating with no inlet vane is largely due to the separated and turbulent airflow entering the fan over the small-radius bellmouth. Note that the stress peaks at resonant points are not increased as much as the stress level at fan speeds between resonant points. This observation would be expected, since the stress level between resonant points is largely determined by the magnitude of airflow turbulence.

DISCUSSION OF TURBINE BUCKET STRESSES

Turbine bucket vibratory stresses can be divided into two categories. The alternating stress imposed by the gas loading of the partial admission design is one, while the other consists of resonant vibration in the bucket's fundamental modes. The overall stress level data in Figures 270 through 276 include contributions from both categories.

The characteristic of gradually increasing stress level with increasing fan speed and the occurrence of stress peaks at certain fan speed is to some extent similar to blade stress data. The stress peaks are more numerous, however, and they are more difficult to correlate with physical

obstructions to the gas flow.

Two additional observations can be made by studying the overall bucket stress data: (1) Operating at reduced scroll areas significantly lowered the level and peaking characteristics of the bucket stress. (2) A relatively large change occurred in stress activity after run 7, Figure 270.

The data from the LF2 demonstrator test are shown in Figure 270 with LF2/VAS results, and the general level of stress is the same for the two tests. All bucket stress data gathered after run 7 indicate stress levels from 1.5 to 2 times as large as those recorded in Figure 270.

This difference is not understood at the present time, but further analysis of the stress data may uncover the reason for this situation. Analysis of the data to this point has indicated that the stress level is correct and not an instrumentation recording or calibration error.

The natural vibratory mode of most significance is the first flexural mode as indicated in Figure 277. The first flexural frequency has a tendency to be lower as fan speed is increased because the effect of reduced material stiffness at higher operating temperatures more than offsets the stiffening effect of centrifugal force. Because bucket stress peaks did not seem to be related to physical disturbances occurring as "n"-per-revolution excitation, spectrum analyses were made of the bucket stress signal at several fan speeds. The results of the spectrum analyses have been shown in Figures 278 through 280. At each fan speed, the data reveal components of stress at every multiple of the one-cycle-per-revolution frequency up to 40 cycles per revolution. The existence of this multitude of frequencies at even multiples of the one-per-revolution frequency and the amplitude distribution indicates that the stress peaks in the spectrum analysis data represent the sinusoidal components of the one-per-revolution stress caused by the essentially square-wave loading of the partial admission turbine design.

The one-per-revolution component amplitude should increase linearly with fan speed squared, since it is proportional to the torque input to the fan. The data in Figure 281 from runs 7 and 11 show that this stress component does increase linearly.

The stress components in a band near the first flexural frequency, 980 cycles, have relatively high stress amplitude because of their proximity to resonance. The bucket's response near resonance has provided the opportunity to evaluate damping characteristics in the LF2/VAS turbine as described in one of the following sections of discussion of test results.

Scroll area changes have a large influence on turbine bucket stress levels. This can be seen very readily in the changing amplitude and wave form of the stress signal at different scroll areas shown in Figure 284.

The reduction of scroll area results in higher amplitude, partial-admission

loading on the turbine for a given fan speed, since the torque input to the fan must be provided by fewer turbine buckets in the active arc. This effect is shown in Figure 282, where the fundamental harmonic of the one-per-revolution stress is shown in a ratio form as a function of scroll actuator position. The anticipated square-wave stress level is shown in the figure for comparison. The large discrepancy is a result of the data reduction technique which provides the fundamental sinusoidal component amplitude rather than the square-wave amplitude. This effect tends to cancel the actual increase in partial admission stress as the length of the admission arc is reduced.

In Figure 283 the overall stress level is shown to be significantly lowered when the scroll area is reduced and fan speed is held constant. This reduction occurs in spite of the increased level of the partial admission load discussed in the previous paragraph. This improvement in the bucket stress level may be a result of changing the effective wave form of the partial admission loading or of eliminating a region of turbulent gas flow near the scroll ends as the scroll area is closed down. It is possible that an improvement in the vane splitter-nozzle flow characteristics could help to reduce the bucket stress level obtained during operation at 100-percent scroll area.

As noted before, the transient operation did not increase the stress levels above those experienced for steady-state operation at equivalent test points. On this basis, as long as vibratory stresses are within limits established by semi-infinite life criteria throughout the operating range, no detrimental effect is indicated by the transient data. However, if resonant points at certain fan speeds within the anticipated operating region cause stresses high enough for marginal part life, the repeated cycling through the resonant point could be damaging after a period of time.

DISCUSSION OF TORQUE BAND STRESSES

The torque band function in the LF2 rotor is to transmit tangential driving forces from the turbine admission arc to the fan blades operating in the inactive arc. By transmitting this force through a continuous band at the blade tips, the fan blades are not subjected to the large stresses induced by transmitting this force as a bending moment.

The partial admission torque force produces all the alternating stresses observed in the torque band. The manner in which this torque band force varies during a revolution of the rotor is quite different from the turbine bucket's partial admission force. While the turbine bucket has a square-wave type loading due to sudden application and removal of gas flow at the scroll ends, the torque band load varies in a nearly sinusoidal manner.

In Figure 286 the overall torque band stress level is shown to increase as the scroll area is reduced and fan speed is maintained constant. As dis-

cussed for the turbine bucket, this increase in amplitude is necessary to impart the same rotor torque in the smaller admission arc. In Figure 287, where effective area is used instead of scroll actuator position, the reduction of the scroll area by a factor of one-half results in a stress increase of approximately two. This is in keeping with the assumption that the one-cycle-per-revolution partial admission stress is inversely proportional to the admission arc area for constant fan speed. This assumption was used in arriving at the estimated curve in Figure 282 for turbine bucket stress. The data reduction technique has no cancelling effects on the sinusoidal stress signal from the torque band strain gage similar to that noted for the square-wave signal of the turbine bucket.

DISCUSSION OF ROTATING COMPONENT TEMPERATURES

In Figure 289 the rotor component temperatures are shown as a function of core engine exhaust gas temperature. From these data the turbine bucket temperature is approximately 0.78 of the engine exhaust gas temperature, the torque band temperature is approximately 0.42 of the engine exhaust gas temperature, and the blade tip tang temperature is approximately 0.35 of the engine exhaust gas temperature. The scroll area is at 100-percent open for the above temperature ratios; however, the data in Figure 290 show no significant change in component temperatures as the scroll area is changed with engine EGT held constant. Note that these data are obtained at different fan speeds, since the smaller scroll areas result in reduced fan speeds at constant engine power. Any extension of these data to larger scroll areas must be adjusted to take this speed variation into account.

The bearing temperatures were monitored primarily as safety instrumentation. The data in Figure 293 show quite a variation in temperature versus fan speed depending upon the history of the test run. Another influence on bearing temperatures is the test duration. Operating temperatures were lower during the latter test runs than during the initial runs. This has been a typical experience with grease-packed bearings in lift fan rotors and is attributed to a "run-in" effect required to establish proper lubricant volume and movement among the rolling elements.

The tunnel gas temperatures measured aft of the turbine in the enclosed flow path on the inactive side of the fan are important in determining the temperature environment of rotor turbine components during a portion of their rotation. As shown in Figure 295, the tunnel gas temperature varies from 0.16 to 0.23 of the engine EGT, depending upon circumferential location.

The circumferential variation shown in Figure 296 would indicate that the turbine gas carried into the tunnel with the turbine buckets is rapidly cooled by a circulation of fan air through the air seals.

TURBINE BUCKET RESPONSE CHARACTERISTICS

Relative response of the turbine bucket system at resonance can be obtained by use of the spectrum analysis characteristics given in Figures 278, 279, and 280. The procedure used in obtaining the response of the turbine bucket is described below:

First, it was assumed that the turbine bucket flexural response is defined by the equation

$$A/A_o = \frac{1}{[1 - (\frac{\omega}{\omega_o})^2 + j 2\zeta \frac{\omega}{\omega_o}]}$$

where ω = the impressed frequency of the exciting force

ω_o = the bucket natural frequency

ζ = the damping factor

At resonance the response is as follows:

$$(A/A_o)_{\text{resonance}} = \frac{1}{2\zeta}$$

Also, at low values of $\frac{\omega}{\omega_o}$ the response is approximately unity.

The second assumption is that the level of any exciting force due to the scroll discharge flow pattern varies directly with fan speed squared and that the ratio of a particular harmonic to the fundamental is a constant. This assumption is based on the ideal fan performance laws which state that turbine torque is proportional to fan speed squared for a given configuration.

Making use of these assumptions, it is possible to trace a particular harmonic or group of harmonics through the resonance condition of the turbine bucket and therefore obtain the turbine bucket damping coefficient. The procedure is iterative, but for the sake of explanation, assume that the first iteration has shown that the bucket resonance frequency is 965 cycles per second and the damping coefficient is low, perhaps 0.01 or 0.02. Now, to trace the 24th harmonic through the spectrum analysis, begin at the lowest fan speed condition of 1900 revolutions per minute. At this speed, the frequency of this harmonic is as follows.

$$F = \frac{1900}{60} (24) = 760$$

From the spectrum analysis the stress level at 760 cycles per second is about 400 pounds per square inch and the frequency ratio ω/ω_0 is 0.788. At this frequency, the response ratio A/A_0 is about 2.64 based on the equation representing the bucket response. The exciting force is then 400 divided by 2.64 or equivalent to 151 psi. Now let us look at a higher speed point at a fan speed of 2440 revolutions per minute. At this speed the frequency of the 24th harmonic is 976 cycles per second. The stress level at this frequency from Figure 280 is 7400 pounds per square inch. Relating the first stress level of 151 and correcting for fan speed effects, the response level of the turbine bucket to the 24th harmonic is obtained as follows:

$$A/A_0 = \frac{7400}{151} \left(\frac{1900}{2440} \right)^2 = 29.7$$

This relative response then represents a single data point as shown on Figure 337 that was plotted at 976 cycles per second and 2440 revolutions per minute.

This procedure was repeated for each of the data points shown in the figure. The best fairing of the data results in the curve as shown. At resonance of 968 cycles per second, the relative response ratio is 50. This infers a damping coefficient of 0.01 for the turbine bucket system.

HARMONIC ANALYSIS OF TURBINE EXCITING FORCES

A second type of performance information may be obtained using the results of the spectrum analysis in conjunction with the bucket response characteristics just previously described. Assuming that the bucket response is as shown in Figure 337, each of the levels of the harmonics shown in the spectrum analysis may be reduced to an equivalent level as a percentage of the fundamental. The fundamental is the relative high stress level between 30 and 80 cycles per second. From each spectrum analysis the level of the n^{th} harmonic is read from the data, and the relative level as compared to the fundamental is obtained as follows:

$$\text{Relative Amplitude} = \frac{A_n/A_1}{A/A_0}$$

where A_n = level of n^{th} harmonic

A_1 = level of fundamental

A/A_0 = turbine bucket relative response factor calculated at the frequency of the n^{th} harmonic

This procedure was used to obtain the characteristics shown in Figure 338 for the three high-speed conditions. The results show the following trends:

The second and third harmonics are high and about 20 to 25 percent of the fundamental.

Harmonics above the 15th that are in the range of turbine bucket resonance have a nearly constant amplitude of between 4 and 6 percent of the fundamental.

For the 10th and 16th harmonic conditions, one set of data indicated higher than normal levels. These two conditions happen to coincide with the fan blade first flexural and first torsional frequencies. This appears to be blade vibration exciting the turbine buckets.

The above analysis is the case for a partial admission scroll of 168 degrees arc. Closing down the arc by using the variable area scroll appears to change the level of these exciting forces significantly. However, at the time of this report, this type of detailed analysis had not been completed.

THE J85/LF2 ANALOG COMPUTER SIMULATION

An analog computer simulation of the J85/LF2 variable area scroll fan system was developed and run. The analog tests were done in two parts.

The first analog operation, in October and November 1965, was to determine objective dynamic thrust control performance for the hardware demonstration. The second analog operation, conducted following the LF2 fan hardware tests, was run to add to and extrapolate the data obtained from the hardware test so that a complete definition of the LF2 power transfer system could be obtained. The two analog simulations were nearly identical except that the second analog simulation included a more sophisticated duct circuit which more accurately calculated the duct total pressure losses during power transfer gas flow modulation.

The results of the second analog operation are reported in this section. Several LF2 fan hardware test points were run to insure that the analog system would indeed duplicate the LF2 system. The analog system simulated J85/J4 engines (dry J85-13), while the hardware test used engines having lower power levels. The only correction to the analog system that was required to duplicate the hardware test results was the change in fan available power level.

Thus, a true analog representation of the J85/LF2 fan system has been achieved as substantiated by actual full-scale LF2 hardware tests, and dynamic thrust control performance has been extrapolated to design objective levels of variable area scroll admission arc. Principal analog results were:

1. The LF2 fan hardware test results have been accurately duplicated by the analog simulation.
2. The extrapolation of the LF2 hardware test results to a 200-degree arc of admission system has been accurately predicted by the analog simulation.
3. Analytically determined fan dynamic response has been verified by the analog simulation.
4. A fan thrust time constant of 0.31 second for small (5 percent) step changes in area about the design point has been demonstrated. Realistic values of scroll hydraulic actuation and control system dynamics were included.
5. Use of a jazzer can reduce this value of fan thrust time constant to as low as one-half the basic value without overshoot.
6. A fan thrust time constant of about 0.25 second can be obtained for height control using small step changes of fan area with a jazzer.
7. A fan thrust time constant of 0.10 second can be obtained for height control using small step changes of the engine throttles.

THE ANALOG FACILITY

Figure 339 shows a section of the General Electric, Evendale, analog computer laboratory.

THE SYSTEM SIMULATION

Figure 340 shows a simplified block diagram of the analog system. The system simulated one engine, two fans, and associated ducting. The engine output was doubled to represent a two-engine system. Duct dynamics were incorporated by using the duct to satisfy the continuity of flow. Flow, temperature, and pressure were the principal parameters coupling the engine and fans. The simulation required the use of 4 computer consoles, and used 130 amplifiers, 10 function generators, 4 electronic maps, and 21 multipliers. Four quarter-square multipliers were used, two of which were borrowed from the General Electric, Philadelphia, analog computer laboratory for this simulation.

The J85/J4 Core Engine Simulation

The simulation of the core engine was based on a model having an aft fan, with a balance made on engine discharge (station 51) variables. Pressure, P_{51} , was an input to the engine; temperature, T_{51} , and flow, W_{51} , were output quantities. Figure 341 shows the engine block diagram and Figure 342 shows the engine analog wiring diagram.

Steady-state engine performance is shown in Table X, which lists the principal engine performance parameters as functions of engine speed.

Engine internal cycle transient data were generated using the digital computer decks of Evendale and Lynn. The engine discharge corrected flow, $W_{51} \sqrt{\theta_2} / \delta_2$, was defined as a function of speed by

$$W_{51} \sqrt{\theta_2} / \delta_2 = \xi_1$$

where

ξ_1 = the function tabulated in Table XI.

The compressor discharge corrected static pressure, P_{s3} / δ_2 , was defined as a function of speed and fuel flow by

$$P_{s3} / \delta_2 = \gamma_1 + \gamma_2$$

where

γ_1 and γ_2 = functions tabulated in Table XI.

The steady-state corrected engine discharge pressure, P_{51}^{ss} / δ_2 , was defined as a function of speed and fuel flow by

$$P_{51}^{ss}/\theta_2 = \phi_1 + \phi_2$$

where

ϕ_1 and ϕ_2 = functions tabulated in Table XI.

The corrected engine discharge temperature, T_{51}/θ_2 , was defined as a function of engine speed, fuel flow, and engine transient discharge pressure by

$$T_{51}/\theta_2 = 520 + \gamma_2 [\gamma_1 + \Delta P_{51} (\partial T_{51}/\partial P_{51})]$$

where

γ_1 and γ_2 = functions tabulated in Table XI.

ΔP_{51} = the difference between the instantaneous value and the steady-state value of engine discharge pressure during an engine transient.

$\partial T_{51}/\partial P_{51}$ = the instantaneous value of the partial derivative of discharge temperature with respect to discharge pressure with speed and fuel flow held constant. This derivative is shown in Figure 343.

The engine unbalanced torque, Q_e , is defined by the expression

$$Q_e = \Delta P_{51} (\partial Q_e/\partial P_{51})$$

where

ΔP_{51} = the difference between the instantaneous value and the steady-state value of engine discharge pressure during an engine transient.

$\partial Q_e/\partial P_{51}$ = the derivative of engine unbalanced torque with respect to discharge pressure with speed and fuel flow held constant. This derivative is shown in Figure 344.

The engine speed was found by integrating the unbalanced torque:

$$N_e = C J_e Q_e/s$$

where

N_e = engine speed, rpm

C = conversion constant for units

J_e = engine polar moment of inertia, lb-ft-sec²

Q_e = engine unbalanced torque, ft-lb

s = Laplacian operator, d/dt

The Duct Simulation

Figure 345 shows the analog block diagram for the duct. Figure 346 shows the duct analog wiring diagram. Continuity of flow was satisfied by use of the gas law in the form

$$P_{52} = RT_{52}/Vol \int_0^t (W_{in} - W_{out}) dt$$

where

P_{52} = crossover duct entrance total pressure, psia

R = gas constant, ft-lb/lb-°R

Vol = duct volume, ft³

W_{in} = flow into the duct from the engines, lb/sec

W_{out} = flow absorbed by the fans, lb/sec

The total pressure drop in the crossover ducts and scrolls (P_{54}/P_{52}) is shown in Figure 347. The pressure drop was calculated by assuming total pressure loss coefficients (\bar{w}) of

Diverter Valve: 0.24

Crossover Duct: 0.35

Scroll: 0.55

This pressure loss coefficient, \bar{w} , is defined as the total pressure loss between two stations divided by the difference in total and static pressures at the upstream station. In symbols

$$\bar{w} = (P_{T1} - P_{T2}) / (P_{T1} - P_{S1})$$

where

P_T = total pressure, psia

P_S = static pressure, psia

and where subscripts 1 and 2 denote the upstream and downstream stations, respectively.

The Lift Fan Simulation

Figure 348 shows the fan block diagram. The two fans were identical. Figures 349 through 352 are the wiring diagrams for the two fans. Figure 353 shows the wiring diagram for the fan area control. The tip turbine map is shown in Figures 354 and 355. The map defines the tip turbine energy function, $\Delta h/h$, and the percentage value of the tip turbine flow function, $\% \phi_{54}$. The map operating line is shown in Figure 356. The fan design point is given in Table XII.

The map value of the enthalpy function $(\Delta h)_{map}$ was corrected by

$$W_{54} (\Delta h)_{corr} = \underbrace{0.988 W_{54} (\Delta h)_{map}}_{(1)} - \delta_2 \underbrace{[8.501 (N_F/1000) + 7.955 (1 - F) (N_F/1000)^3]}_{(2) + (3)}$$

where

$W_{54} (\Delta h)_{corr}$ = fan absorbed energy, Btu/sec

$W_{54} (\Delta h)_{map}$ = turbine available energy, Btu/sec

and where the three corrections are

- o 0.988 for leakage and efficiency.
- o end loss, proportional to fan speed.
- o windage loss, with the $(1 - F)$ term proportional to turbine arc of admission and with a second term proportional to the cube of fan speed.

The tip turbine discharge temperature, T_{55} , was found by

$$T_{55} = T_{54} - (\Delta h)_{map}/c_p$$

where

c_p = specific heat ratio, a constant in this simulation

The turbine exit area, A_{58} , was proportional to the turbine nozzle area, A_{54} . A discharge pressure loss coefficient, \bar{w}_{55} , of 0.06 was assumed. The turbine downstream conditions were found by satisfying the continuity equation.

The fan torque was found by using the fan laws. The turbine torque was found by using the relation

$$HP_T = (778/550) W_{54} (\Delta h)_{corr} = 2\pi N_F T_T / 33,000$$

where

HP_T = turbine horsepower

N_F = fan speed, rpm

T_T = turbine torque, ft-lb

The fan speed, N_F , was found by integrating the unbalanced torque:

$$T_T - T_F = (2\pi/60) J_O (d/dt)(N_F)$$

where

T_T = turbine torque, ft-lb

T_F = fan torque, ft-lb

J_O = fan rotor polar moment of inertia, 21.5 lb-ft-sec²

The fan thrust was found from the fan laws. The turbine thrust was found from the thrust function, $F_T/W_{58}\sqrt{T_{58}}$: an input function of P_{58}/P_{amb} .

Analog Fan Area Defined

Fan area refers to the variable area of the turbine scroll nozzles. Figure 357 relates the analog fan area to arc of admission and to tip turbine flow for J85/J4 engines at 100-percent speed. An analog area of 100 percent corresponds to the design point area of 96.22 square inches of Table XII and a tip turbine flow equal to 90 percent of the discharge flow of one engine. At this design point, the fan speed is 2740 rpm and the fan lift is 7525 pounds.

Figure 358 relates analog area to the J85/LF2 test hardware scroll actuator stroke.

Steady-State Fan Performance

The solid lines of Figure 359 show steady-state fan speed as a function of analog fan area, as measured on the analog simulation. The dashed lines show the fan speed as measured in the hardware test. These test values are lower than the analog values because of the lower energy of the engines used for the hardware test. The circles are points taken from Figure 313 and represent extrapolation of these hardware test data to the full J85/J4 engine power level of 100-percent engine speed. There is good correlation between the extrapolated hardware test data and analog data.

The solid lines of Figure 360 show fan lift versus fan analog area. The circles are points from Figure 314, and show the extrapolation of hardware test data to the full J85/J4 engine power level at 100-percent engine speed. The extrapolated hardware test data show that the test hardware slightly exceeded the quoted LF2 lift performance level.

Figure 361 shows fan lift versus fan speed. The solid line is the analog data from Figures 359 and 360. Shown for comparison are data from four test hardware runs, with and without stator stiffening rings. The test hardware slightly exceeded the quoted J85/LF2 lift level. Again, there is good correlation between analog and hardware test performance.

Effect of Actuator Slew Rate

The effect of actuator slew rate (time required for full stroke of the scroll area actuator) was investigated on the analog by performing step changes in fan area of 5 percent and 15 percent from an initial fan area of 100 percent. The results are shown in Figure 362. The hardware test

actuator had a slew rate of about 0.20 second. The slew rates shown in Figure 362 are for analog area changes equivalent to full stroke of the test hardware actuator. The fan time constants for the larger fan area steps are more affected by the value of actuator slew rate. There is only a small effect on the fan time constants for changes in actuator slew rate between 0 seconds (instantaneous response) and 0.20 second. As slew rate increases above 0.20 second, the effect of slew rate becomes more pronounced.

Fan Response to Area Step Changes Without a Jazzer

Figure 363 shows a recorder trace of typical analog fan response to a step change in fan area without a jazzer. Figures 364 and 365 show the analog results for fan speed time constants for positive and negative step changes in fan area at 100-percent engine speed. The slight scatter in the data is due to the inability to measure more accurately the time constants from the analog chart recorder traces. Figure 366 summarizes these data. The solid line denotes a positive area change (step-up) in fan area, and the dashed line denotes a negative change (step-down) in fan area. The fan responds quicker to a step-up than to a step-down in fan area. This is explained by referring to Figures 359 and 360. Fan speed and thrust are nonlinear functions of fan area, so that a step-down in fan area requires a larger speed and thrust change than does an equal-size step-up in fan area. At 100-percent fan area, the fan speed and thrust time constants are 0.31 second, which agrees with previously calculated values.

Figures 367 and 368 compare the analog and the hardware test results for fan speed time constants for step changes in fan area without a jazzer. Shown are the fan speed time constants versus initial fan speed for three sizes of step changes in fan area. The hollow symbols and the lines are analog results, and include the analog data from Figures 364 and 365. The solid symbols denote hardware test data for two engine power settings from Figures 215 and 216, and use the same symbols as on those figures. Scatter is evident in the hardware test data, probably due to reingestion or cross-flow effects. Even so, there is good correlation between the analog and hardware test results.

Figures 369 and 370 show the analog results for fan thrust time constants for positive and negative step changes in fan area at 100-percent engine speed. Figure 371 summarizes these results. Again, the fan responds faster to positive than to negative area changes. Figure 372 shows these analog fan thrust time constants as functions of initial fan speed.

Fan Response to Step Changes With a Jazzer

The jazzer was explained on page 6. Figure 373 shows a recorder trace of typical fan response to step changes in fan area with a jazzer.

Figures 374 and 375 show the analog fan speed and fan thrust time constants as functions of the two jazzer parameters, jazzer magnification factor, M , and jazzer washout rate, τ_j , for step changes of +5 percent and +10 percent

from the 100-percent design area. The points on the ordinate (at $\tau_j = 0$) are from Figures 364 and 369 for no jazzer. The effect of the jazzer is clearly evident; even small values of washout rate significantly lower the value of fan time constant. Fan thrust leads fan speed when a jazzer is used, so that the fan thrust time constants are lower than the fan speed time constants.

For a given value of jazzer magnification, increasing the value of jazzer washout will lower the fan time constant until an apparent minimum value of fan time constant is reached. Further increases in the washout rate have no effect on the time constant. However, increases in washout rate for a given magnification factor do increase the amount of fan speed and thrust overshoot. Therefore, the washout rate should be chosen, in combination with the magnification factor, so that the fan time constant is a minimum while the fan response overshoot is kept to an acceptable level.

It can be shown that when

$$(1 + m) \tau_j = \tau_{fan}$$

where

m = jazzer magnification factor

τ_j = jazzer washout rate, seconds

τ = fan speed or thrust time constant, seconds

overshoot would just be impending; i.e., any change in τ_j to make the product term $(1 + m) \tau_j$ larger than τ_{fan} would cause some overshoot in the fan response. The dashed lines on Figures 374 and 375 show this product term $(1 + m) \tau_j$. For a +5-percent step change in fan area, a jazzer magnification factor of 1 will decrease the fan thrust time constant by 30 percent, while a jazzer magnification factor of 4 will decrease the fan thrust time constant by about 52 percent without fan thrust overshoot.

Fan Steady-State Frequency Response

Figures 376 through 380 compare the hardware test data and analog data for 5 runs without a jazzer. These figures are copies of Figures 197 through 201, with the analog data superposed. There is good correlation between the hardware test results and the analog results.

Figures 381 through 383 show the analog results for three area changes about the design area of 100 percent without a jazzer, at 100-percent engine speed. The fan speed and thrust time constants agree with those on Figures 363 and 371 for step inputs, showing that the analog data are consistent and repeatable.

Figures 384 through 386 compare the hardware test data and analog data for three runs with a jazzer. These figures are copies of Figures 203 through 205, with analog data superposed. Again, there is good correlation between the analog results and hardware test results.

Figures 387 through 390 show the analog results for a fan area change of 100 percent ± 5 percent at 100-percent engine speed for jazzer magnification factors from 1 to 4. The jazzer washout rate was chosen to give between 30 percent and 40 percent overshoot, as seen by the positive values of attenuation.

Figure 391 shows typical analog area response with overshoot. Shown are the jazzer output area and the actuator output area. The input area has a constant amplitude, while the jazzer output area has an increasing amplitude due to the effect of the jazzer. The actuator follows the jazzer signal until a frequency is reached which saturates the actuator; i.e., the actuator is no longer able to follow the jazzer command because of the slew rate limit of the actuator.

Figures 392 and 393 show the analog results for a fan area change of 100 percent ± 10 percent with jazzer magnification factors 1 and 3. For these runs, the jazzer washout rate was chosen to avoid overshoot.

Figure 394 summarizes the results of steady-state frequency response of the fan at 100-percent area. Shown are fan speed and thrust time constants as functions of jazzer magnification factor, m . The two effects of the jazzer are to decrease the fan time constants and to cause the fan thrust response to lead the fan speed.

The effect of the jazzer on fans for roll control is summarized in Figure 395. Shown are the fan speed and thrust time constants for three lines of fan response labeled a, b, c,

where

a = fan response to step inputs with no overshoot (the dashed lines of Figure 374)

b = fan response to step inputs with overshoot, with τ_j chosen to match the values of line c, from Figure 394

c = fan steady-state frequency, from Figures 387 through 390.

Lines b and c are not coincident because during step inputs the actuator is always saturated, while for steady-state frequency response the actuator need not be saturated. The effect of actuator response (slew rate) on fan time constants is thus seen to be significant when a jazzer is used. (Recall that Figure 362 showed that actuator slew rates between 0 and 0.20 second had only a small effect on fan response without a jazzer.)

Lines a and b show the decrease in fan time constant possible with overshoot. Some overshoot in fan response may be acceptable even desirable. However, excessive overshoot will be objectionable.

Fan for Height Control

Aircraft height control can be obtained by either small changes in engine throttle setting or by small changes in total fan area. Each of these methods will be discussed.

Using fans for height control, the areas of the two fans are opened or closed together collectively so that no roll control force is generated while the total area change is sensed by the engine causing a change in total fan lift. Figure 396 shows a recorder trace of typical engine and fan response to step changes in fan area for height control.

Figure 397 shows the steady-state fan speed and thrust, and Figure 398 shows the steady-state engine speed and exhaust gas temperature, T_{51} , as functions of fan area. The J85/J4 droop governor causes the decrease in engine speed shown on Figure 398. The stray data point on Figures 397 and 398 at 97-percent fan area is suspect; it could be an incorrect reading or it could indicate that one of the engine cycle functions of Table XI was incorrectly programmed. The analog data for fan response to decreases in fan area below 100 percent are therefore suspect.

Figure 399 shows the fan speed and thrust time constants for step changes in fan area about the design point, at 100-percent engine speed. The initial fan area was 100 percent, while the size and direction (sign) of the step change are indicated on the abscissa.

Figure 400 shows similar analog data for step changes in fan area. Here the initial area is indicated on the abscissa; the final area was 100 percent.

The trends in Figures 399 and 400 are the same: for area changes above 100 percent area, the fan time constants are unaffected by step size or direction, while for area changes below 100 percent area, the fan time constants are quite sensitive to step size and direction. Even with a jizzer, the thrust time constant is high. This is partly explained by Figure 398. The fan performance is quite sensitive to exhaust gas temperature, T_{51} , but T_{51} changes opposite (in sign) to fan area; therefore, it opposes the fan response demanded by the area change. (This is true regardless of the suspect data point on Figures 397 and 398.) Figure 401 shows the effect of jizzer washout rate on fan response using fans for height control.

Engines for Height Control

Figure 402 shows a recorder trace of typical analog response of the engine and fan to step changes in engine throttle setting for height control.

Figure 403 shows the time constants for engine speed, fan speed, and fan thrust for step changes in engine throttle position. A fan thrust time constant of 0.10 second can be obtained for small step changes of engine throttle position. The J85/J4 engine control causes the fuel flow and

exhaust gas temperature to overshoot as though a jazzer were used, as is evident in Figure 402. This causes rapid fan response. In fact, for small throttle changes, the fan thrust and speed response are more rapid than the engine speed response; i.e., the fan beats the engine on-speed.

COMPARISON OF GAS POWER TRANSFER AND THRUST SPOILING CONTROL SYSTEMS

Thrust spoiling using the exit louver system was the method of control used in the XV/5A aircraft. Control is obtained by pinching together the fan louvers, thereby causing a change of fan lift with no change of power being delivered to the fan.

The LF2/VAS system uses the principle of gas power transfer to modulate the lift of the lift fan propulsion systems. The variable area scroll is the device that permits the transfer of power between fans. The following section compares the steady-state and dynamic performance of these two systems.

The results of the demonstration test and analog simulation were used to obtain the variation of fan lift with gas power transfer for the variable area scroll system. This performance is shown in Figure 407 as the percent change in fan lift as a function of percent change in design fan turbine flow. For a system using two lift fans for roll control, the combined system lift and control forces can be obtained using Figure 407. The resulting control effectiveness of gas power transfer is shown in Figure 408 as a function of percent of design fan turbine flow modulation.

Comparison of control effectiveness of thrust spoiling and gas power transfer must be made at an equivalent control force parameter. This comparison is shown in Figure 408. The performance of the gas power transfer system, variable area scroll, was obtained from Figure 407. The performance of the thrust spoiling system is simply the lift loss required to produce the desired control force. The figure clearly shows the different lift losses experienced when using gas power transfer and thrust spoiling.

Figure 409 is a comparison of the dynamic response of the two methods of control. The response of the gas power transfer system was obtained from the analog simulation results shown in Figure 374. The time constant for the thrust spoiling system was designed to be 0.095 second for the XV-5A system. This time constant is simply the time constant of the exit louver actuator system. The thrust response of the fan is assumed to be instantaneous for this type of control.

Comparison of the dynamic response of the two systems shows that the time constant for the gas power transfer system approaches but does not become less than that for thrust spoiling. A good comparison would be time constants of 0.15 to 0.20 second for gas power transfer and 0.075 to 0.10 second for thrust spoiling. The higher time constant of gas power transfer should be adequate for normal aircraft control systems, especially when consideration is given to the small lift losses that accompany this type of control system using gas power transfer.

CONCLUSIONS

The results of the test program and analog simulation indicated the conclusions summarized below:

VARIABLE AREA SCROLL

1. Power transfer for thrust control of lift fan systems can be obtained by using the variable area scroll for gas power transfer.
2. The variable area scroll using turbine nozzle splitter vanes for area control is an acceptable design based on mechanical and aerodynamic performance. Deficiencies in turbine nozzle effective area of the variable area scroll were observed. Further aerodynamics tests will be required to fully explore this problem.
3. Fan dynamic response can be accurately predicted using analog simulation of the complete fan system.
4. Fan thrust time constants for the LF2 system are 0.31 second for roll control at a design speed of 100 percent. The time constant can be reduced to 0.15 second using a jazzier. Compared to estimated requirements of VTOL aircraft, the time constant of 0.31 second would be marginal while the 0.15 second time constant should be acceptable.
5. Fan thrust time constants for height control are much shorter when using engines for control than when using fan area. The time constant using engines for control will be about 0.10 second. Height control using fan area with the jazzier will have time constants of about 0.25 second. The 0.25 second time constant would be marginal for height control of a VTOL aircraft while the 0.10 second value should be acceptable.
6. Fan scroll actuation forces for the splitter vane design are very low and compatible with existing linear hydraulic actuator design capability.

FAN AERODYNAMIC PERFORMANCE

1. Performance of the LF2 system indicated a lift of 7900 pounds at 2750 revolutions per minute. This level of performance meets or exceeds objective levels established by the X353-5B system.
2. The LF2 system appears to be more sensitive to fan discharge throttling than the X353-5B system. This type of performance does not represent a serious design deficiency but is a performance problem that may warrant further investigation.
3. The LF2 fan system was very sensitive to inlet vane orientation.

Further investigations of effects of fan inlet geometry on fan performance are required to fully explain the problem.

FAN MECHANICAL PERFORMANCE

1. Fan blade stresses were as expected and within normal operating limits. Incorporation of the variable area scroll in the fan system did not significantly affect fan blade stresses.
2. Excessive turbine bucket stresses existed in the LF2 rotor fan conditions of maximum area scroll and high fan speeds. Reduction of scroll area and fan speed produced significant reduction of turbine bucket stress.
3. Fan front frame structural temperatures may be a problem in future fan designs as indicated by higher than allowable temperatures during the demonstrator test program. Cooling air was used to reduce these temperatures.

BIBLIOGRAPHY

1. Alford, G.C., Mechanical Design Report - LF2 Demonstration Test, Lift Fan Systems Operation, General Electric Company, Cincinnati, Ohio, December 1965
2. Austin, C., X353-5 Turbine Scroll Mechanical Design, General Electric Company Report No. R59FPD812, Cincinnati, Ohio, April 1, 1960
3. Beeler, E.F., Volk, L.J., Lift Fan Propulsion System - V/STOL Aircraft Control, Society of Automotive Engineers Publication 650831, Los Angeles, California, October 4, 1965
4. General Electric Company, X353-5B Propulsion System Flightworthiness Test Report, Lift Fan Flight Research Aircraft Program, Contract DA 44-177-TC-715 Report, General Electric Company, Cincinnati, Ohio, January 1963
5. MacKay, A.H., X353-5B Rear Frame Mechanical Design, General Electric Company Report No. R60FPD605, Cincinnati, Ohio, December 1960
6. Matson, E.H., General Performance Curves and Tabulations, General Electric Company Report No. DF52AGT723, Cincinnati, Ohio, March 11, 1952
7. Robinett, D.V., Performance Report - LF2 Demonstration Test, Lift Fan Systems Operation, General Electric Company, Cincinnati, Ohio, December 1965
8. Weatherwax, W.F., Design and Test of a Variable Area Turbine Nozzle, General Electric Company Report No. R55AGT83, Cincinnati, Ohio, February 22, 1955
9. Webb, G., LF2 Lightweight Front Frame Design, Lift Fan Systems Operation, General Electric Company, Cincinnati, Ohio, April 1, 1960

APPENDIX

DATA REDUCTION PROCEDURES

All parameters used in the calculation of engine and fan system aerodynamic performance were recorded by the digital data system. The punch tape data from the digital recorder were used for input to two computer programs. A "quick-look", time-sharing computer program converted the digital data to engineering units, calculated average values of pressures and temperatures, and performed a few additional calculations. The same digital tape was used for input to another program compiled especially for the needs of LF2 data reduction. It performed the same functions as the time-sharing program, but the calculation portion of this program was not limited, as it was in the time-sharing program. This program accomplished all needed calculations to complete the data reduction requirements of the LF2 system.

Engine Inlet Airflow

The inlet bellmouth flow calibration was performed as a part of the engine checkout procedure. The characteristics of the engine inlet bellmouths were assumed to be the same, and the boundary layer total pressure instrumentation was installed in the engine 2 inlet, only. Both inlet bellmouths contained four static pressure elements and three total temperature elements.

The following procedure was used to determine the bellmouth flow calibration characteristics. Assume that static pressure is constant over the whole area and equal to the average measured value. The mainstream total pressure is assumed to be equal to ambient pressure. Calculate flow per unit at each of the boundary layer total pressure stations and in the mainstream. Perform the summation, $\sum \left(\frac{W}{A} \right) (dA)$, over the total flow area to determine actual flow. Repeat the same calculation to determine a theoretical flow value assuming constant inlet total pressure equal to ambient pressure across the complete area. The bellmouth flow coefficient is equal to the actual calculated flow divided by the theoretical value.

The bellmouth flow calibration characteristic is generated by calculating airflow for a range of values of ΔP , ambient total pressure minus static pressure, and multiplying calculated flow by the flow coefficient.

The long bulletnose was designed for the J85-5 engine installation and would not fit on engine 1, which was the YJ85-5 engine. Therefore, an additional correlation of long versus short bulletnose was necessary. The assumption was made that engine 2 corrected flow versus corrected speed characteristic would be identical for long and short bulletnose installations. Using the bellmouth calibration characteristic to determine airflow, and comparing calculated airflow values at the same corrected engine speed, the correction factor for the short bulletnose calculation is 1.066. If the full effect of the area change in the plane of the instrumentation

were assumed, the correction factor for the short bulletnose would be 1.084. The full effect of the area change is not felt due to the close proximity of the short bulletnose to the instrumentation plane. The engine 2 airflow calibration curves for both long and short bulletnose are presented in Figure 404.

Engine Turbine Discharge Conditions

Engine turbine discharge gas flow, $W_{5.1}$, is calculated as follows:

$$W_{5.1} = W_2 - W_{IB} + W_f$$

Compressor interstage bleed air, W_{IB} , is a function of corrected engine speed and compressor inlet temperature. Fuel flow, W_f , is measured with a calibrated fuel potter.

Exhaust gas temperatures are determined from calibration curves of indicated harness temperature versus measured average tailpipe temperature.

The elements of the turbine discharge total pressure rakes are spaced to be in the center of equal areas. The arithmetic average is used in the calculations and represents the average value.

Dump System Flow Calculations

Existing total pressure and total temperature rakes were used in the ducts of the dump system, and the elements were not spaced in centers of equal areas. The gas flow in the dump ducts was determined by calculating the flow per unit area at each total pressure element and then summing (W/A) (ΔA) over the complete area. In the flow calculation, average static pressure and turbine discharge exhaust gas temperature with the calibration correction were used. The measured dump duct temperature was reliable initially and showed close agreement with calibrated exhaust gas temperature. During later runs, several dump temperature elements failed and exhaust gas temperature proved to be the more consistent and reliable indication of dump temperature.

Flow Split

The turbine discharge flow of each engine is distributed to the fan scroll, the overboard dump, the diverter valve seal leakage, and the bleed nozzle. The flow to the fan scroll is calculated as follows:

$$W_{5.3} = W_{5.1} - W_L - W_D - W_B$$

where

$$W_{5.3} = \text{flow to fan scroll inlet}$$

$$W_L = \text{diverter valve leakage}$$

W_D = flow to overboard dump

W_B = flow to bleed nozzle

The calculation of engine turbine discharge flow and overboard dump flow has been described previously. Diverter valve leakage flow is assumed to be a constant 0.8 percent of turbine discharge flow. The bleed nozzle flow is calculated for choked flow at maximum engine power using the relation

$$\frac{W_B \sqrt{T_{5.1}}}{P_{tB} A_{eB}} = \text{constant} = 0.521$$

where

$T_{5.1}$ = turbine discharge exhaust gas temperature with calibration correction, degrees Rankine

P_{tB} = bleed nozzle inlet total pressure, pounds per square inch absolute

A_{eB} = bleed nozzle effective area, square inches

Bleed nozzle inlet total pressure is calculated by correcting turbine discharge total pressure for diverter valve and cross duct loss coefficients. To get effective area of the bleed nozzle, a flow coefficient of 0.985 was assumed:

$$A_{eB} = (0.985) (A_B)$$

Engine 1 bleed nozzle area was 18.7 square inches and the flow was calculated to be 16.55 percent of the turbine discharge flow. Engine 2 bleed flow was 11.89 percent of turbine discharge flow for a bleed nozzle area of 12.7 square inches. Flow to the fan expressed as a percentage of turbine discharge flow was calculated as follows:

$$\frac{W_{5.31}}{W_{5.11}} = (1 - 0.008 - \frac{W_{D1}}{W_{5.11}} - 0.1655)$$

$$\frac{W_{5.32}}{W_{5.12}} = (1 - 0.008 - \frac{W_{D2}}{W_{5.12}} - 0.1189)$$

Horsepower Calculation

Energy levels in terms of ideal gas horsepower are used in the presentation of fan system performance. Ideal gas horsepower is the power that could be utilized in an ideal expansion of the gas from one set of conditions to another; for example, the engine discharge flow when expanding from turbine discharge pressure to ambient pressure. The equation for this ideal horsepower is

$$HP_{5.1} = \frac{778.26}{550} C_P T_{5.1} W_{5.1} \left[1 - \left(\frac{P_{t5.1}}{P_a} \right)^{\frac{\gamma-1}{\gamma}} \right]$$

Available fan horsepower as used in this report is defined as

$$FHP_{5.1} = \left(\frac{W_{5.31}}{W_{5.11}} \right) HP_{5.11} + \left(\frac{W_{5.32}}{W_{5.12}} \right) HP_{5.12}$$

Lift and Thrust Correction for Bleed Nozzles

Bleed nozzles installed on the pitch fan legs of the cross ducts produce thrust that contributes to both the horizontal and the vertical measured values. The gas flow in each bleed nozzle was assumed to be a constant percentage of the engine discharge flow, and the procedure for determining these values was described earlier under "Flow Split".

Conical nozzle thrust is calculated from the thrust function, $F_g/W_g\sqrt{T_t}$, presented as a function of nozzle pressure ratio in Reference 6. Horizontal and vertical thrust components for each bleed nozzle were calculated using a thrust coefficient of 0.99. The bleed nozzles are directed downward at an angle of 16.5 degrees from vertical, and the engine 1 bleed nozzle is directed forward while the engine 2 bleed nozzle is directed aft. Using measured data from run 17, Figures 405 and 406 were generated to show the bleed nozzle lift and thrust contributions to the system measurements as a function of core engine corrected speed.

Since the bleed nozzles are directed in opposite directions from the standpoint of horizontal thrust components, Figure 406 represents the difference between the two components. The resulting thrust component is shown as positive and has the same direction as the horizontal component of exit lower thrust for positive vector angles.

Correction Parameters

Throughout the data analysis and presentation, measured parameters were corrected to standard atmospheric conditions. These corrections are similar to those used in all parametric presentation of jet engine performance. The correction factors are defined as follows:

$$\theta_2 = \frac{T_{t2}}{518.688} \quad (T_{t2} \text{ in degrees Rankine})$$

$$\theta_{10} = \frac{T_{t10}}{518.688} \quad (T_{t10} \text{ in degrees Rankine})$$

$$\delta_2 = \frac{P_{t2}}{14.696} \quad (P_{t2} \text{ in pounds per square inch})$$

$$\delta_{10} = \frac{P_{t10}}{14.696} \quad (P_{t10} \text{ in pounds per square inch})$$

Fan and engine inlet total pressures are both assumed to be identical to ambient pressure, and the δ_2 and δ_{10} corrections are equal.

Corrected Performance

The above correction parameters, referred to standard temperature and pressure, were then used in computing corrected performance as listed below:

Corrected rotational speed	$\frac{N}{\sqrt{\theta}}$
Corrected airflow	$\frac{W/\theta}{\delta}$
Corrected thrust	F/δ
Corrected lift	L/δ
Corrected temperature	T/θ
Corrected pressure	P/δ
Corrected fuel flow	$W_f/\delta\sqrt{\theta}$
Corrected horsepower	$HP/\delta\sqrt{\theta}$

Flow Coefficient and Pressure Coefficient

Fan aerodynamic performance is usually presented in terms of flow coefficient and pressure coefficient. These parameters were computed using the following equations:

$$\text{Pressure Coefficient: } \Psi_{10.6} = \frac{2}{(\gamma-1)(M_T)^2} \left[\left(\frac{P_{t10.6}}{P_a} \right)^{\frac{\gamma-1}{\gamma}} - 1 \right]$$

$$\text{Flow Coefficient: } \phi_{10.3} = \sqrt{\frac{2}{(\gamma-1)(M_T)^2} \left[1 - \left(\frac{P_{s10.3}}{P_a} \right)^{\frac{\gamma-1}{\gamma}} \right]}$$

where

M_T = fan tip Mach number

$P_{t10.6}$ = fan rotor discharge total pressure

$P_{s10.3}$ = fan rotor inlet static pressure

P_a = ambient pressure

Fan tip Mach number is the ratio of fan tip speed, U_T , to fan inlet sonic velocity based on inlet total temperature:

$$M_T = \frac{U_T}{\sqrt{\gamma g R T_{t10.6}}} = \frac{\pi D_F \frac{NF}{60}}{\sqrt{\gamma g R T_{t10.6}}}$$

Fan inlet static pressures and fan bulletnose static pressures were converted to flow coefficient form for data presentation purposes. Similarly, fan rotor discharge total pressures and fan hub, dishpan, static pressures were converted to pressure coefficient form.

Pressure Loss Coefficients

Pressure loss coefficients are used to define the losses in the ducting from engine discharge to scroll nozzle inlets and to the overboard dump measuring station. The loss coefficients were calculated as follows:

$$\bar{w}_S = \frac{P_{t5.1} - P_{sS}}{q_{5.1}}$$

$$\bar{w}_D = \frac{P_{t5.1} - P_{tD}}{q_{5.1}}$$

where

$P_{t5.1}$ = engine turbine discharge total pressure

P_{sS} = scroll nozzle inlet static pressure

P_{tD} = dump total pressure

$q_{5.1}$ = turbine discharge dynamic head

The scroll nozzle inlet static pressure elements were located at the ends of each scroll arm; and when the scroll is partially closed, δ_S less than 80 percent, it was assumed to be an indication of total pressure.

TABLE I

MATERIAL PROPERTIES FOR COMPONENTS USED IN VARIABLE AREA SCROLL

Material	80% Stress Rupture, psi	% Elongation
Hastelloy X	15,200	36
Inconel X	35,000	5
L-605	22,500	16
René 41	55,000	6

TABLE II

VARIABLE AREA SCROLL MECHANISM AND ACTUATION COMPONENT WEIGHTS

Component	Quantity	Weight, Pounds
Biconvex Splitter Vanes	24	1.55
Flat Splitter Vanes	12	1.30
Journals and Housings	72	3.99
Levers	24	0.56
Bellcranks	12	0.78
Roller Bearings and Nuts	19	0.24
Tie Bars - Aft	6	0.29
Tie Bars - Forward	6	0.21
Slide Brackets	12	2.82
Cam Tracks	6	2.19
Mechanical Subtotal		13.93
Serrated Connector	2	0.19
Couples	2	0.16
Link Support Bracket	1	0.31
Actuator Support Bracket	1	1.80
Retainer	1	0.20
Forward Link	1	1.06
Aft Link	1	3.27
Miscellaneous Bolts	-	0.69
Actuation Subtotal		7.68
Nonflight Type Actuator		6.50
TOTAL		28.11

TABLE III
LIST OF TEST INSTRUMENTATION

TEMPERATURES				
Description	Symbol	Number	Units	Readout
Engine 1 Inlet	T _{t2.01}	3	MV	Digital
Engine 2 Inlet	T _{t2.02}	3	MV	Digital
Engine 1 Turbine Discharge (Harness)	T _{t5.11}	1	°C	Control Panel
		1	MV	Digital & Sanborn
Engine 2 Turbine Discharge (Harness)	T _{t5.12}	1	°C	Control Panel
		1	MV	Digital & Sanborn
Engine Tailpipe (Installed on either engine as needed)	T _{t6}	32	MV	Digital
Fan Inlet	T _{t10}	12	MV	Digital
Engine 1 Dump	T _{tD1}	9	MV	Digital
Engine 2 Dump	T _{tD2}	9	MV	Digital
Engine 1 Potter Fuel Temperature	T _{p1}	1	MV	Digital
Engine 2 Potter Fuel Temperature	T _{p2}	1	MV	Digital
Ambient Temperature	T _a	2	MV	Digital
Fan Ball Bearing	T _{UF}	1	°F	S-O-M
Fan Roller Bearing	T _{LF}	1	°F	S-O-M
Fan Rotating Temperature	T _{FR}	3	°F	S-O-M
	T _{FF}	3	°F	S-O-M
Fan Front Frame Temperature	T _S	3	°F	S-O-M
Fan Rear Frame Air Seal	T _{SA}	4	°F	S-O-M
Fan Scroll Actuation	T _{LT1}	1	°F	S-O-M
Engine 1 Lube Tank Temperature				

TABLE III (Cont'd)
LIST OF TEST INSTRUMENTATION

TEMPERATURES					
Description	Symbol	Number	Units	Readout	
Engine 2 Lube Tank Temperature	T _{LT2}	1	°F	S-O-M	
Hydraulic Tank Temperature	T _{HT}	1	°F	S-O-M	
PRESSURES					
Engine 2 Inlet Total (Used only during engine checkout)	P _{t2.0}	10	MV	Digital	
Engine 1 Inlet Static	P _{s2.01}	2	MV	Digital	
Engine 2 Inlet Static	P _{s2.02}	2	MV	Digital	
Engine 1 Turbine Discharge	P _{t5.11}	14	MV	Digital	
Engine 2 Turbine Discharge	P _{t5.12}	14	MV	Digital	
Fan Inlet Statics	P _{s10}	28	MV	Digital	
Fan Bulletrnose Static	P _{BNS}	6	MV	Digital	
Fan Rotor Discharge Total	P _{t10.6}	28	MV	Digital	
Hub Statics	P _{sF}	4	MV	Digital	
Engine 1 Dump Total	P _{tD1}	13	MV	Digital	
Engine 2 Dump Total	P _{tD2}	13	MV	Digital	
Engine 1 Dump Static	P _{sD1}	3	MV	Digital	
Engine 2 Dump Static	P _{sD2}	3	MV	Digital	
Engine 1 Scroll Internal Static	P _{SA1}	1	MV	Digital	
Engine 2 Scroll Internal Static	P _{SA2}	1	MV	Digital	
Engine 1 Compressor Discharge Static	P _{s3.01}	1	"Hg	Control Panel	

TABLE III (Cont'd)

LIST OF TEST INSTRUMENTATION

PRESSURES				
Description	Symbol	Number	Units	Rea'tout
Engine 2 Compressor Discharge Static	P _{s3.02}	1	"Hg	Control Panel
Engine 1 Lube In	P _{L1}	1	PSIG	Control Panel
Engine 2 Lube In	P _{L2}	1	PSIG	Control Panel
Engine 1 Fuel Manifold	P _{f1}	1	PSIG	Control Panel
Engine 2 Fuel Manifold	P _{f2}	1	PSIG	Control Panel
Engine 1 Starter Air	P _{AS1}	1	PSIG	Control Panel
Engine 2 Starter Air	P _{AS2}	1	PSIG	Control Panel
Facility - Starter Air Pressure	P _{ASF}	1	PSIG	Control Panel
Facility - Fuel in Pressure	P _{FF}	1	PSIG	Control Panel
Facility Hydraulic System	P _H	1	PSIG	Control Panel
MISCELLANEOUS				
Engine 1 Fuel Flow	W _{f1}	1	lb/hr	Digital Berkeley Sanborn
Engine 2 Fuel Flow	W _{f2}	1	lb/hr	Digital Berkeley Sanborn
Engine 1 Speed	N _{e1}	1	rpm	Digital Berkeley Sanborn
Engine 2 Speed	N _{e2}	1	rpm	Digital Berkeley Sanborn

TABLE III (Cont'd)
LIST OF TEST INSTRUMENTATION

MISCELLANEOUS				
Description	Symbol	Number	Units	Readout
Fan Speed	N_F	1	rpm	Digital Berkeley Sanborn
Scroll Actuator Position	δ_S	1	MV	Digital Sanborn
Dump Valve Actuator Position	δ_D	1	MV	Digital Sanborn
Vertical Lift	L	3	Pounds	Digital Control Panel Sanborn
Horizontal Thrust	F	2	Pounds	Digital Control Panel
Wind Velocity	W_V	1	mph	Chart (Bldg. 401)
Wind Direction	W_D	1	Degrees	Chart (Bldg. 401)
Engine 1 Vibrations	CFV1	4	Mils	Control Panel (70-Cycle Filter)
	CFH1			
	TV1			
	TH1			
Engine 2 Vibrations	CFV2	4	Mils	Control Panel (70-Cycle Filter)
	CFH2			
	TV2			
	TH2			
Fan Vibrations	BNA	3	Mils	Control Panel (10-Cycle Filter)
	Radial			BNA on Sanborn
	Tangential			

TABLE III (Cont'd)

LIST OF TEST INSTRUMENTATION

MISCELLANEOUS				
Description	Symbol	Number	Units	Readout
Engine Throttle Position (1 per engine)		2	Degrees	Control Panel
Diverter Valve Position (1 per engine)		2	Degrees	Control Panel
Rotor Gages		9	psi	Stress Recording Equipment Scopes & Tape
		(Blade)		
		3		
		(Bucket)		
		2		
		(Torque Band)		
Bulletnose Strain Gage (long bulletnose only)		1	psi	Scopes & Tape
Pan Front Frame Main Strut ss Gages		2	psi	Digital
Pan Rear Frame Dynamic Gages		4	psi	Scopes & Tape
Scroll Actuation System		2	psi	Scopes & Tape

TABLE IV

SUMMARY OF TEST RUNS

Run	Date	Readings	Average Wind Conditions		Description
			Velocity Direction		
			Miles Per Hour	Degrees From North	
1	6/08/66	1-9	11	300	Checkout of core engine in #2 position, J85-GE-5, S/N 231233. With nozzle area set at 111.8 square inches, performance data taken at speeds from 75 to 100%.
2	6/10/66	10-27	16	40	Performance data recorded at speed settings from 75 to 100% at nozzle areas of 114.8 and 117.8 square inches.
3	6/13/66	-	-	-	Checkout of core engine in #1 position, J85-GE-5, S/N 230729. Vib limits were exceeded; no performance data recorded.
	6/15/66	-	-	-	Investigation of vib problem; no performance data recorded.
4	8/12/66	28-46	4	300	Checkout of core engine in #1 position, YJ85-GE-5, S/N 230105. Performance data recorded at nozzle areas of 117.8 and 120.8 square inches.
5	8/26/66	47-53	7	235	Two-engine familiarization in jet mode; performance data recorded at 90 to 100% speed. Tailpipe trim areas were 117.8 and 113.8 square inches for core engines #1 and #2, respectively. Began fan mechanical checkout. Loss of strain gage instrumentation at 75% fan speed necessitated shutdown.

TABLE IV (Cont'd)
SUMMARY OF TEST RUNS

Run	Date	Readings	Average Wind Conditions		Description
			Velocity Miles Per Hour	Direction Degrees From North	
6	8/29/66	54-56	11	160	Fan mechanical checkout to full engine power; maximum fan speed obtained was 2425 rpm. Cooling air jets were installed prior to this run and were used on this and all successive runs to cool the fan front frame. Dump valve system hung up, but operated satisfactorily after it cooled off.
7	9/01/66	57-61	2	190	Fan aerodynamic performance; stator stiffener rings not installed. Noted high fan inlet temperatures recorded at two screen thermocouple locations. Scroll actuator set for maximum open scroll area during this run.
8	9/02/66	62	10	270	Began variable area scroll calibration. Dump valve system hung up.
9	8/23/66	63-69	16	330	Configuration changes before run 9 included: (1) adjusted diverter valve linkage on #2 core engine to reduce hot gas leakage, (2) installed rear frame stator stiffener rings, (3) accomplished load cell calibrations, and (4) reworked dump system. Recorded fan performance at maximum scroll area. Started calibration of variable area scroll but ran out of dump system capability. Reached choked flow condition in #1 core engine dump duct so further opening of valve had no effect on engine trim.

TABLE IV (Cont'd)
SUMMARY OF TEST RUNS

Run	Date	Readings	Average Wind Conditions		Description
			Velocity Miles Per Hour	Direction Degrees From North	
10	9/26/66	70-75	6	130	Bleed nozzles installed in place of blank-off plates on pitch fan ports of cross ducts. Performance data taken at 95% core engine speed and scroll actuator positions from maximum open to full closed using dump system to trim to same EGT at each point.
11	9/29/66	76-82	25	240	Repeated variable area scroll calibration (see run 10) at 100% core engine speed.
12	10/04/66	83-87	20	240	Scroll actuator position versus dump valve position was programmed into the control system. The variable area system was positioned manually from full open to full closed and back to full open with data recorded on Sanborn traces. Set scroll position to 76% o° stroke and recorded fan performance at exit louver settings from 0 to 36°.
13	10/06/66	88	5	330	Fan transient performance at 95% core engine speed. Scroll actuator position at 50% with ±20% sine wave input. Varied sine wave frequency from 0.1 to 7 cycles per second. Above 2 cycles per second, the amplitude of the sine wave motion of the scroll actuator began to decrease as expected. This is a saturation condition where the actuator slew rate capability is exceeded and it is no longer able to follow the input command.

TABLE IV (Cont'd)

SUMMARY OF TEST RUNS

Run	Date	Readings	Average Wind Conditions			Description
			Velocity	Direction	Miles	
			Per Hour	Degrees		
			From North			
14	10/10/66	89-98	9	270	Fan transient performance at 95 and 100% core engine speed. All sine wave out-of-phase data completed per test plan.	
15	10/26/66	99-108	11	15	Cracks in two turbine buckets were discovered after last run. These buckets were removed. Installed three thermocouples to measure in vicinity of rear frame air seal. Set up movie camera to photograph hydraulic system gages for indication of actuation forces. The following was accomplished: (1) at 100% core engine power, the scroll actuator was moved slowly from 90% to 0% and back to 90% for movies of the hydraulic pressure gage, (2) commanded out-of-phase step inputs and in-phase step inputs at 100% core engine power, (3) made engine throttle step inputs with scroll actuator setting of 80%, (4) in-phase step inputs repeated at 100% core engine speed, (5) repeated out-of-phase step inputs at 95% core engine power, and (6) obtained fan performance data at 100% core engine speed and scroll area from 80% to 0%.	
16	10/27/66	109-127	4	270	Fan transient performance with jasper included both out-of-phase step inputs and sine wave inputs at 100% core engine power. Scroll actuator hung up just before the last scheduled point was to be taken. Obtained fan performance at 95% core engine power for scroll areas from 0 to 80%. At louver setting of	

TABLE IV (Cont'd)

SUMMARY OF TEST RUNS

Run	Date	Readings	Average Wind Conditions		Description
			Velocity Miles Per Hour	Direction Degrees From North	
17	10/28/66	128-133	8	180	<p>20°, set core engine speed to 95%, took data reading, then varied core engine speed from 95 to 100 to 90 to 95%. The procedure was repeated for the 0 to 80% scroll settings. At a louver setting of 36°, the same procedure of taking readings at 95% core engine speed, doing a 95 to 100 to 90 to 95% core engine speed excursion for a series of scroll settings from 0 to 80% was repeated.</p> <p>Fan performance at 80% scroll setting.</p> <p>Fan performance at -7° louver setting at scroll settings from 0 to 80% and 95% engine speed. Engine speed excursion from 95 to 100 to 90 to 95% for transient stress data was repeated at each scroll setting as done previously in run 16.</p> <p>Covered slip ring cavity and took fan performance data at scroll setting of 80%.</p> <p>Tape spaced around blade tip tang and took fan performance data at 80% scroll setting.</p> <p>Performance series of core engine throttle transient from 99, 98, 97, 96, and 95% to 100% speed for a series of scroll areas from 0 to 60% for stress analysis.</p>
		134-138	8	180	
		139-145	12	240	
		146-152	8	200	

TABLE IV (Cont'd)

SUMMARY OF TEST RUNS

Run	Date	Readings	Average Wind Conditions			Description
			Velocity Miles Per Hour	Direction		
				Degrees From North	Degrees	
18	10/29/66	153-160	12	360	Tape around blade tip tangs has been removed. Inlet vane quadrant from 3 to 6 o'clock was raised approximately 0.5 inch and rotated 4° open. Fan performance taken at 80% scroll setting.	
		161-171	12	360	Removed exit louvers and repeated fan performance at 80% scroll as well as at 0 to 80% scroll at 100% core engine speed.	
		172-176	18	360	Removed inlet vane and ran fan performance. Took data at scroll settings from 0 to 80%; all at about 1750-rpm fan speed. Could not go higher in fan speed due to high stress levels.	
19	10/31/66	177-187	10	210	Circular vane reinstalled in original position. RTV sealant added to honeycomb structure just above rotor on hot side (improved forward air seal). Took fan performance at 80% scroll setting as well as 0 to 80% scroll setting at 100% core engine power.	
		188-200	10	210	Removed stator stiffener rings and repeated previous fan performance run.	

TABLE V

STRESS RATIOS* FOR GAGE LOCATIONS

Mode	Location of Maximum Stress	Stress Ratio				
		Gage 1	Gage 2	Gage 3	Gage 4	Gage 5
1st Flexural	Airfoil Tip, Convex Side at 0.60" From Tip, 1.5" From Trailing Edge	0.15	0.67	1.00	0.60	0.60
2nd Flexural	Airfoil Root, Concave Side at 0.5" From Trailing Edge, and Convex Side at 2.0" From Trailing Edge	0.62	0.58	0.46	0.50	1.00
1st Torsional	Airfoil Trailing Edge, Concave Side, 5.5" From Root and 13.5" From Root	0.92	0.80	0.78	0.92	0.40
30, 20 and Gyro	Airfoil Root at Leading Edge	0.87	0.65	0.10	0.22	-

*Stress ratio is the ratio of stress at the gage location to the maximum stress in the blade.

TABLE VI
EFFECTS OF TEST CONFIGURATION ON LIFT
MEASURED AT A FAN SPEED OF 2300 RPM

Lift	Run	Configuration Changes						
		Stiffener Rings	Inlet Vane	Louvers	Dishpan Hole	Seal Improved	Bleed Nozzles	Scroll Position
5560	7	Out	Down	On	Open	No	No	100%
5430	9	In	"	"	"	"	"	"
5360	11	"	"	"	"	"	Yes	~ 70%
5320	15	"	"	"	"	"	"	~ 60%
5360	17	"	"	"	"	"	"	80%
5380	17	"	"	"	Closed	"	"	80%
5210	18	"	Raised	"	"	"	"	80%
5500	18	"	"	Off	"	"	"	80%
Low	18	"	Out	"	"	"	"	80%
5720	19	"	Down	"	"	Yes	"	80%
5760	19	Out	"	"	"	"	"	80%

TABLE VII

COMPARISONS OF LIFT INCREMENTS AT 2300 RPM

Configuration Changes	Lift Increments
Installing Stator Stiffener	-2.3%
Installing Bleed Nozzles (Estimated Effects of 100% to 70% Scroll Area is about 1.8%)	-1.3%
Covering Slip Ring Hole	+0.4%
Raising Inlet Vane	-3.1%
Removing Exit Louvers	+5.6%
Improving Forward Air Seal	+0.7%
Removing Stiffener Rings (Second Time)	+0.6%
Best Estimate of LF2 Performance:	
Base Lift at 2300 rpm	5580 Pounds
Cover Hole (+0.4%)	<u>22 Pounds</u>
Total	5582 Pounds

TABLE VIII

SUMMARY OF BLADE STRESS RESONANT POINTS
 LF2/VAS ($\delta_g = 100\%$)($\beta_v = 0^\circ$)

Fan Speed N_F rpm	η/Rev	Frequency cps	Mode	Peak Stress Level 1,000 psi		
				Gage 1	Gage 3	Gage 4
1150	16	308	1st Flexural	-	4.0	5.0
1400	20	470	2nd Flexural	4.0	6.5	8.5
1610	12	325	1st Flexural	-	5.5	9.0
1800	20	610	1st Torsional	5.0	-	8.0
1850	16	498	2nd Flexural	10.0	10.0	10.0
1965	3	95	3 Theta	9.0	5.0	7.5
2090	10	352	1st Flexural	-	8.0	12.0
2300	14	536	2nd Flexural	6.5	9.0	12.0
2380	16	628	1st Torsional	6.0	-	10.5

TABLE IX

LF2 AND X353-5B VECTORING CHARACTERISTICS AT CONSTANT INPUT GAS HORSEPOWER

Parameter	LF2 ($\delta_s = 80\%$)			X353-5B ($\delta_s = 100\%$)		
Indicated Louver Angle, β_v	20.0	30.0	37.0	17.7	27.2	33.2
Actual Turning Angle, β_v	22.0	32.0	39.0	22.0	32.0	39.0
Fan Speed Ratio, N_F/N_{F_0}	1.0	1.025	1.053	1.007	1.016	1.027
Lift Ratio, L/L_0	0.891	0.783	0.703	0.934	0.847	0.769
Thrust to Lift Ratio, F/L_0	0.357	0.490	0.565	0.374	0.530	0.618
Total Lift Ratio, L_T/L_0	0.96	0.924	0.902	1.006	0.999	0.987

TABLE X
STEADY STATE J85/J4 CORE ENGINE PERFORMANCE DATA

<u>%Ne</u>	<u>P_{s3}</u>	<u>T_{s1}</u>	<u>P₅₁</u>	<u>W₅₁</u>	<u>W_f</u>	<u>W₂</u>	<u>W_f/P_{s3}</u>
100	95.28	1795	36.41	44.85	2928	44.04	30.73
99	93.69	1759	35.80	44.55	2818	43.76	30.08
98	91.84	1726	35.10	44.08	2706	43.33	29.46
97	89.60	1695	34.27	43.38	2583	42.66	28.83
96	87.18	1665	33.39	42.58	2469	41.90	28.32
95	84.34	1634	32.37	41.57	2343	41.19	27.78
90	69.16	1498	27.21	35.64	1762	37.46	25.48
85	58.31	1437	24.05	30.76	1430	33.73	24.52
80	48.65	1378	21.53	26.25	1147	30.42	23.58
75	43.82	1390	20.39	23.53	1043	27.53	23.80
70	38.68	1407	19.26	20.59	935	24.31	24.17

TABLE XI
ANALOG ENGINE CYCLE PARAMETERS

$\frac{W_F/b_2/\sqrt{g_2}}{}$	ϕ_1	γ_1	ψ_1
0	0	0	520
940	4.60	8.74	890
1043	5.55	10.00	993
1150	6.56	11.25	1093
1430	9.06	14.40	1351
1762	12.02	18.00	1651
2343	17.05	23.60	2166
2928	21.74	29.05	2654
3550	24.40	34.05	3141

$\frac{XN_0/\sqrt{g_2}}{}$	ϕ_2	γ_2	ψ_2	ξ_1
70	14.70	29.94	1.0000	20.59
75	14.84	33.80	0.8754	23.53
80	14.99	37.40	0.7866	26.23
85	15.00	43.90	0.6786	30.76
90	15.19	51.20	0.5923	35.64
95	15.32	60.70	0.5141	41.57
100	14.67	66.25	0.4804	44.85
105	14.30	70.50	0.4680	45.60

TABLE XII
ANALOG FAN DESIGN POINT DATA

Nozzle Area, A_{54} , inches ²	96.22
Nozzle Area, A_{54} , percent	100
Turbine Exit Area, A_{58} , inches ²	303.2
Turbine Flow, W_{54} , pounds/second	40.04
Turbine Flow Ratio, $W_{54}/44.50$	0.90
Engine Discharge Pressure, P_{51} , psia	36.41
Diverter Valve Discharge Pressure, P_{52} , psia	35.32
Nozzle Discharge Pressure, P_{54} , psia	33.73
Bucket Discharge Pressure, P_{55} , psia	16.25
Duct Pressure Drop, P_{54}/P_{52}	0.955
Turbine Pressure Ratio, P_{54}/P_{55}	2.078
Engine Discharge Temperature, T_{51} , degrees Rankine	1795
Nozzle Discharge Temperature, T_{54} , degrees Rankine	1795
Bucket Discharge Temperature, T_{55} , degrees Rankine	1539
Nozzle Flow Function, ϕ_{54}	0.5227
Nozzle Flow Function, ϕ_{54} , percent	100
Turbine Torque, T_T , foot-pounds	7320
Fan Torque, T_F , foot-pounds	7320
Turbine Horsepower, HP_T	3976
Fan Horsepower, HP_F	3819
Windage Loss, horsepower	124
End Loss, horsepower	33
Fan Speed N_F , rpm	2740
Turbine Energy Function, $(\Delta h/h)$ map	0.1427
Turbine Energy, (Δh) map, Btu/second	71.05
Fan Lift, pounds	6715
Turbine Lift, pounds	810
Total Lift, pounds	7525

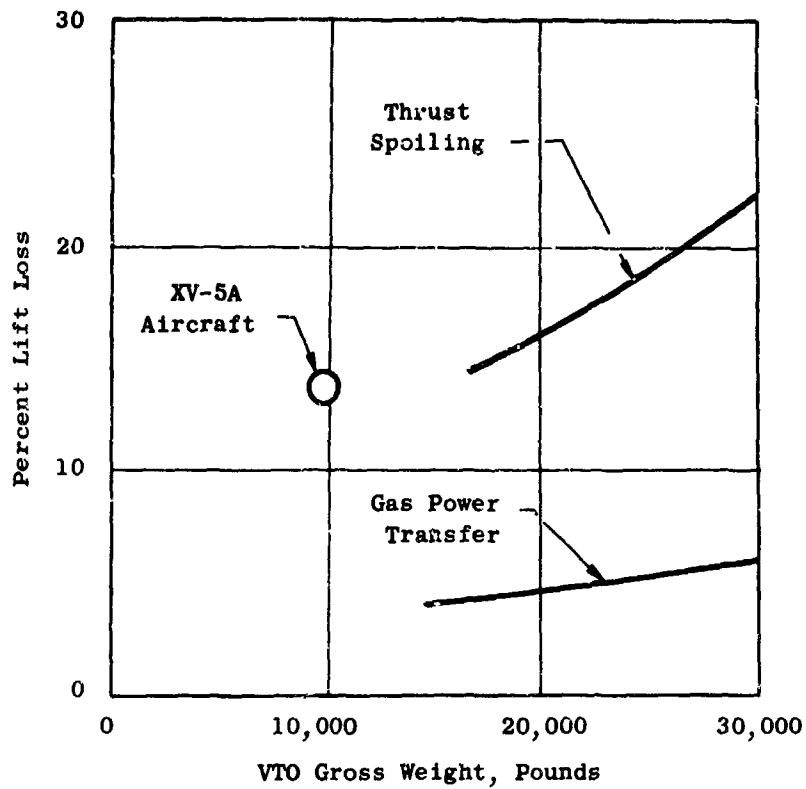


Figure 1. Comparison of Lift Losses for Full Roll Control.

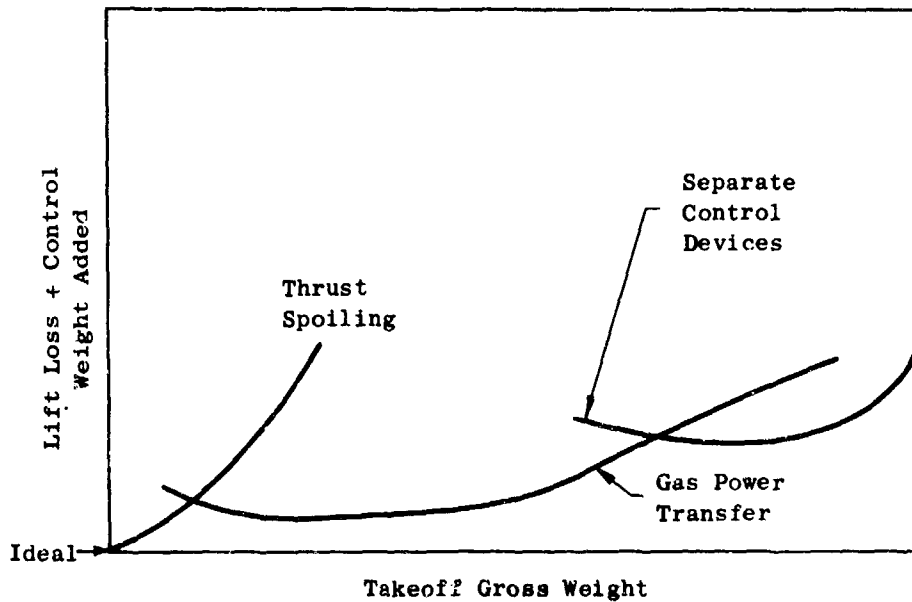


Figure 2. V/STOL Aircraft Control Efficiency Comparison.

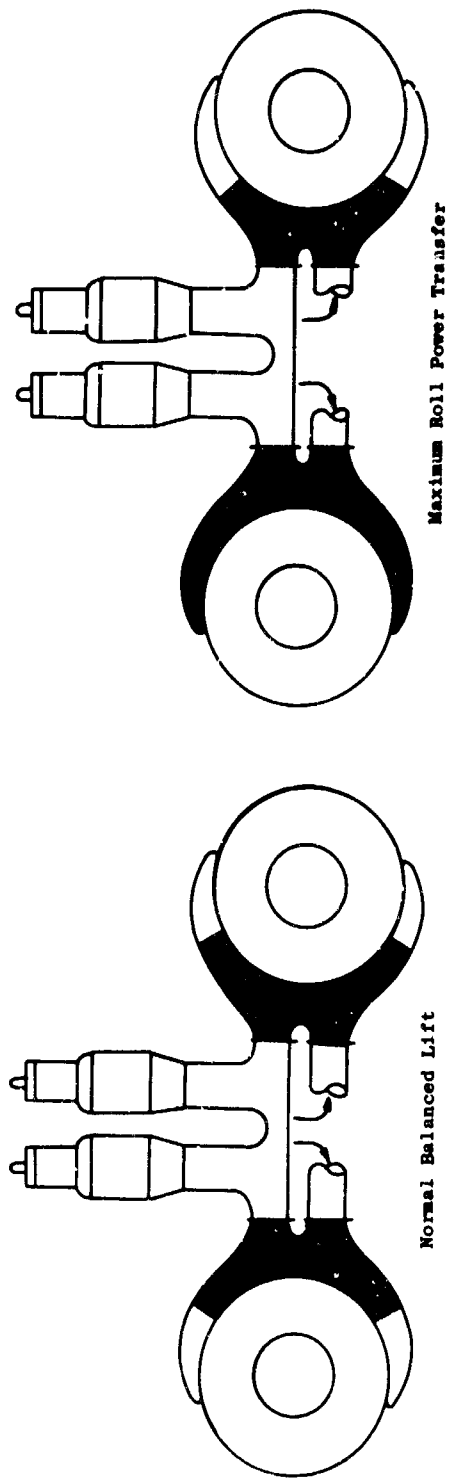


Figure 3. Power Transfer for Roll Control.

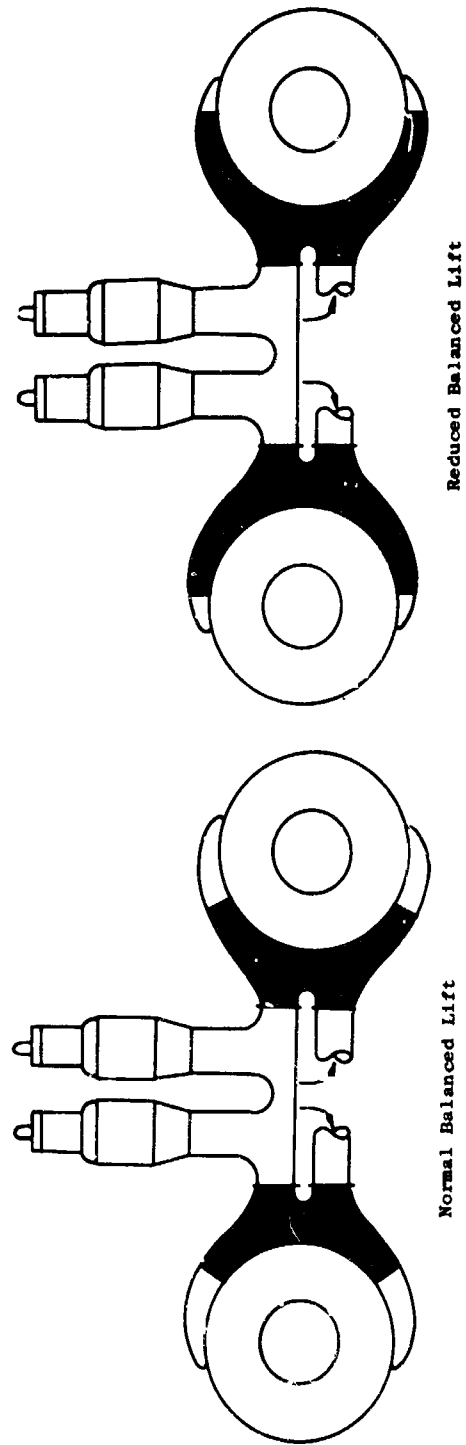
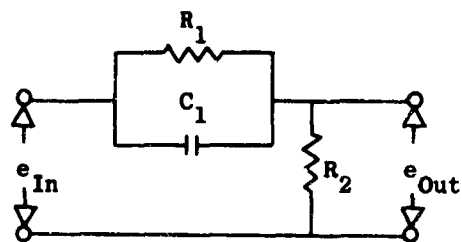
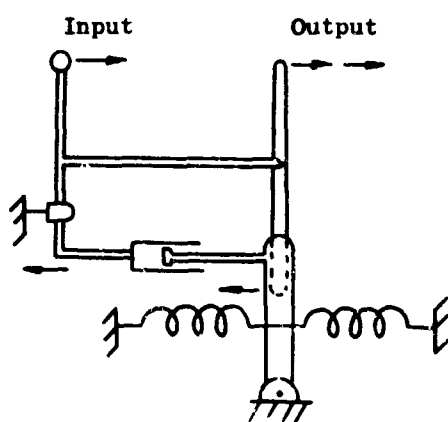


Figure 4. Variable Area for Height Control.



Electrical Circuit



Mechanical System

Figure 5. Electrical and Mechanical Jazzer Systems.

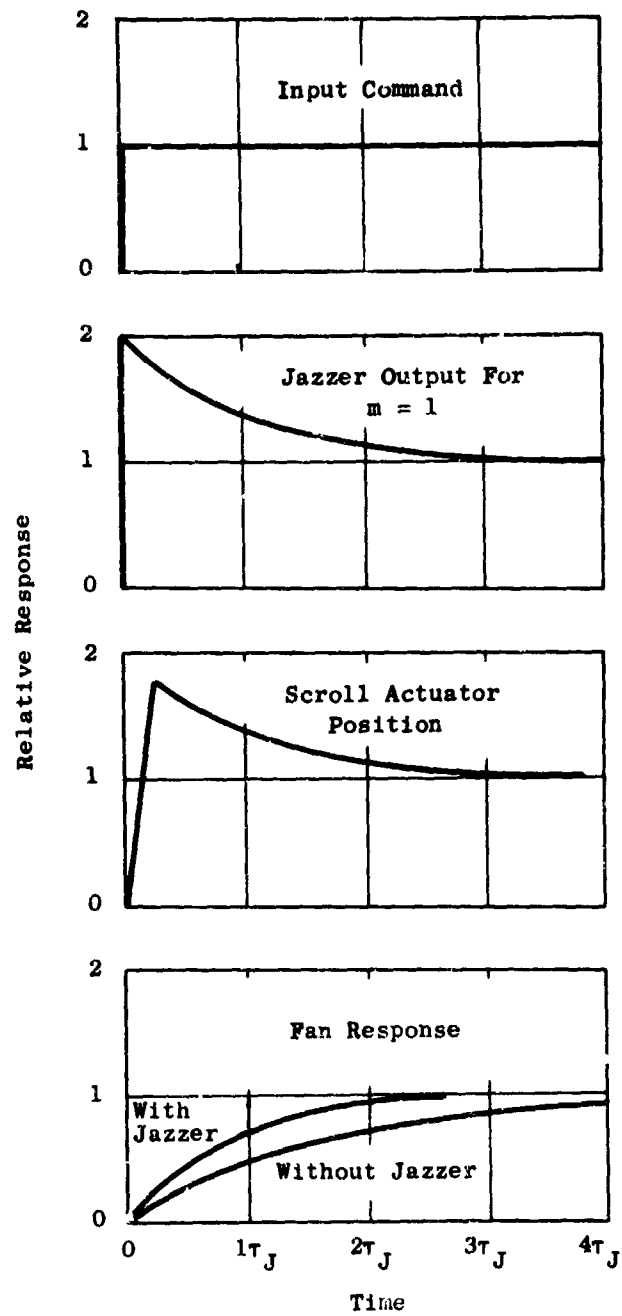


Figure 6. Typical Response Characteristics for a Step Input Showing Effects of Jazzer.

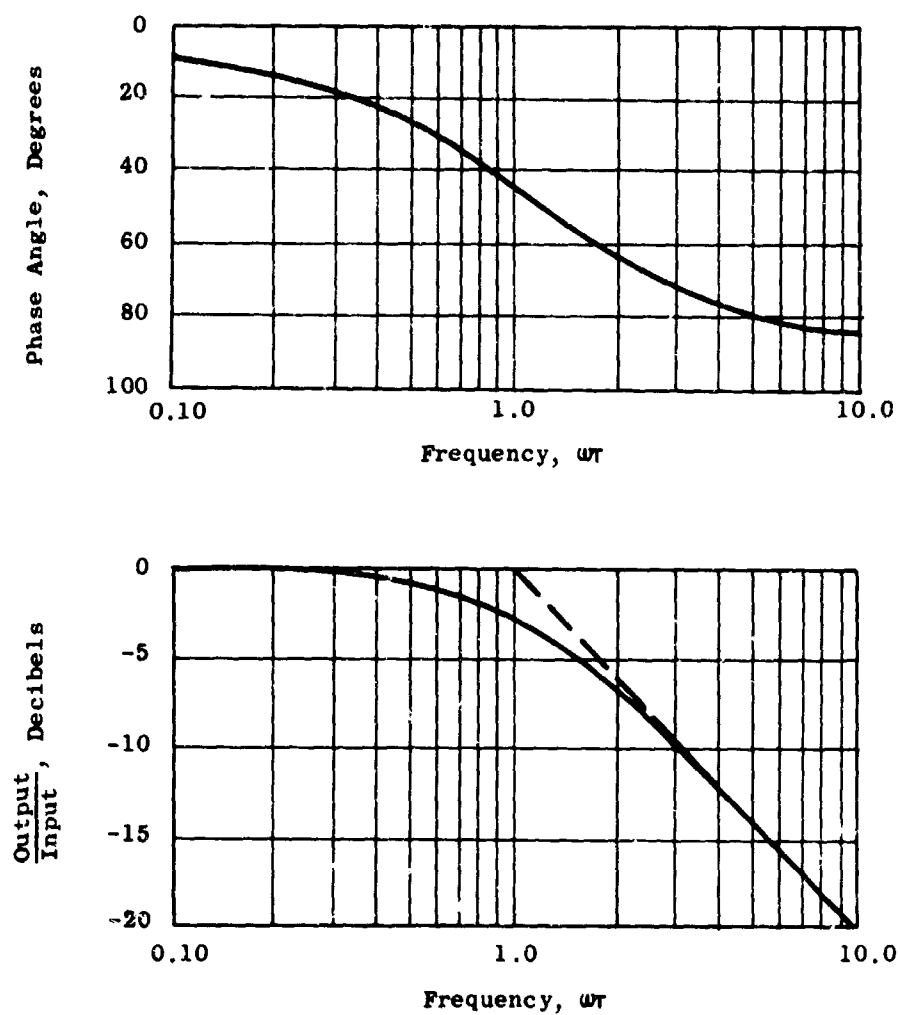


Figure 7. Typical Attenuation and Phase Angle Characteristics of a Single Time Constant System.

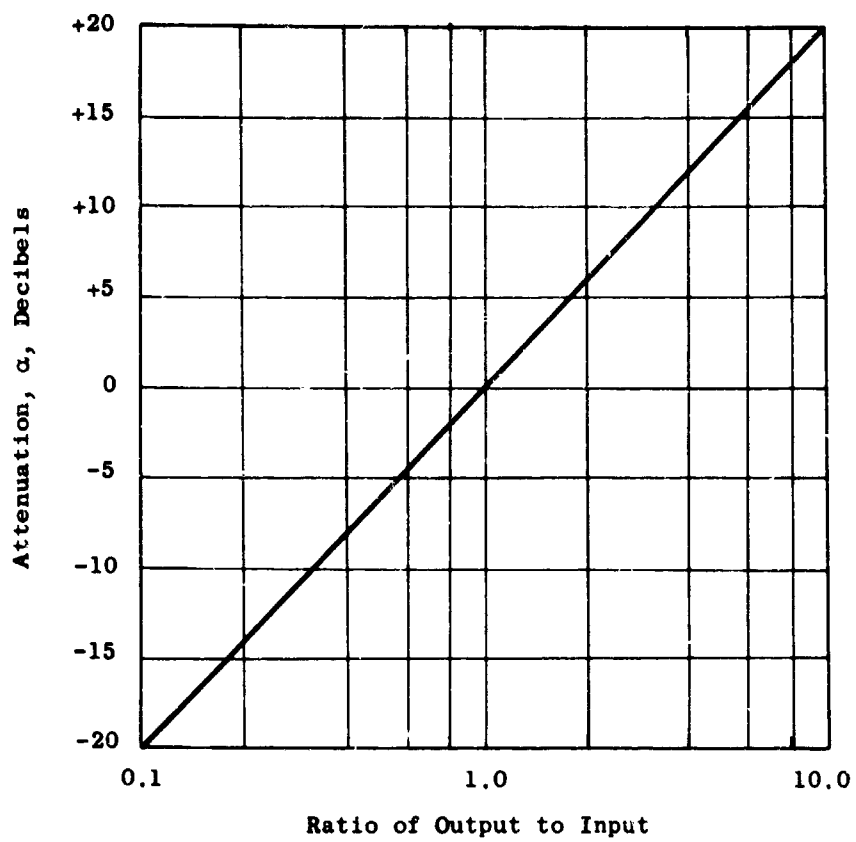


Figure 8. Decibel Conversion Chart.

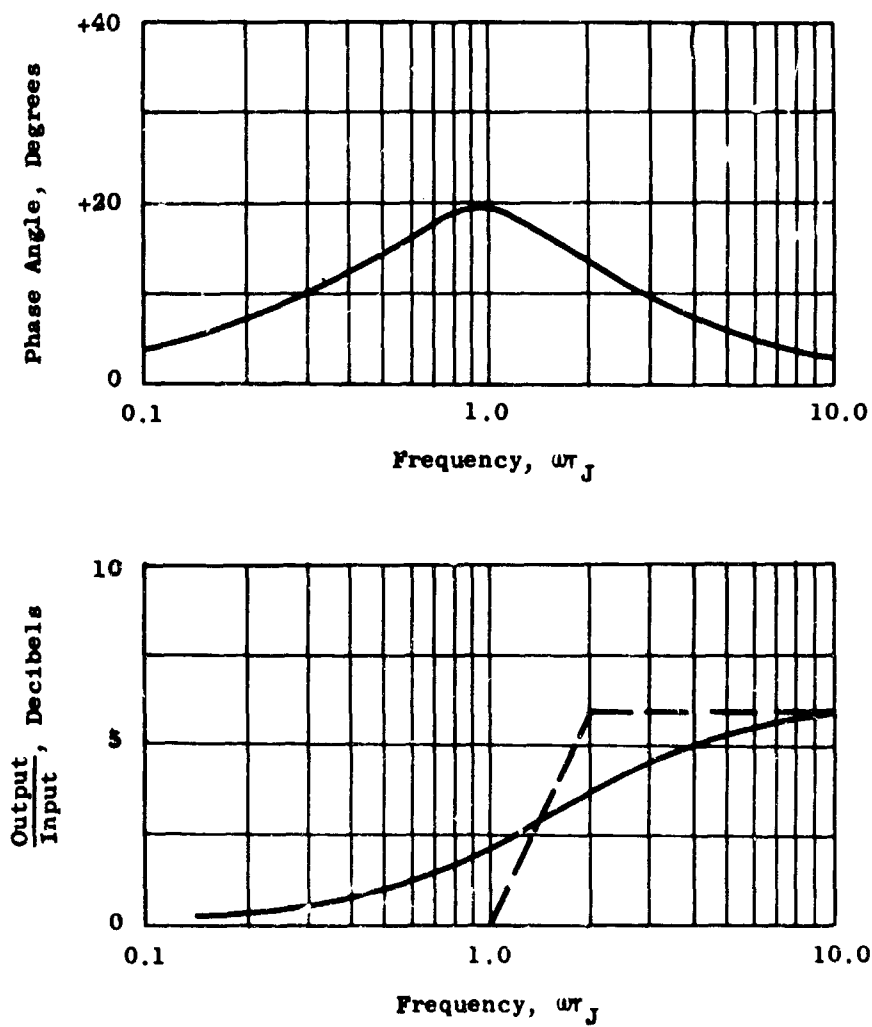


Figure 9. Typical Attenuation and Phase Angle Characteristics for a Jazzer With a Magnification Factor, m , of 1.0.

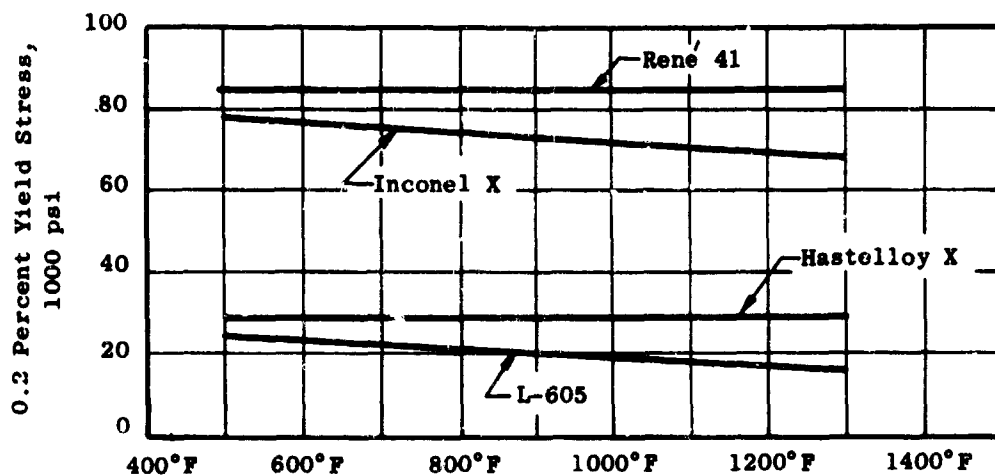


Figure 10. 0.2 Percent Yield Strength For Materials Used in Variable Area Scroll Assembly.

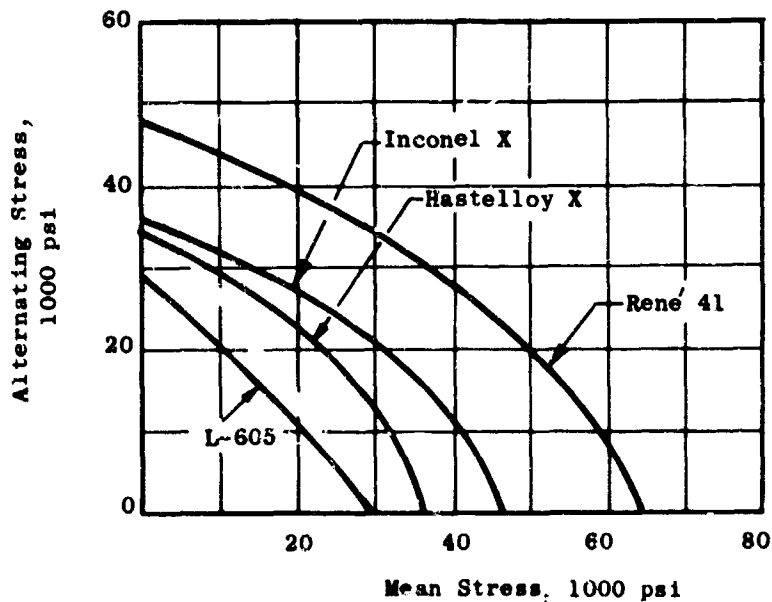


Figure 11. Stress Range Diagram for Materials Used in Variable Area Scroll Assembly.

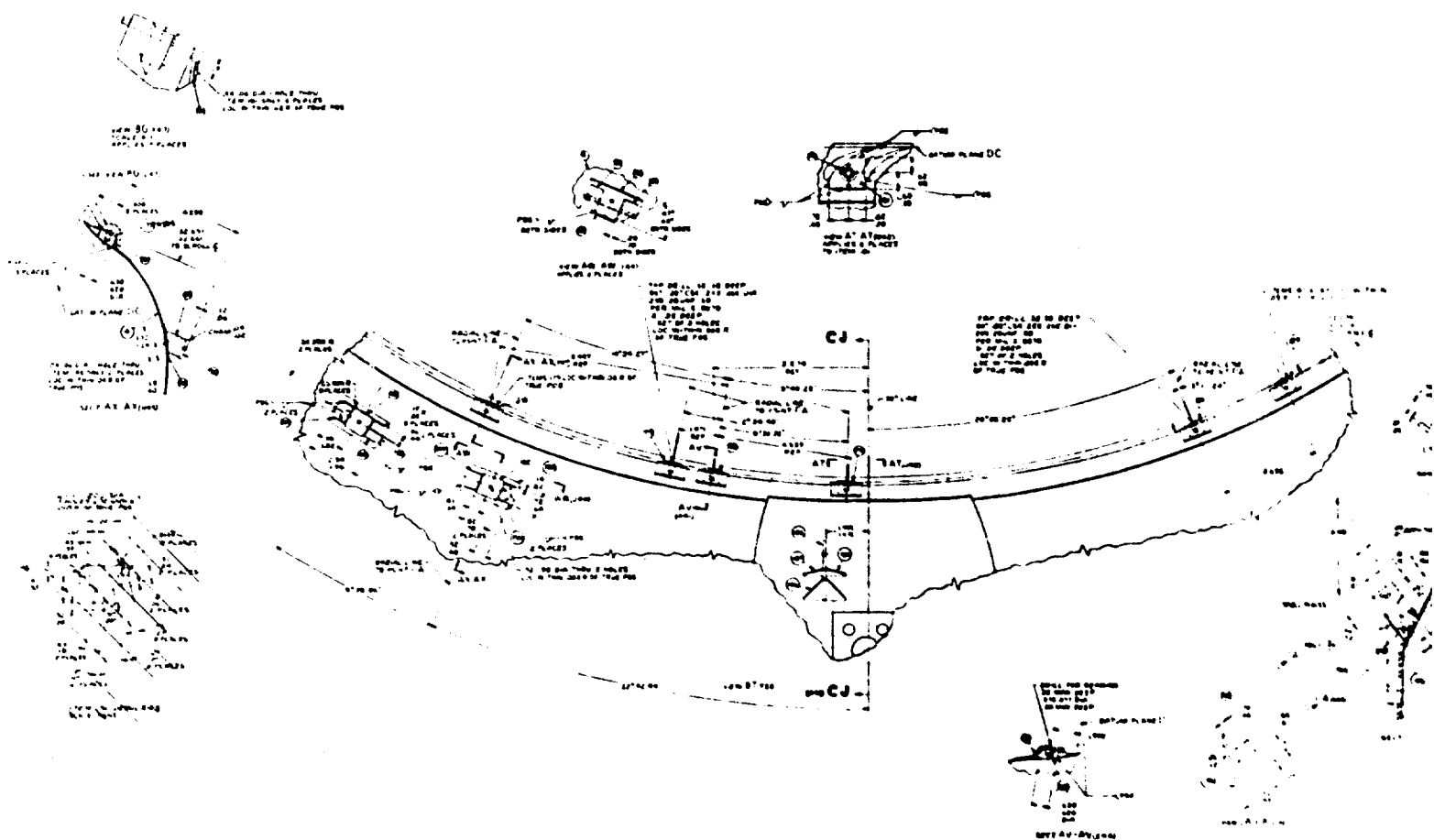
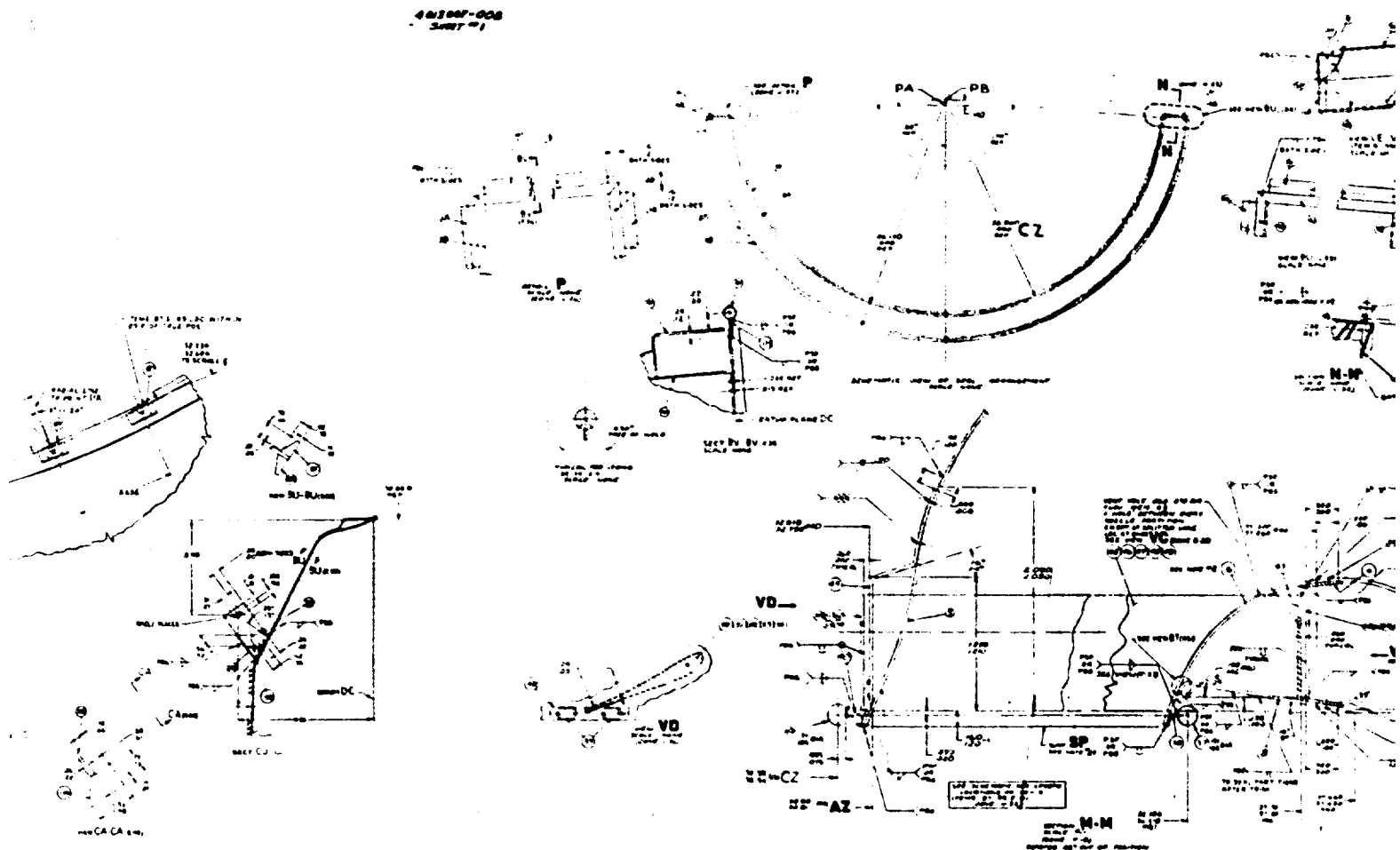


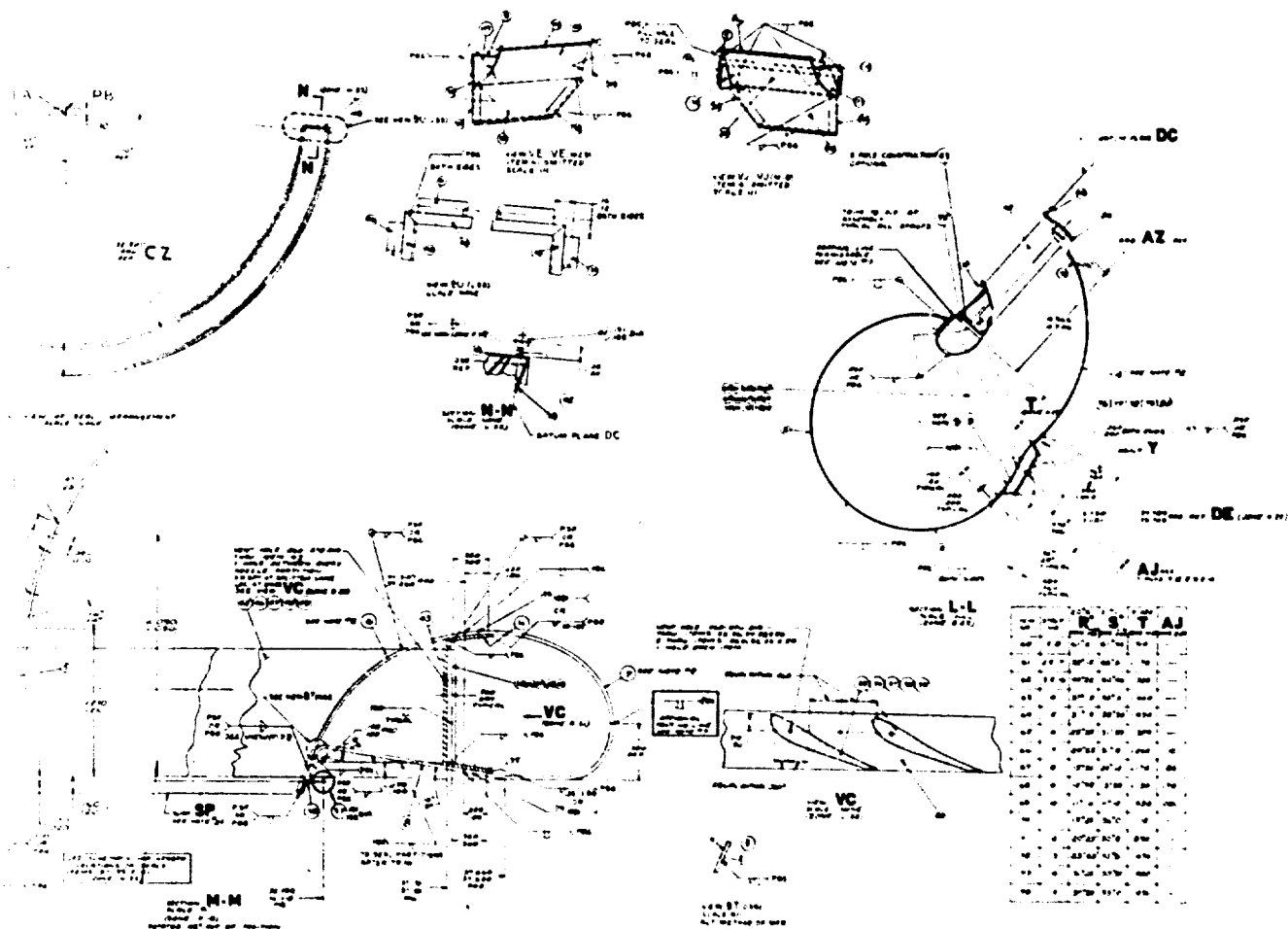
Figure 12. Scroll (Drawing 4013007-008, Sheet 1).

A

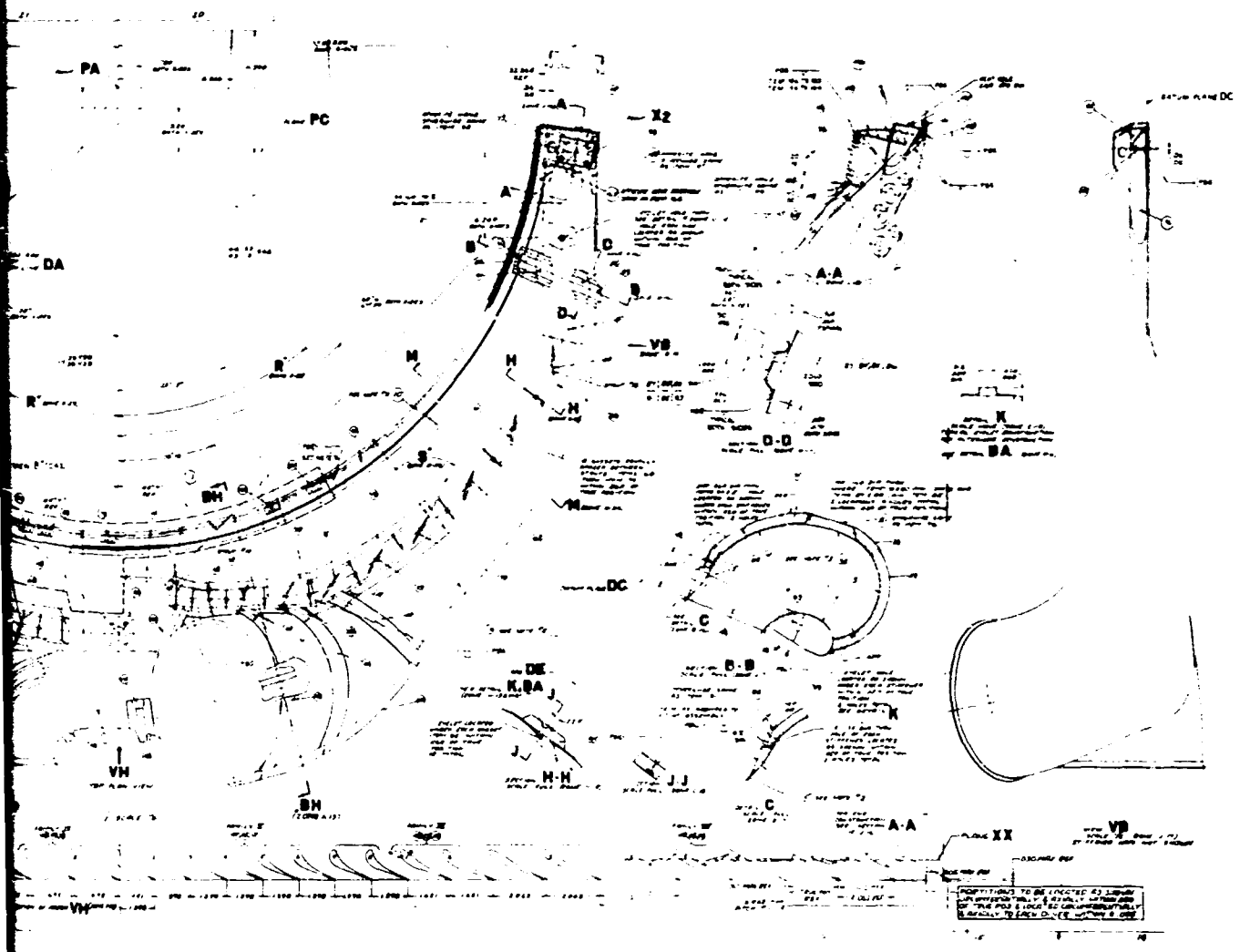
44300F-000
- 300000



B



e



B

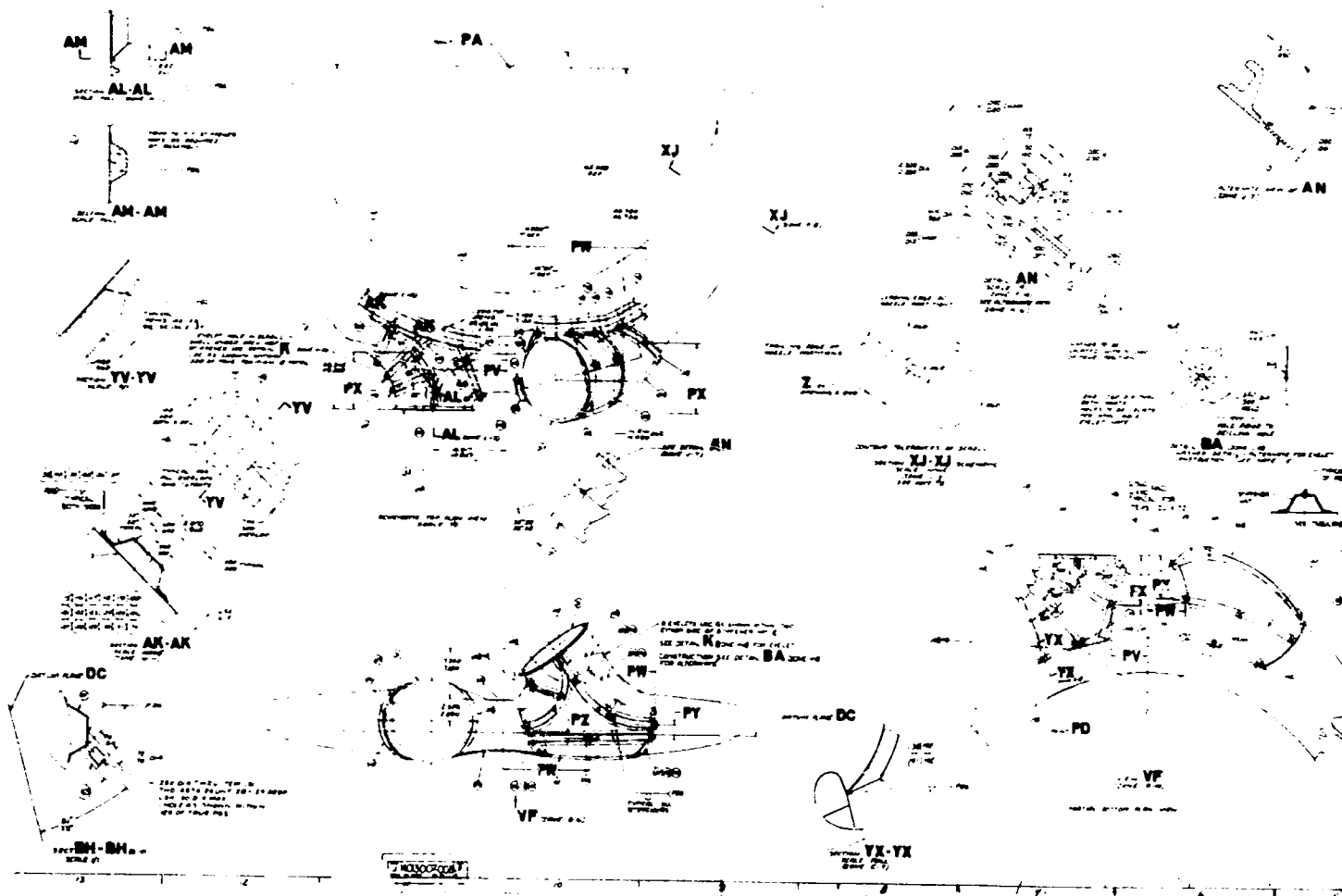
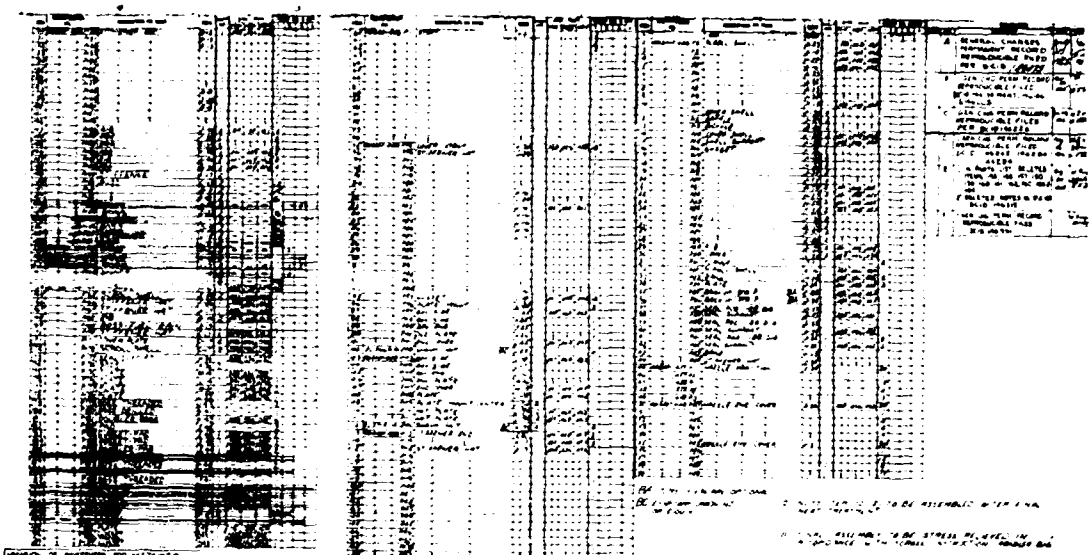
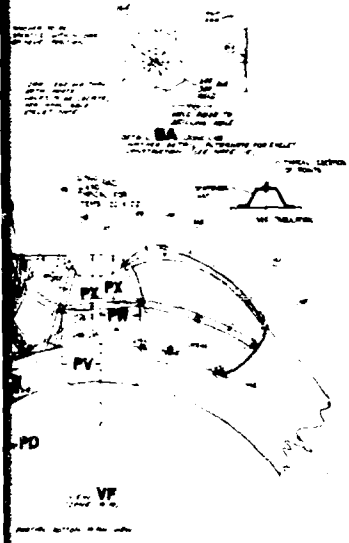


Figure 12. (Cont'd).



24. DETAIL PLANE DC

ITEM	DESCRIPTION	QTY	UNIT
1
2
3
4
5
6
7
8
9
10
11
12
13
14
15
16
17
18
19
20
21
22
23
24
25
26
27
28
29
30
31
32
33
34
35
36
37
38
39
40
41
42
43
44
45
46
47
48
49
50

24. DETAIL PLANE DC

25. DETAIL PLANE DC

26. DETAIL PLANE DC

27. DETAIL PLANE DC

28. DETAIL PLANE DC

29. DETAIL PLANE DC

30. DETAIL PLANE DC

31. DETAIL PLANE DC

32. DETAIL PLANE DC

33. DETAIL PLANE DC

34. DETAIL PLANE DC

35. DETAIL PLANE DC

36. DETAIL PLANE DC

37. DETAIL PLANE DC

38. DETAIL PLANE DC

39. DETAIL PLANE DC

40. DETAIL PLANE DC

41. DETAIL PLANE DC

42. DETAIL PLANE DC

43. DETAIL PLANE DC

44. DETAIL PLANE DC

45. DETAIL PLANE DC

46. DETAIL PLANE DC

47. DETAIL PLANE DC

48. DETAIL PLANE DC

49. DETAIL PLANE DC

50. DETAIL PLANE DC

1. DETAIL PLANE DC

2. DETAIL PLANE DC

3. DETAIL PLANE DC

4. DETAIL PLANE DC

5. DETAIL PLANE DC

6. DETAIL PLANE DC

7. DETAIL PLANE DC

8. DETAIL PLANE DC

9. DETAIL PLANE DC

10. DETAIL PLANE DC

11. DETAIL PLANE DC

12. DETAIL PLANE DC

13. DETAIL PLANE DC

14. DETAIL PLANE DC

15. DETAIL PLANE DC

16. DETAIL PLANE DC

17. DETAIL PLANE DC

18. DETAIL PLANE DC

19. DETAIL PLANE DC

20. DETAIL PLANE DC

21. DETAIL PLANE DC

22. DETAIL PLANE DC

23. DETAIL PLANE DC

24. DETAIL PLANE DC

25. DETAIL PLANE DC

26. DETAIL PLANE DC

27. DETAIL PLANE DC

28. DETAIL PLANE DC

29. DETAIL PLANE DC

30. DETAIL PLANE DC

31. DETAIL PLANE DC

32. DETAIL PLANE DC

33. DETAIL PLANE DC

34. DETAIL PLANE DC

35. DETAIL PLANE DC

36. DETAIL PLANE DC

37. DETAIL PLANE DC

38. DETAIL PLANE DC

39. DETAIL PLANE DC

40. DETAIL PLANE DC

41. DETAIL PLANE DC

42. DETAIL PLANE DC

43. DETAIL PLANE DC

44. DETAIL PLANE DC

45. DETAIL PLANE DC

46. DETAIL PLANE DC

47. DETAIL PLANE DC

48. DETAIL PLANE DC

49. DETAIL PLANE DC

50. DETAIL PLANE DC

B

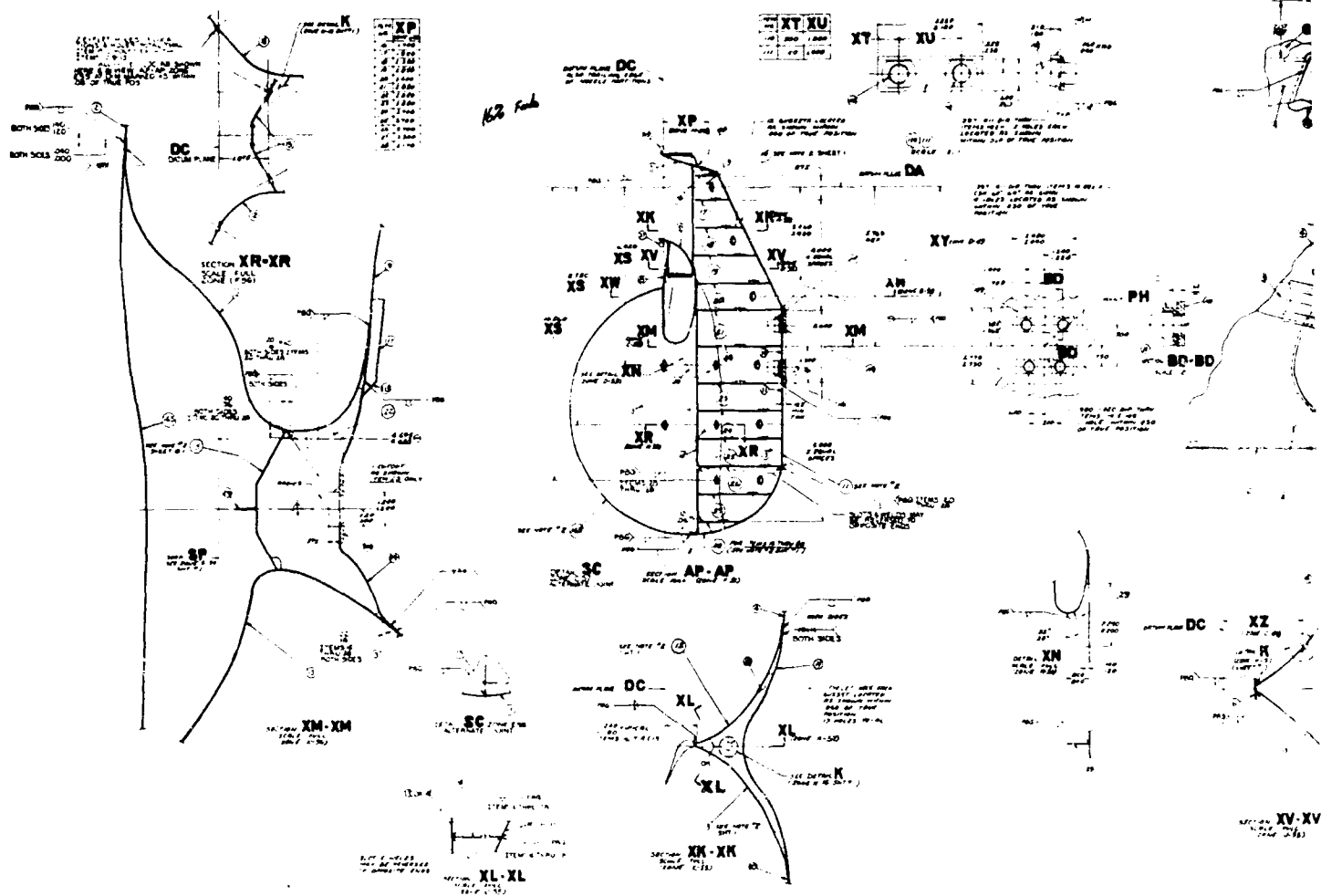
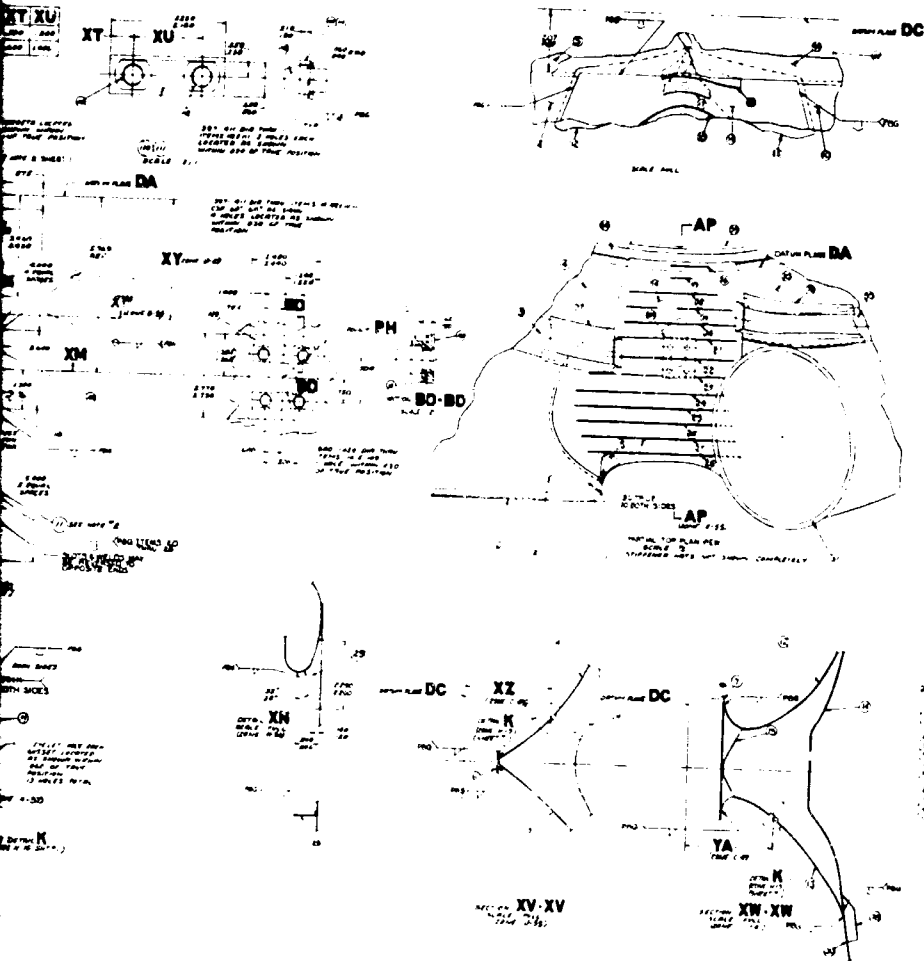


Figure 13. Scroll (Drawing 4013007-008, Sheet 2).

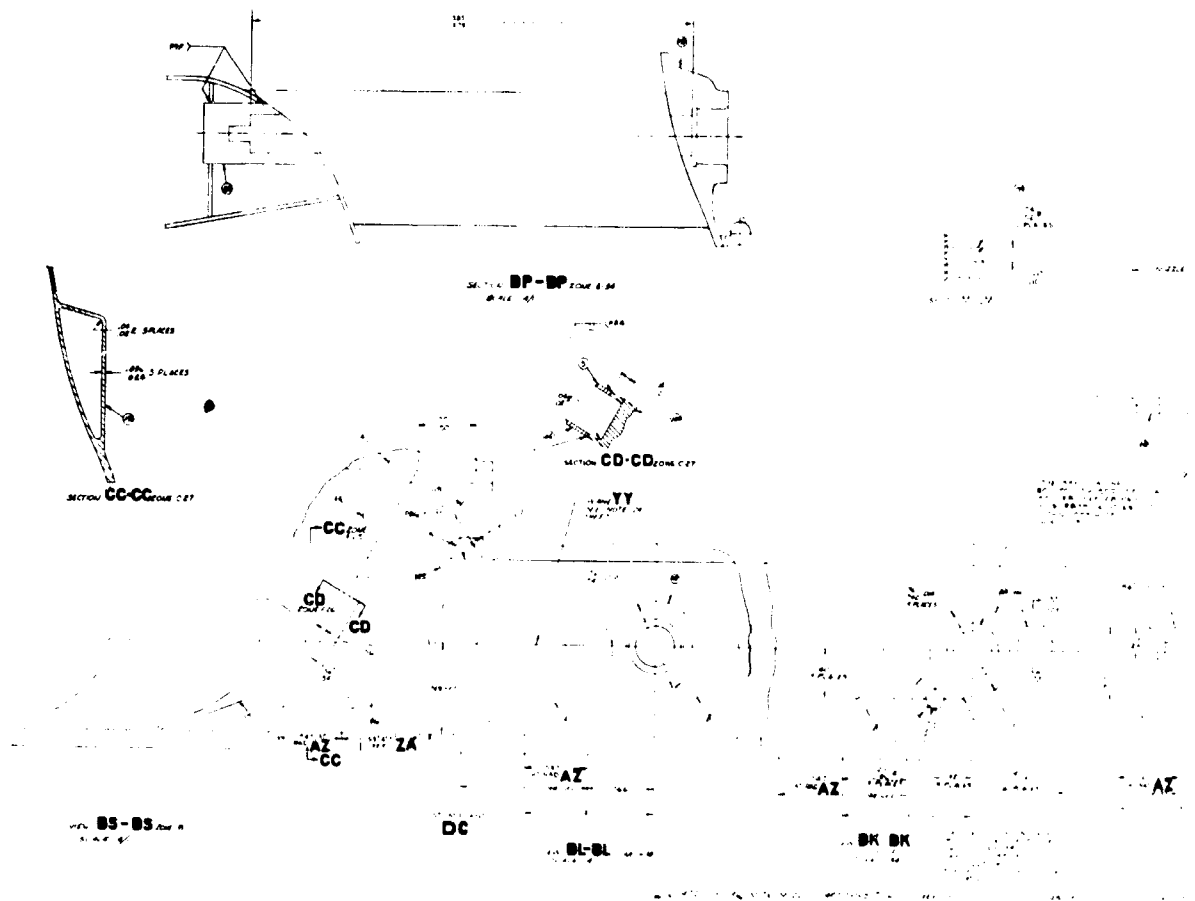


2).

B

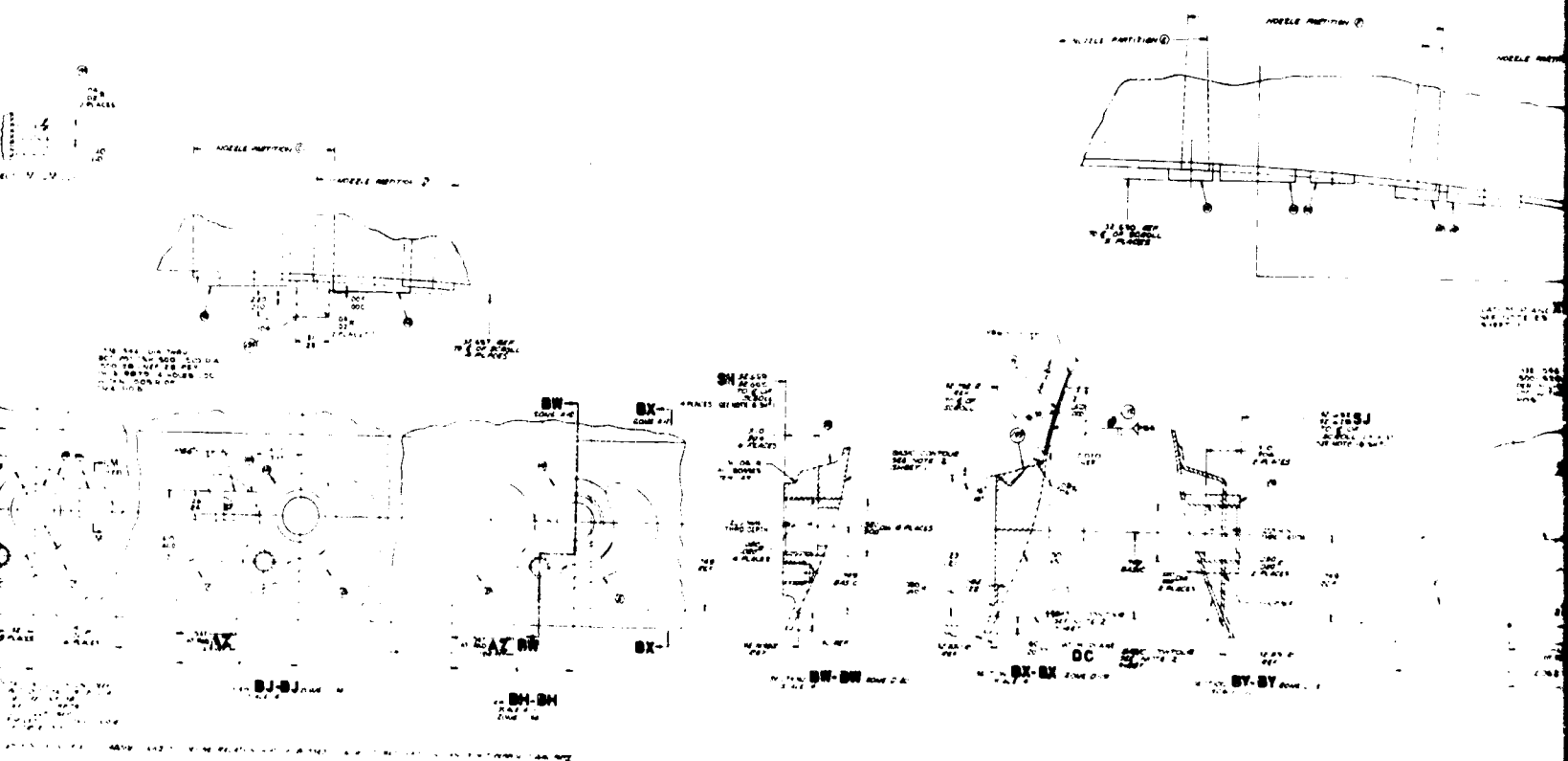


141



A

Figure 13. (Cont'd).



B

1	2	3	4	5	6	7	8	9	10	11	12	13	14	15	16	17	18	19	20	21	22	23	24	25	26	27	28	29	30	31	32	33	34	35	36	37	38	39	40	41	42	43	44	45	46	47	48	49	50	51	52	53	54	55	56	57	58	59	60	61	62	63	64	65	66	67	68	69	70	71	72	73	74	75	76	77	78	79	80	81	82	83	84	85	86	87	88	89	90	91	92	93	94	95	96	97	98	99	100	101	102	103	104	105	106	107	108	109	110	111	112	113	114	115	116	117	118	119	120	121	122	123	124	125	126	127	128	129	130	131	132	133	134	135	136	137	138	139	140	141	142	143	144	145	146	147	148	149	150	151	152	153	154	155	156	157	158	159	160	161	162	163	164	165	166	167	168	169	170	171	172	173	174	175	176	177	178	179	180	181	182	183	184	185	186	187	188	189	190	191	192	193	194	195	196	197	198	199	200	201	202	203	204	205	206	207	208	209	210	211	212	213	214	215	216	217	218	219	220	221	222	223	224	225	226	227	228	229	230	231	232	233	234	235	236	237	238	239	240	241	242	243	244	245	246	247	248	249	250	251	252	253	254	255	256	257	258	259	260	261	262	263	264	265	266	267	268	269	270	271	272	273	274	275	276	277	278	279	280	281	282	283	284	285	286	287	288	289	290	291	292	293	294	295	296	297	298	299	300	301	302	303	304	305	306	307	308	309	310	311	312	313	314	315	316	317	318	319	320	321	322	323	324	325	326	327	328	329	330	331	332	333	334	335	336	337	338	339	340	341	342	343	344	345	346	347	348	349	350	351	352	353	354	355	356	357	358	359	360	361	362	363	364	365	366	367	368	369	370	371	372	373	374	375	376	377	378	379	380	381	382	383	384	385	386	387	388	389	390	391	392	393	394	395	396	397	398	399	400	401	402	403	404	405	406	407	408	409	410	411	412	413	414	415	416	417	418	419	420	421	422	423	424	425	426	427	428	429	430	431	432	433	434	435	436	437	438	439	440	441	442	443	444	445	446	447	448	449	450	451	452	453	454	455	456	457	458	459	460	461	462	463	464	465	466	467	468	469	470	471	472	473	474	475	476	477	478	479	480	481	482	483	484	485	486	487	488	489	490	491	492	493	494	495	496	497	498	499	500	501	502	503	504	505	506	507	508	509	510	511	512	513	514	515	516	517	518	519	520	521	522	523	524	525	526	527	528	529	530	531	532	533	534	535	536	537	538	539	540	541	542	543	544	545	546	547	548	549	550	551	552	553	554	555	556	557	558	559	560	561	562	563	564	565	566	567	568	569	570	571	572	573	574	575	576	577	578	579	580	581	582	583	584	585	586	587	588	589	590	591	592	593	594	595	596	597	598	599	600	601	602	603	604	605	606	607	608	609	610	611	612	613	614	615	616	617	618	619	620	621	622	623	624	625	626	627	628	629	630	631	632	633	634	635	636	637	638	639	640	641	642	643	644	645	646	647	648	649	650	651	652	653	654	655	656	657	658	659	660	661	662	663	664	665	666	667	668	669	670	671	672	673	674	675	676	677	678	679	680	681	682	683	684	685	686	687	688	689	690	691	692	693	694	695	696	697	698	699	700	701	702	703	704	705	706	707	708	709	710	711	712	713	714	715	716	717	718	719	720	721	722	723	724	725	726	727	728	729	730	731	732	733	734	735	736	737	738	739	740	741	742	743	744	745	746	747	748	749	750	751	752	753	754	755	756	757	758	759	760	761	762	763	764	765	766	767	768	769	770	771	772	773	774	775	776	777	778	779	780	781	782	783	784	785	786	787	788	789	790	791	792	793	794	795	796	797	798	799	800	801	802	803	804	805	806	807	808	809	810	811	812	813	814	815	816	817	818	819	820	821	822	823	824	825	826	827	828	829	830	831	832	833	834	835	836	837	838	839	840	841	842	843	844	845	846	847	848	849	850	851	852	853	854	855	856	857	858	859	860	861	862	863	864	865	866	867	868	869	870	871	872	873	874	875	876	877	878	879	880	881	882	883	884	885	886	887	888	889	890	891	892	893	894	895	896	897	898	899	900	901	902	903	904	905	906	907	908	909	910	911	912	913	914	915	916	917	918	919	920	921	922	923	924	925	926	927	928	929	930	931	932	933	934	935	936	937	938	939	940	941	942	943	944	945	946	947	948	949	950	951	952	953	954	955	956	957	958	959	960	961	962	963	964	965	966	967	968	969	970	971	972	973	974	975	976	977	978	979	980	981	982	983	984	985	986	987	988	989	990	991	992	993	994	995	996	997	998	999	1000	1001	1002	1003	1004	1005	1006	1007	1008	1009	1010	1011	1012	1013	1014	1015	1016	1017	1018	1019	1020	1021	1022	1023	1024	1025	1026	1027	1028	1029	1030	1031	1032	1033	1034	1035	1036	1037	1038	1039	1040	1041	1042	1043	1044	1045	1046	1047	1048	1049	1050	1051	1052	1053	1054	1055	1056	1057	1058	1059	1060	1061	1062	1063	1064	1065	1066	1067	1068	1069	1070	1071	1072	1073	1074	1075	1076	1077	1078	1079	1080	1081	1082	1083	1084	1085	1086	1087	1088	1089	1090	1091	1092	1093	1094	1095	1096	1097	1098	1099	1100	1101	1102	1103	1104	1105	1106	1107	1108	1109	1110	1111	1112	1113	1114	1115	1116	1117	1118	1119	1120	1121	1122	1123	1124	1125	1126	1127	1128	1129	1130	1131	1132	1133	1134	1135	1136	1137	1138	1139	1140	1141	1142	1143	1144	1145	1146	1147	1148	1149	1150	1151	1152	1153	1154	1155	1156	1157	1158	1159	1160	1161	1162	1163	1164	1165	1166	1167	1168	1169	1170	1171	1172	1173	1174	1175	1176	1177	1178	1179	1180	1181	1182	1183	1184	1185	1186	1187	1188	1189	1190	1191	1192	1193	1194	1195	1196	1197	1198	1199	1200	1201	1202	1203	1204	1205	1206	1207	1208	1209	1210	1211	1212	1213	1214	1215	1216	1217	1218	1219	1220	1221	1222	1223	1224	1225	1226	1227	1228	1229	1230	1231	1232	1233	1234	1235	1236	1237	1238	1239	1240	1241	1242	1243	1244	1245	1246	1247	1248	1249	1250	1251	1252	1253	1254	1255	1256	1257	1258	1259	1260	1261	1262	1263	1264	1265	1266	1267	1268	1269	1270	1271	1272	1273	1274	1275	1276	1277	1278	1279	1280	1281	1282	1283	1284	1285	1286	1287	1288	1289	1290	1291	1292	1293	1294	1295	1296	1297	1298	1299	1300	1301	1302	1303	1304	1305	1306	1307	1308	1309	1310	1311	1312	1313	1314	1315	1316	1317	1318	1319	1320	1321	1322	1323	1324	1325	1326	1327	1328	1329	1330	1331	1332	1333	1334	1335	1336	1337	1338	1339	1340	1341	1342	1343	1344	1345	1346	1347	1348	1349	1350	1351	1352	1353	1354	1355	1356	1357	1358	1359	1360	1361	1362	1363	1364	1365	1366	1367	1368	1369	1370	1371	1372	1373	1374	1375	1376	1377	1378	1379	1380	1381	1382	1383	1384	1385	1386	1387	1388	1389	1390	1391	1392	1393	1394	1395	1396	1397	1398	1399	1400	1401	1402	1403	1404	1405	1406	1407	1408	1409	1410	1411	1412	1413	1414	1415	1416	1417	1418	1419	1420	1421	1422	1423	1424	1425	1426	1427	1428	1429	1430	1431	1432	1433	1434	1435	1436	1437	1438	1439	1440	1441	1442	1443	1444	1445	1446	1447	1448	1449	1450	1451	1452	1453	1454	1455	1456	1457	1458	1459	1460	1461	1462	1463	1464	1465	1466	1467	1468	1469	1470	1471	1472	1473	1474	1475	1476	1477	1478	1479	1480	1481	1482	1483	1484	1485	1486	1487	1488	1489	1490	1491	1492	1493	1494	1495	1
---	---	---	---	---	---	---	---	---	----	----	----	----	----	----	----	----	----	----	----	----	----	----	----	----	----	----	----	----	----	----	----	----	----	----	----	----	----	----	----	----	----	----	----	----	----	----	----	----	----	----	----	----	----	----	----	----	----	----	----	----	----	----	----	----	----	----	----	----	----	----	----	----	----	----	----	----	----	----	----	----	----	----	----	----	----	----	----	----	----	----	----	----	----	----	----	----	----	----	-----	-----	-----	-----	-----	-----	-----	-----	-----	-----	-----	-----	-----	-----	-----	-----	-----	-----	-----	-----	-----	-----	-----	-----	-----	-----	-----	-----	-----	-----	-----	-----	-----	-----	-----	-----	-----	-----	-----	-----	-----	-----	-----	-----	-----	-----	-----	-----	-----	-----	-----	-----	-----	-----	-----	-----	-----	-----	-----	-----	-----	-----	-----	-----	-----	-----	-----	-----	-----	-----	-----	-----	-----	-----	-----	-----	-----	-----	-----	-----	-----	-----	-----	-----	-----	-----	-----	-----	-----	-----	-----	-----	-----	-----	-----	-----	-----	-----	-----	-----	-----	-----	-----	-----	-----	-----	-----	-----	-----	-----	-----	-----	-----	-----	-----	-----	-----	-----	-----	-----	-----	-----	-----	-----	-----	-----	-----	-----	-----	-----	-----	-----	-----	-----	-----	-----	-----	-----	-----	-----	-----	-----	-----	-----	-----	-----	-----	-----	-----	-----	-----	-----	-----	-----	-----	-----	-----	-----	-----	-----	-----	-----	-----	-----	-----	-----	-----	-----	-----	-----	-----	-----	-----	-----	-----	-----	-----	-----	-----	-----	-----	-----	-----	-----	-----	-----	-----	-----	-----	-----	-----	-----	-----	-----	-----	-----	-----	-----	-----	-----	-----	-----	-----	-----	-----	-----	-----	-----	-----	-----	-----	-----	-----	-----	-----	-----	-----	-----	-----	-----	-----	-----	-----	-----	-----	-----	-----	-----	-----	-----	-----	-----	-----	-----	-----	-----	-----	-----	-----	-----	-----	-----	-----	-----	-----	-----	-----	-----	-----	-----	-----	-----	-----	-----	-----	-----	-----	-----	-----	-----	-----	-----	-----	-----	-----	-----	-----	-----	-----	-----	-----	-----	-----	-----	-----	-----	-----	-----	-----	-----	-----	-----	-----	-----	-----	-----	-----	-----	-----	-----	-----	-----	-----	-----	-----	-----	-----	-----	-----	-----	-----	-----	-----	-----	-----	-----	-----	-----	-----	-----	-----	-----	-----	-----	-----	-----	-----	-----	-----	-----	-----	-----	-----	-----	-----	-----	-----	-----	-----	-----	-----	-----	-----	-----	-----	-----	-----	-----	-----	-----	-----	-----	-----	-----	-----	-----	-----	-----	-----	-----	-----	-----	-----	-----	-----	-----	-----	-----	-----	-----	-----	-----	-----	-----	-----	-----	-----	-----	-----	-----	-----	-----	-----	-----	-----	-----	-----	-----	-----	-----	-----	-----	-----	-----	-----	-----	-----	-----	-----	-----	-----	-----	-----	-----	-----	-----	-----	-----	-----	-----	-----	-----	-----	-----	-----	-----	-----	-----	-----	-----	-----	-----	-----	-----	-----	-----	-----	-----	-----	-----	-----	-----	-----	-----	-----	-----	-----	-----	-----	-----	-----	-----	-----	-----	-----	-----	-----	-----	-----	-----	-----	-----	-----	-----	-----	-----	-----	-----	-----	-----	-----	-----	-----	-----	-----	-----	-----	-----	-----	-----	-----	-----	-----	-----	-----	-----	-----	-----	-----	-----	-----	-----	-----	-----	-----	-----	-----	-----	-----	-----	-----	-----	-----	-----	-----	-----	-----	-----	-----	-----	-----	-----	-----	-----	-----	-----	-----	-----	-----	-----	-----	-----	-----	-----	-----	-----	-----	-----	-----	-----	-----	-----	-----	-----	-----	-----	-----	-----	-----	-----	-----	-----	-----	-----	-----	-----	-----	-----	-----	-----	-----	-----	-----	-----	-----	-----	-----	-----	-----	-----	-----	-----	-----	-----	-----	-----	-----	-----	-----	-----	-----	-----	-----	-----	-----	-----	-----	-----	-----	-----	-----	-----	-----	-----	-----	-----	-----	-----	-----	-----	-----	-----	-----	-----	-----	-----	-----	-----	-----	-----	-----	-----	-----	-----	-----	-----	-----	-----	-----	-----	-----	-----	-----	-----	-----	-----	-----	-----	-----	-----	-----	-----	-----	-----	-----	-----	-----	-----	-----	-----	-----	-----	-----	-----	-----	-----	-----	-----	-----	-----	-----	-----	-----	-----	-----	-----	-----	-----	-----	-----	-----	-----	-----	-----	-----	-----	-----	-----	-----	-----	-----	-----	-----	-----	-----	-----	-----	-----	-----	-----	-----	-----	-----	-----	-----	-----	-----	-----	-----	-----	-----	-----	-----	-----	-----	-----	-----	-----	-----	-----	-----	-----	-----	-----	-----	-----	-----	-----	-----	-----	-----	-----	-----	-----	-----	-----	-----	-----	-----	-----	-----	-----	-----	-----	-----	-----	-----	-----	-----	-----	-----	-----	-----	-----	-----	-----	-----	-----	-----	-----	-----	-----	-----	-----	-----	-----	-----	-----	-----	-----	-----	-----	-----	-----	-----	-----	-----	-----	-----	-----	-----	-----	-----	-----	-----	-----	-----	-----	-----	-----	-----	-----	-----	-----	-----	-----	-----	-----	-----	-----	-----	-----	-----	-----	-----	-----	-----	-----	-----	-----	-----	-----	-----	-----	-----	-----	-----	-----	-----	-----	-----	-----	-----	-----	-----	-----	-----	-----	-----	-----	-----	-----	-----	-----	-----	-----	-----	-----	-----	-----	-----	-----	-----	-----	-----	-----	-----	-----	-----	-----	-----	-----	-----	-----	-----	-----	-----	-----	-----	-----	-----	-----	-----	-----	-----	-----	-----	-----	-----	-----	-----	-----	-----	-----	-----	-----	-----	-----	-----	-----	-----	-----	-----	-----	-----	-----	-----	-----	-----	-----	-----	-----	-----	-----	-----	-----	-----	-----	-----	-----	-----	-----	-----	-----	-----	-----	-----	-----	-----	-----	-----	-----	-----	-----	-----	-----	-----	-----	-----	-----	-----	-----	-----	-----	-----	-----	-----	-----	-----	-----	-----	-----	-----	-----	-----	-----	-----	-----	-----	-----	-----	-----	-----	-----	-----	-----	-----	-----	-----	-----	------	------	------	------	------	------	------	------	------	------	------	------	------	------	------	------	------	------	------	------	------	------	------	------	------	------	------	------	------	------	------	------	------	------	------	------	------	------	------	------	------	------	------	------	------	------	------	------	------	------	------	------	------	------	------	------	------	------	------	------	------	------	------	------	------	------	------	------	------	------	------	------	------	------	------	------	------	------	------	------	------	------	------	------	------	------	------	------	------	------	------	------	------	------	------	------	------	------	------	------	------	------	------	------	------	------	------	------	------	------	------	------	------	------	------	------	------	------	------	------	------	------	------	------	------	------	------	------	------	------	------	------	------	------	------	------	------	------	------	------	------	------	------	------	------	------	------	------	------	------	------	------	------	------	------	------	------	------	------	------	------	------	------	------	------	------	------	------	------	------	------	------	------	------	------	------	------	------	------	------	------	------	------	------	------	------	------	------	------	------	------	------	------	------	------	------	------	------	------	------	------	------	------	------	------	------	------	------	------	------	------	------	------	------	------	------	------	------	------	------	------	------	------	------	------	------	------	------	------	------	------	------	------	------	------	------	------	------	------	------	------	------	------	------	------	------	------	------	------	------	------	------	------	------	------	------	------	------	------	------	------	------	------	------	------	------	------	------	------	------	------	------	------	------	------	------	------	------	------	------	------	------	------	------	------	------	------	------	------	------	------	------	------	------	------	------	------	------	------	------	------	------	------	------	------	------	------	------	------	------	------	------	------	------	------	------	------	------	------	------	------	------	------	------	------	------	------	------	------	------	------	------	------	------	------	------	------	------	------	------	------	------	------	------	------	------	------	------	------	------	------	------	------	------	------	------	------	------	------	------	------	------	------	------	------	------	------	------	------	------	------	------	------	------	------	------	------	------	------	------	------	------	------	------	------	------	------	------	------	------	------	------	------	------	------	------	------	------	------	------	------	------	------	------	------	------	------	------	------	------	------	------	------	------	------	------	------	------	------	------	------	------	------	------	------	------	------	------	------	------	------	------	------	------	------	------	------	------	------	------	------	------	------	------	------	------	------	------	------	------	------	------	------	------	------	------	------	------	------	------	------	------	------	------	------	------	------	------	------	------	------	------	------	------	------	------	------	------	------	------	------	------	------	------	------	------	------	------	------	------	------	------	------	------	------	------	---

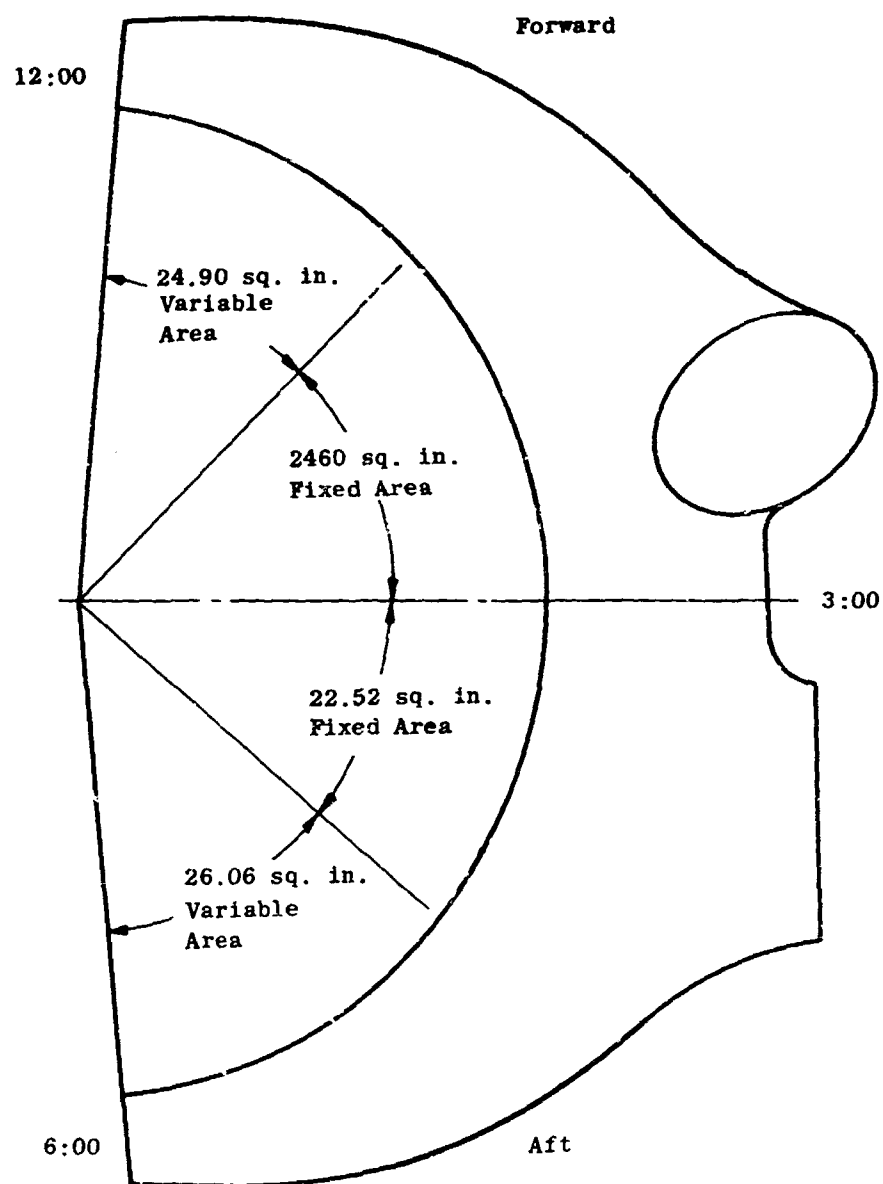


Figure 14. Physical Fixed and Variable Scroll Turbine Area.

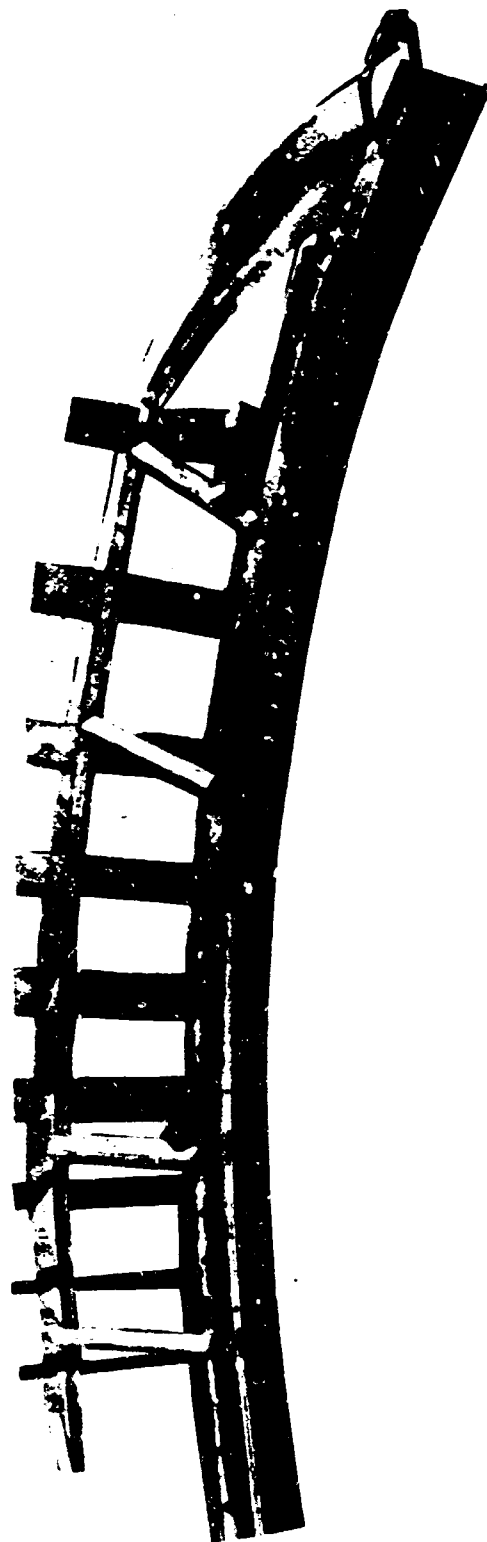


Figure 15. Nozzle Diaphragm During Manufacturing.

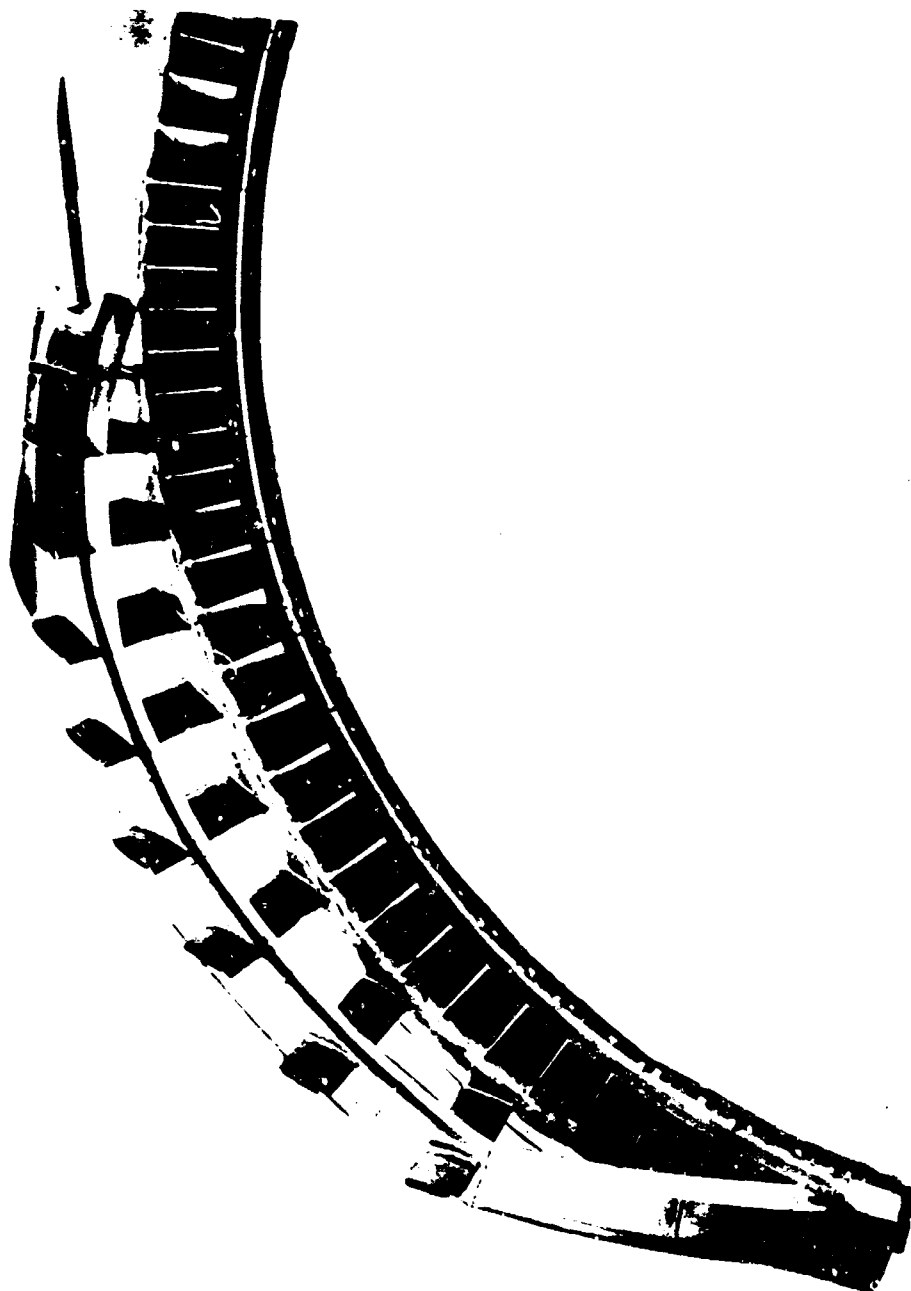


Figure 16. Nozzle Diaphragm During Manufacturing.

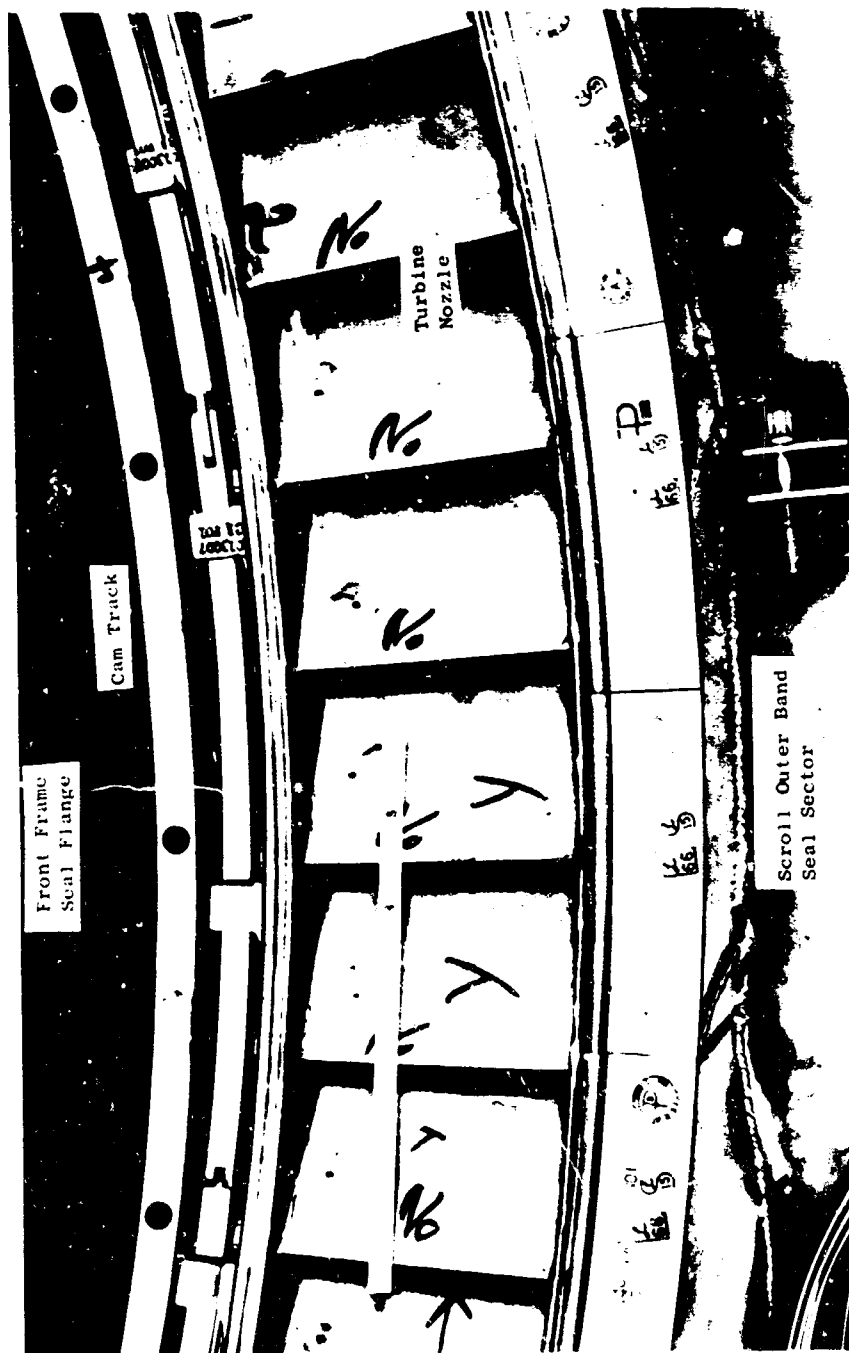


Figure 17. Scroll Mechanism and Front Frame Flange.

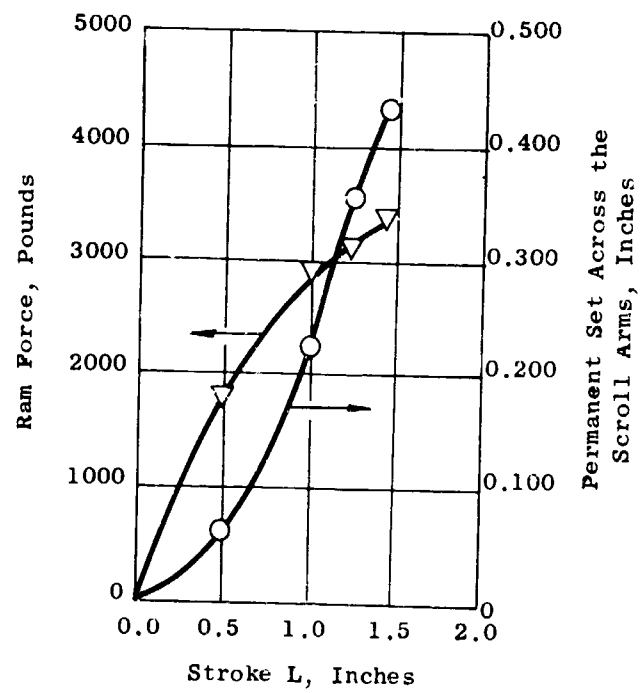
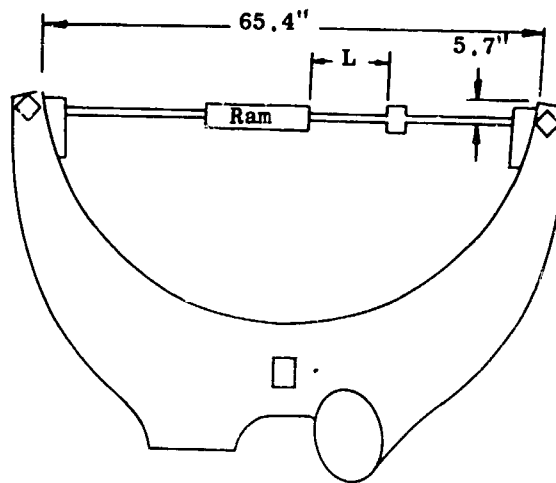


Figure 18. Enlarging the Scroll Arms for Assembly.

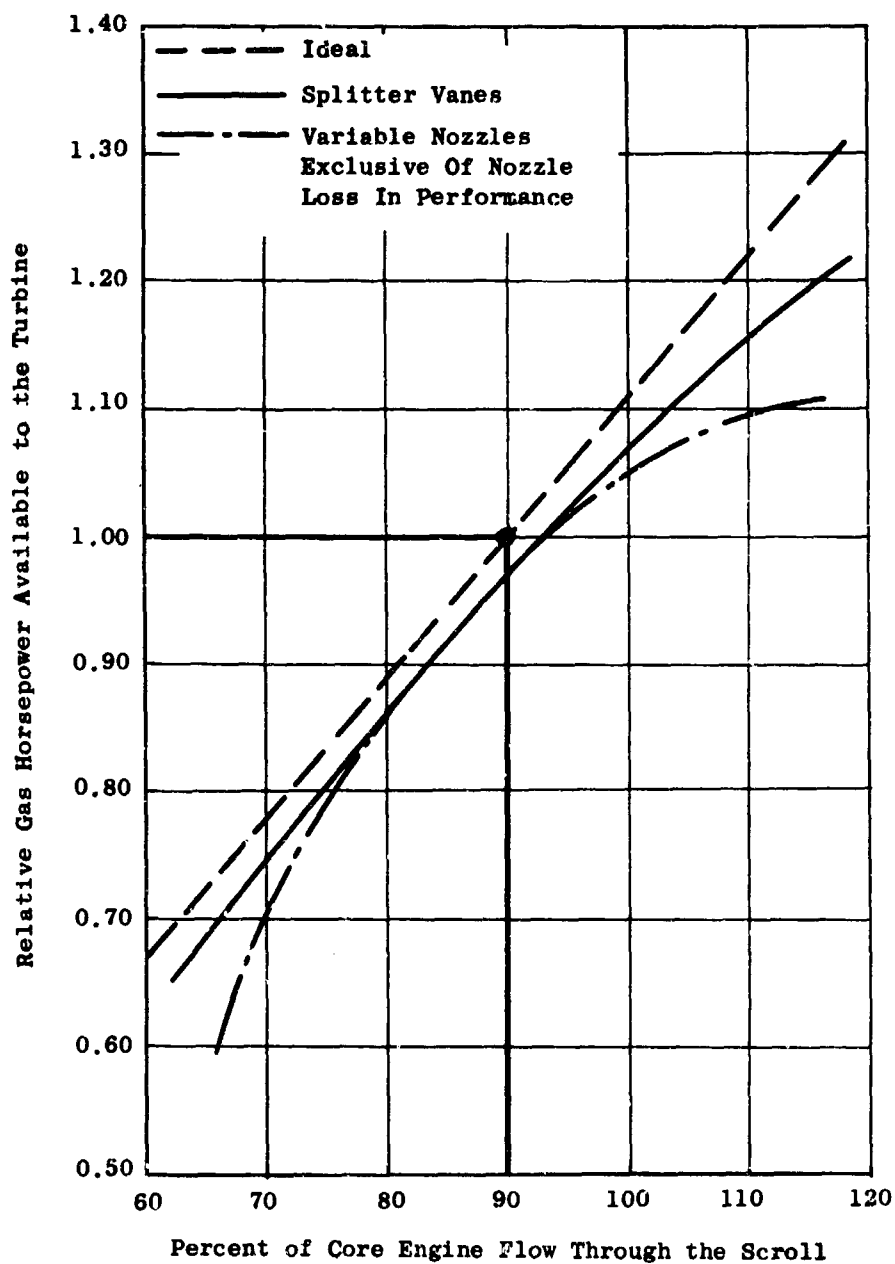


Figure 19. Comparison of Performance of the Two Methods of Nozzle Area Control.

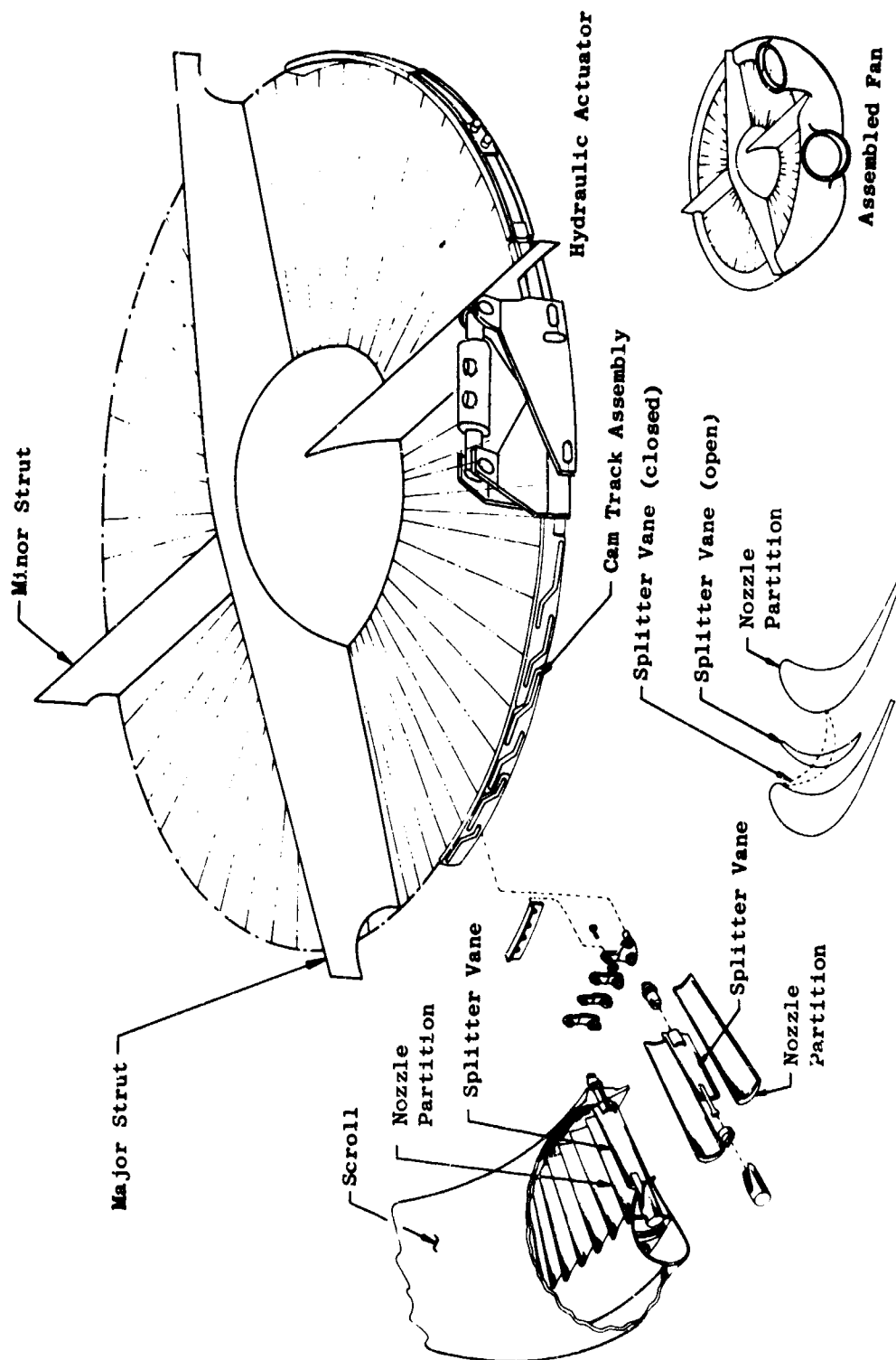


Figure 20. Variable Area Scroll Actuation.

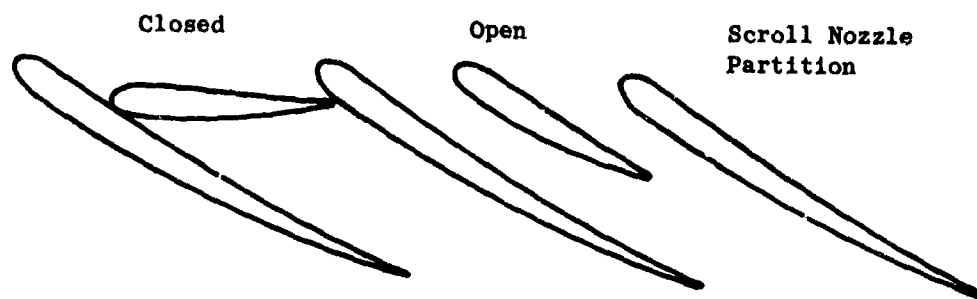


Figure 21. Flat Splitter Vanes for Scroll.

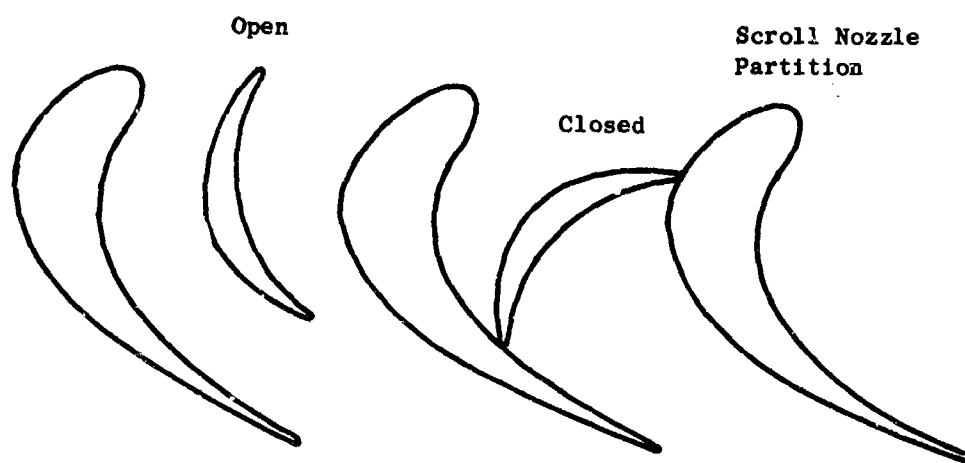


Figure 22. Biconvex Splitter Vanes for Scroll.

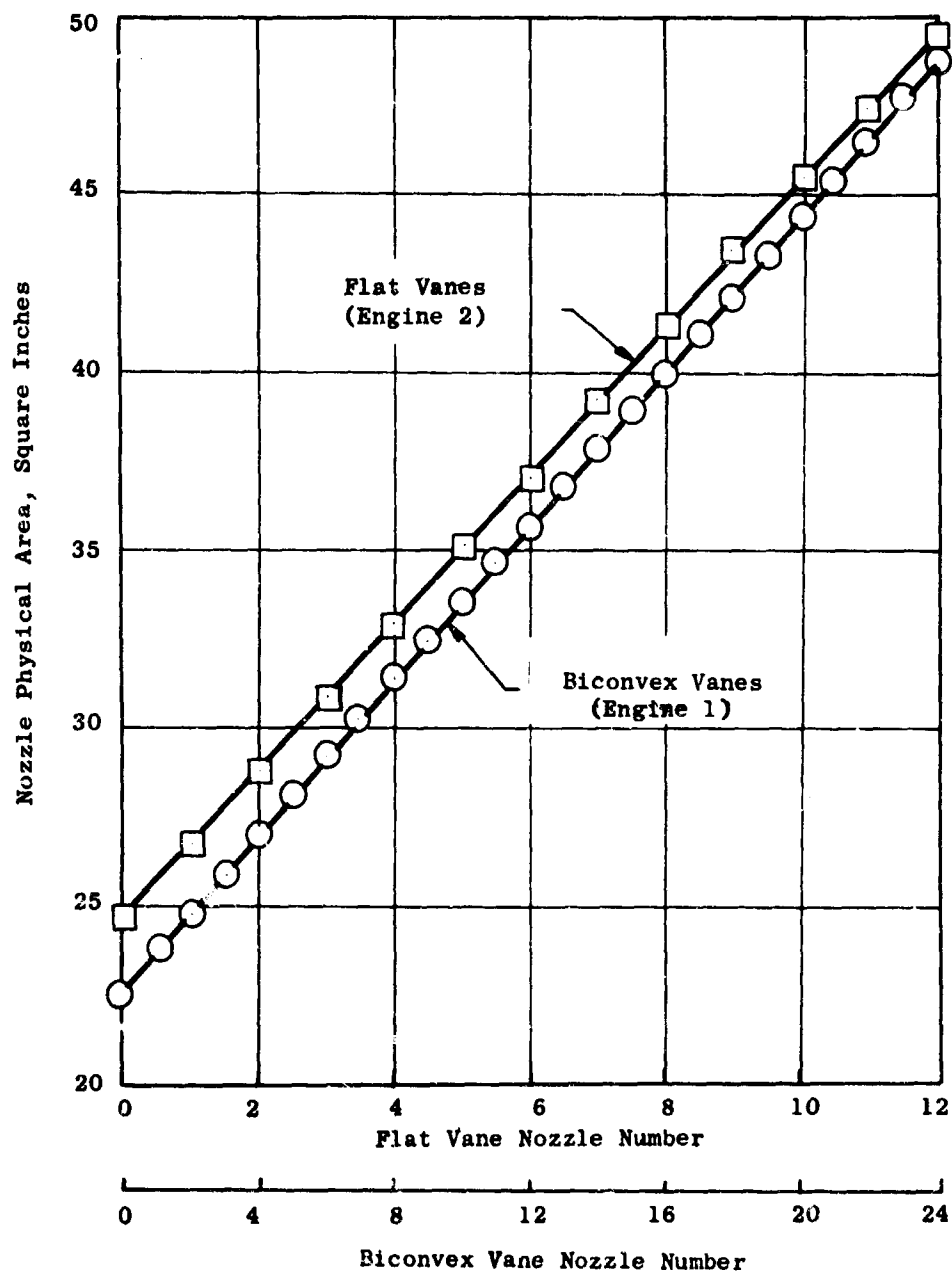


Figure 23. Scroll Nozzle Physical Area Distribution.

ITEM	IDENTIFICATION NO	DESCRIPTION
1		ASSY
2	4013007-640 201	SHAFT
3	4013007-640 202	INSERT
4	4012001-453 203	VANE BLA

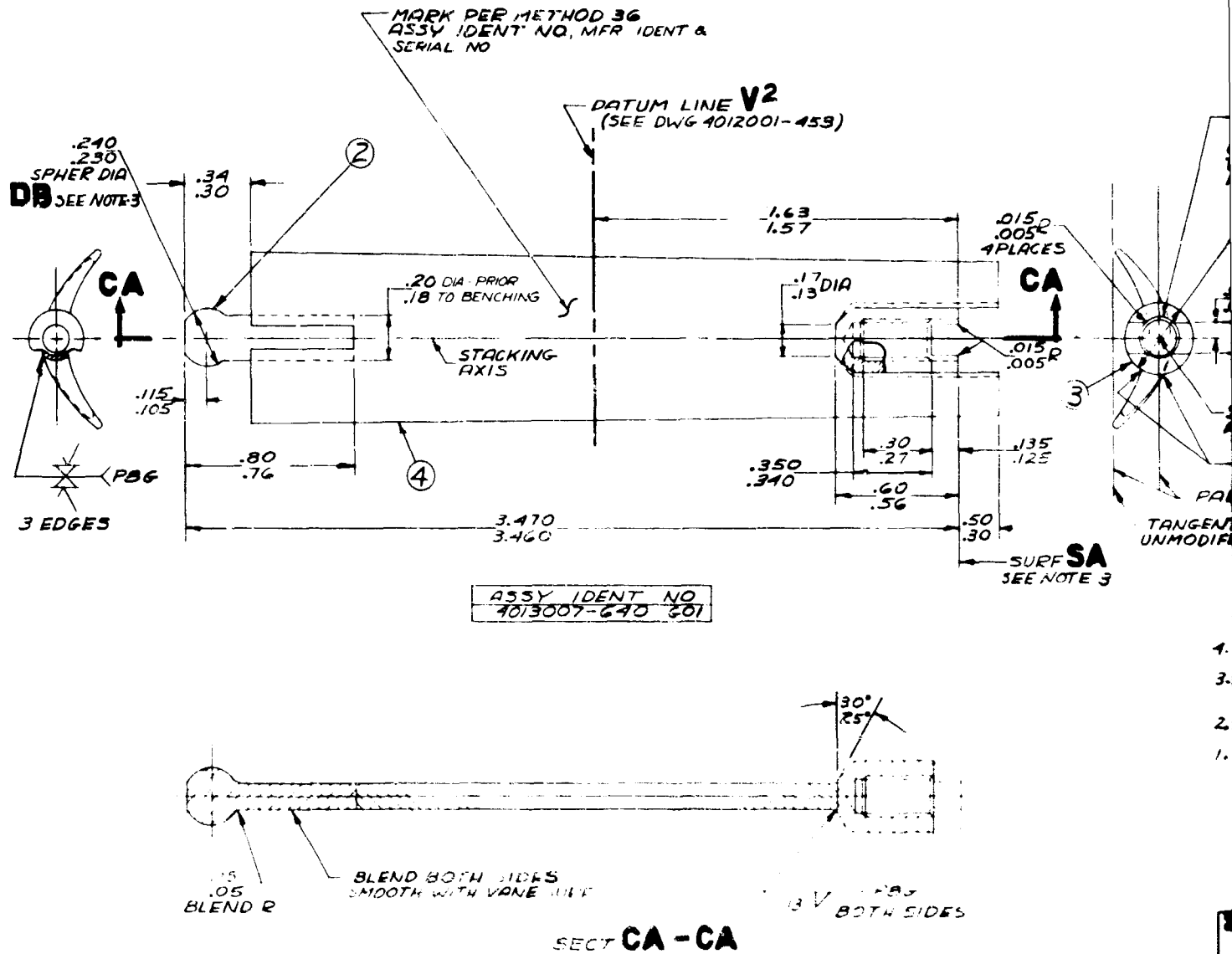


Figure 24. Splitter Vane - Aft (Drawing 4013007-640).

ITEM	IDENTIFICATION NO.	ASST
1		
2	4013007-639P01	SH
3	-639P02	IN
4	4013007-454P02	VZ

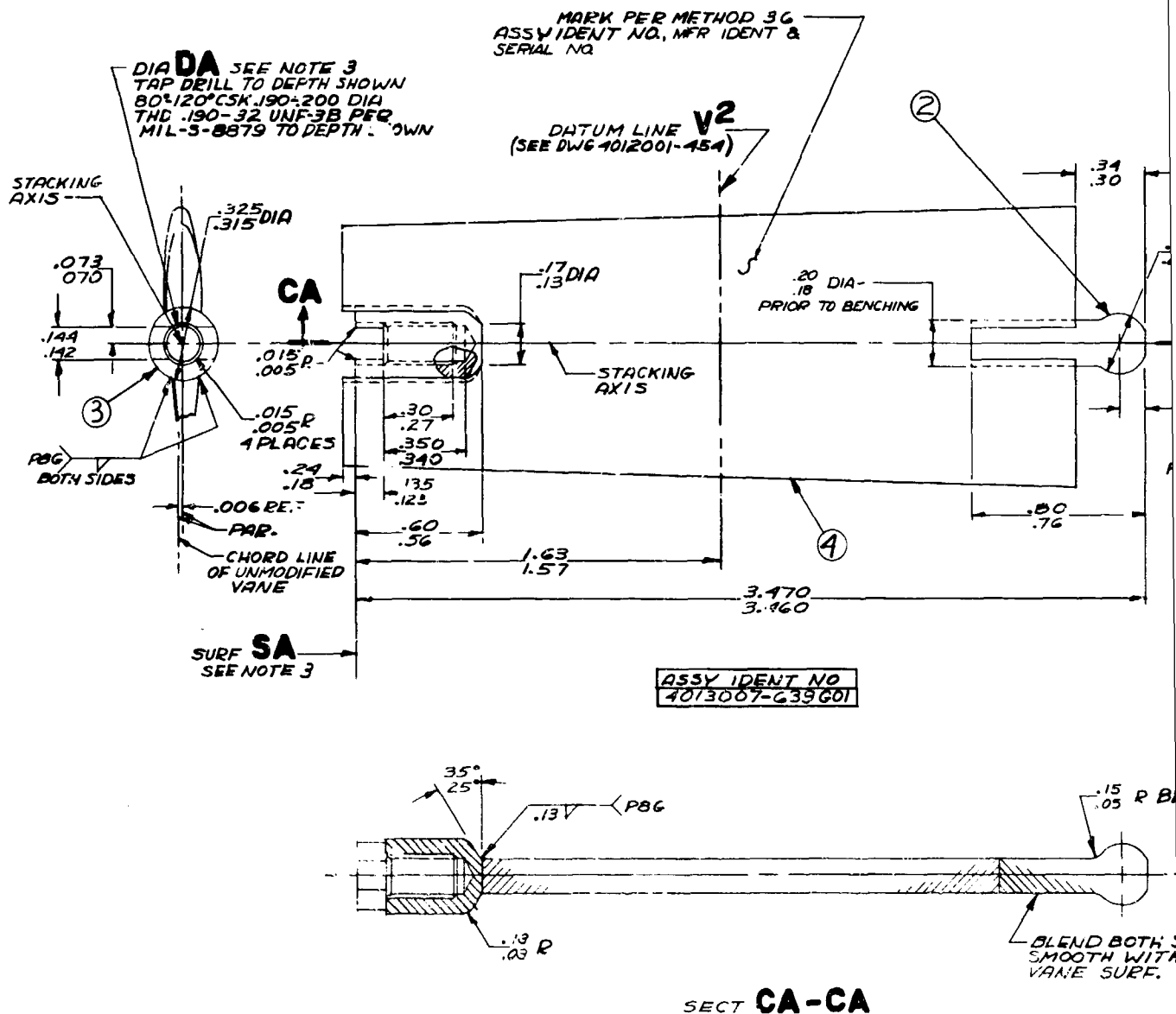
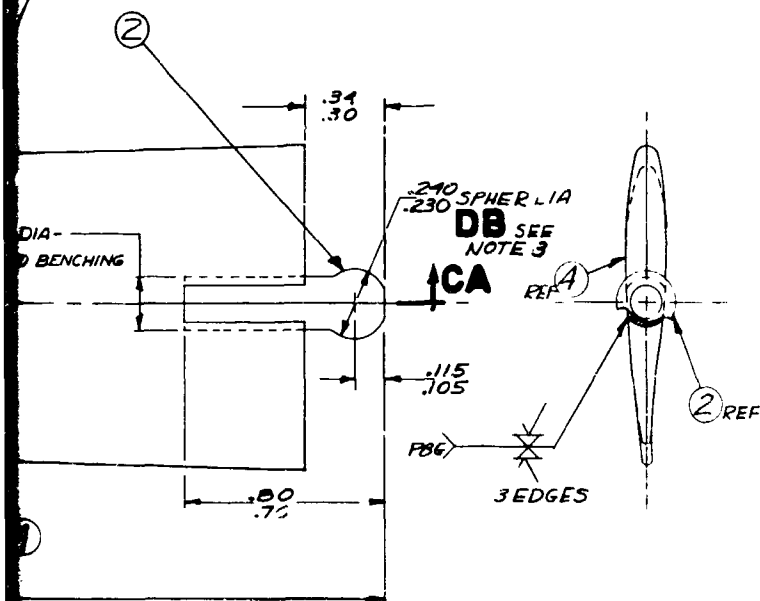


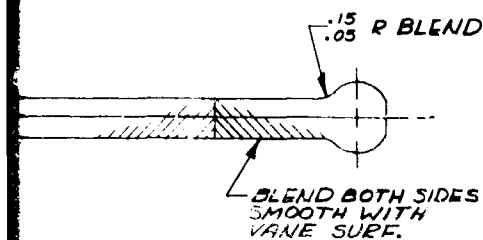
Figure 25. Splitter Vane - Forward (Drawing 4013007-639).

IDENTIFICATION		DESCRIPTION OR NAME	ZONE	GROUP NO. & QTY					REVISIONS	
ITEM	NO			1	2	3	4	DATE	BY	CHKD
1		ASST	B-6	1						
2	1013007-639P01	SHEET	D-1	1						
3	1013007-639P02	INSERT	C-2	1						
4	1012001-454P02	VANE BLANK	B-3	1						



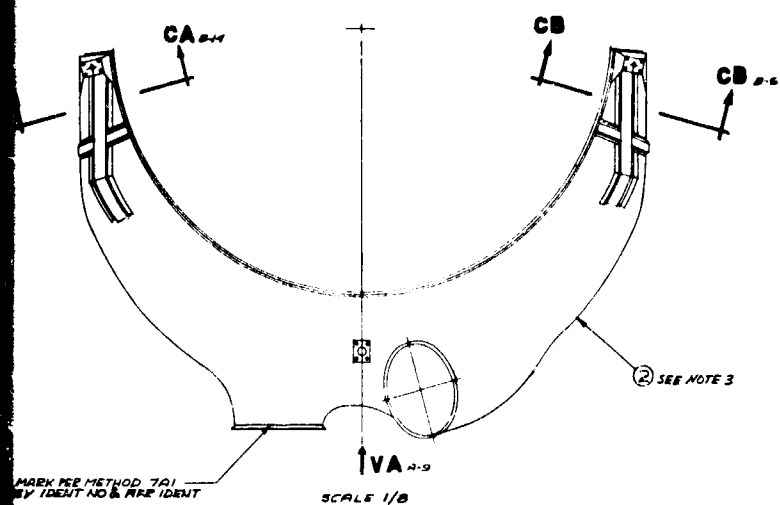
4. STRESS RELIEVE FOR 1 HR AT 1800°F ± 25°
3. SURF SA TO BE SQUARE WITH AXIS OF DIA DA
WITHIN .002 F.I.R. AXIS OF DIA DA TO BE CON
WITH DIA DB WITHIN .005 F.I.R.
2. POG FILLER MATL AMS579B

1. MUST CONFORM TO:
 SI 212,010 (INTERPRETATION OF DWG)
 M501A (WELDING SPEC)
 P23TF2 (MARKING SPEC)
 P3TF2 CL(B) (FLUOR PENETRANT INSP)
 P29TF7 CL-(B) (FLUOR ACCEPTABILITY LIMITS)



(FILL IN OFFICIALS SPECIFIED DIMENSIONS ARE IN INCHES)		QTR TYPE DETAIL-ASSY		GENERAL ELECTRIC ADVANCED ENGINE AND TECHNOLOGY DEPT. CINCINNATI, OHIO, U.S.A.	
ALL PURPOSES 637 MAT. HASTELLOY-X AMS 5754-E		DISCREPANCIES 12/2/66 1-6-66 1-8-66 1-10-66 1-11-66 1-12-66 1-13-66 1-14-66 1-15-66 1-16-66 1-17-66 1-18-66 1-19-66 1-20-66 1-21-66 1-22-66 1-23-66 1-24-66 1-25-66 1-26-66 1-27-66 1-28-66 1-29-66 1-30-66 1-31-66 1-32-66 1-33-66 1-34-66 1-35-66 1-36-66 1-37-66 1-38-66 1-39-66 1-40-66 1-41-66 1-42-66 1-43-66 1-44-66 1-45-66 1-46-66 1-47-66 1-48-66 1-49-66 1-50-66 1-51-66 1-52-66 1-53-66 1-54-66 1-55-66 1-56-66 1-57-66 1-58-66 1-59-66 1-60-66 1-61-66 1-62-66 1-63-66 1-64-66 1-65-66 1-66-66 1-67-66 1-68-66 1-69-66 1-70-66 1-71-66 1-72-66 1-73-66 1-74-66 1-75-66 1-76-66 1-77-66 1-78-66 1-79-66 1-80-66 1-81-66 1-82-66 1-83-66 1-84-66 1-85-66 1-86-66 1-87-66 1-88-66 1-89-66 1-90-66 1-91-66 1-92-66 1-93-66 1-94-66 1-95-66 1-96-66 1-97-66 1-98-66 1-99-66 1-100-66 1-101-66 1-102-66 1-103-66 1-104-66 1-105-66 1-106-66 1-107-66 1-108-66 1-109-66 1-110-66 1-111-66 1-112-66 1-113-66 1-114-66 1-115-66 1-116-66 1-117-66 1-118-66 1-119-66 1-120-66 1-121-66 1-122-66 1-123-66 1-124-66 1-125-66 1-126-66 1-127-66 1-128-66 1-129-66 1-130-66 1-131-66 1-132-66 1-133-66 1-134-66 1-135-66 1-136-66 1-137-66 1-138-66 1-139-66 1-140-66 1-141-66 1-142-66 1-143-66 1-144-66 1-145-66 1-146-66 1-147-66 1-148-66 1-149-66 1-150-66 1-151-66 1-152-66 1-153-66 1-154-66 1-155-66 1-156-66 1-157-66 1-158-66 1-159-66 1-160-66 1-161-66 1-162-66 1-163-66 1-164-66 1-165-66 1-166-66 1-167-66 1-168-66 1-169-66 1-170-66 1-171-66 1-172-66 1-173-66 1-174-66 1-175-66 1-176-66 1-177-66 1-178-66 1-179-66 1-180-66 1-181-66 1-182-66 1-183-66 1-184-66 1-185-66 1-186-66 1-187-66 1-188-66 1-189-66 1-190-66 1-191-66 1-192-66 1-193-66 1-194-66 1-195-66 1-196-66 1-197-66 1-198-66 1-199-66 1-200-66 1-201-66 1-202-66 1-203-66 1-204-66 1-205-66 1-206-66 1-207-66 1-208-66 1-209-66 1-210-66 1-211-66 1-212-66 1-213-66 1-214-66 1-215-66 1-216-66 1-217-66 1-218-66 1-219-66 1-220-66 1-221-66 1-222-66 1-223-66 1-224-66 1-225-66 1-226-66 1-227-66 1-228-66 1-229-66 1-230-66 1-231-66 1-232-66 1-233-66 1-234-66 1-235-66 1-236-66 1-237-66 1-238-66 1-239-66 1-240-66 1-241-66 1-242-66 1-243-66 1-244-66 1-245-66 1-246-66 1-247-66 1-248-66 1-249-66 1-250-66 1-251-66 1-252-66 1-253-66 1-254-66 1-255-66 1-256-66 1-257-66 1-258-66 1-259-66 1-260-66 1-261-66 1-262-66 1-263-66 1-264-66 1-265-66 1-266-66 1-267-66 1-268-66 1-269-66 1-270-66 1-271-66 1-272-66 1-273-66 1-274-66 1-275-66 1-276-66 1-277-66 1-278-66 1-279-66 1-280-66 1-281-66 1-282-66 1-283-66 1-284-66 1-285-66 1-286-66 1-287-66 1-288-66 1-289-66 1-290-66 1-291-66 1-292-66 1-293-66 1-294-66 1-295-66 1-296-66 1-297-66 1-298-66 1-299-66 1-300-66 1-301-66 1-302-66 1-303-66 1-304-66 1-305-66 1-306-66 1-307-66 1-308-66 1-309-66 1-310-66 1-311-66 1-312-66 1-313-66 1-314-66 1-315-			

B



IDENT NO
PART-IDENT

BENCHED
BOSS

OPEN POS

CLEARANCE IN
POS

VIEW VC C-8 C-12 NO SCALE
RESTORE LEADING & TRAILING EDGES
TO A SMOOTH RADIUS AFTER BENCHING

CLOSED POS

OPEN POS

VC

3/8 REF

0.000-0.010 CLEARANCE
IN CLOSED POS

32.030 R
EFF

MATCH MARK BLANKED
VANE AND ITS BOSS

POS. OF CLEARANCE - AS NOTE 2
WITH LEADING EDGE IN OPEN POS
WITH TRAILING EDGE IN CLOSED
WITH ITEMS 3 & 4 MOUNTED
TOGETHER

LEADING EDGE
DOWN POSITION

0.000-0.010 CLEARANCE WITH
ITEM 15 MOUNTED ADAPT

CB-CB
FILE 4/1

VIEW VA E-10 SCALE FULL

7-641).

B

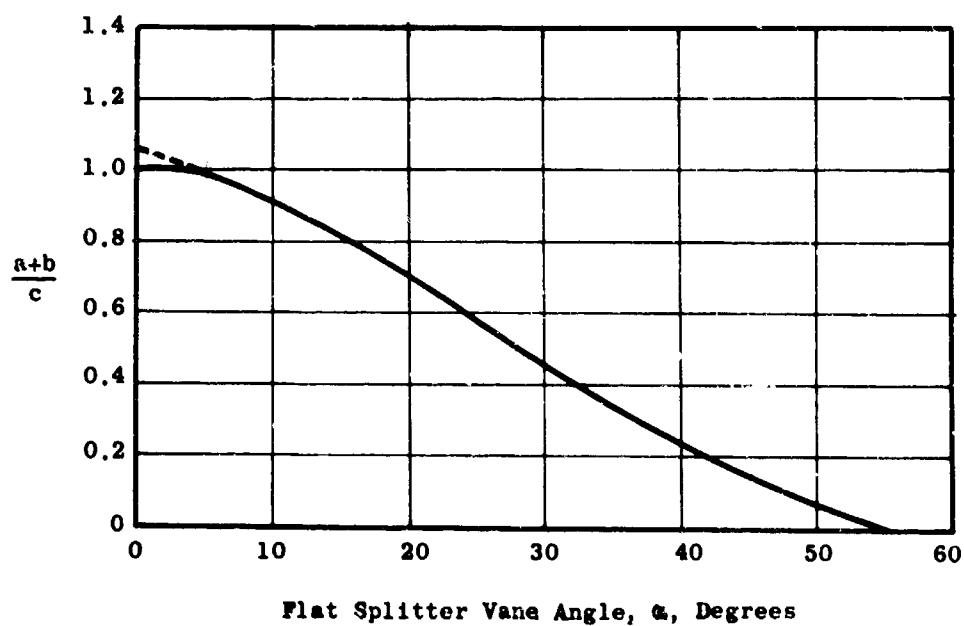
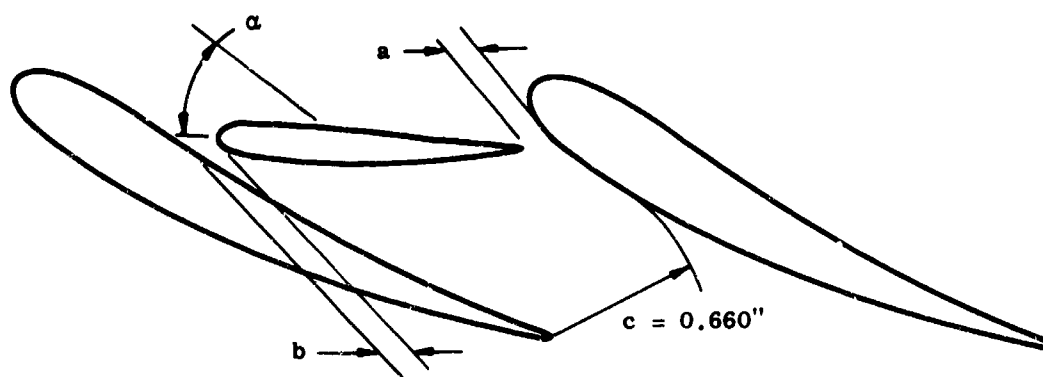


Figure 27. Flat Splitter Vane Throat Ratio.

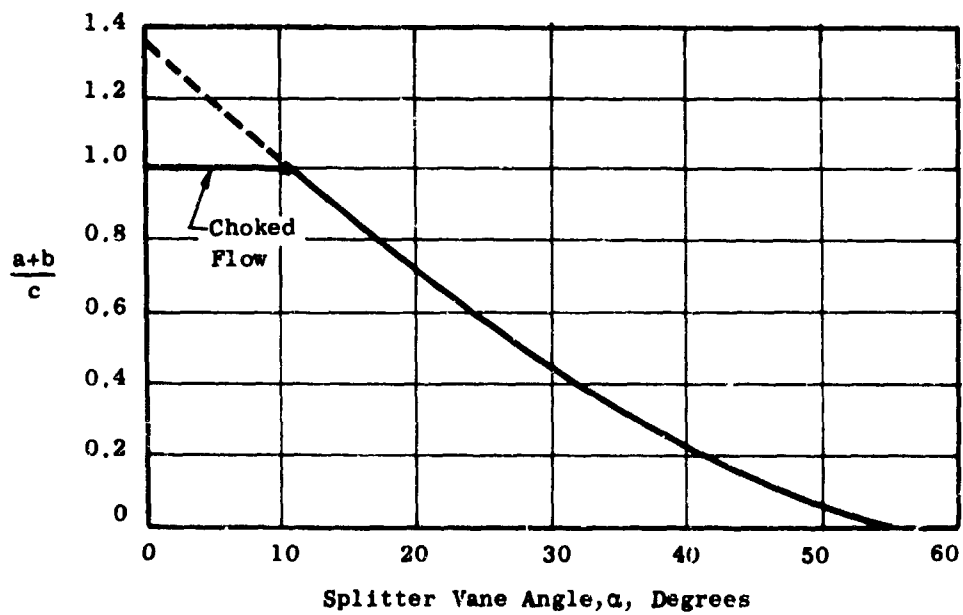
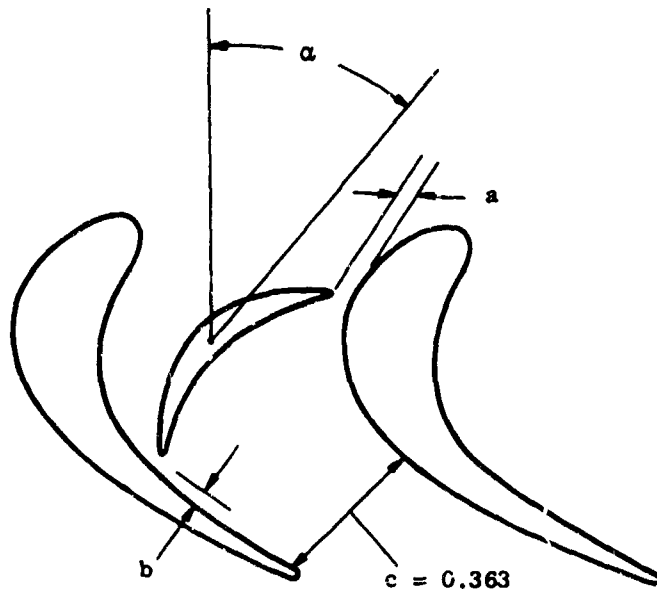


Figure 28. Biconvex Splitter Vane Throat Ratio.

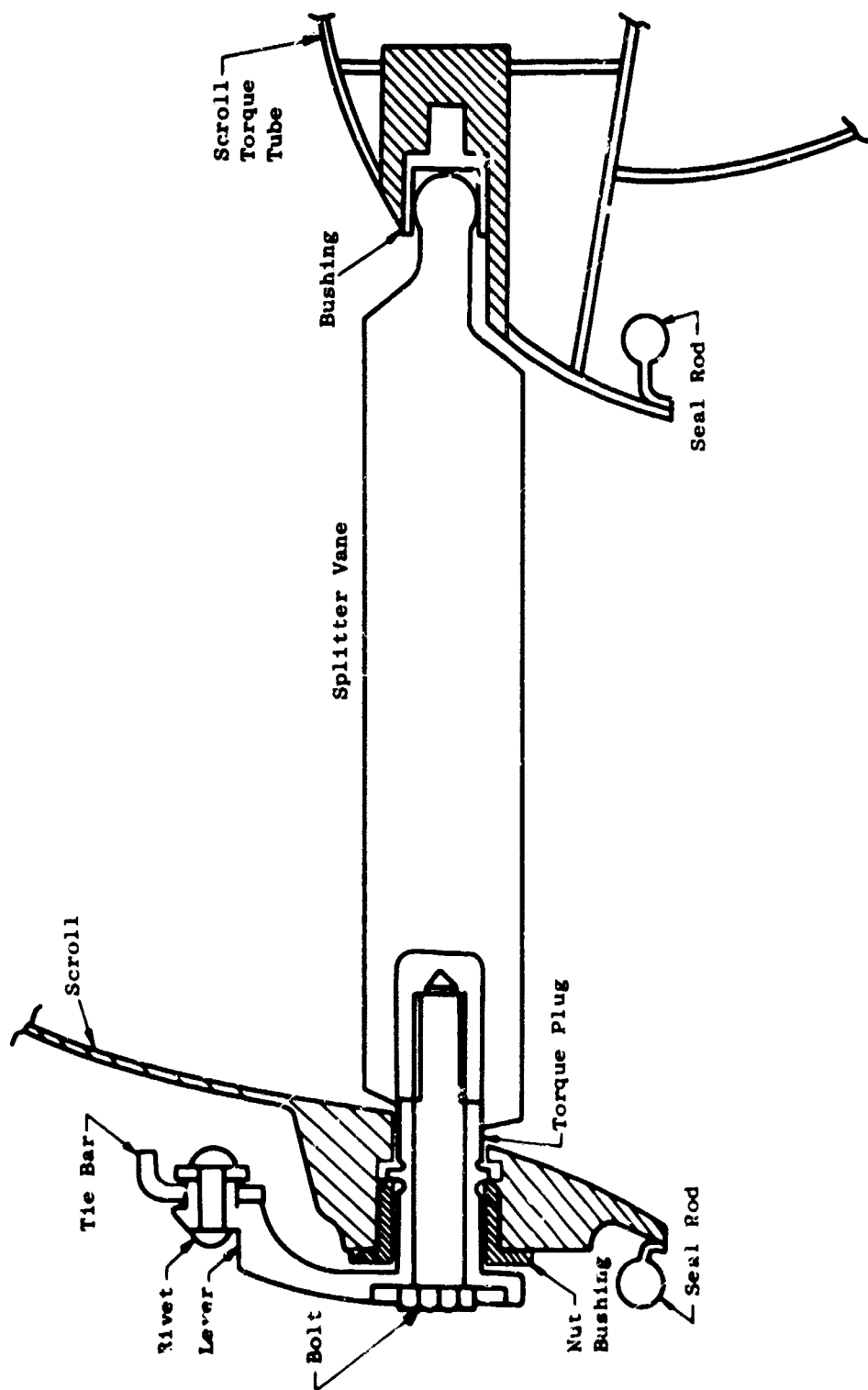
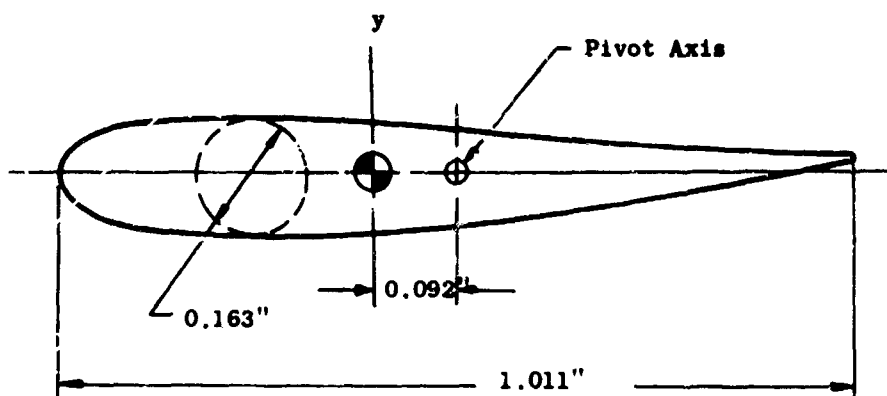


Figure 29. Splitter Vane Assembled in Scroll.



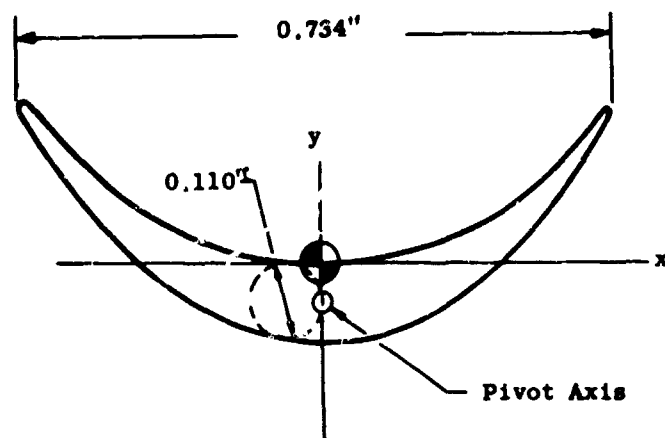
$$I_X = 0.000158 \text{ in}^4$$

$$I_y = 0.00569 \text{ in}^4$$

$$K_{SV} = 0.000624 \text{ in}^6$$

$$A = 0.106 \text{ in}^2$$

Figure 30. Flat Splitter Vane Section Properties.



$$I_x = 0.000239 \text{ in}^4$$

$$I_y = 0.00219 \text{ in}^4$$

$$K_{SV} = 0.000154 \text{ in}^6$$

$$A = 0.0628 \text{ in}^2$$

Figure 31. Biconvex Splitter Vane Section Properties.

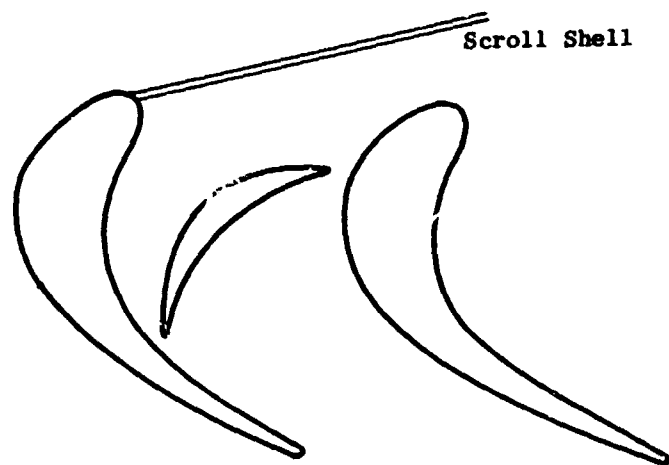


Figure 32. Biconvex Splitter at End of Scroll Arm.

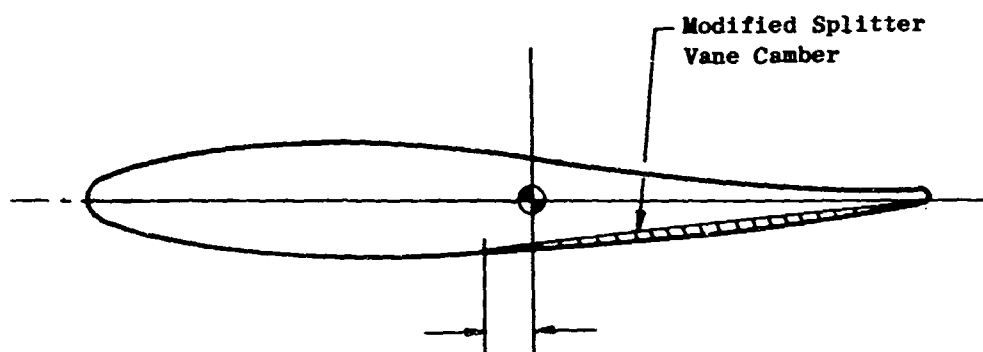


Figure 33. Rework of Flat Splitter Vane Camber.

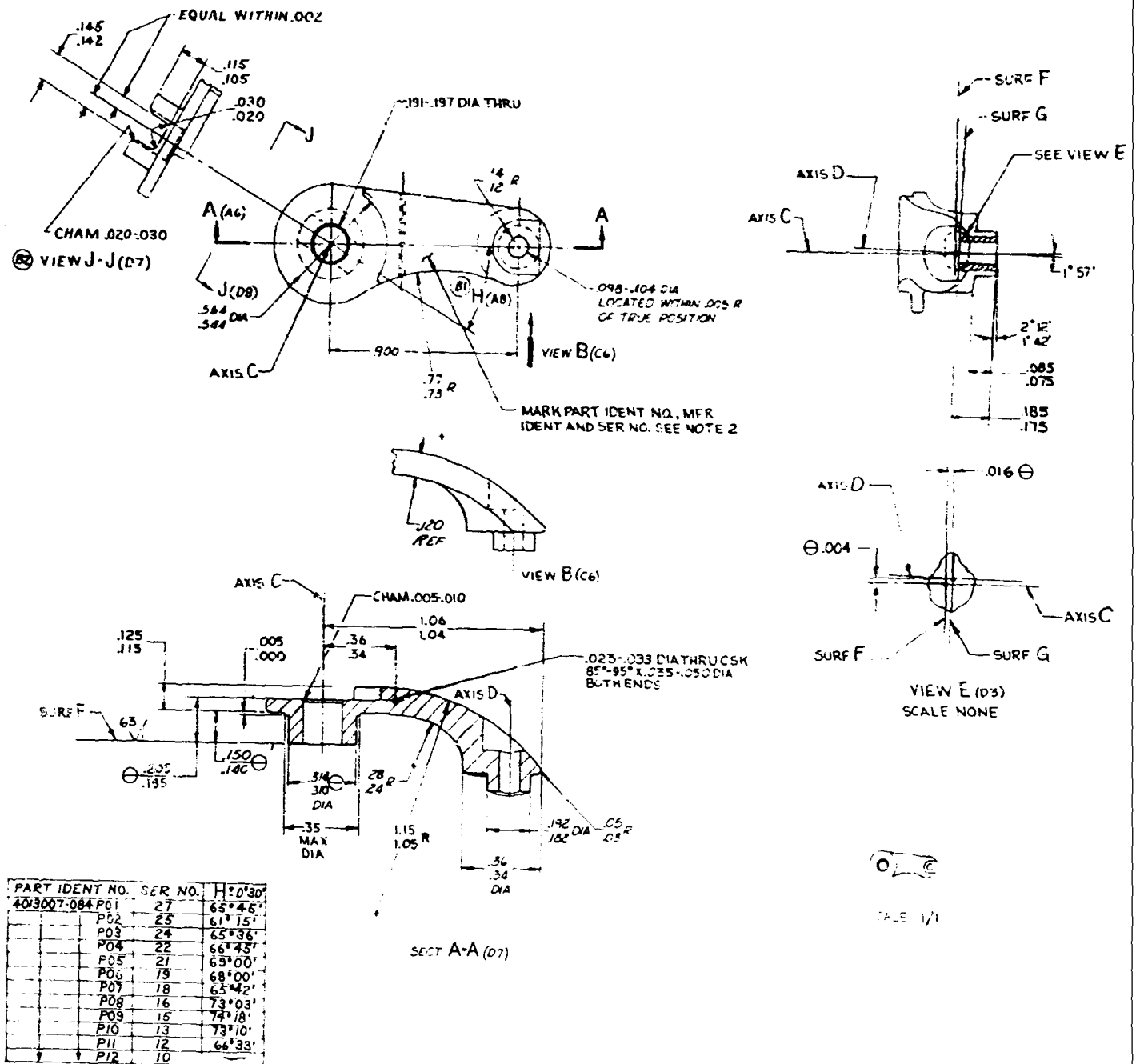
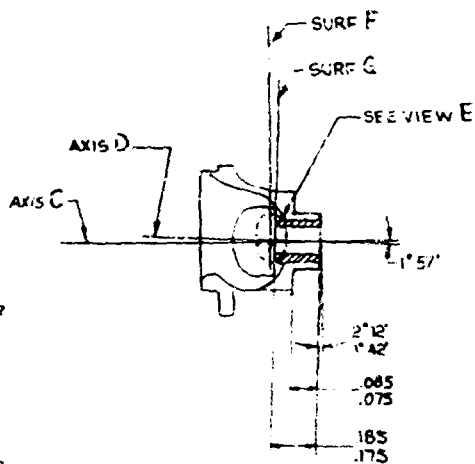
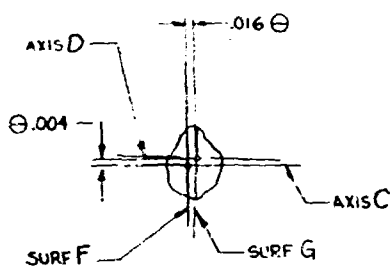


Figure 34. Aft Lever (Drawing 4013007-084).



DIA
WITHIN .005 R
POSITION

Q. MFR
SEE NOTE 2



VIEW E (03)
SCALE NONE

DIATHRU CSM
55-.050 DIA



SCALE 1/1

REV	DATE	DESCRIPTION	BY	CHKD
A3A		(1) MATL WAS C50T53E		
B2		(2) DELETED NOTES 4&5		
B2		(3) ADDED NOTE 7 PEU D-CID 146188		
C6		(4) ADDED ANGLE		
D8		(5) ADDED VIEW J-J		
A5		(6) ADDED P02 THRU P12		
A5		(7) WAS FMF4013007-100 DCID 146319		

7. ANNEAL AT 1750°F ±25° FOR 1/2 HR & AIR
COOL, AGE AT 1350°F ±25° FOR 8 HRS &
FURNACE COOL AT 25°F PER HR TO 1150°F THEN
AIRCOOL. ANNEAL & AGE IN A PROTECTIVE
ATMOSPHERE

8. ALL INSIDE AND CORNER RADIUS TO BE .015-.005 UNLESS
OTHERWISE SPECIFIED

⊖

⊖

3. PART MUST CONFORM TO PSOT04 (FLUOR PENETRANT INSP.)
ONLY THE FOLLOWING INDICATIONS ARE ACCEPTABLE AND
THEY MUST NOT BE CLOSER THAN .30.
A) ALL INDICATIONS .032 LG OR LESS
B) INDICATIONS .033-.002 LG NOT INTERPRETED AS
CRACKS

2. MARK PER P23TF2 METHOD 2C1

1. HUS. CONFORM TO

SI-212.010 (INTERPRETATION OF DNG)

070

DETAIL		GENERAL ELECTRIC	
ADVANCED ENGINE AND TECHNOLOGY DEPT. CHICAGO, ILL. U.S.A.		LEVER-AFT, RECESSED	
UPPER P-027 IN SH-3705 DIMENSIONS ARE IN INCHES	ALL SURFACES 125 WHL AMS 5667	FOR G.C. USE ONLY SIMILAR TO NONE LW 4013007-149 WHL E02-002 FME 4013007-457D	SIZE CODE 4013007-084 D 4013007-084
SCALE 4/1		SHEET	

B

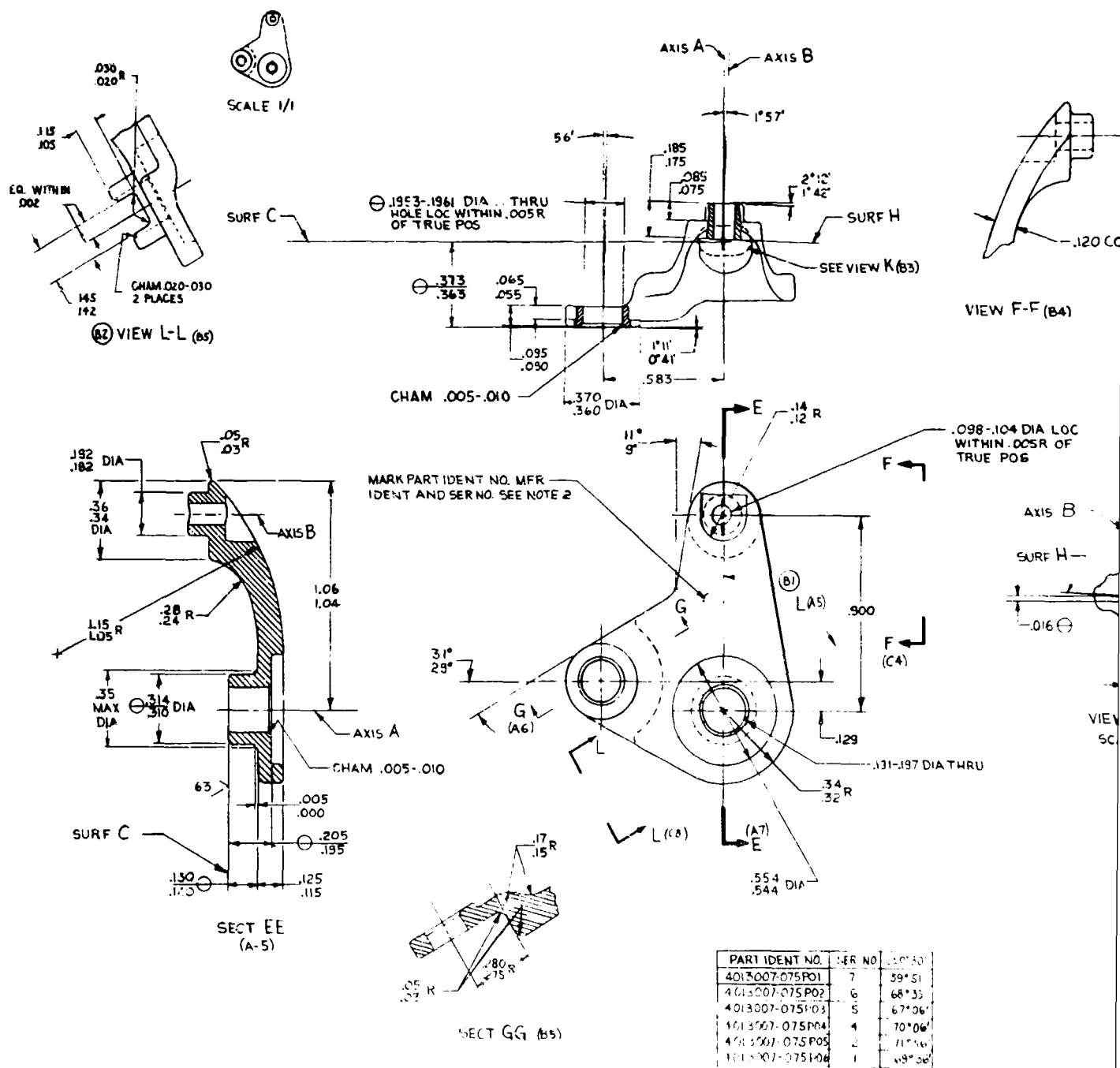
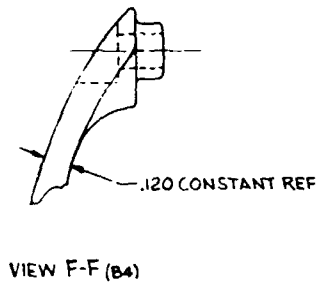
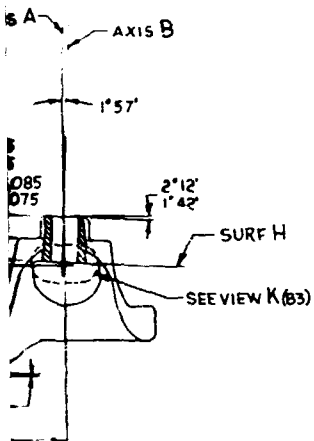
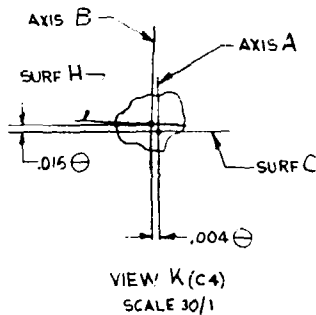
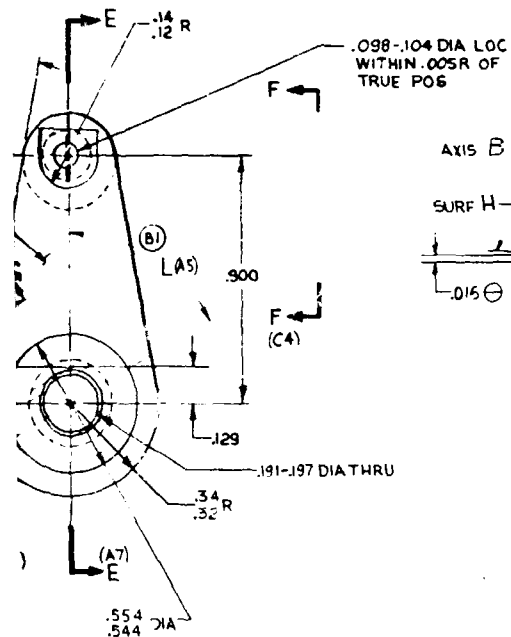


Figure 35. Aft Bellcrank (Drawing 4013007-075).



REV	DATE	DESCRIPTION	BY	CHKD
A	11/1/65	1) MATL WAS C50T53E 2) DELETE NOTES 4&5 3) ADDED NOTE 7 PER D-CID 146189	W. J. ...	W. J. ...
B5 C8	11/1/65	1) ANGLE ADDED 2) VIEW L-L ADDED 3) PARTS P02 THRU P06 ADDED 4) WAS FMF 4013007-100 D-CID 146316	W. J. ...	W. J. ...



7. ANNEAL AT 1750°F ± 25°F FOR 1/2 HR & AIR COOL.
AGE AT 1350°F ± 25°F FOR 8 HRS & FURNACE COOL
AT 25°F PER HR TO 1150°F THEN AIR COOL. USE OF
A PROTECTIVE ATMOSPHERE IS REQUIRED

8. ALL INSIDE AND CORNER RADII TO BE .015-.005 UNLESS
OTHERWISE SPECIFIED

- ⊖ 3. PART MUST CONFORM TO P3070A (FLUOR PENETRANT INSP) ONLY THE FOLLOWING INDICATIONS ARE ACCEPTABLE AND THEY MUST NOT BE CLOSER THAN .30:
- A) ALL INDICATIONS .032 LG OR LESS
 - B) INDICATIONS .033-.062 LG NOT INTERPRETED AS CRACKS
2. MARK PER P23TF2 METHOD 2C1
1. MUST CONFORM TO
SI-212.010 (INTERPRETATION OF DNG 1)

PART IDENT NO.	SER NO.	± 0° 30'
4013007-075P01	7	59° 51'
4013007-075P02	6	68° 33'
4013007-075P03	5	67° 06'
4013007-075P04	4	70° 06'
4013007-075P05	2	71° 36'
4013007-075P06	1	69° 36'

DETAIL		GENERAL ELECTRIC	
UNLESS OTHERWISE SPECIFIED DIMENSIONS ARE IN INCHES		ADVANCED ENGINE AND TECHNOLOGY DEPT. CONCORD, MASS., U.S.A.	
DESIGN	NO. 5-13-65	BELL CRANK-AFT	
CHG. NO. 5-13-65	8-9-65		
DATE 5-13-65	8-9-65	D 4013007-075	
DATE 8-9-65	8-9-65		
FOR G.E. USE ONLY		SCALE 4/1	
DRAWN BY NONE		SHEET	
LVL 4013007-149			
P02-002			
P02-002-130			

B

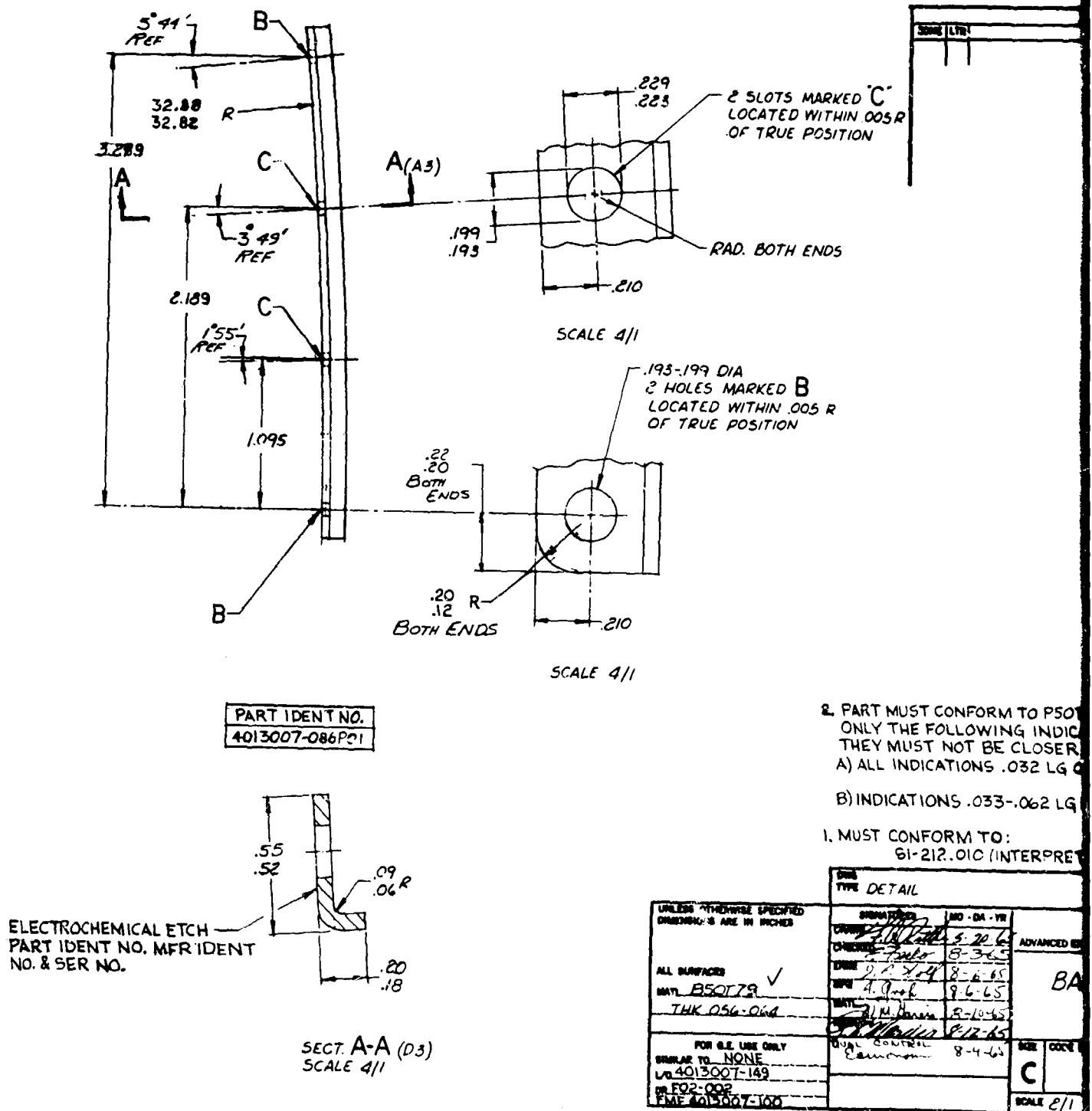
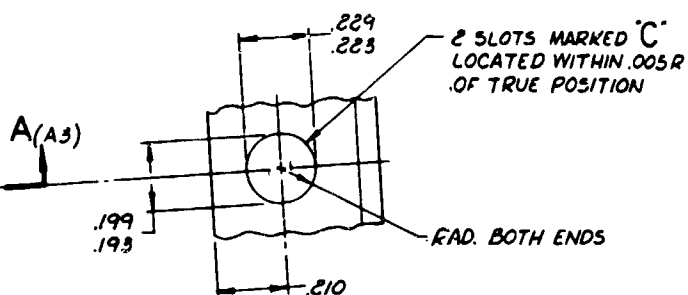
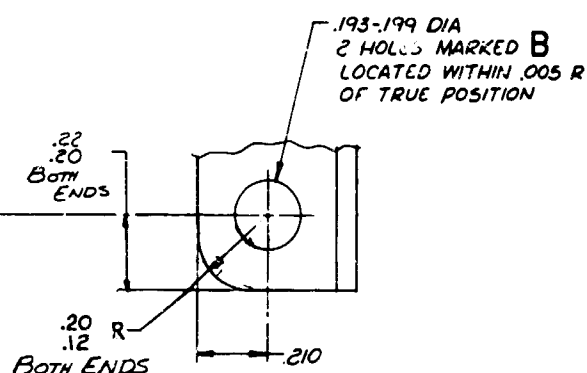


Figure 36. Aft Tie Bar (Drawing 4013007-086).

REVISIONS			
NO.	DATE	DESCRIPTION	APPROVED

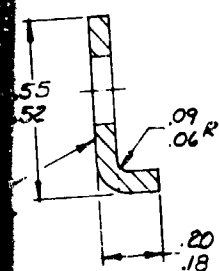


SCALE 4/1



SCALE 4/1

RT IDENT NO.
3007-086P01



SECT. A-A (D3)
SCALE 4/1

2. PART MUST CONFORM TO P5078A (FLUOR PENETRANT INSP)
ONLY THE FOLLOWING INDICATIONS ARE ACCEPTABLE AND
THEY MUST NOT BE CLOSER THAN .30:
A) ALL INDICATIONS .032 LG OR LESS.
B) INDICATIONS .033-.062 LG NOT INTERPRETED AS CRACKS.

1. MUST CONFORM TO:
61-212.010 (INTERPRETATION OF DWG)

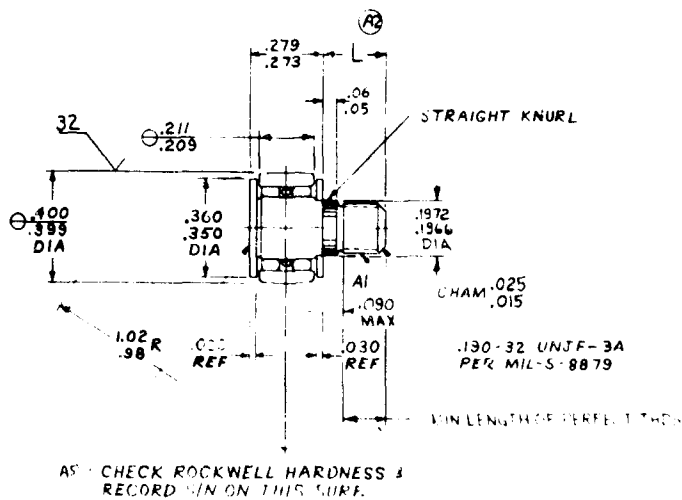
UNLESS OTHERWISE SPECIFIED DIMENSIONS ARE IN INCHES		DATE TYPE DETAIL		GENERAL ELECTRIC ADVANCED ENGINE AND TECHNOLOGY DEPT. CINCINNATI, OHIO, U.S.A.	
ALL SURFACES MATERIAL THK 056-064	✓ B50779	DATE 5-20-65	DATE 3-3-65	BAR-AFT, TIE	
FOR G.E. USE ONLY SIMILAR TO 4013007-149	✓ F02-002	DATE 8-6-65	DATE 8-6-65	C 4013007-086	
DATE 4013007-100	DATE 8-4-65	SCALE 2/1 BY SHEET SHEET			

Aft Tie Bar (Drawing 4013007-086).

B

ENDURANCE REQUIREMENTS			
CONDITION	NORMAL LOAD LB	SPEED IN./SEC	% OF RUNNING TIME CYCLE
STATIC 1	56	0	1
STATIC 2	178	0	5
SLOW MODULATION 1	80	3	15
SLOW MODULATION 2	135	5	30
SLOW MODULATION 3	200	5	30
FAST MODULATION 1	80	10	4
FAST MODULATION 2	135	10	7.5
FAST MODULATION 3	200	10	7.5

RUNNING TIME CYCLE (COOL TO 300°F BEFORE NEXT CYCLE)	
CYCLE TIME (MIN)	NO. OF CYCLES
150	1
30	5
10	105
5	330



A3
 PART IDENT NO.
 4013007-040 P01 210 111
 4013007-040 P02 210 120

Figure 37. Roller Bearing (Drawing 4013007-040).



Figure 38. Front Frame Gussets Modified for Cam Tracks.

N = Load on Cam Follower

μ = Friction Coefficient

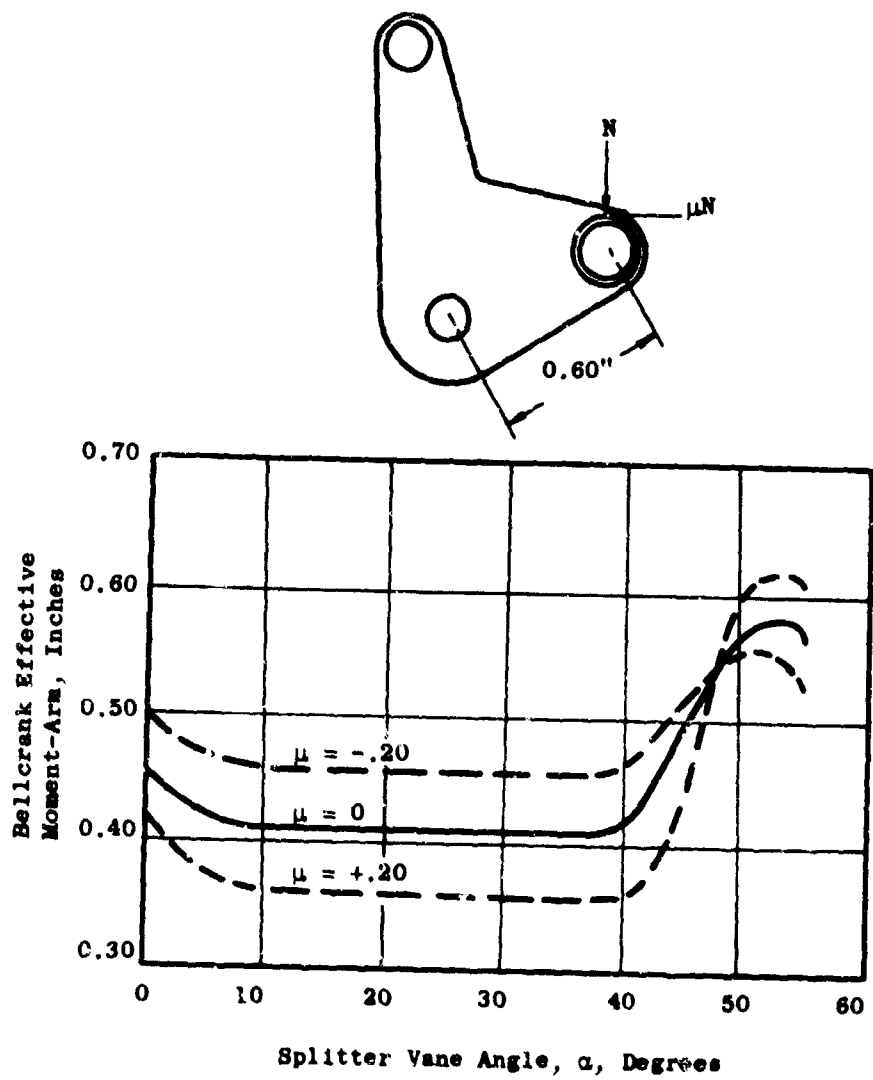


Figure 39. Forward Bellcrank Moment Arm, Flat Splitter Vanes.

N = Load on Cam Follower

μ = Friction Coefficient

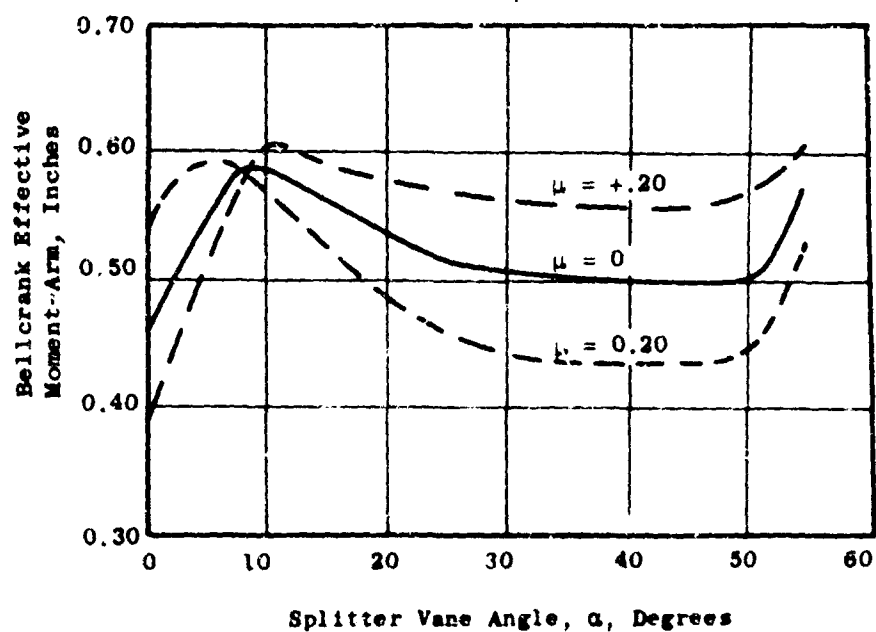
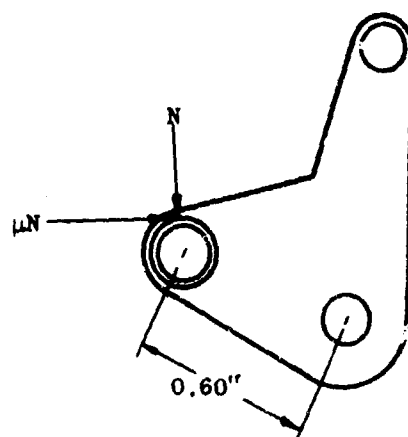
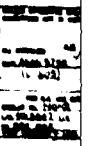
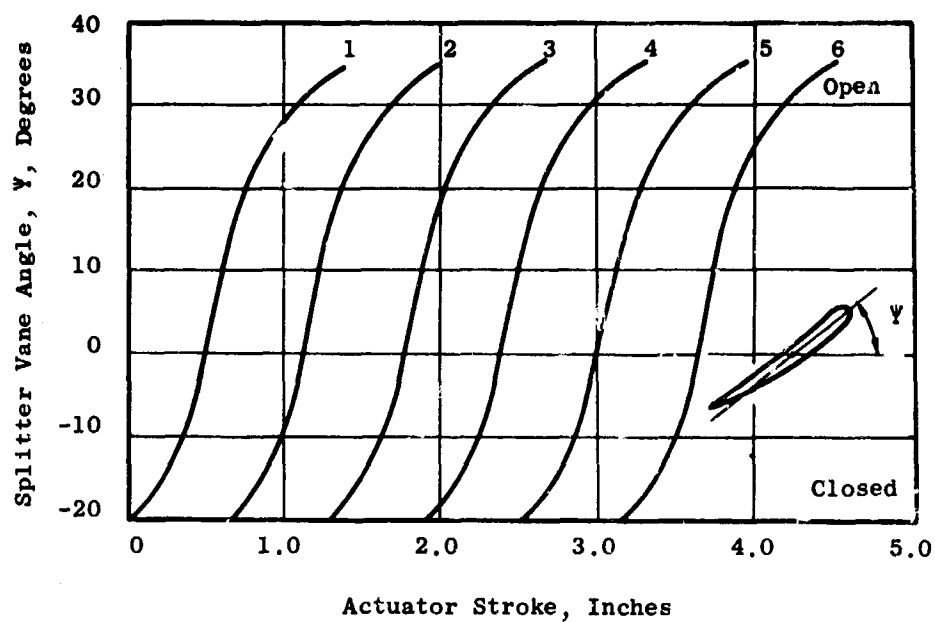


Figure 40. Aft Bellcrank Moment Arm, Biconvex Splitter Vanes.





A



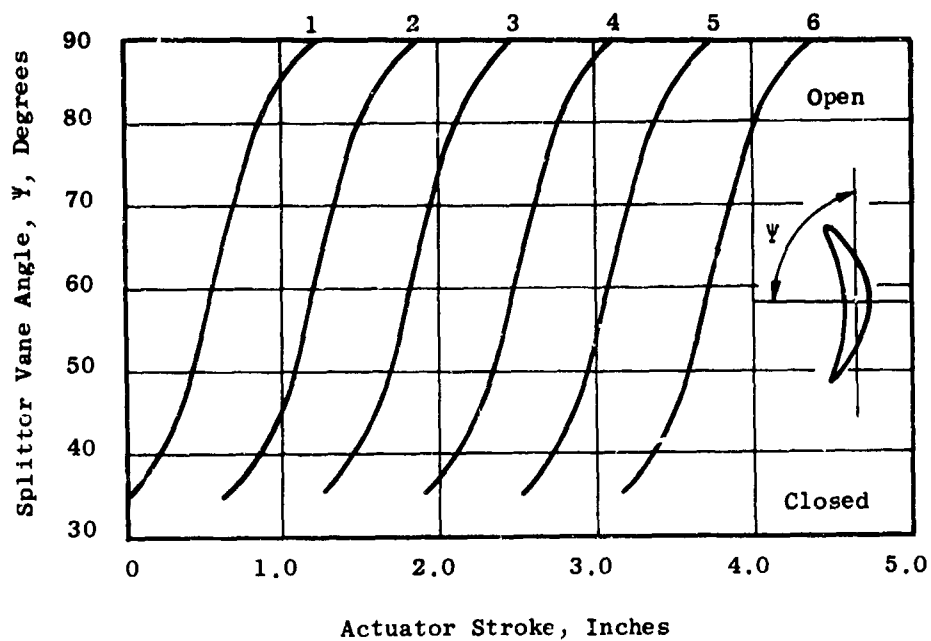
$\Psi = 35^\circ$ Splitter Vanes Open

$\Psi = -20^\circ$ Splitter Vanes Closed

Group	Measured Scroll Nozzle Area, Square Inches (Total of Two Vanes)
1*	4.219
2	4.073
3	4.185
4	4.176
5	4.180
6	3.968

*Group 1 Starts at Center of Scroll.

Figure 44. Flat Splitter Vane Rotation Sequence.



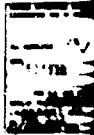
$\Psi = 90^\circ$ Splitter Vane

$\Psi = 35^\circ$ Splitter Vane

Group	Measured Scroll Nozzle Area	
	Square Inches (Total of Four Vanes)	
1*	4.478	
2	4.368	
3	4.287	
4	4.285	
5	4.349	
6	4.288	

*Group 1 Starts at Center of Scroll.

Figure 43. Biconvex Splitter Vane Rotation Sequence.



A

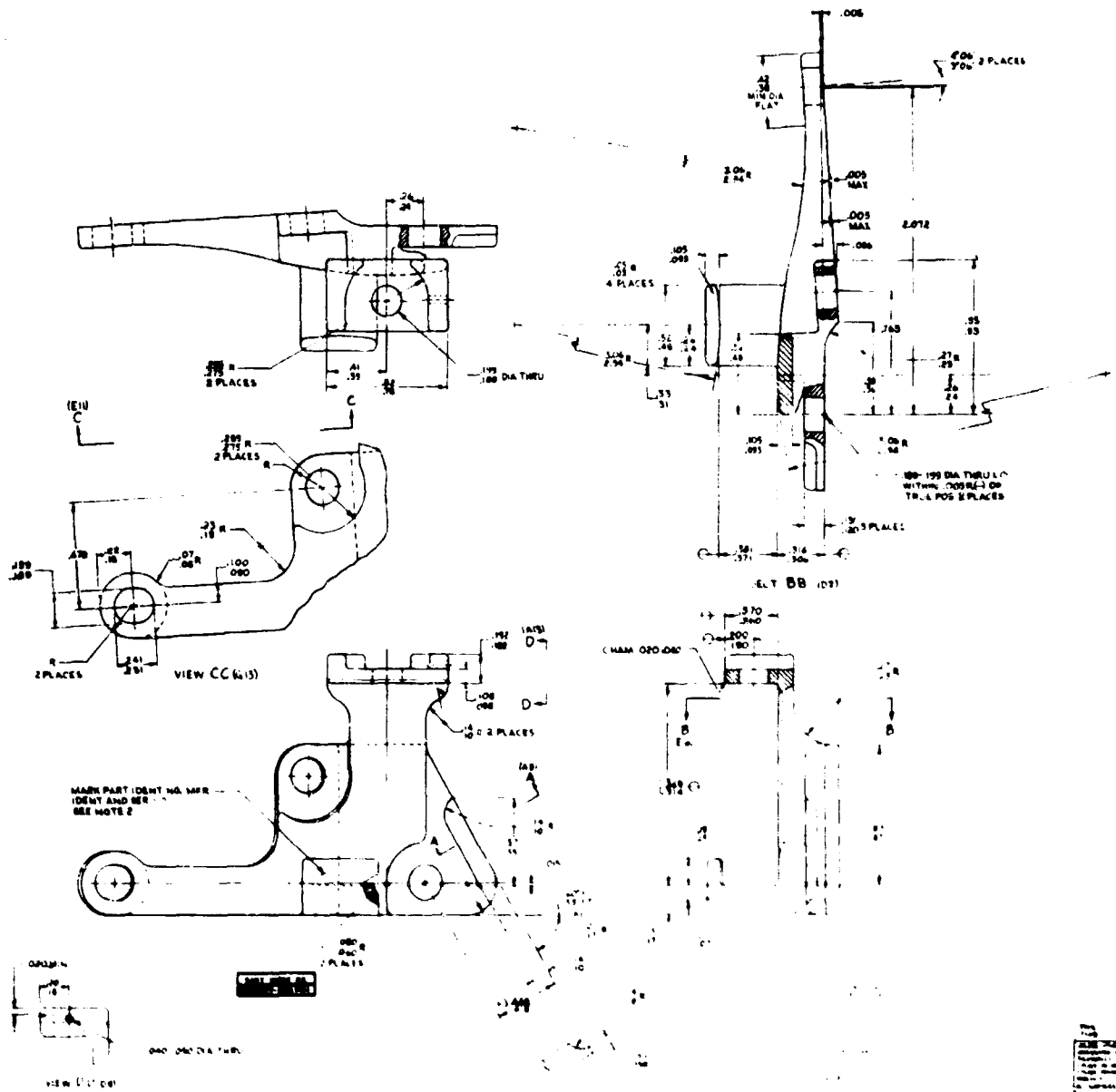


Figure 47. Forward Cam Track Bracket (Drawing 4013007-033).

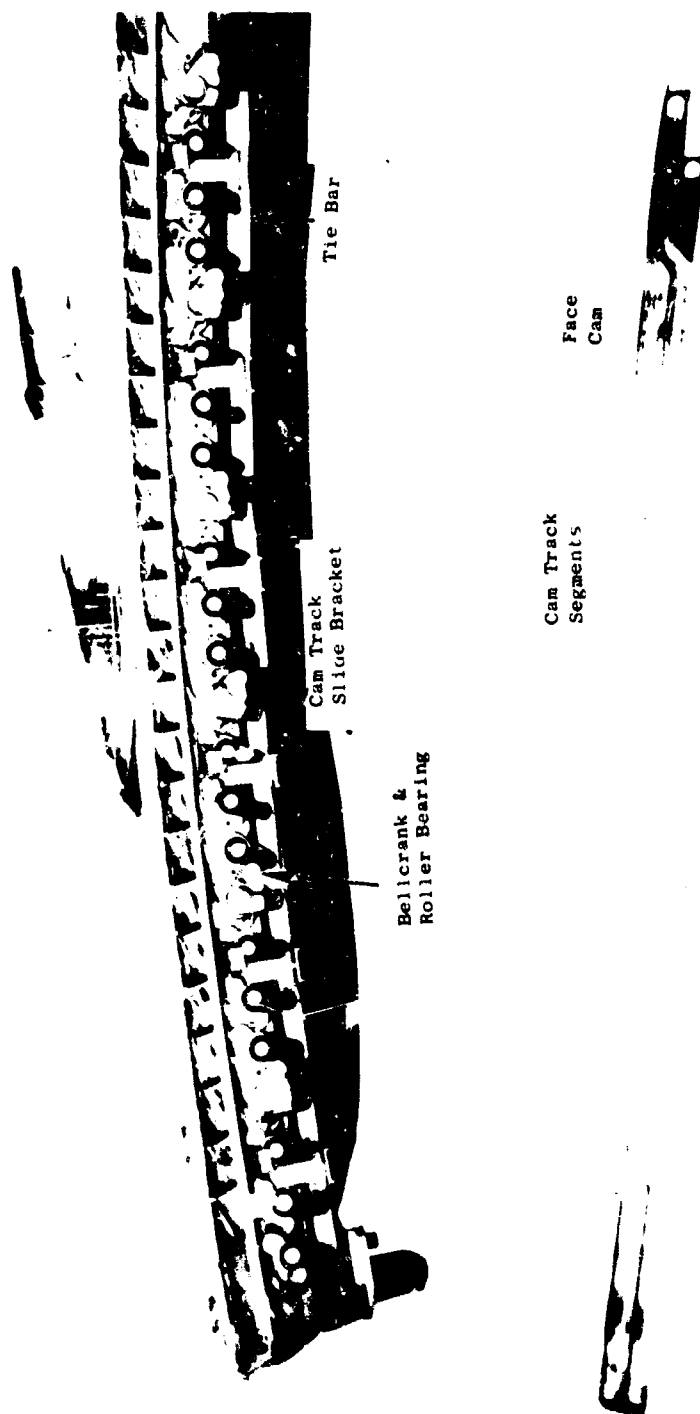


Figure 48. Cam Tracks Disassembled From Scroll.

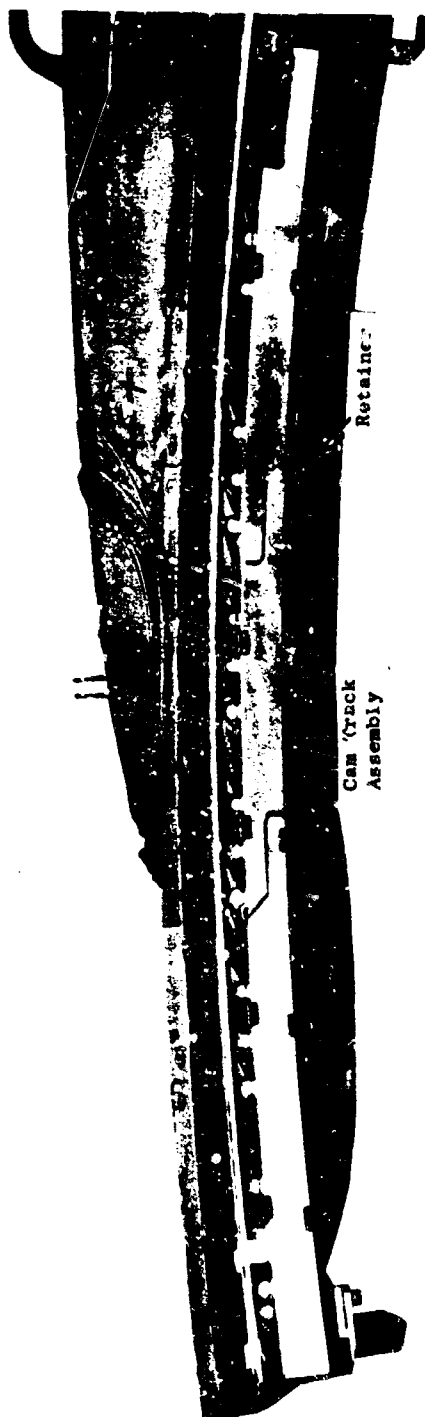
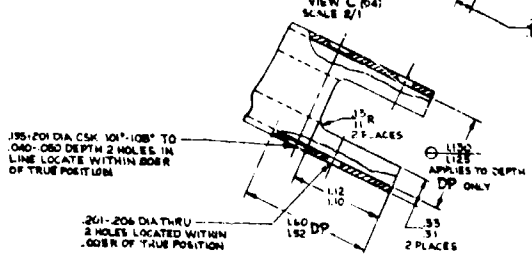
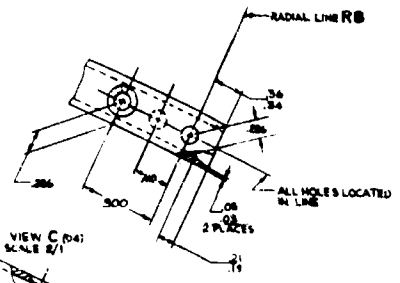
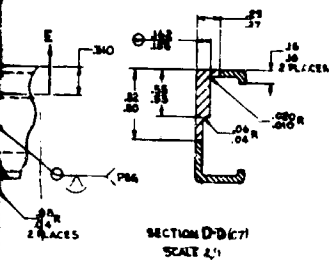
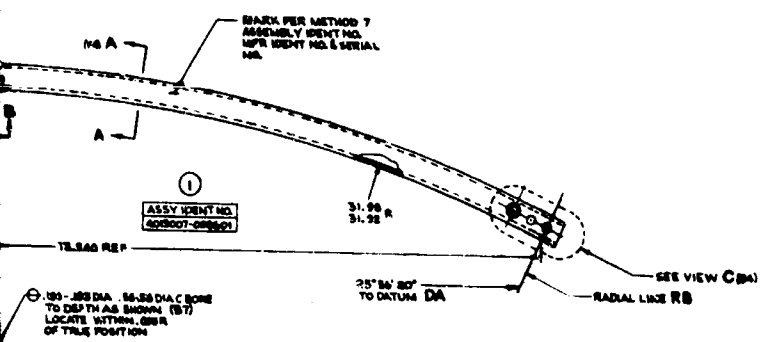
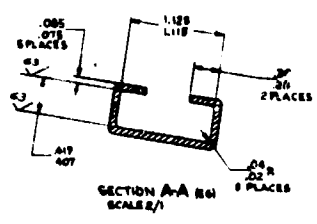


Figure 49. Cam Tracks Assembled to Scroll.

REV	DESCRIPTION	DATE	BY	CHKD
1	ISSUED FOR FAB	10/1/58	WJ	WJ
2	REVISION	10/1/58	WJ	WJ
3	REVISION	10/1/58	WJ	WJ
4	REVISION	10/1/58	WJ	WJ



4. MUST CONFORM TO PERMANENT IDENTIFICATION
5. MUST BE IDENTIFIED BY PERMANENT IDENTIFICATION
6. MUST BE IDENTIFIED BY PERMANENT IDENTIFICATION
7. MUST BE IDENTIFIED BY PERMANENT IDENTIFICATION
8. MUST BE IDENTIFIED BY PERMANENT IDENTIFICATION
9. MUST BE IDENTIFIED BY PERMANENT IDENTIFICATION
10. MUST BE IDENTIFIED BY PERMANENT IDENTIFICATION
11. MUST BE IDENTIFIED BY PERMANENT IDENTIFICATION
12. MUST BE IDENTIFIED BY PERMANENT IDENTIFICATION
13. MUST BE IDENTIFIED BY PERMANENT IDENTIFICATION
14. MUST BE IDENTIFIED BY PERMANENT IDENTIFICATION
15. MUST BE IDENTIFIED BY PERMANENT IDENTIFICATION
16. MUST BE IDENTIFIED BY PERMANENT IDENTIFICATION
17. MUST BE IDENTIFIED BY PERMANENT IDENTIFICATION
18. MUST BE IDENTIFIED BY PERMANENT IDENTIFICATION
19. MUST BE IDENTIFIED BY PERMANENT IDENTIFICATION
20. MUST BE IDENTIFIED BY PERMANENT IDENTIFICATION

INSEPARABLE ASSY		4013007-098
REV	DESCRIPTION	DATE
1	ISSUED FOR FAB	10/1/58
2	REVISION	10/1/58
3	REVISION	10/1/58
4	REVISION	10/1/58

Forward Link (Drawing 4013007-098).

B



B

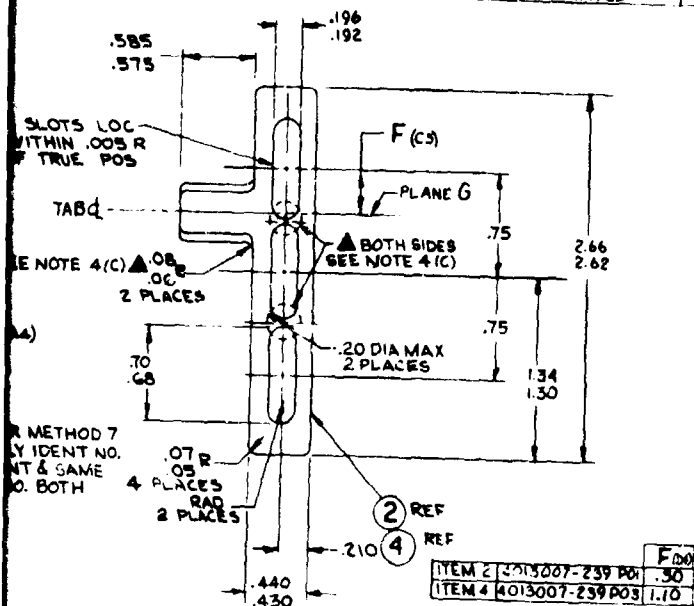


Figure 32. Forward and Alt Links.

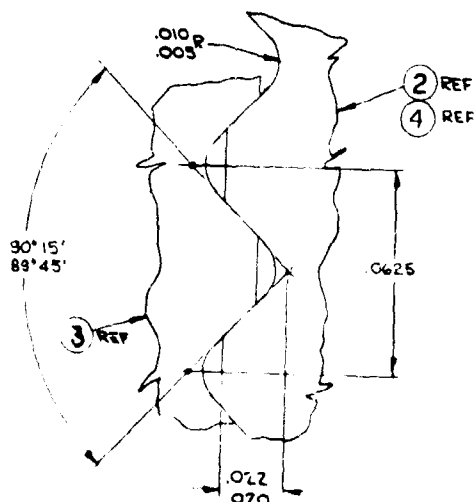
197

A

ITEM	REVISION	DESCRIPTION OR NAME	ZONE	GROUP NO & QTY	REVISION	DESCRIPTION	DATE	BY
1	4013007-239 P01	POST - SERRATED	C6	1	1			
2	4013007-239 P02	SERRATED PLATE	D6	1	1			
3	4013007-239 P03	POST - SERRATED	D6	1	1			
4	4013007-239 P04	POST - SERRATED	D6	1	1			



- MUST CONFORM TO PSOTBA (FLUOR PENETRANT INSP) ONLY THE FOLLOWING INDICATIONS ARE ACCEPTABLE AND THEY MUST NOT BE CLOSER THAN .30.
 - ALL INDICATIONS .032 LG OR LESS.
 - INDICATIONS .033-.062 LG NOT INTERPRETED AS CRACKS
 - NO INDICATIONS ALLOWED IN AREAS MARKED ▲ (ZONES C4-A6-B6-C5-A7)
- DIMENSION D MUST BE MET WITH ITEM 2 & 3 MATED ALONG SERRATED SURFACE.
- STRESS RELIEF ANNEAL AT 1950°F ±25°F FOR 1/2 HOUR AIRCOOL. AGE AT 1350°F ±25°F FOR 8 HOURS. FURNACE COOL AT 25°F PER HOUR TO 1150°F AIRCOOL STRESS RELIEF & AGE IN A PROTECTIVE ATMOSPHERE.
- MUST CONFORM TO:
 - SL212-010 (INTERPRETATION OF DWG)
 - P2TF2 (IDENTIFICATION MARKING) SEE ZONE C5



VIEW A (c)
SCALE 50/1
6 SERRATIONS PER
INCH LOCATED WITHIN
.001 OF TRUE POSITION

MATCHED PARTS		GENERAL ELECTRIC	
ALL DIMENSIONS 125	AM5547	ADVANCED ENGINE AND TECHNOLOGY DEPT. CHENNAI, INDIA, U.S.A.	
CONNECTOR, SERRATED		D	
4013007-239		D	
D		D	

B

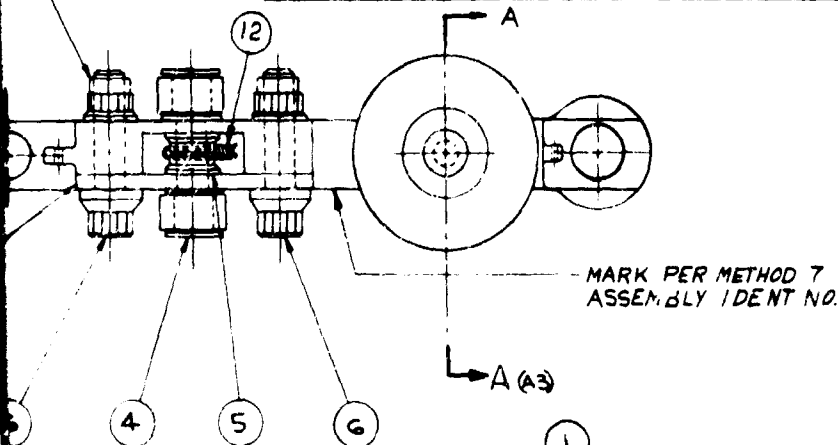


Figure 54. Serrated Connector Assembled to Alt Link.

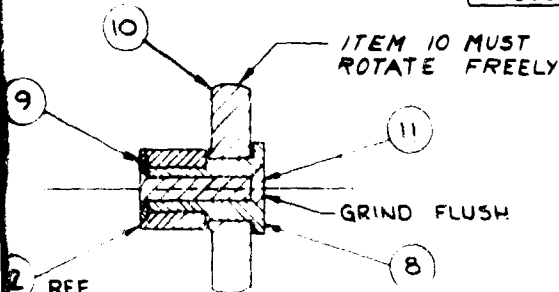
UNION N J OR EQUIV

ENKINTOWN PA OR EQUIV

ITEM	IDENTIFICATION NO	DESCRIPTION OR NAME	ZONE	GROUP NO & QTY				REVISIONS			DATE	APPROVED
				01	02	03	04	REVISION				
1	4013007-101401	ASSY, LINK SUPPORT		X				D3	A	1) ITEM 6 WAS EW80420-3-6	April 29, 1966	[Signature]
2	4013007-102P01	BRACKET-LINK SUPPORT	D4	1				D3		2) ITEM 8 WAS 4013007-105P02		
3	4013007-103P01	PLATE	C4	1				D3		3) ITEM 11 WAS AN 123666		
4	4013007-040P01	BEARING, ROLLER	D4	2						CID 146263		
5	4013007-055	NUT	B3	2								
6	4013007-24/P01	BOLT	B4	2								
7	LH 34/7-02	NUT	A	D4	2							
8	4013007-105P01	BUSHING	A3	1								
9	4013007-104P01	WASHER	B4	1								
10	4013007-107P01	WHEEL	B4	1								
11	AN 123627	RIVET	B3	1								
7	R11B6P003	NUT	B	D4	ALT							
12	R297P02	LOCKWIRE	C3	AR								



ASSY IDENT NO.
4013007-101G01



SECT A-A(C3)

- 3 TORQUE REQUIREMENTS AT ASSEMBLY SHALL BE:
ITEM 6 TO 25 TO 30 IN-LBS
- 2 LOCKWIRE ITEM 5 TOGETHER PER AEROSPACE STANDARD AS 567. LOCKWIRE MUST NOT PROTRUDE FROM ITEM 2 CAVITY
- 1 MUST CONFORM TO
SI 212 010 INTERPRETATION OF DWG)
F29TF1 (FORMED RIVETS)
AS 567 (LOCKWIRE) (SEE NOTE 2)
P12TF2 (TORQUE SPEC) (SEE NOTE 3)
P23TF2 (IDENTIFICATION MARKING) SEE ZONE C3

294

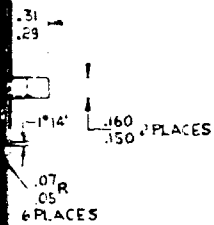
UNLESS OTHERWISE SPECIFIED DIMENSIONS ARE IN INCHES		SIGNATURES		REV. NO. - DATE		GENERAL ELECTRIC ADVANCED ENGINE AND TECHNOLOGY DEPT. CINCINNATI, OHIO, U.S.A.	
ALL SURFACES		L. SANBORN		5-26-65		ASSEMBLY FWD LINK SUPPORT	
DATE		DATE		DATE		DATE	
FOR G.E. USE ONLY		DATE		DATE		DATE	
DRAWING NO. 4013007-101		DATE		DATE		DATE	
REV. NO. 002		DATE		DATE		DATE	
DATE 4013007-100		DATE		DATE		DATE	
C 07482		4013007-101		SCALE 2/1		SHEET	

Support Assembly (Drawing 4013007-101).

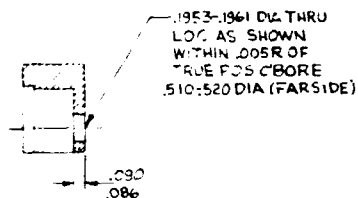
201

B

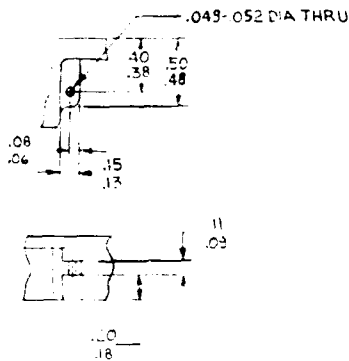
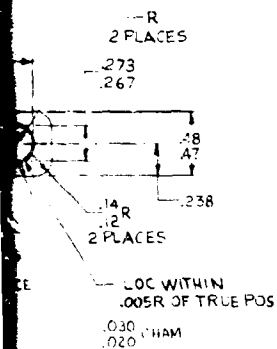
.001-.009 DIA THRU
SF 35-39 FARSIDE
TO DEPTH SHOWN (A6)
2 HOLES LOC WITHIN
CCS OF TRUE POS



SEE VIEW C (A4)



SECT BB (C)



VIEW C (B5)

- 5 AXIS E SHOWN TO BE PERPENDICULAR TO SURFACE F
- 4 PRIOR TO FINISH MACHINING IN PROCESS ANNEALING SHALL BE AT 1500°F PLUS OR MINUS 25°F FOR 1/2 HOUR AIR COOL
- 3 PART MUST CONFORM TO F5078A (FLUOR PENETRANT INSP) ONLY THE FOLLOWING INDICATIONS ARE ACCEPTABLE AND THEY MUST NOT BE CLOSER THAN .50:
 - A) ALL INDICATIONS .032 LG OR LESS
 - B) INDICATIONS .033-.062 LG NOT INTERPRETED AS CRACKS.
- 2 ALL INSIDE & CORNER RADII TO BE .005-.015 UNLESS OTHERWISE SPECIFIED.
- 1 MUST CONFORM TO:
 - 51-212,010 (INTERPRETATION OF DWG)

027

DRAWING TYPE DETAIL		NO. - DA - YR	
SIGNATURES		GENERAL ELECTRIC	
DESIGNED BY: [Signature]		ADVANCED ENGINE AND TECHNOLOGY DEPT. CINCINNATI, OHIO, U.S.A.	
CHECKED BY: [Signature]		BRACKET-LINK SUPPORT	
DATE: 8-8-65		SIZE: D	
DATE: 7-7-65		CODE: 07482	
DATE: 9-9-65		REF: 40:3007-102	
DATE: 8-14-65		SCALE: 2/1	
DATE: 7-12-65		BY: [Signature]	
DATE: 7-14-65		SHEET: [Blank]	
DATE: 7-14-65		[Blank]	

97-102).

B

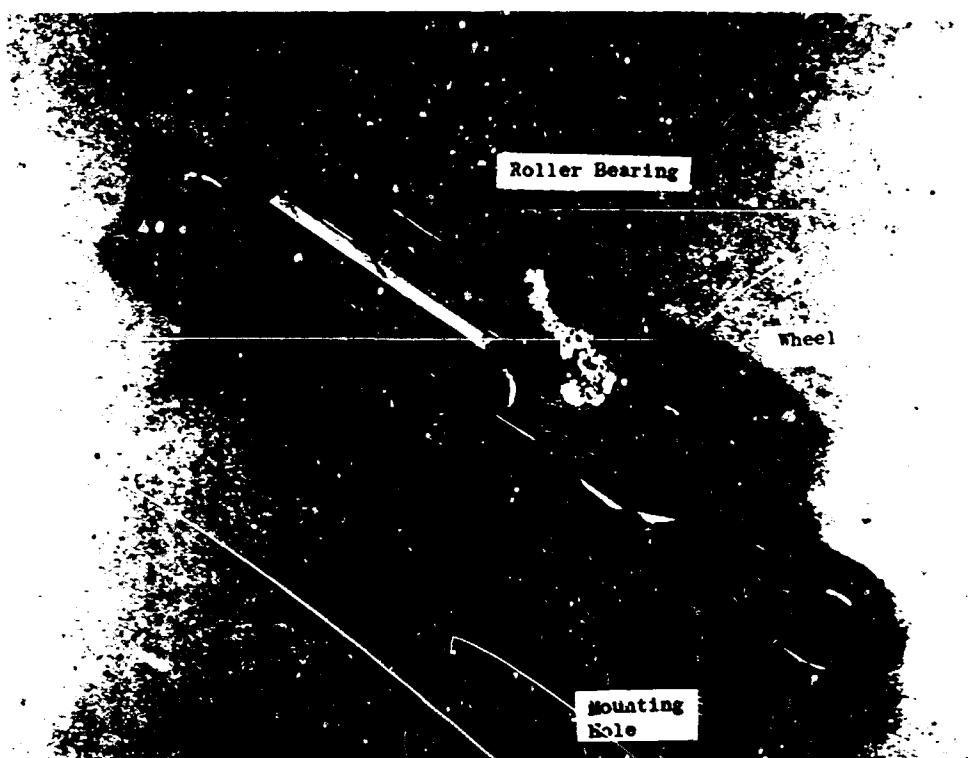


Figure 57. Link Support Assembly.

NOTE
ANY ADJUSTMENT IN CONFIGURATION WHICH EXCEEDS
THE OVERALL DIMENSIONS SHOWN HERE, MUST BE
APPROVED BY THE GENERAL ELECTRIC CO.

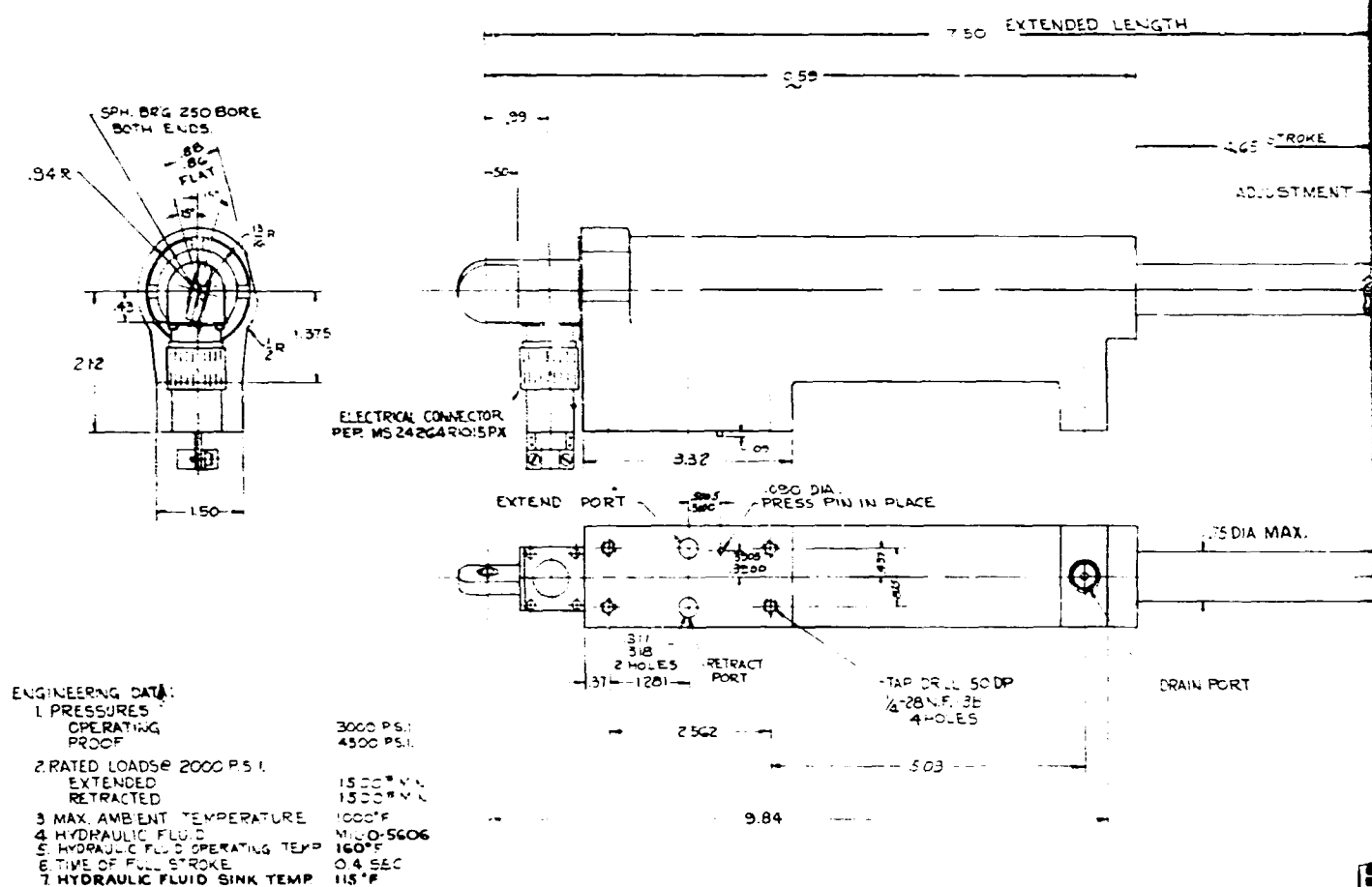
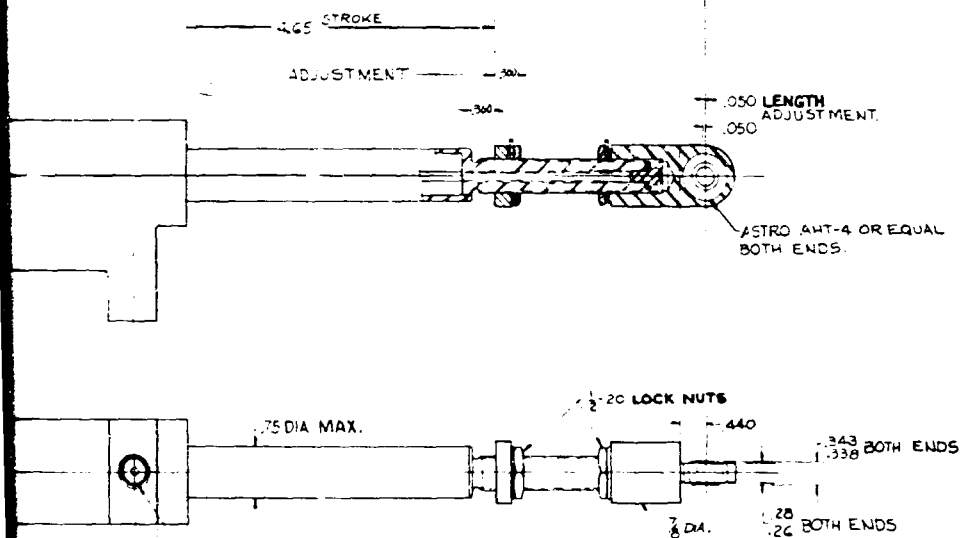


Figure 58. Test Actuator (Drawing 4013016-178).

SOURCE OF SUPPLY		
G.E. PART IDENT. NO.	VENDOR NO.	VENDOR
401301G-178-P01		

URATION WHICH EXCEEDS
AS SHOWN HERE, MUST BE
RAL ELECTRIC CO.

50 EXTENDED LENGTH



50 DP
B

DRAIN PORT

NOTE!
2 PISTON ROD COOLING FLOW MUST BE PROVIDED
1. PROVIDE POSITION TRANSDUCER WITHIN ACTUATOR

DESIGN TYPE		GENERAL ELECTRIC	
SIGNATURE		ADVANCED ENGINE AND TECHNOLOGY DEPT. CINCINNATI, OHIO, U.S.A.	
DATE		ACTUATOR, SCROLL MECHANISM	
FOR G.E. USE ONLY		D 401301G-178	
SCALE 1/1		BY EEL	

B

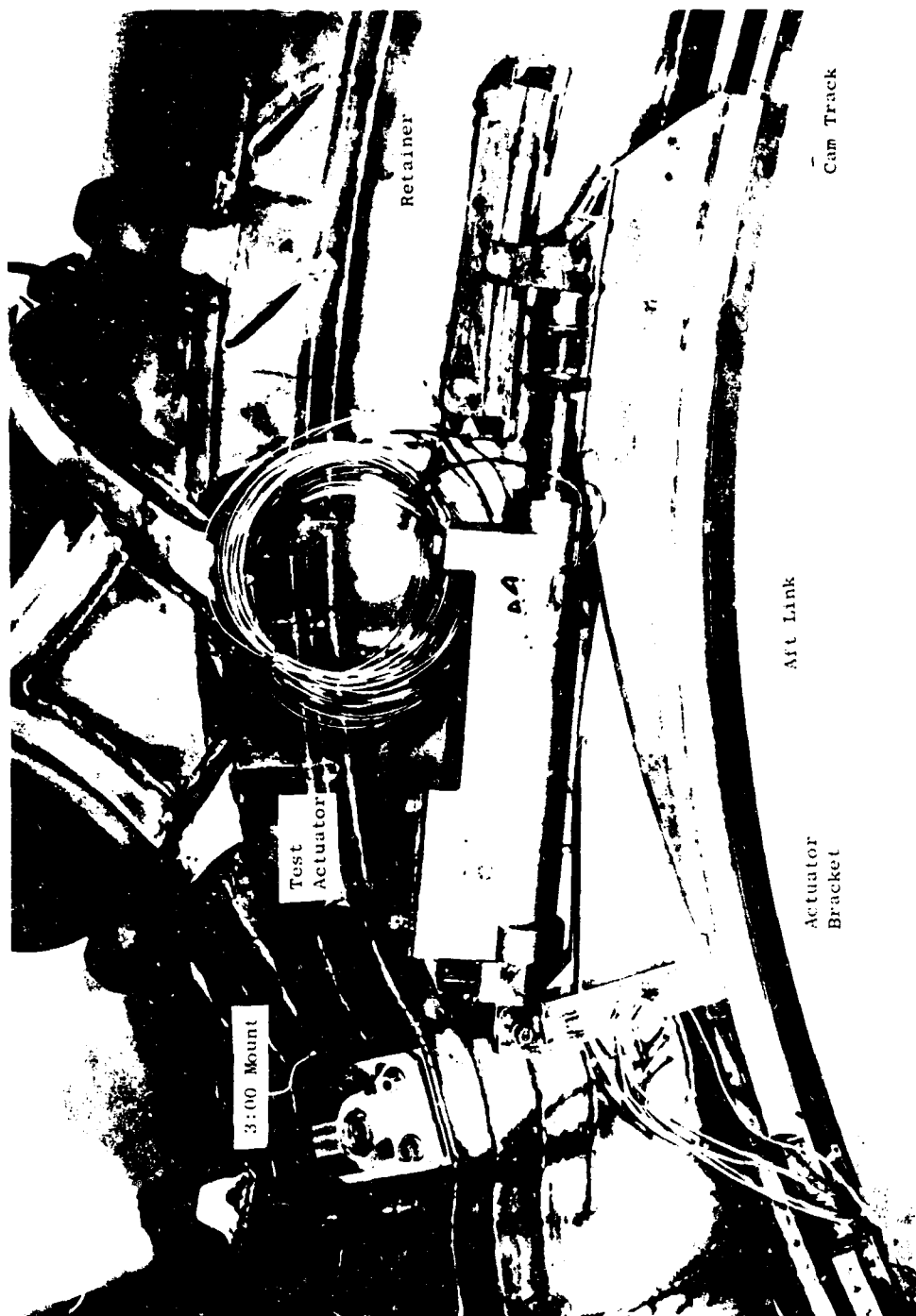


Figure 59. Actuator and Drive Links.

ITEM NO.	DESCRIPTION	UNIT	VAL
1	CARRIER TO SEAL OVERLAP	INCH	0.00
2	CARRIER TO SEAL GAP	INCH	0.00
3	TOOTH PITCH TO SEAL	INCH	0.00
4	CARRIER TWO TIP RADIUS	INCH	0.00
5	BLADE TO TORQUE BAND GAP	INCH	0.00
6	CARRIER TO SCROLL INNER	INCH	0.00
7	CARRIER TO SCROLL OUTER	INCH	0.00
8	CARRIER AFT LIP RADIUS	INCH	0.00
9	CARRIER TURNING HILL INNER	INCH	0.00
10	CARRIER TURNING HILL OUTER	INCH	0.00
11	CARRIER SCROLL TO REAR FRAME	INCH	0.00
12	INNER SEAL ENGAGEMENT	INCH	0.00
13	INNER SEAL ENGAGEMENT	INCH	0.00
14	SCROLL INNER HOLE RADIUS	INCH	0.00
15	SCROLL OUTER HOLE RADIUS	INCH	0.00
16	SCROLL OUTER SEAL ENGAGEMENT	INCH	0.00
17	OUTER SEAL GROWTH	INCH	0.00
18	SCROLL SEAL GROWTH	INCH	0.00
19	BLADE TIP TO STATOR	INCH	0.00
20	AFT CARRIER LIP TO REAR FRAME	INCH	0.00
21	CARRIER INNER TURNING HILL	INCH	0.00
22	CARRIER TO TURNING STATOR	INCH	0.00
23	CARRIER OUTER TURNING HILL	INCH	0.00
24	SPACER REAR FRAME TO REAR FRAME	INCH	0.00
25	SHFT 3.00 INCH	INCH	0.00
26	SHFT TO SPEED SENSOR	INCH	0.00
27	PROBE TO SENSOR OVERLAP	INCH	0.00
28	PROBE TO SENSOR GAP	INCH	0.00
29	SHFT SPEED SENSOR	INCH	0.00
30	SCROLL END MOUNT	INCH	0.00
31	SCROLL END MOUNT	INCH	0.00
32	SCROLL END MOUNT SHIM	INCH	0.00

ITEM NO.	DESCRIPTION	UNIT	VAL
33	SEAL CORNER CLEARANCE	INCH	0.00
34	PAW AFT END W/BLADE	INCH	0.00
35	PAW AFT END W/BLADE	INCH	0.00
36	PAW AFT END W/BLADE	INCH	0.00
37	PAW AFT END W/BLADE	INCH	0.00
38	PAW AFT END W/BLADE	INCH	0.00
39	PAW AFT END W/BLADE	INCH	0.00
40	PAW AFT END W/BLADE	INCH	0.00
41	SLIP RING DRIVE TO REAR FRAME	INCH	0.00
42	SLIP RING DRIVE TO RETAINER BOLT	INCH	0.00
43	SLIP RING DRIVE TO RETAINER BOLT	INCH	0.00
44	SLIP RING DRIVE TO RETAINER BOLT	INCH	0.00
45	SLIP RING DRIVE TO RETAINER BOLT	INCH	0.00
46	SLIP RING DRIVE TO RETAINER BOLT	INCH	0.00
47	SLIP RING DRIVE TO RETAINER BOLT	INCH	0.00
48	SLIP RING DRIVE TO RETAINER BOLT	INCH	0.00
49	SLIP RING DRIVE TO RETAINER BOLT	INCH	0.00
50	SLIP RING DRIVE TO RETAINER BOLT	INCH	0.00
51	SLIP RING DRIVE TO RETAINER BOLT	INCH	0.00

L RADIAL DIM
 A AXIAL DIM

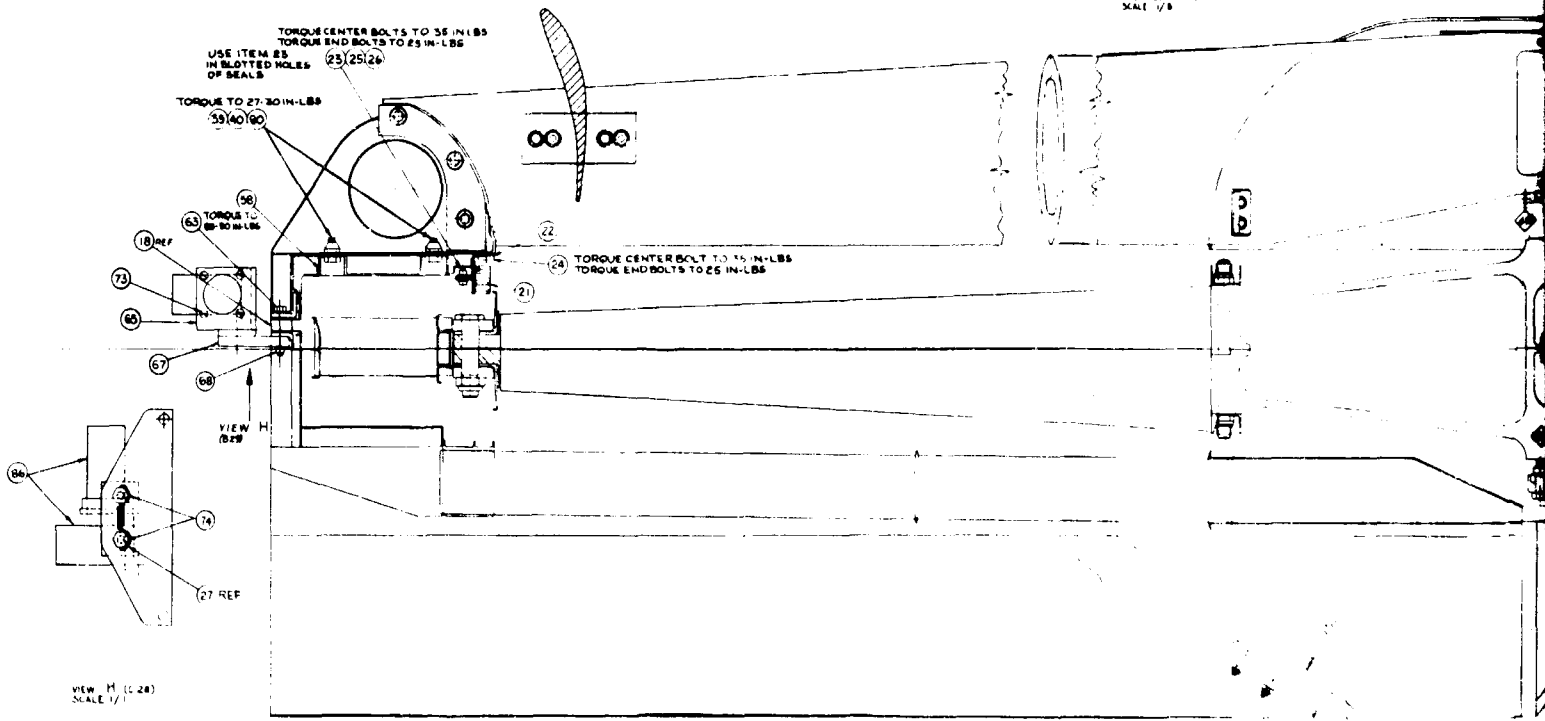
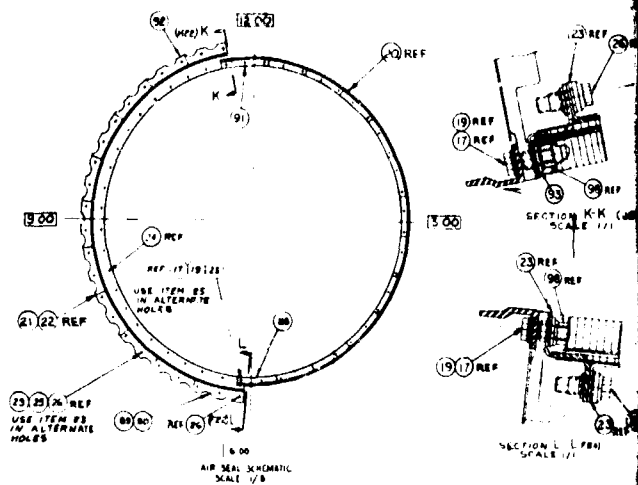
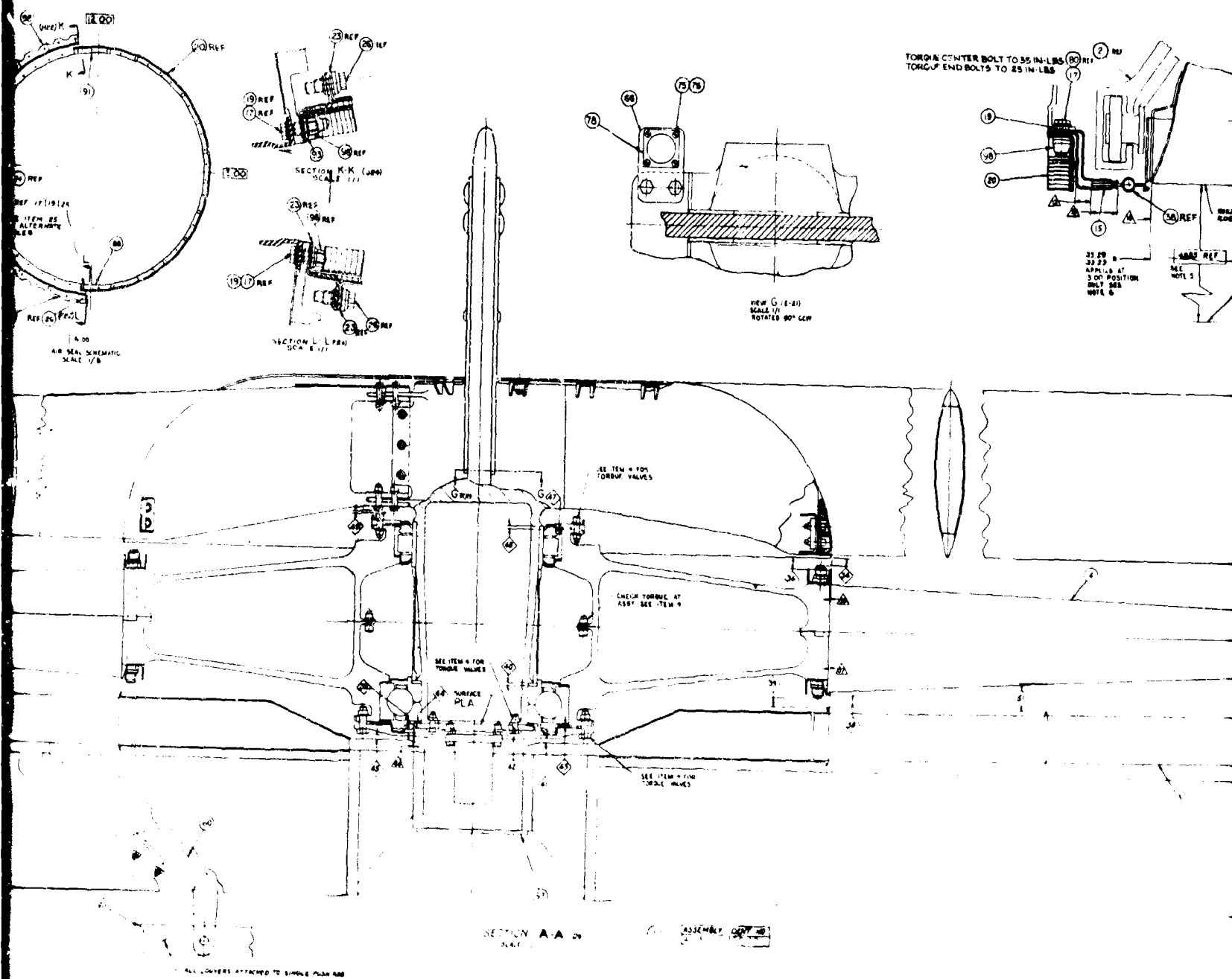
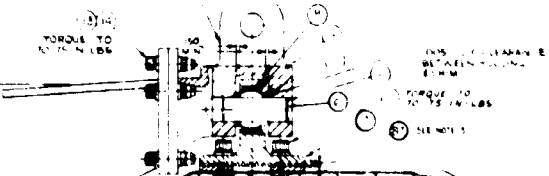
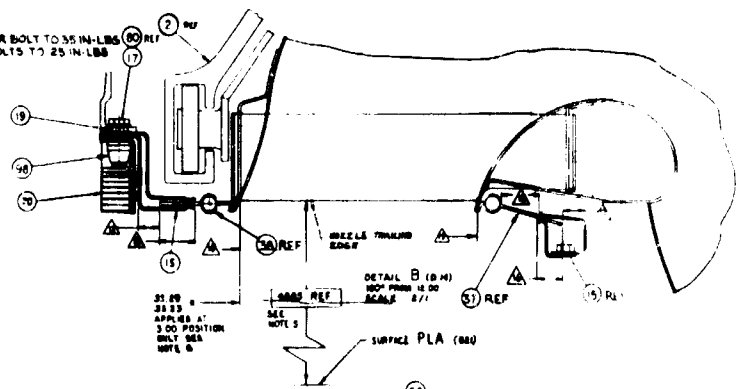


Figure 62. LF2 Fan Assembly (Drawing 4013007-300).



ALL COVERS ATTACHED TO SINGLE PLAN ARE

TORQUE CENTER BOLT TO 35 IN-LBS
TORQUE END BOLTS TO 25 IN-LBS



DETAIL B (0 41)



100



215

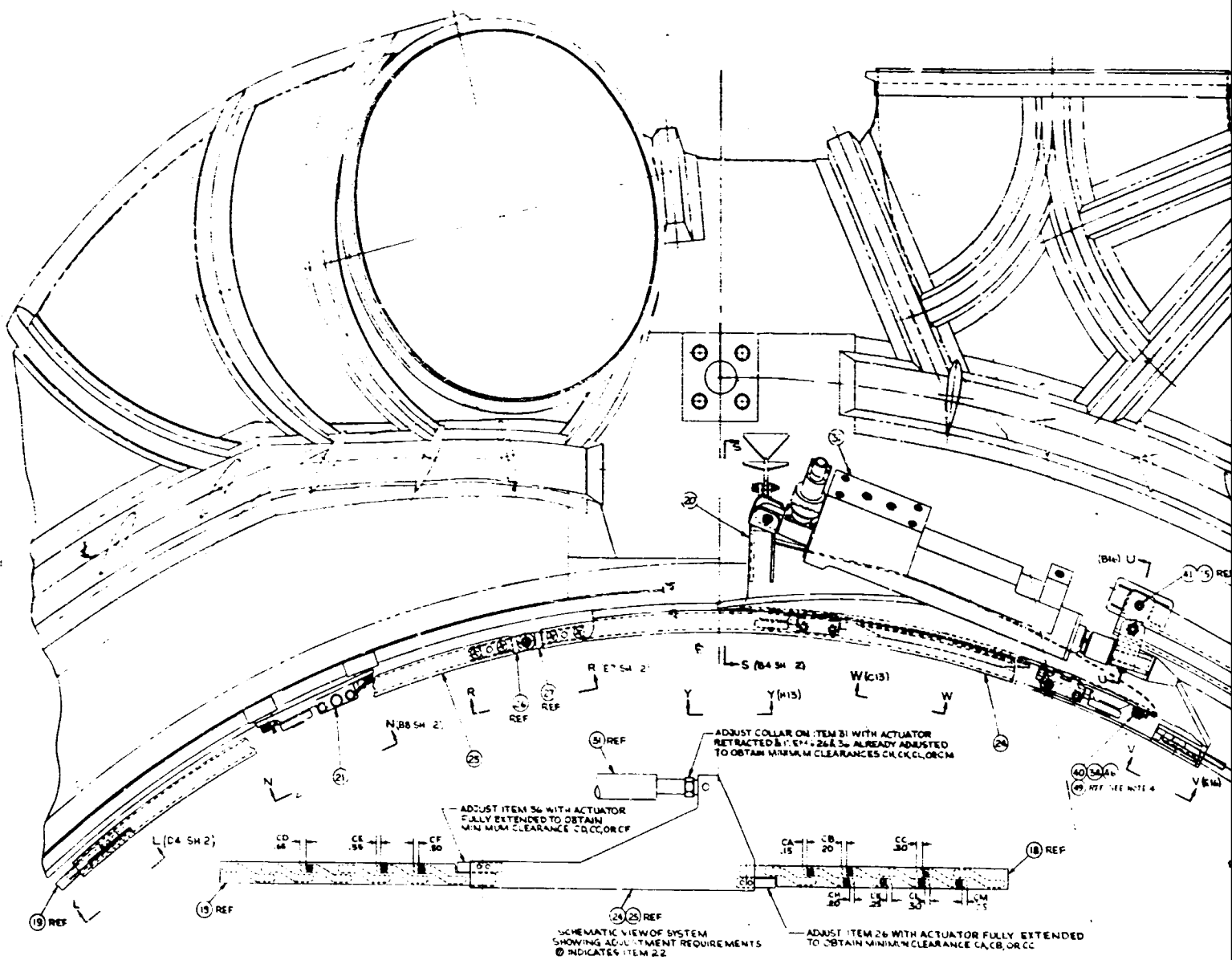
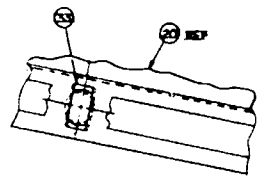
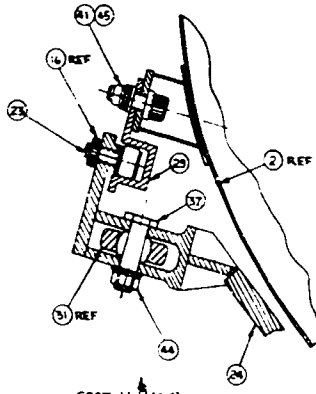
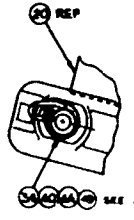
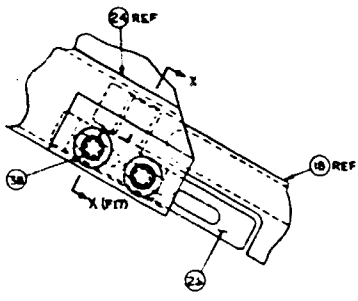
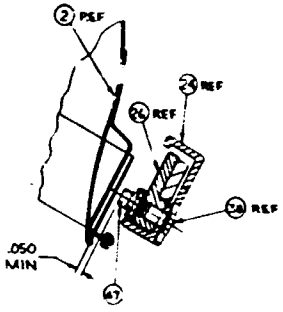
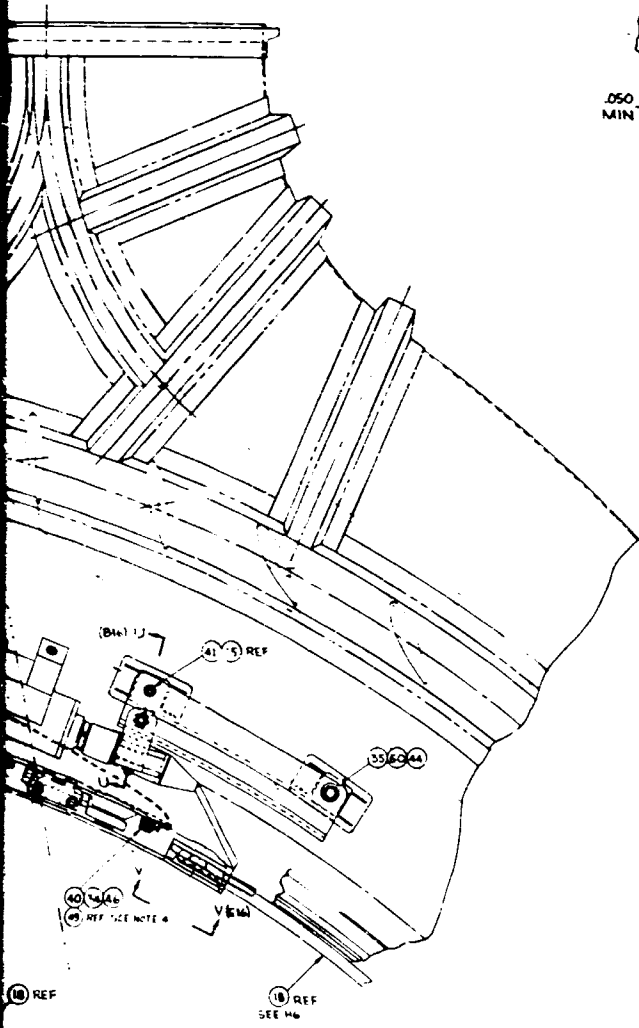


Figure 63. Variable Area Scroll Assembly (Drawing 4013007-450, Sheet 1).



EXTENDED
SC

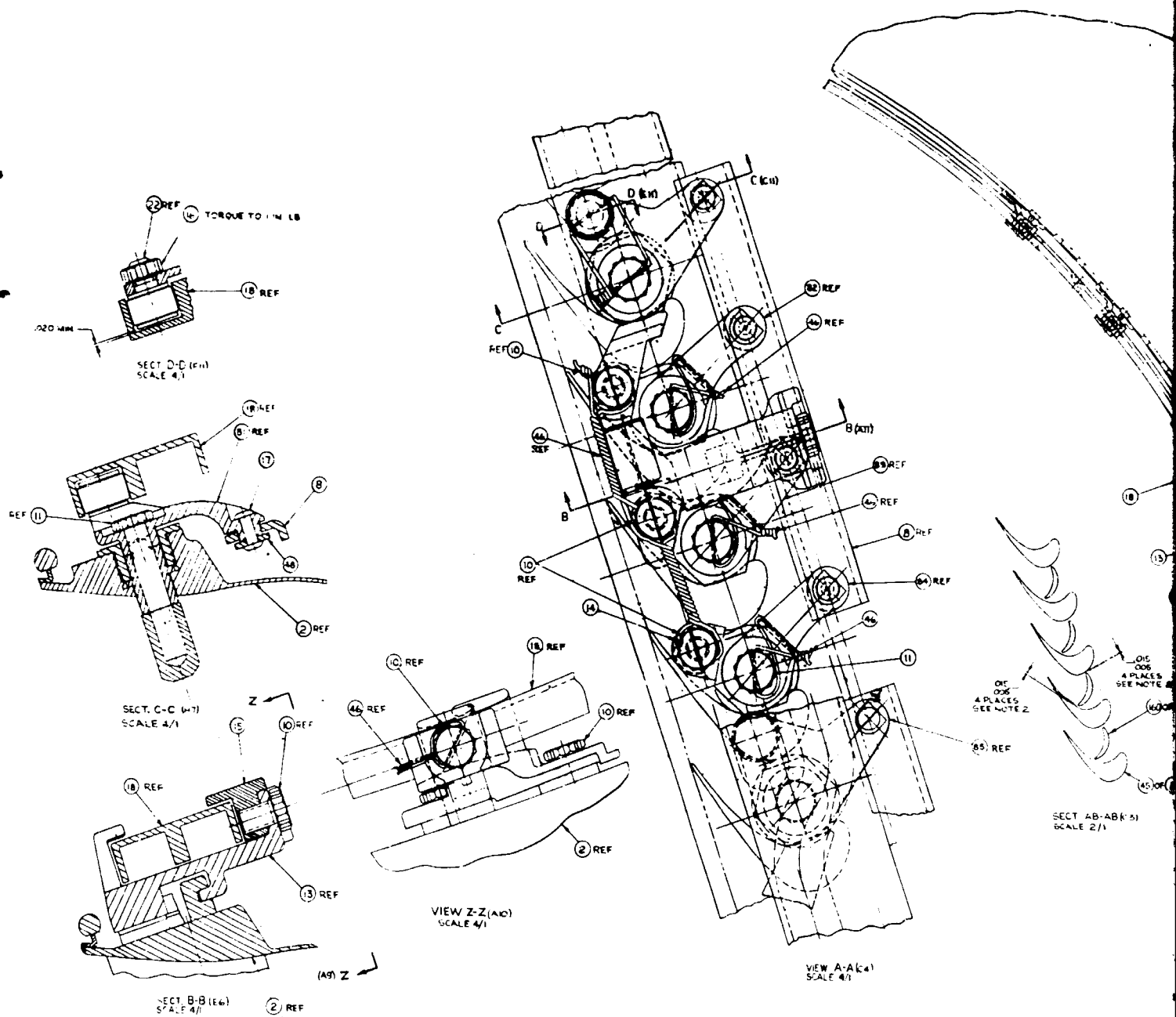
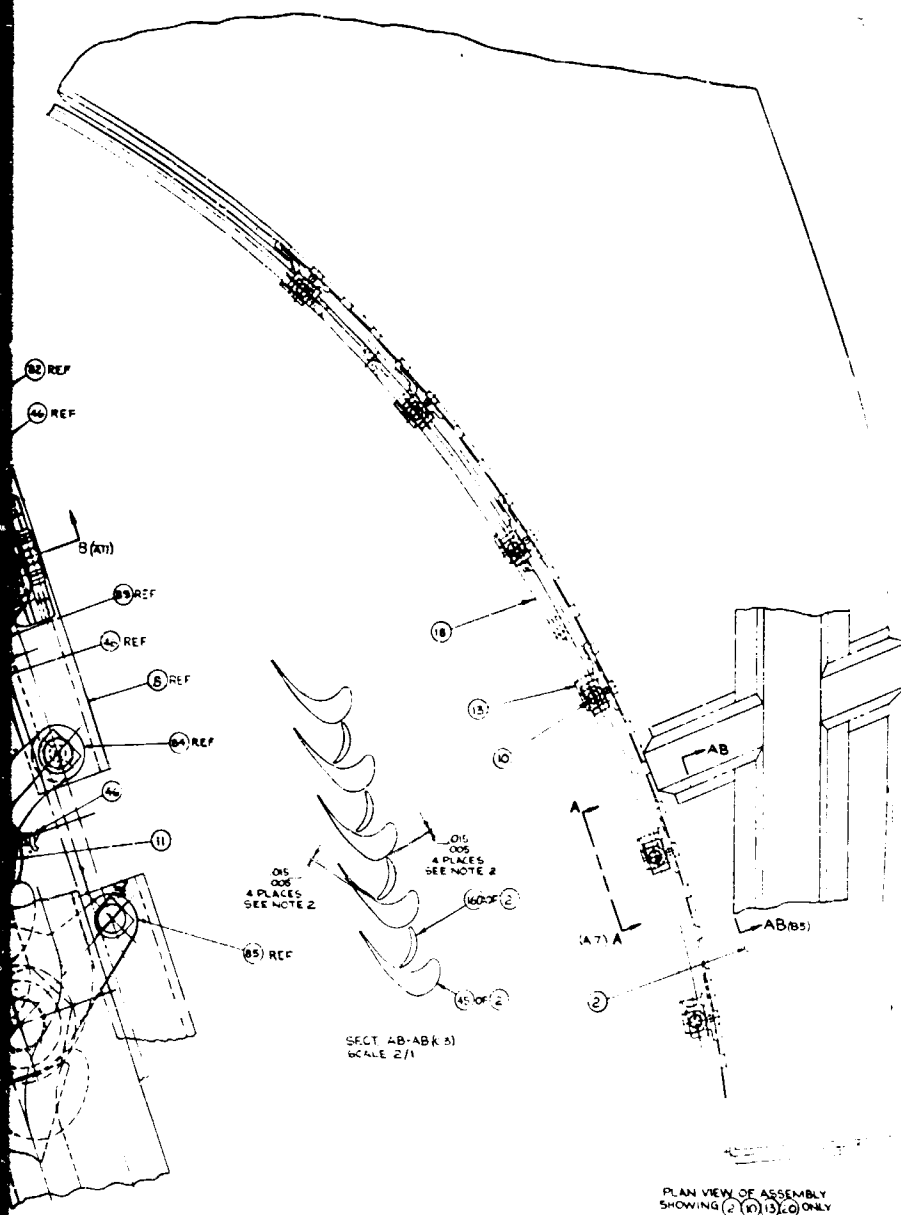


Figure 63. (Cont'd).

A

REVISIONS		DATE	BY	APP
1	17 DEC 68	1968	17	17
2	17 DEC 68	1968	17	17
3	17 DEC 68	1968	17	17
4	17 DEC 68	1968	17	17
5	17 DEC 68	1968	17	17
6	17 DEC 68	1968	17	17
7	17 DEC 68	1968	17	17
8	17 DEC 68	1968	17	17
9	17 DEC 68	1968	17	17
10	17 DEC 68	1968	17	17
11	17 DEC 68	1968	17	17
12	17 DEC 68	1968	17	17
13	17 DEC 68	1968	17	17
14	17 DEC 68	1968	17	17
15	17 DEC 68	1968	17	17
16	17 DEC 68	1968	17	17
17	17 DEC 68	1968	17	17
18	17 DEC 68	1968	17	17
19	17 DEC 68	1968	17	17
20	17 DEC 68	1968	17	17
21	17 DEC 68	1968	17	17
22	17 DEC 68	1968	17	17
23	17 DEC 68	1968	17	17
24	17 DEC 68	1968	17	17
25	17 DEC 68	1968	17	17
26	17 DEC 68	1968	17	17
27	17 DEC 68	1968	17	17
28	17 DEC 68	1968	17	17
29	17 DEC 68	1968	17	17
30	17 DEC 68	1968	17	17
31	17 DEC 68	1968	17	17
32	17 DEC 68	1968	17	17
33	17 DEC 68	1968	17	17
34	17 DEC 68	1968	17	17
35	17 DEC 68	1968	17	17
36	17 DEC 68	1968	17	17
37	17 DEC 68	1968	17	17
38	17 DEC 68	1968	17	17
39	17 DEC 68	1968	17	17
40	17 DEC 68	1968	17	17
41	17 DEC 68	1968	17	17
42	17 DEC 68	1968	17	17
43	17 DEC 68	1968	17	17
44	17 DEC 68	1968	17	17
45	17 DEC 68	1968	17	17
46	17 DEC 68	1968	17	17
47	17 DEC 68	1968	17	17
48	17 DEC 68	1968	17	17
49	17 DEC 68	1968	17	17
50	17 DEC 68	1968	17	17
51	17 DEC 68	1968	17	17
52	17 DEC 68	1968	17	17
53	17 DEC 68	1968	17	17
54	17 DEC 68	1968	17	17
55	17 DEC 68	1968	17	17
56	17 DEC 68	1968	17	17
57	17 DEC 68	1968	17	17
58	17 DEC 68	1968	17	17
59	17 DEC 68	1968	17	17
60	17 DEC 68	1968	17	17
61	17 DEC 68	1968	17	17
62	17 DEC 68	1968	17	17
63	17 DEC 68	1968	17	17
64	17 DEC 68	1968	17	17
65	17 DEC 68	1968	17	17
66	17 DEC 68	1968	17	17
67	17 DEC 68	1968	17	17
68	17 DEC 68	1968	17	17
69	17 DEC 68	1968	17	17
70	17 DEC 68	1968	17	17
71	17 DEC 68	1968	17	17
72	17 DEC 68	1968	17	17
73	17 DEC 68	1968	17	17
74	17 DEC 68	1968	17	17
75	17 DEC 68	1968	17	17
76	17 DEC 68	1968	17	17
77	17 DEC 68	1968	17	17
78	17 DEC 68	1968	17	17
79	17 DEC 68	1968	17	17
80	17 DEC 68	1968	17	17
81	17 DEC 68	1968	17	17
82	17 DEC 68	1968	17	17
83	17 DEC 68	1968	17	17
84	17 DEC 68	1968	17	17
85	17 DEC 68	1968	17	17
86	17 DEC 68	1968	17	17
87	17 DEC 68	1968	17	17
88	17 DEC 68	1968	17	17
89	17 DEC 68	1968	17	17
90	17 DEC 68	1968	17	17
91	17 DEC 68	1968	17	17
92	17 DEC 68	1968	17	17
93	17 DEC 68	1968	17	17
94	17 DEC 68	1968	17	17
95	17 DEC 68	1968	17	17
96	17 DEC 68	1968	17	17
97	17 DEC 68	1968	17	17
98	17 DEC 68	1968	17	17
99	17 DEC 68	1968	17	17
100	17 DEC 68	1968	17	17



5. ITEMS 11, 22, 40, 38, THREADS TO BE COATED WITH "REL-PRO" LUBRICANT (C.F. 800)
4. USE WASHER ITEM 49 BETWEEN BUSHING ITEM 34 & BOLT HEAD ITEM 40
3. WITH THE BELL CRANK ENGAGED IN ITEM 19, ROTATED TO "MAX CCW POSITION" 0.05 MIN CLEARANCE MUST EXIST BETWEEN THE LEADING EDGE & TRAILING EDGE OF WARE WITH THE NOZZLE POSITION A WITH THE LEVER ATTACHED TO THE BELL CRANK. USAB ITEM 9. THE SAME CONDITIONS MUST BE MET
2. WITH THE BELL CRANK ENGAGED IN ITEM 19, ROTATED TO "MAX CCW POSITION" 0.05 MIN CLEARANCE MUST EXIST BETWEEN THE LEADING EDGE & TRAILING EDGE OF THE VANE WITH THE NOZZLE POSITION A WITH THE LEVER ATTACHED TO THE BELL CRANK. USAB ITEM 9. THE SAME CONDITIONS MUST BE MET
1. MUST CONFORM TO:
 - 5/ 212-000 (INTERPRETATION OF DWG)
 - P25T1 (FORMED RIVETS)
 - AS567 (LOCKWIRE)
 - P12F2 (TORQUE SPEC)

ASSEMBLY		GENERAL ELECTRIC	
DATE	17 DEC 68	BY	17
APP	17	APP	17
VARIABLE AREA		SCROLL ASSEMBLY	
ITEM NO.	07482	ITEM NO.	4013007-450
REV	1	REV	1

B

[illegible]

C

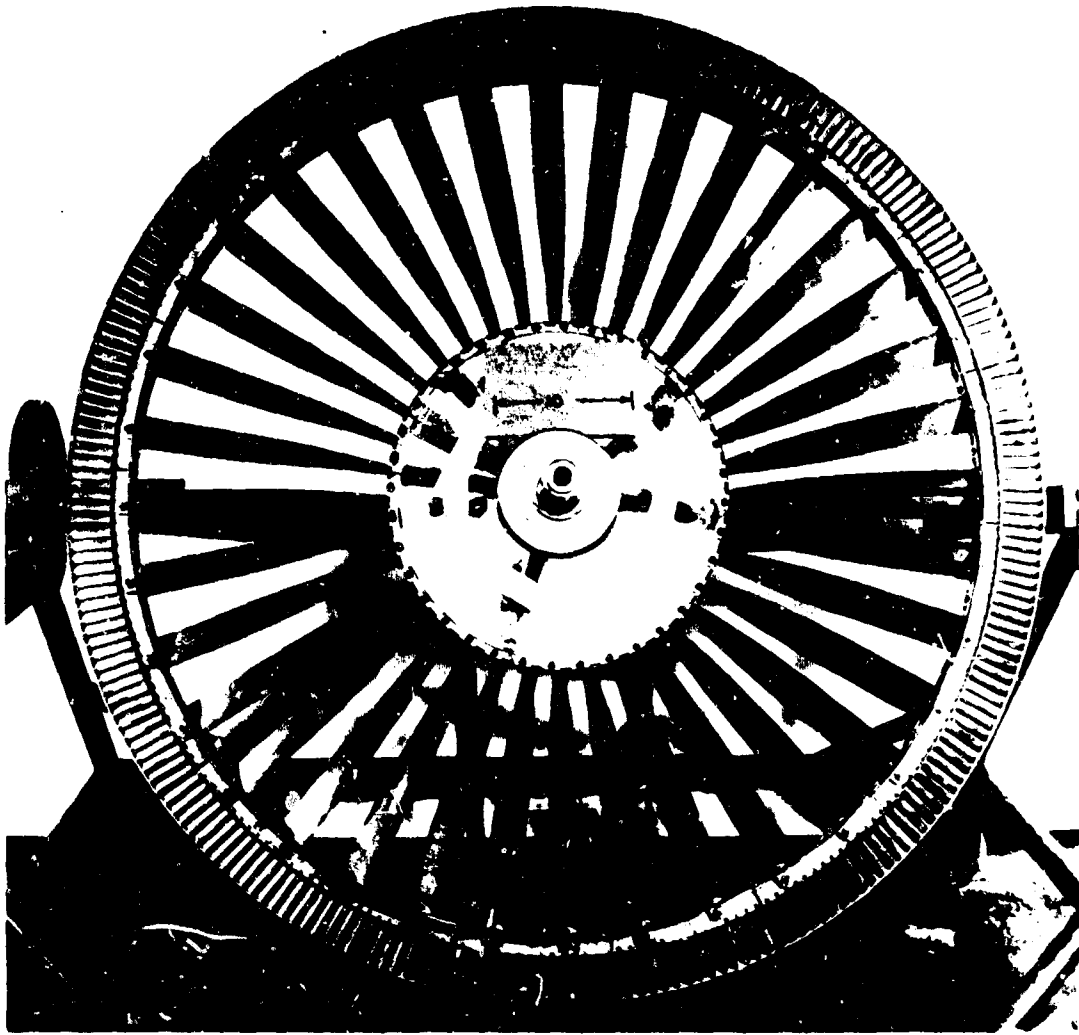


Figure 65. Photograph of LF2 Rotor Assembly.

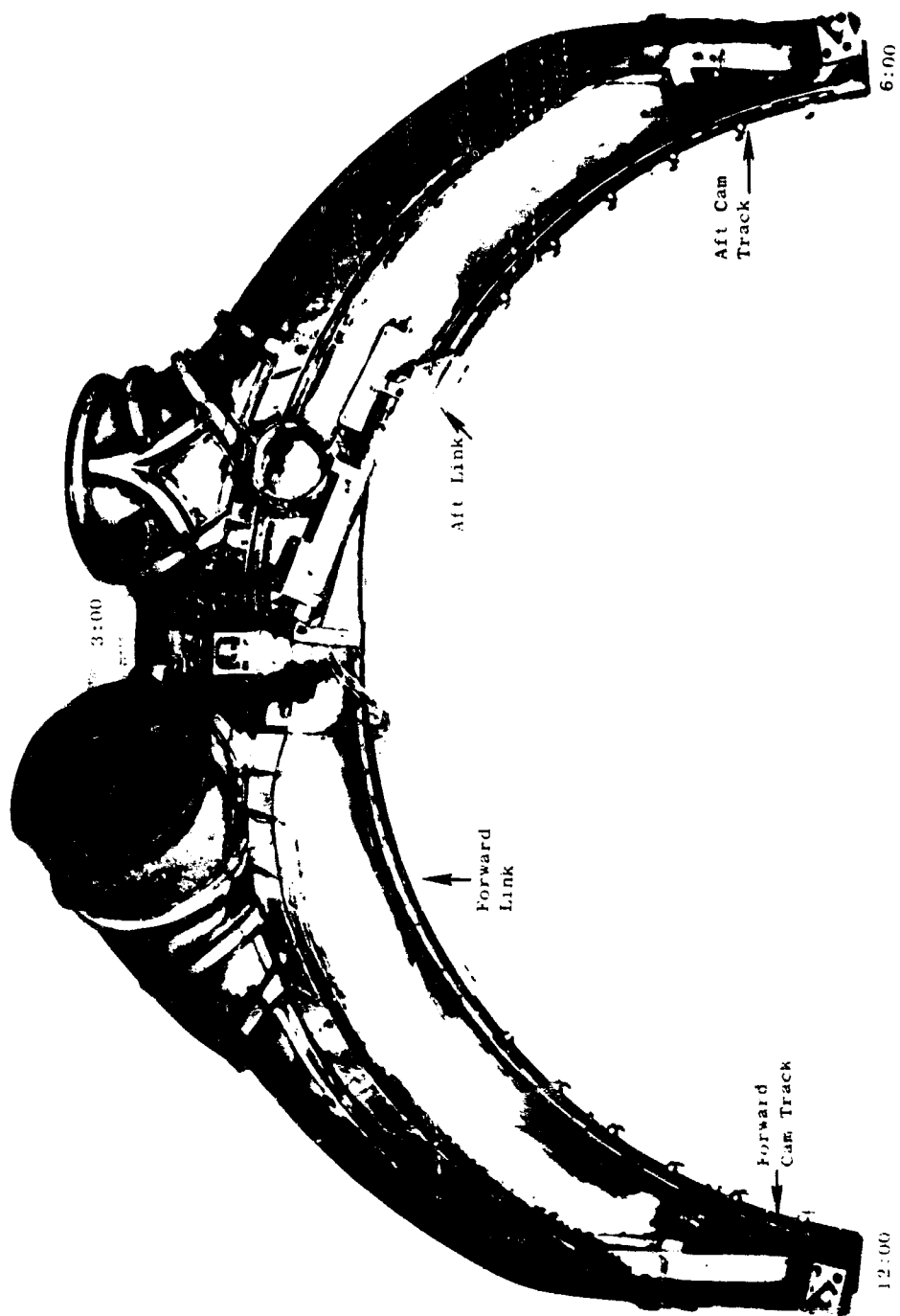


Figure 66. Top View of Variable Area Scroll Assembly.

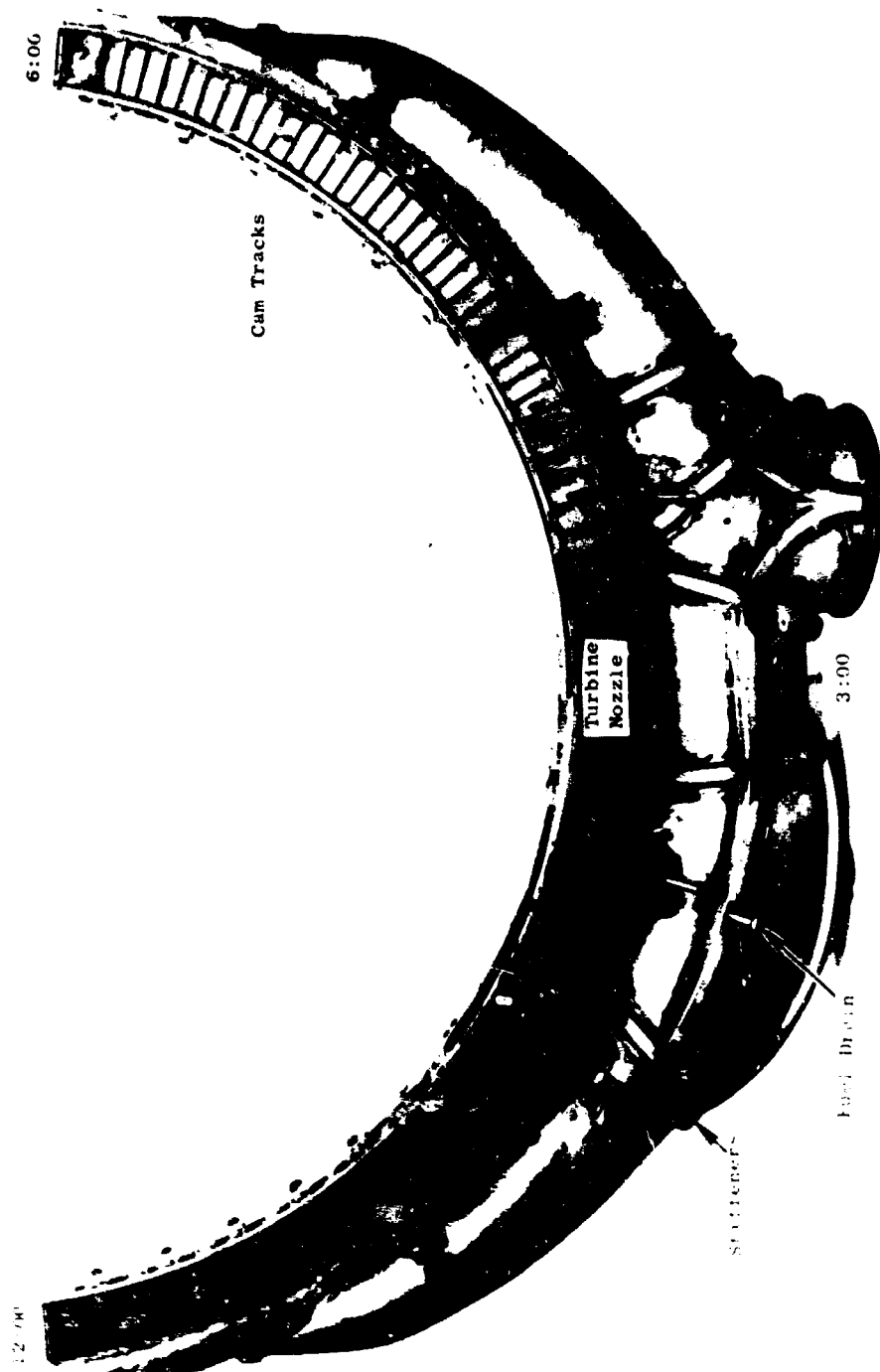
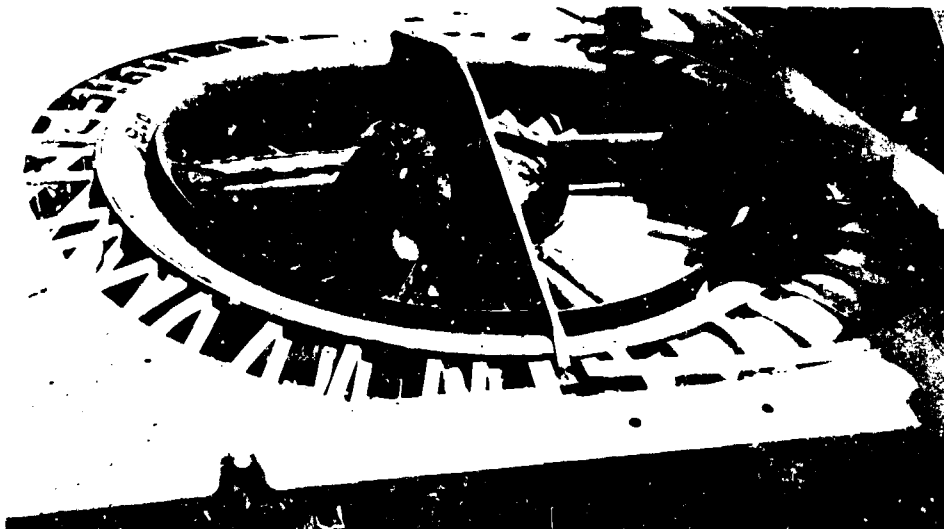


Figure 67. Bottom View of Variable Area Scroll Assembly.



a. Top View of Fan.



b. View Looking at Bottom of Fan.

Figure 68 Photograph of LF2/VAS Assembly Installed in Test Facility.

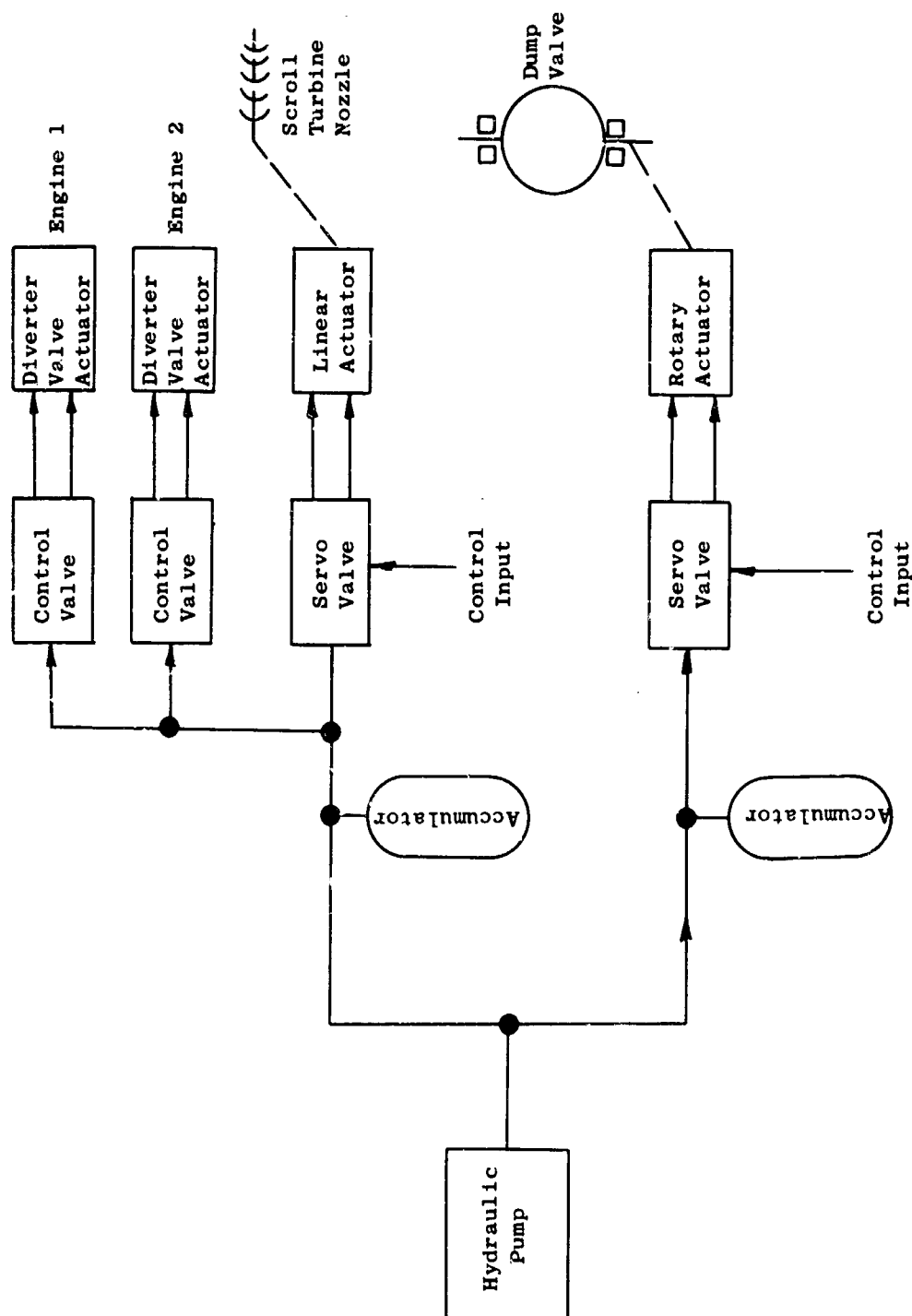


Figure 69. Hydraulic System Block Diagram.

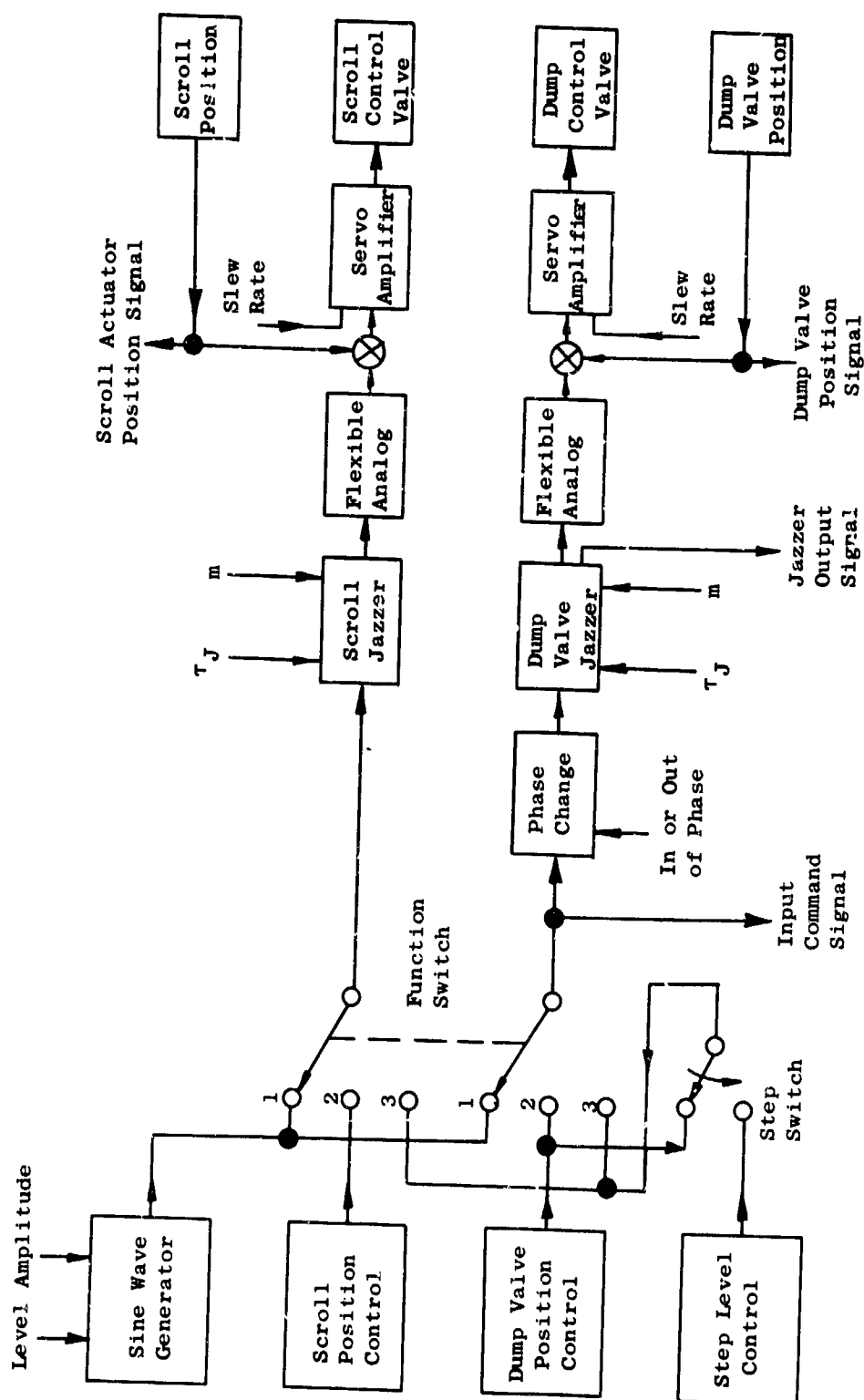


Figure 70. Control System Block Diagram.

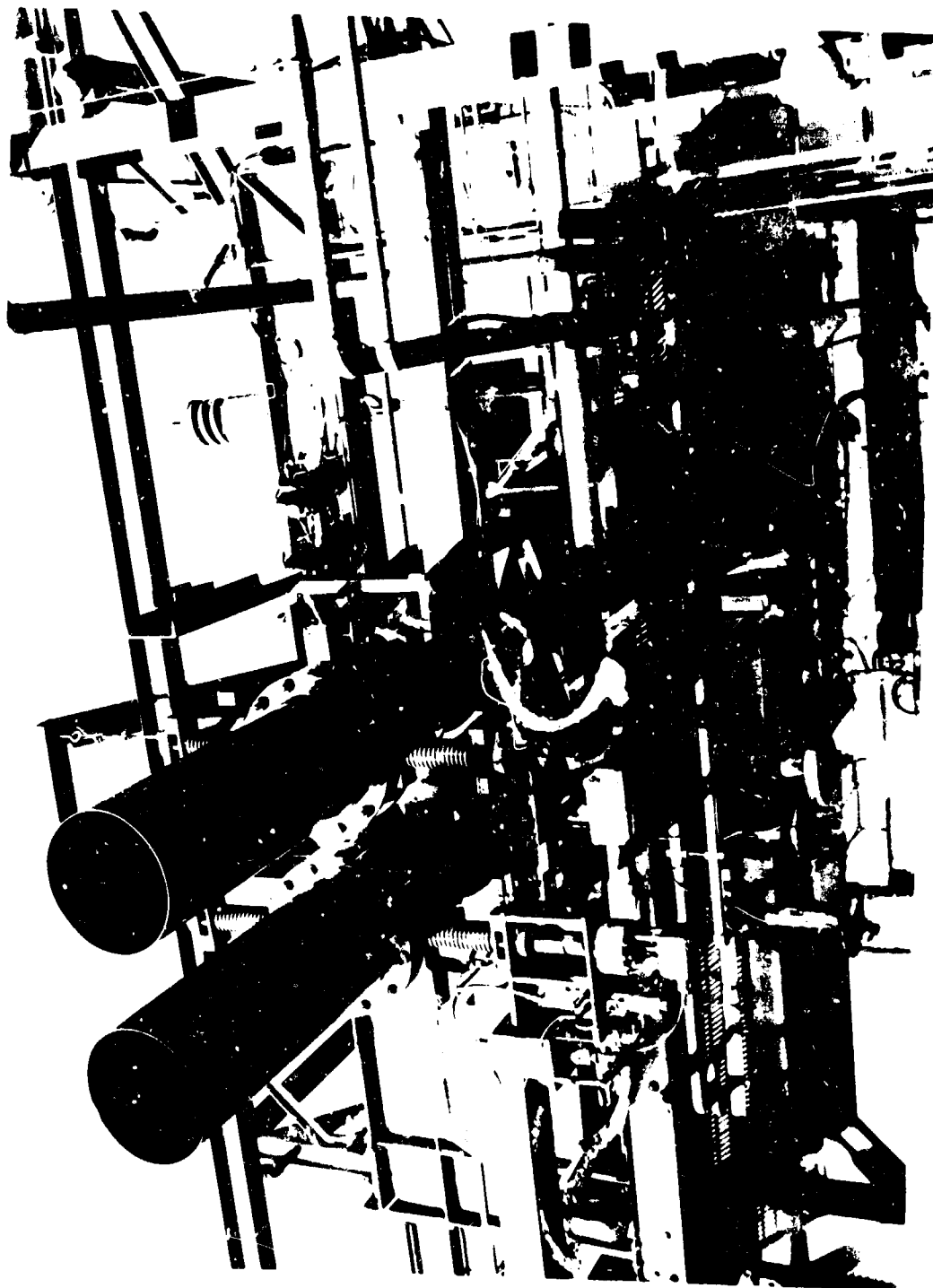
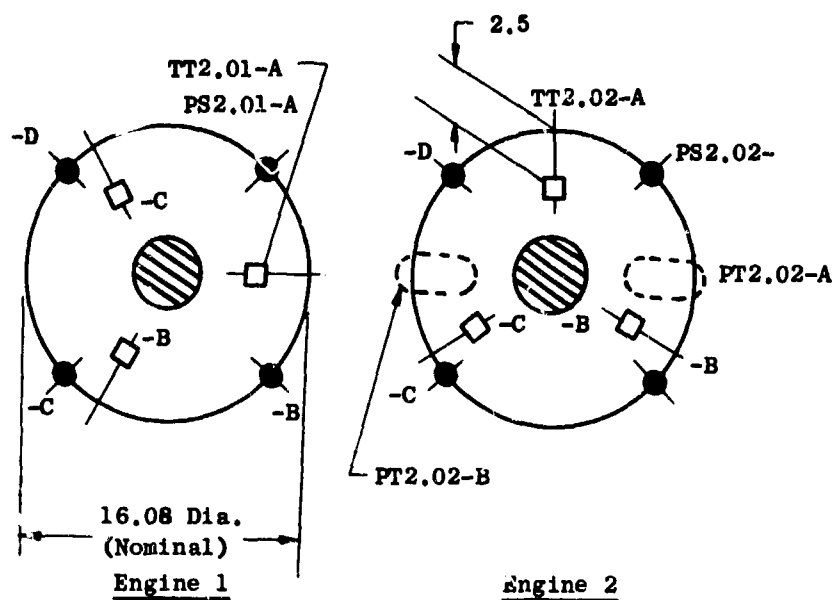


Figure 71. Photograph of Overboard Dump Valve System.



Note: View shown looking upstream.

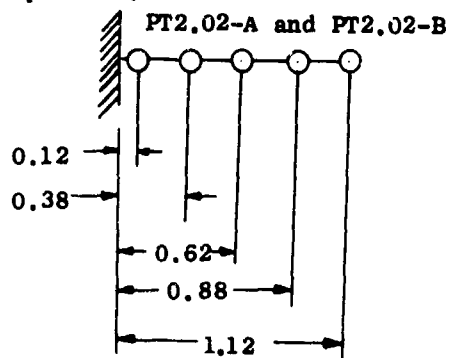


Figure 72. Core Engine Inlet Instrumentation - Station 2.0.

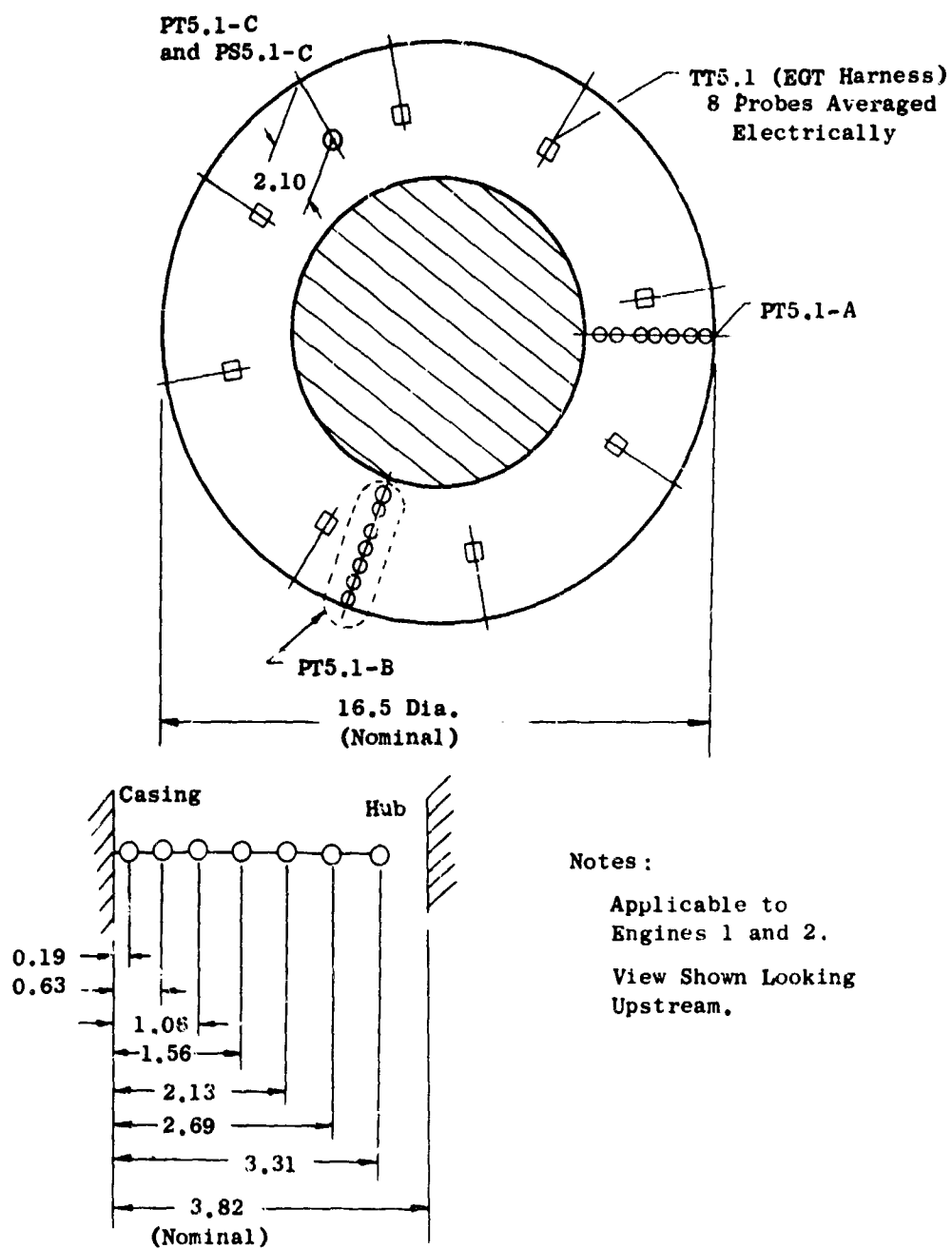
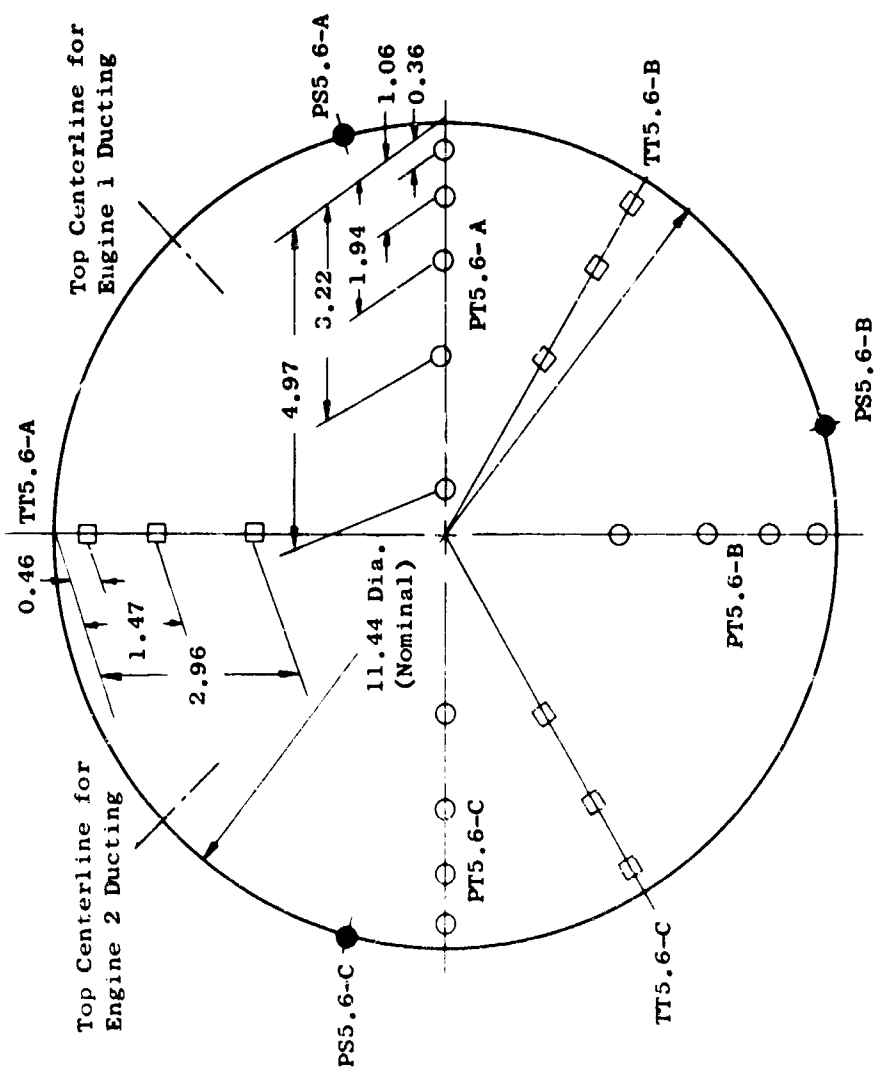
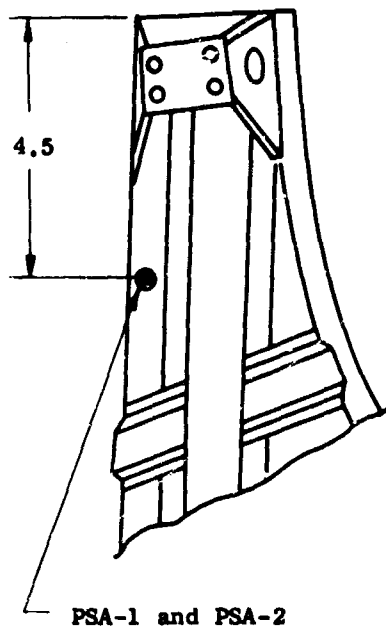


Figure 73. Core Engine Turbine Discharge Instrumentation - Station 5.1.



Notes:
 Instrumentation as Shown Applicable to Both Engine Ducting Systems.
 View Shown Looking Upstream.

Figure 75. Overboard Dump Ducting Instrumentation - Station 5.6.



Notes:

PSA-1 and PSA-2 are Scroll Internal Static Pressure Taps.

PSA-1 Located at 12 o'clock Position on Scroll and
PSA-2 Located at 6 o'clock Position.

Figure 76. Scroll Duct Static Pressure Instrumentation.

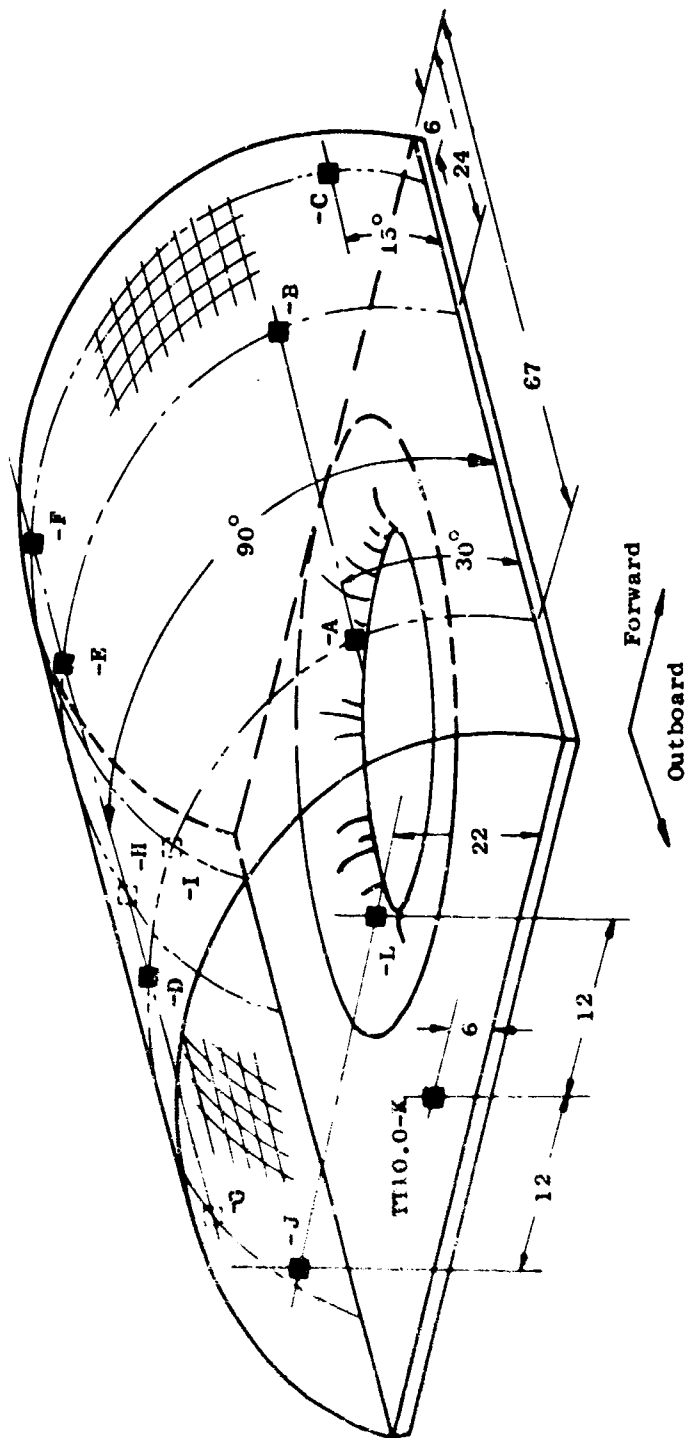
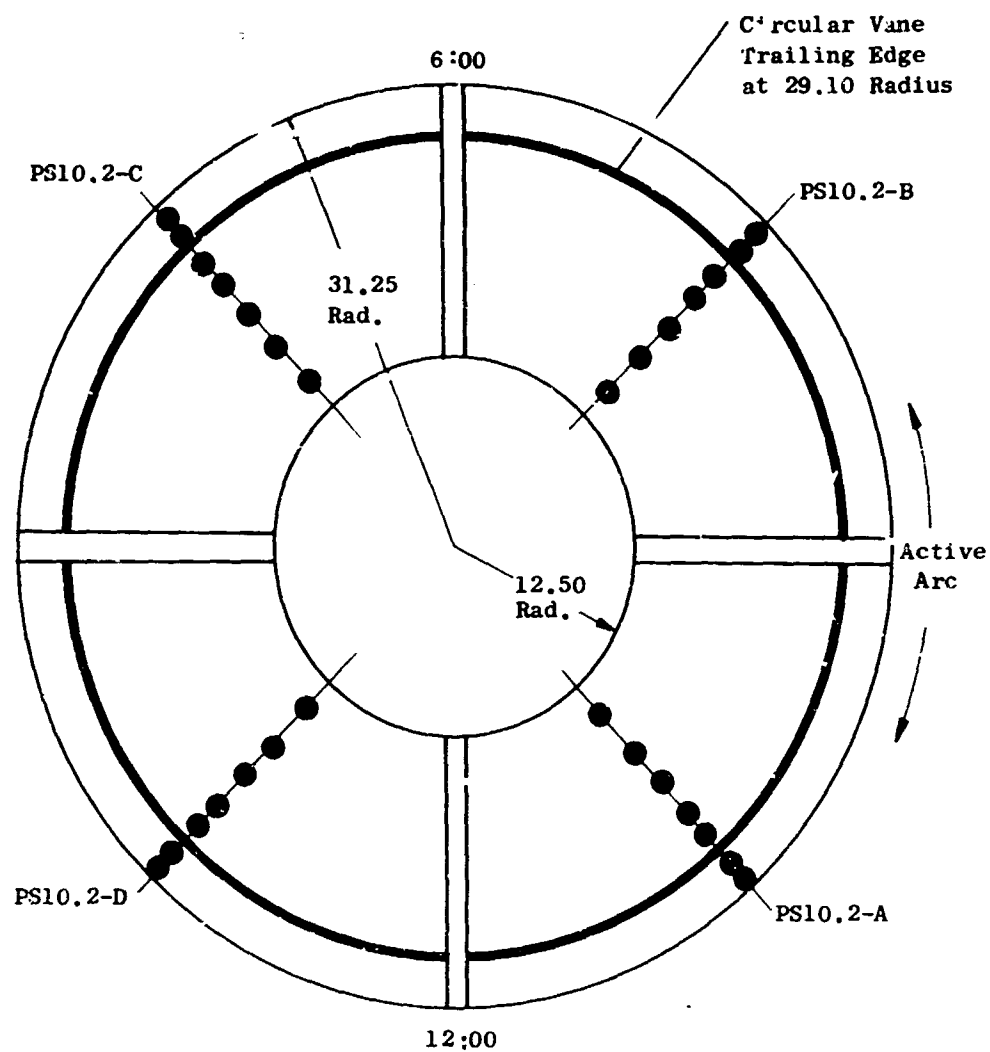


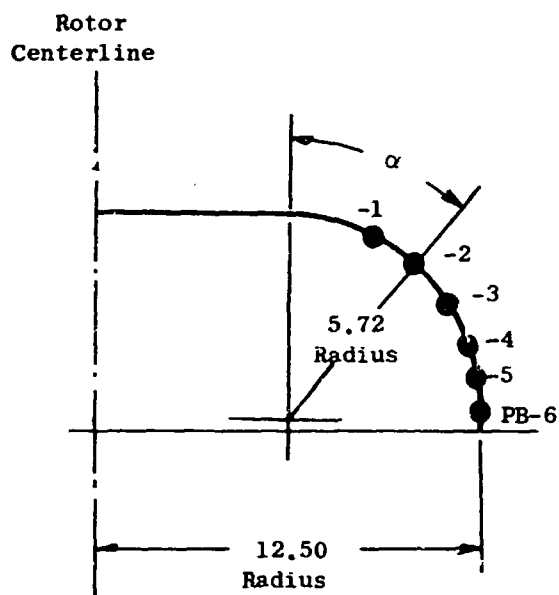
Figure 77. Fan Inlet Screen Instrumentation - Station 10.0.



Note: View Shown Looking Upstream.

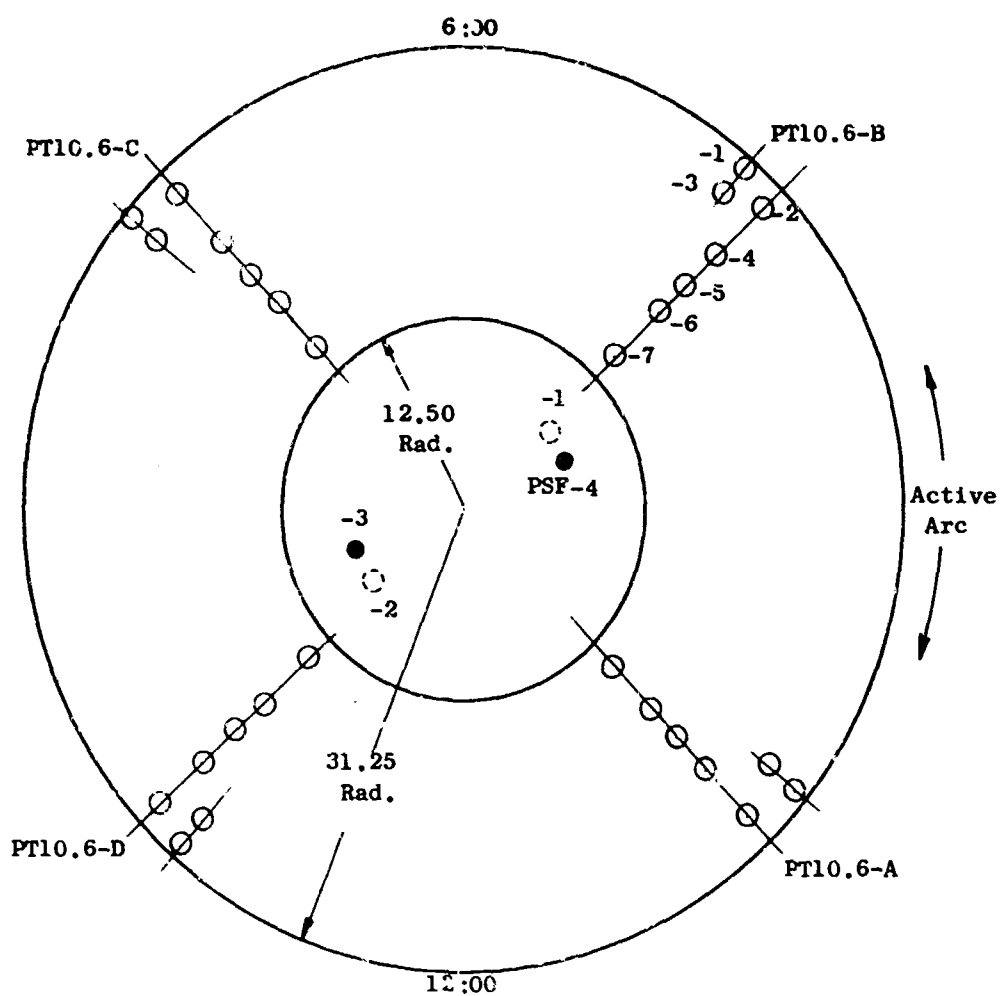
Rake	-1	-2	-3	-4	-5	-6	-7
-A	0.50	1.25	4.25	6.12	8.69	12.75	16.75
-B	0.50	1.12	3.88	6.00	8.81	12.25	17.06
-C	0.69	1.38	3.38	5.88	8.63	12.63	16.38
-D	0.50	1.25	3.63	5.06	8.56	12.44	16.38

Figure 78. Fan Inlet Instrumentation - Station 10.2.



<u>Pressure</u>	<u>α, Degrees</u>	<u>Radius, Inches</u>
-1	25	8.64
-2	40	11.14
-3	55	12.33
-4	67.5	13.04
-5	77.5	12.40
-6	87.5	12.50

Figure 79. Fan Bullethead Pressure Instrumentation.



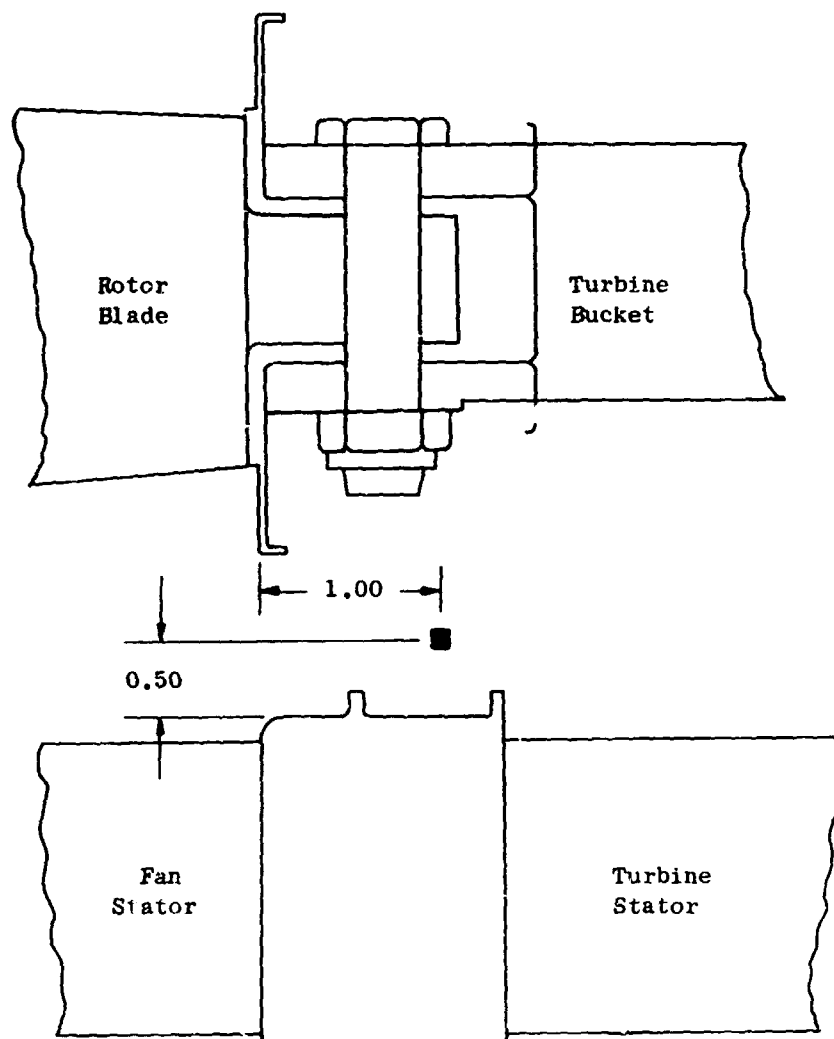
Notes:

View Shown Looking Upstream.

PSF-1 and PSF-2 are on Upper Surface of Hub. PSF-3 and PSF-4 are on Lower Surface.

Rake	-1	-2	-3	-4	-5	-6	-7
-A	29.8	28.7	-	25.0	21.6	18.6	14.9
-B	30.0	28.8	27.9	24.8	21.4	18.6	14.7
-C	29.7	28.4	-	24.8	21.4	18.8	14.9
-D	30.0	28.3	28.0	24.8	21.4	18.8	15.0

Figure 80. Rotor Discharge Pressure Instrumentation - Station 10.6.



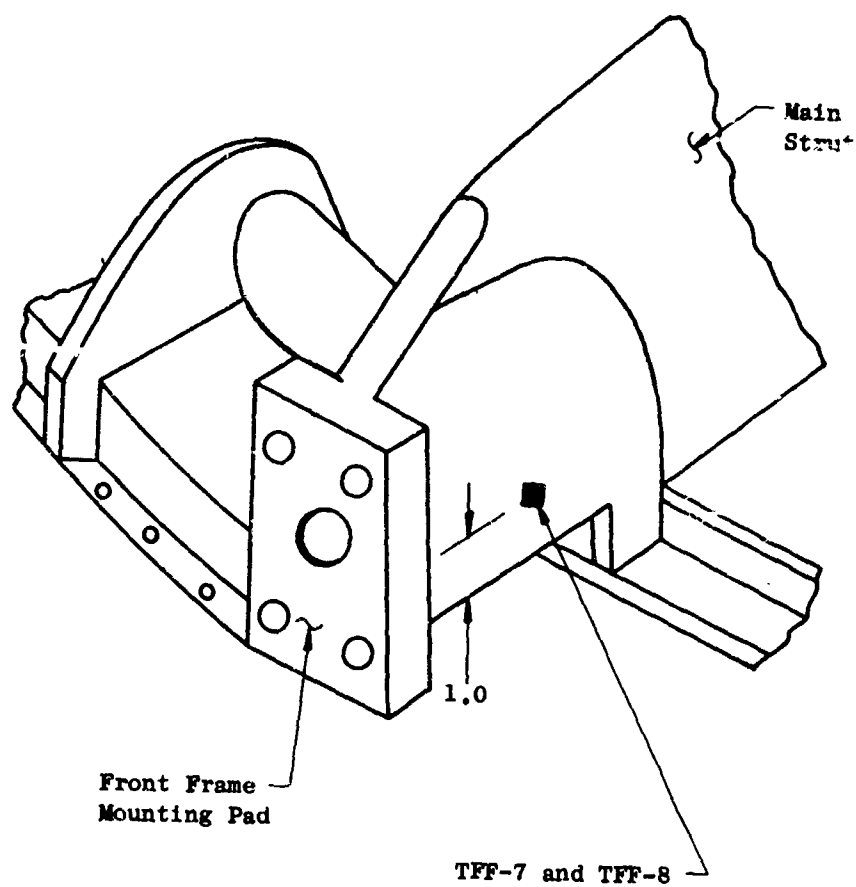
Notes:

TS-1 located at 90 degree position measured clockwise looking downstream.

TS-2 located at 210 degree position.

TS-3 located at 330 degree position.

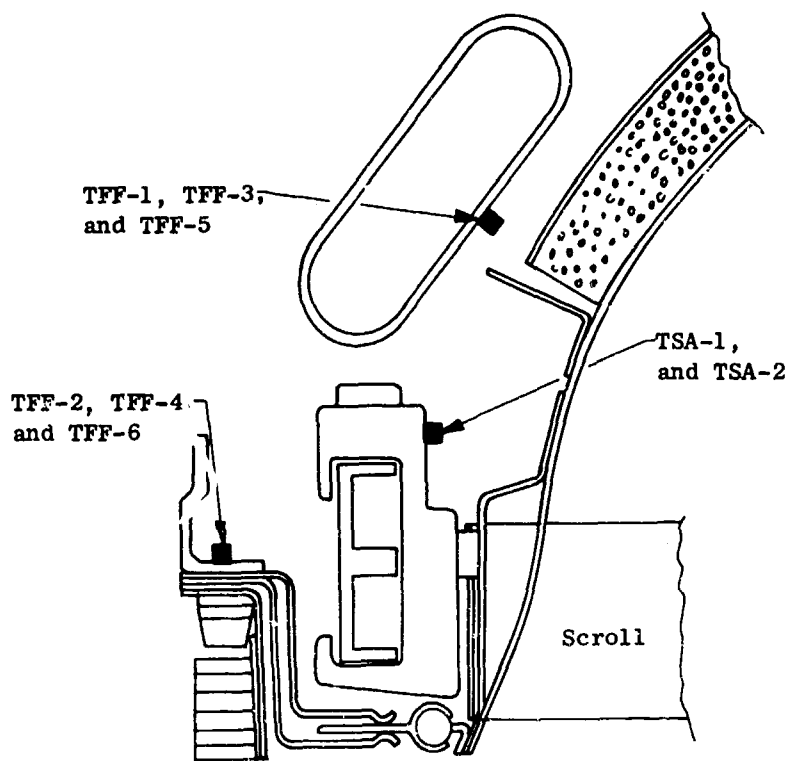
Figure 81. Seal Temperature Instrumentation Location.



Notes:

TFF-7 and TFF-8 are located as shown on the 12 o'clock and 6 o'clock mount positions, respectively.

Figure 82. Front Frame Main Strut Temperature Instrumentation,



Notes:

TFF-1 and TFF-2 are located at 30 degrees from 12 o'clock position (looking down on fan inlet).

TFF-3 and TFF-4 are located at 100 degrees.

TFF-5 and TFF-6 are located at 150 degrees.

TSA-1 and TSA-2 are located on cam track brackets at 20 degrees and 160 degrees, respectively.

Figure 83. Front Frame and Actuation Structure Temperature Instrumentation.

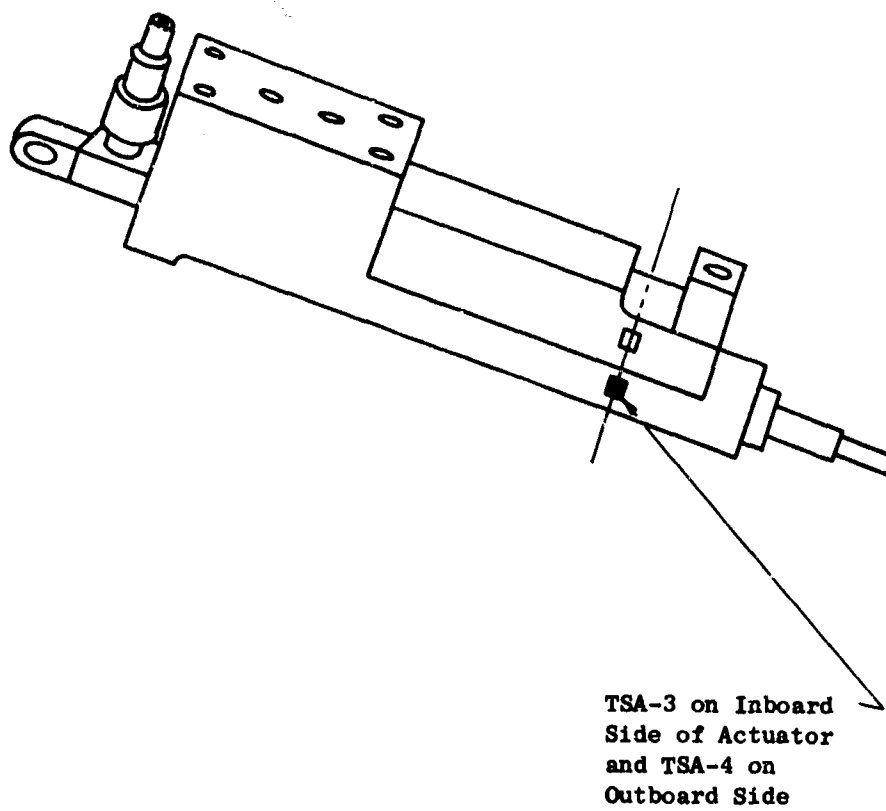
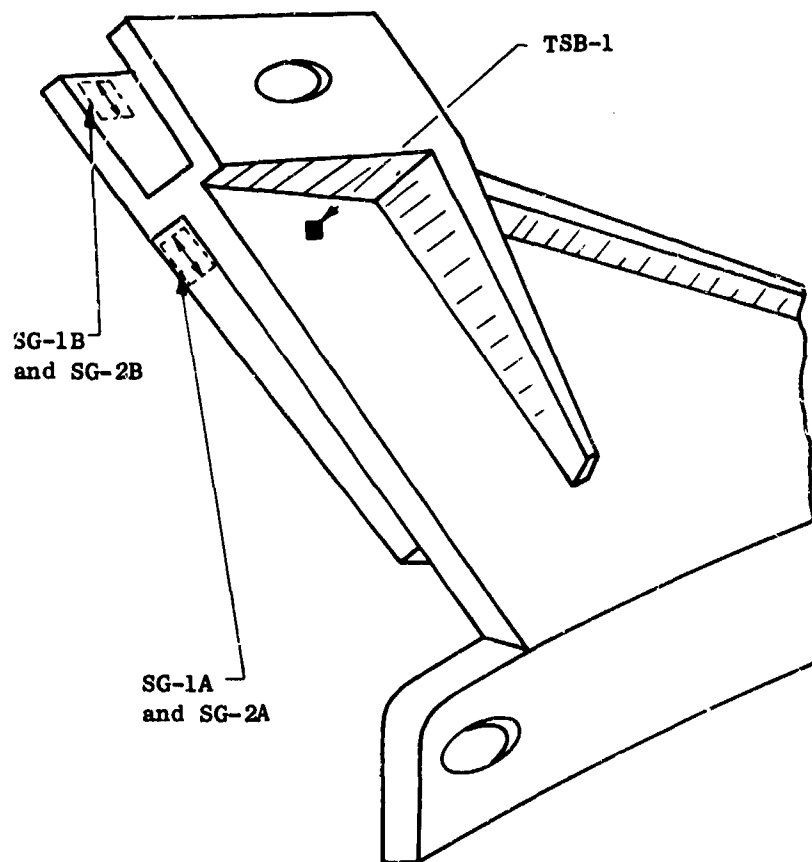


Figure 84. Variable Area Scroll Actuator Temperatures.



Notes :

SG-1A and SG-1B are located as shown.

SG-2A and SG-2B are located on opposite sides of structure.

SG-1A and SG-2A are active gages and SG-1B and SG-2B are temperature compensating gages.

Figure 85. Scroll Actuator Bracket Instrumentation.

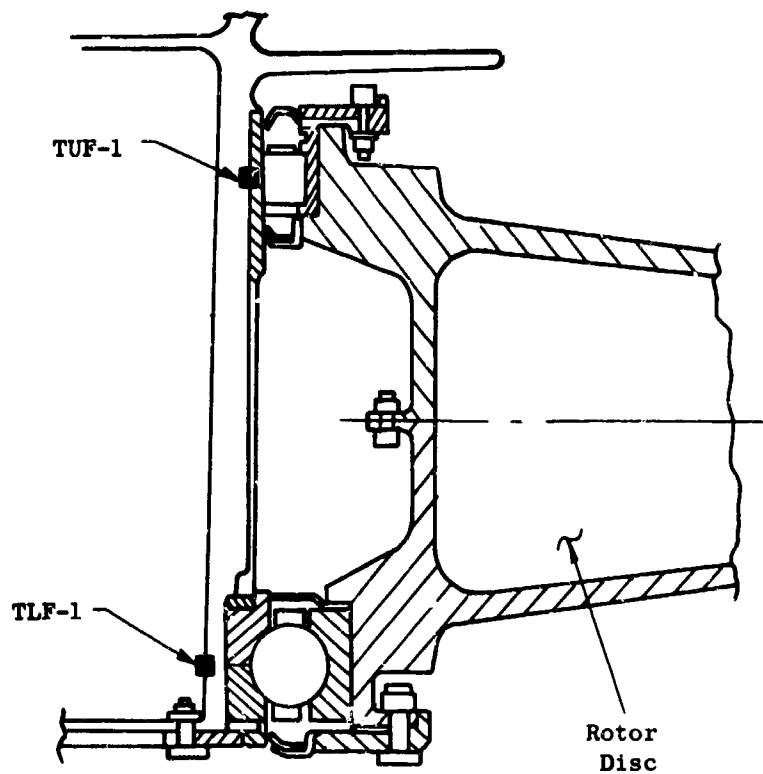


Figure 86. Fan Bearing Temperature Instrumentation.

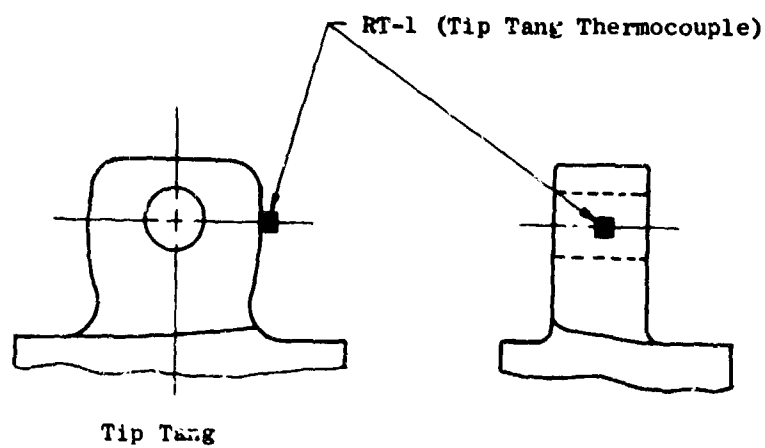
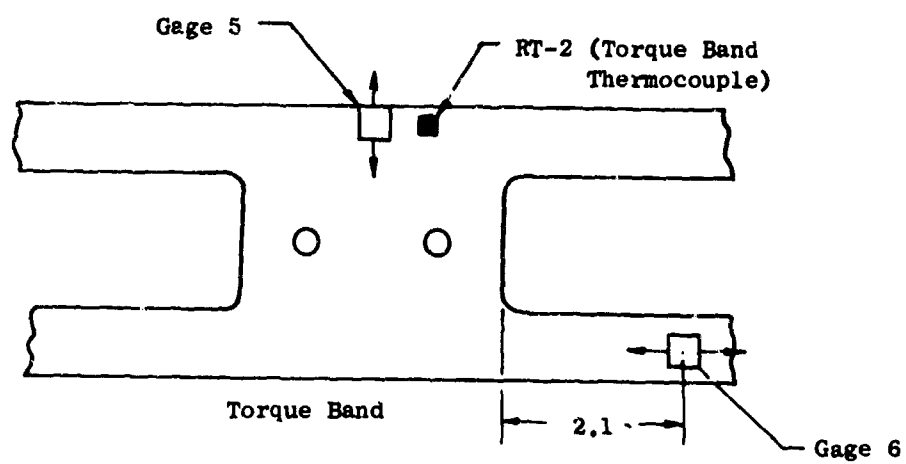
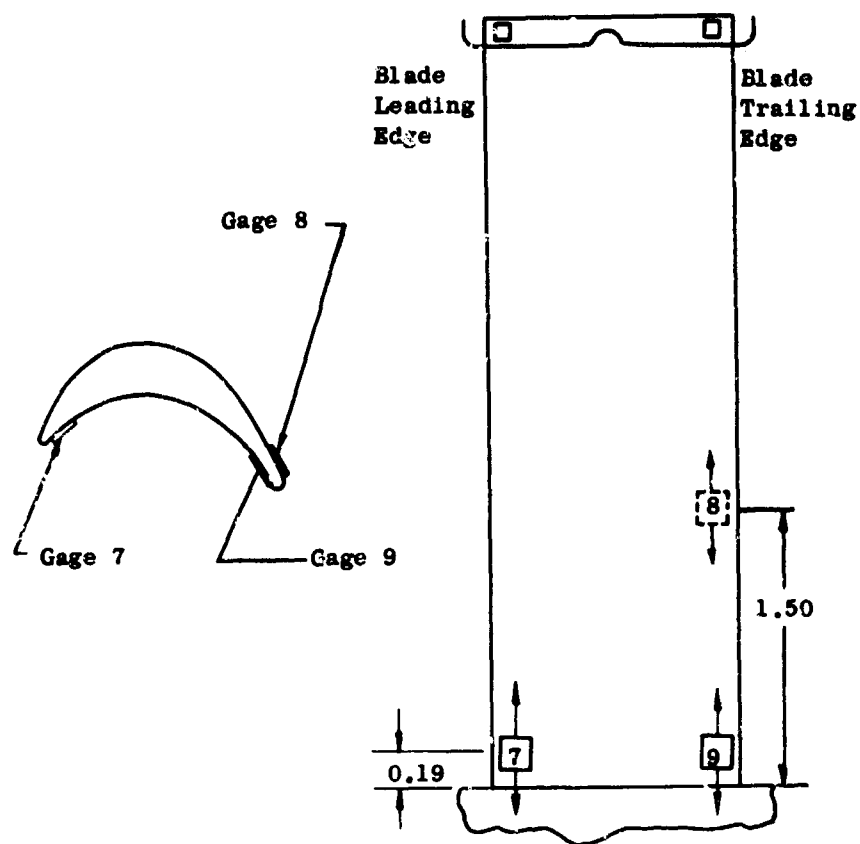
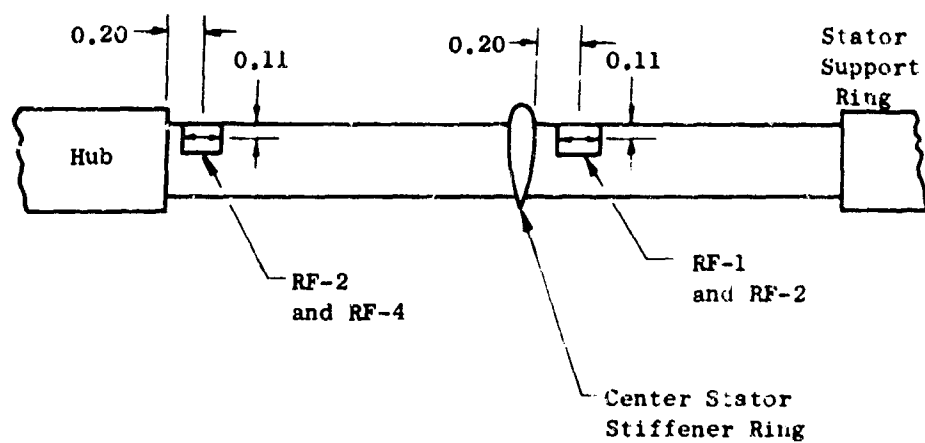


Figure 87. Torque Band and Tip Tang Instrumentation.



Note: Bucket thermocouple (RT-3) is located at the gage 7 location.

Figure 88. Turbine Bucket Instrumentation Location.



Notes:

Gages RF-1 and RF-2 are located at 3 o'clock position on fan looking downstream (vane 22).

Gages RF-3 and RF-4 are located at 9 o'clock position on fan looking downstream (vane 66).

Figure 89. Rear Frame Strain Gage Instrumentation.

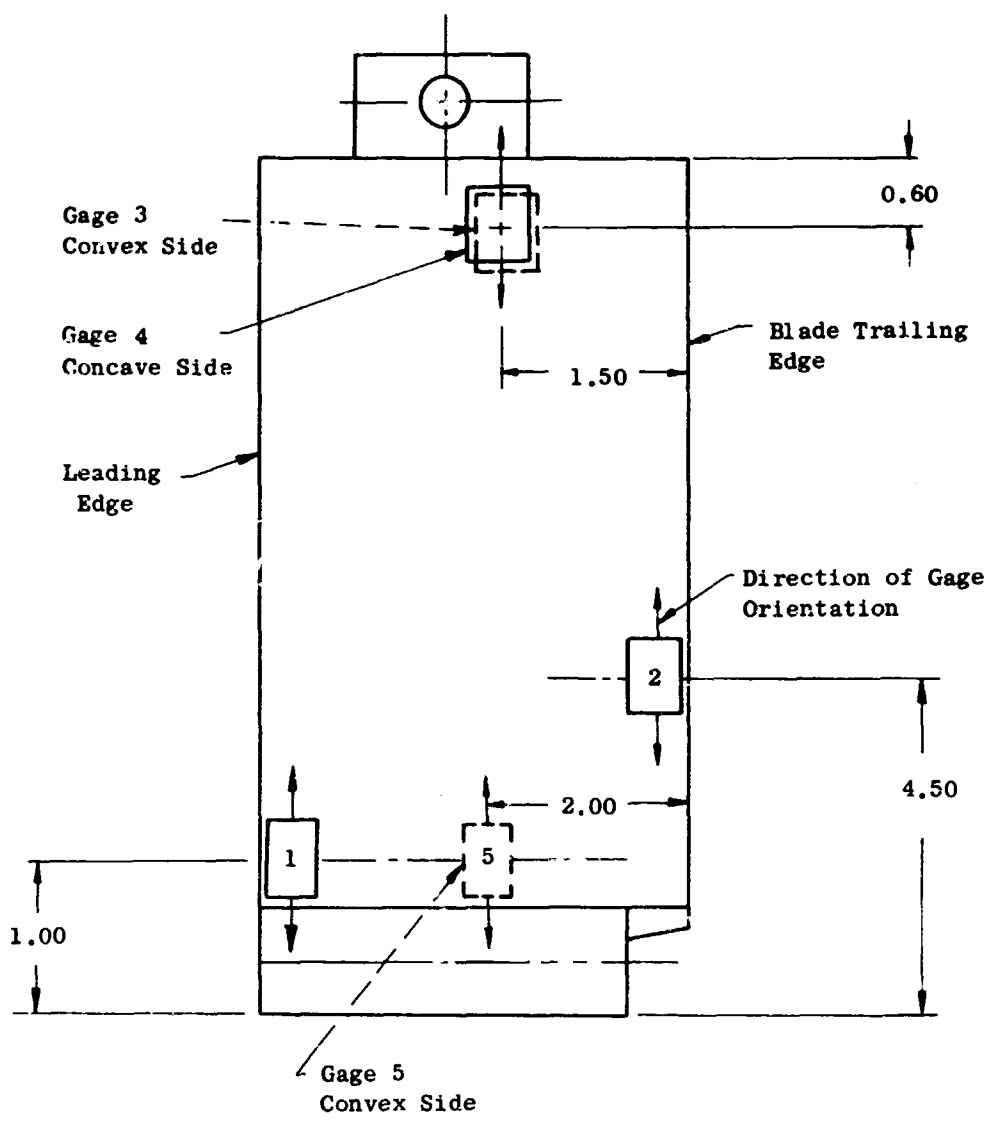


Figure 90. Fan Blade Strain Gage Locations.

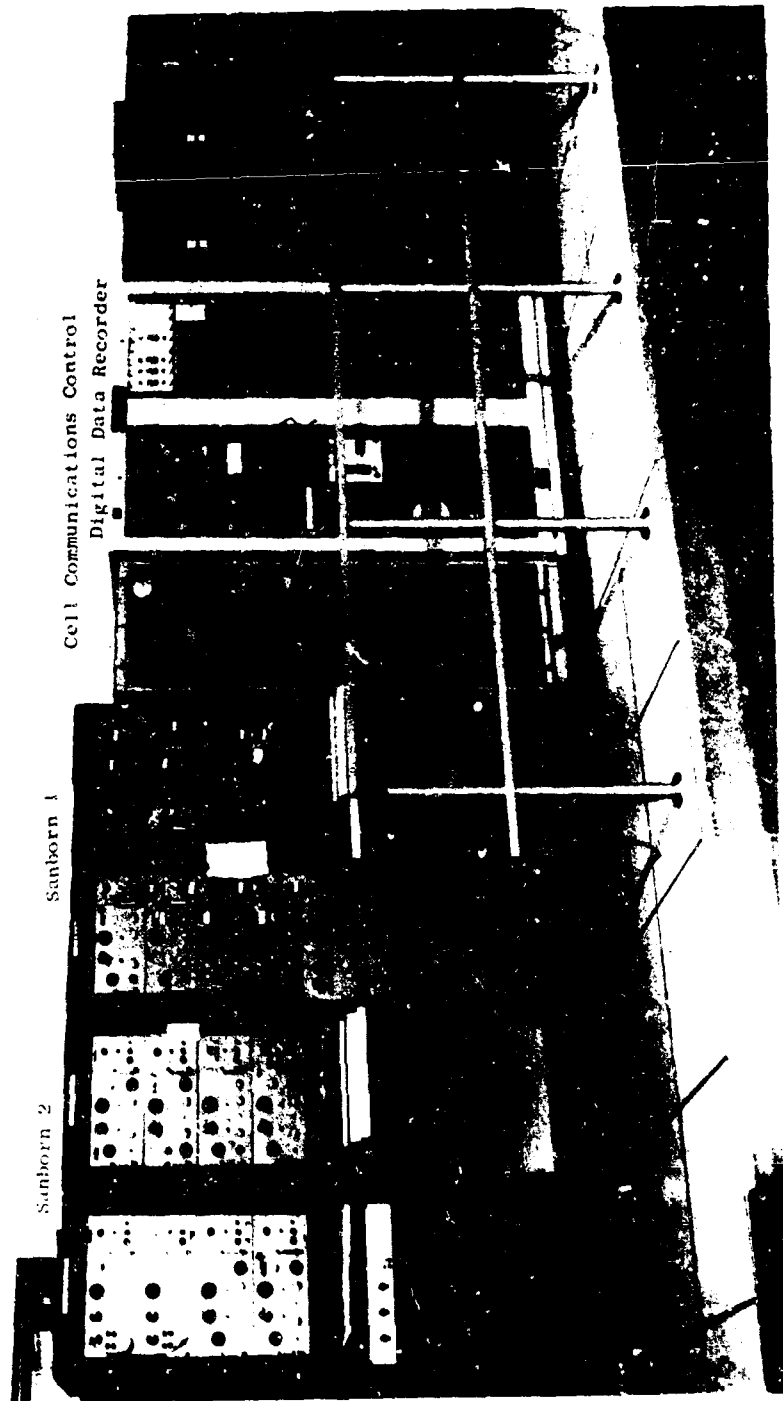


Figure 91. Lift Fan Test Facility Control Room, East Wall.



Figure 92. Lift Fan Test Facility Control Room, South Wall.

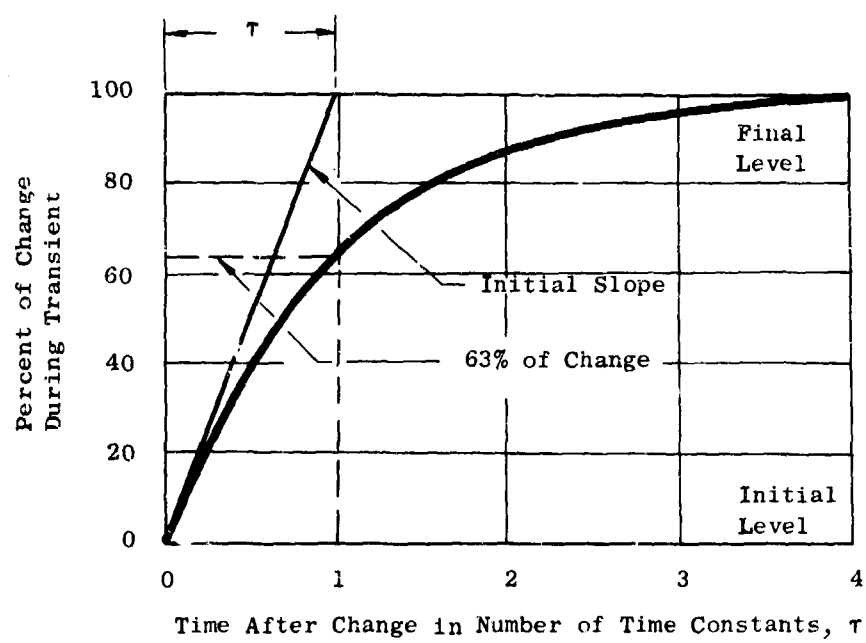


Figure 93. Graphical Representation of Two Definitions of Time Constant.

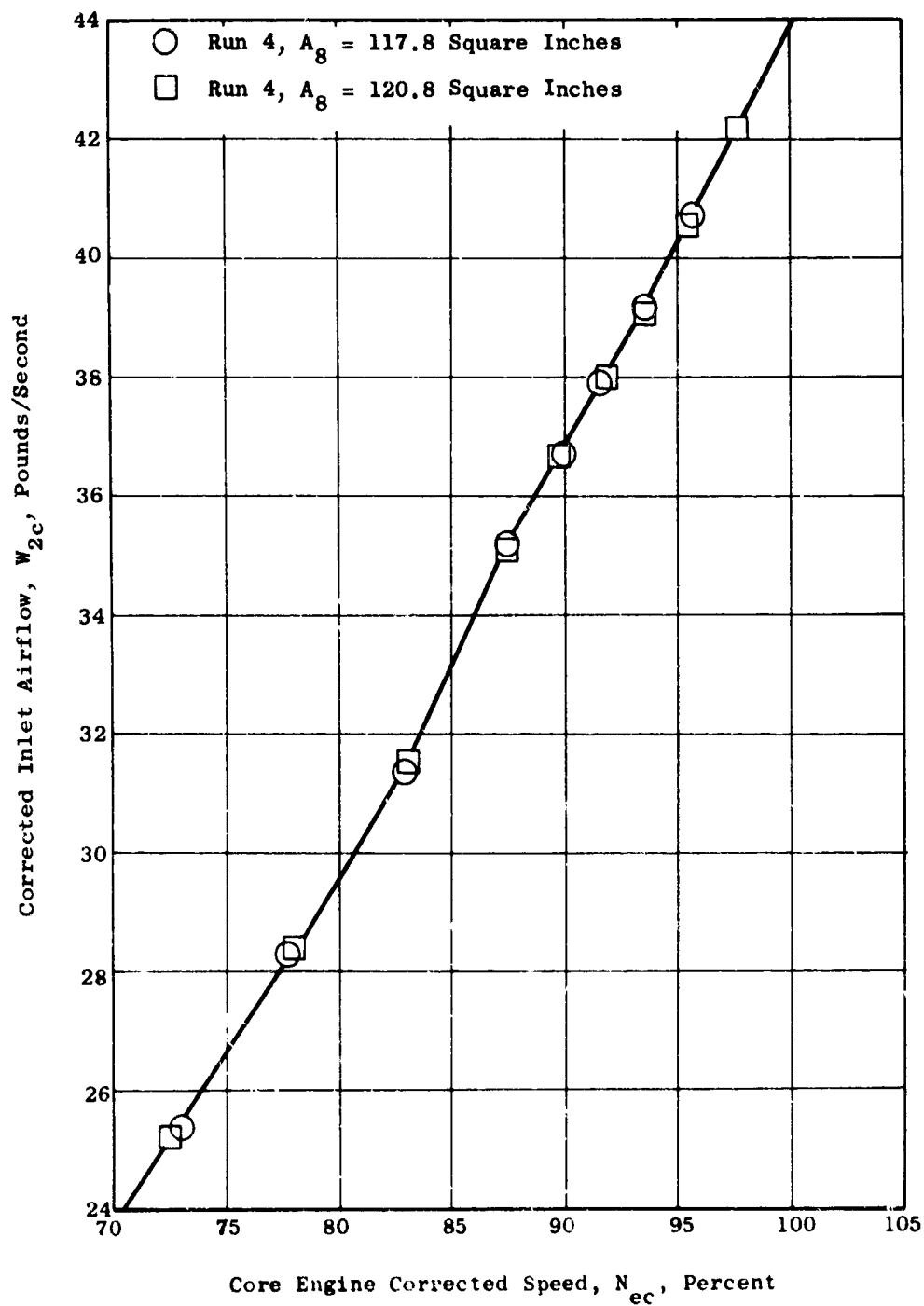


Figure 94. Cruise Mode Compressor Inlet Airflow for Engine 1, YJ85-GE-5, S/N 23G105.

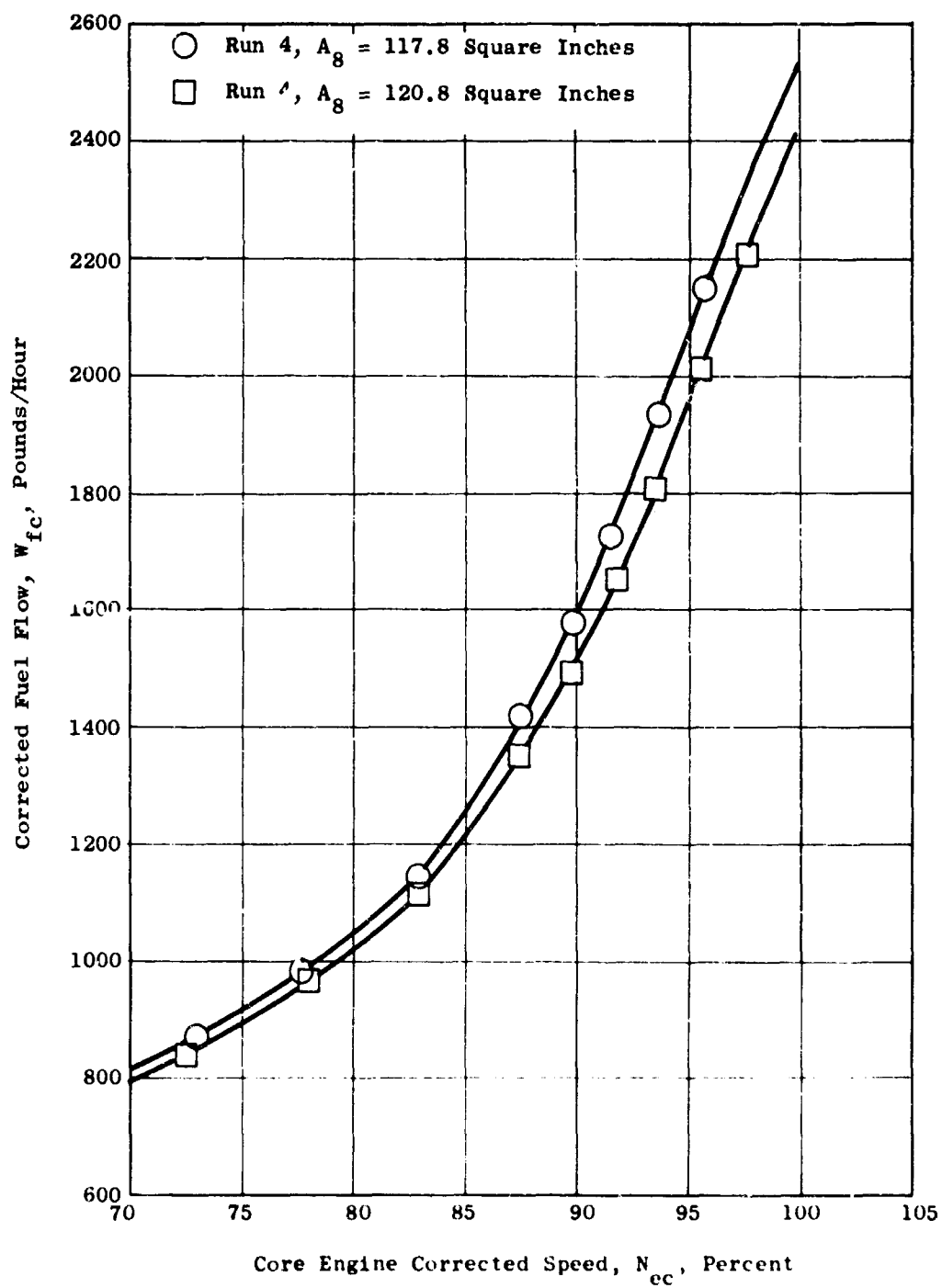


Figure 95. Cruise Mode Fuel Flow for Engine 1, YJ85-GE-5, S/N 230105.

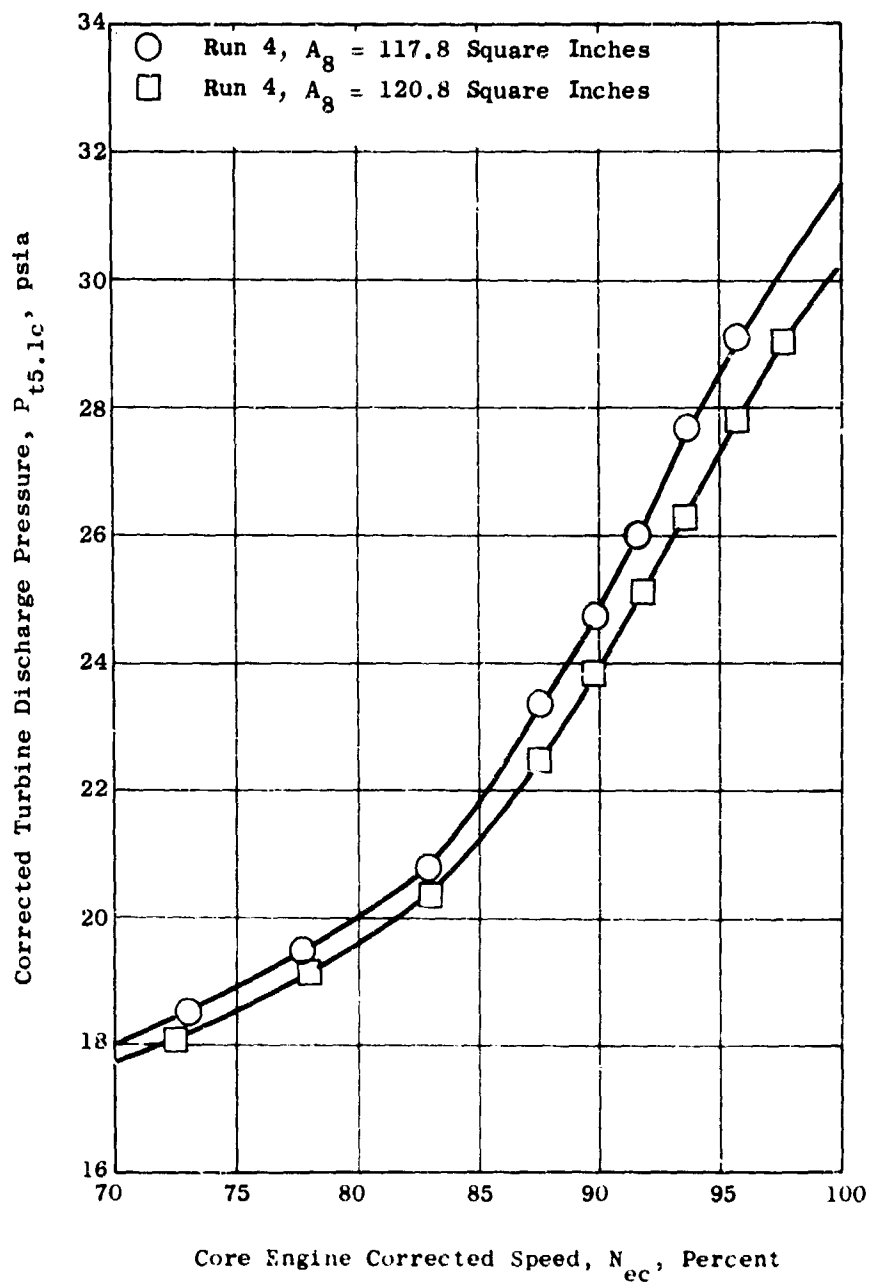


Figure 96. Cruise Mode Turbine Discharge Pressure for Engine 1, YJ85-GE-5, S/N 230105.

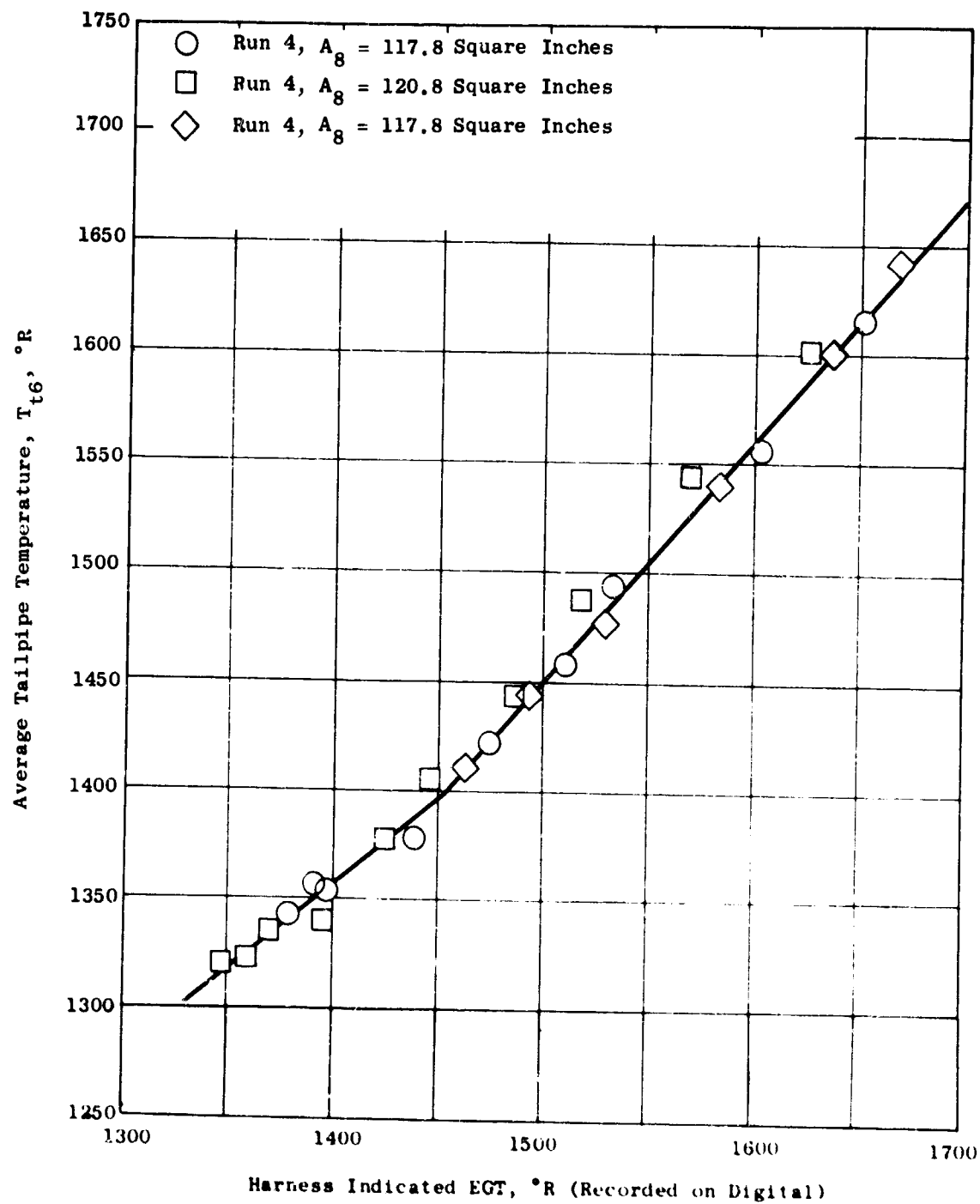


Figure 97. Calibration of Indicated EGT on Digital Recorder on Engine 1, YJ85-GE-5, S/N 230105.

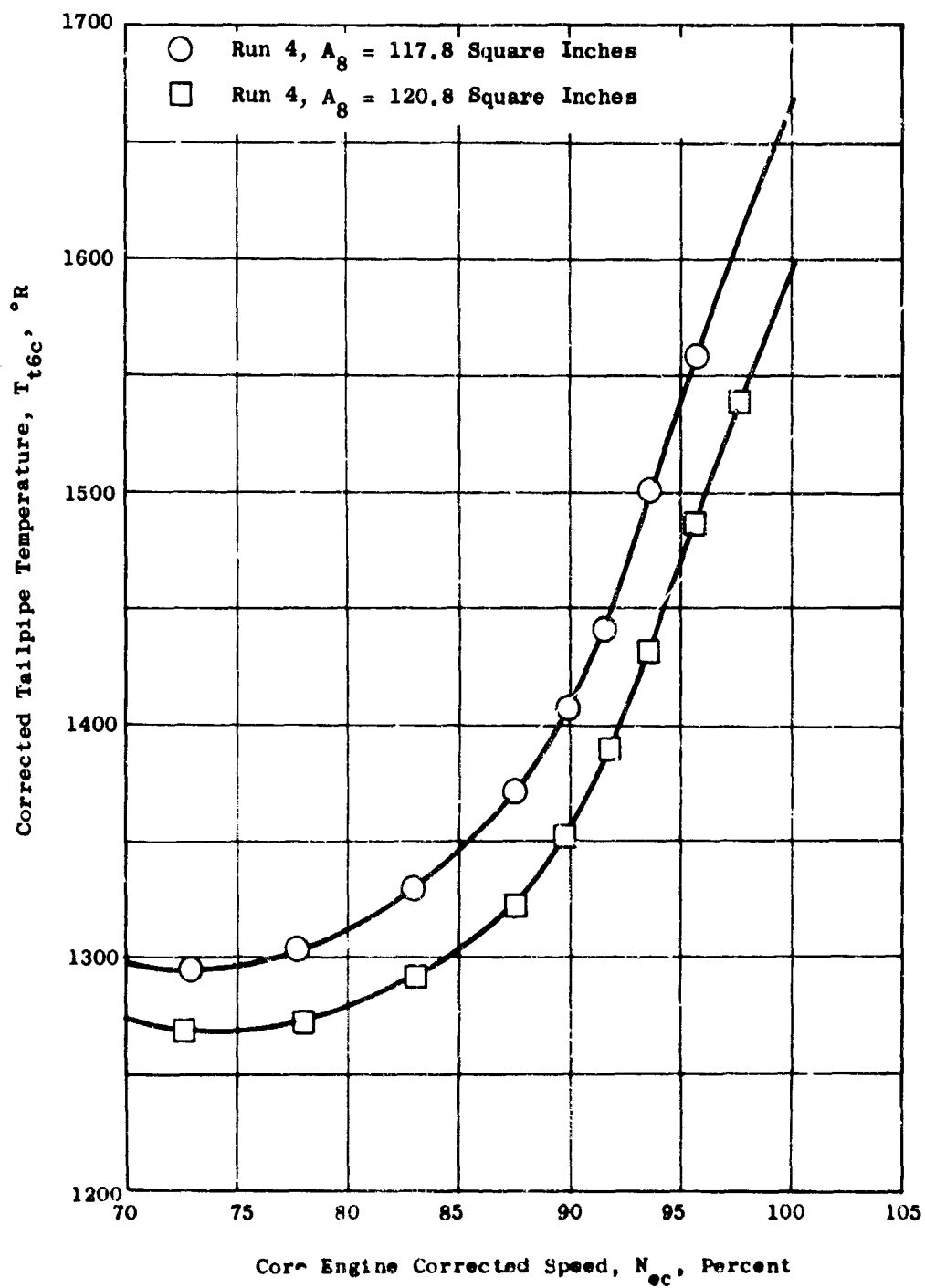


Figure 98. Cruise Mode Tailpipe Temperature for Engine 1, YJ85-GE-5, S/N 230105.

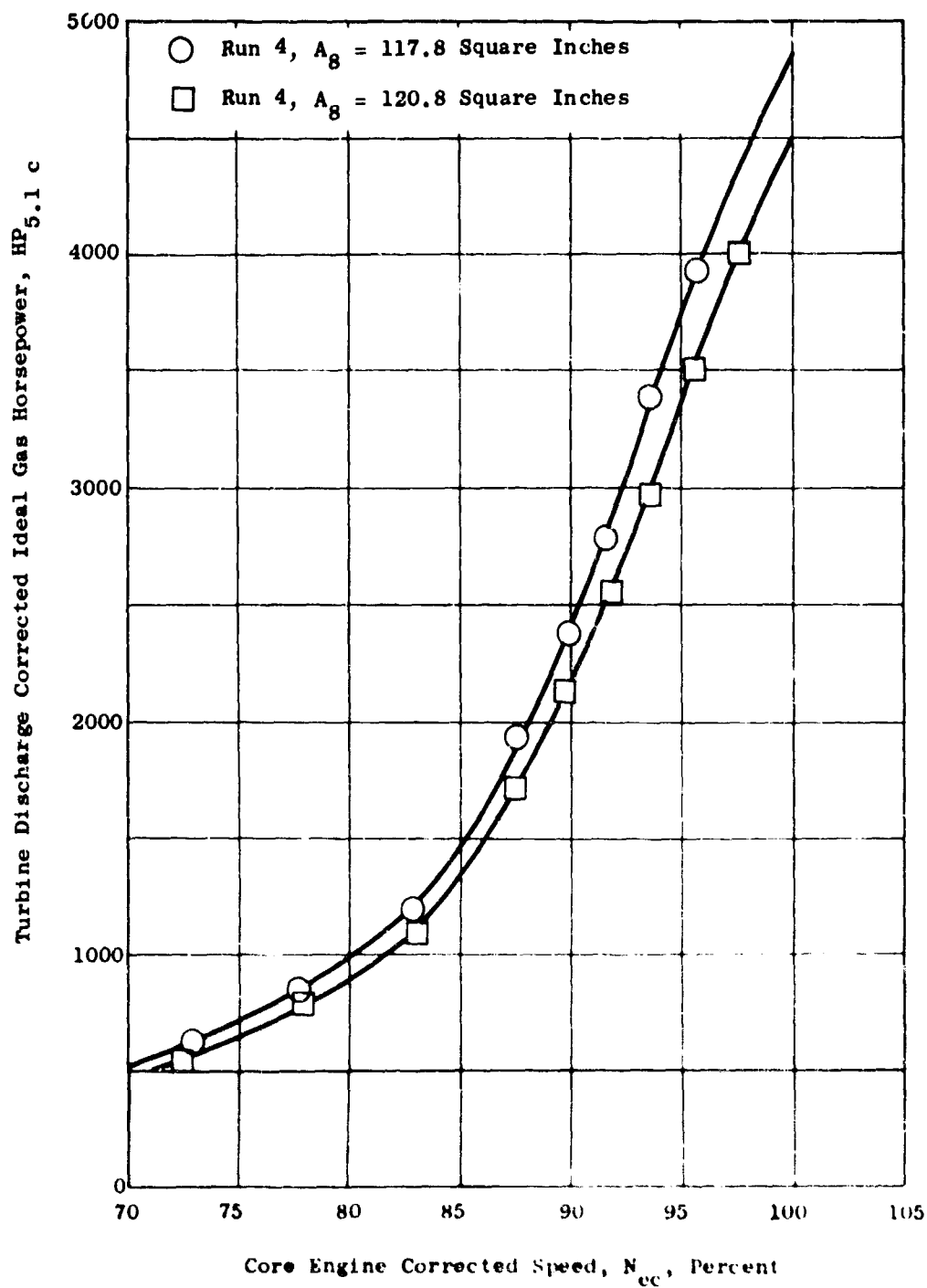


Figure 99. Cruise Mode Turbine Discharge Ideal Gas Horsepower for Engine 1, YJH5-GE-5, S N 230105.

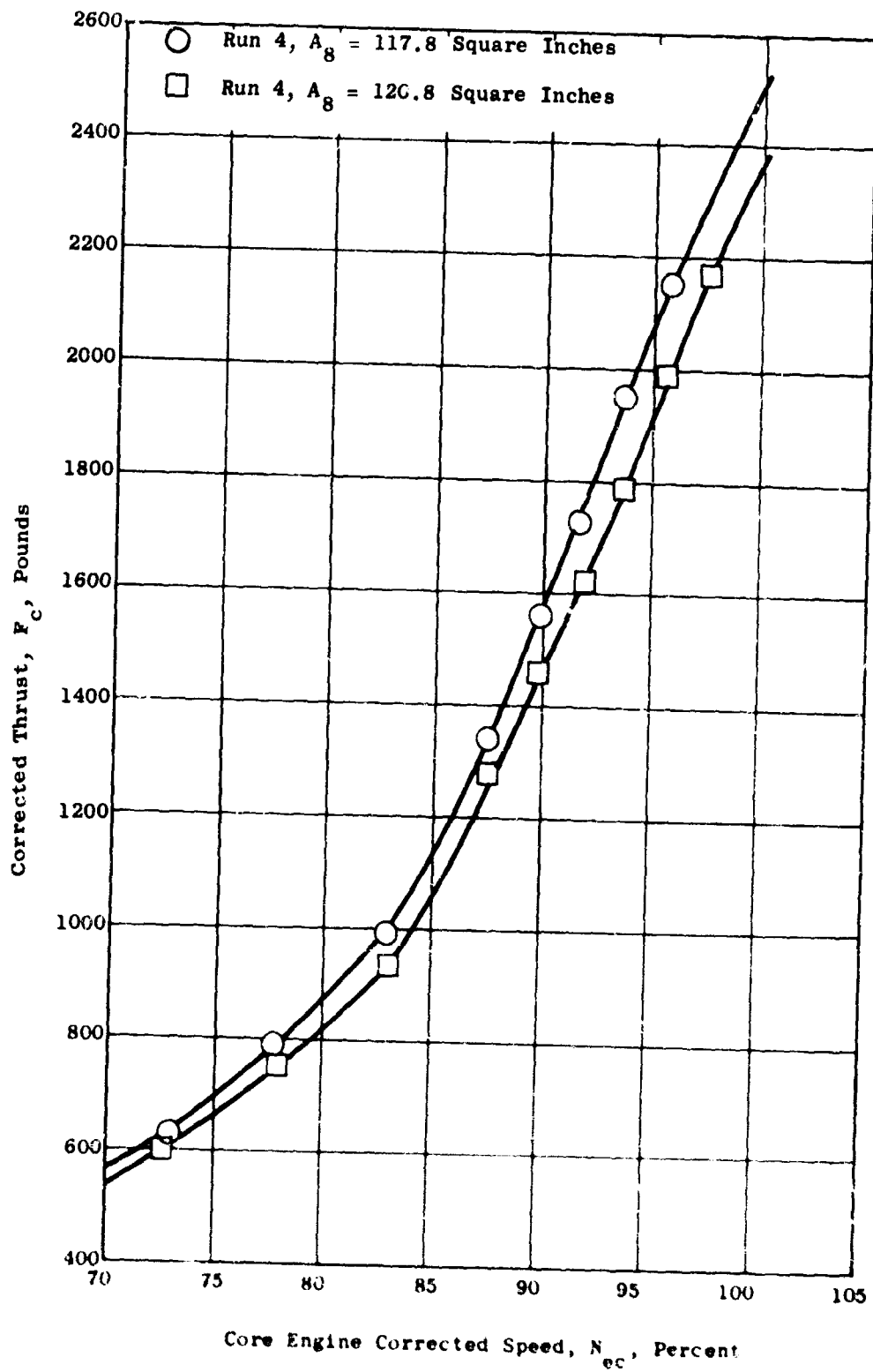


Figure 100. Cruise Mode Thrust for Engine 1, YJH5-GE-5, S/N 25105.

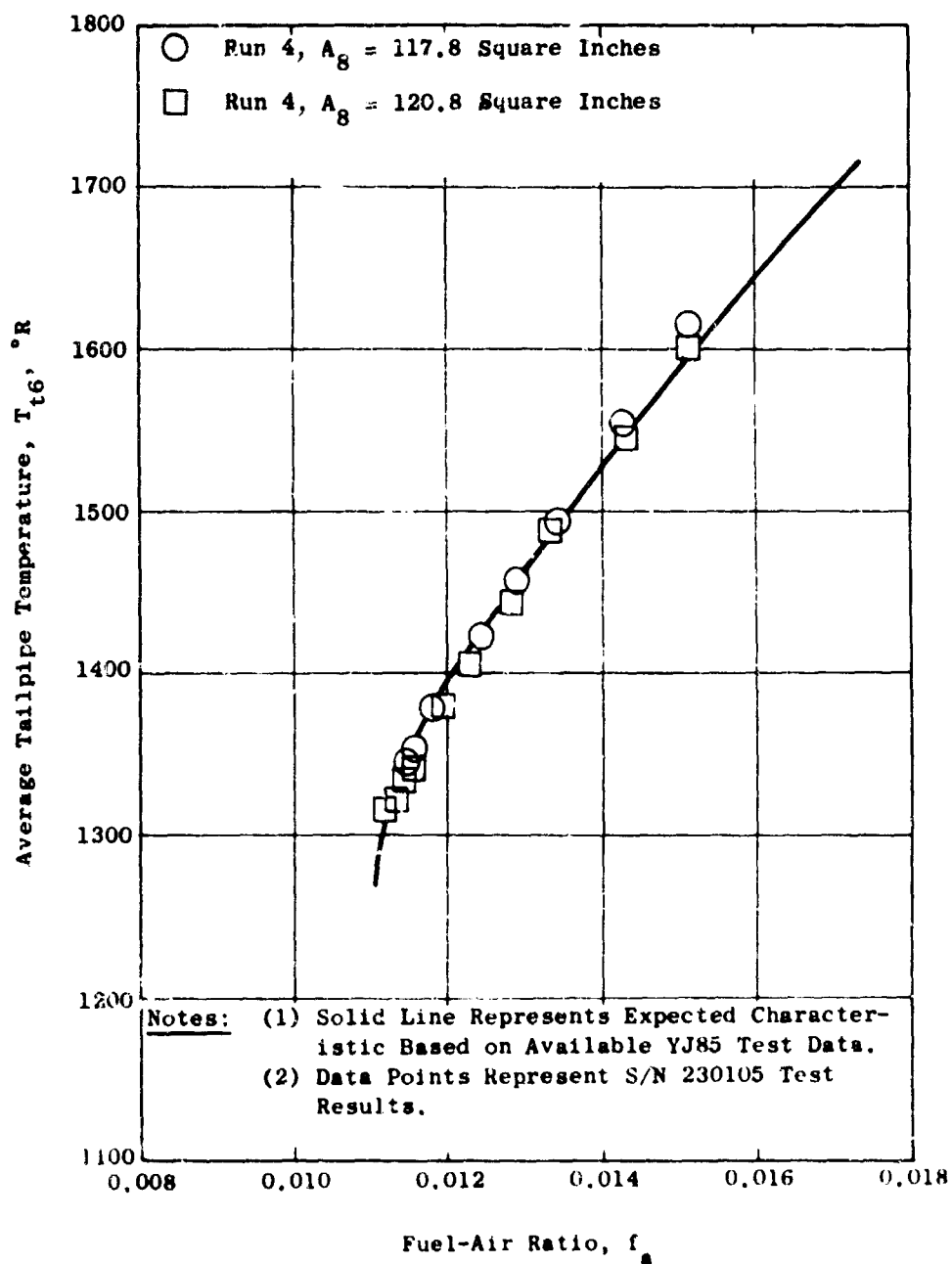


Figure 101. Correlation of Average Tailpipe Temperature With Fuel-Air Ratio for Engine 1, YJ85-GE-5, S/N 230105.

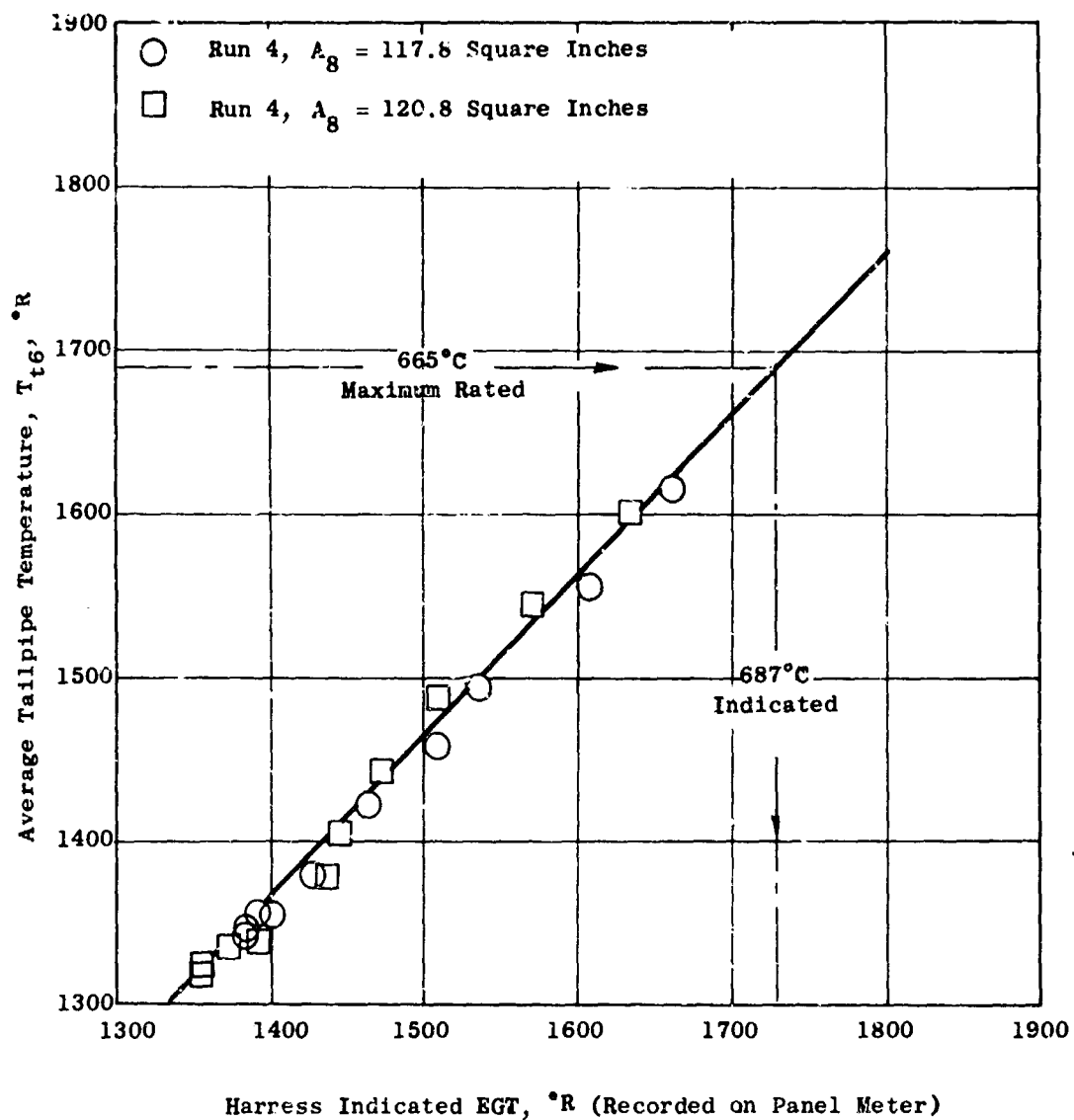


Figure 102. Calibration of Indicated EGT on Panel Meter for Engine 1, YJ85-GE-5, S/N 230105.

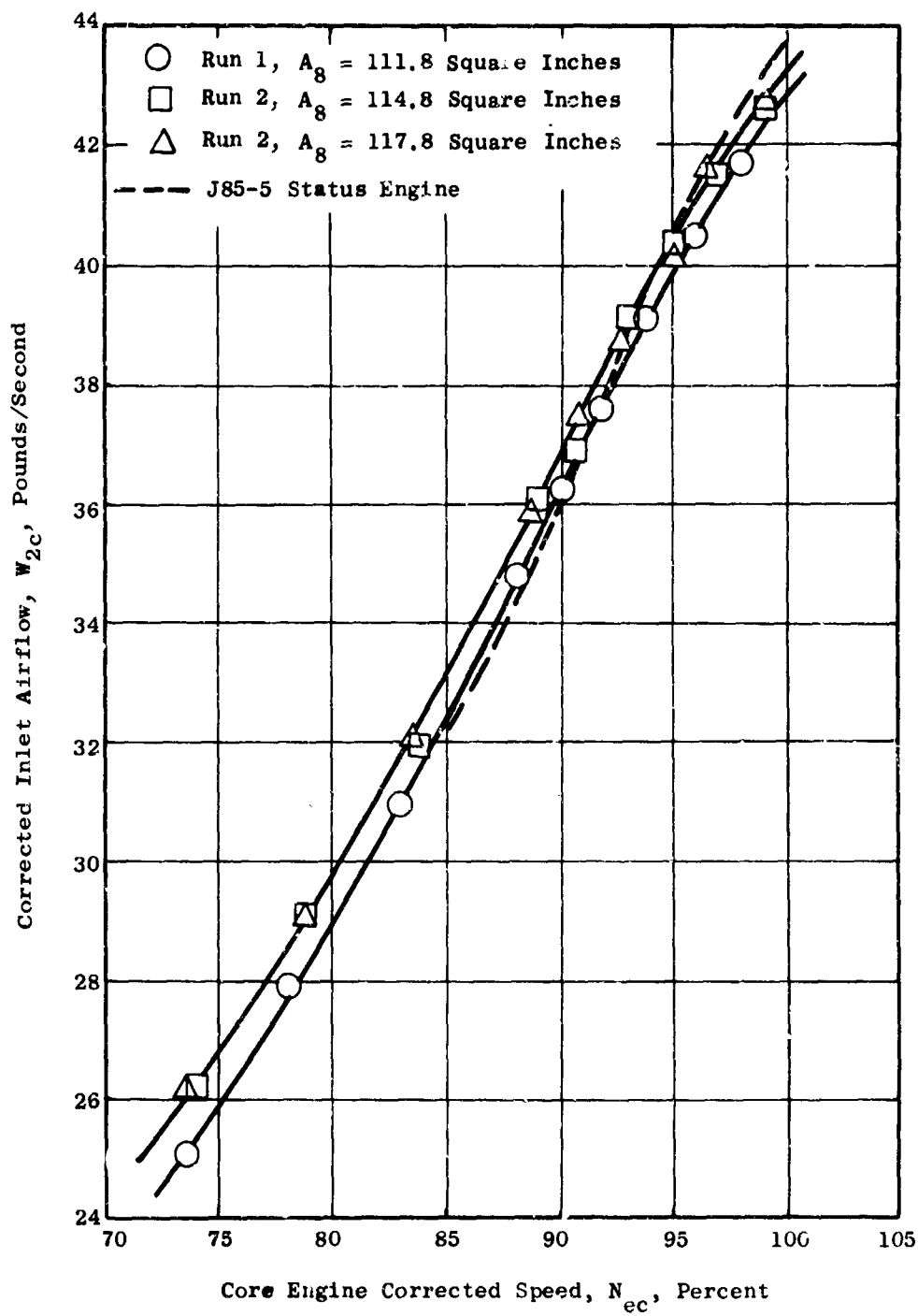


Figure 103. Cruise Mode Compressor Inlet Airflow for Engine 2, J85-GE-5, S/N 231233.

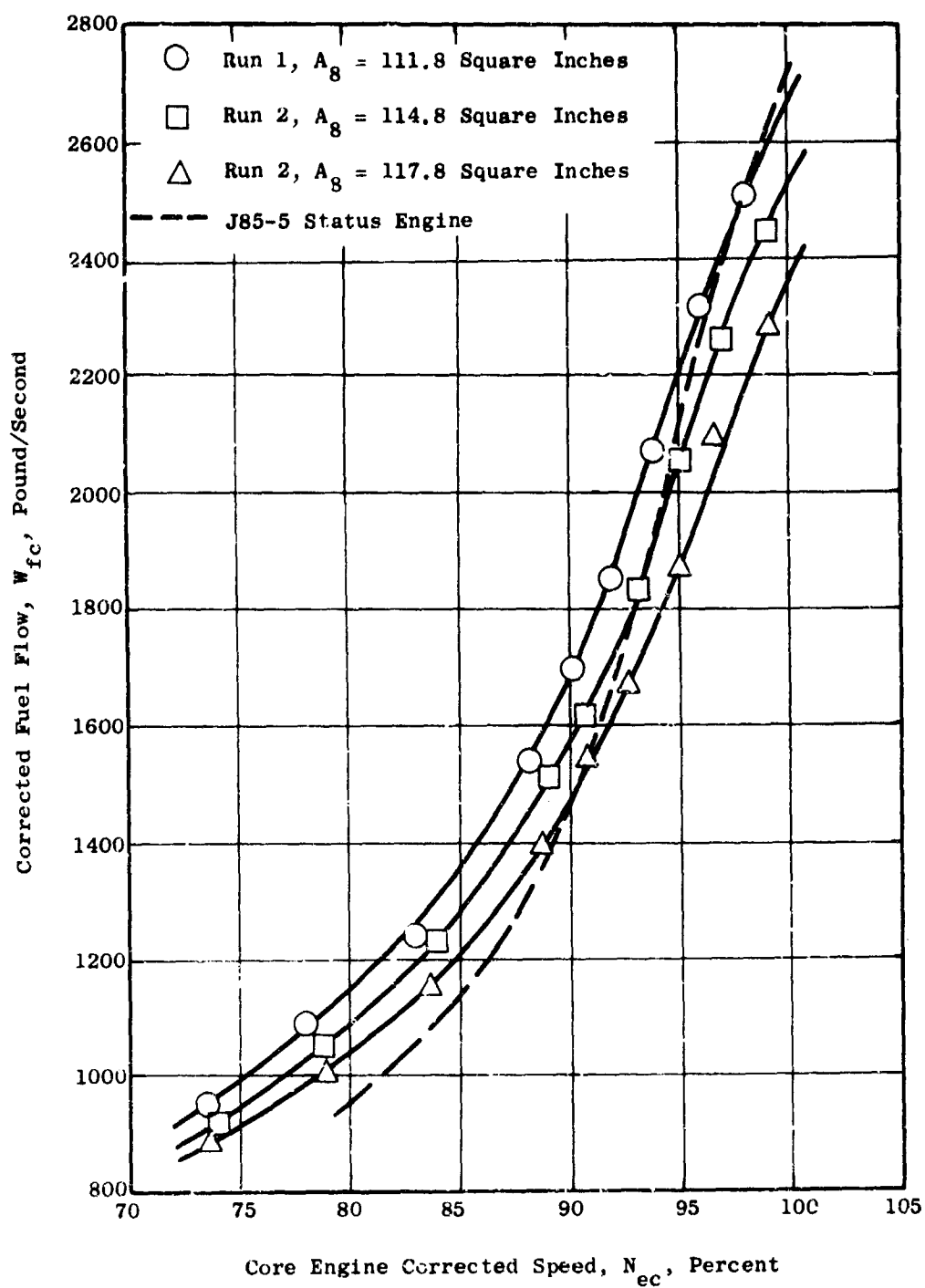


Figure 104. Cruise Mode Fuel Flow for Engine 2, J85-GE-5, S/N 231233.

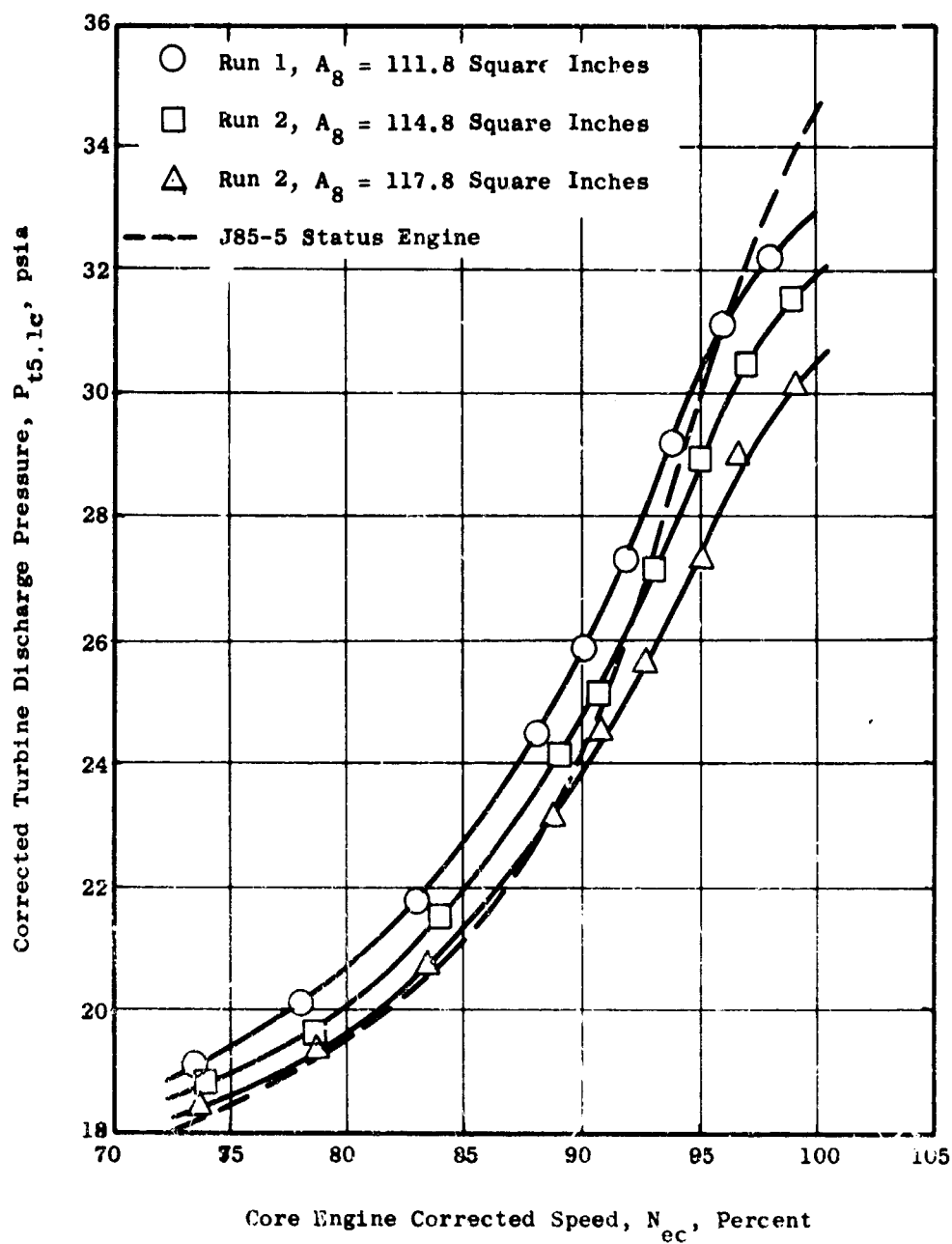


Figure 105. Cruise Mode Turbine Discharge Pressure for Engine 2, J85-GE-5, S/N 231233.

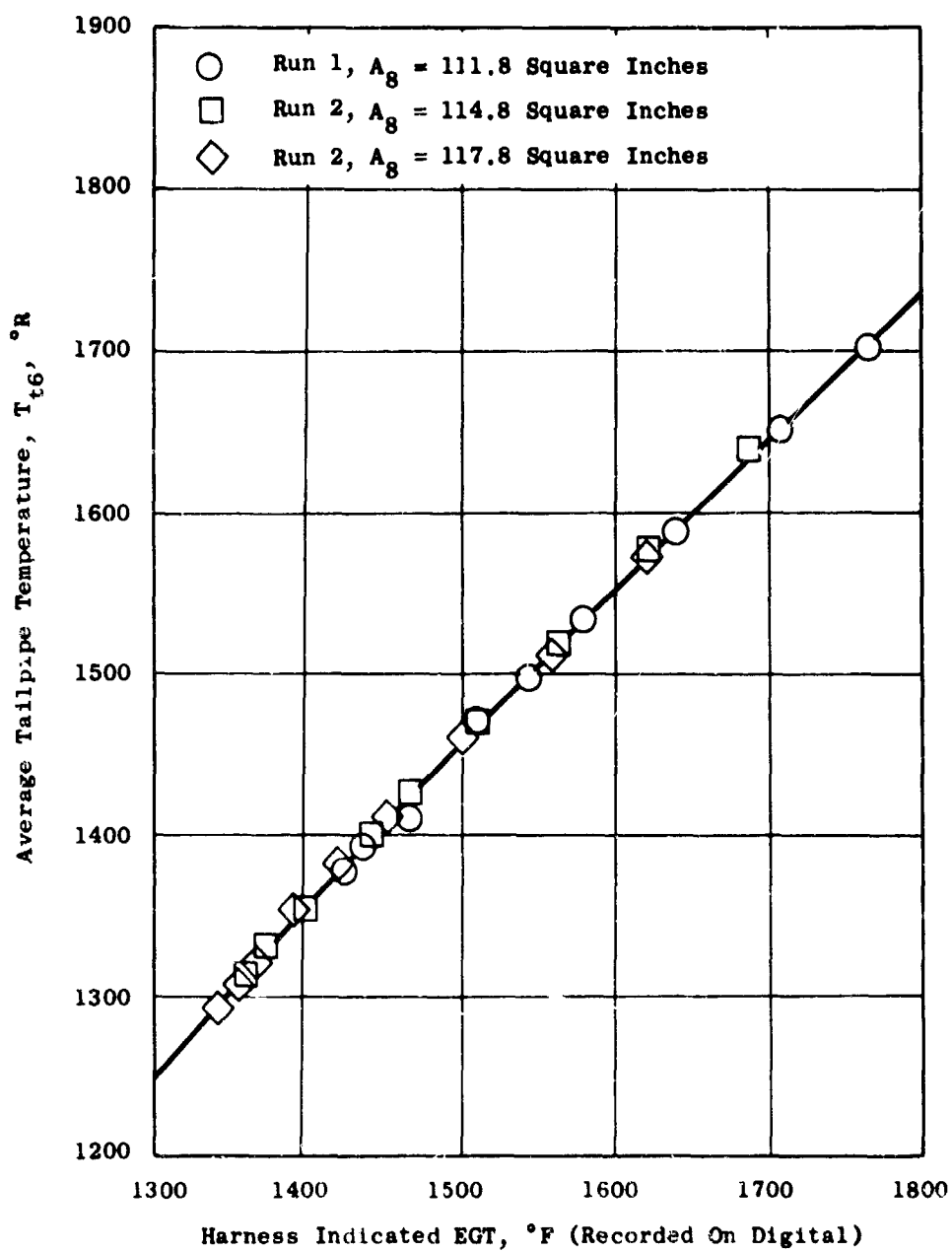


Figure 106. Calibration of Indicated EGT on Digital Recorder on Engine 2, J85-GE-5, S/N 231233.

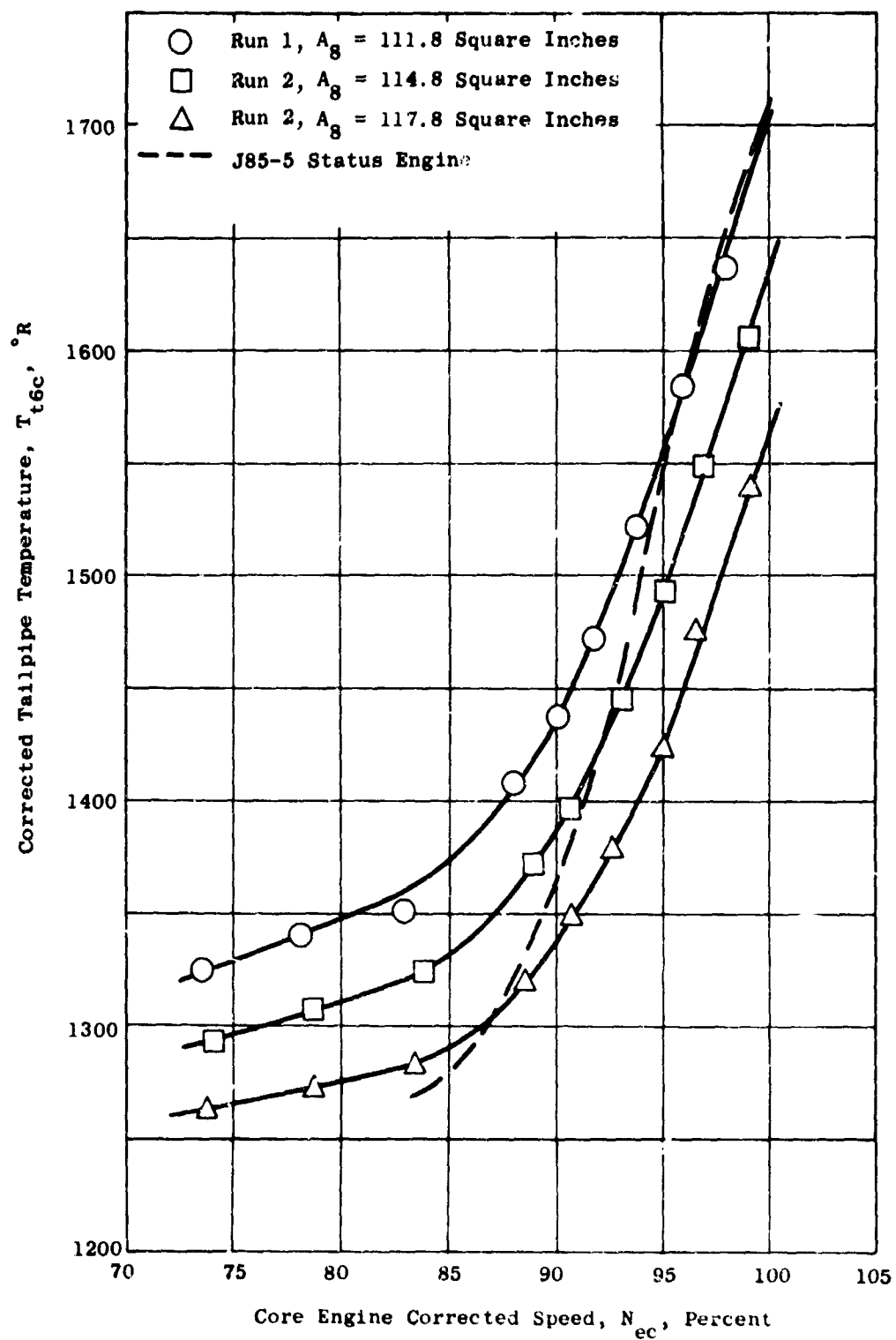


Figure 107. Cruise Mode Tailpipe Temperature for Engine 2, J85-GE-5, S/N 231233.

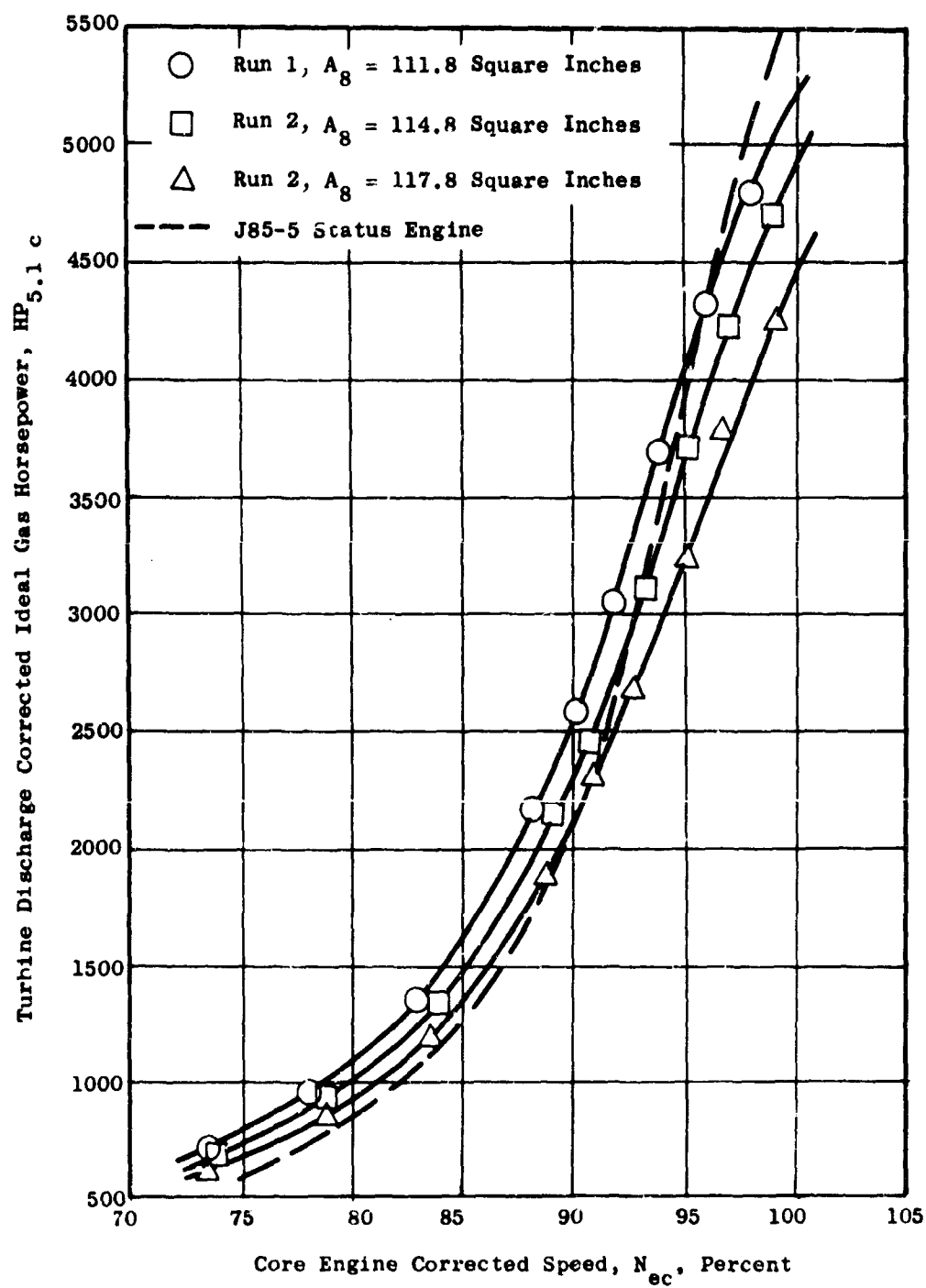


Figure 108. Cruise Mode Turbine Discharge Ideal Gas Horsepower for Engine 2, J85-GE-5, S/N 231233.

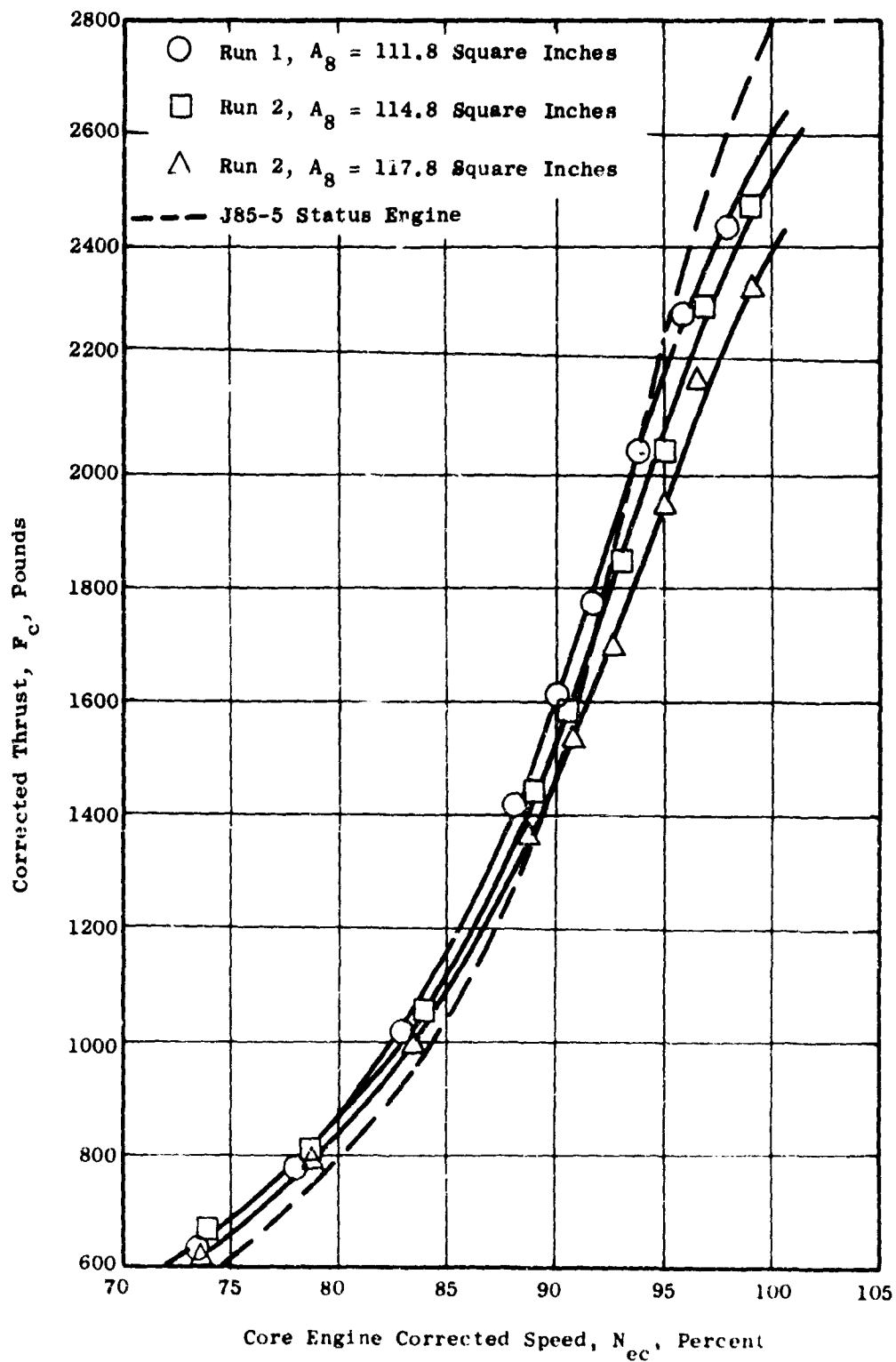


Figure 109. Cruise Mode Thrust for Engine 2, J85-GE-5, S/N 231233.

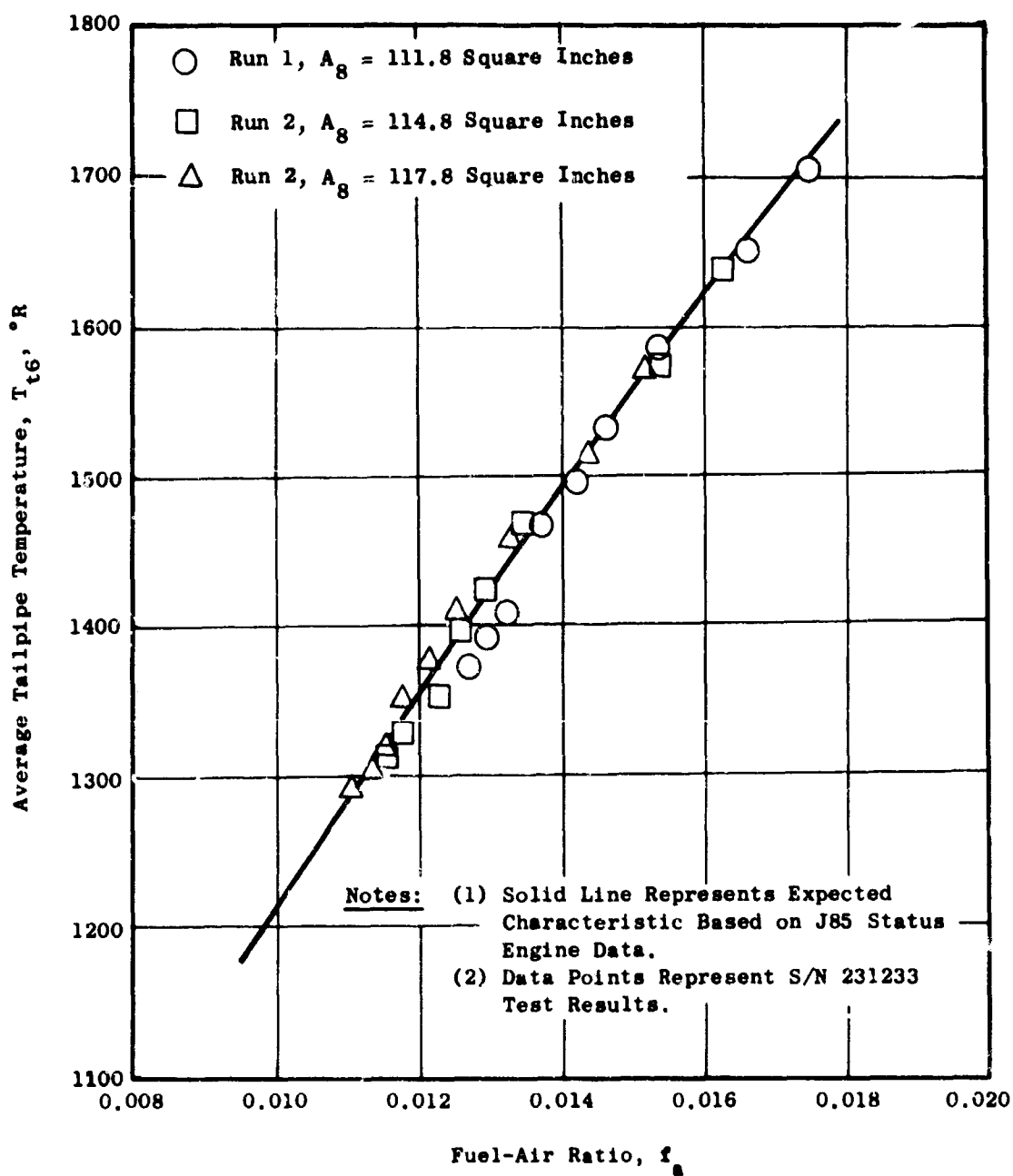


Figure 110. Correlation of Average Tailpipe Temperature With Fuel-Air Ratio for Engine 2, J85-GE-5, S/N 231233.

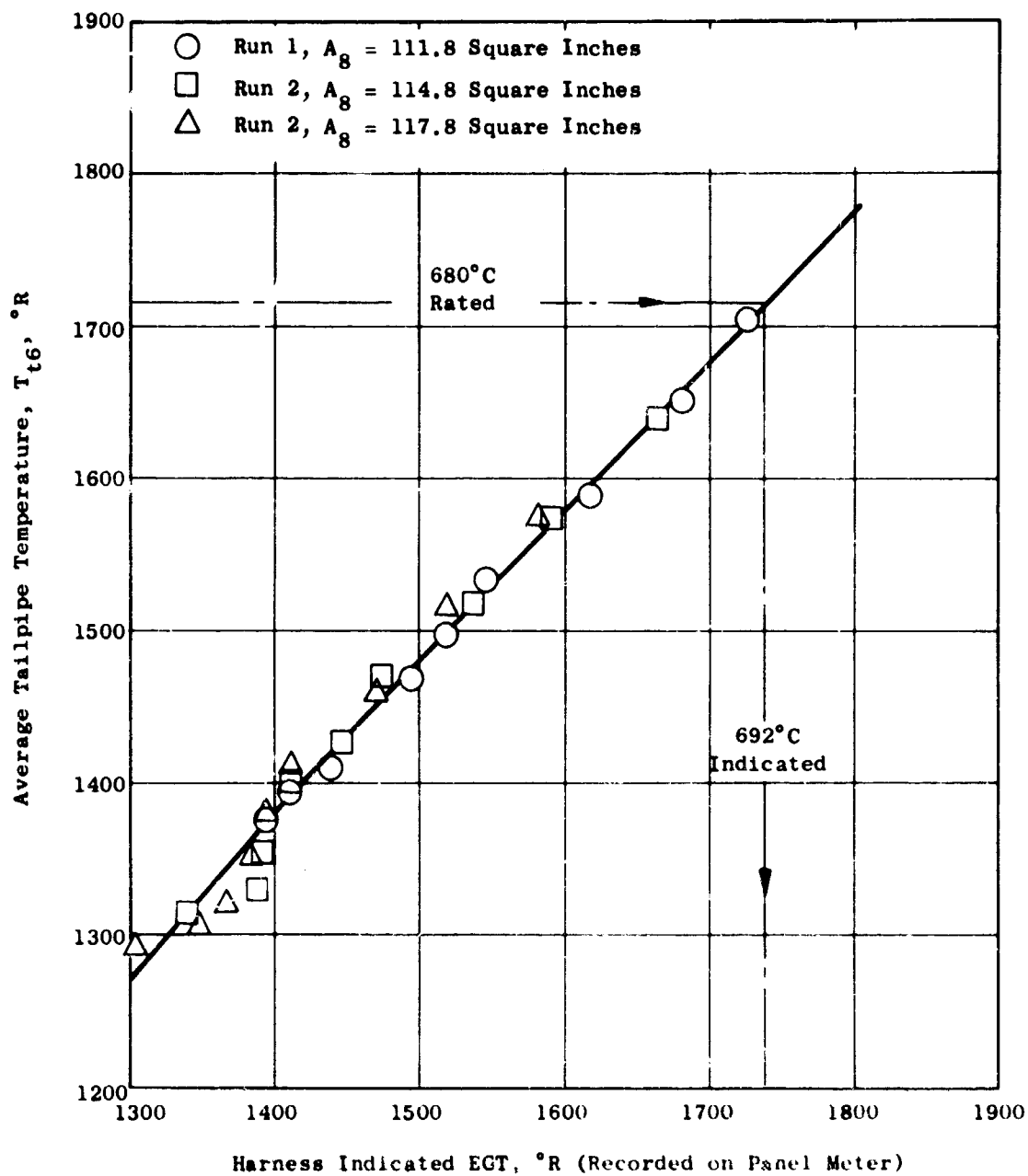


Figure 111. Calibration of Indicated EGT on Panel Meter for Engine 2, J85-GE-5, S/N 231233.

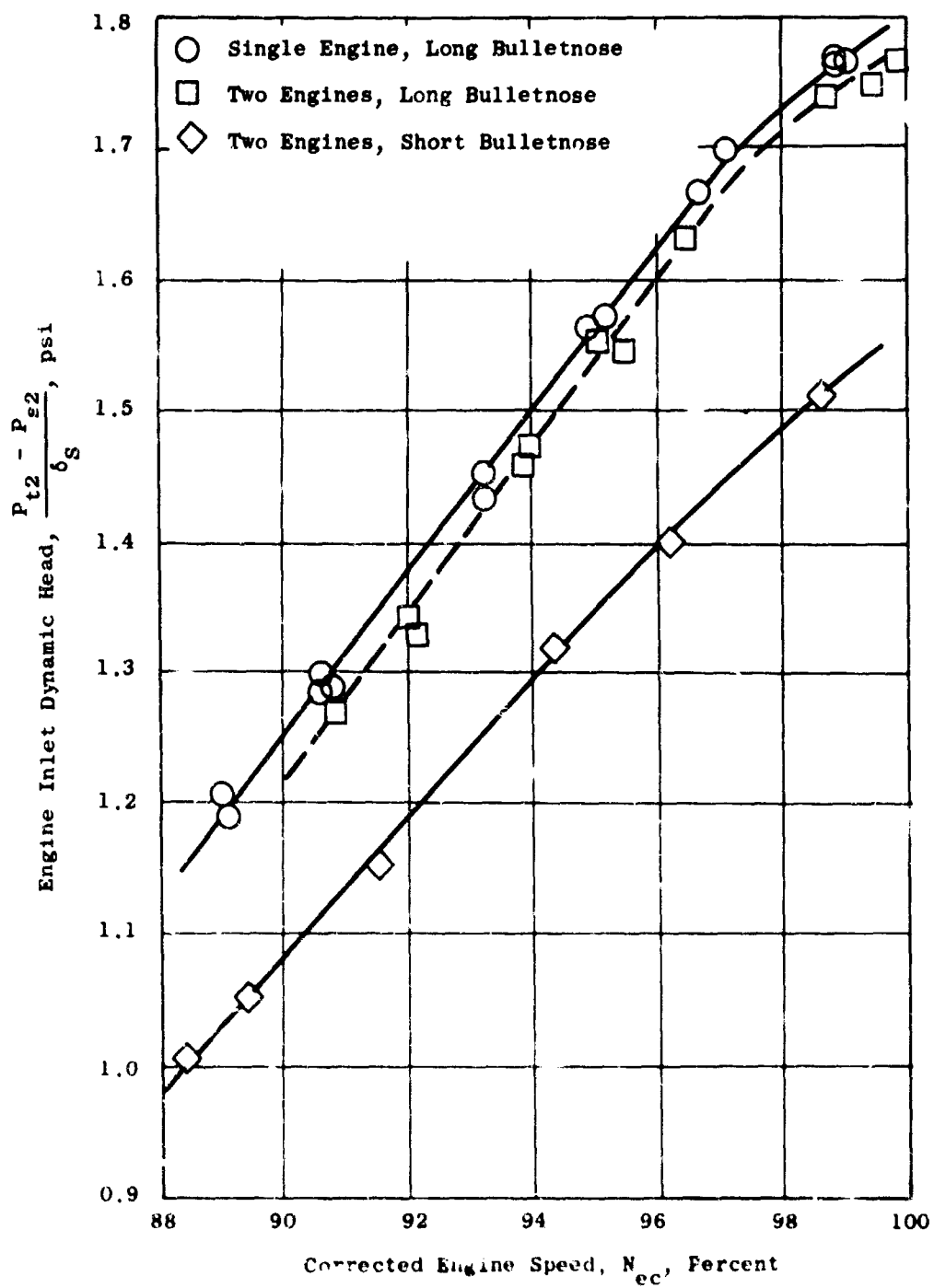


Figure 112. Effect of Bulletnose Configuration on Engine Inlet Dynamic Head.

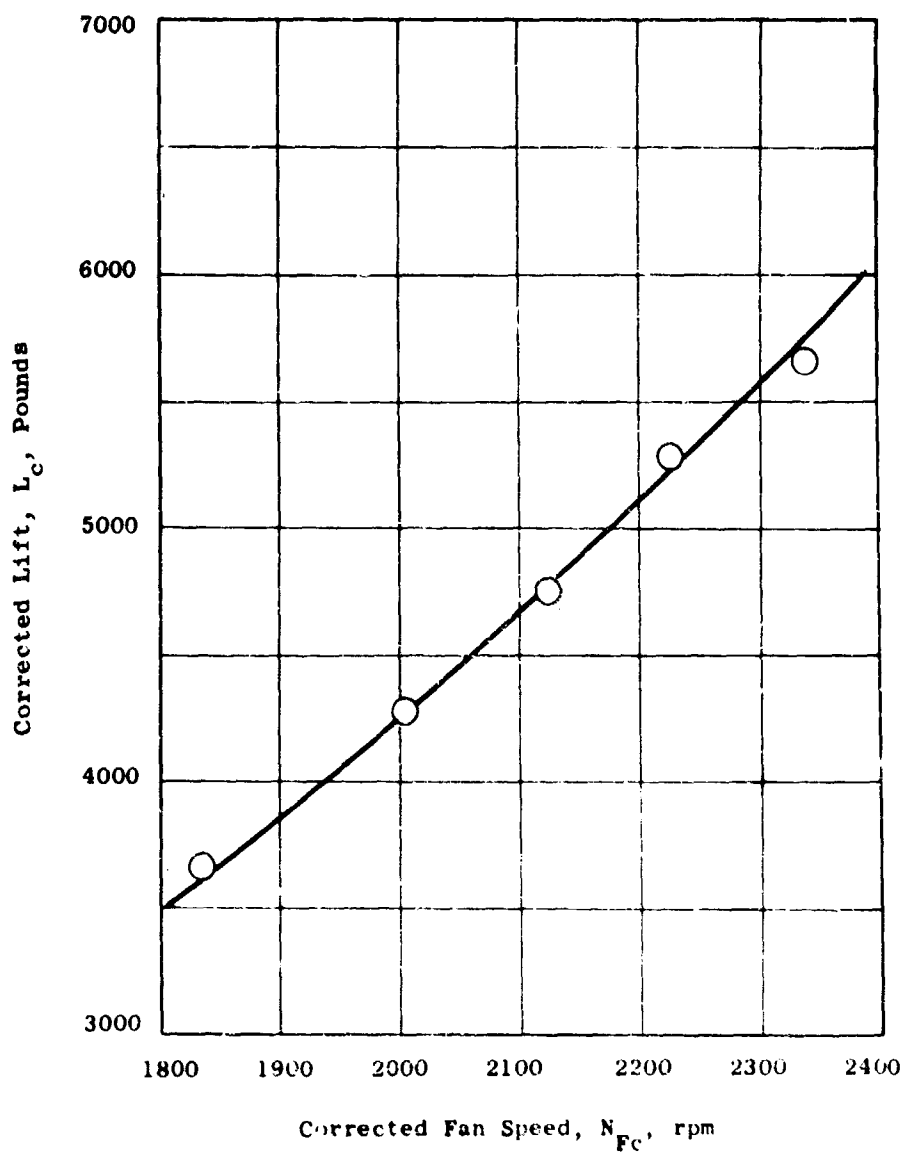


Figure 113. Lift Versus Fan Speed, Run 7, Stator Stiffener Rings Out, $\delta_s = 110$ Percent.

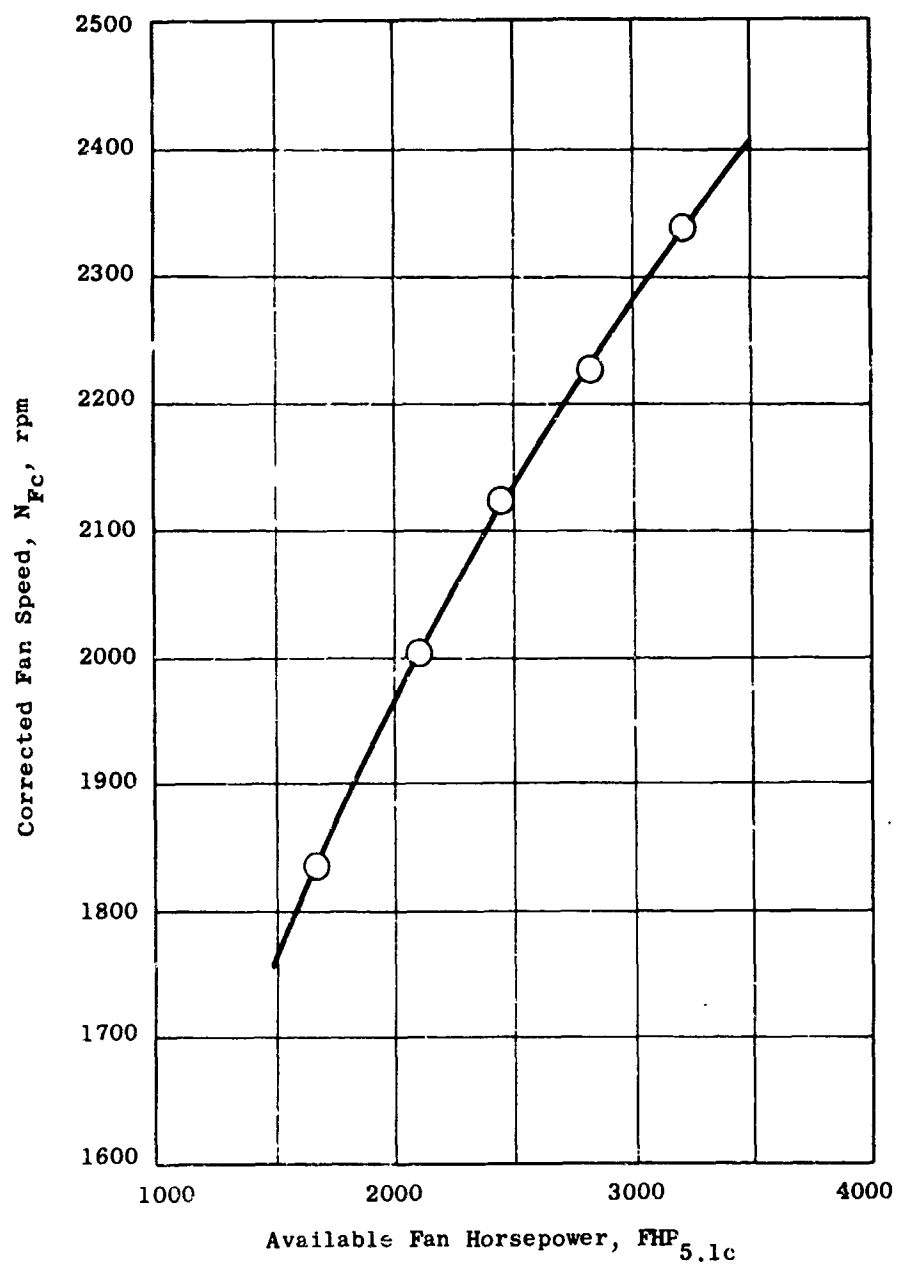


Figure 114. Speed Versus Horsepower, Run 7, Stator Stiffener Rings Out, $\delta_s = 110$ Percent.

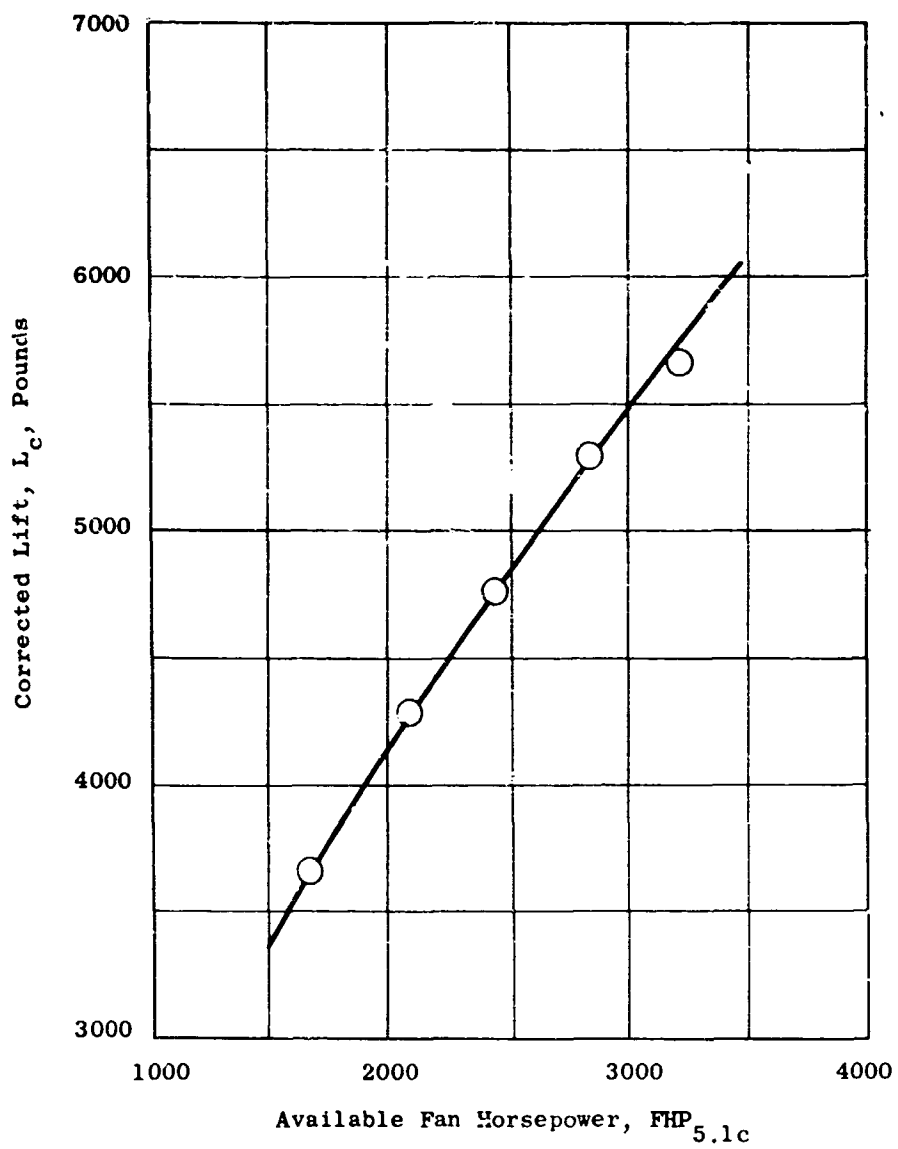


Figure 115. Lift Versus Horsepower, Run 7, Stator Stiffener Rings Out, $\delta_s = 110$ Percent.

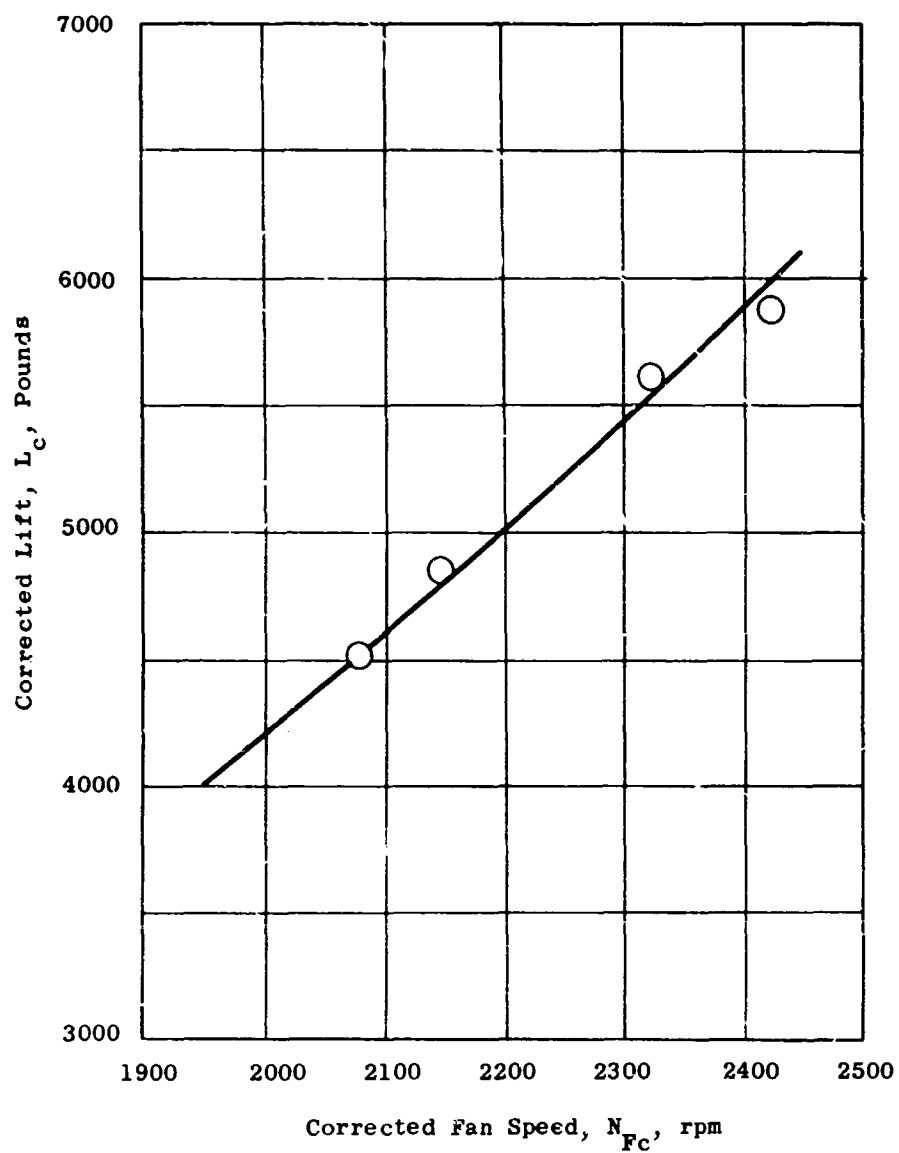


Figure 116. Lift Versus Fan Speed, Run 9, Stator Stiffener Rings In, $\delta_s = 110$ Percent.

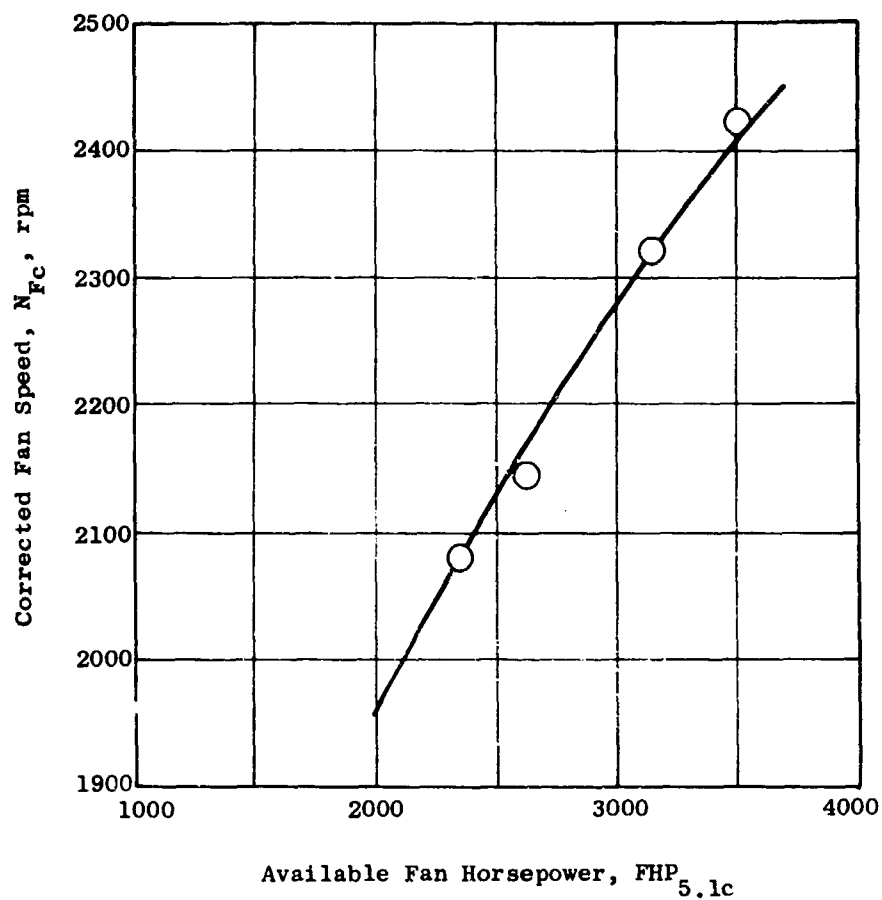


Figure 117. Speed Versus Horsepower, Run 9, Stator Stiffener Rings In, $\delta_s = 110$ Percent.

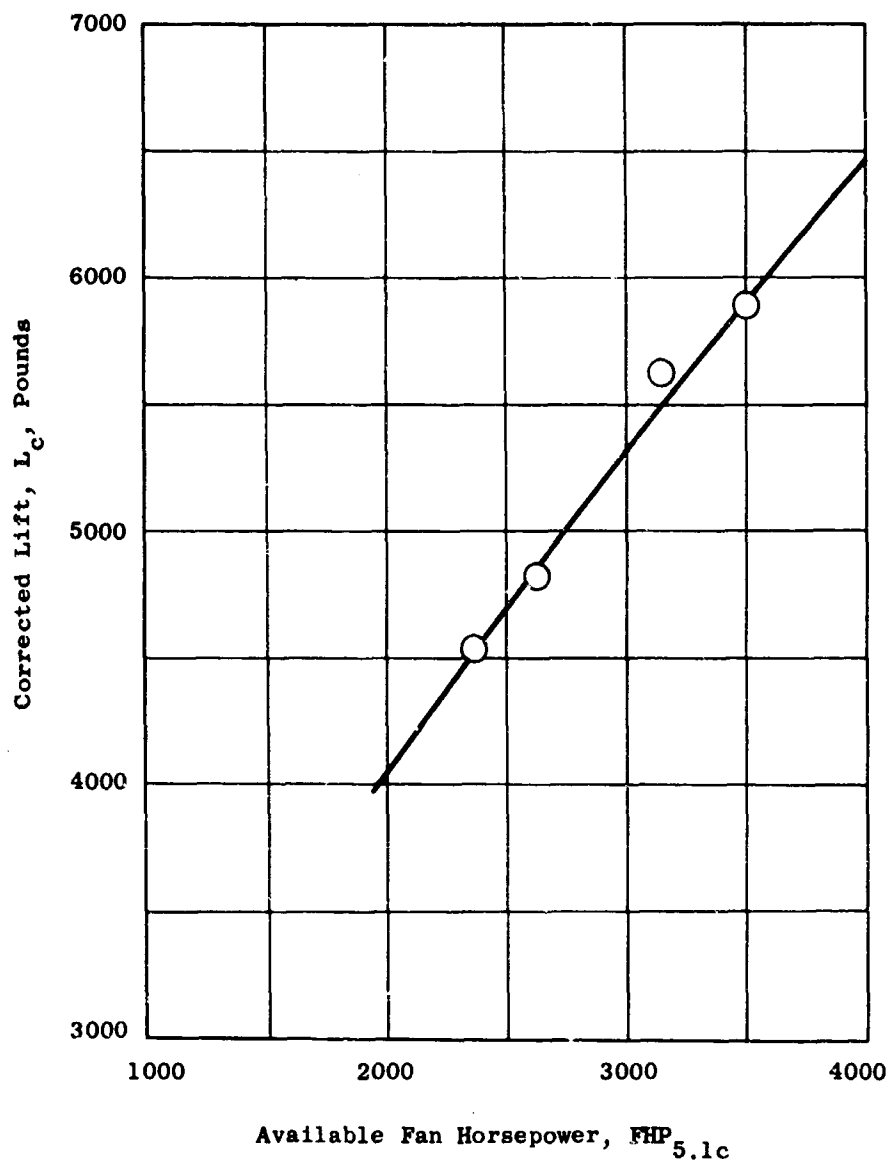


Figure 118. Lift Versus Horsepower, Run 9, Stator Stiffener Rings In, $\delta_s = 110$ Percent.

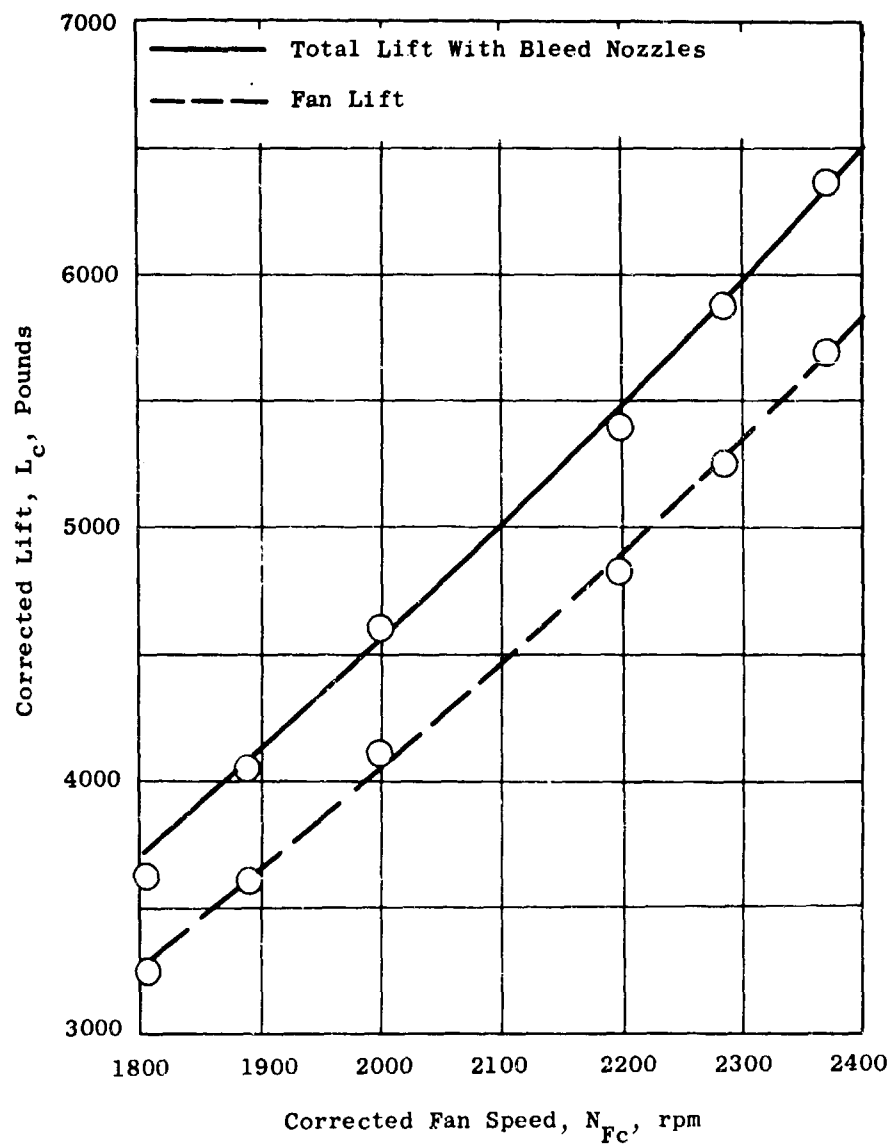


Figure 119. Lift Versus Fan Speed, Run 17, $\delta_s = 80$ Percent, Before and After Bleed Nozzle Correction.

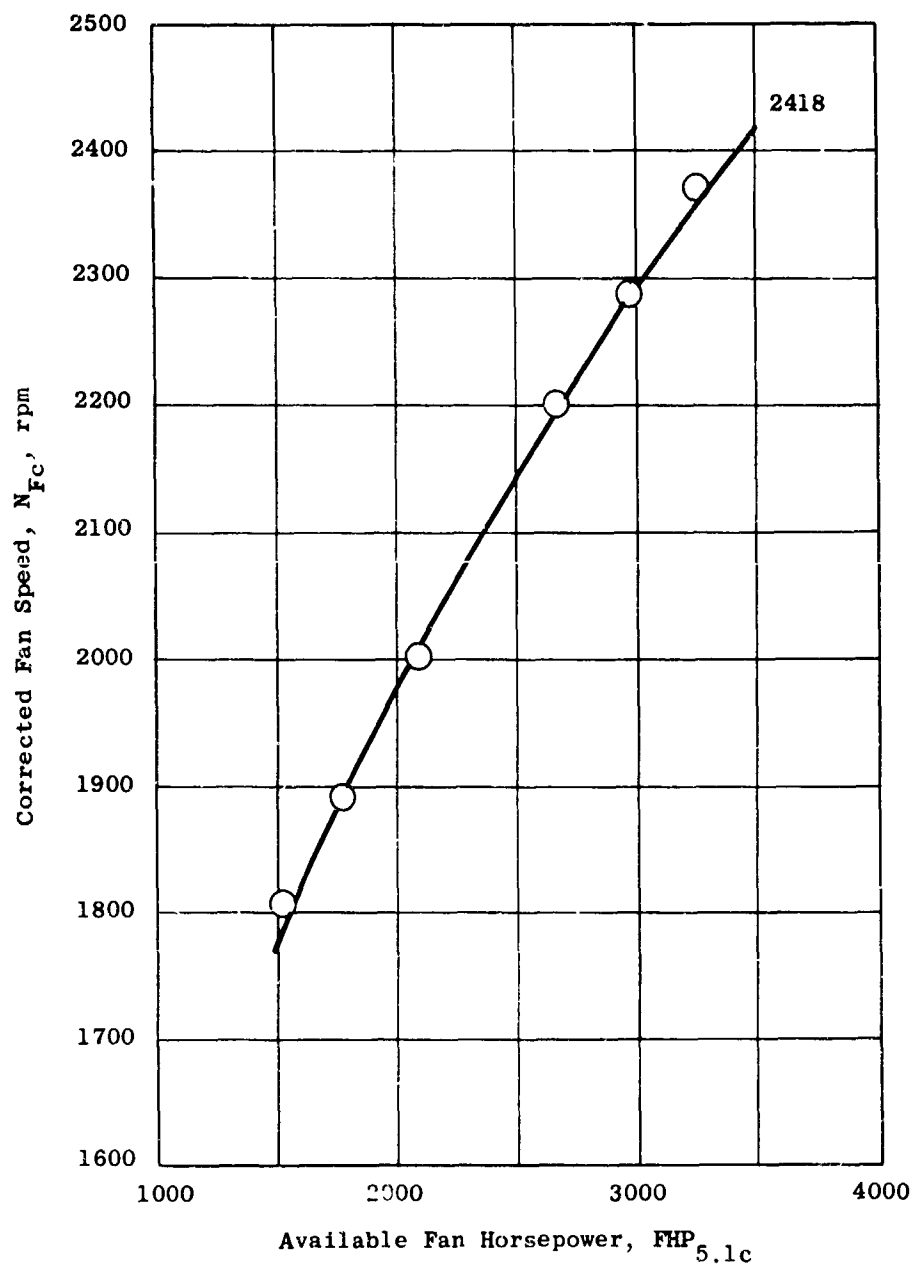


Figure 120. Fan Speed Versus Available Fan Horsepower, Run 17, $\delta_s = 80$ Percent.

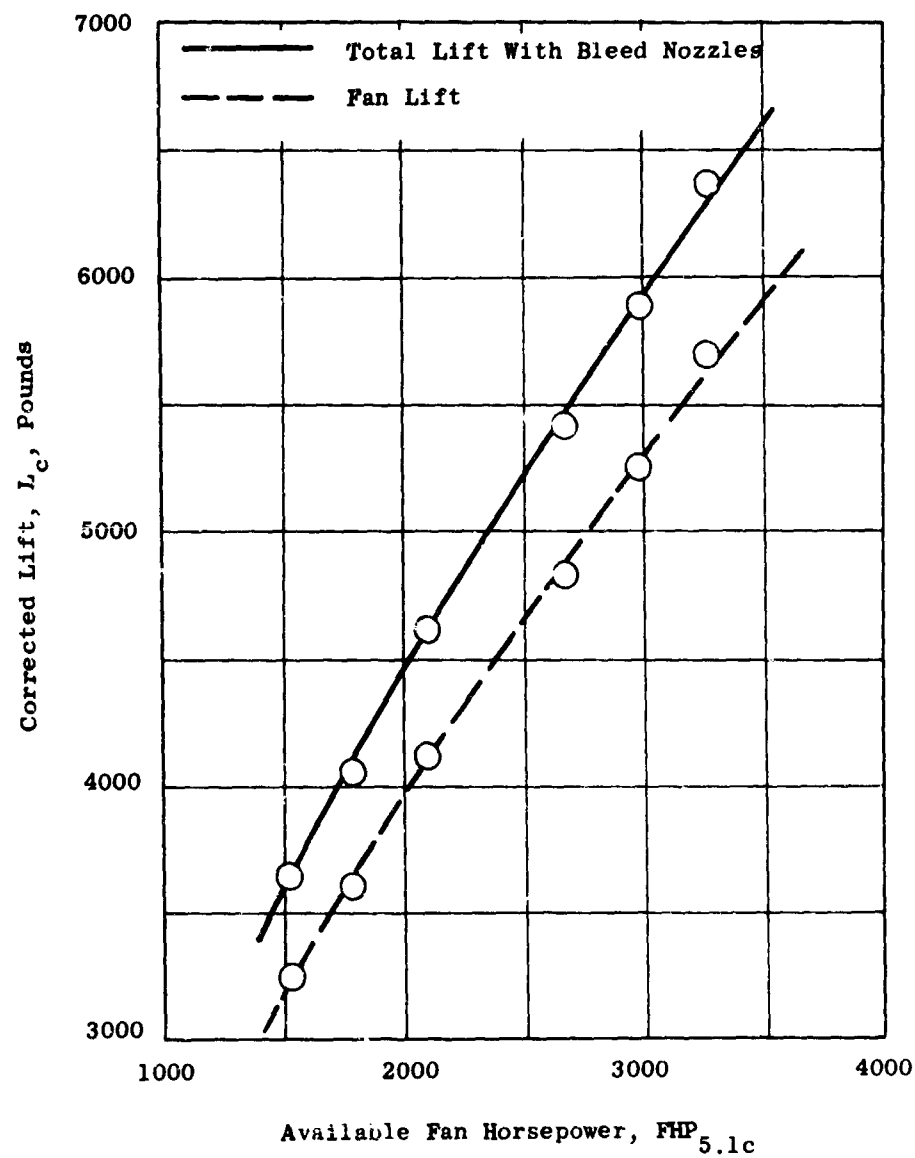


Figure 121. Lift Versus Available Fan Horsepower, Run 17, $\delta_s = 80$ Percent.

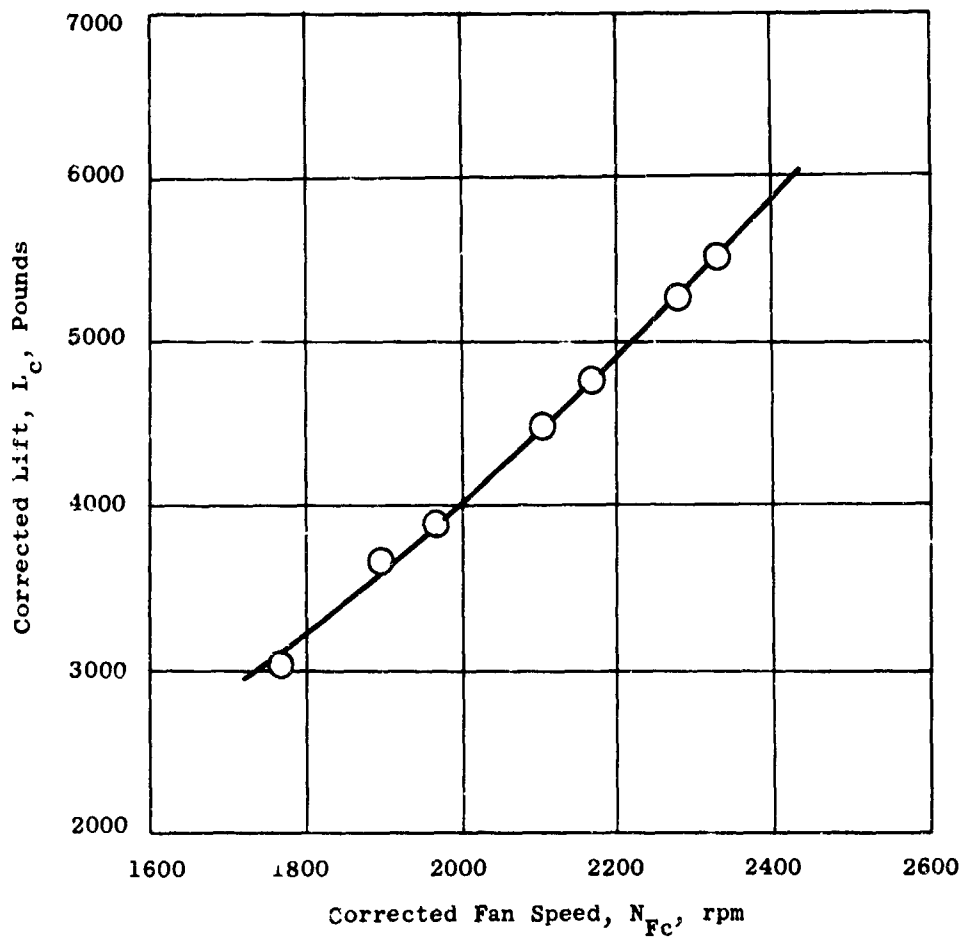


Figure 122. Lift Versus Fan Speed, Run 17, $\delta_s = 80$ Percent, Slip Ring Cavity Covered.

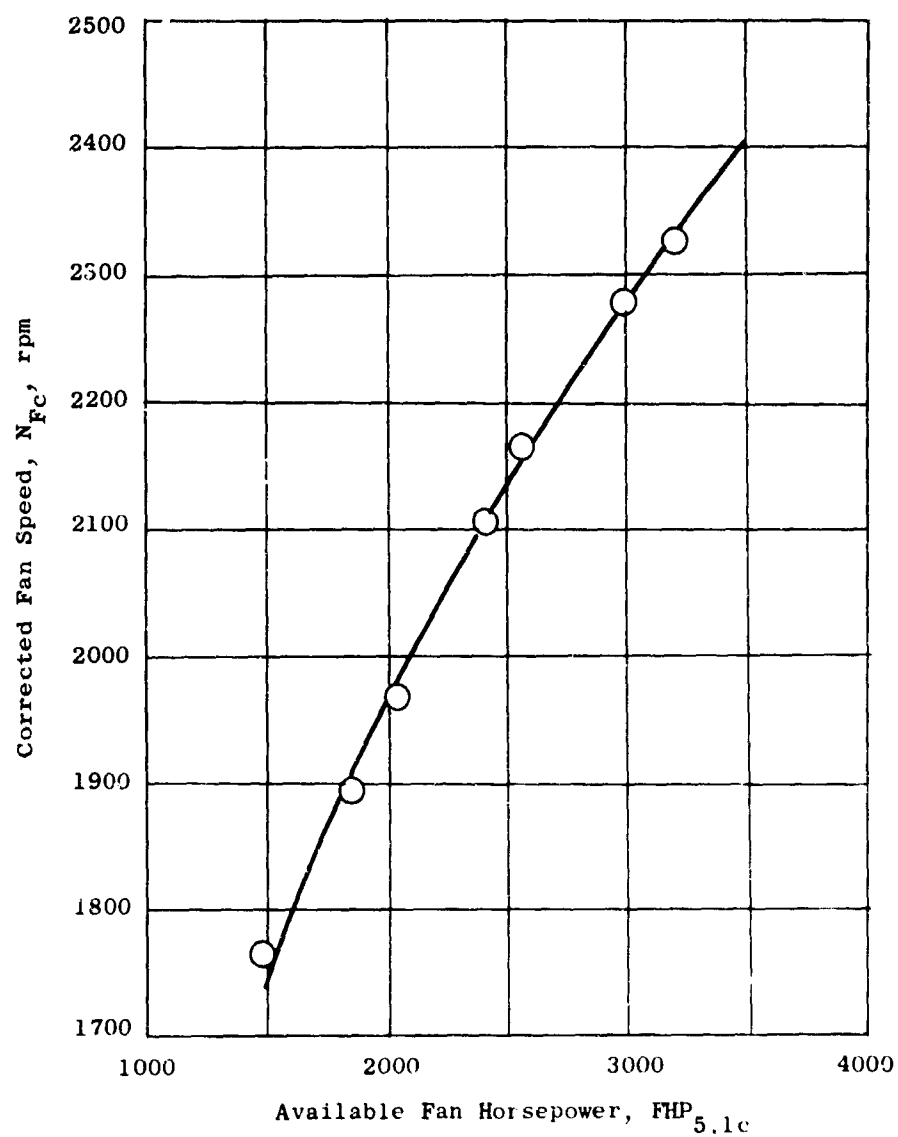


Figure 123. Fan Speed Versus Available Fan Horsepower, Run 17, $\delta_s = 80$ Percent, Slip Ring Cavity Covered.

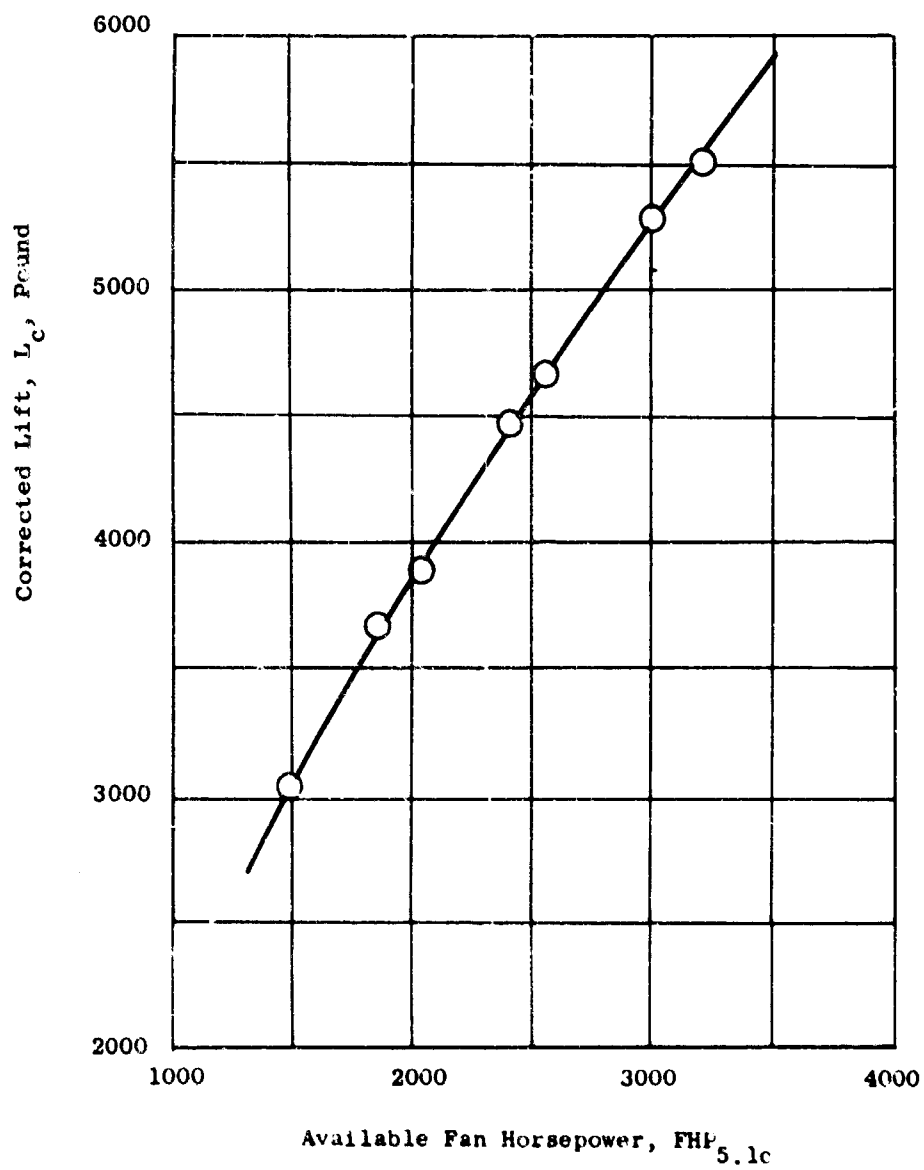


Figure 124. Lift Versus Available Fan Horsepower, Run 17, $\phi_S = 80$ Percent, Slip Ring Cavity Covered.

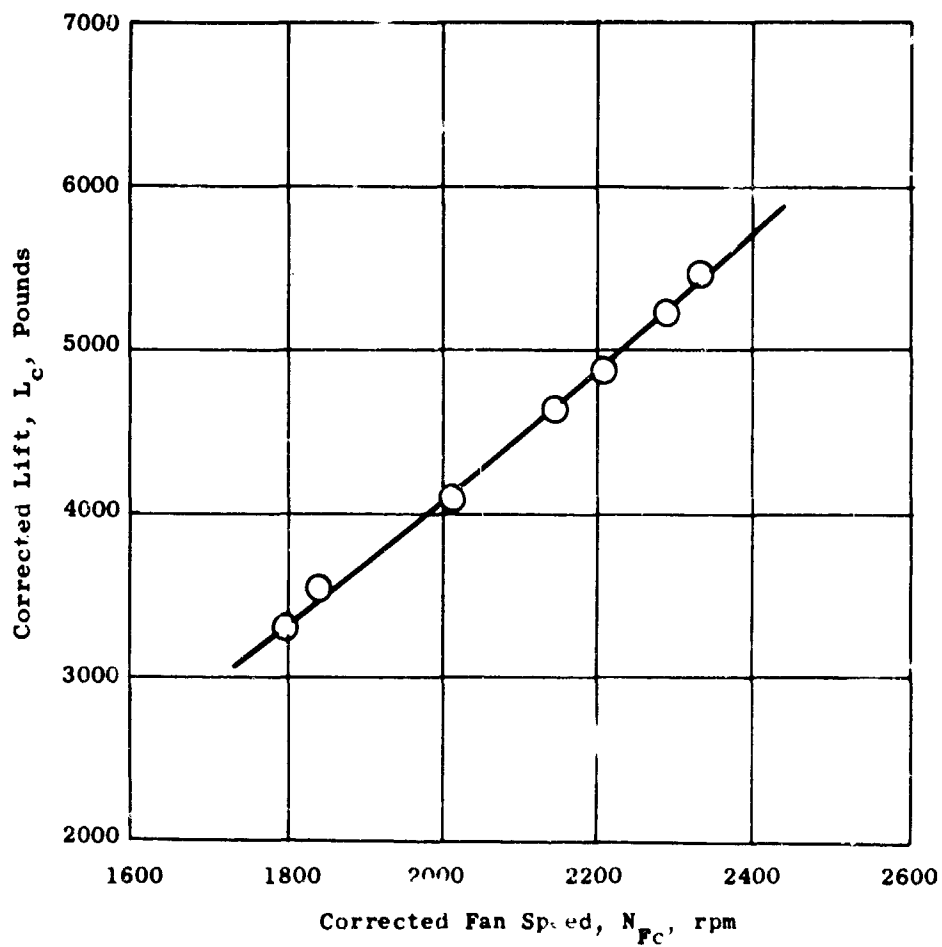


Figure 125. Lift Versus Fan Speed, Run 17, $\delta_S = 80$ Percent, Covered Space Around Blade Tip Tangs.

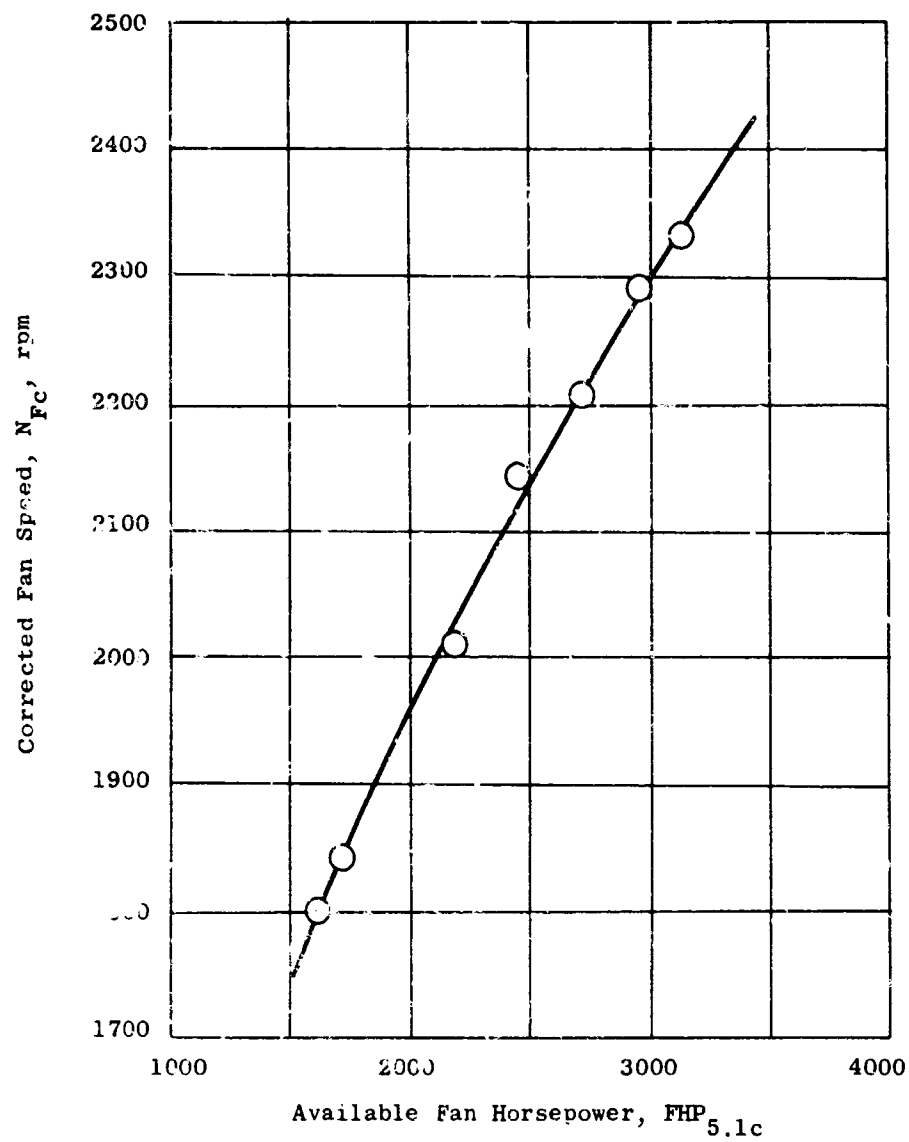


Figure 126. Fan Speed Versus Available Fan Horsepower, Run 17, $\delta_s = 80$ Percent, Covered Space Around Blade Tip Tangs.

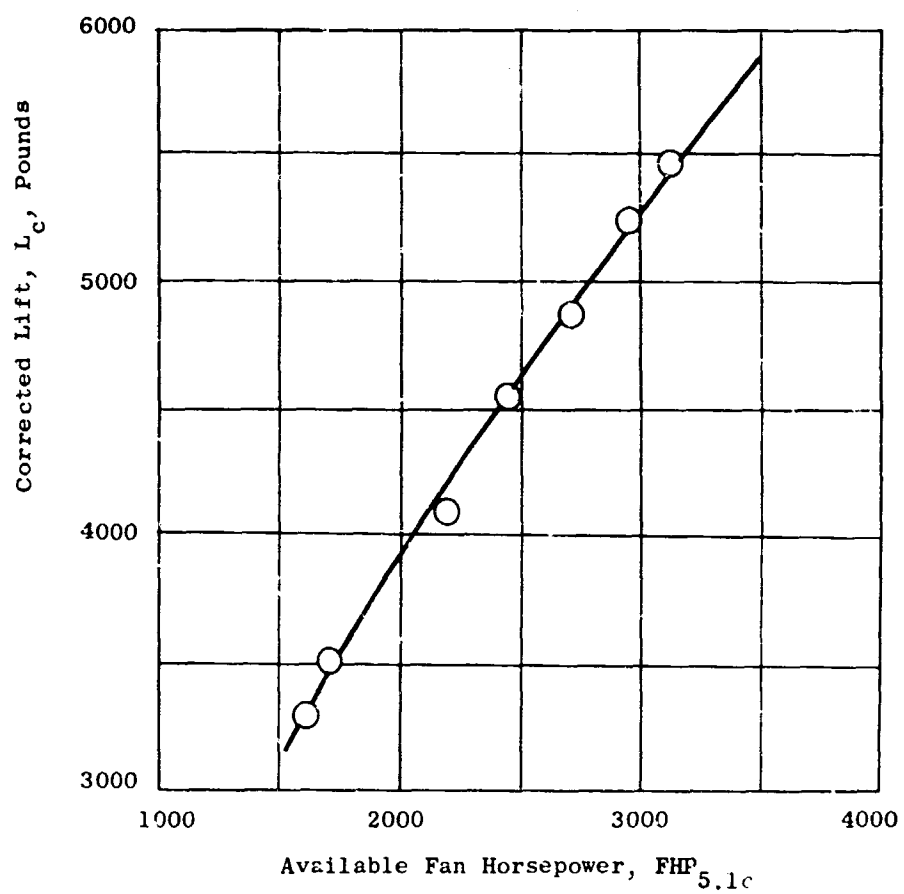


Figure 127. Lift Versus Available Fan Horsepower, Run 17, $\delta_S = 80$ Percent, Covered Space Around Blade Tip Tangs.

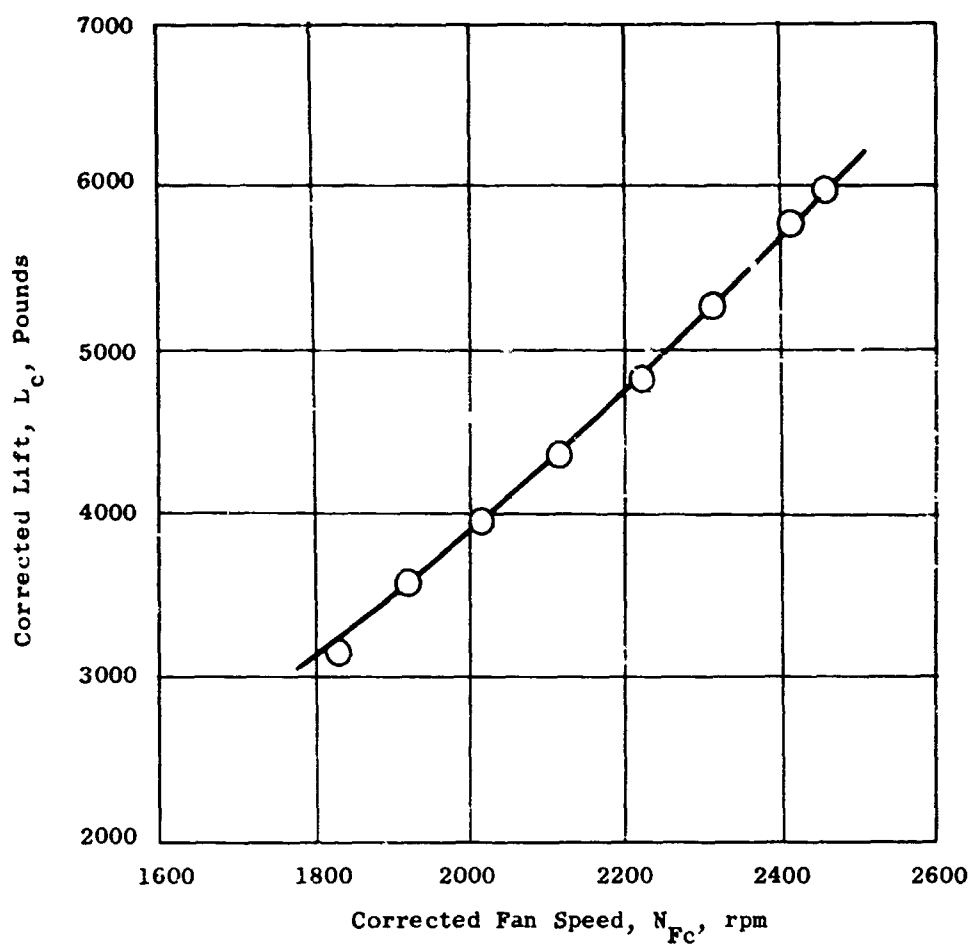


Figure 128. Lift Versus Fan Speed, Run 18, $\delta_s = 80$ Percent, 3 to 6 O'clock Inlet Vane Quadrant Raised.

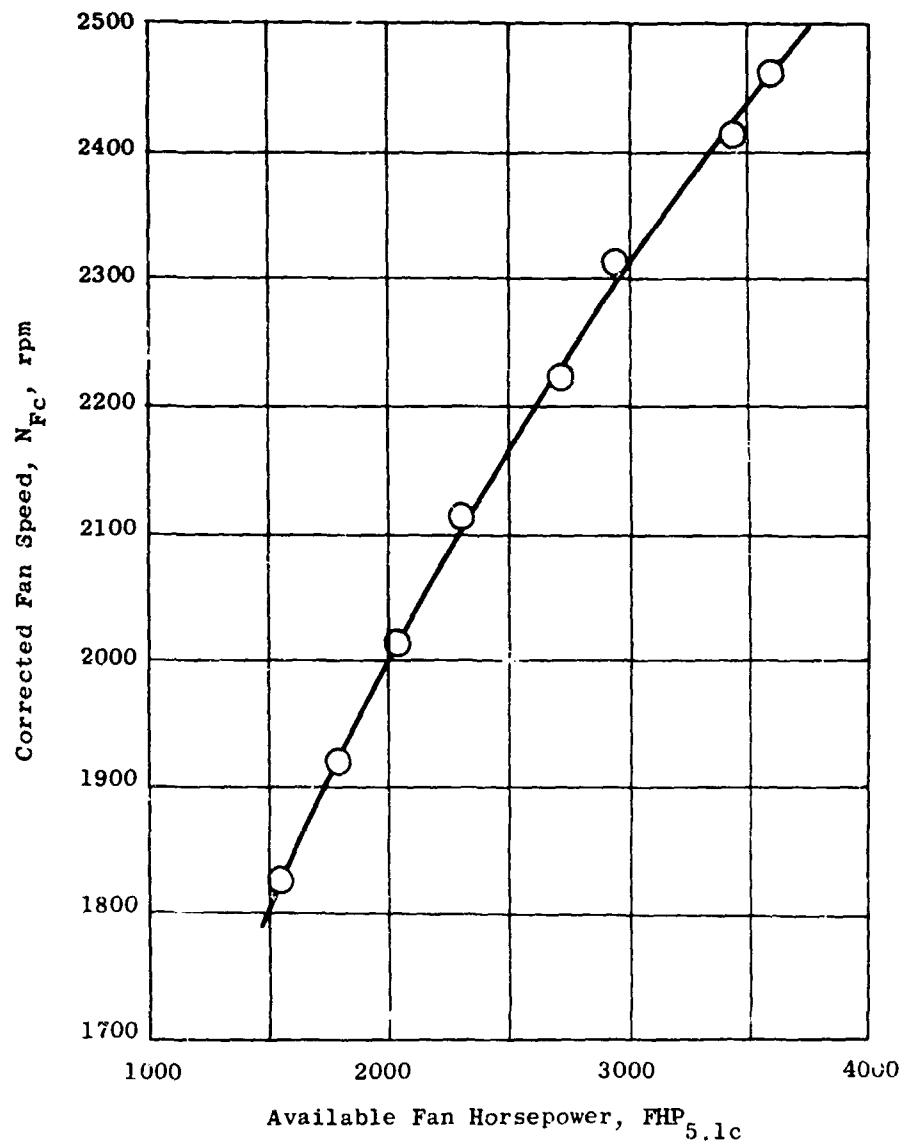


Figure 129. Fan Speed Versus Available Fan Horsepower,
Run 18, $\delta_S = 80$ Percent, 3 to 6 O'clock Inlet
Vane Quadrant Raised.

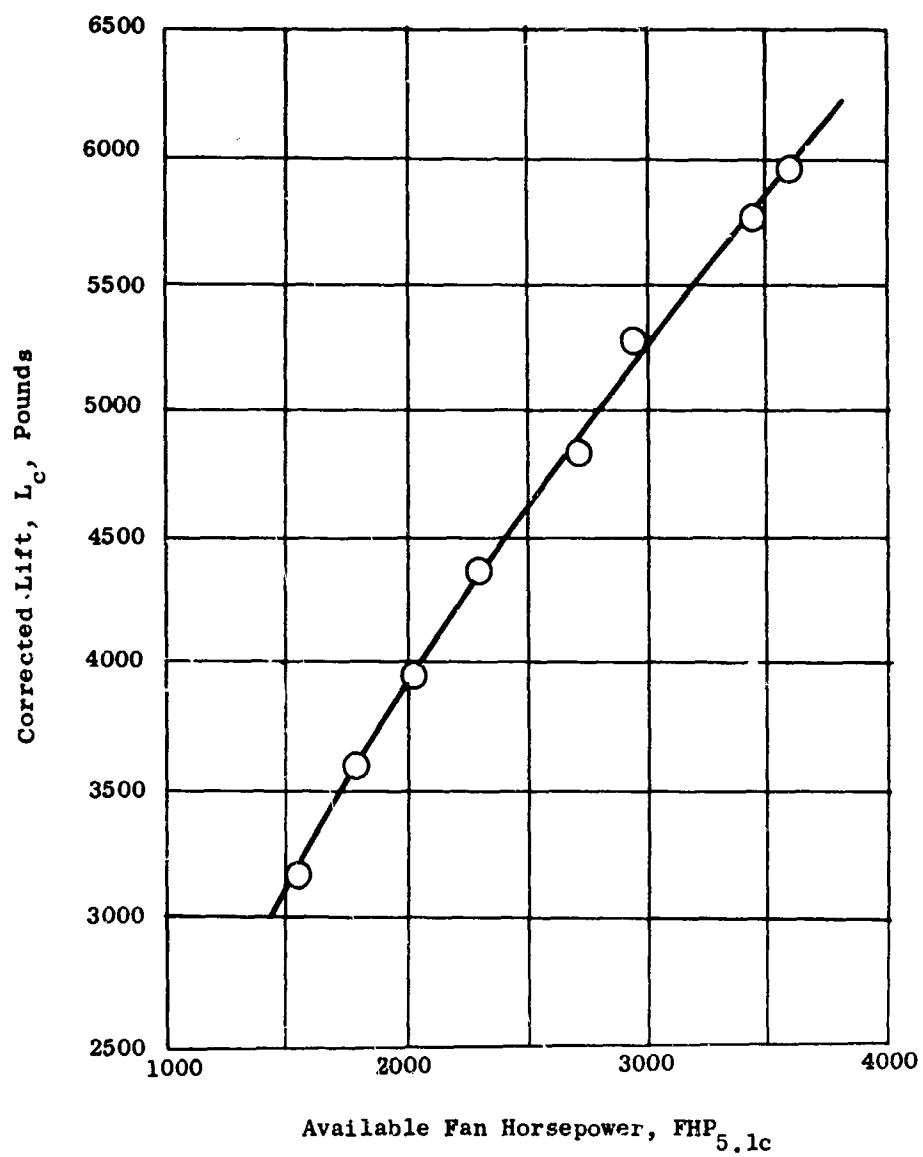


Figure 130. Lift Versus Available Fan Horsepower, Run 18,
 $\delta_S = 80$ Percent, 3 to 6 O'clock Inlet Vane
 Quadrant Raised.

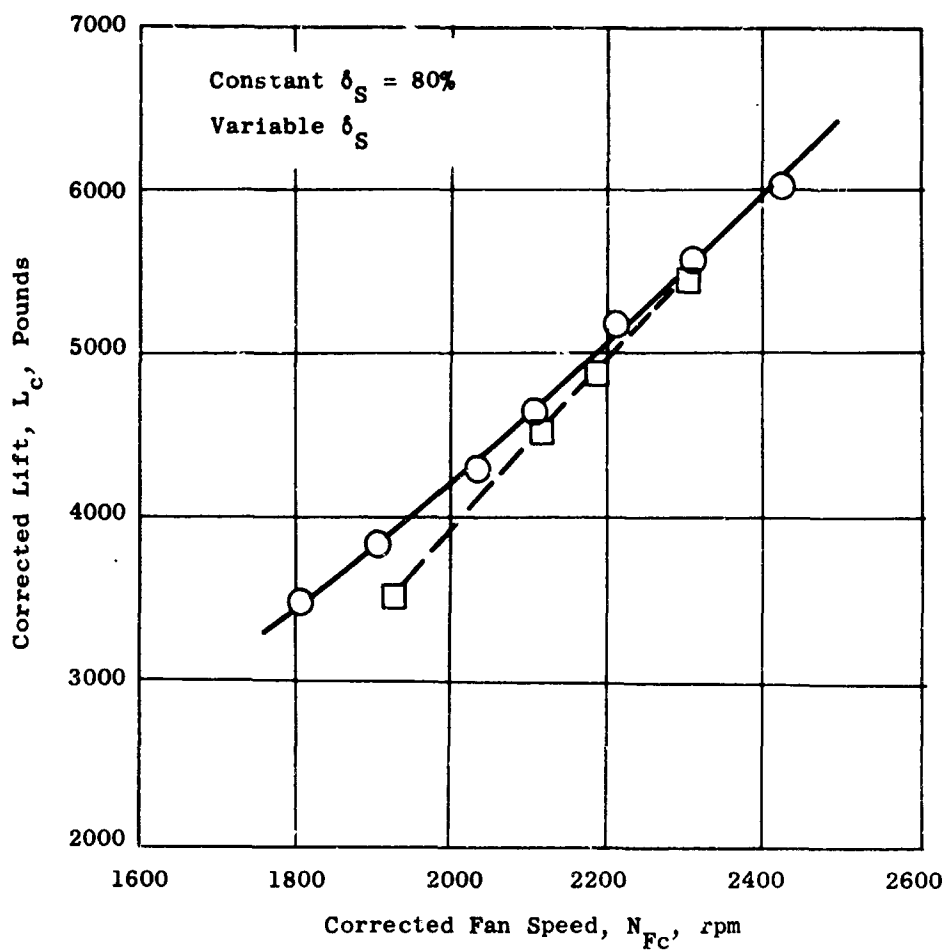


Figure 131. Lift Versus Fan Speed, Run 18, Exit Louvers Removed.

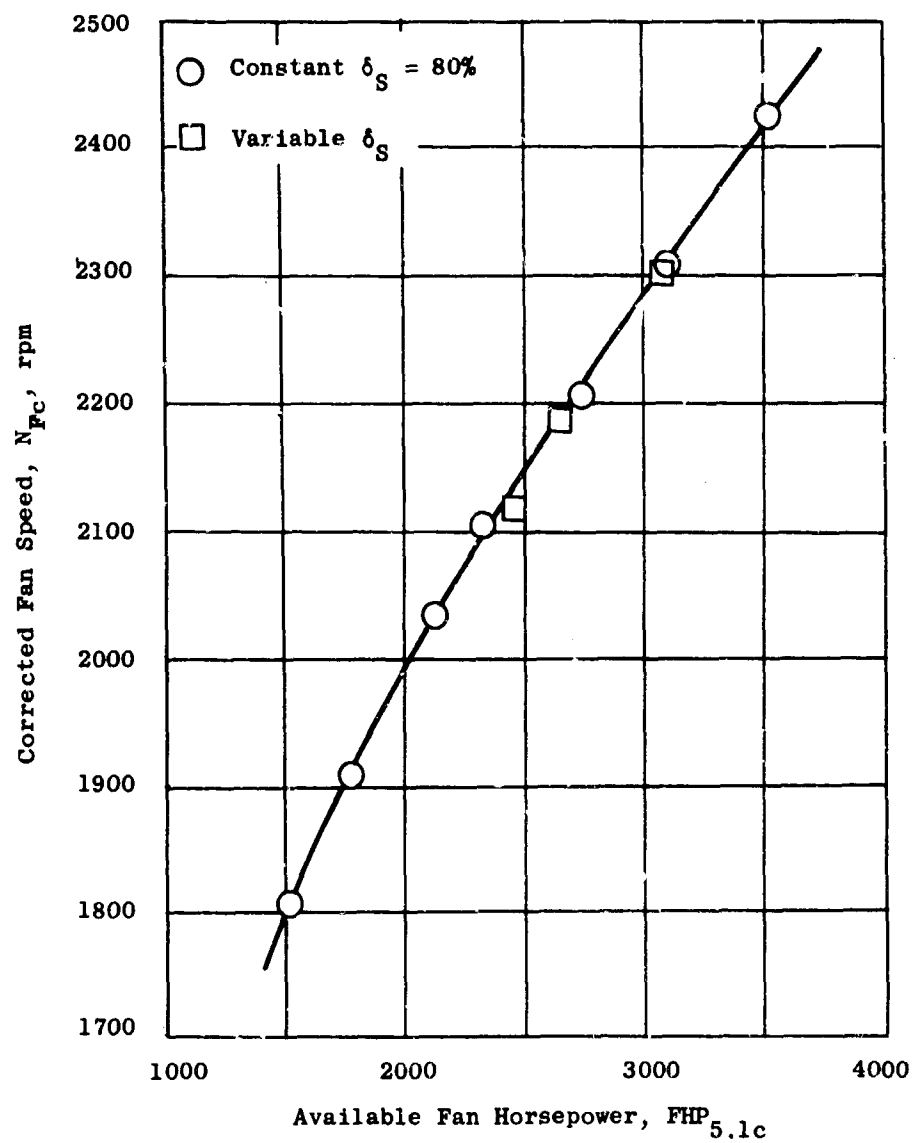


Figure 132. Fan Speed Versus Available Fan Horsepower, Run 18, Exit Louvers Removed.

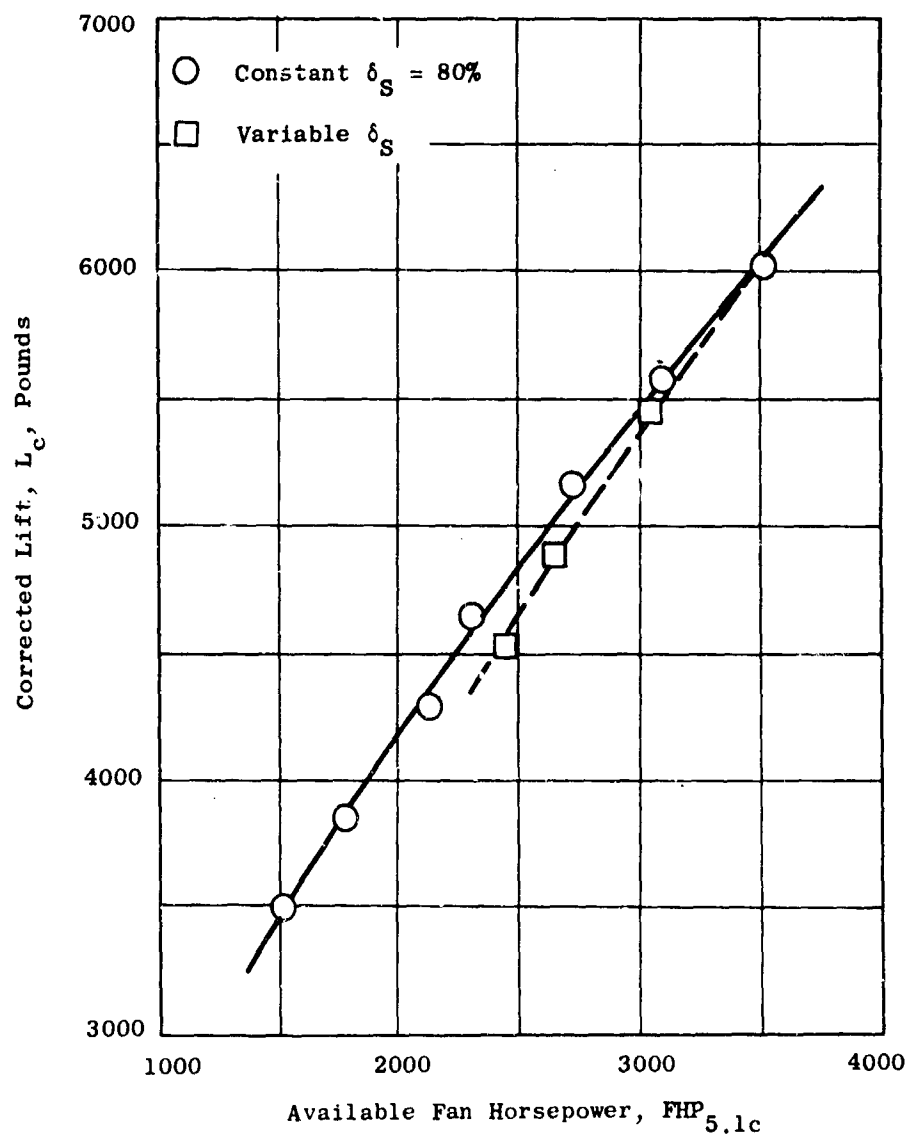


Figure 133. Lift Versus Available Fan Horsepower, Run 18, Exit Louver Removed.

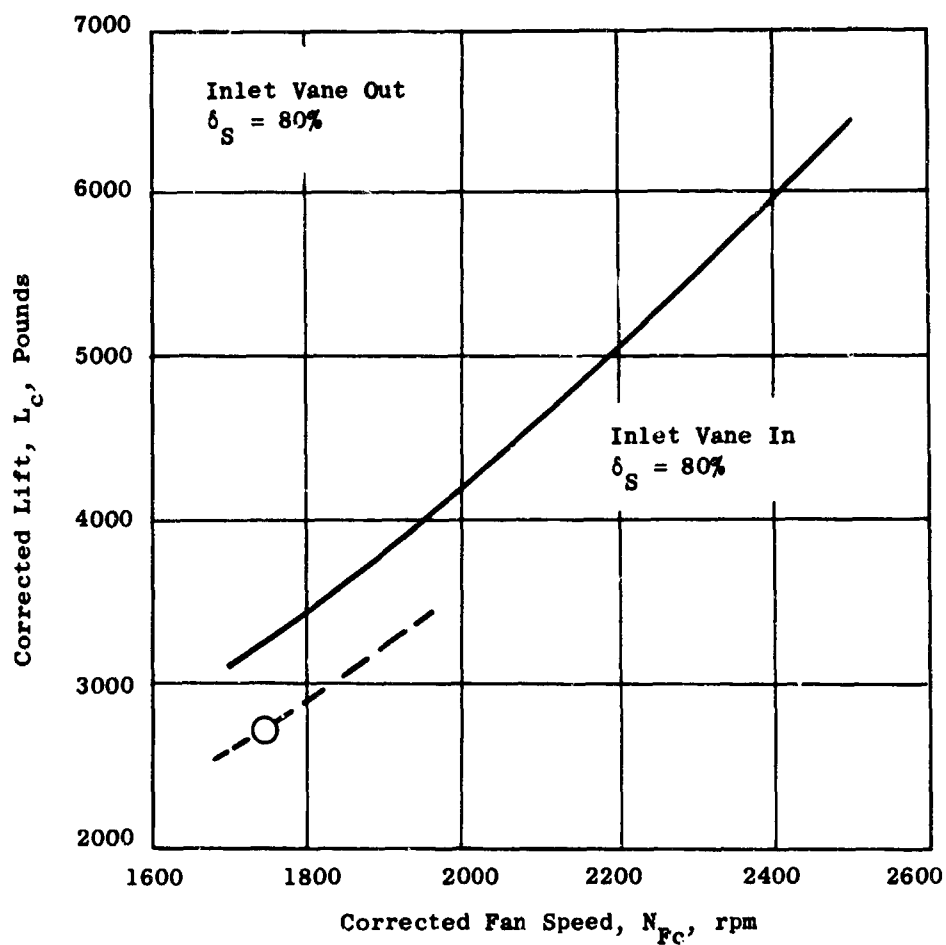


Figure 134. Lift Versus Fan Speed, Run 18, Inlet Vane Out.

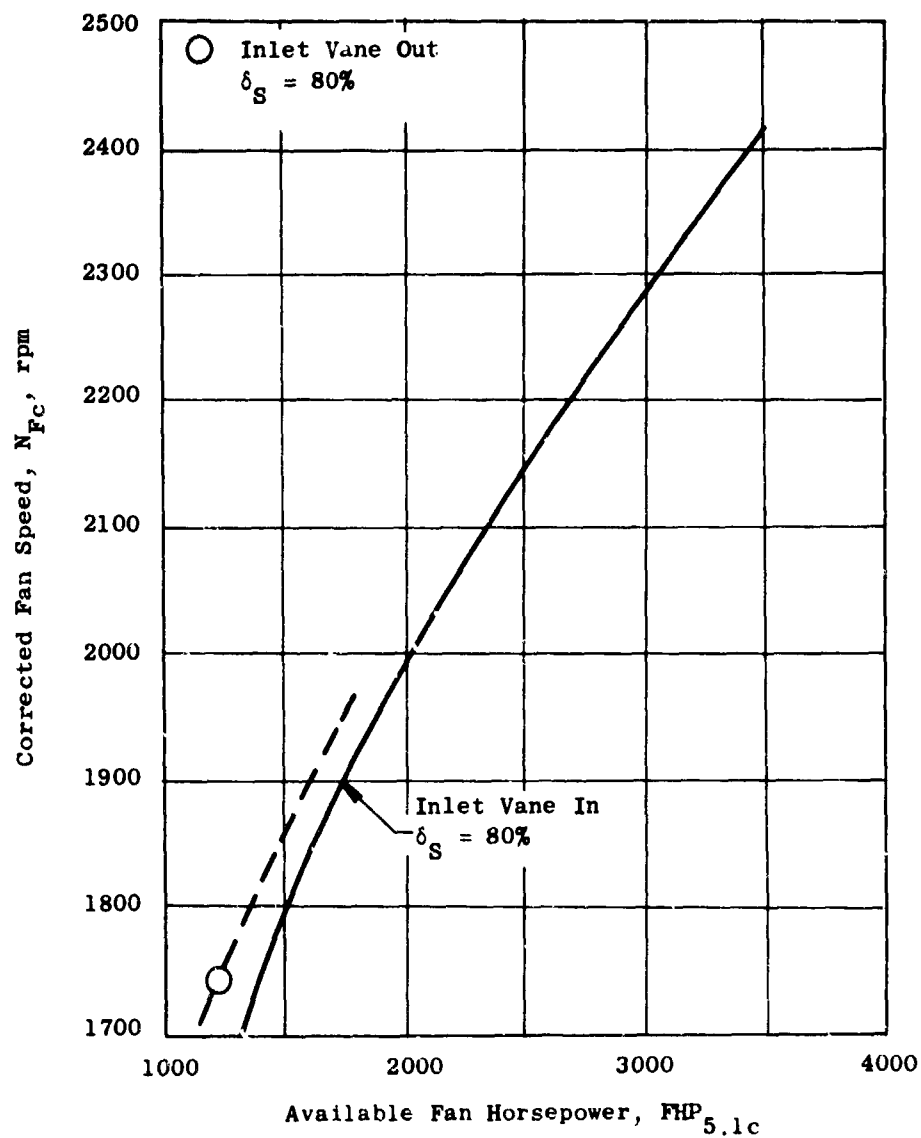


Figure 135. Fan Speed Versus Available Fan Horsepower, Run 18, Inlet Vane Out.

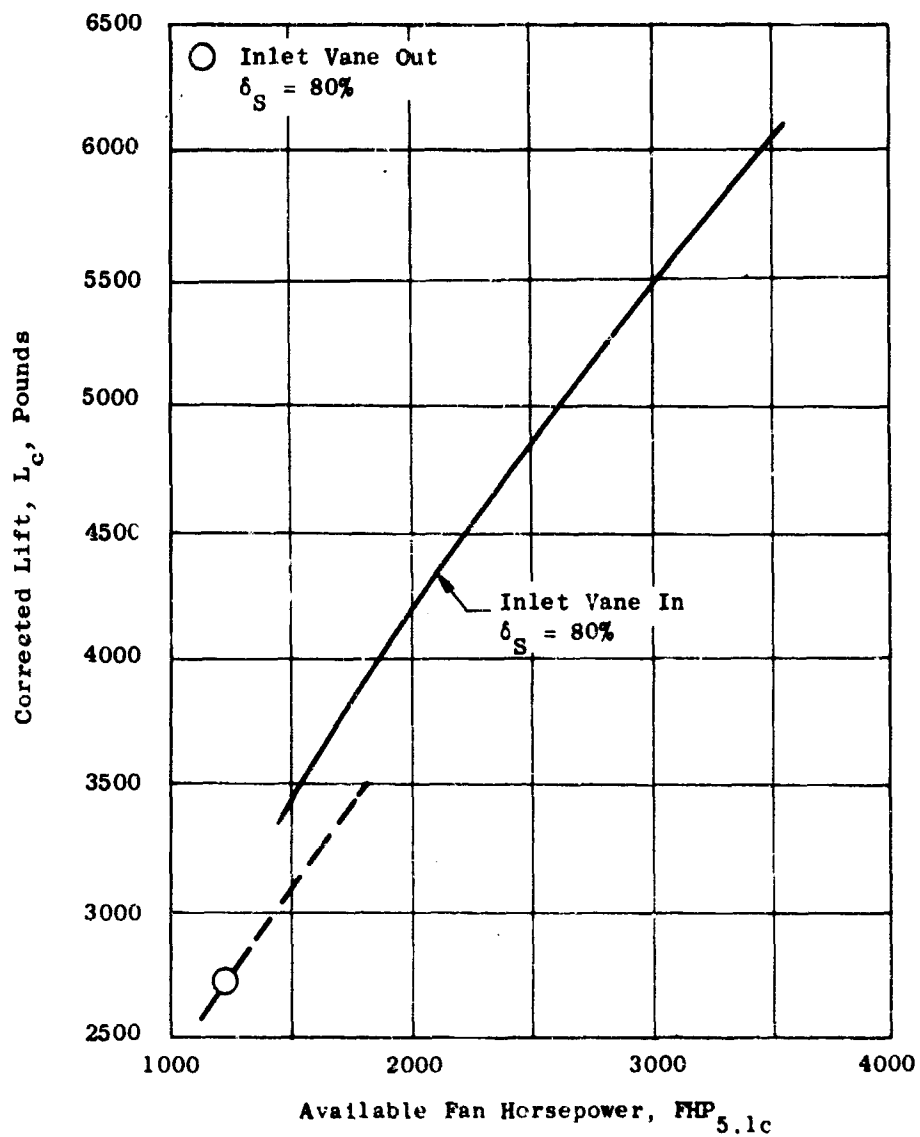


Figure 136. Lift Versus Available Fan Horsepower, Run 18, Inlet Vane Out.

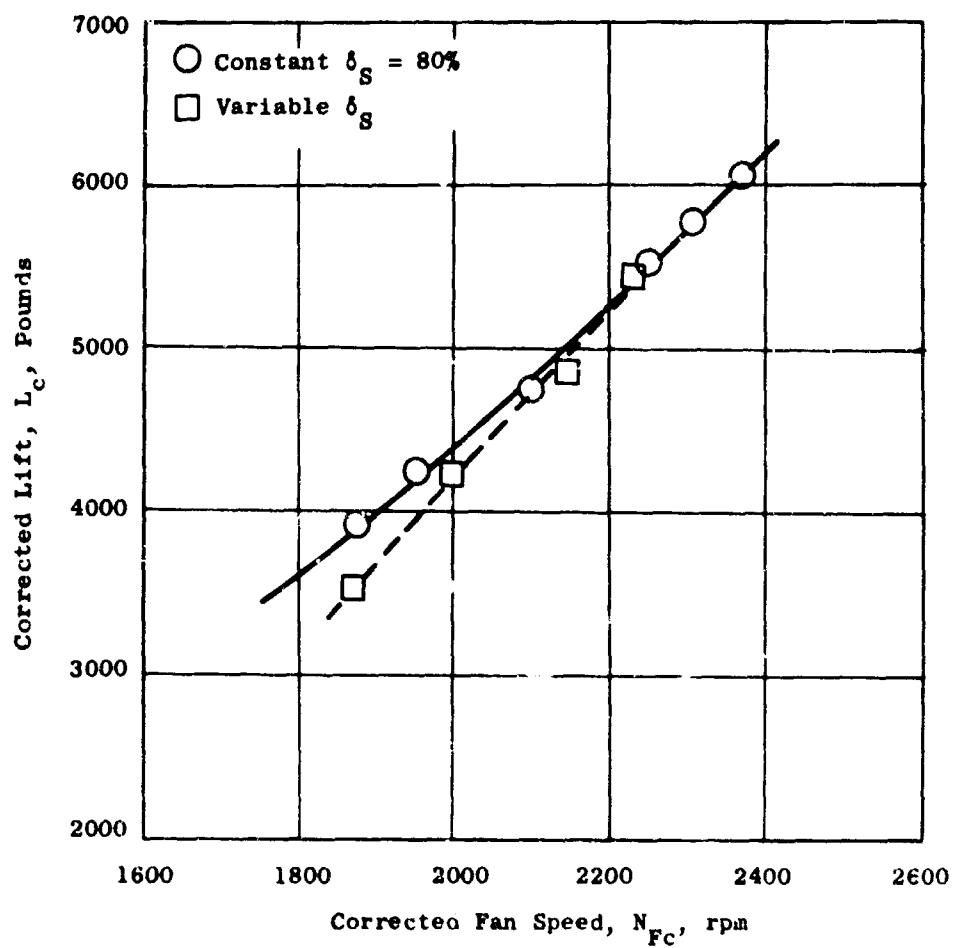


Figure 137. Lift Versus Fan Speed, Run 19, Improved Forward Air Seal.

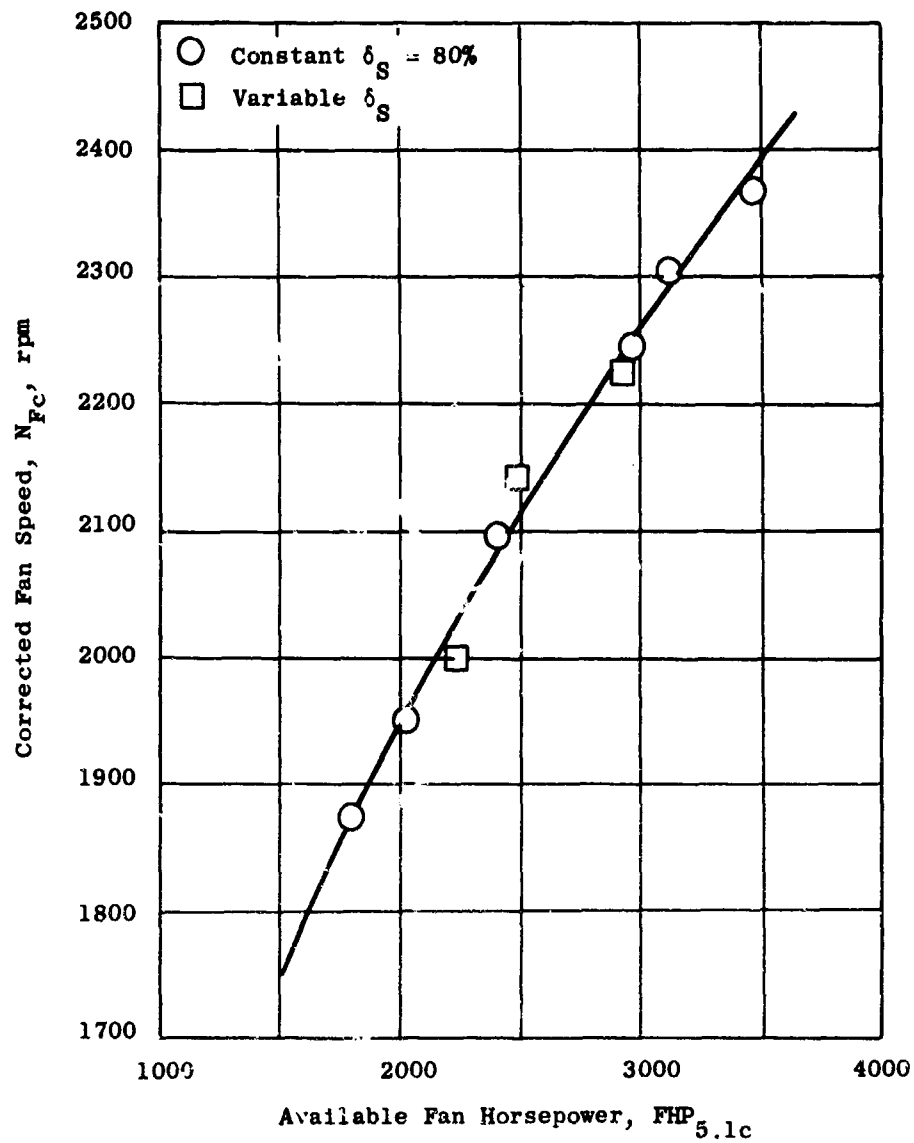


Figure 138. Fan Speed Versus Available Fan Horsepower, Run 19, Improved Forward Air Seal.

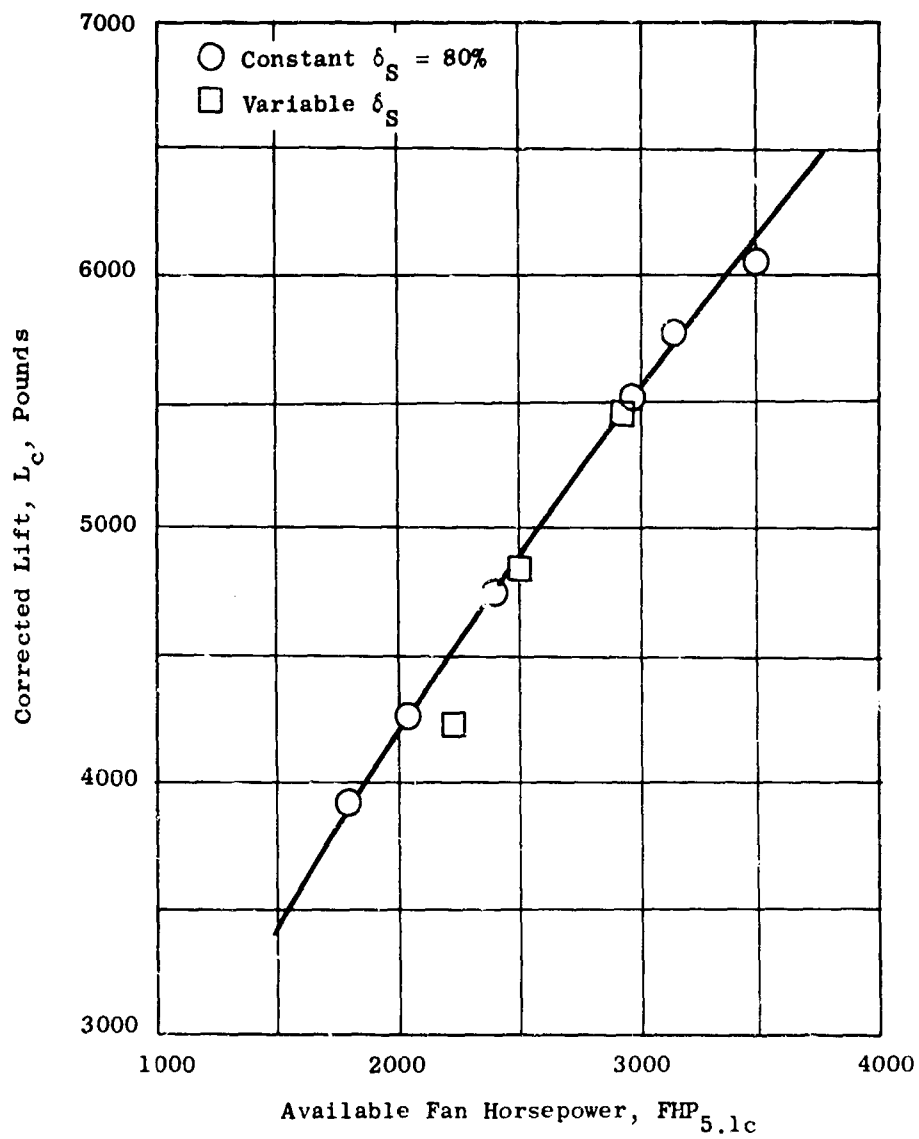


Figure 139. Lift Versus Available Fan Horsepower, Run 19, Improved Forward Air Seal.

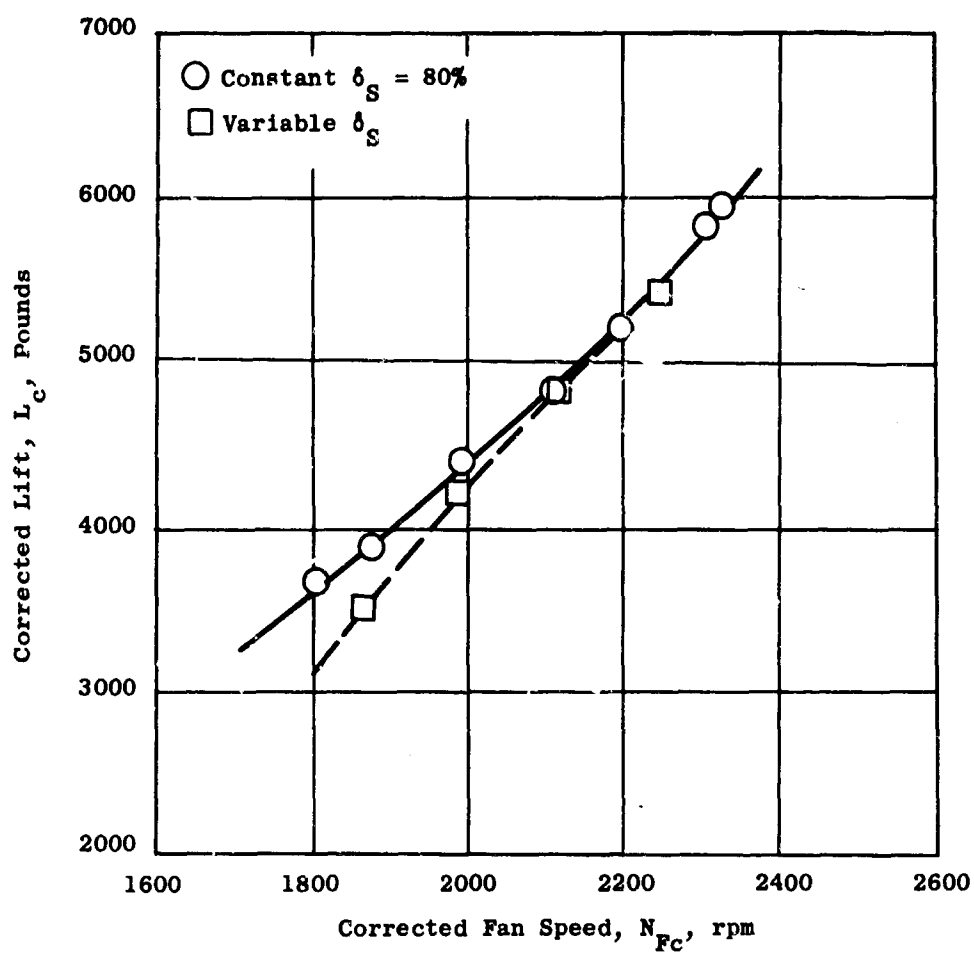


Figure 140. Lift Versus Fan Speed, Run 19, Stator Stiffener Rings Out.

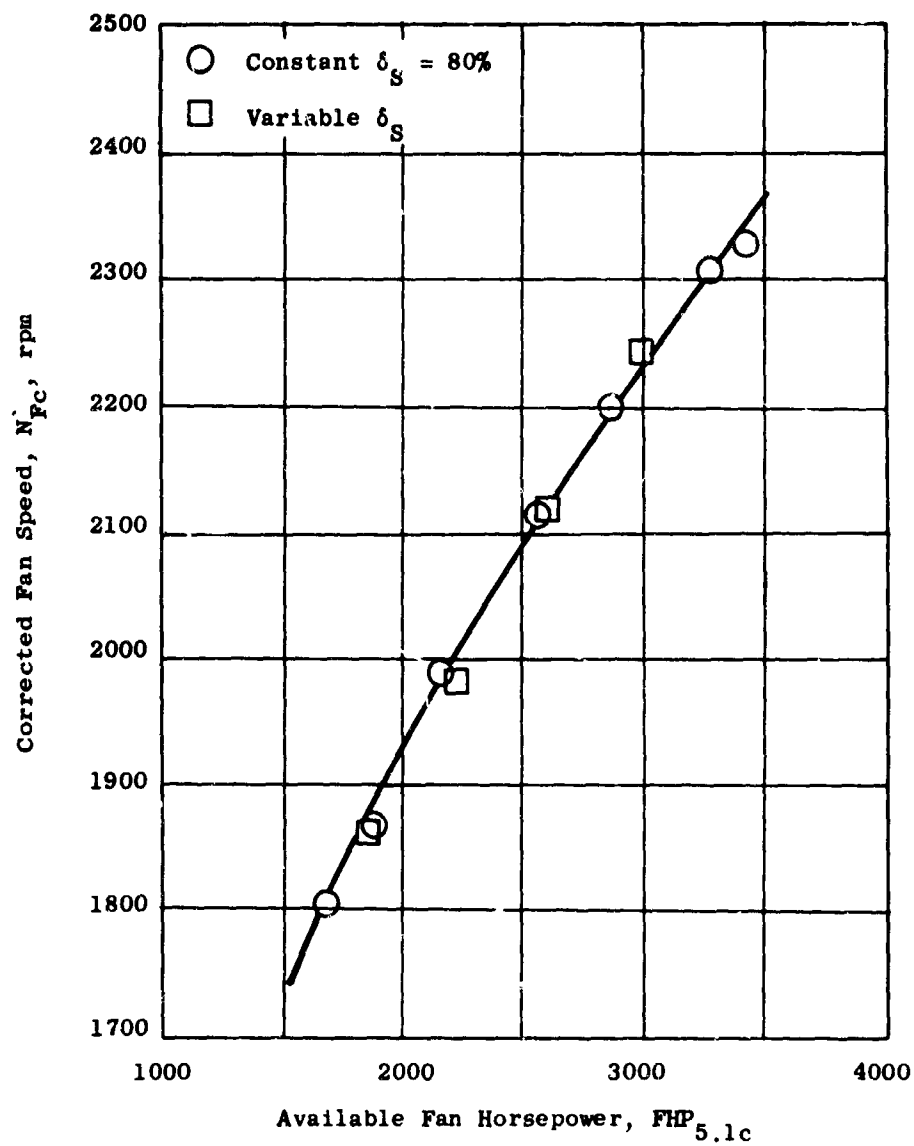


Figure 141. Fan Speed Versus Available Fan Horsepower, Rur 19, Stator Stiffener Rings Out.

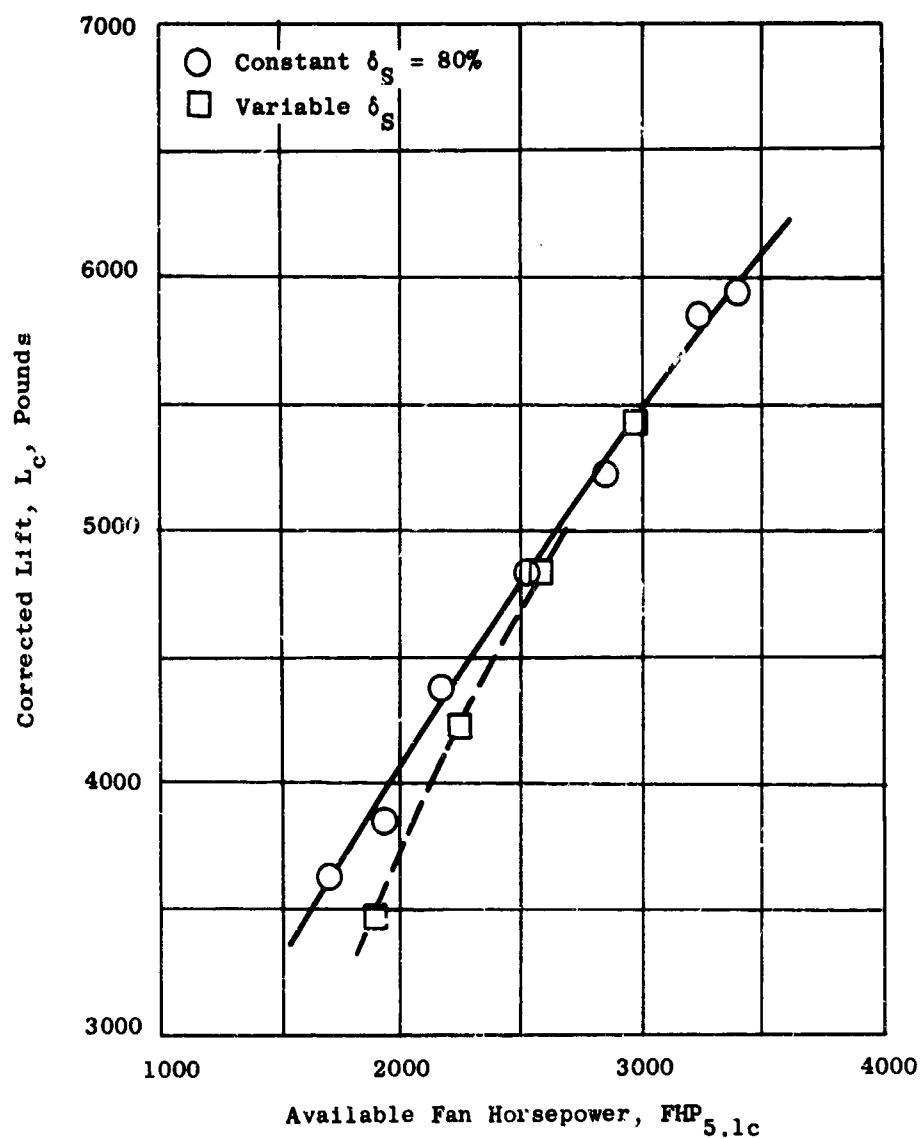


Figure 142. Lift Versus Available Fan Horsepower, Run 19, Stator Stiffener Rings Out.

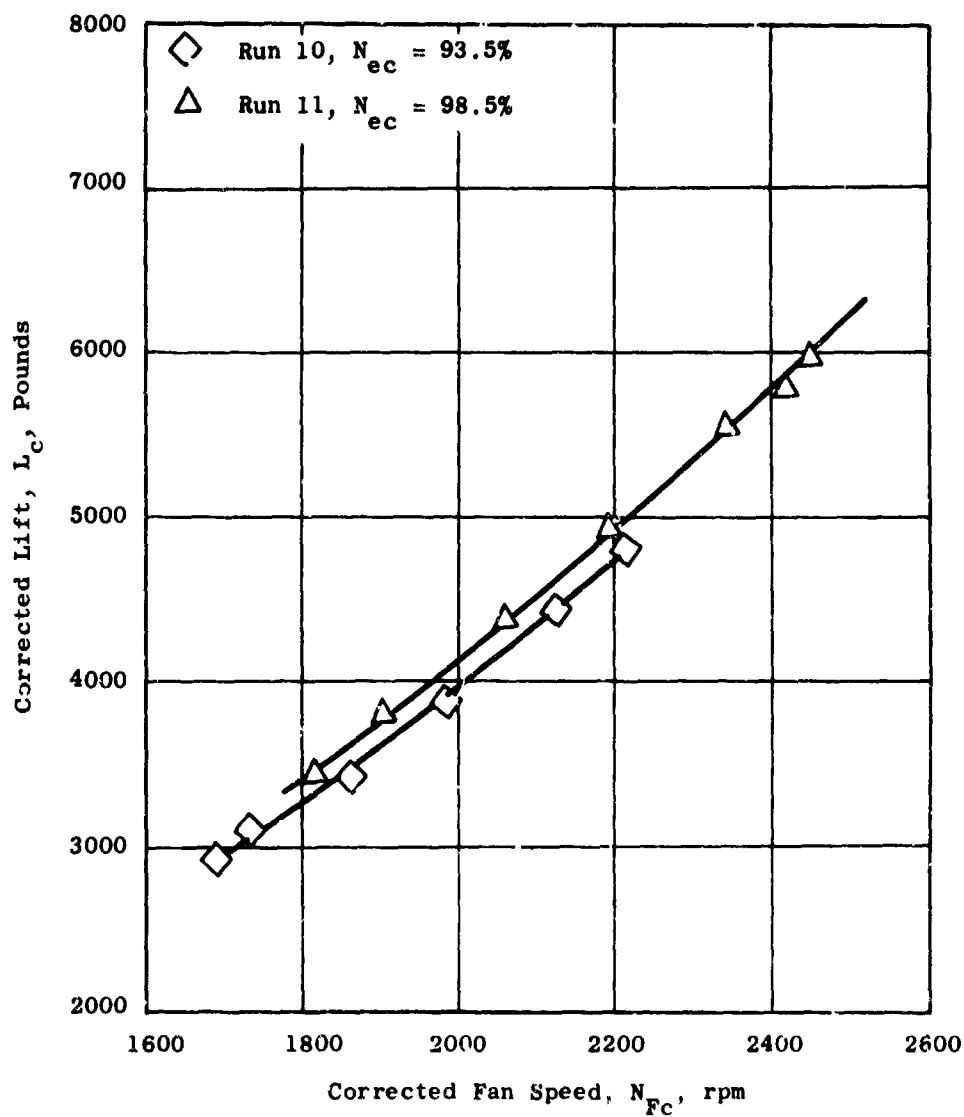


Figure 143. Lift Versus Fan Speed, Runs 10 and 11, Variable δ_s From -8 to 110 Percent.

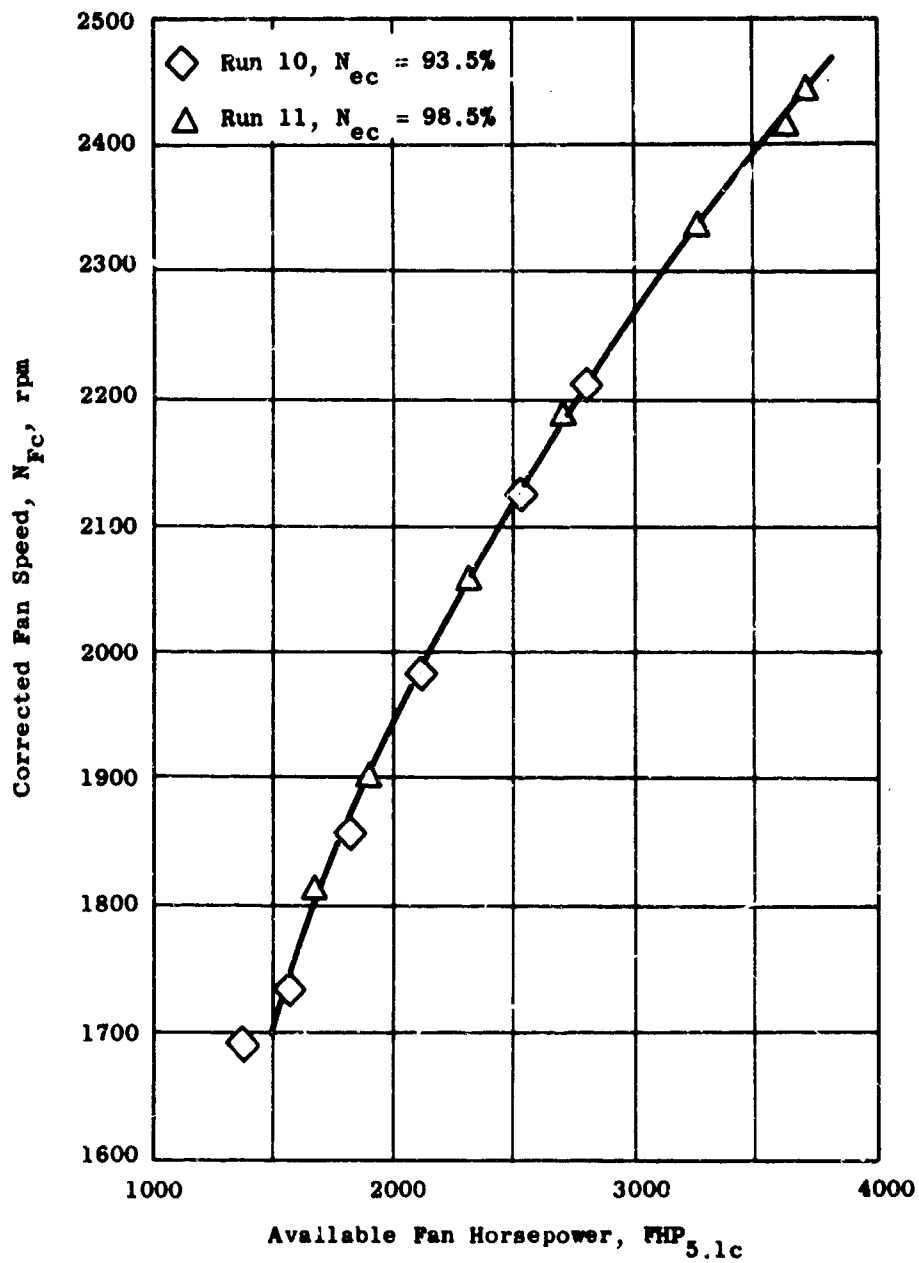


Figure 144. Fan Speed Versus Available Fan Horsepower, Runs 10 and 11, Variable δ_s From -8 to 110 Percent.

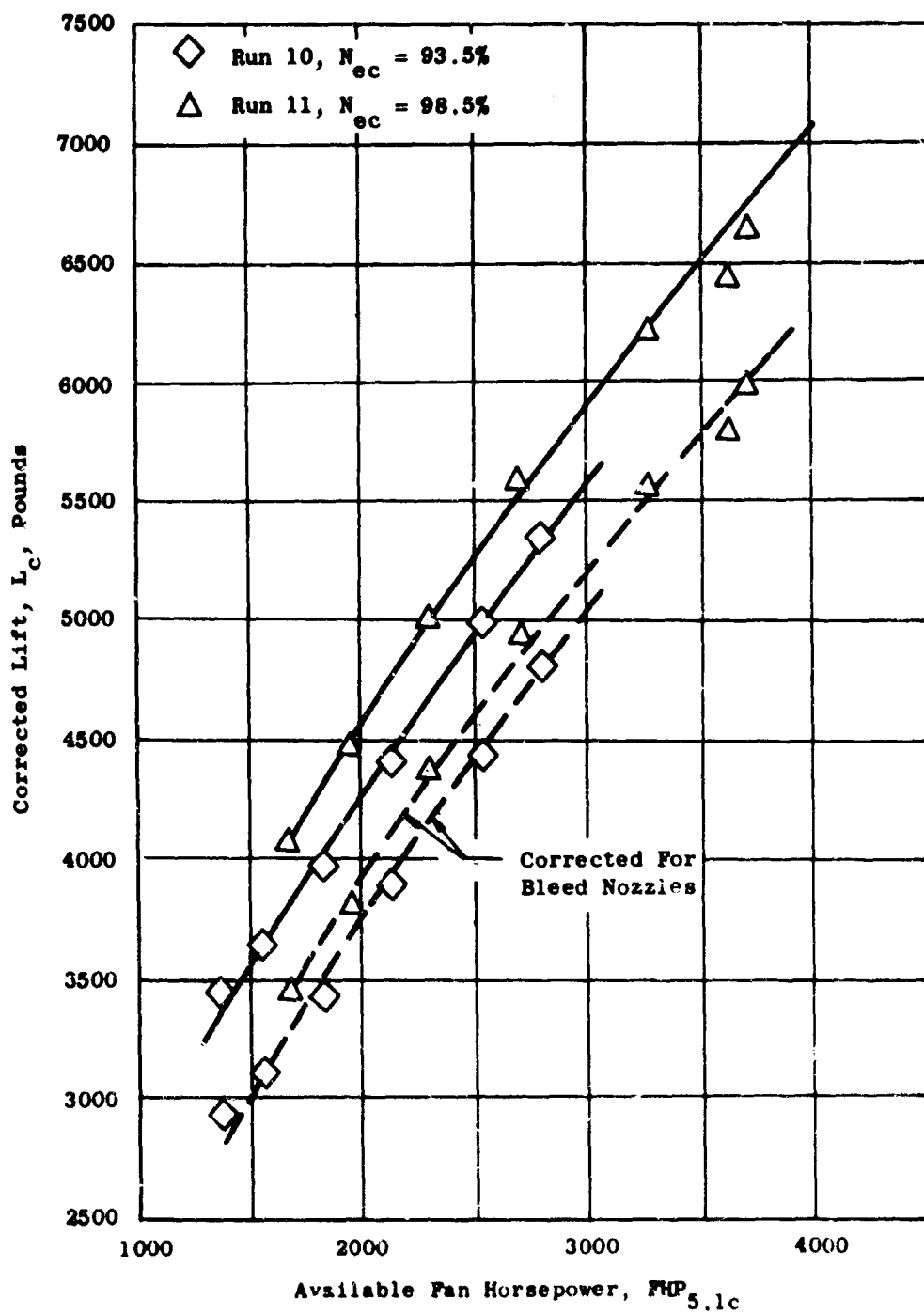


Figure 145. Lift Versus Available Fan Horsepower, Runs 10 and 11, Variable δ_s From -8 to 110 Percent.

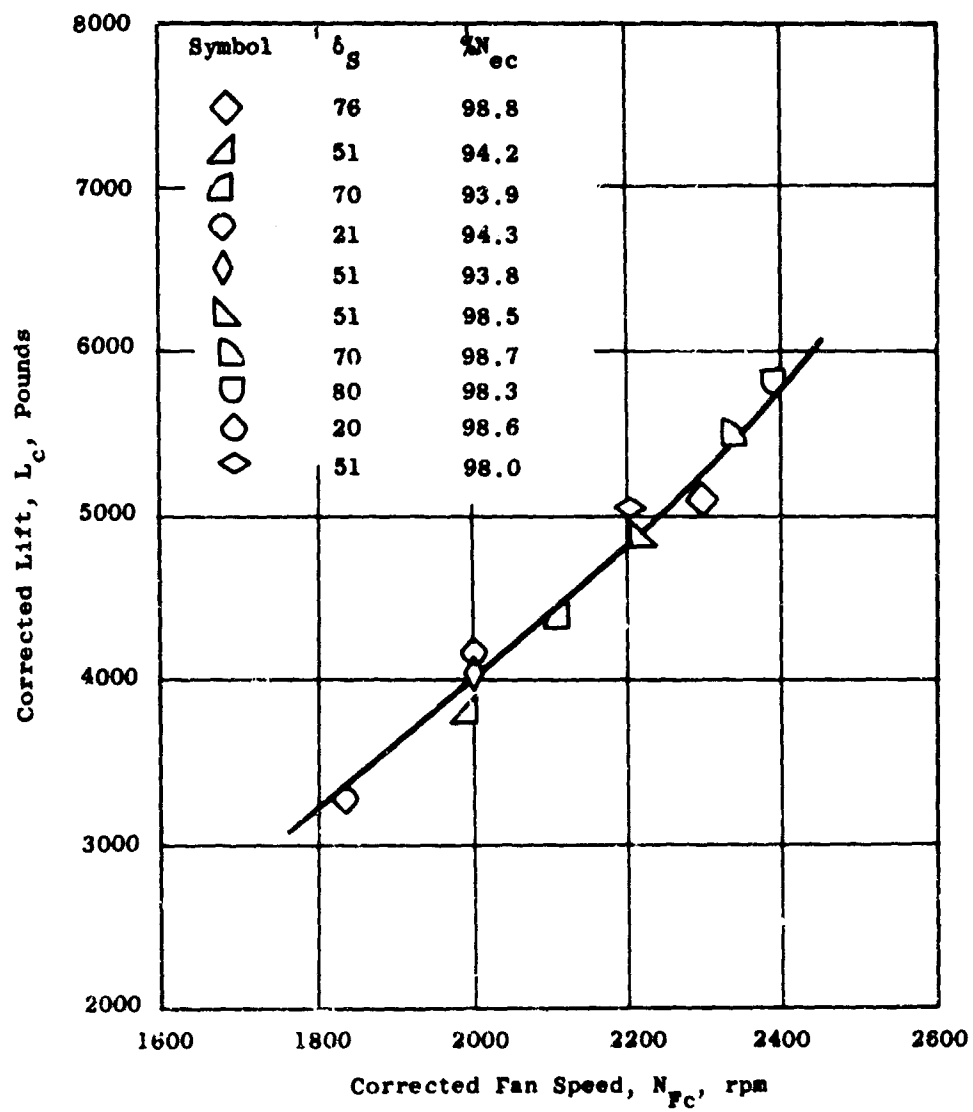


Figure 146. Lift Versus Fan Speed, Runs 12 and 14, Variable δ_s .

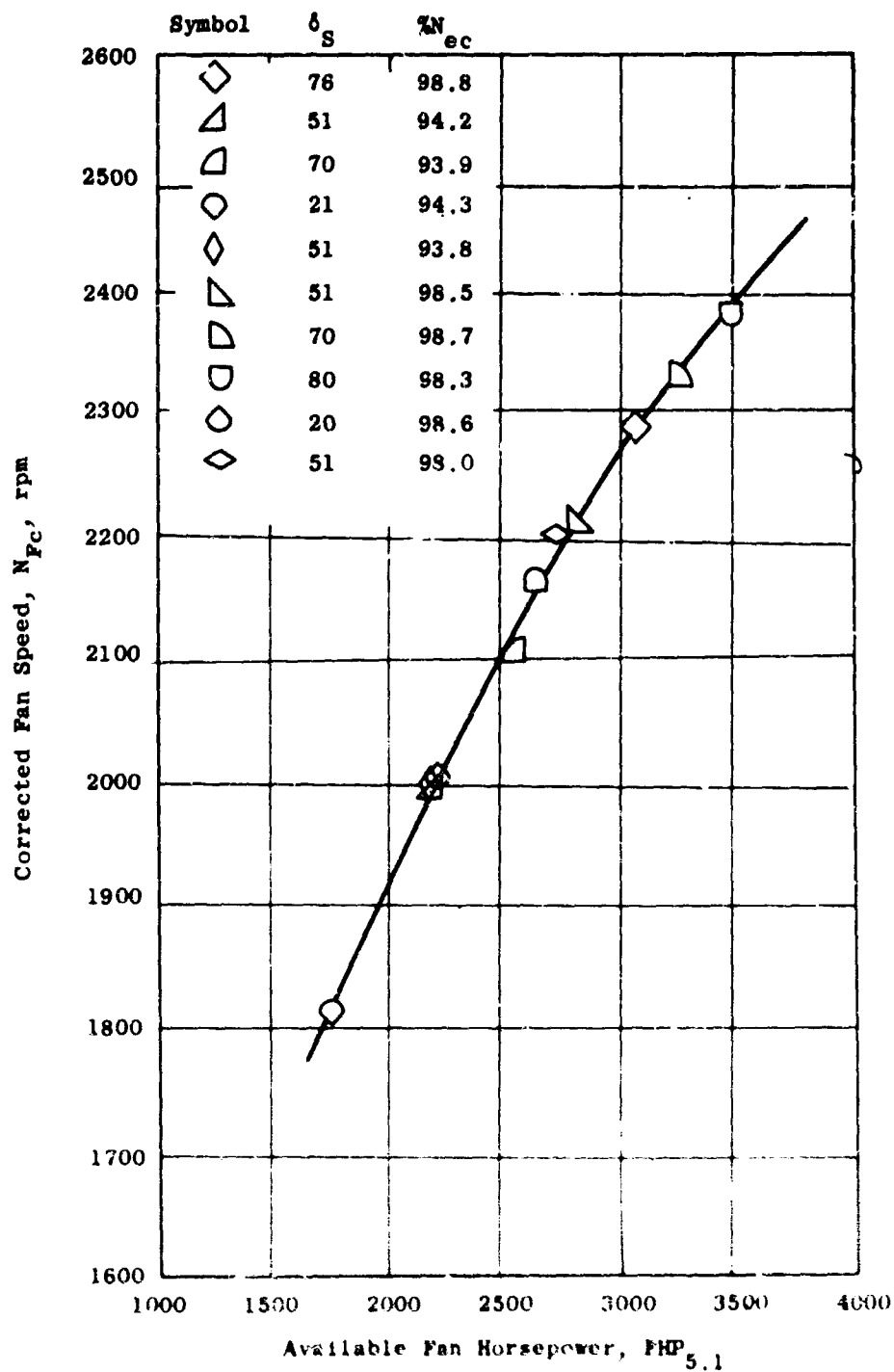


Figure 147. Fan Speed Versus Available Fan Horsepower, Runs 12 and 14, Variable δ_s .

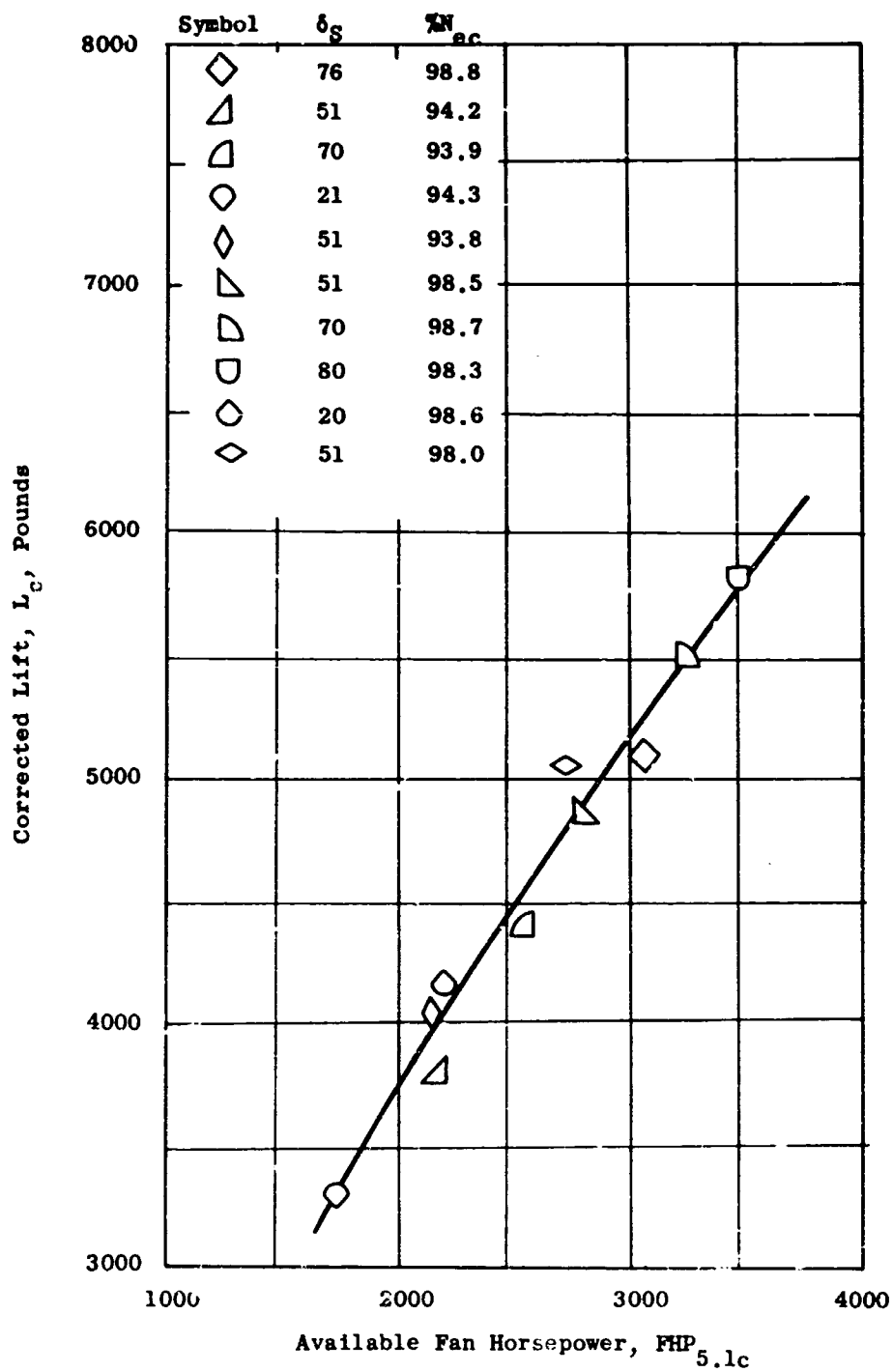


Figure 148. Lift Versus Available Fan Horsepower, Runs 12 and 14, Variable δ_S .

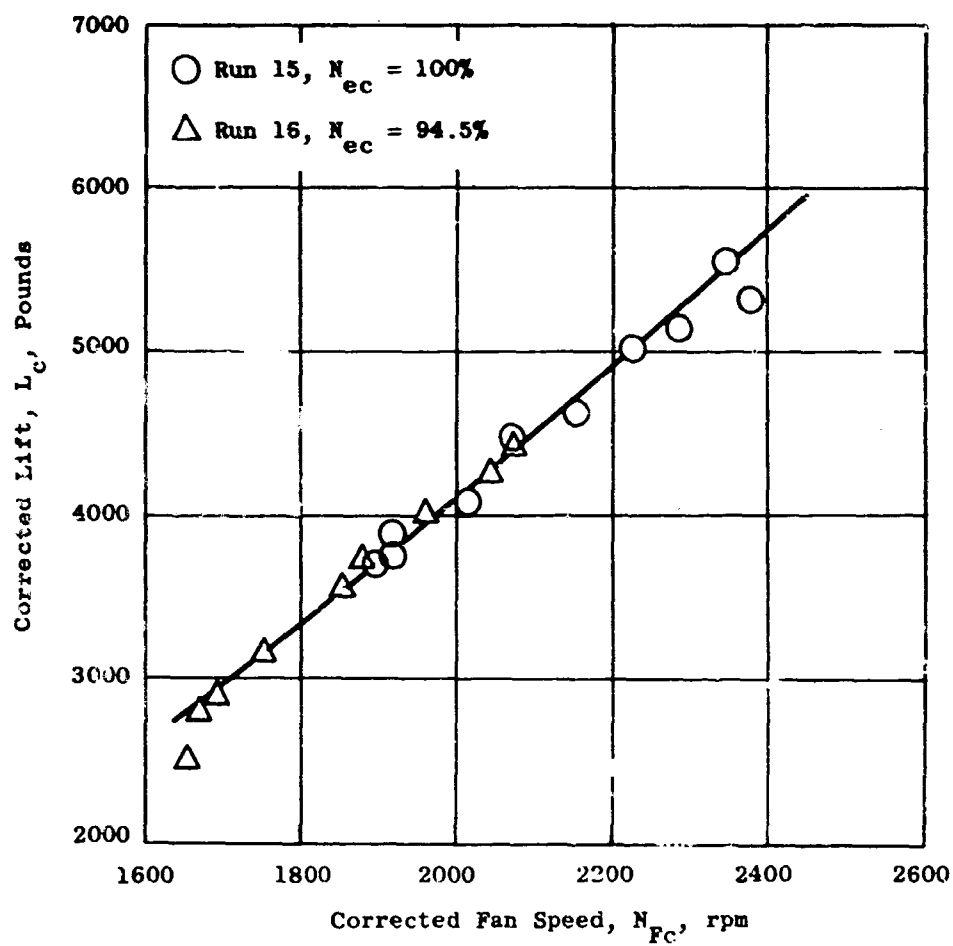


Figure 149. Lift Versus Fan Speed, Runs 15 and 16, Variable δ_s From 0 to 80 Percent, $\beta_v = 0$ Degrees.

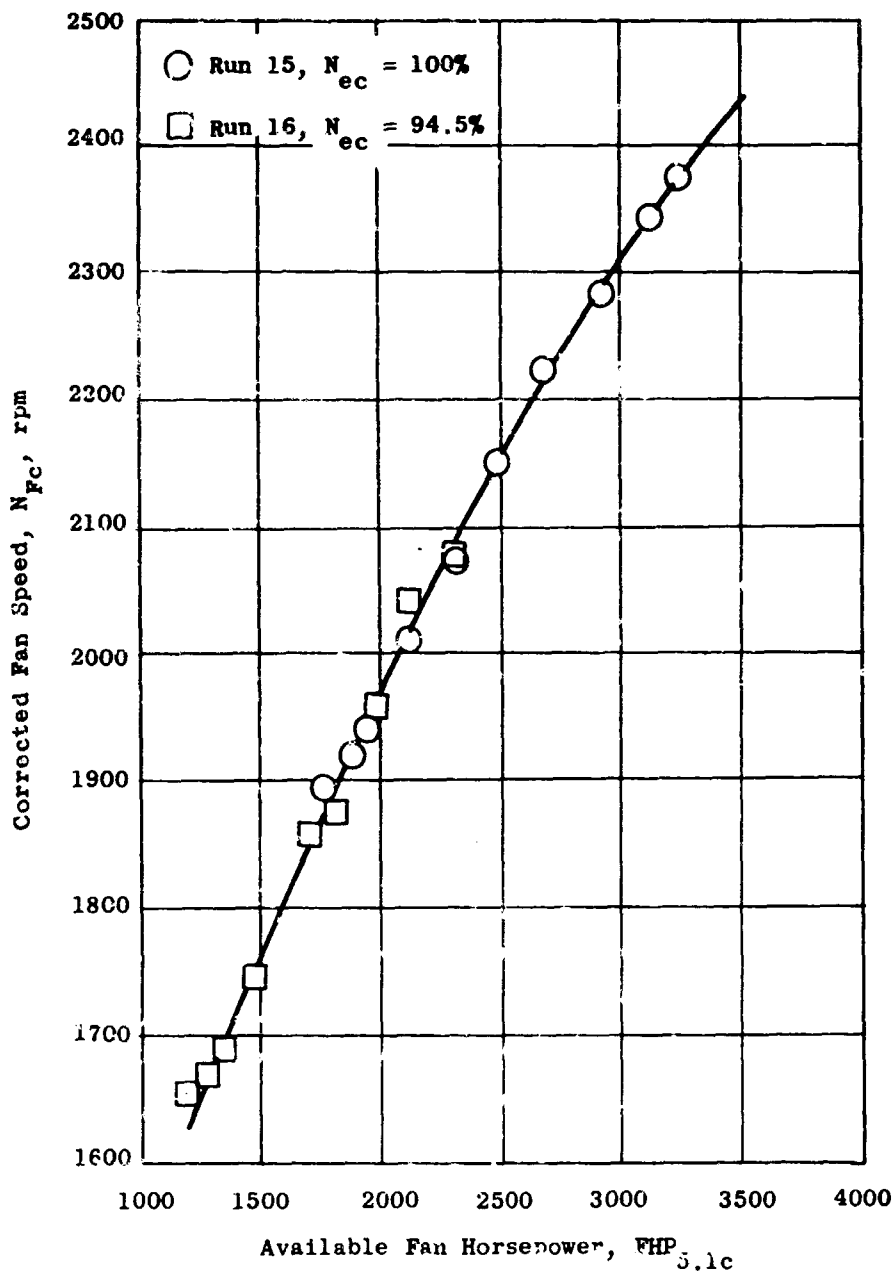


Figure 150. Fan Speed Versus Available Fan Horsepower, Runs 15 and 16, Variable δ_s From 0 to 80 Percent, $\beta_v = 0$ Degrees.

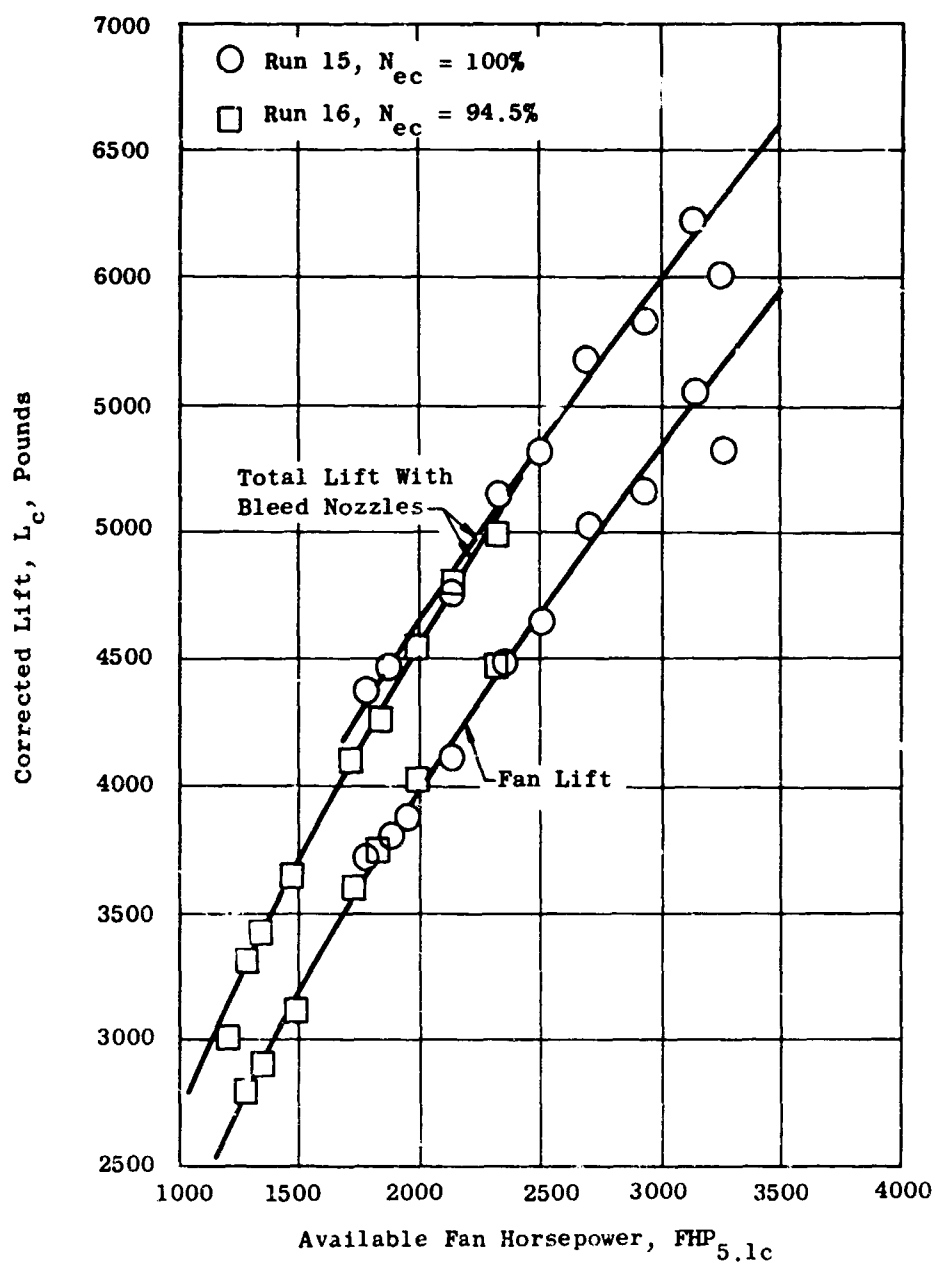


Figure 151. Lift Versus Available Fan Horsepower, Runs 15 and 16, Variable δ_s From 0 to 80 Percent, $\beta_v = 0$ Degrees.

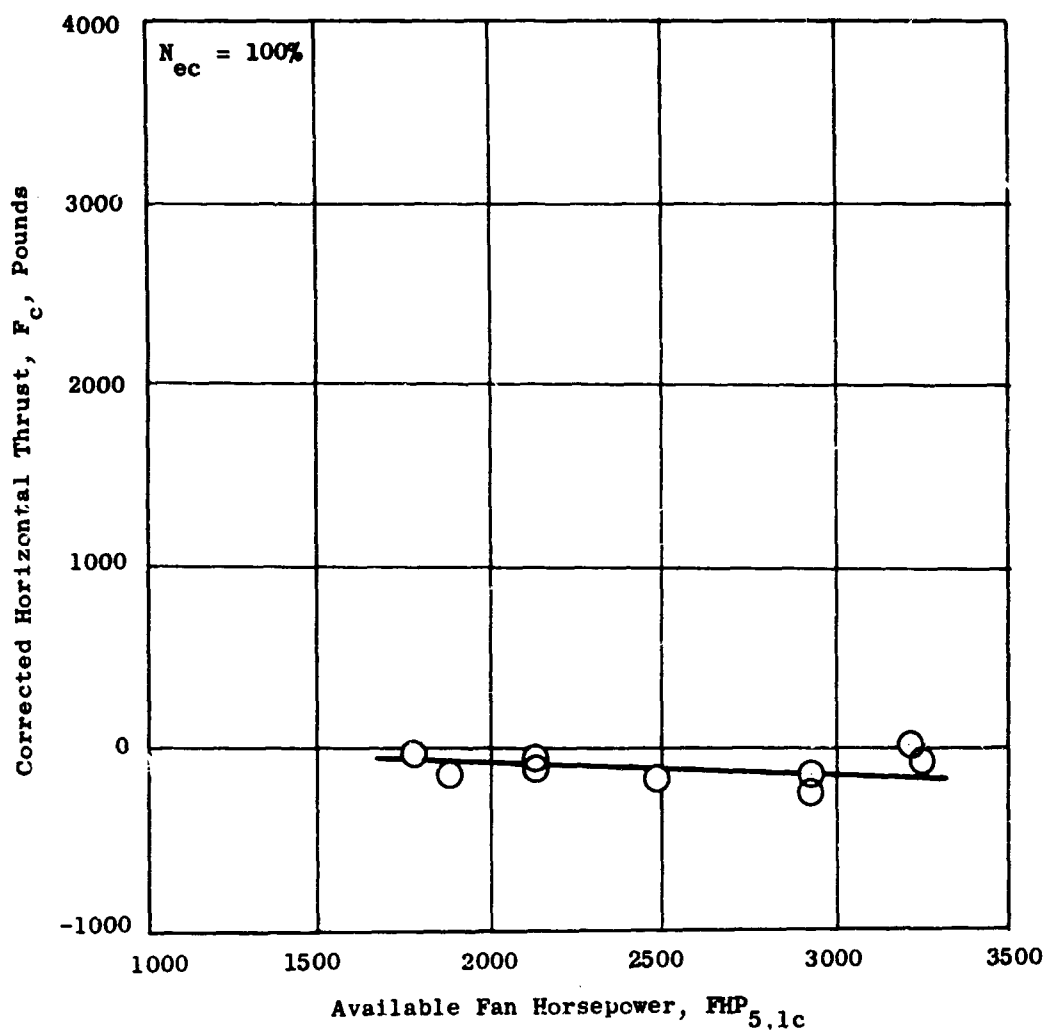


Figure 152. Thrust Versus Available Fan Horsepower, Run 15, Variable δ_s , $\beta_v = 0$ Degrees.

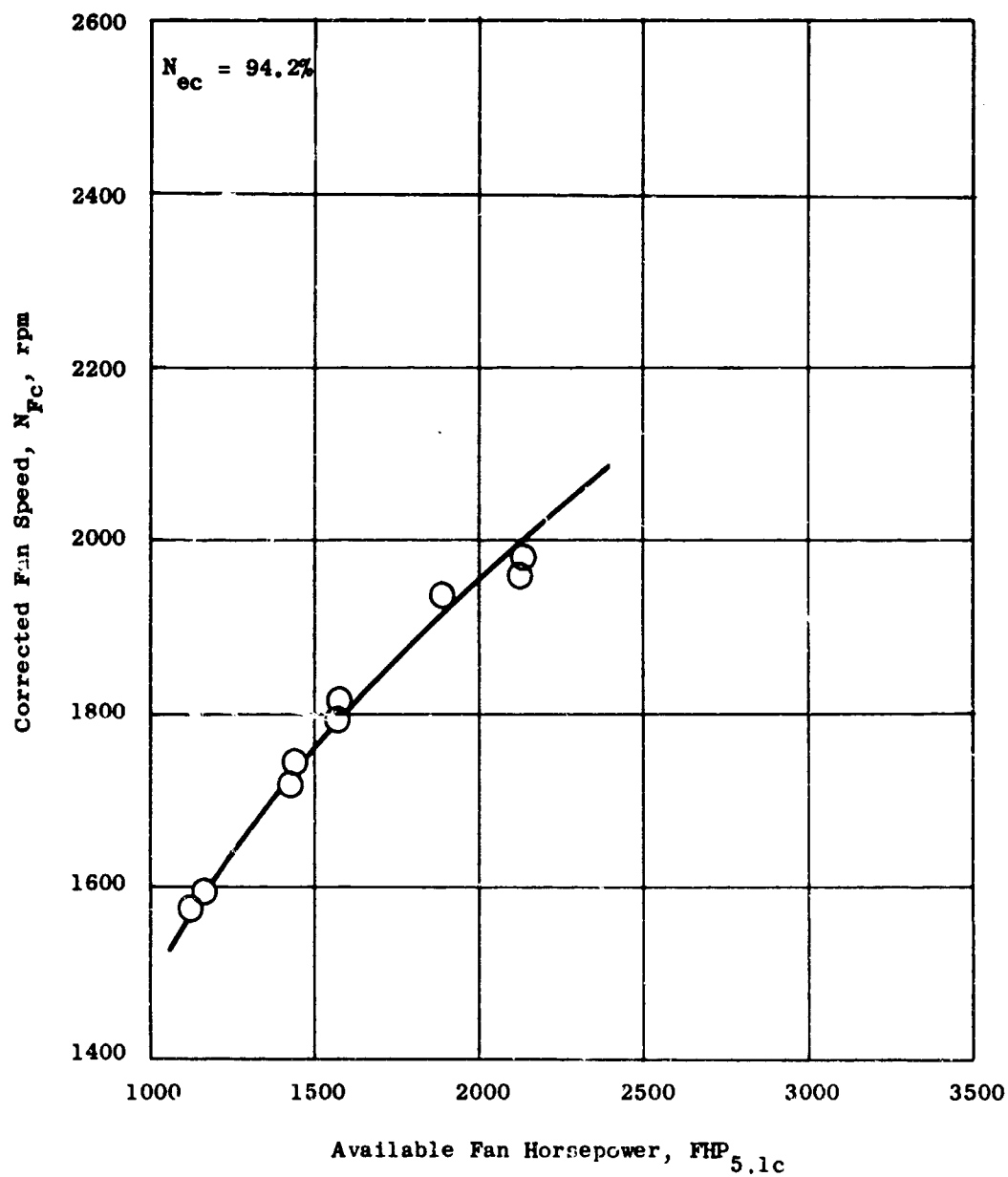


Figure 153. Fan Speed Versus Available Fan Horsepower, Run 17, δ_s Variable From 0 to 80 Percent, $\beta_v = -7$ Degrees.

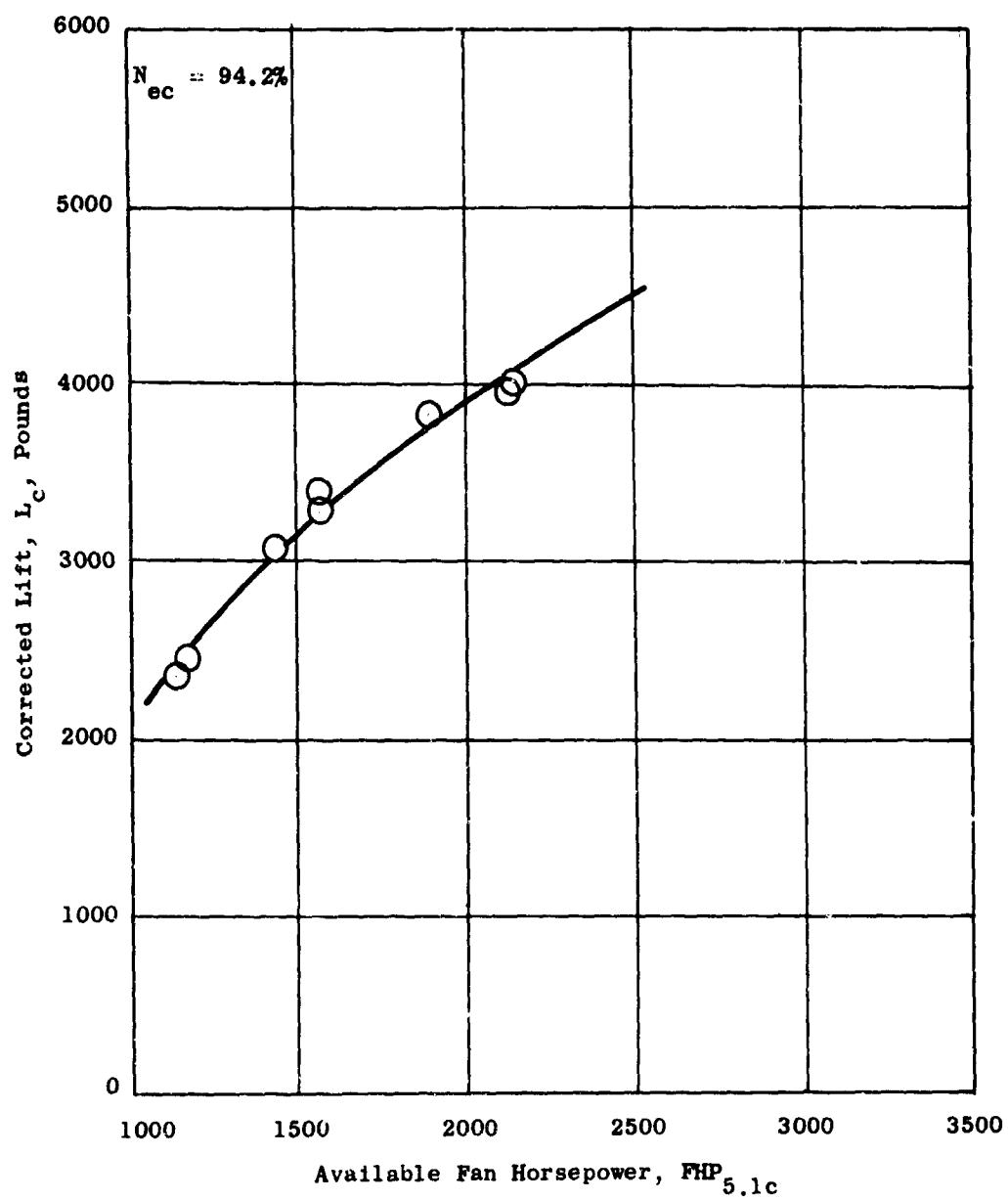


Figure 154. Lift Versus Available Fan Horsepower, Run 17, δ_s Variable From 0 to 80 Percent, $\beta_v = -7$ Degrees.

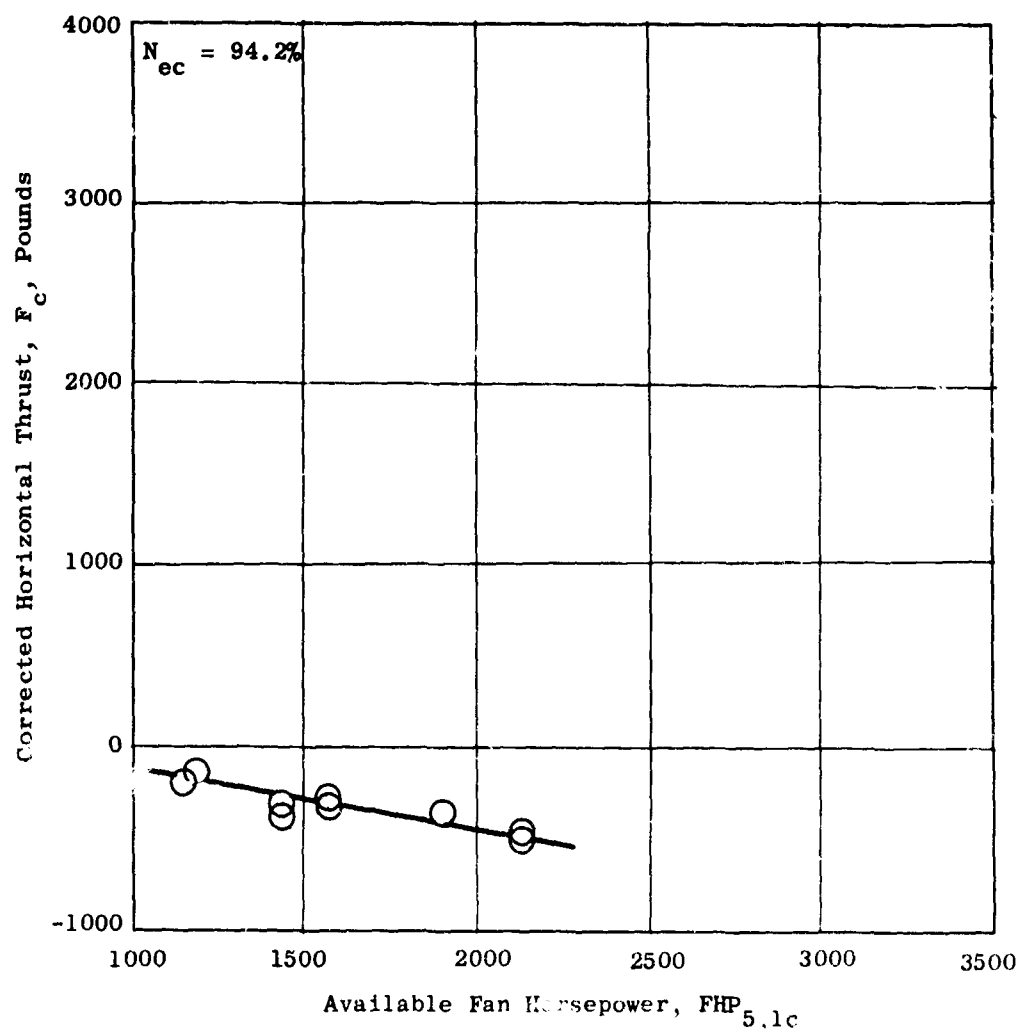


Figure 155. Thrust Versus Available Fan Horsepower,
Run 17, δ_s Variable From 0 to 80 Percent,
 $\beta_v = -7$ Degrees.

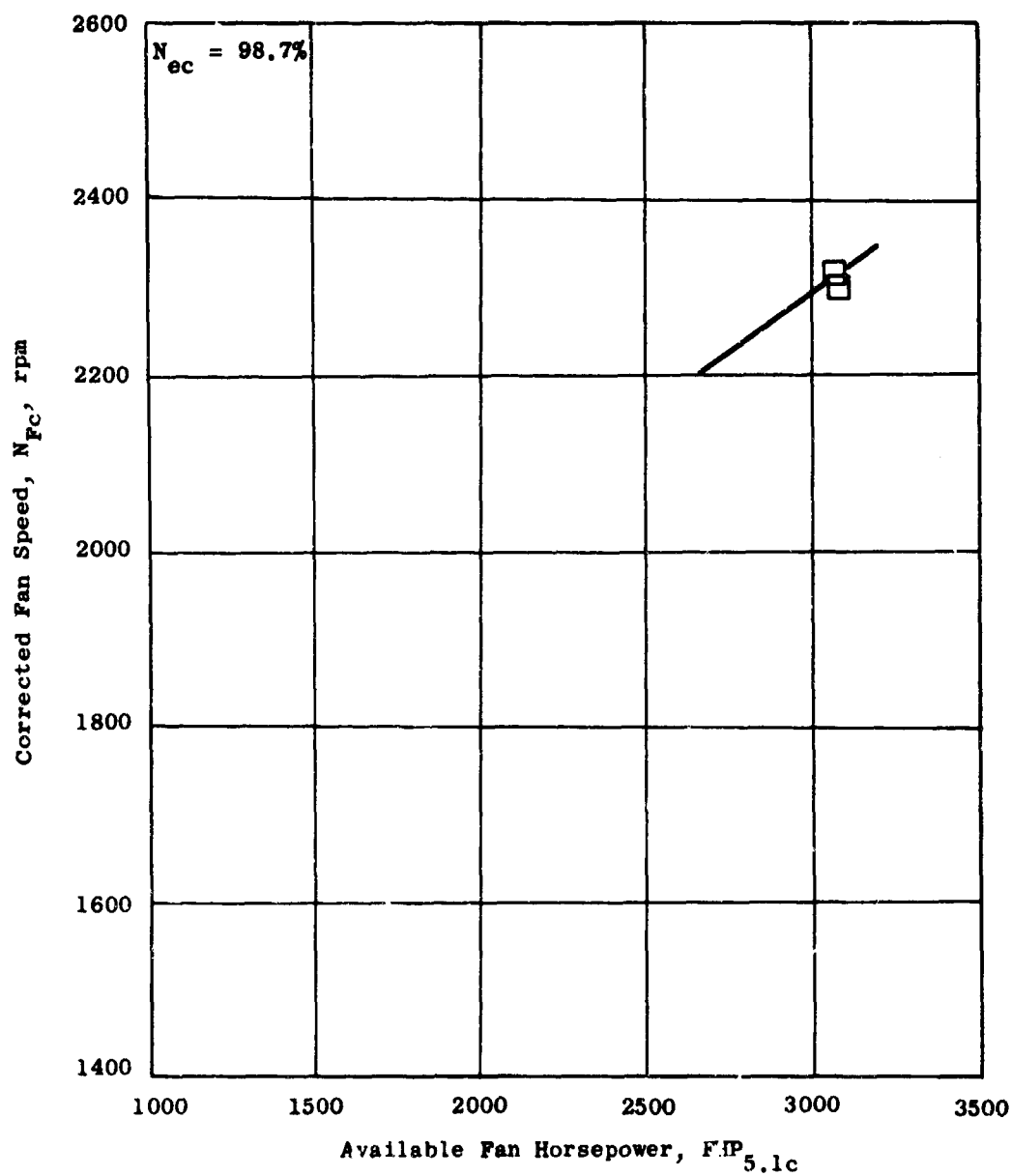


Figure 156. Fan Speed Versus Available Fan Horsepower,
Run 12, $\delta_S = 76$ Percent, $\beta_V = 10$ Degrees.

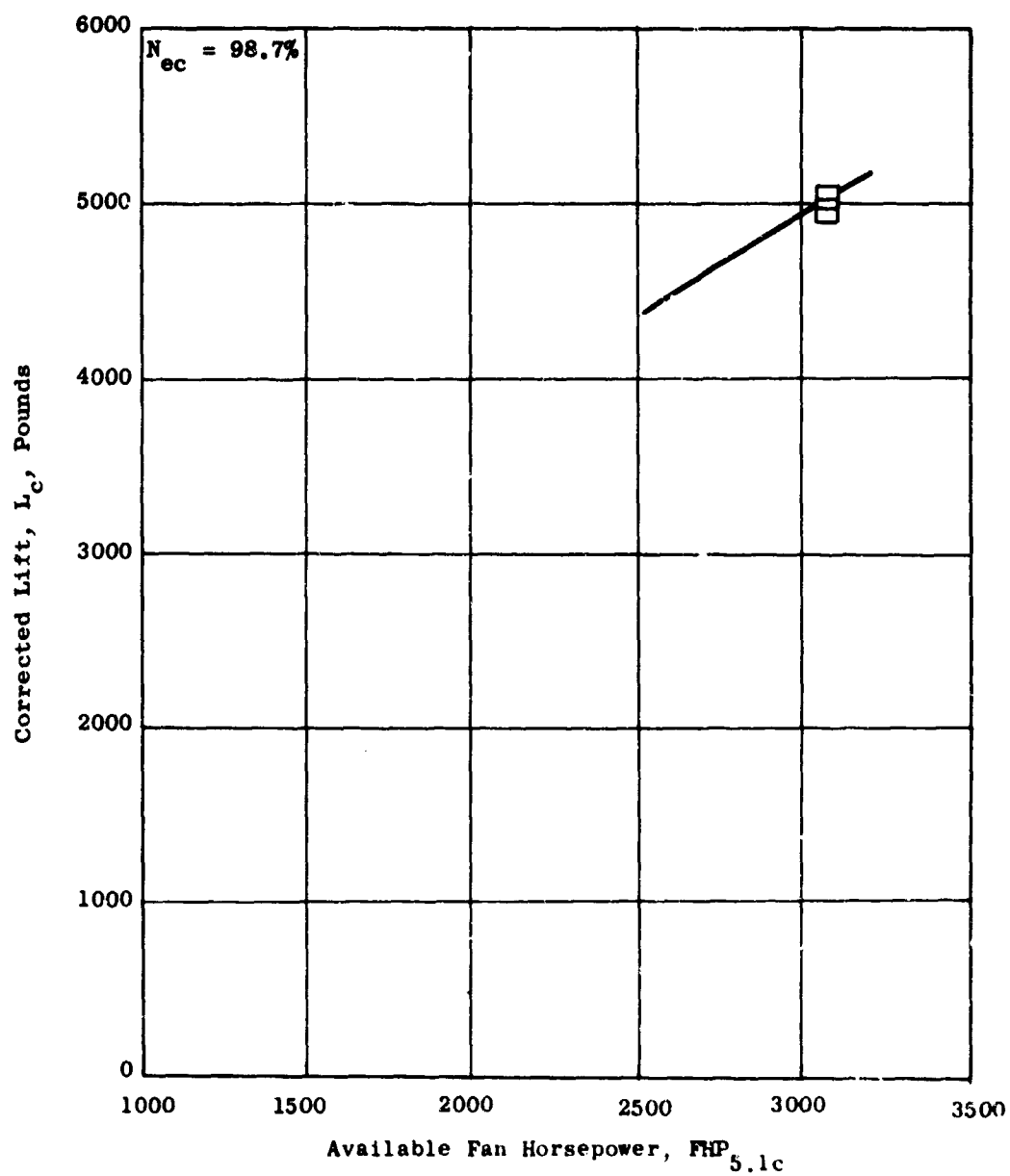


Figure 157. Lift Versus Available Fan Horsepower,
Run 12, $\delta_S = 76$ Percent, $\delta_V = 10$ Degrees.

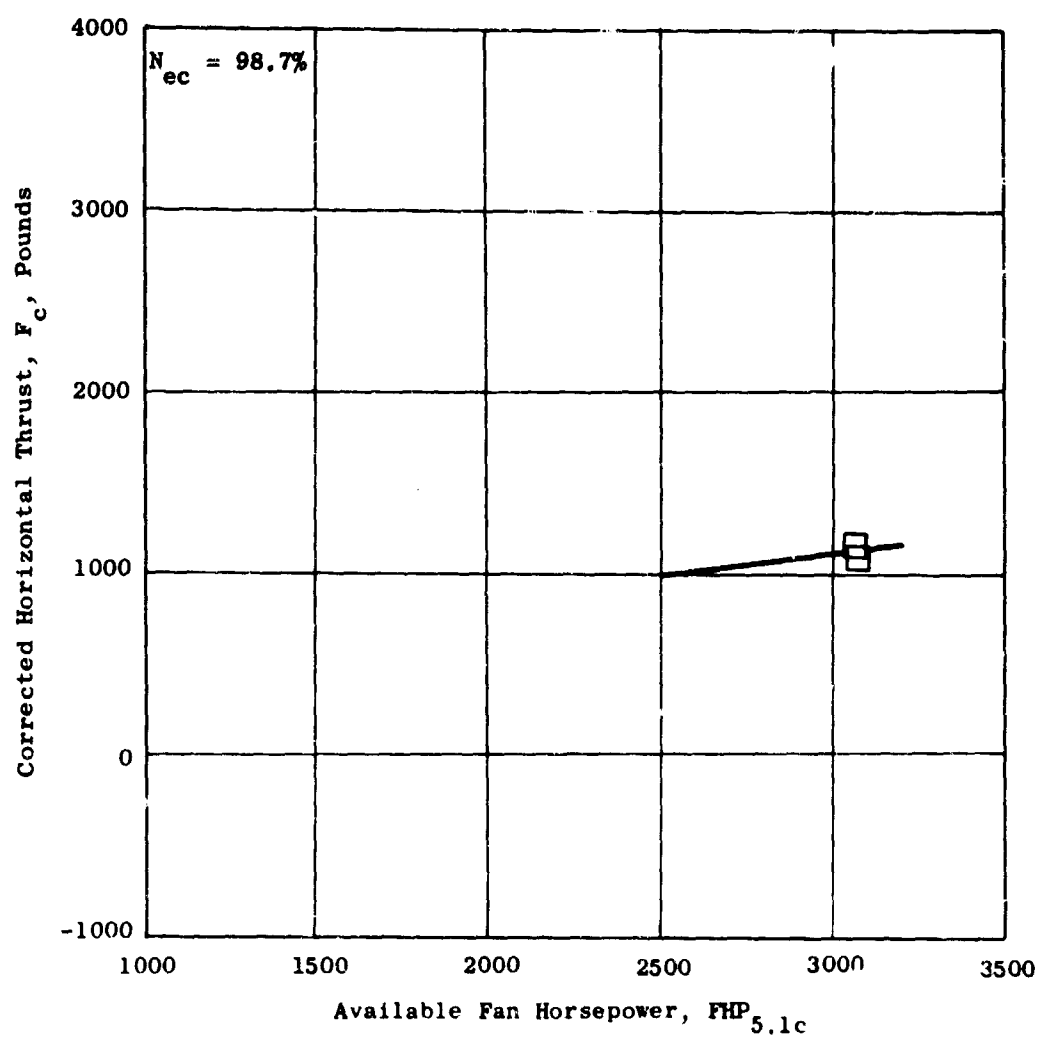


Figure 158. Thrust Versus Available Fan Horsepower,
Run 12, $\delta_S = 76$ Percent, $\alpha_V = 10$ Degrees.

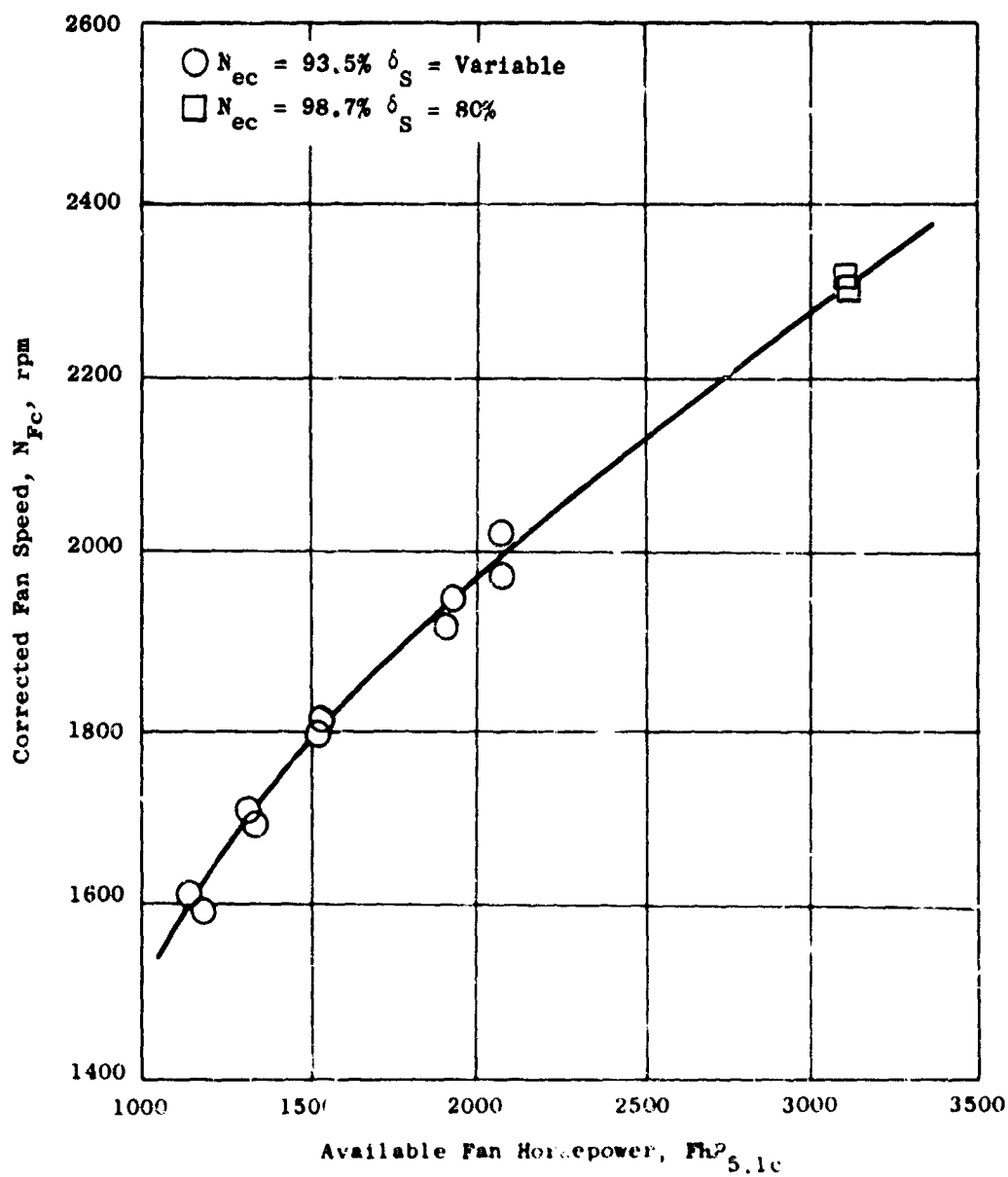


Figure 159. Fan Speed Versus Available Fan Horsepower, Run 16,
 δ_s Variable From 0 to 80 Percent, $\delta_v = 20.5$ Degrees.

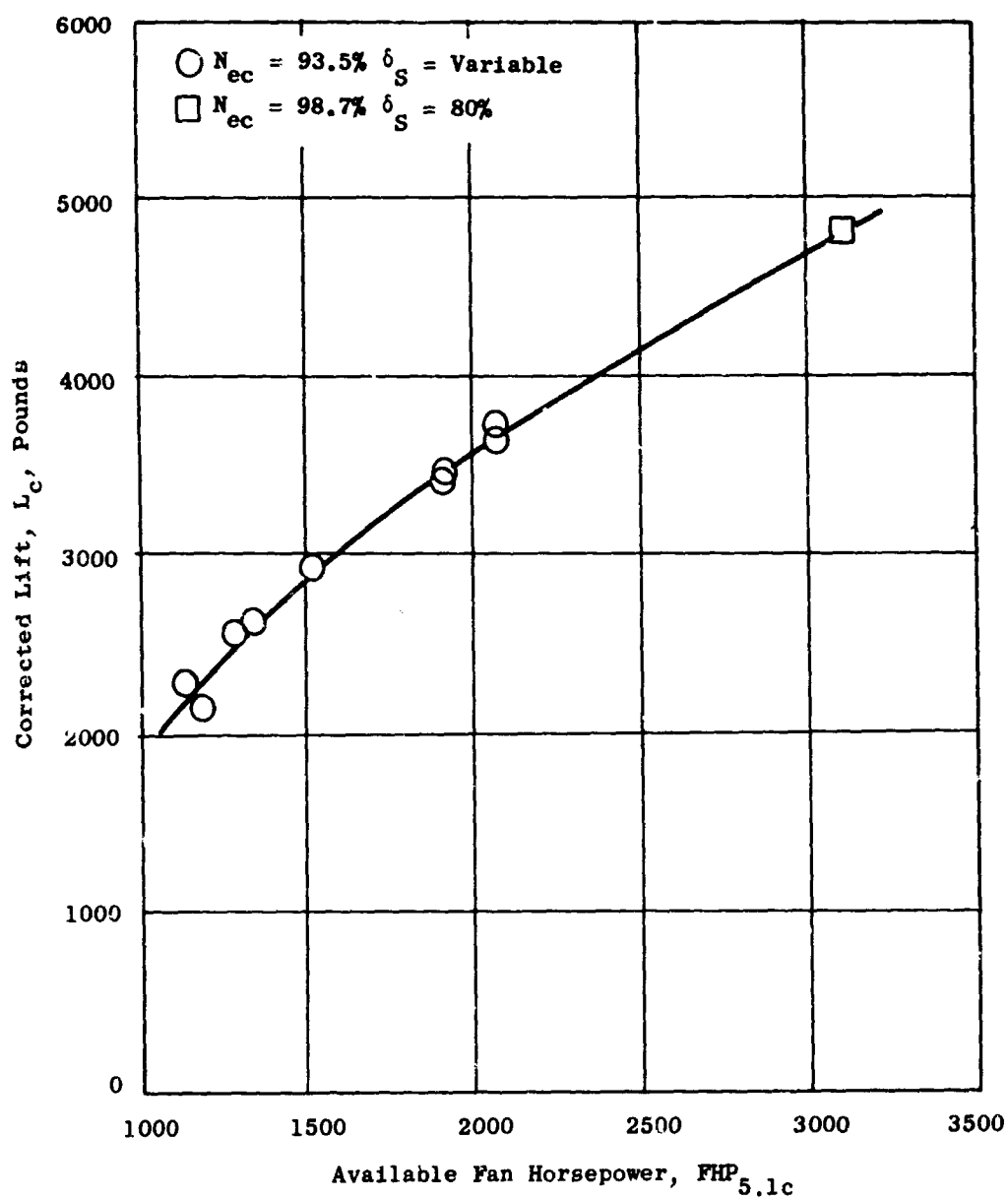


Figure 160. Lift Versus Available Fan Horsepower, Run 16, δ_s Variable From 0 to 80 Percent, $\theta_v = 20.5$ Degrees.

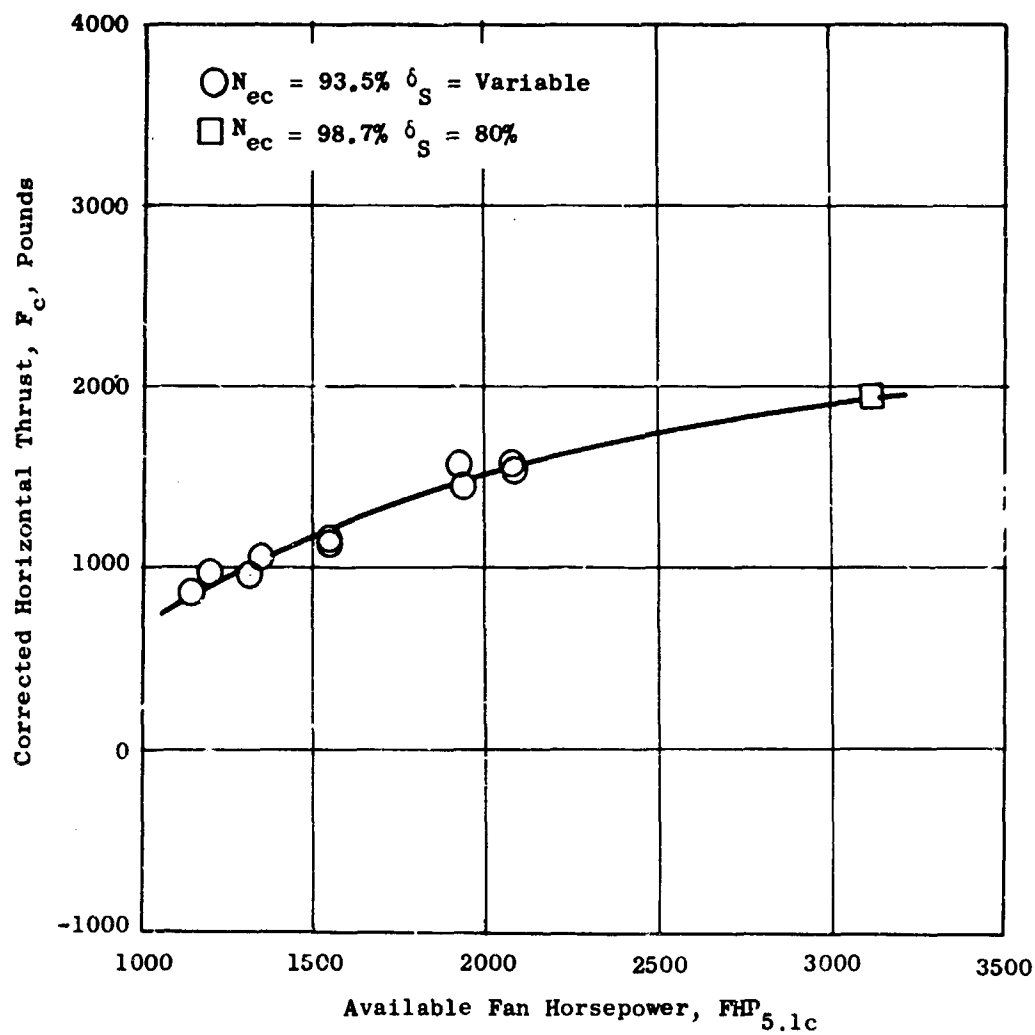


Figure 161. Thrust Versus Available Fan Horsepower, Run 16, δ_s Variable From 0 to 80 Percent, $\beta_v = 20.5^\circ$ Degrees.

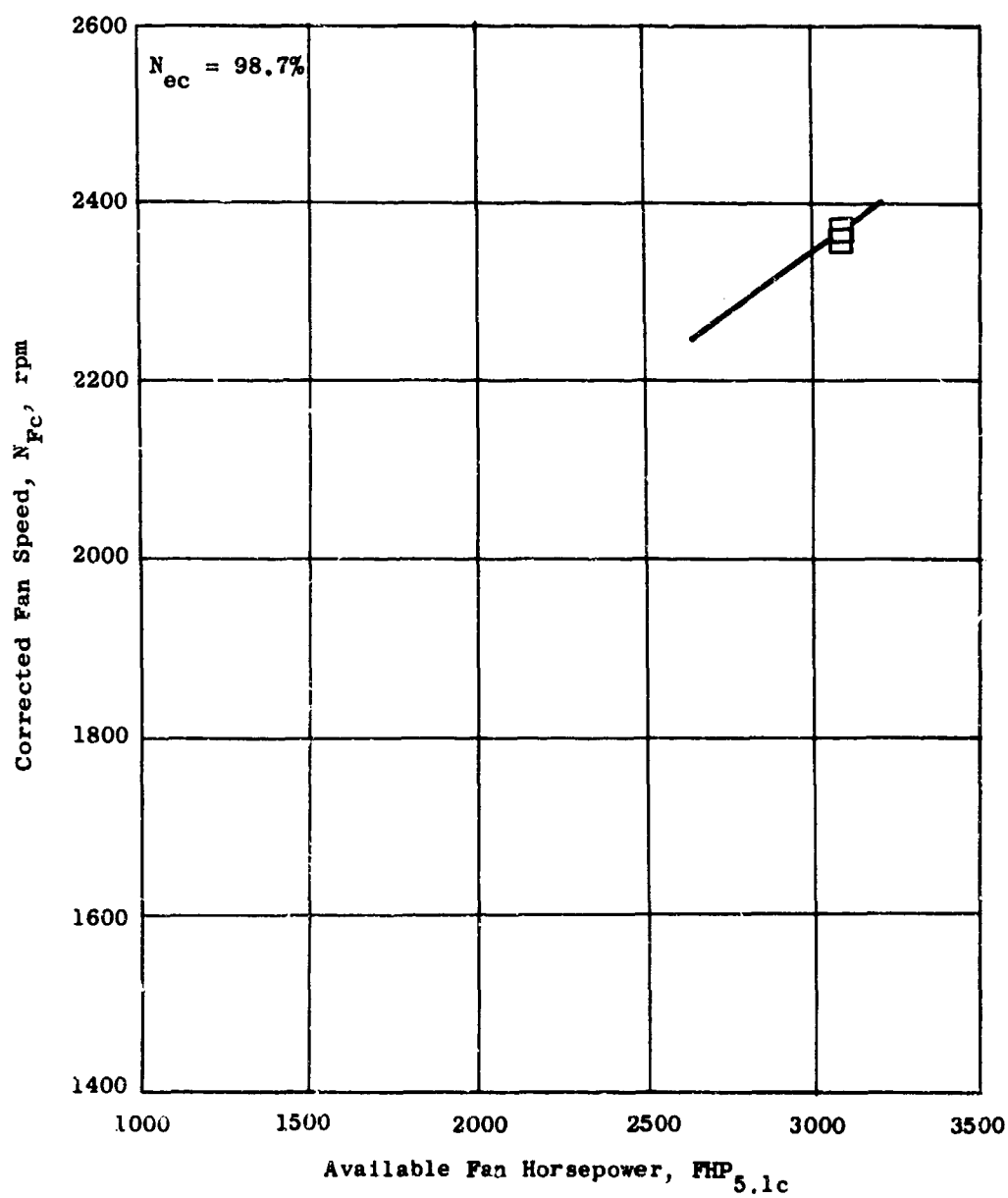


Figure 162. Fan Speed Versus Available Fan Horsepower,
Run 12, $\delta_S = 76$ Percent, $\beta_V = 30$ Degrees.

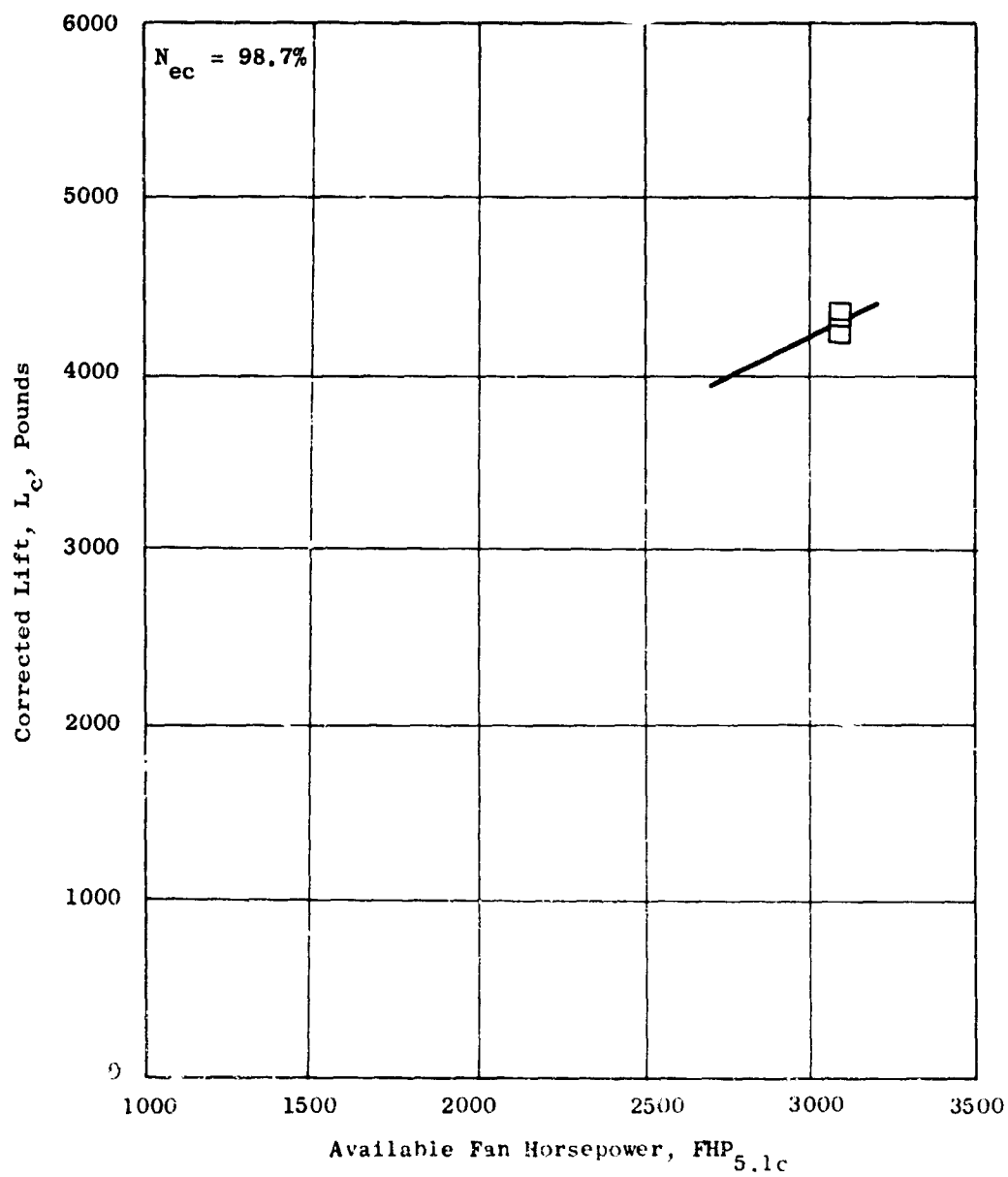


Figure 163. Lift Versus Available Fan Horsepower.
Run 12, $\delta_S = 76$ Percent, $\delta_V = 30$ Degrees.

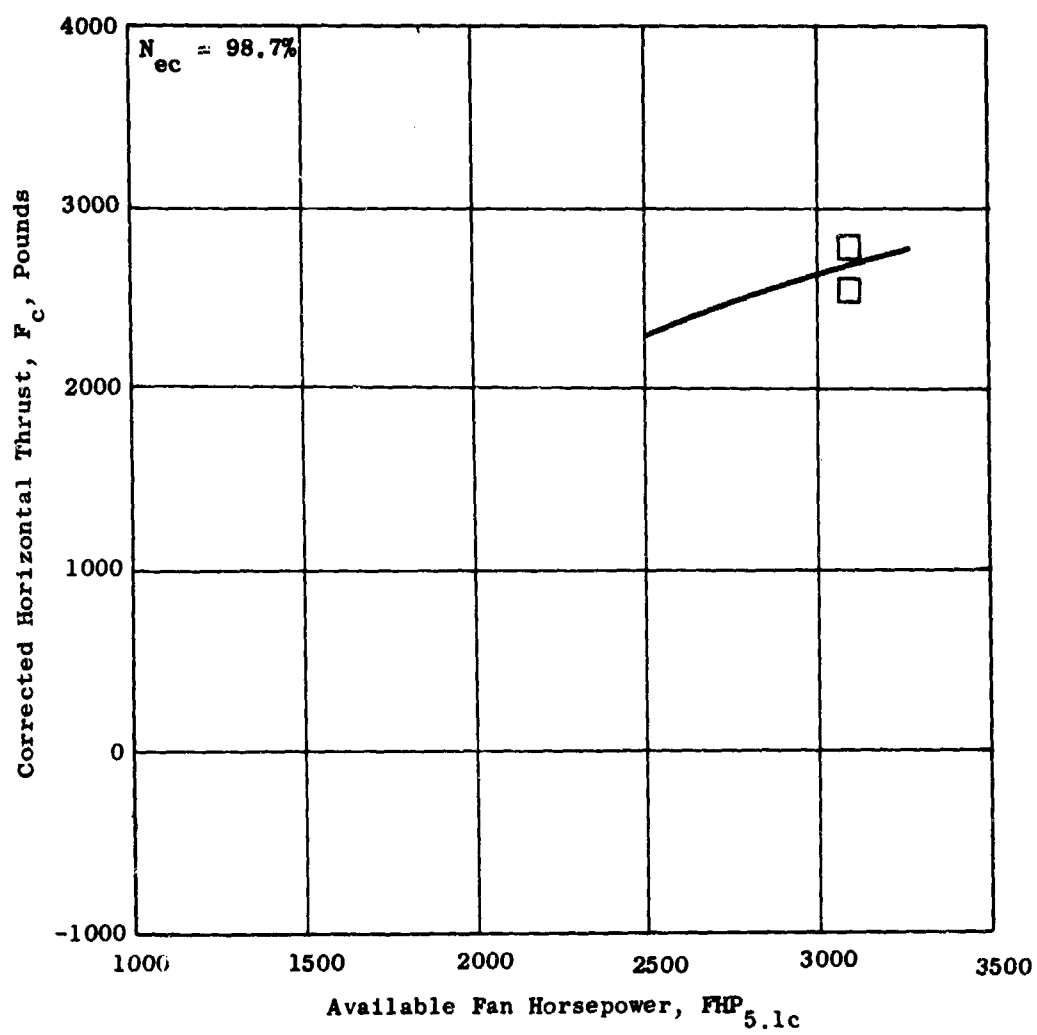


Figure 164. Thrust Versus Available Fan Horsepower,
Run 12, $\delta_s = 76$ Percent, $\beta_v = 30$ Degrees.

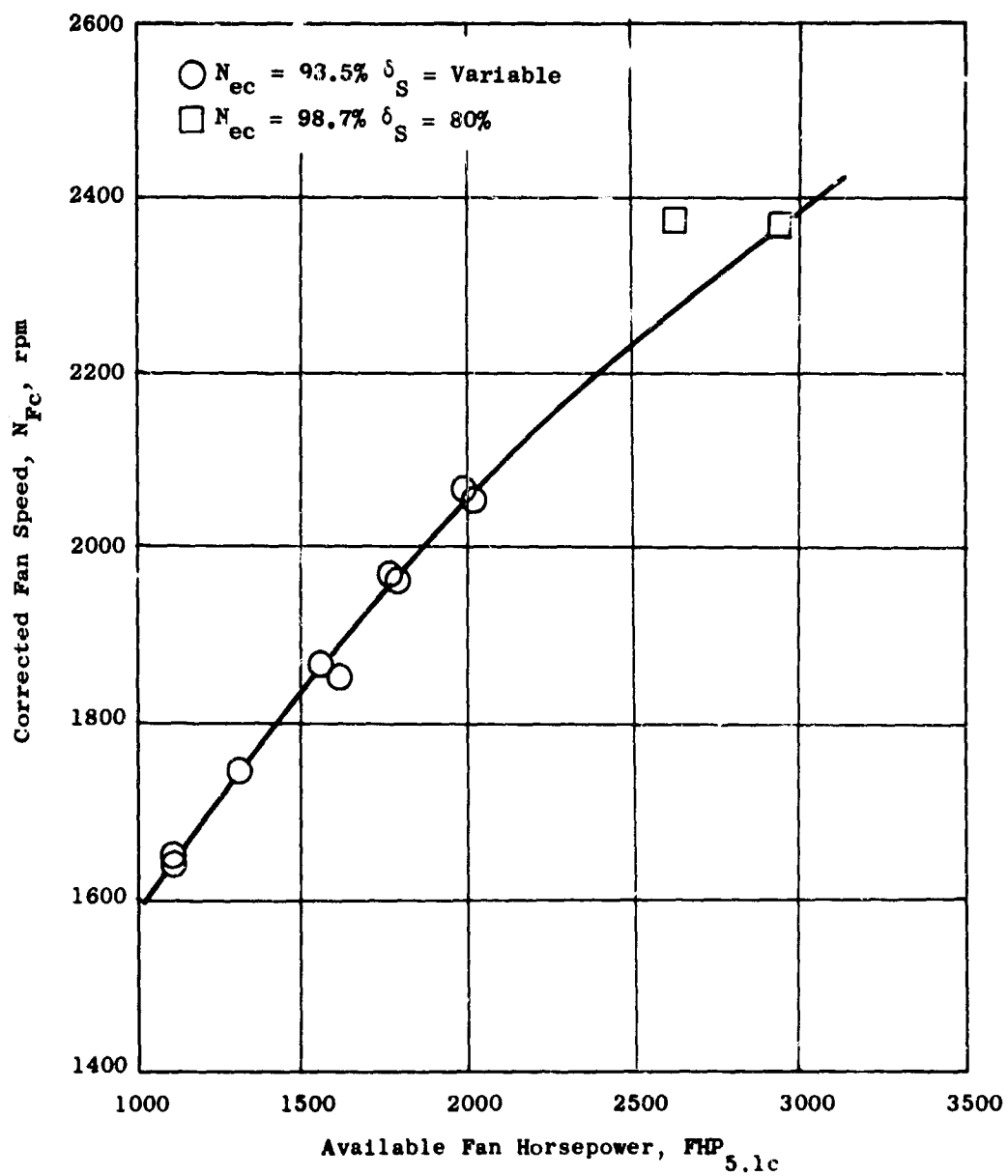


Figure 165. Fan Speed Versus Available Fan Horsepower, Run 16, δ_S Variable From 0 to 80 Percent, $\beta_V = 37$ Degrees.

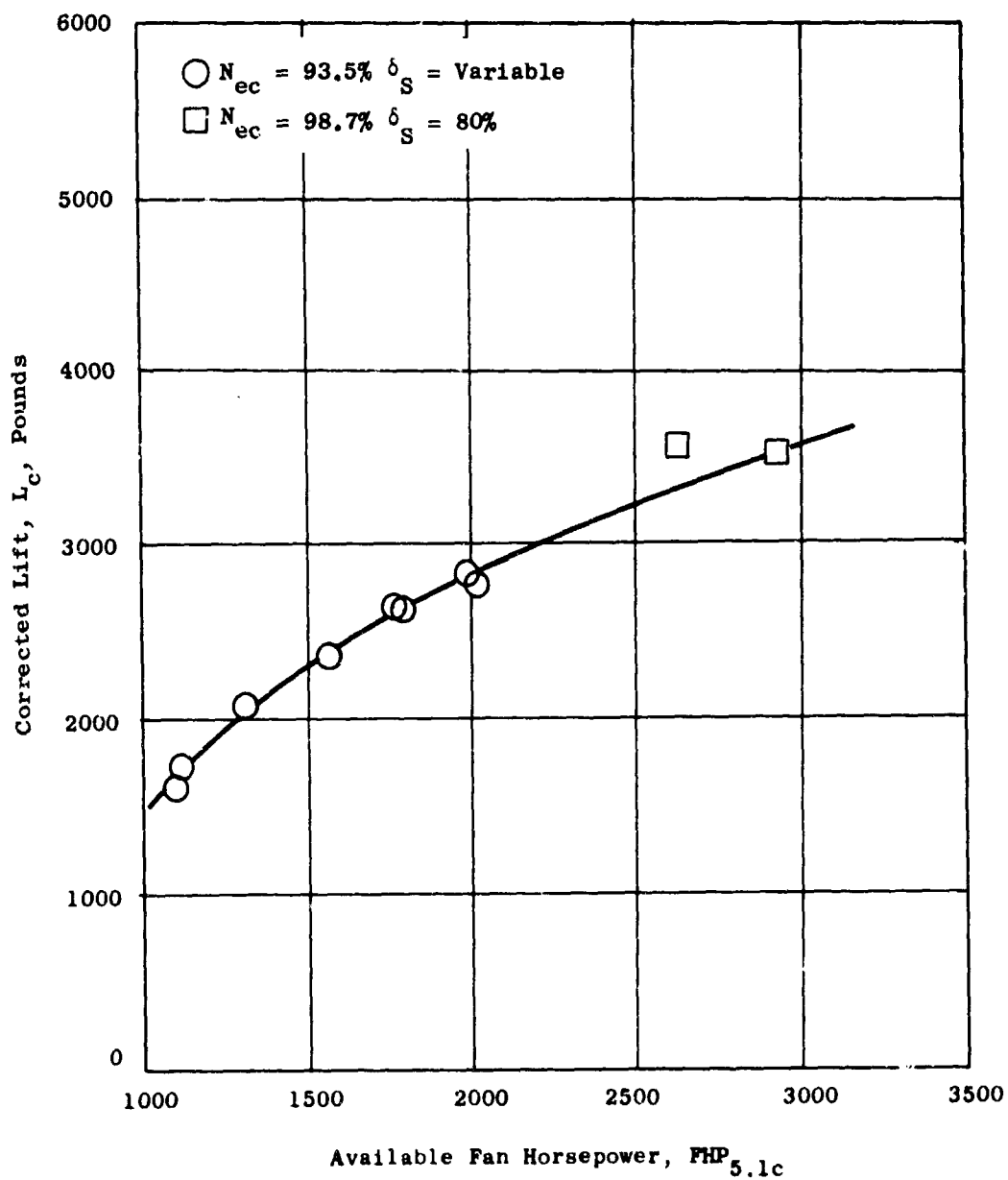


Figure 166. Lift Versus Available Fan Horsepower, Run 16, δ_s Variable From 0 to 80 Percent, $\beta_v = 37$ Degrees.

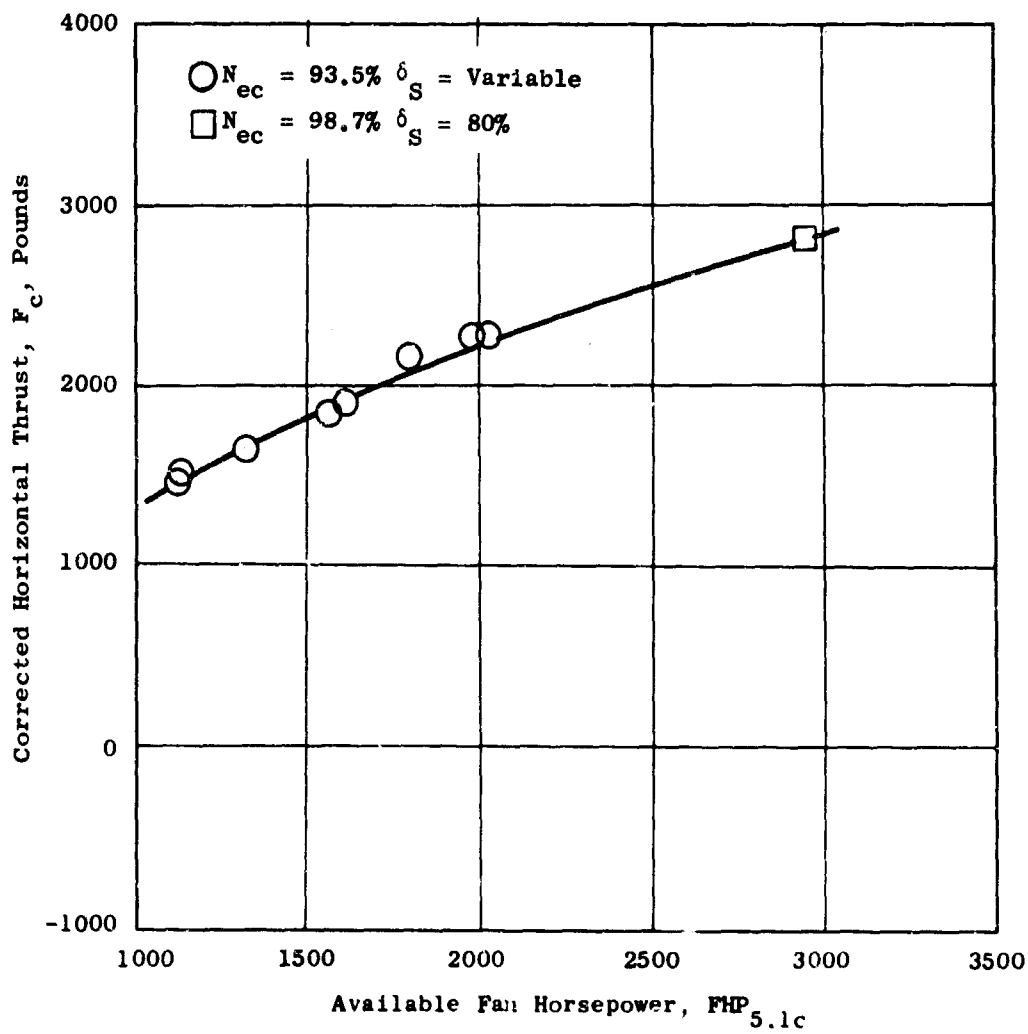


Figure 167. Thrust Versus Available Fan Horsepower,
Run 16, δ_s Variable From 0 to 80 Percent,
 $\beta_v = 37$ Degrees.

Note:

Open Symbols Denote Data As Measured.

Solid Symbols Denote Data Corrected to Rated Exhaust Gas Temperatures.

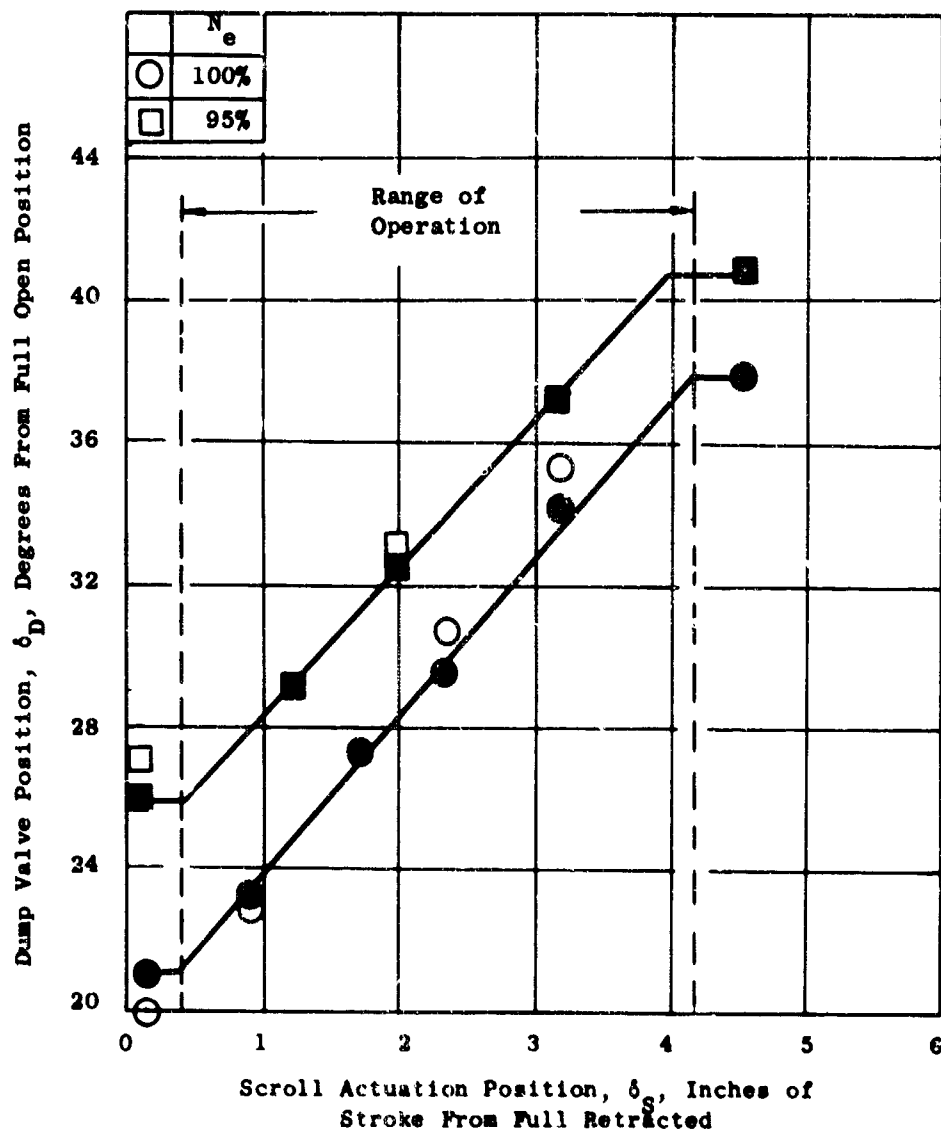


Figure 168. Variation of Scroll Actuator Position and Dump Valve Actuator Position as Required to Maintain Constant Core Engine Operation.

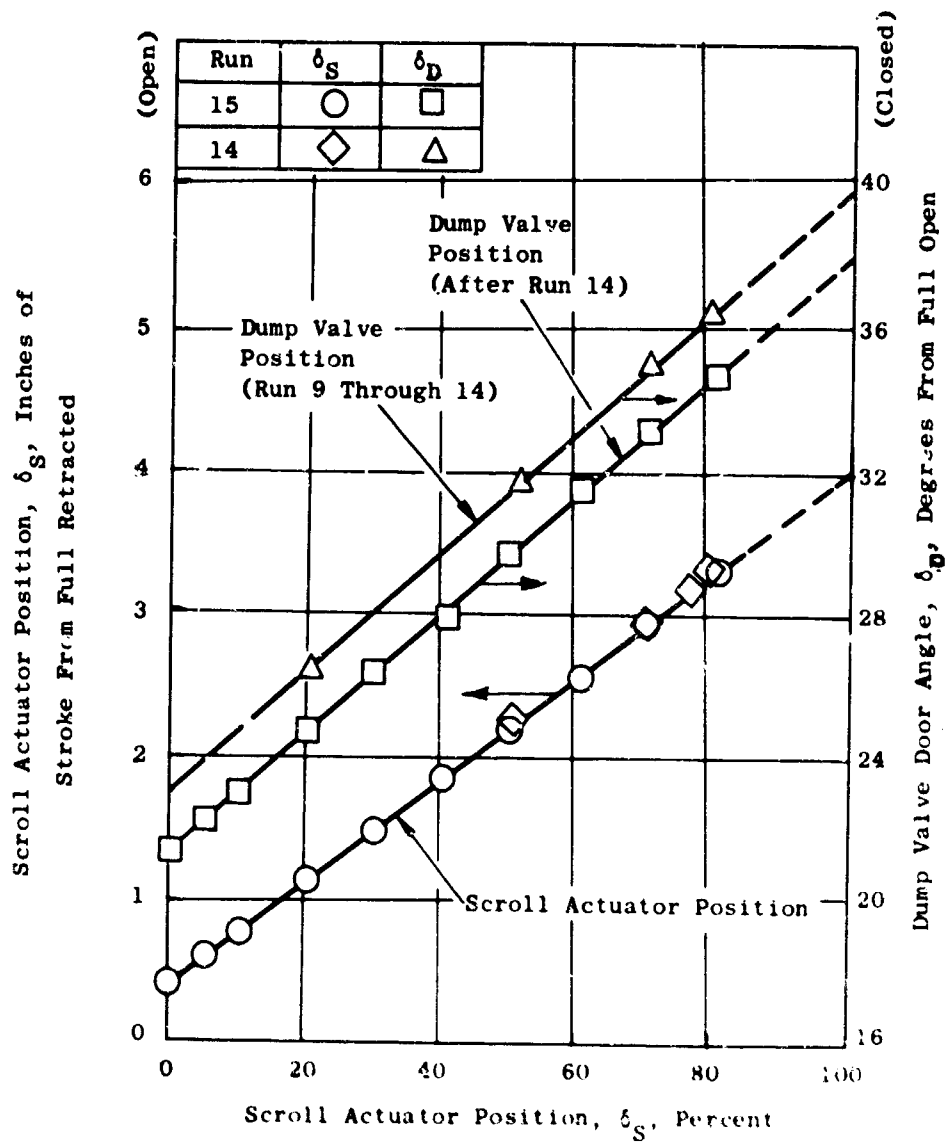


Figure 169. Scroll Actuator and Dump Valve Position Variation With Percent of Scroll Actuator Stroke.

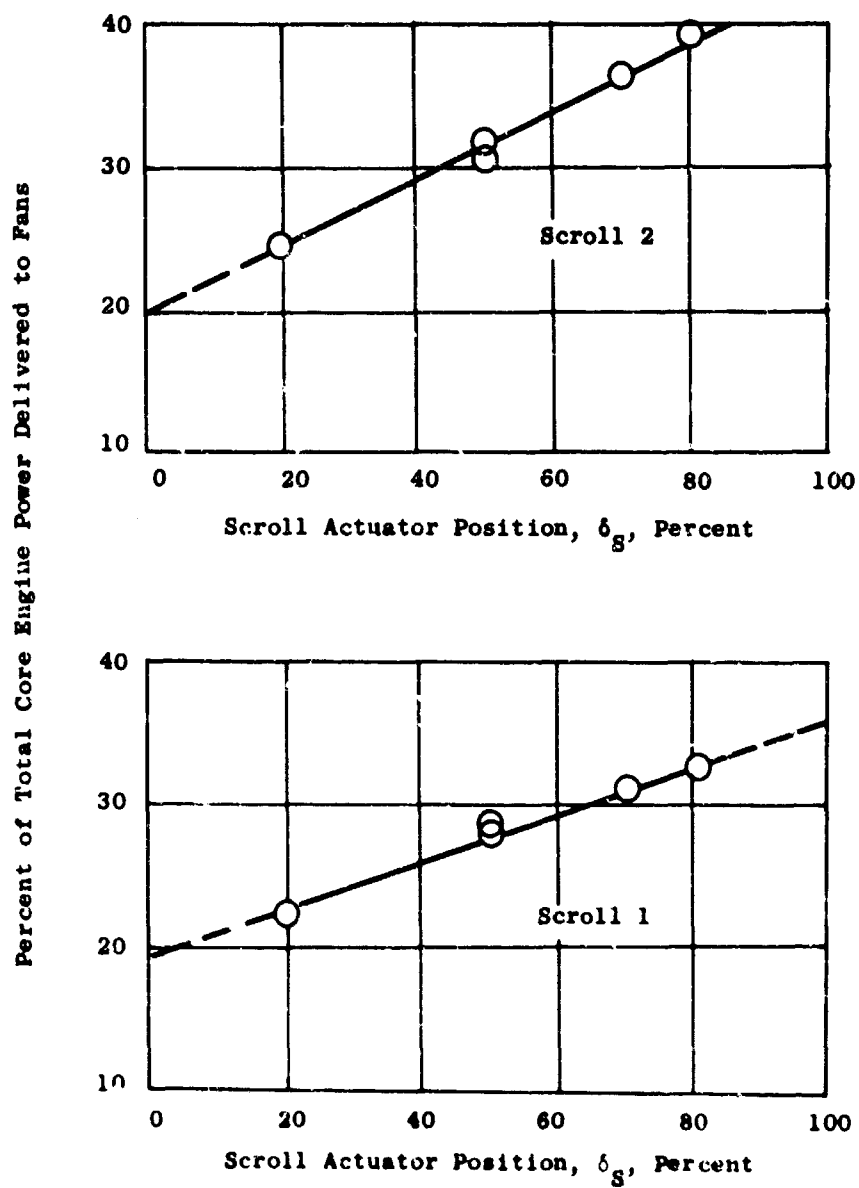


Figure 170. Engine Horsepower Delivered to Fan as a Function of Scroll Position for Initial Rigging.

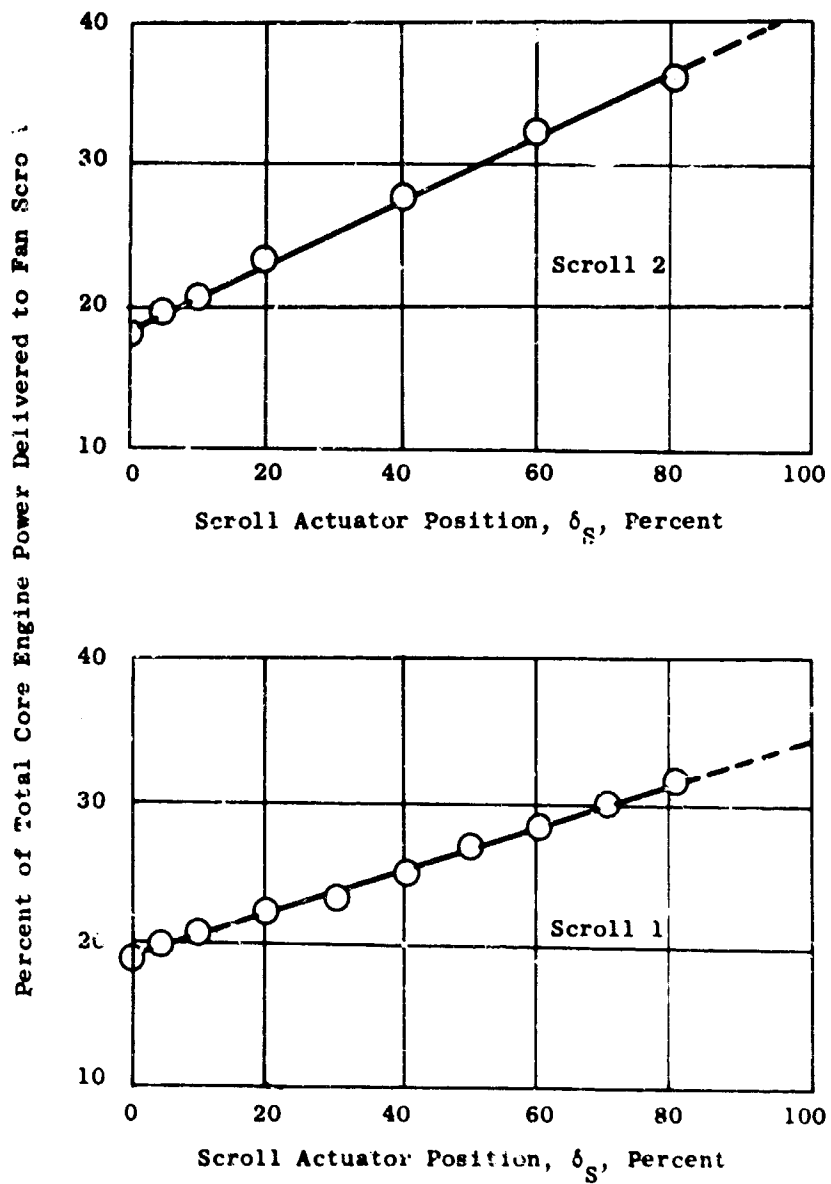


Figure 171. Engine Horsepower Delivered to Fan as a Function of Scroll Position for Final Rigging.

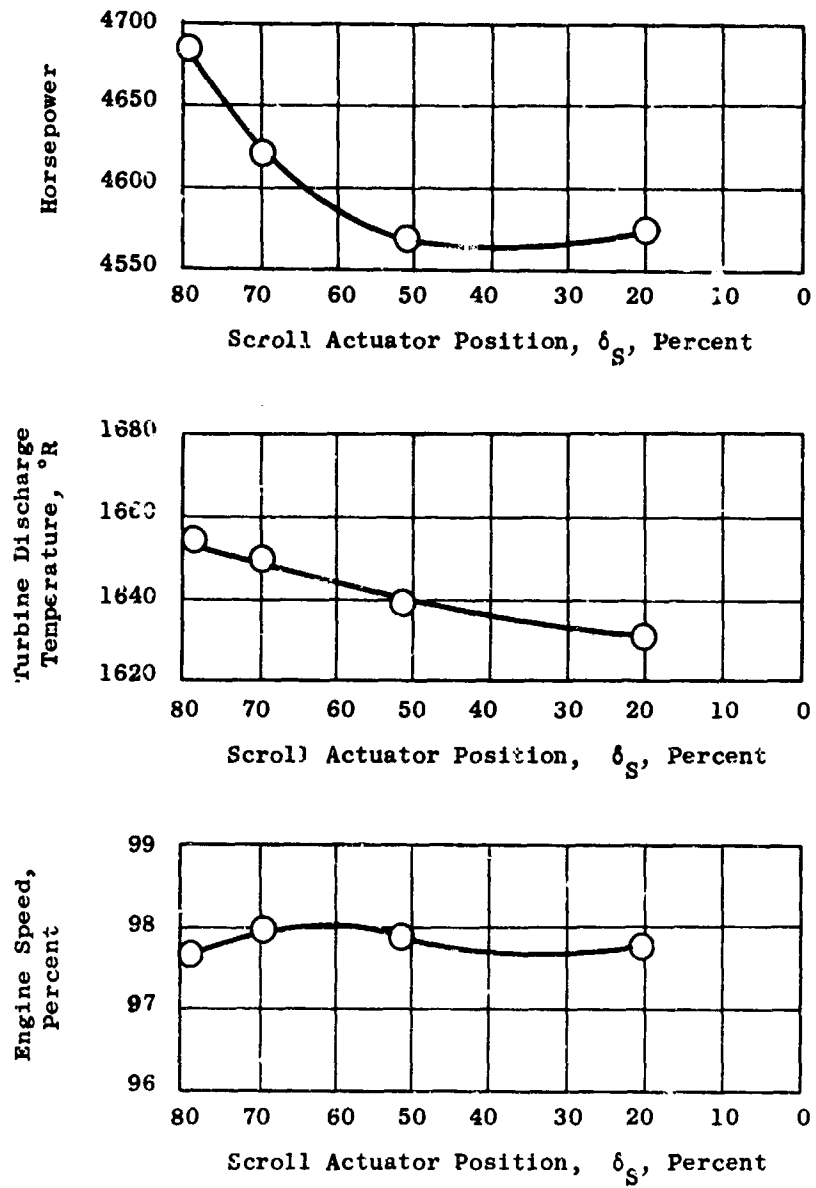


Figure 172. Effects of Scroll Area on Engine 1 Performance for Initial Rigging.

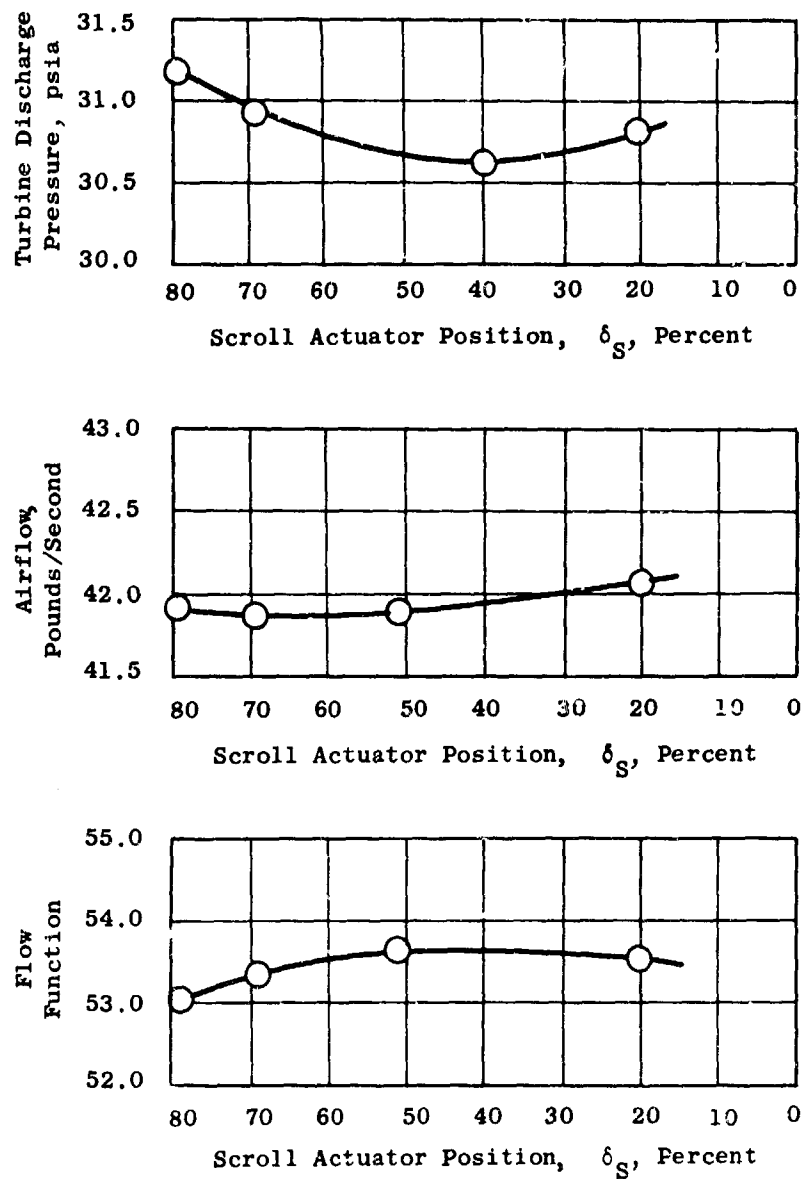


Figure 173. Effects of Scroll Area on Engine 1 Performance for Initial Rigging.

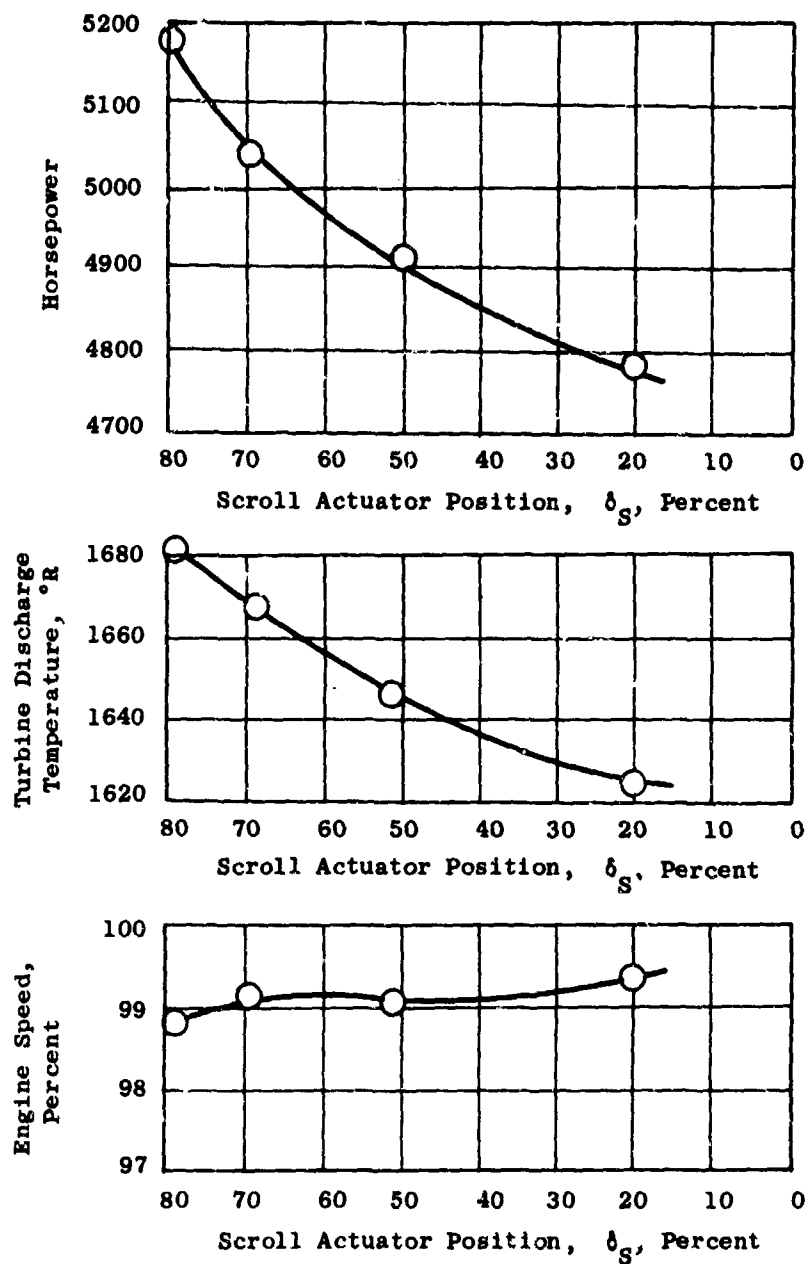


Figure 174. Effects of Scroll Area on Engine 2 Performance for Initial Rigging.

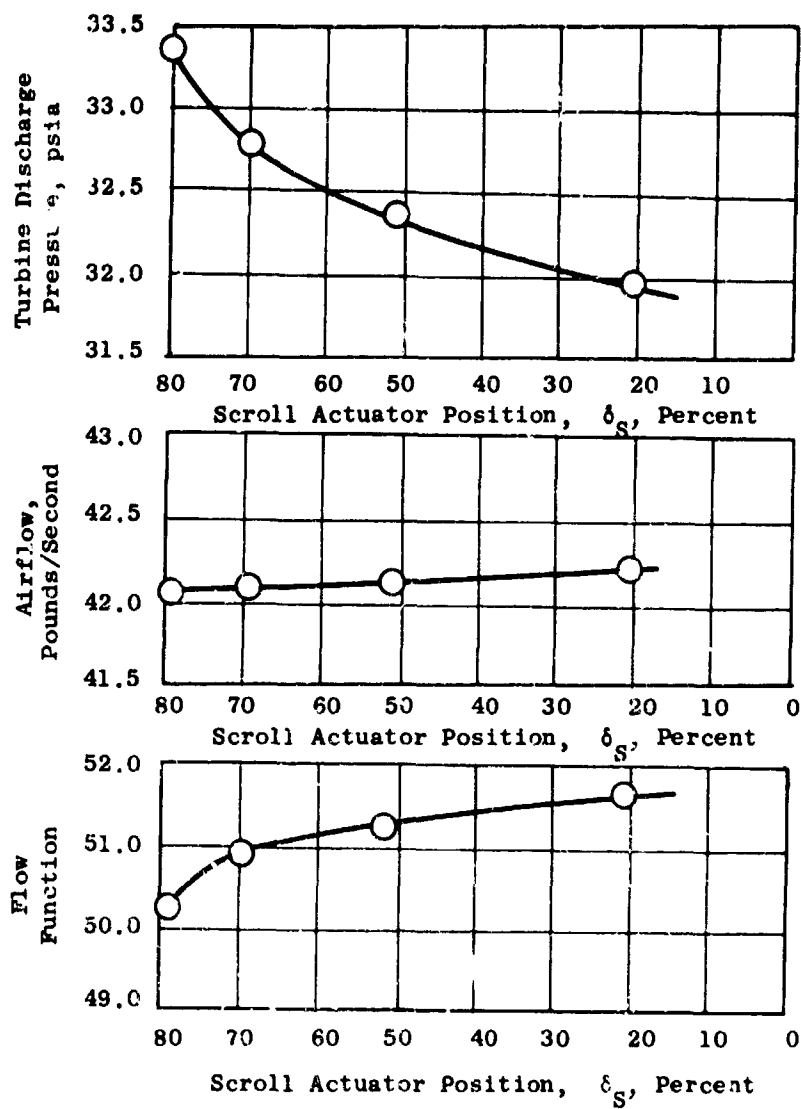


Figure 175. Effects of Scroll Area on Engine 2 Performance for Initial Rigging.

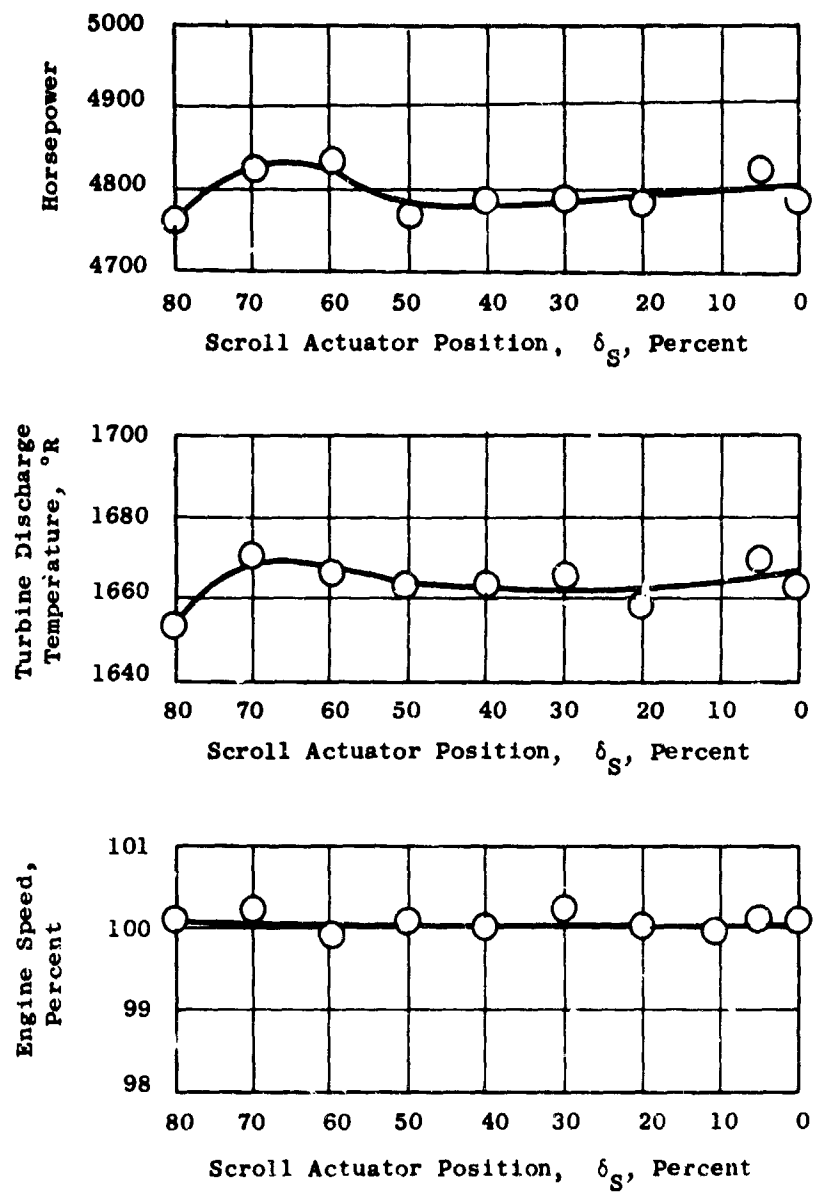


Figure 176. Effects of Scroll Area on Engine 1 Performance for Final Rigging.

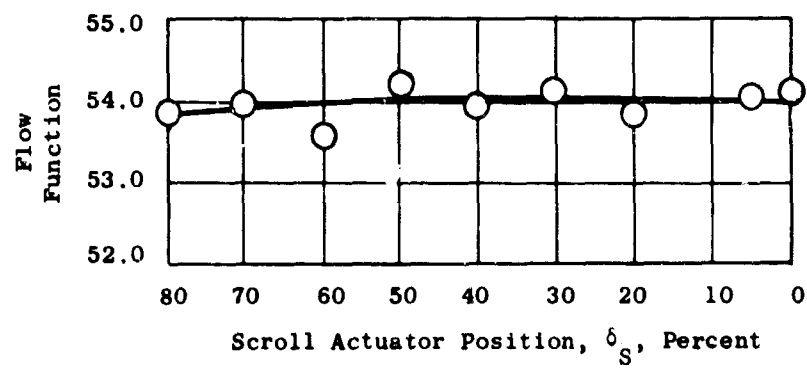
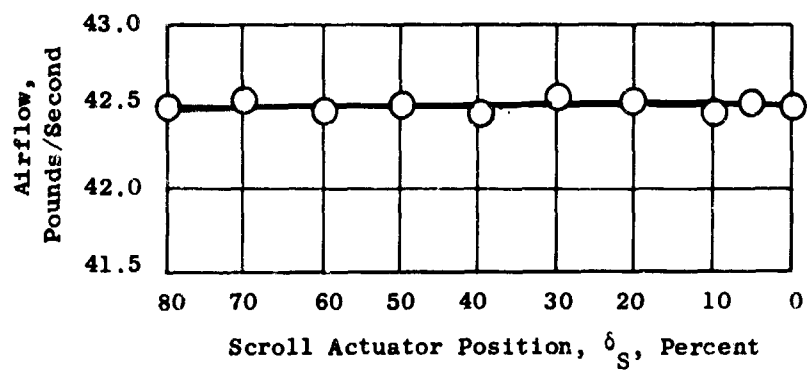
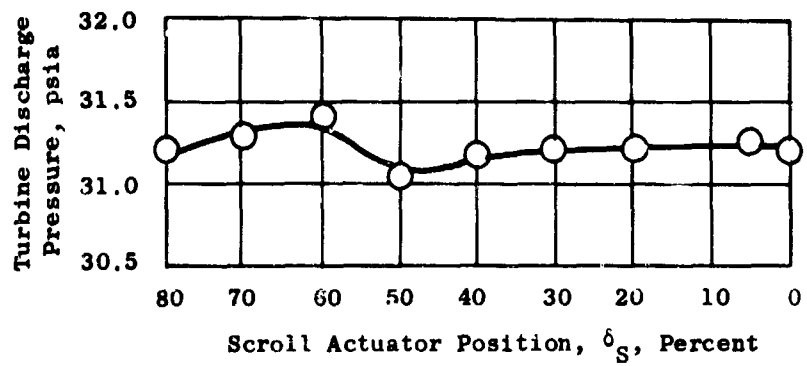


Figure 177. Effects of Scroll Area on Engine 1 Performance for Final Rigging.

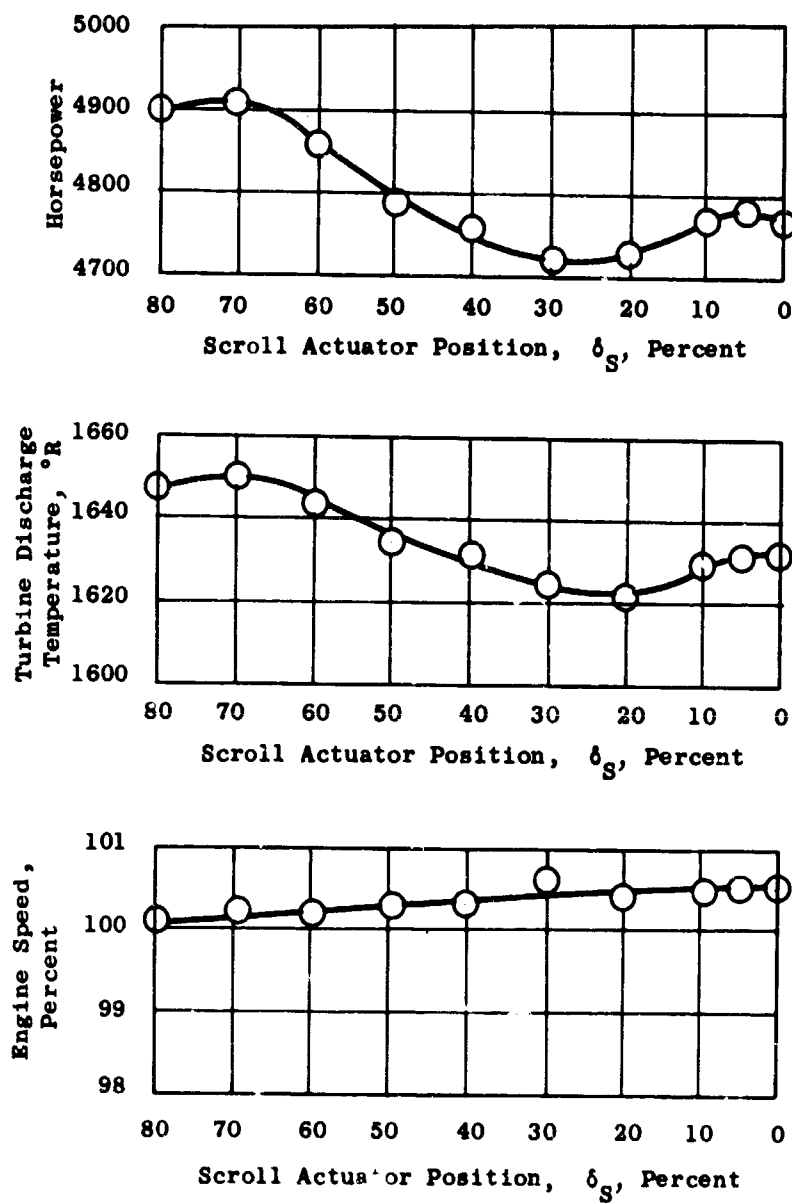


Figure 178. Effects of Scroll Area on Engine 2 Performance for Final Rigging.

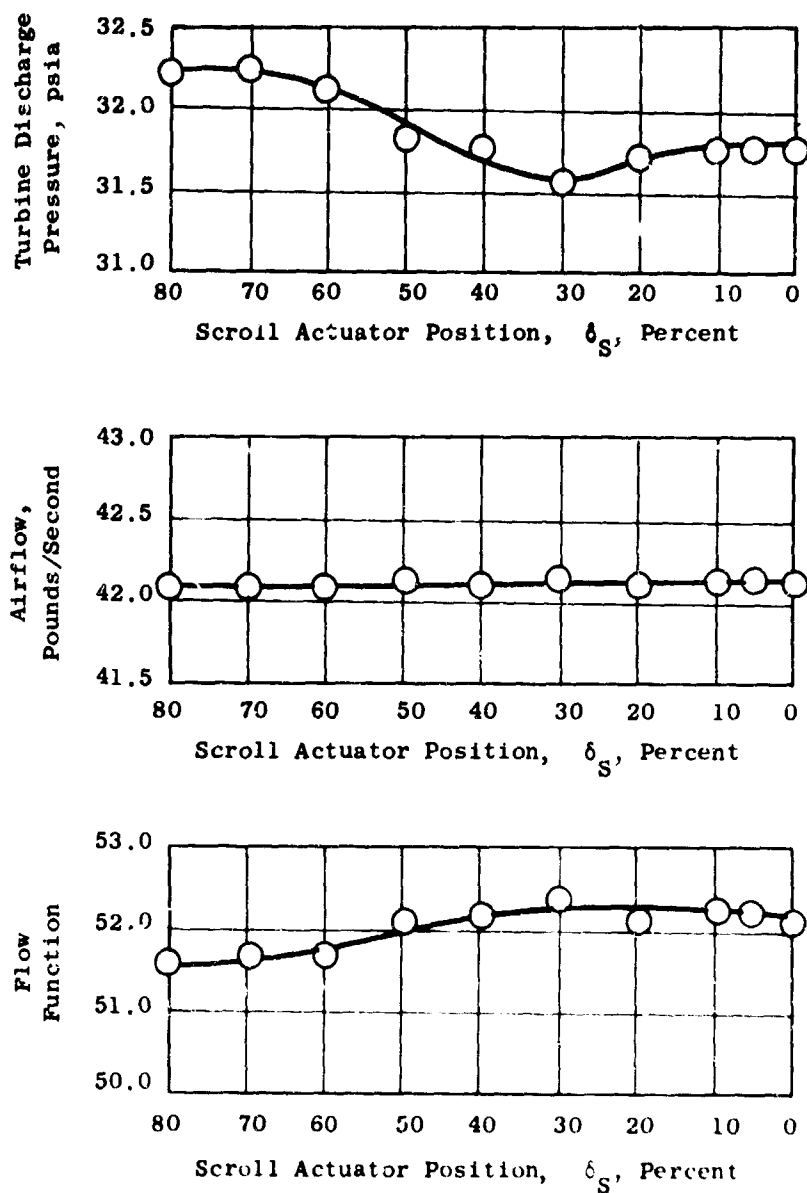


Figure 179. Effects of Scroll Area on Engine 2 Performance for Final Rigging.

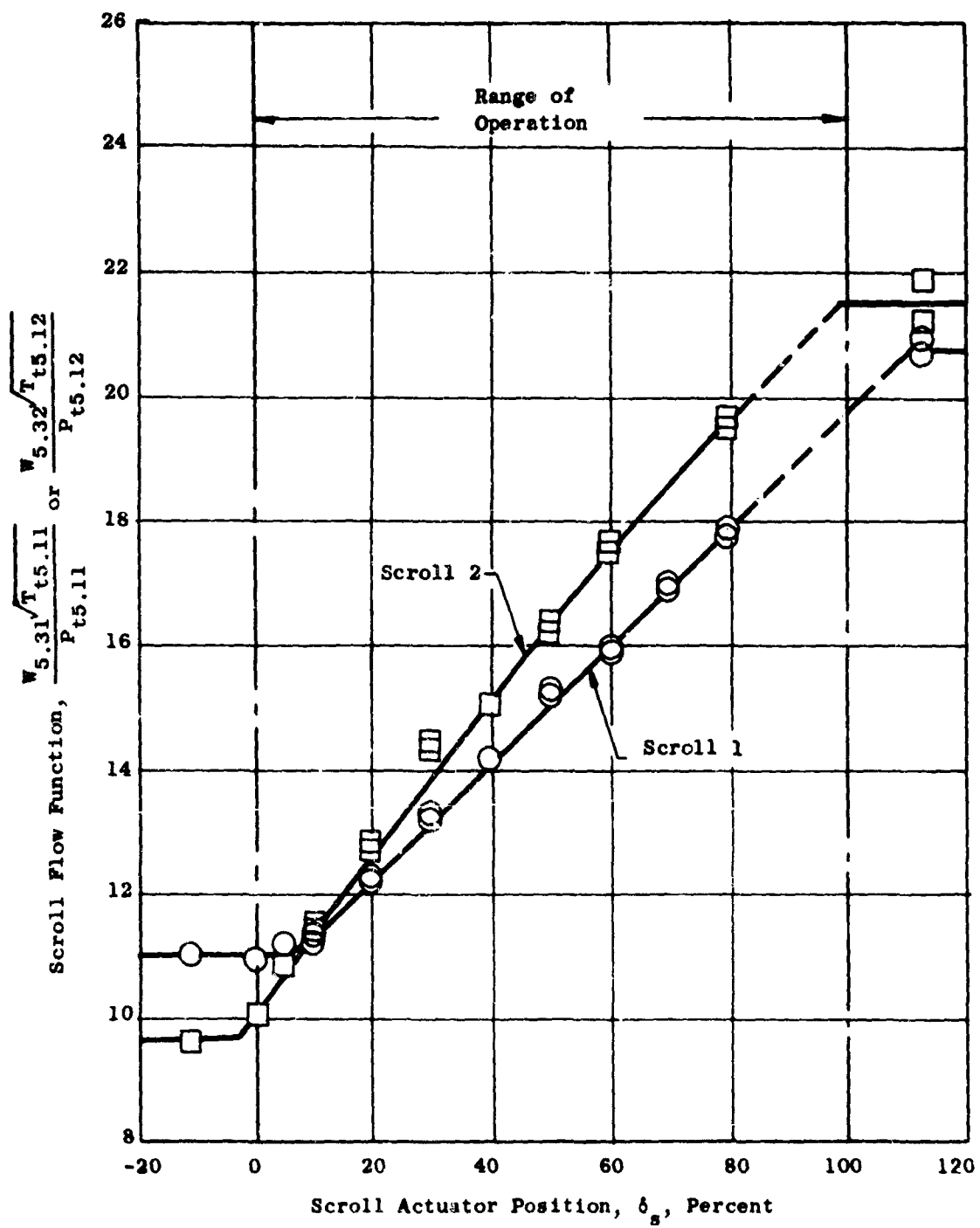


Figure 180. Variation of Scroll Flow Function With Scroll Actuator Position.

Loss Coefficient (Between Engine Discharge
and Ends of Scroll Arms)

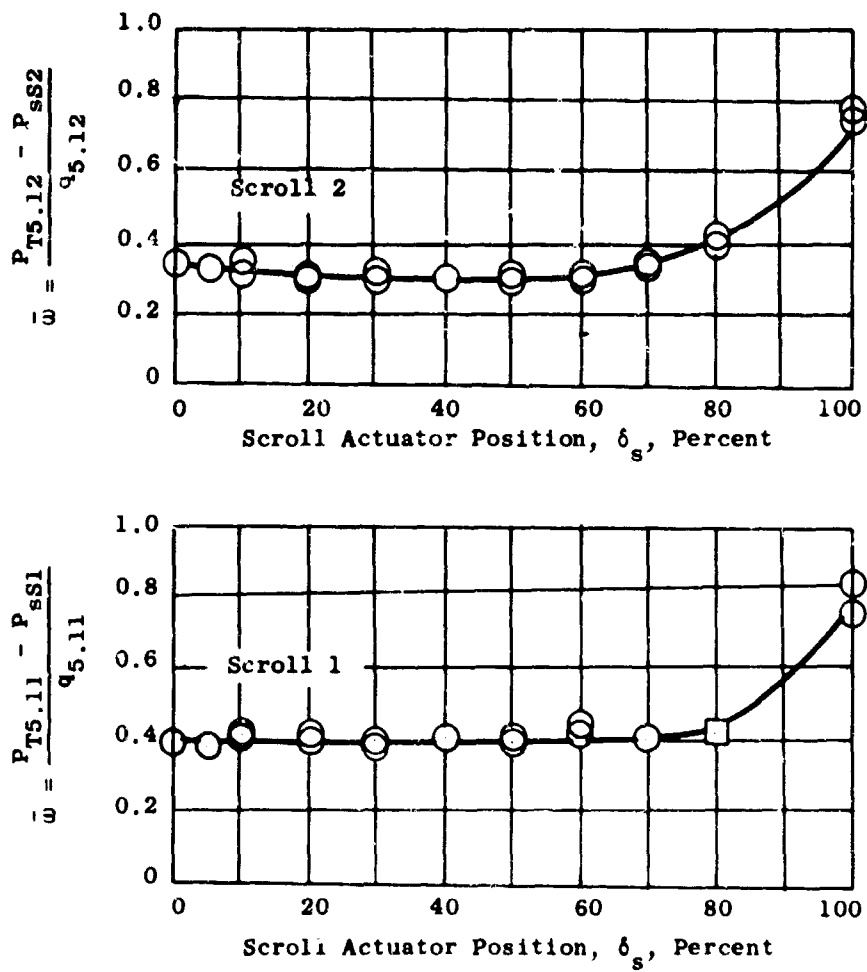


Figure 181. Variation of Scroll Loss Coefficient With Scroll Actuator Position.

Loss Coefficient (Between Engine Discharge and Ends
of Scroll Arms)

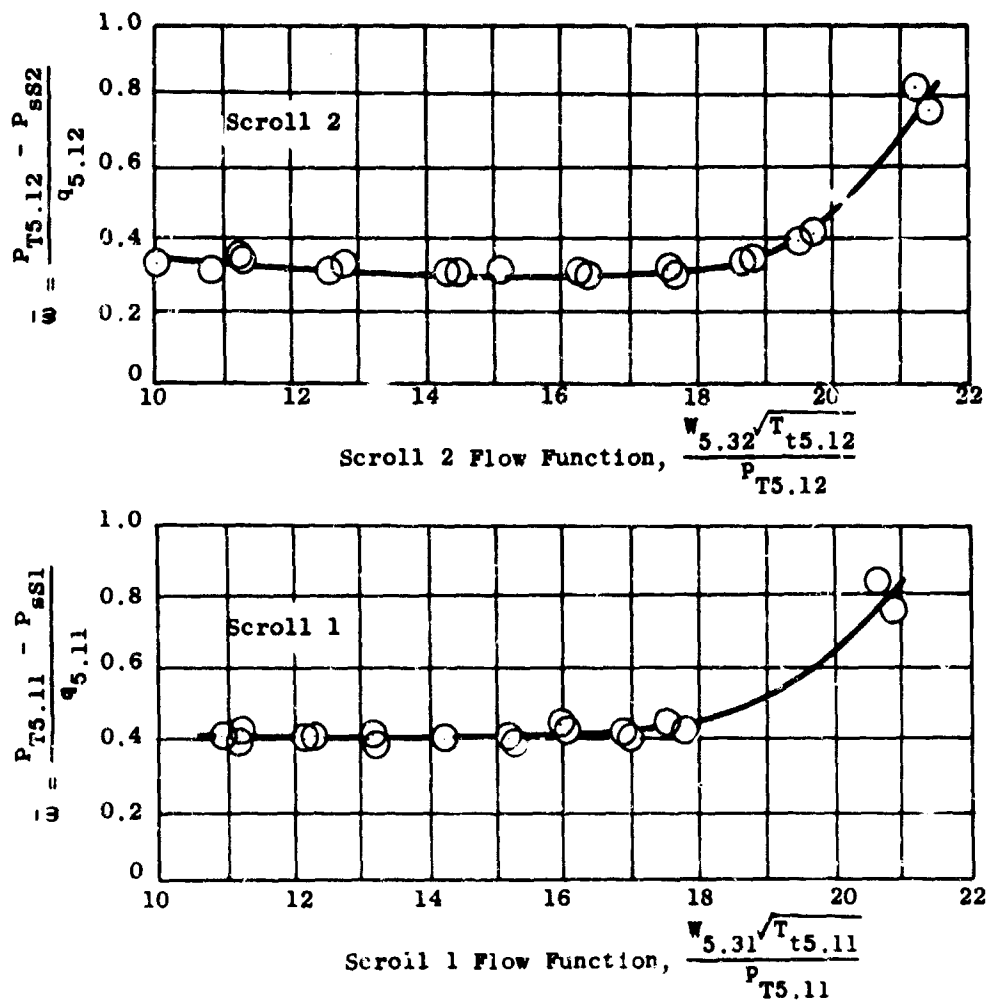


Figure 182. Variation of Scroll Loss Coefficient With Scroll Flow Function.

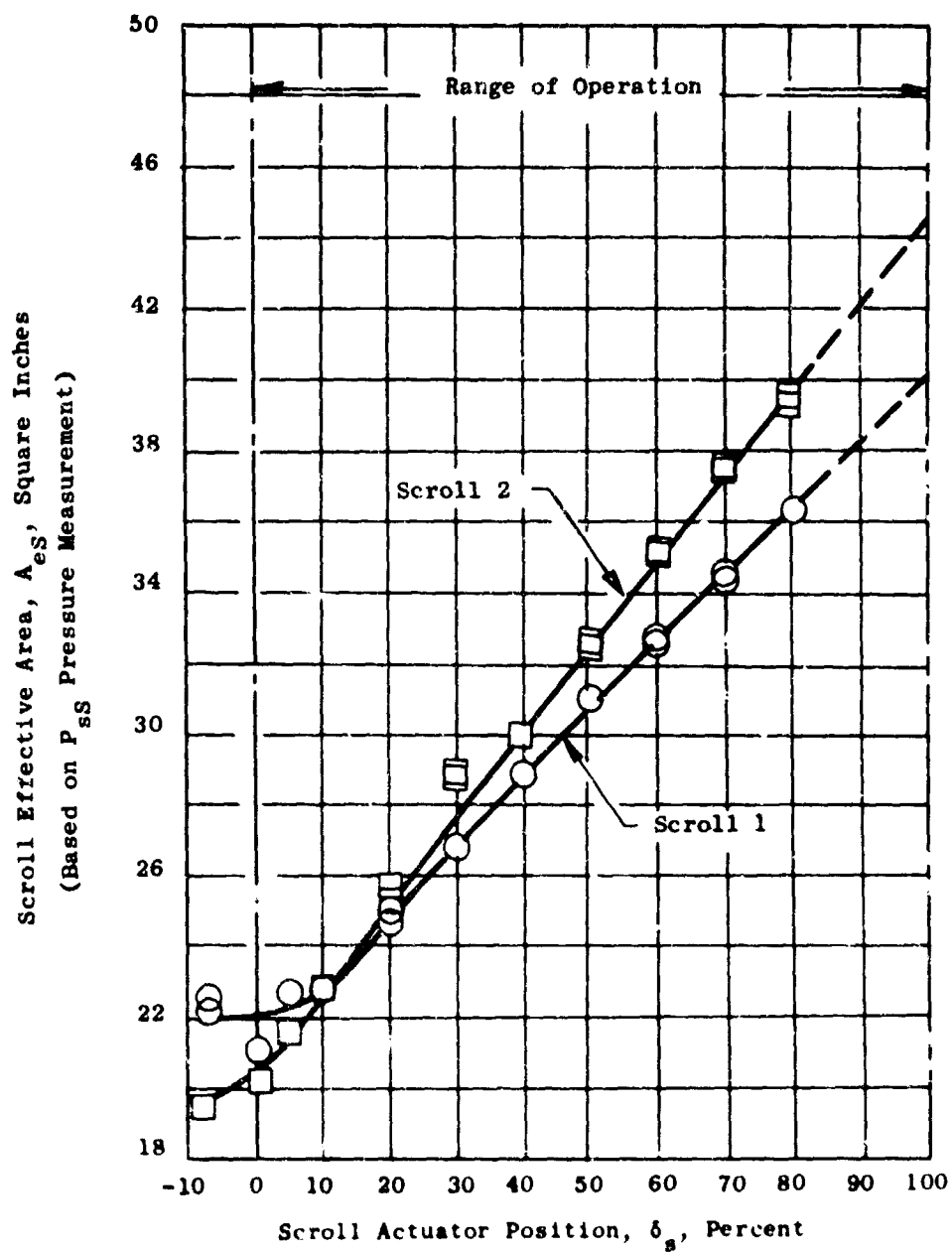


Figure 183. Variation of Scroll Effective Area With Scroll Actuator Position.

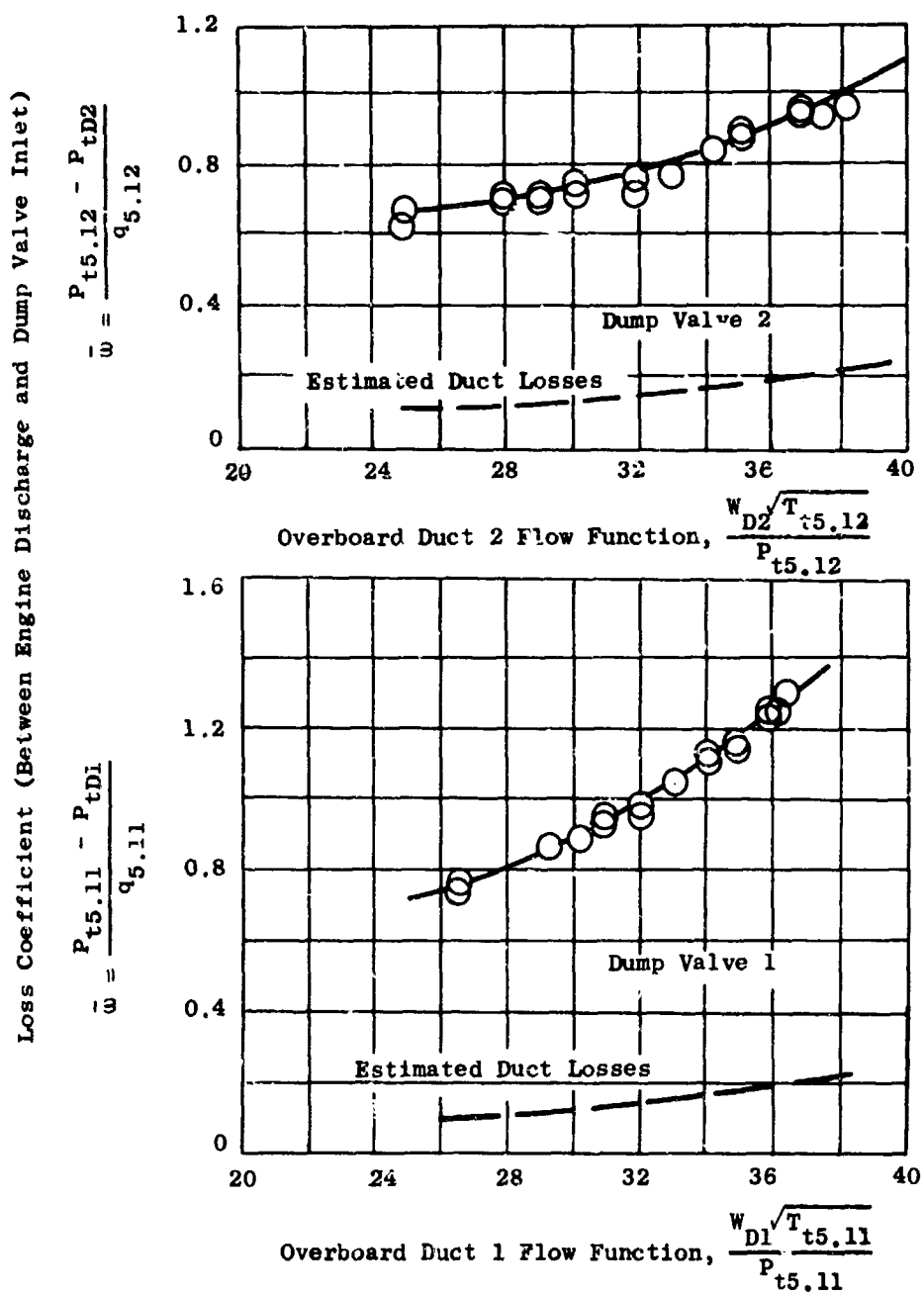


Figure 184. Variation of Overboard Dump System Losses With Flow Function.

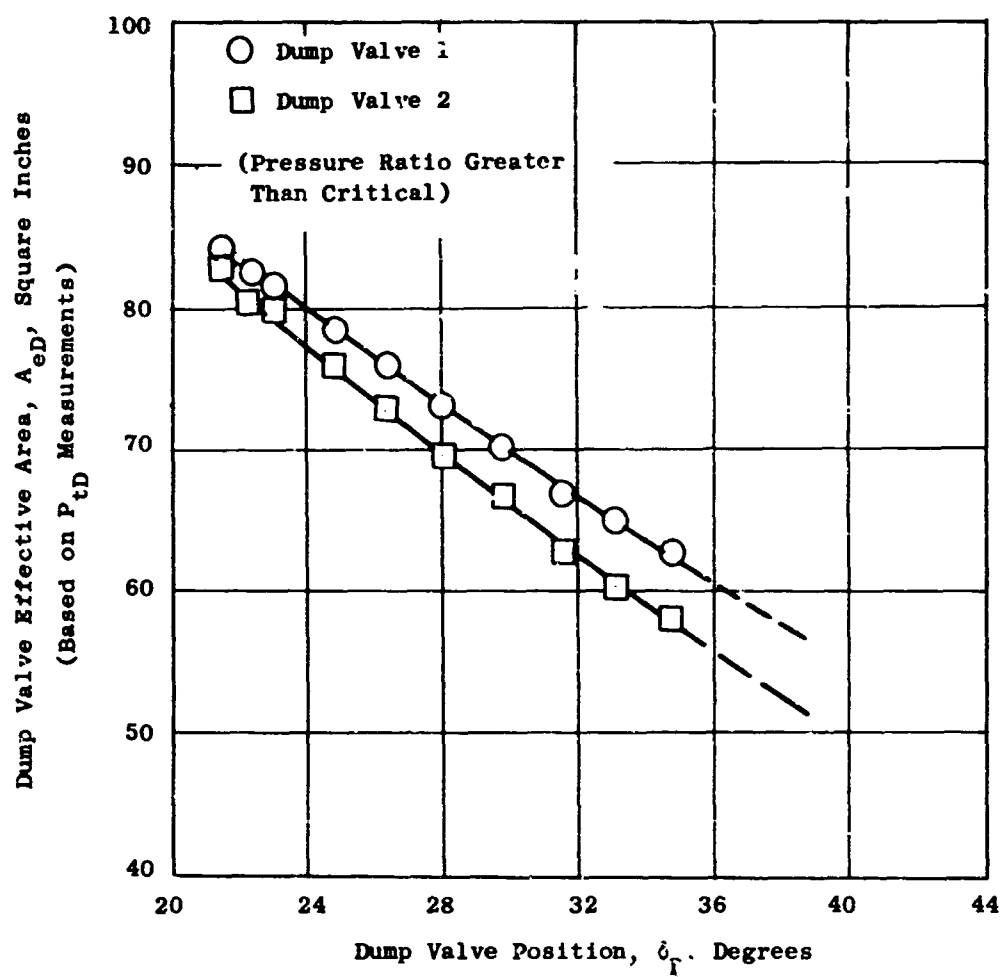


Figure 185. Variation of Dump Valve Effective Area With Position.

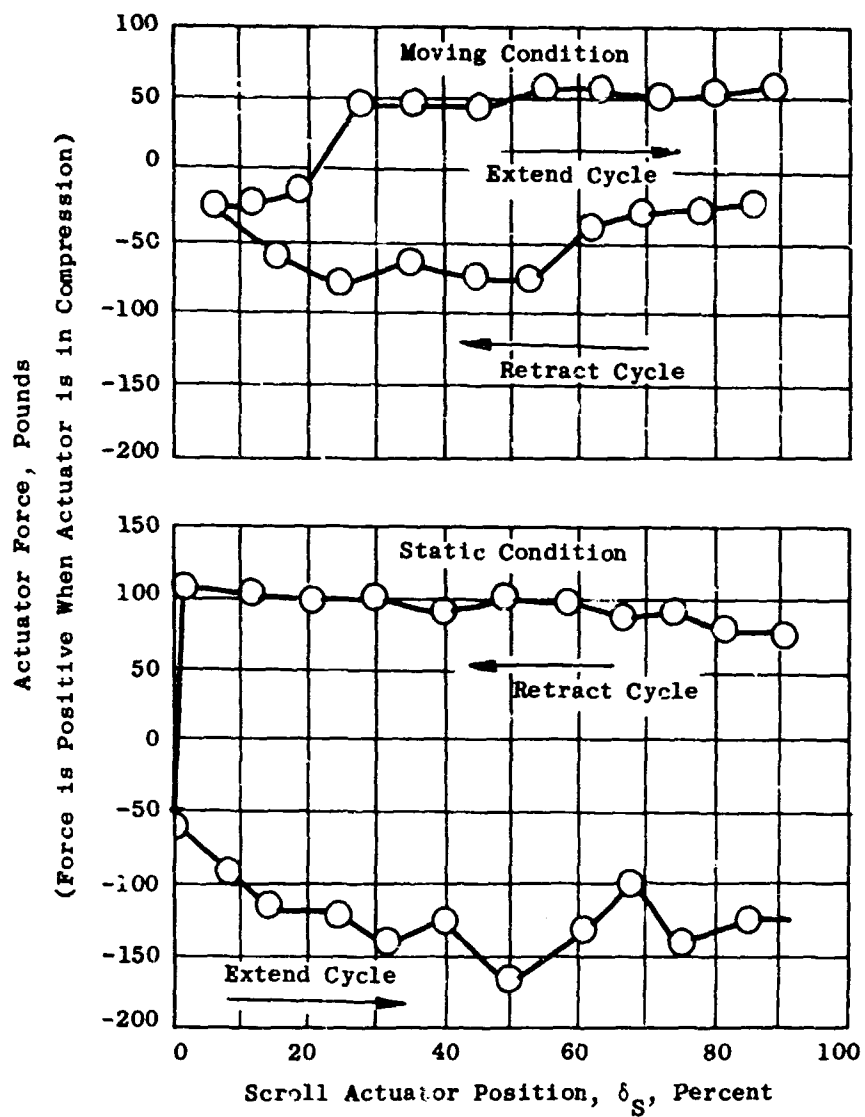


Figure 186. Scroll Actuator Forces Versus Actuator Position.

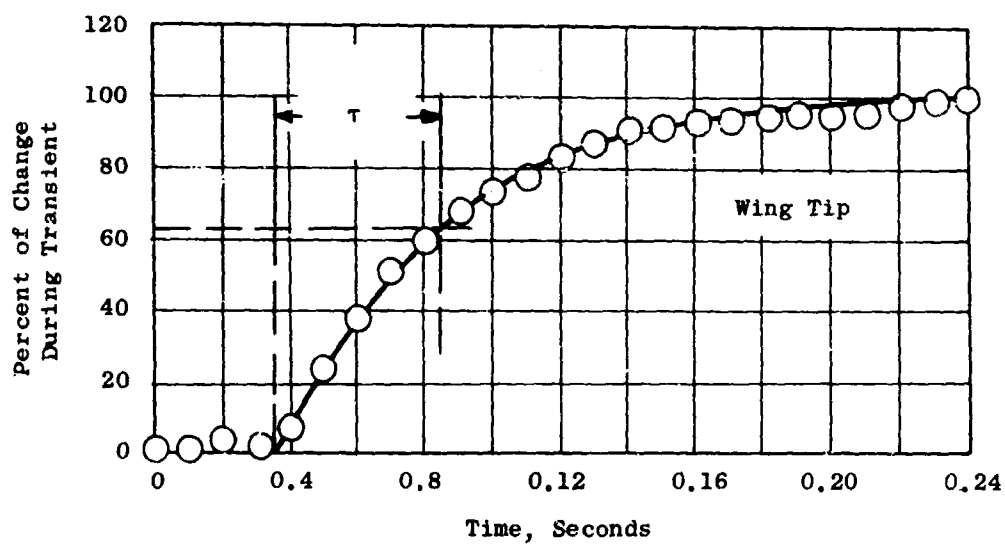
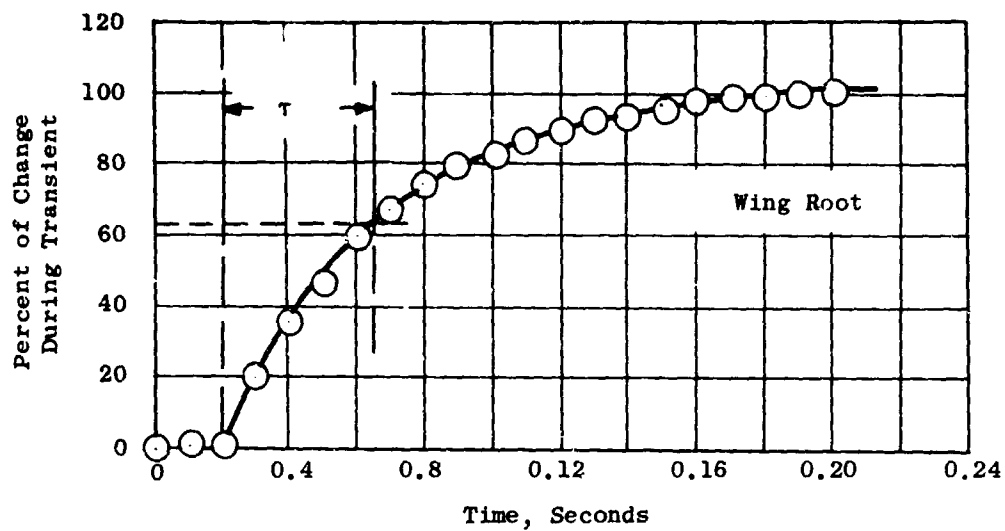


Figure 187. Response of the Vertical Lift Load Cells to a Step Input.

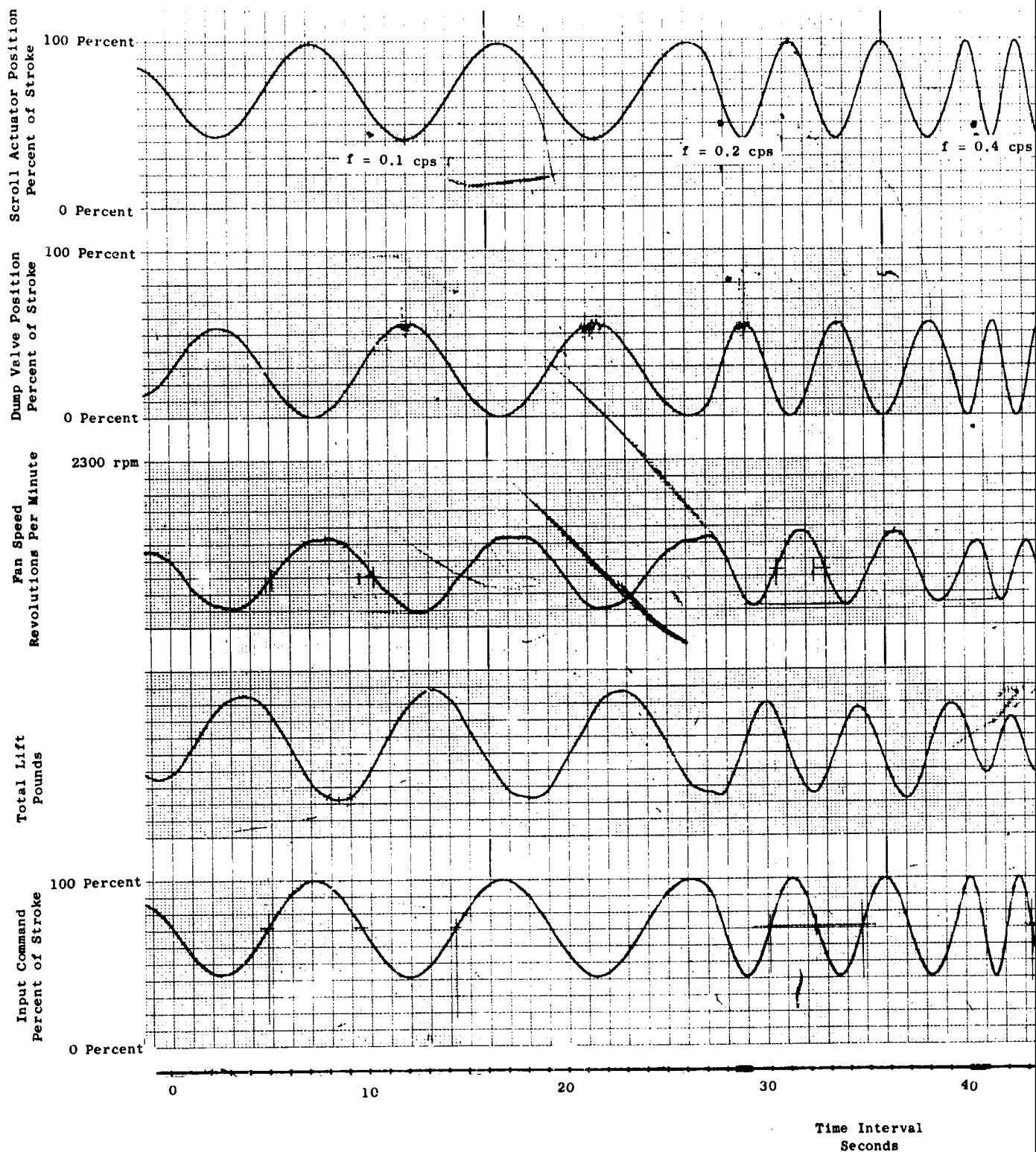
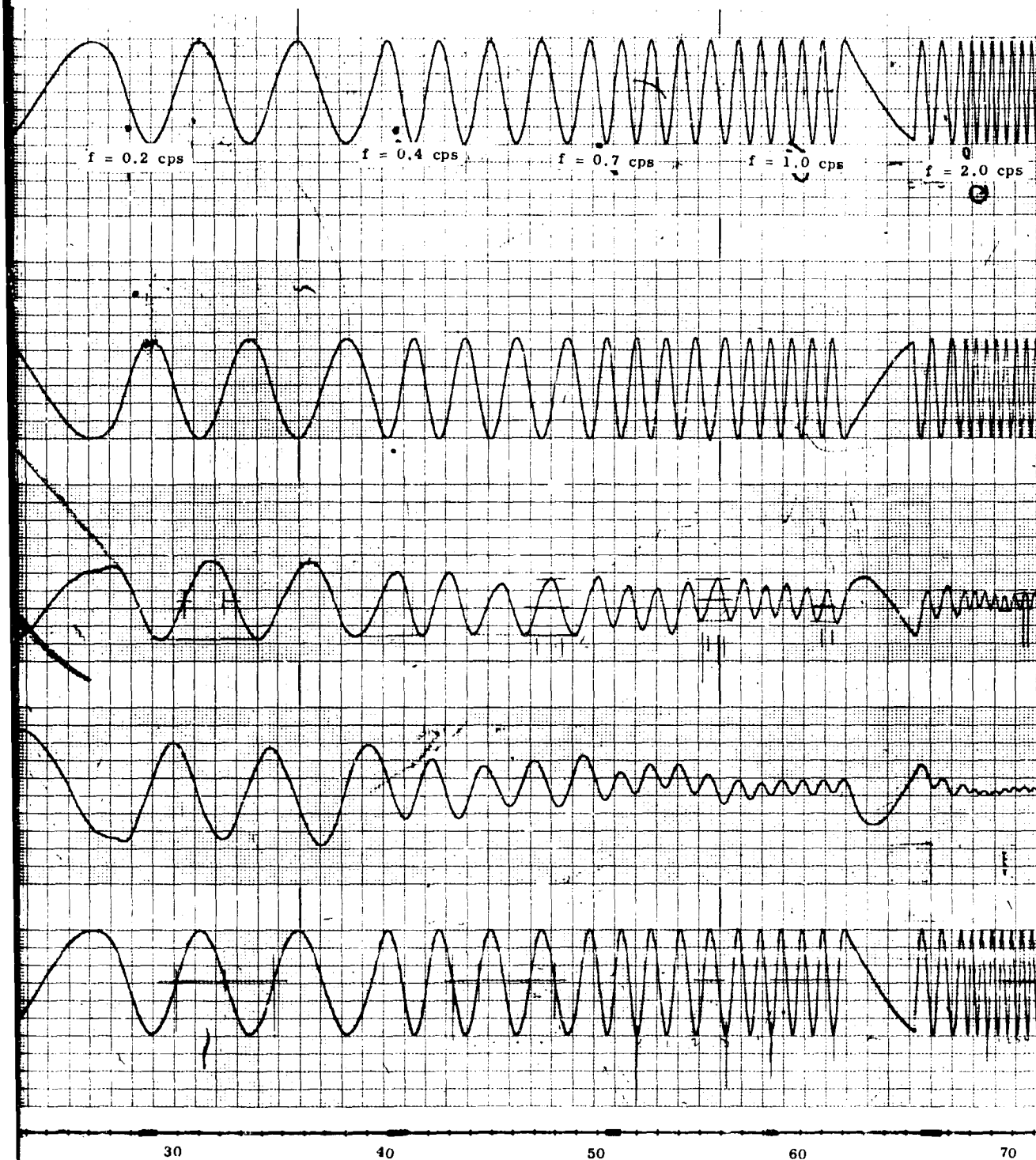


Figure 188. Typical Response Characteristics for a sinusoidal Input of 80 ± 20 Percent, $N_e = 95$ Percent.



Time Interval
Seconds

a sinusoidal input of

B

$N_{Fc} = 1780 \text{ rpm}$ $\delta_s = 20 \pm 20 \text{ Percent}$

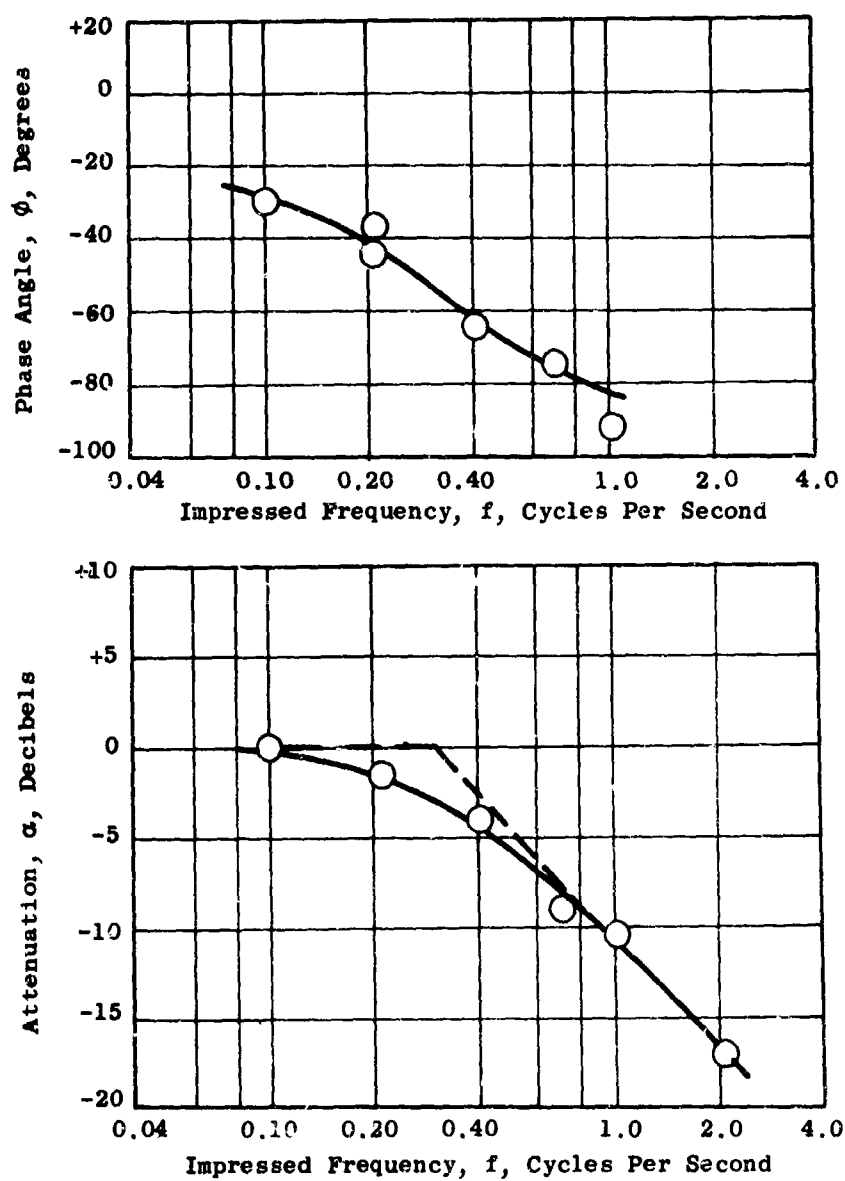


Figure 129. Frequency Response Characteristics Based on Fan Speed, $N_{Fc} = 1780 \text{ rpm}$, $\delta_s = 20 \pm 20 \text{ Percent}$.

$N_{Fc} = 1940 \text{ rpm}$

$\delta_s = 50 \pm 20 \text{ Percent}$

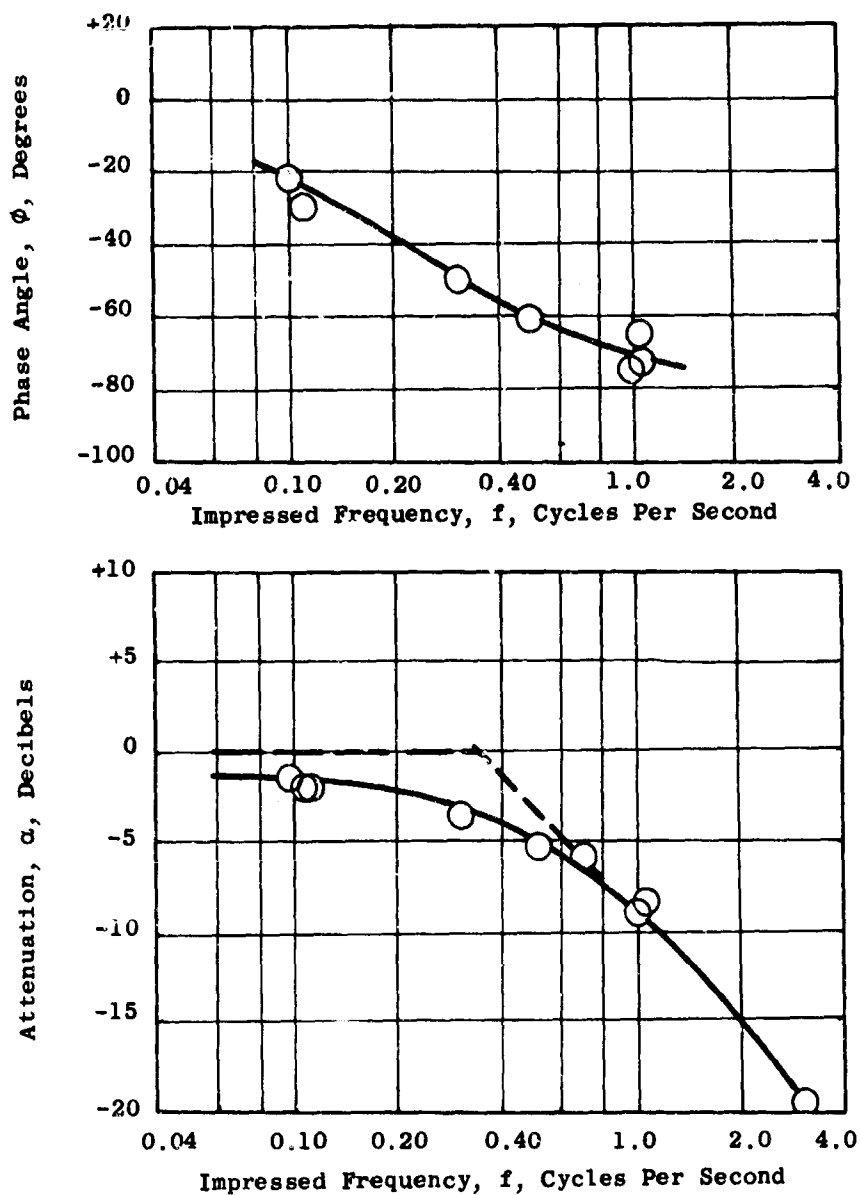


Figure 190. Frequency Response Characteristics Based on Fan Speed, $N_{Fc} = 1940 \text{ rpm}$, $\delta_s = 50 \pm 20 \text{ Percent}$.

$N_{Fc} = 1940 \text{ rpm}$ $\delta_S = 50 \pm 50 \text{ Percent}$

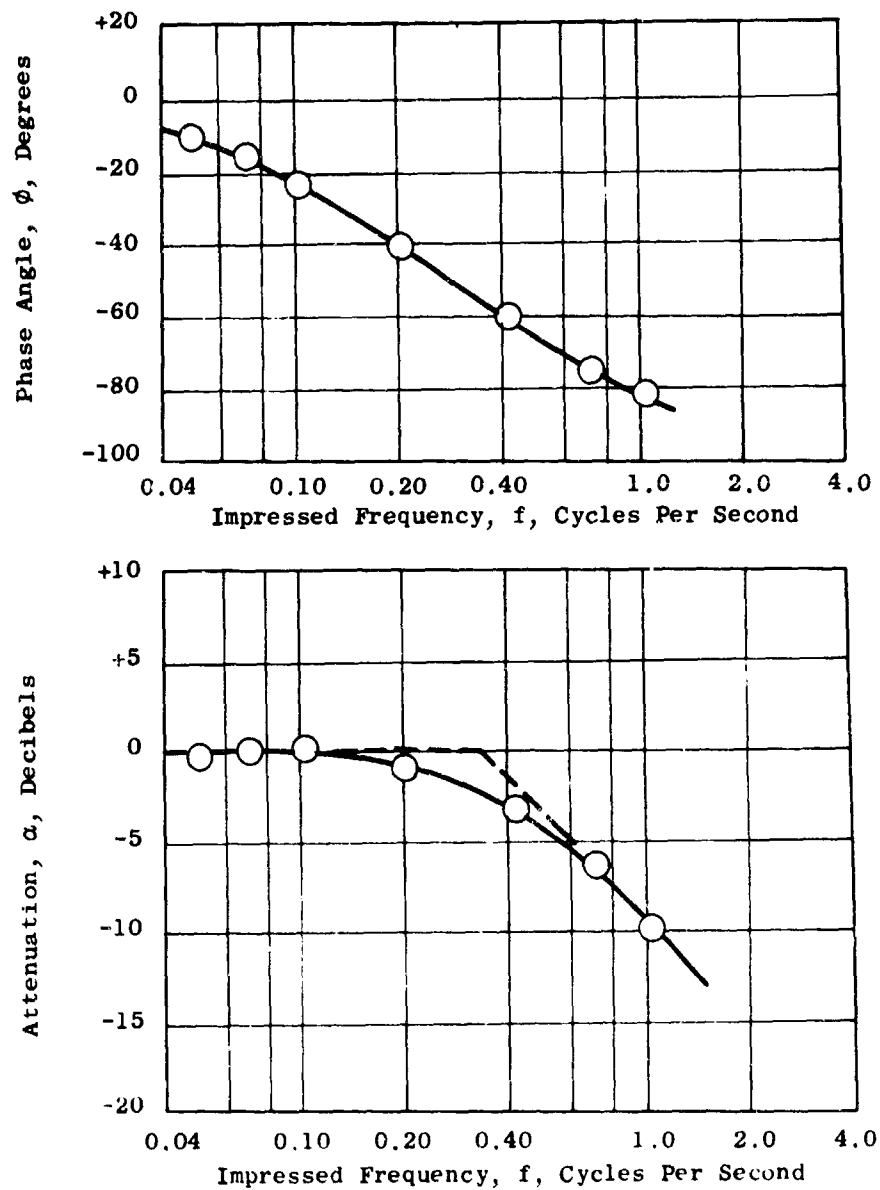


Figure 191. Frequency Response Characteristics Based on Fan Speed, $N_{Fc} = 1940 \text{ rpm}$, $\delta_S = 50 \pm 50 \text{ Percent}$.

$N_{Fc} = 2050 \text{ rpm}$ $\delta_s = 70 \pm 10 \text{ Percent}$

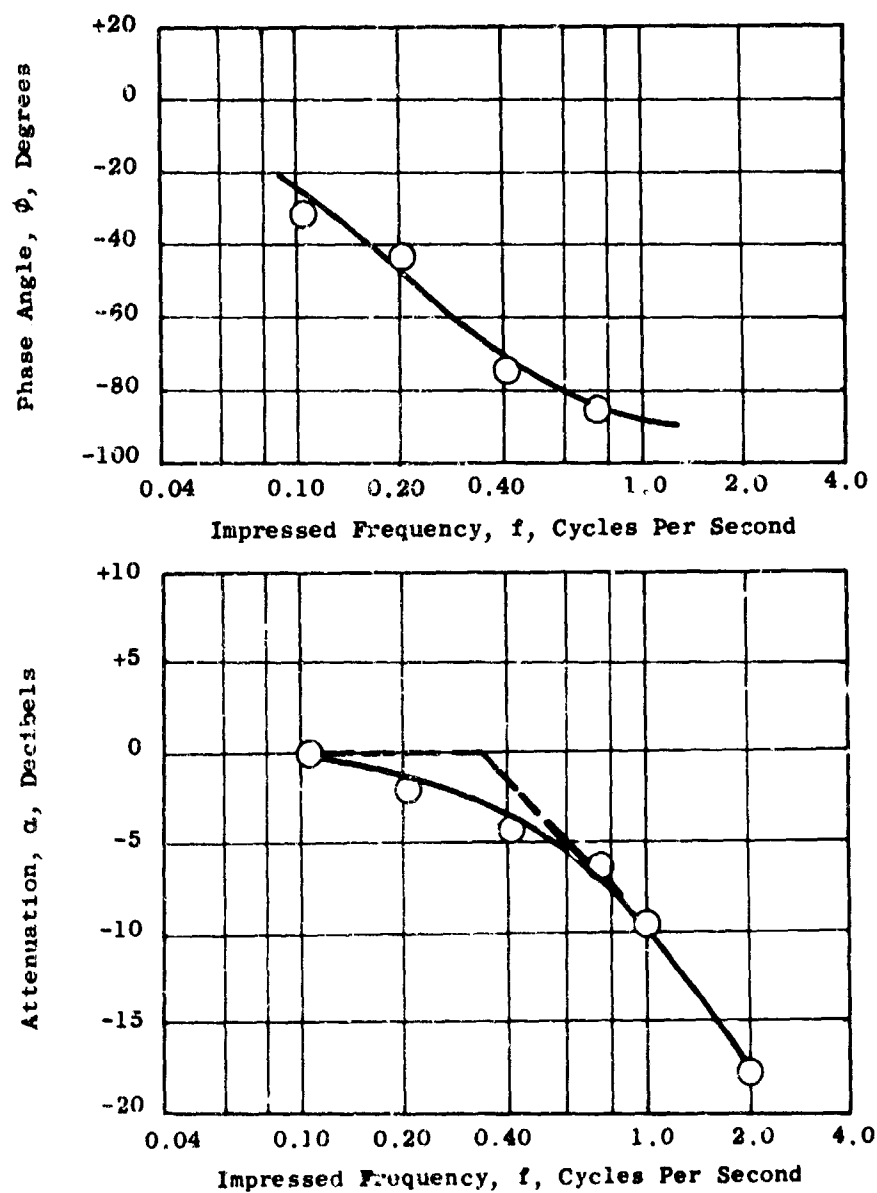


Figure 192. Frequency Response Characteristics Based on Fan Speed, $N_{Fc} = 2050 \text{ rpm}$, $\delta_s = 70 \pm 10 \text{ Percent}$.

$N_{Fc} = 2050 \text{ rpm}$ $\delta_S = 70 \pm 20 \text{ Percent}$

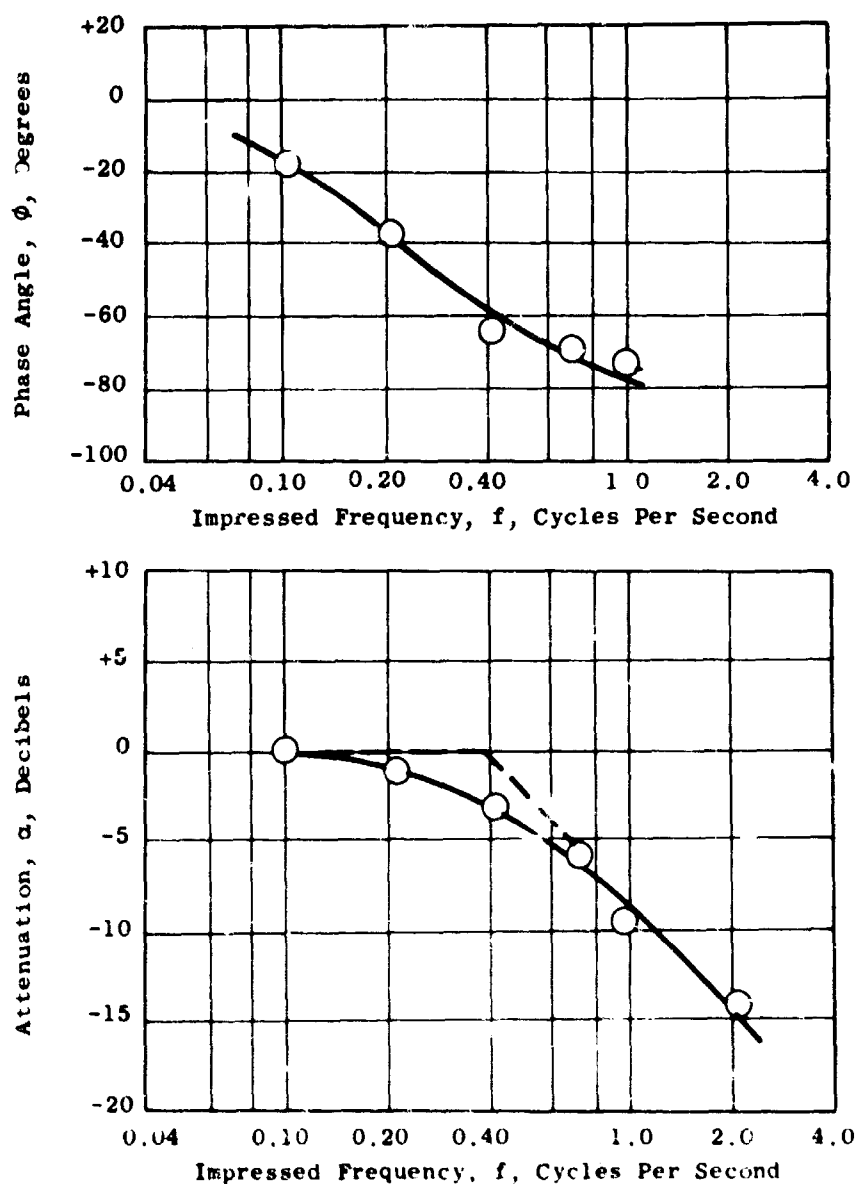


Figure 193. Frequency Response Characteristics Based on Fan Speed, $N_{Fc} = 2050 \text{ rpm}$, $\delta_S = 70 \pm 20 \text{ Percent}$.

$N_{Fc} = 2050 \text{ rpm}$

$\delta_S = 70 \pm 30 \text{ Percent}$

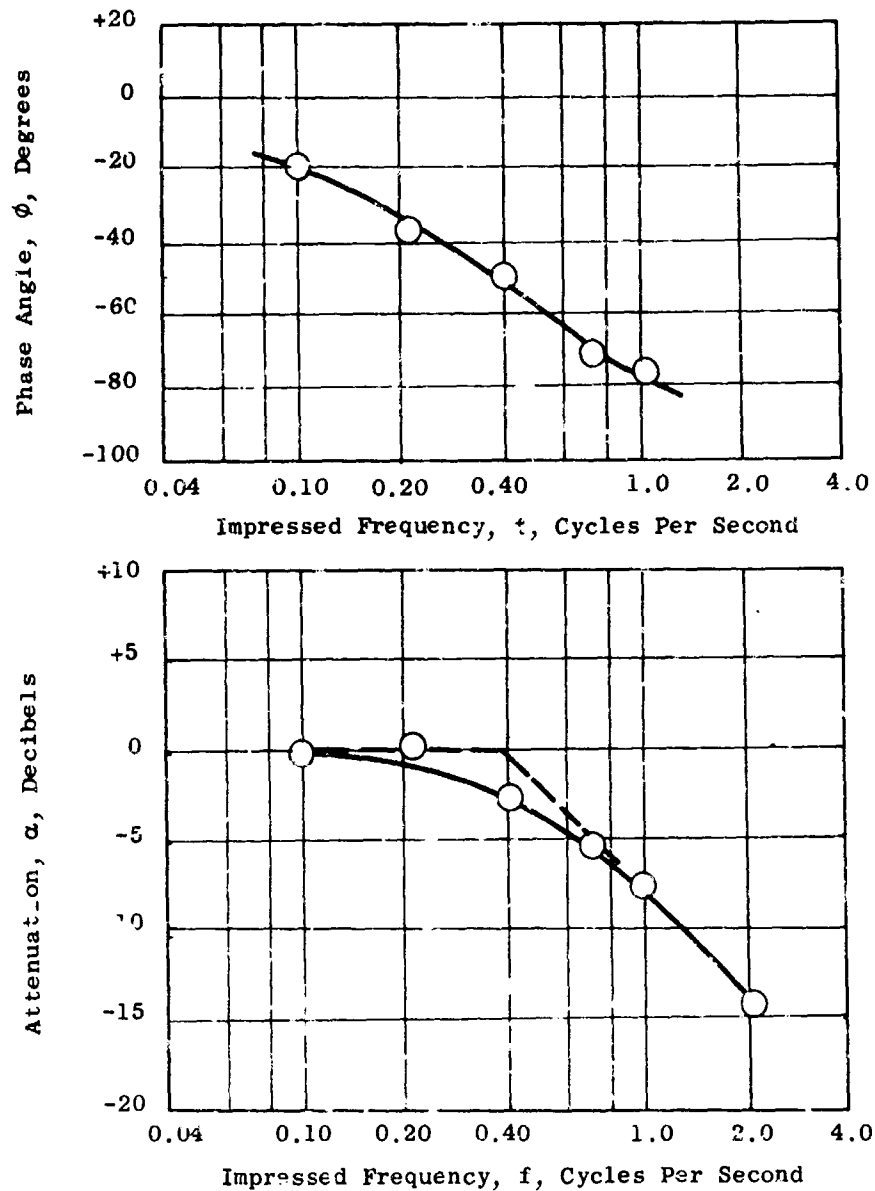


Figure 194. Frequency Response Characteristics Based on Fan Speed, $N_{Fc} = 2050 \text{ rpm}$, $\delta_S = 70 \pm 30 \text{ Percent}$.

$N_{Fc} = 2090 \text{ rpm}$

$\delta_S = 80 \pm 20 \text{ Percent}$

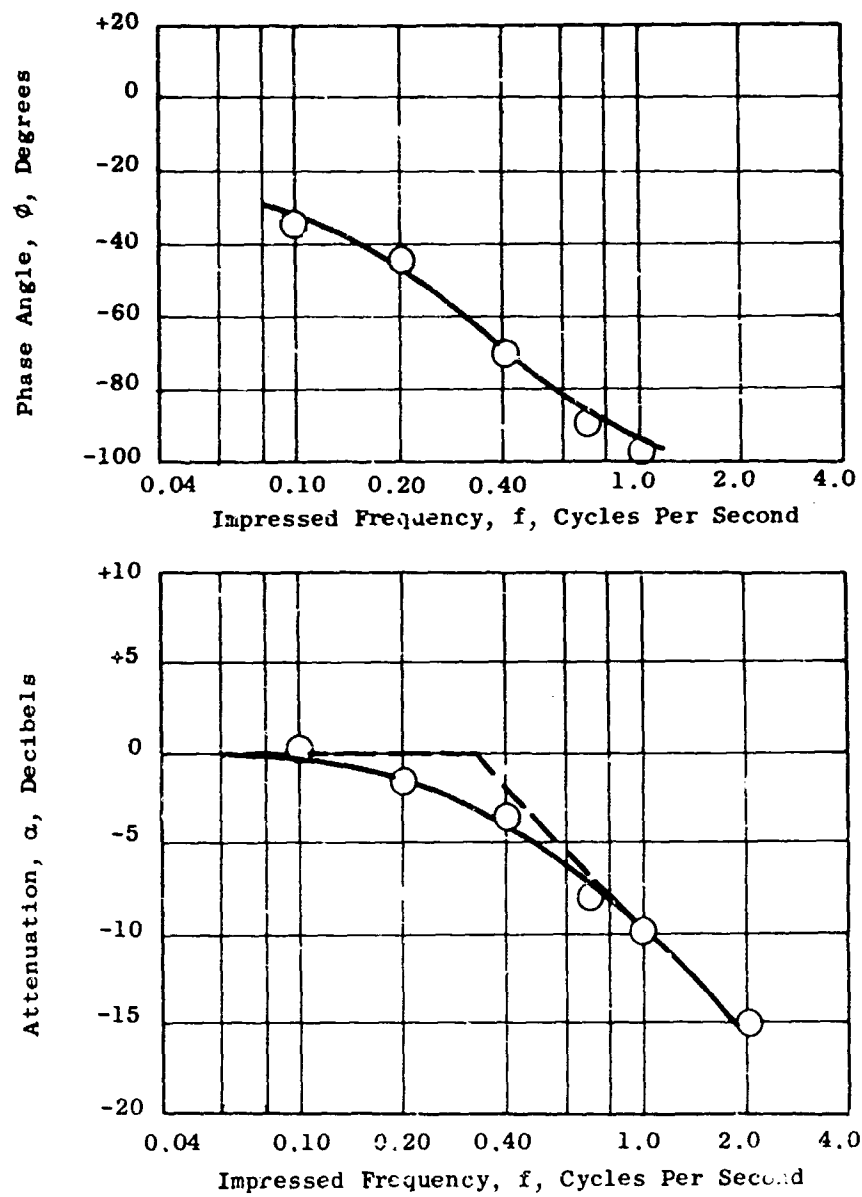


Figure 195. Frequency Response Characteristics Based on Fan Speed, $N_{Fc} = 2090 \text{ rpm}$, $\delta_S = 80 \pm 20 \text{ Percent}$.

$N_{Fc} = 2000 \text{ rpm}$ $\delta_S = 20 \pm 20 \text{ Percent}$

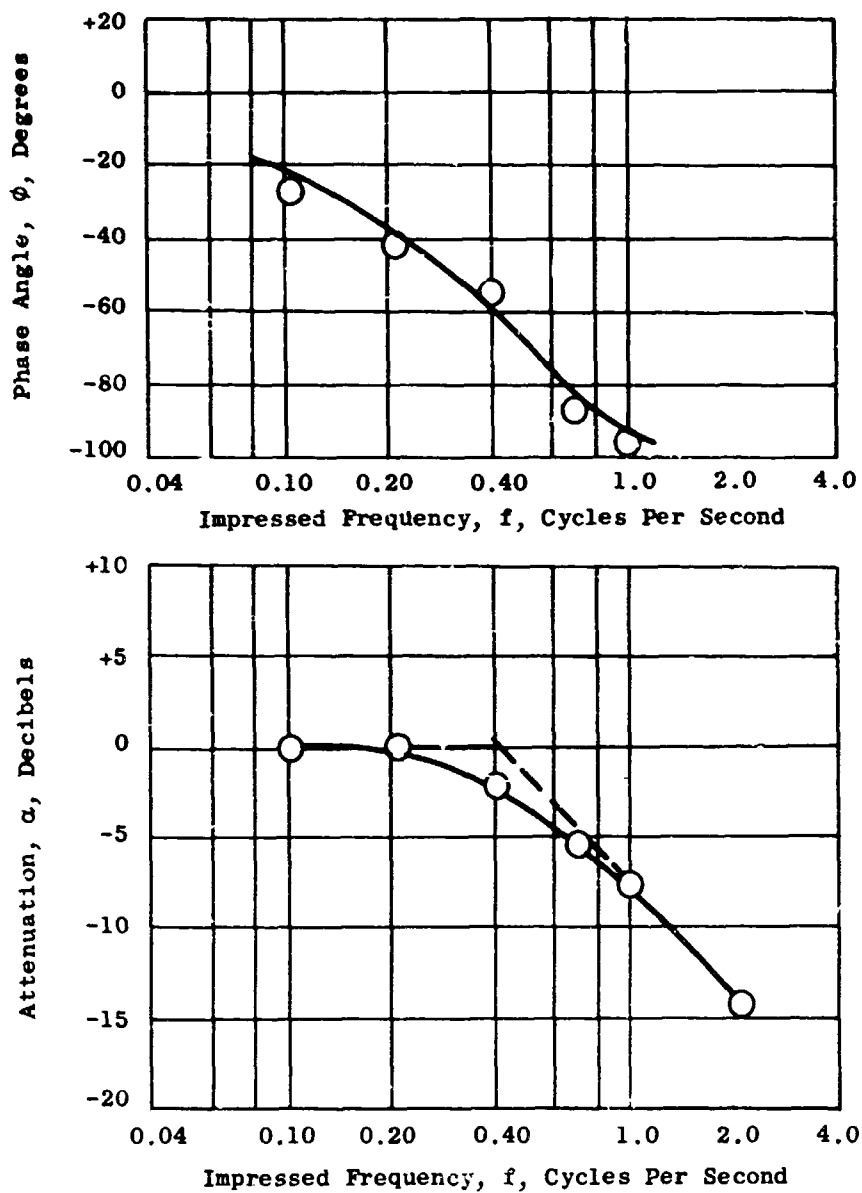


Figure 196. Frequency Response Characteristics Based on Fan Speed, $N_{Fc} = 2000 \text{ rpm}$, $\delta_S = 20 \pm 20 \text{ Percent}$.

$N_{Fc} = 2220 \text{ rpm}$ $\delta_S = 50 \pm 20 \text{ Percent}$

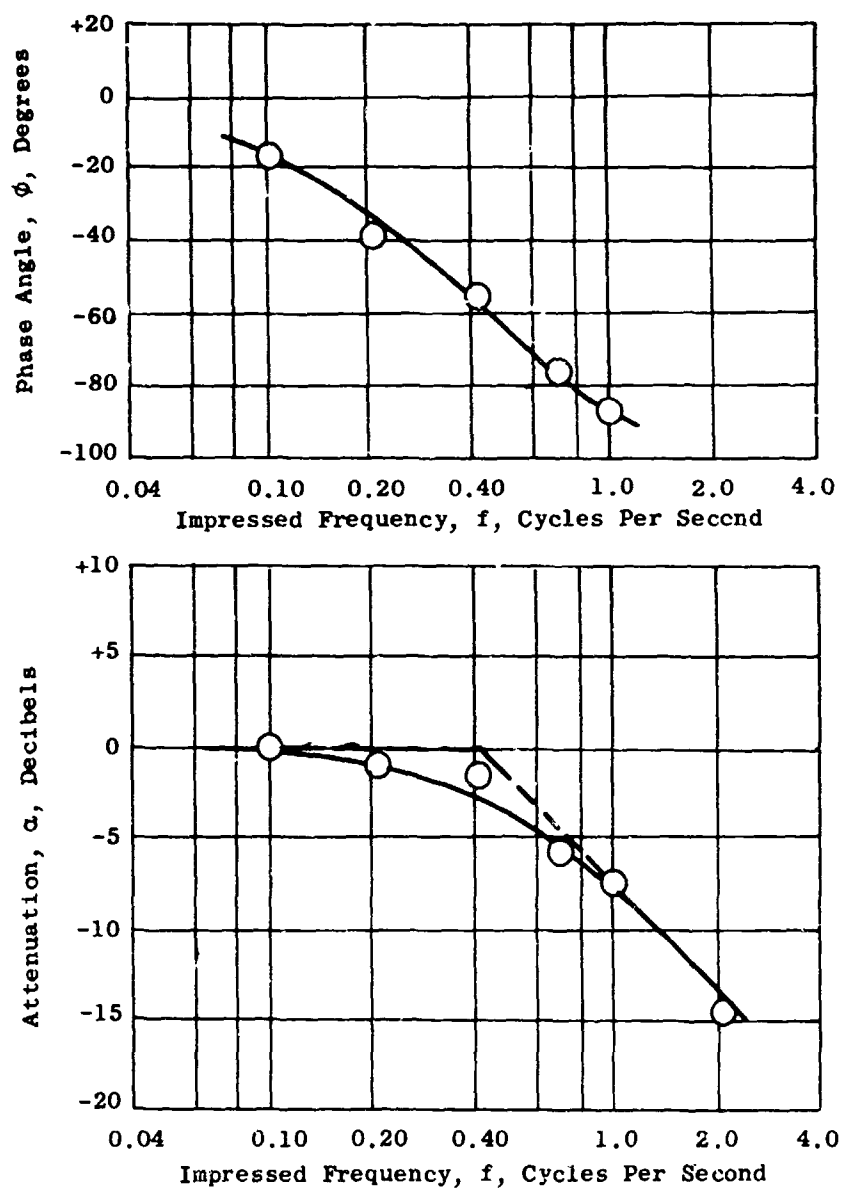


Figure 197. Frequency Response Characteristics Based on Fan Speed, $N_{Fc} = 2220 \text{ rpm}$, $\delta_S = 50 \pm 20 \text{ Percent}$.

$N_{Fc} = 2220 \text{ rpm}$

$\delta_s = 50 \pm 50 \text{ Percent}$

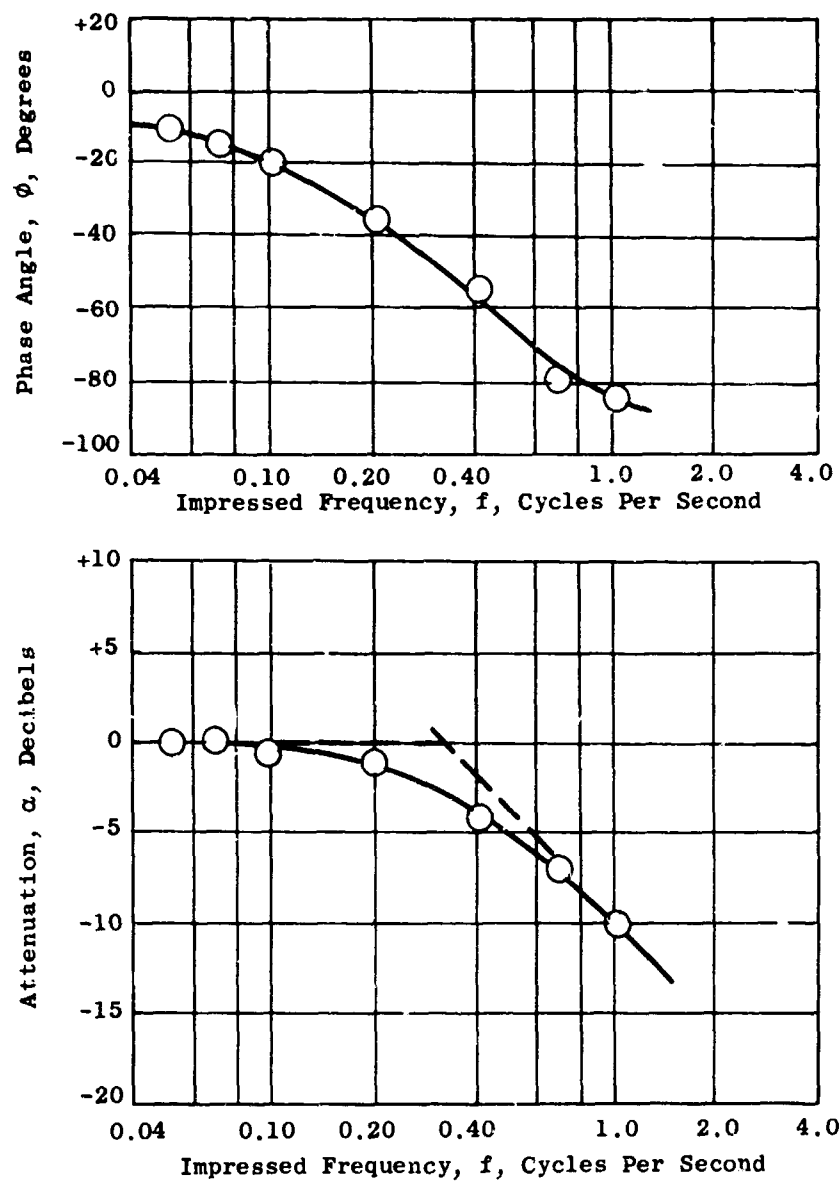


Figure 198. Frequency Response Characteristics Based on Fan Speed, $N_{Fc} = 2220 \text{ rpm}$, $\delta_s = 50 \pm 50 \text{ Percent}$.

$N_{Fc} = 2330 \text{ rpm}$ $\delta_S = 70 \pm 10 \text{ Percent}$

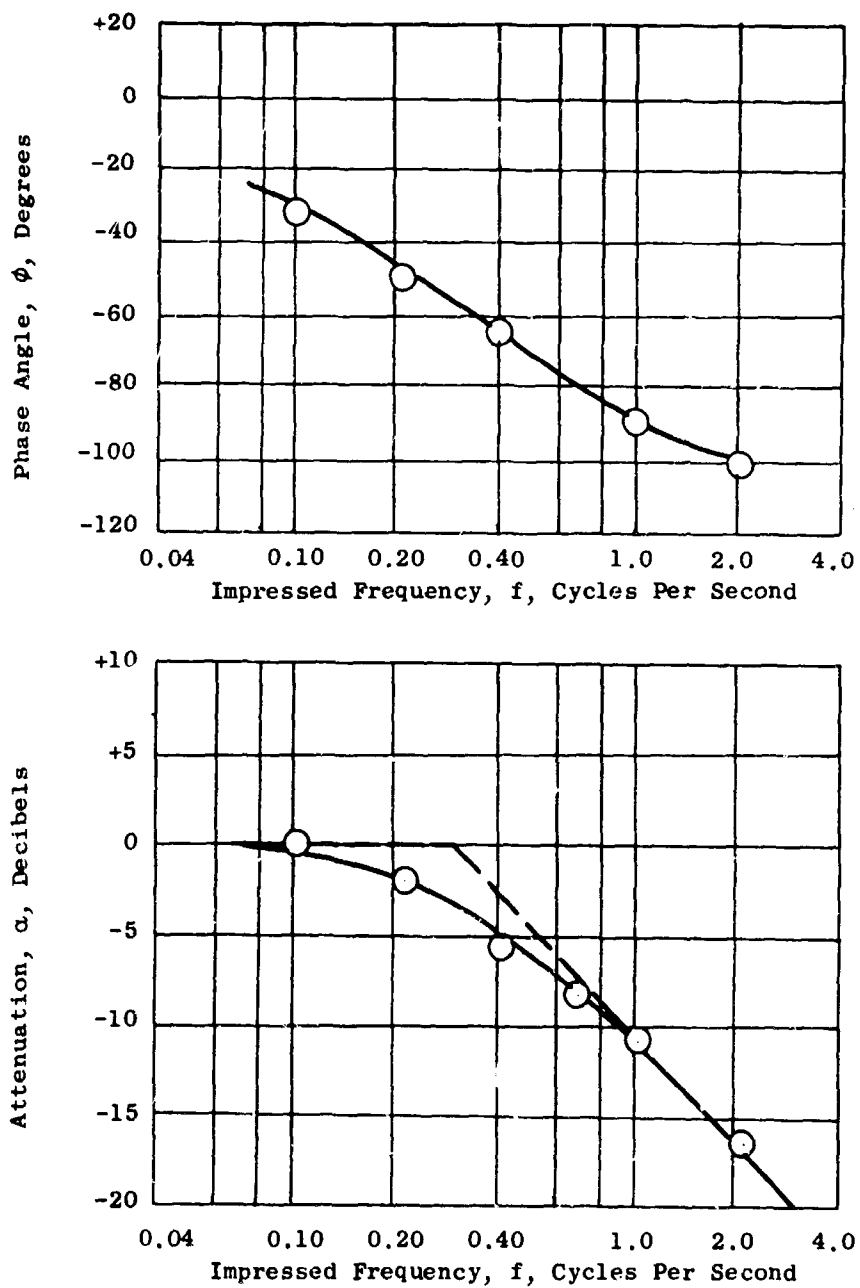


Figure 199. Frequency Response Characteristics Based on Fan Speed, $N_{Fc} = 2330 \text{ rpm}$, $\delta_S = 70 \pm 10 \text{ Percent}$.

$N_{Fc} = 2330 \text{ rpm}$

$\delta_S = 70 \pm 20 \text{ Percent}$

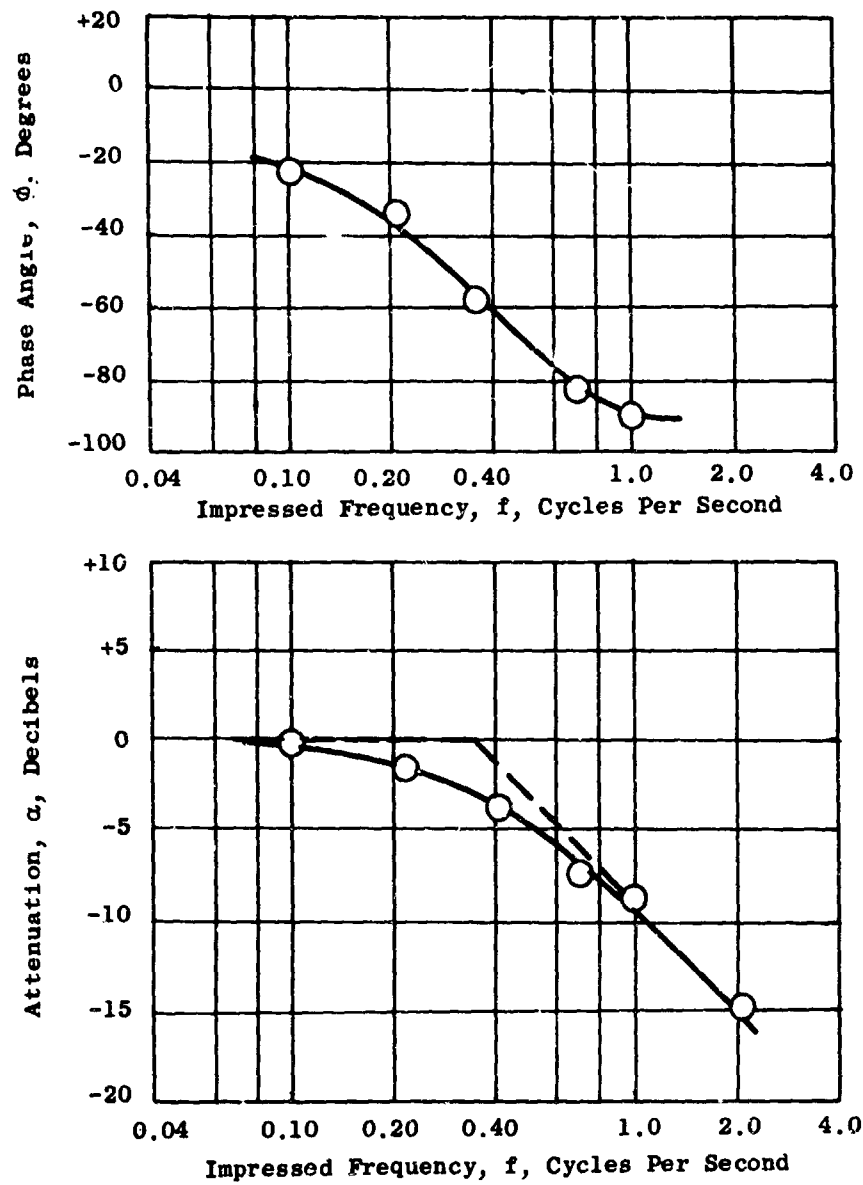


Figure 200. Frequency Response Characteristics Based on Fan Speed, $N_{Fc} = 2330 \text{ rpm}$, $\delta_S = 70 \pm 20 \text{ Percent}$.

$N_{Fc} = 2330 \text{ rpm}$ $\delta_S = 70 \pm 30 \text{ Percent}$

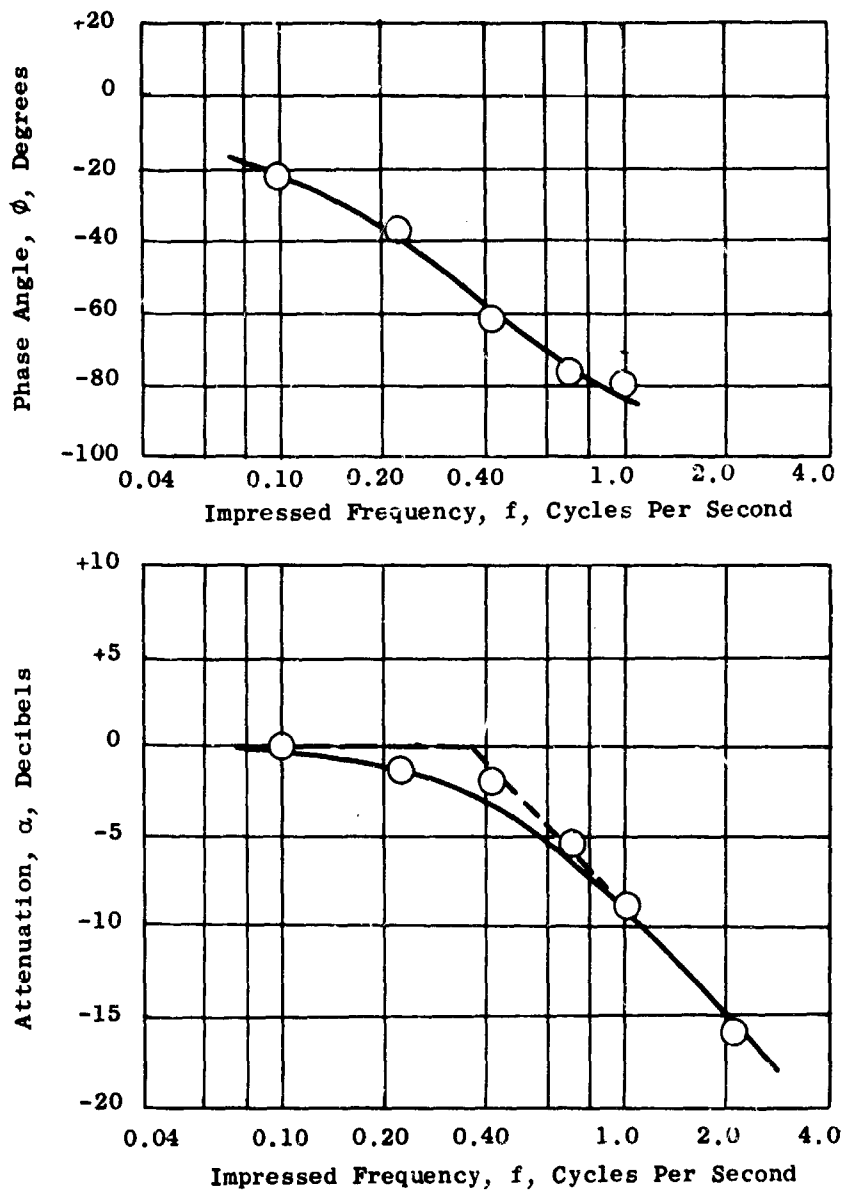


Figure 201. Frequency Response Characteristics Based on Fan Speed, $N_{Fc} = 2330 \text{ rpm}$, $\delta_S = 70 \pm 30 \text{ Percent}$.

$N_{Fc} = 2370 \text{ rpm}$ $\delta_s = 80 \pm 20 \text{ Percent}$

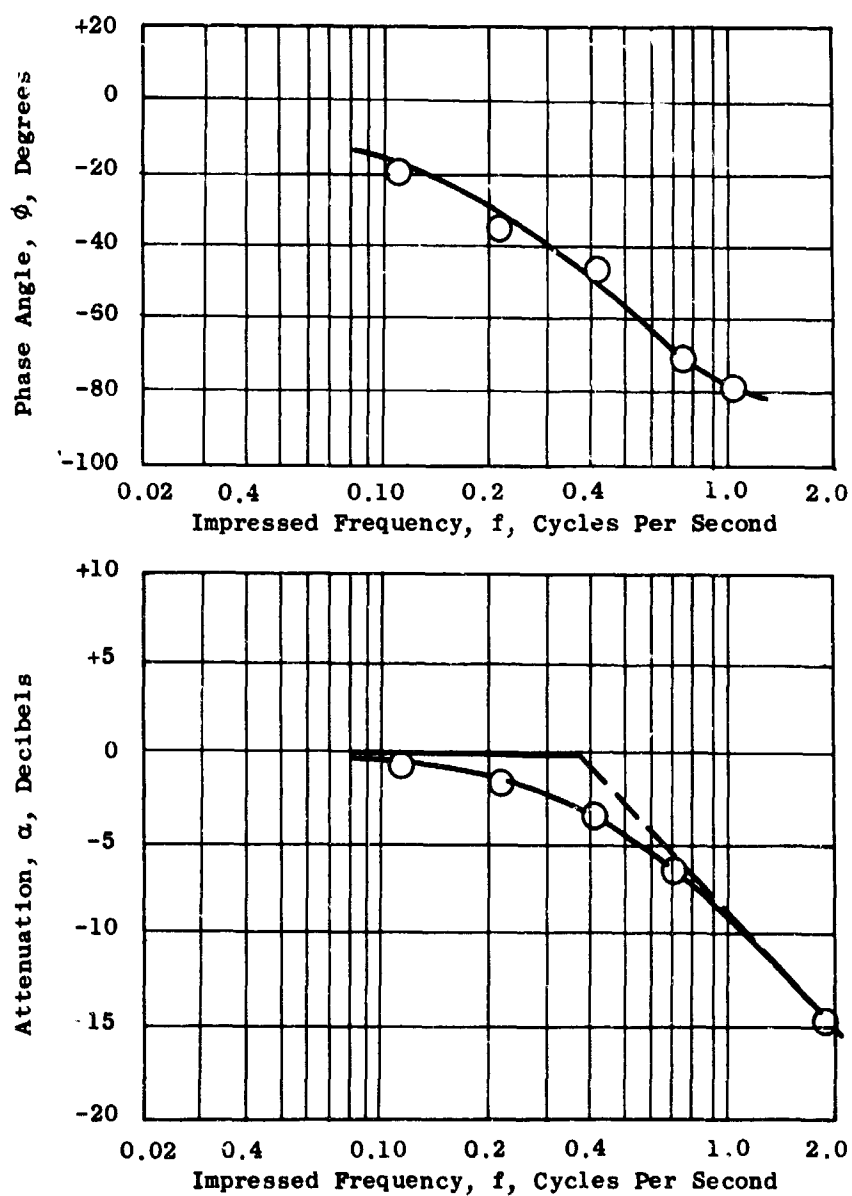


Figure 202. Frequency Response Characteristics Based on Fan Speed, $N_{Fc} = 2370 \text{ rpm}$, $\delta_s = 80 \pm 20 \text{ Percent}$.

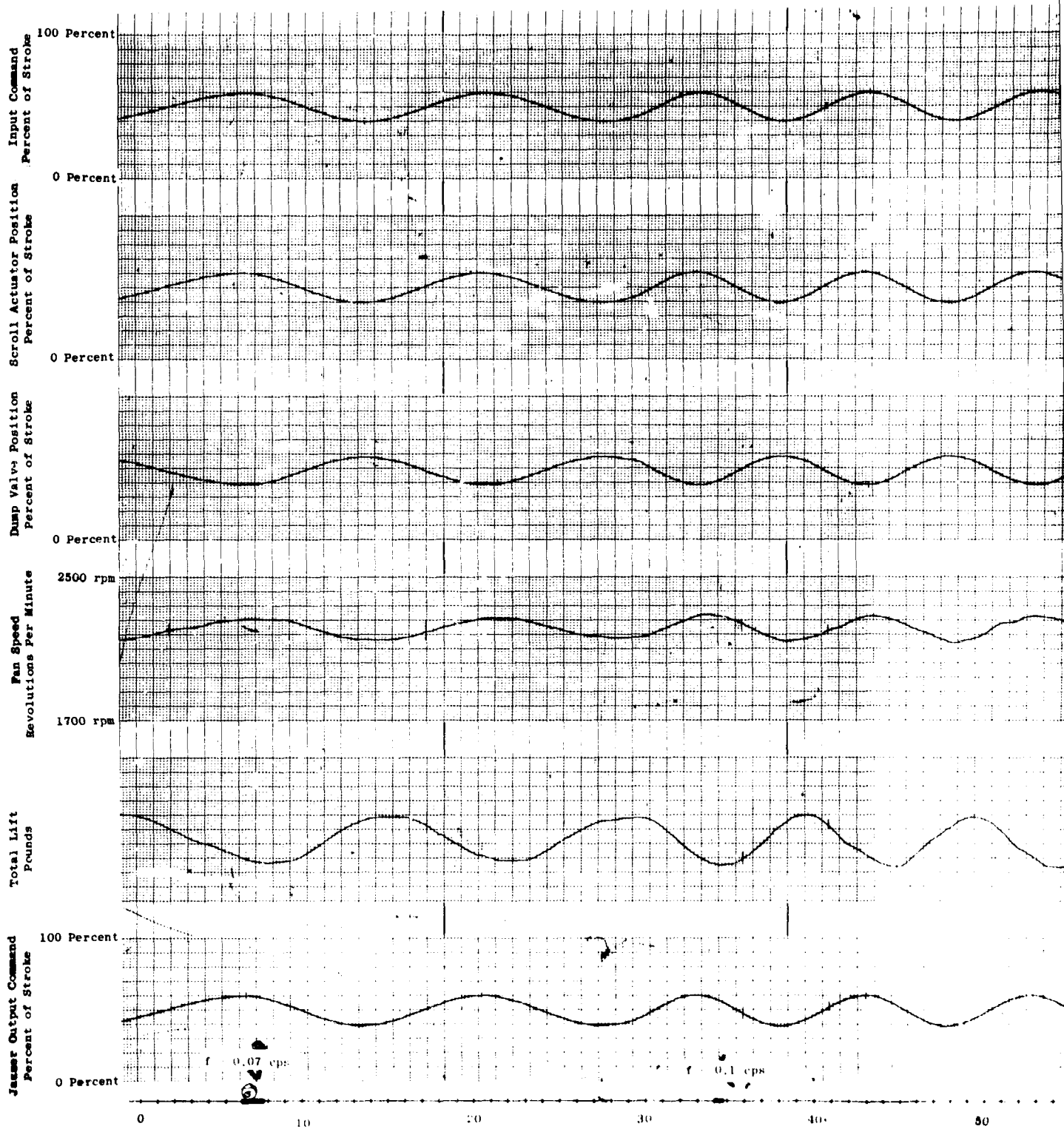
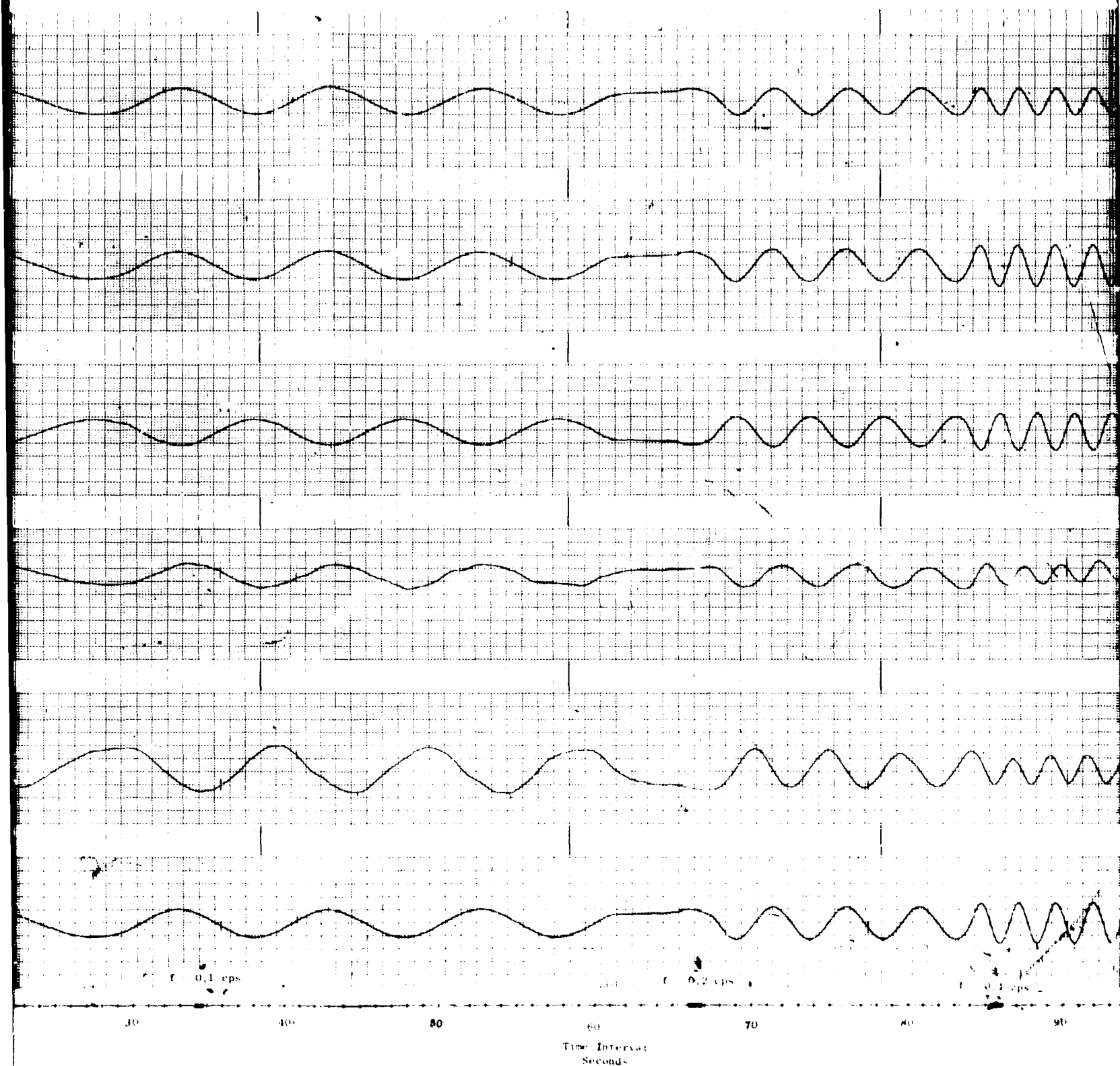


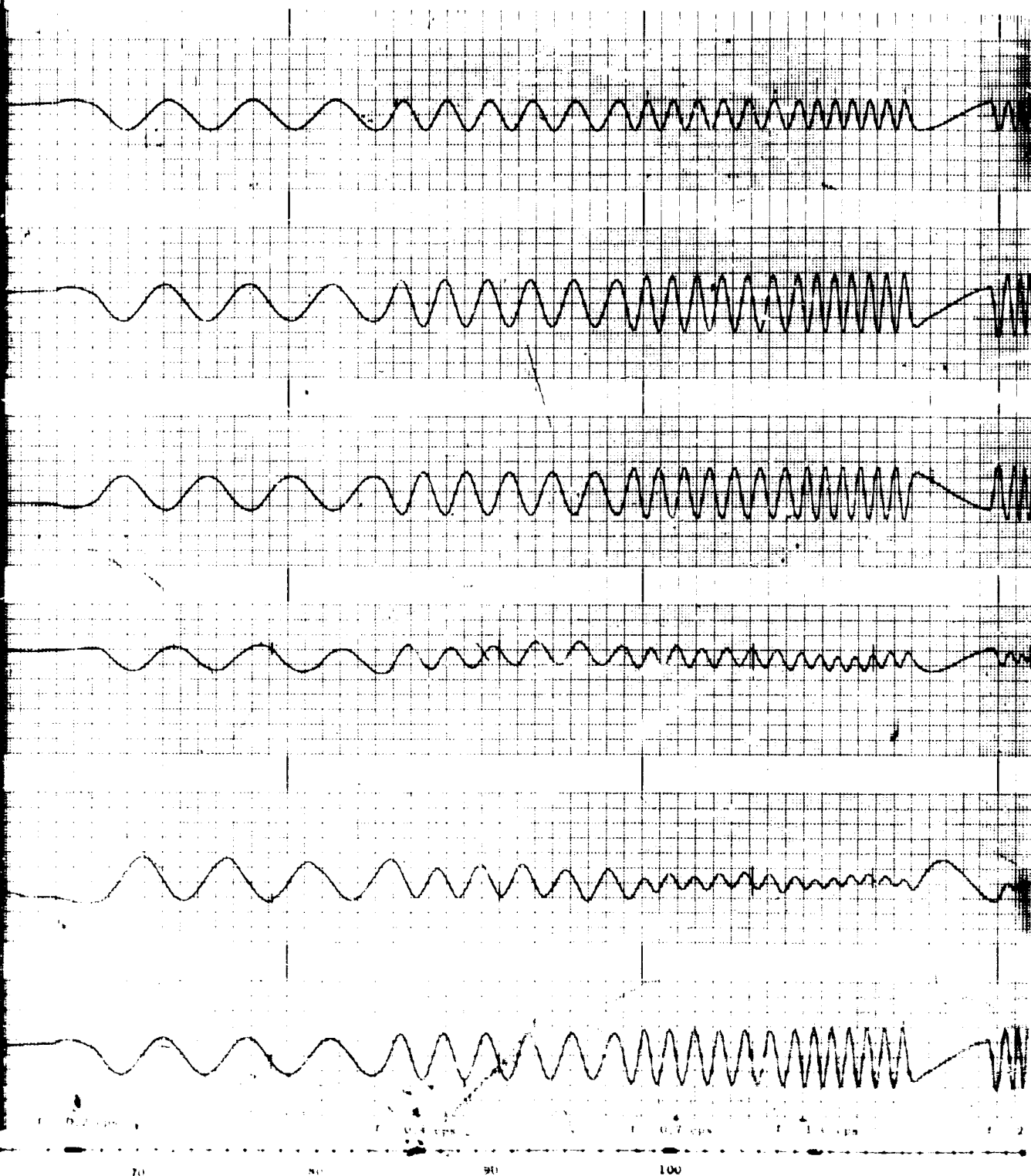
Figure 203. Typical Response Characteristics, With Jazzer m of 1.0, for a Sinusoidal Input of 50 ± 10 Percent, $N_e = 100$ Percent.

A



cs. With Jazzer m of 1.0, for
Percent, $N_e = 100$ Percent.

B



$\tau_J = 0.31$; $m = 1$ (Nominal); $\delta_S = 50 \pm 10$ Percent

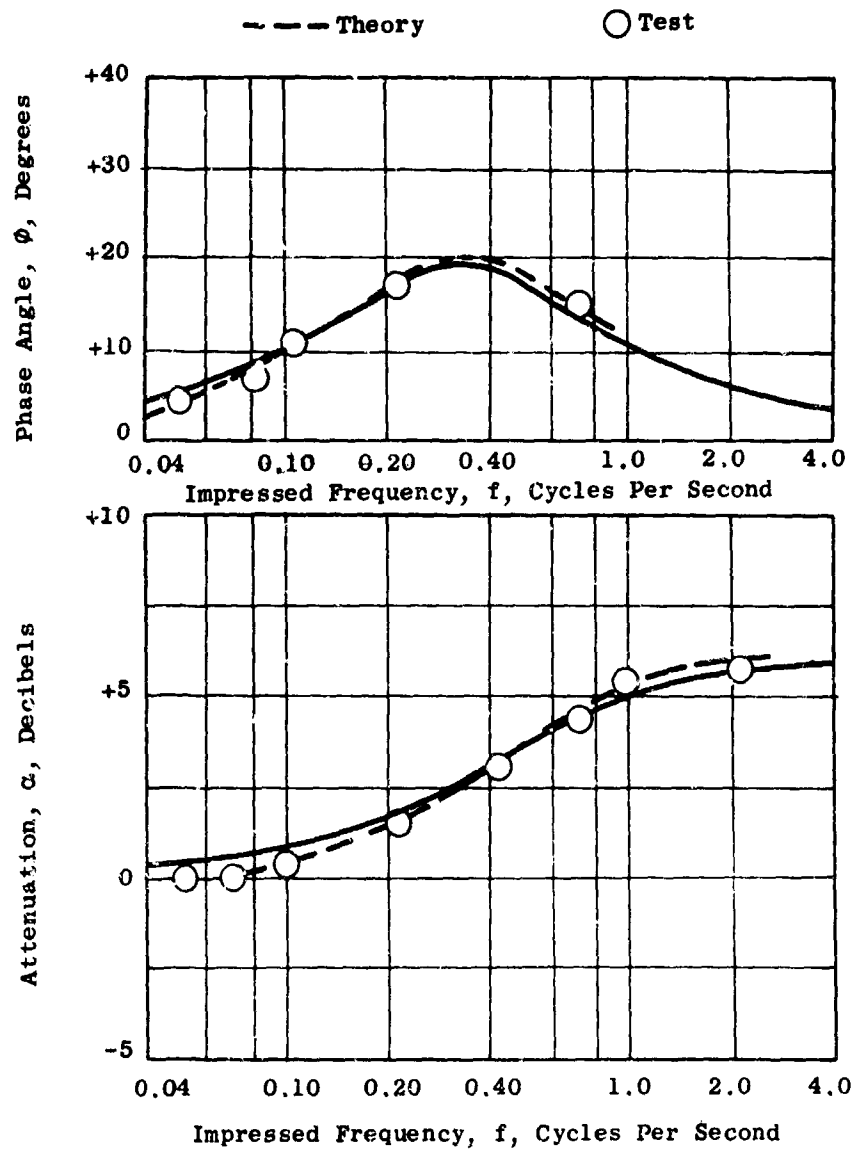


Figure 204. Frequency Response Characteristics of the Jazzer.
 $\tau_J = 0.31$, $m = 1$, $\delta_S = 50 \pm 10$ Percent.

$N_{Fc} = 2220 \text{ rpm}$ $\delta_s = 50 \pm 10 \text{ Percent}$

$\tau_J = 0.31$ $m = 1 \text{ (Nominal)}$

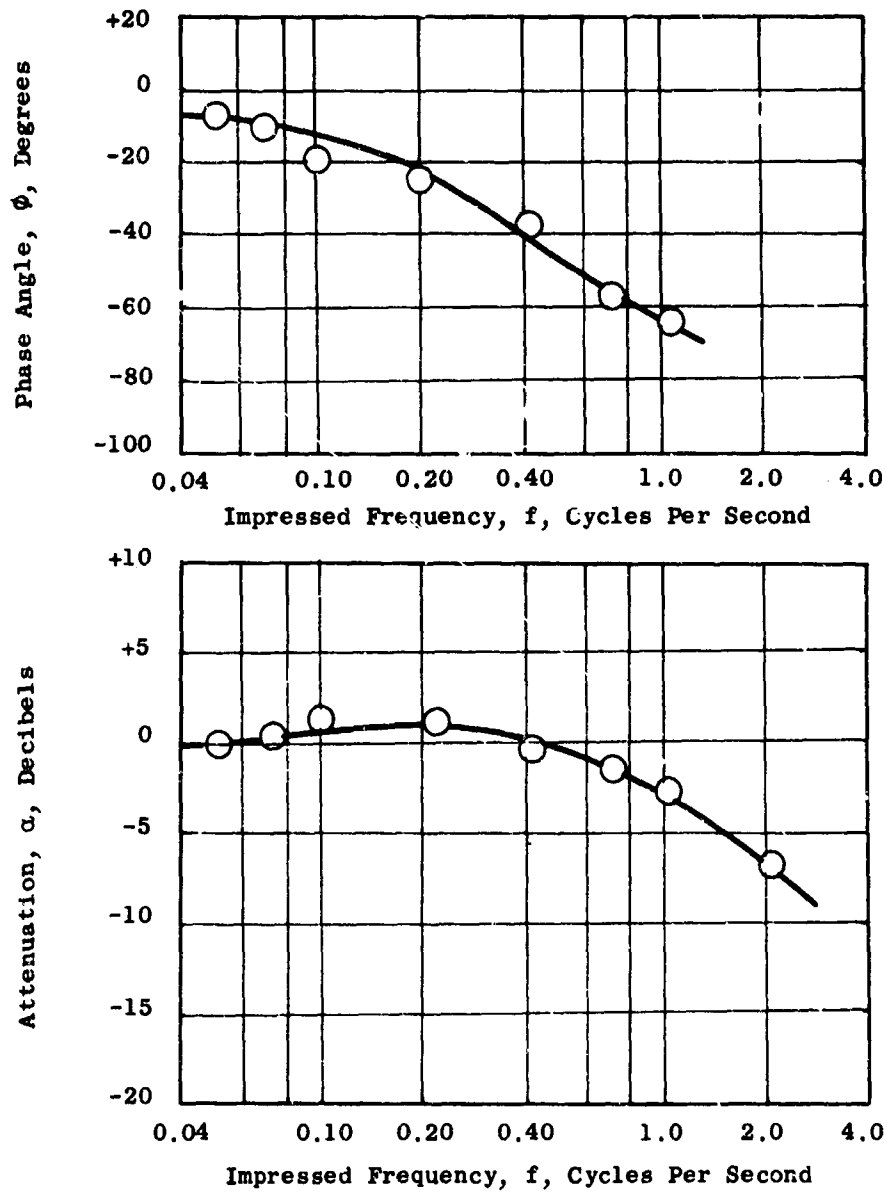


Figure 205. Frequency Response Characteristics With Jazzer, Based on Fan Speed, $N_{Fc} = 2220 \text{ rpm}$, $m = 1$, $\delta_s = 50 \pm 10 \text{ Percent}$.

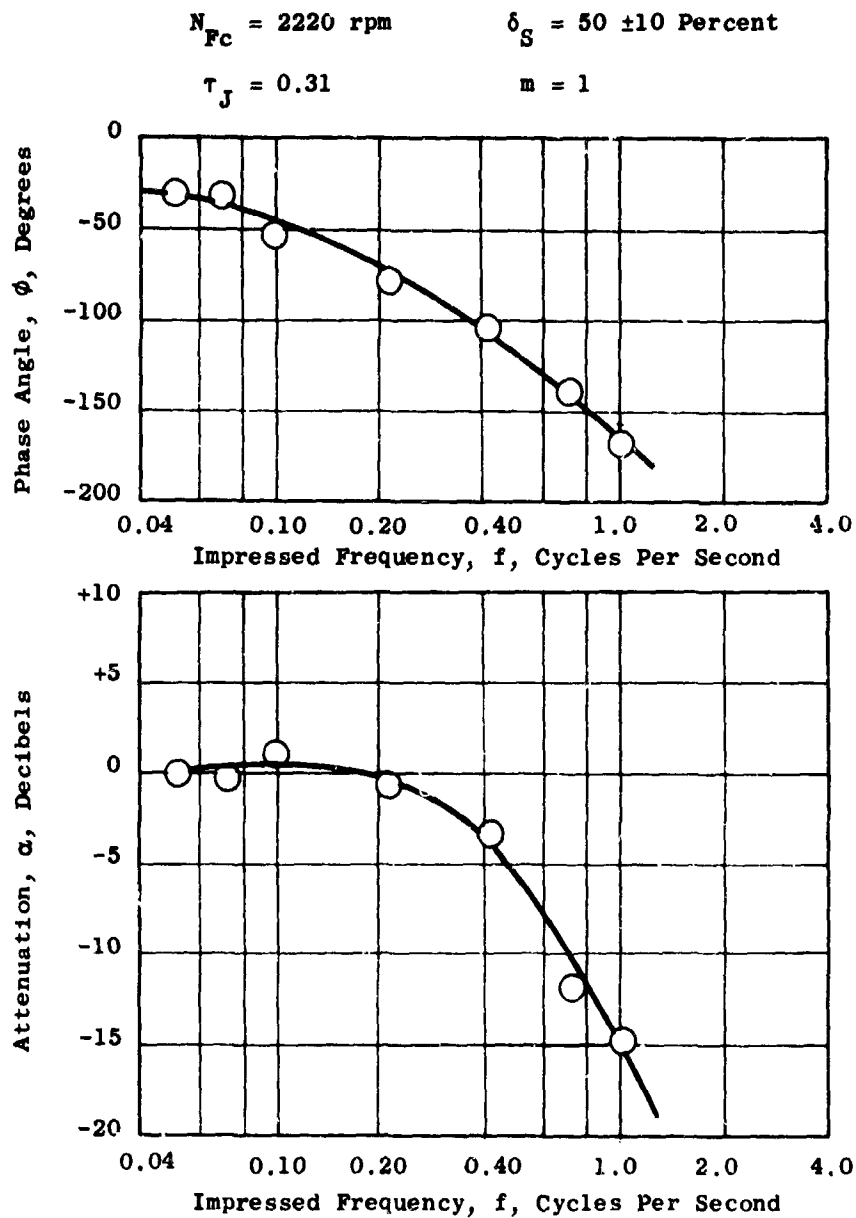


Figure 206. Frequency Response Characteristics With Jazzer, Based on Thrust, $N_{Fc} = 2220 \text{ rpm}$, $m = 1$, $\delta_S = 50 \pm 10 \text{ Percent}$.

$\tau_J = 0.31$; $m = 1$ (Nominal); $\delta_s = 50 \pm 20$ Percent

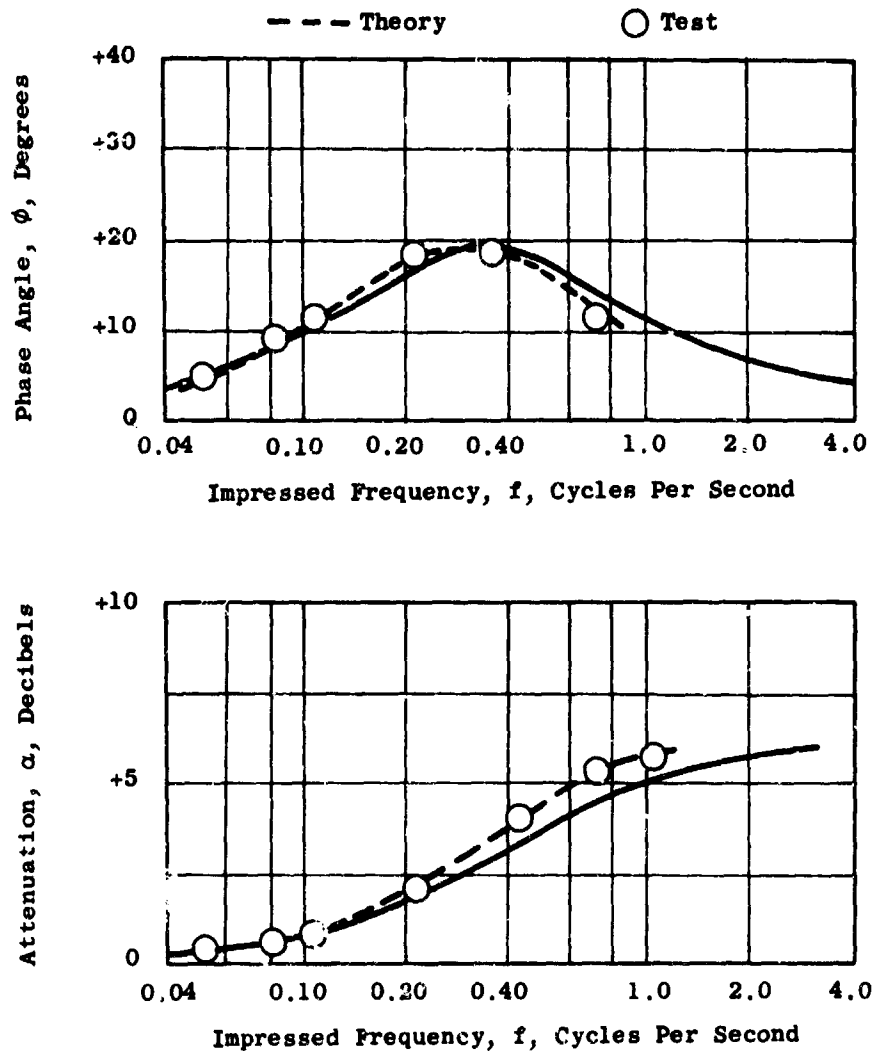


Figure 207. Frequency Response Characteristics of the Jazzer.
 $\tau_J = 0.31$, $m = 1$, $\delta_s = 50 \pm 20$ Percent.

$N_{Fc} = 2220 \text{ rpm}$

$\delta_S = 50 \pm 20 \text{ Percent}$

$\tau_J = 0.31$

$m = 1 \text{ (Nominal)}$

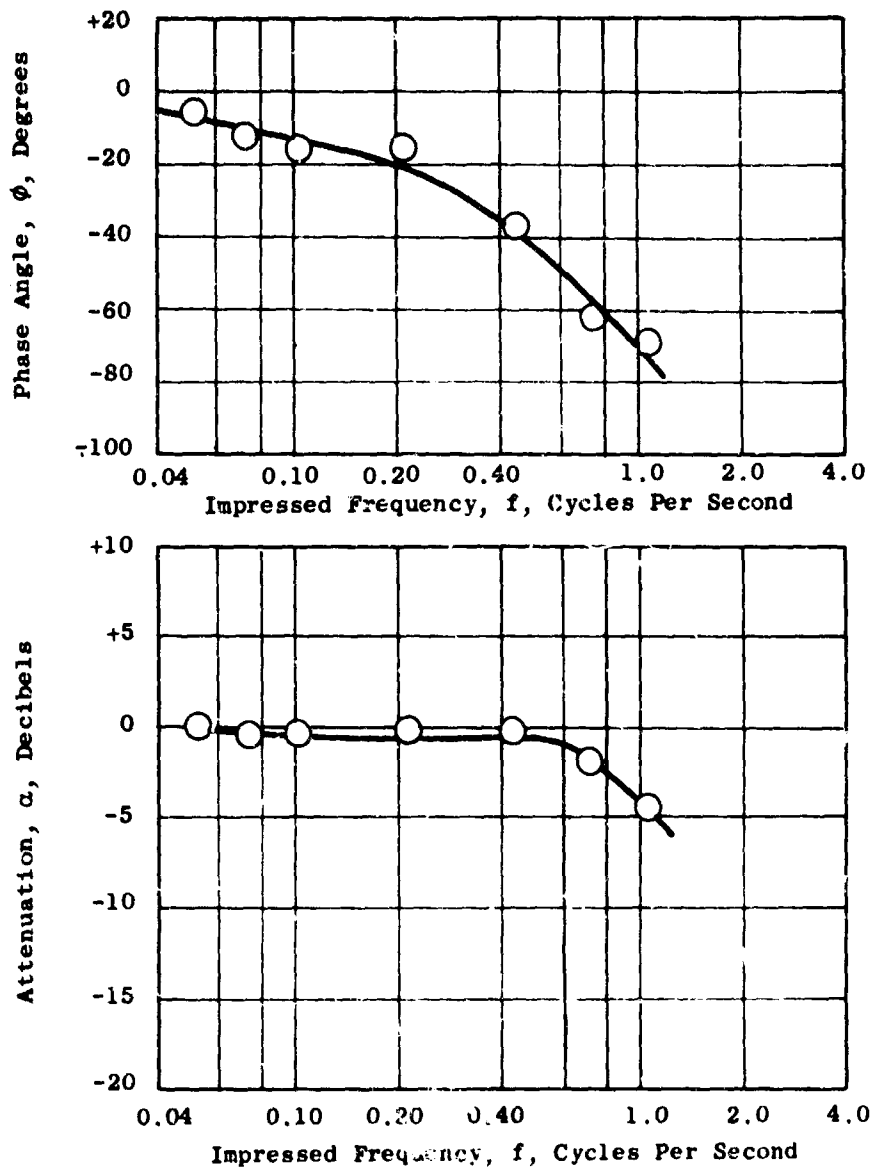


Figure 208. Frequency Response Characteristics With Jazzer, Based on Fan Speed, $N_{Fc} = 2220 \text{ rpm}$, $m = 1$, $\delta_S = 50 \pm 20 \text{ Percent}$.

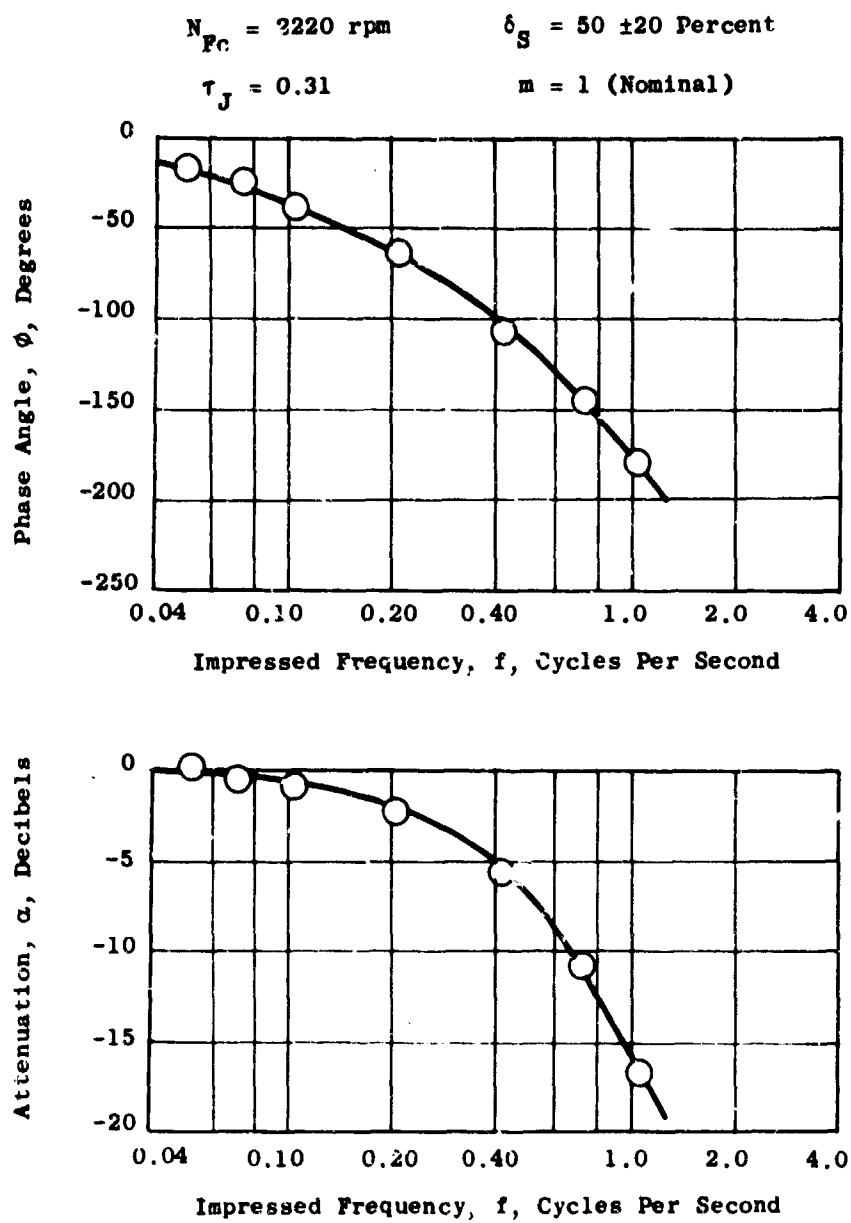


Figure 209. Frequency Response Characteristics With Jazzer.
 Based on Thrust, $N_{Fc} = 2220 \text{ rpm}$, $m = 1$,
 $\delta_S = 50 \pm 20 \text{ Percent}$.

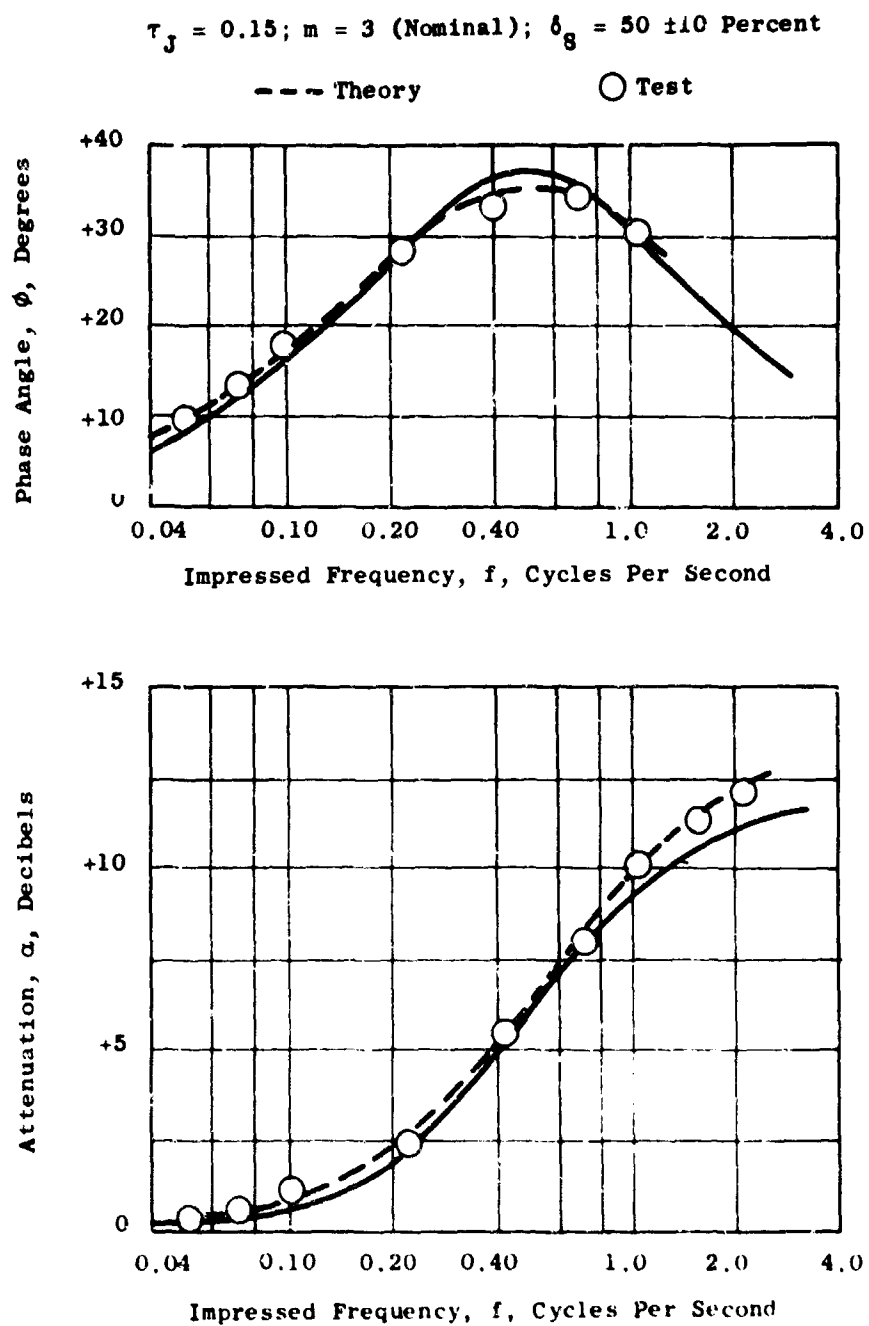


Figure 210. Frequency Response Characteristics of the Jazzer.
 $\tau_J = 0.15$, $m = 3$, $\delta_g = 50 \pm 10$ Percent.

$N_{Fc} = 2220 \text{ rpm}$

$\delta_S = 50 \pm 10 \text{ Percent}$

$\tau_J = 0.15$

$m = 3 \text{ (Nominal)}$

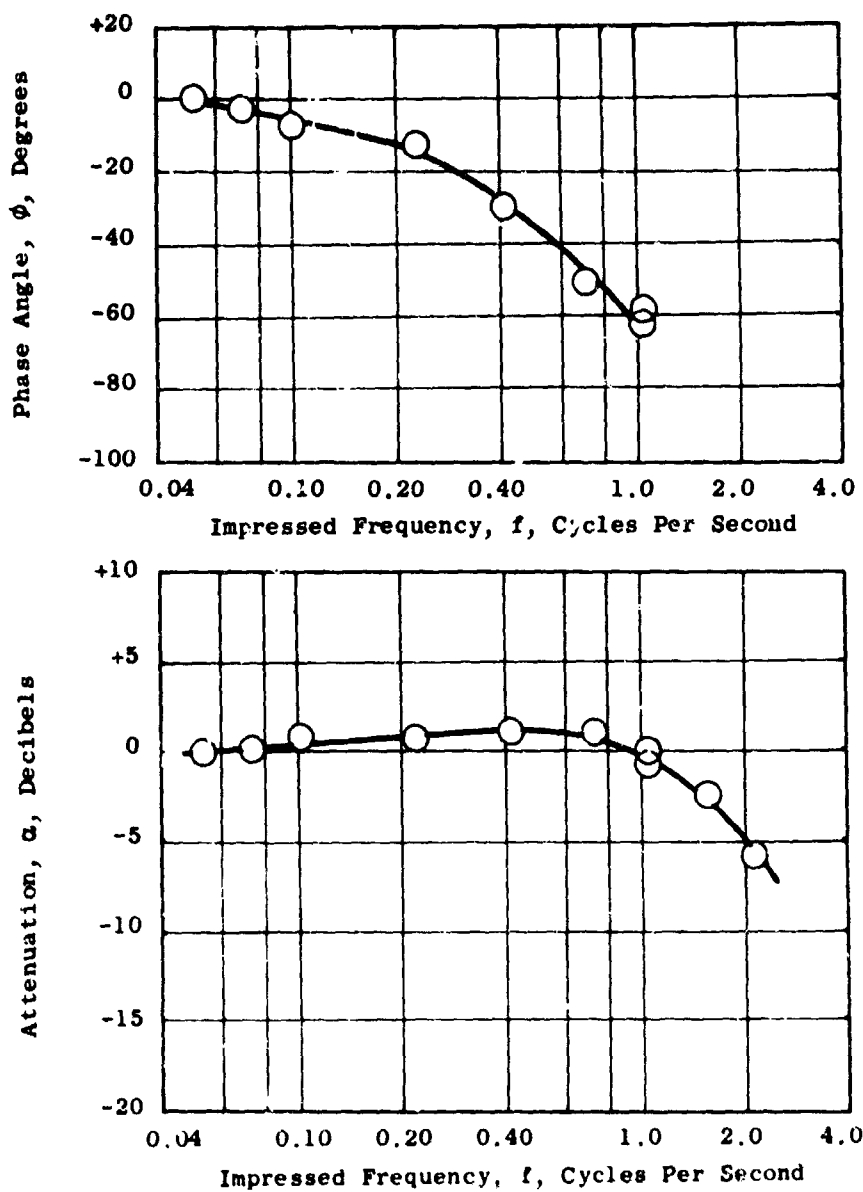


Figure 211. Frequency Response Characteristics With Jazzer, Based on Fan Speed, $N_{Fc} = 2220 \text{ rpm}$, $m = 3$, $\delta_S = 50 \pm 10 \text{ Percent}$.

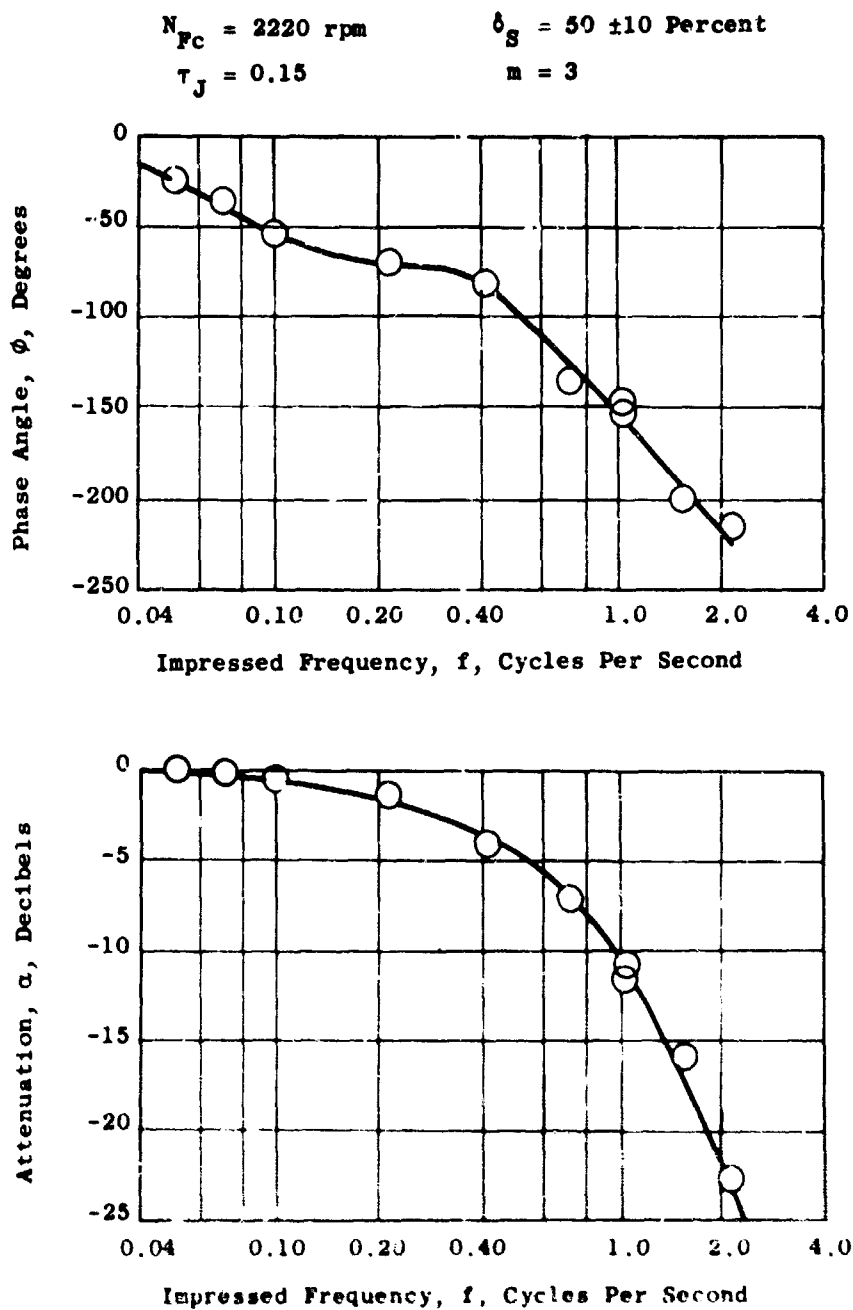


Figure 212. Frequency Response Characteristics With
 Jazzer, Based on Thrust, $N_{Pc} = 2220 \text{ rpm}$,
 $m = 3$, $\delta_S = 50 \pm 10 \text{ Percent}$.

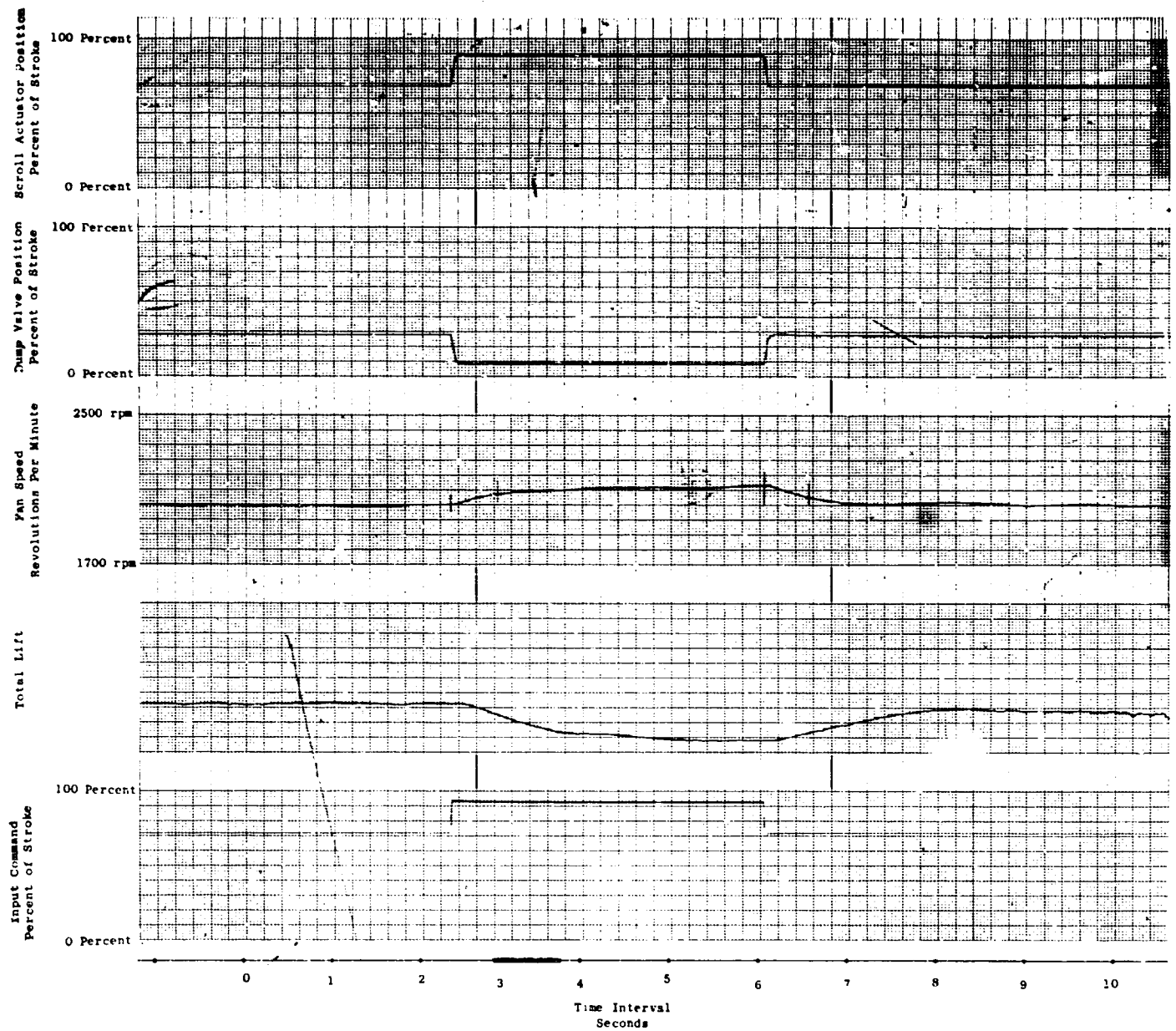


Figure 213. Typical Response Characteristic for a Step Input of ± 20 Percent, $N_e = 100$ Percent.

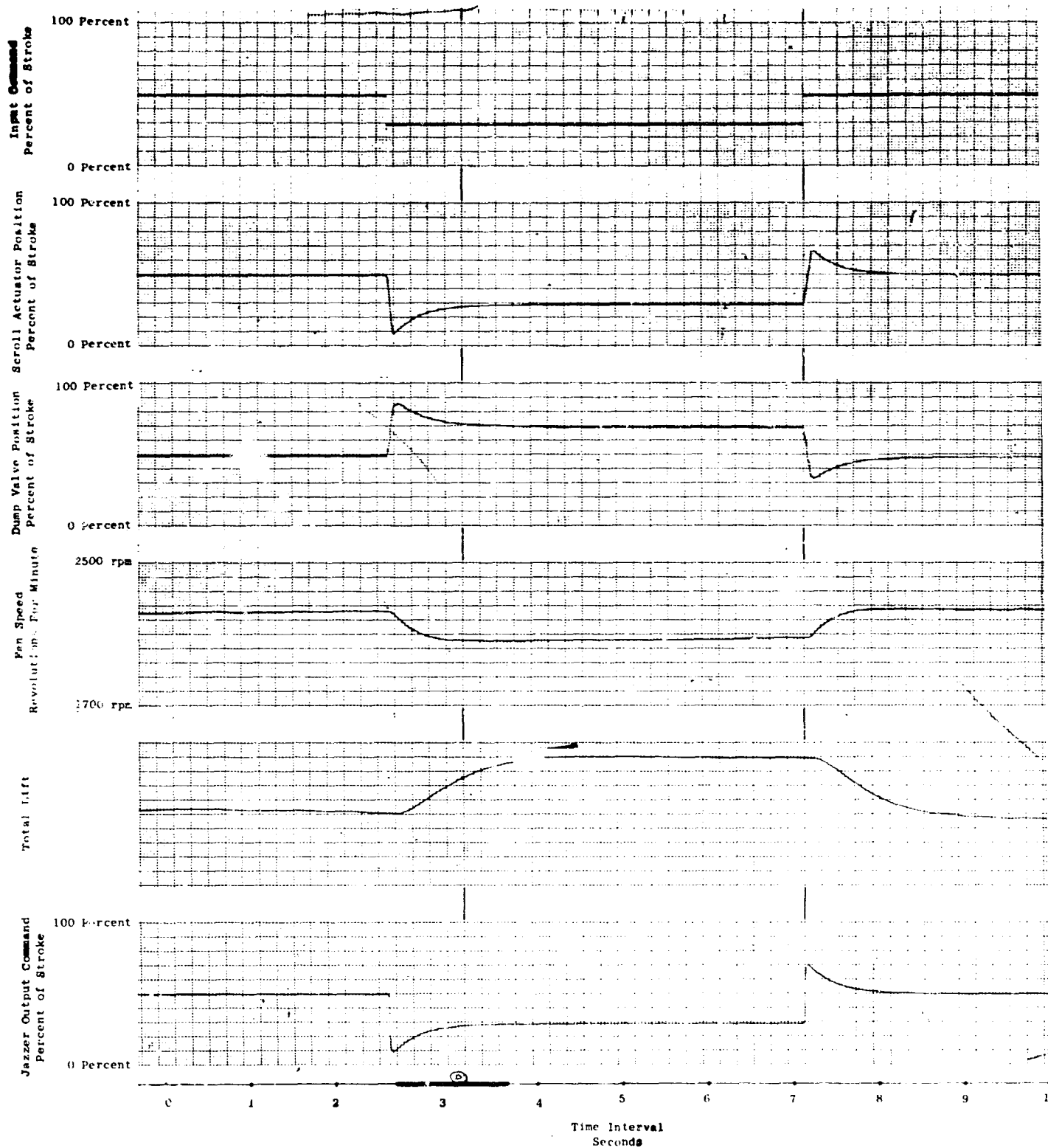
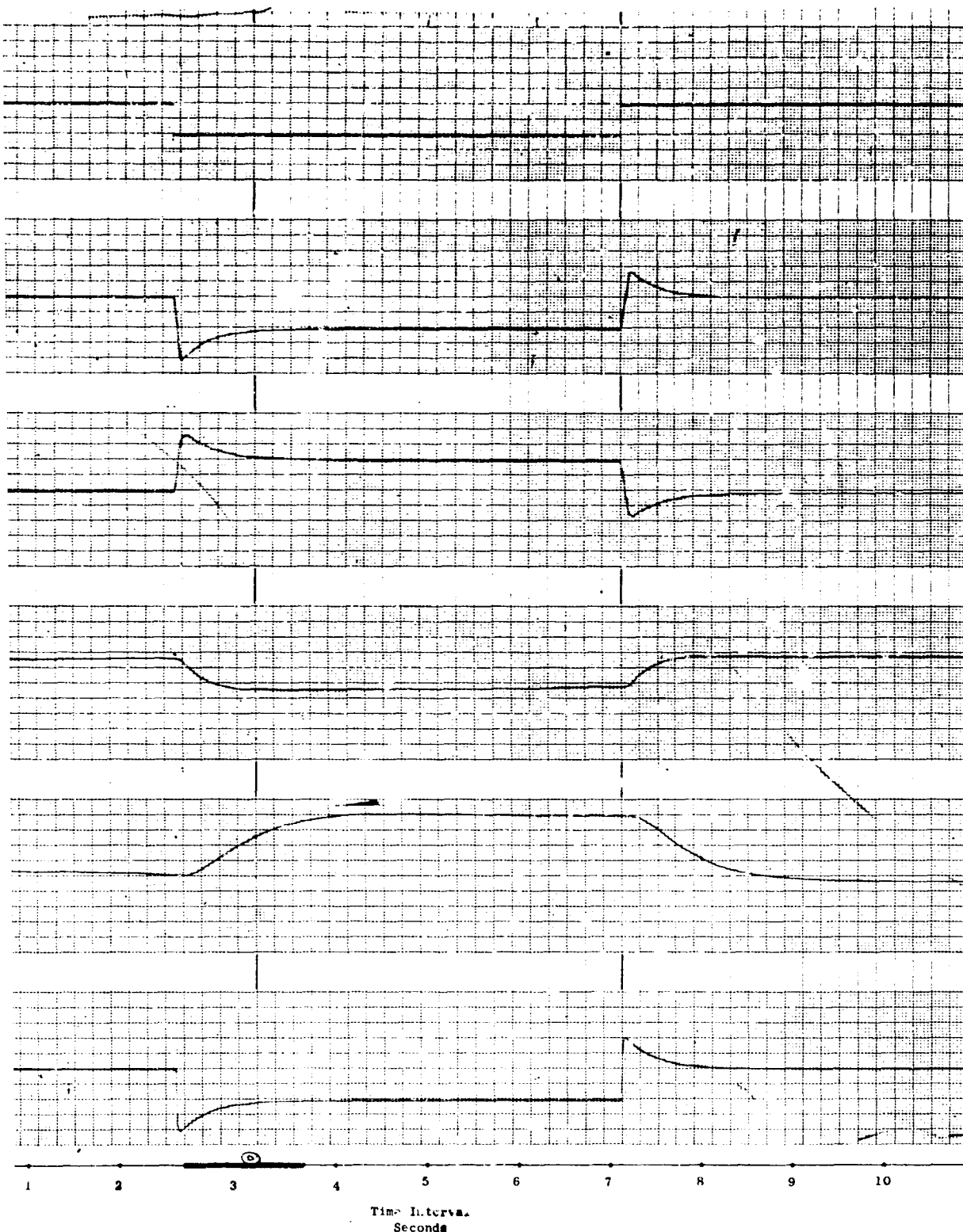


Figure 214. Typical Response Characteristics for a Step Input, With Jazzer m of 3.0, of ± 20 Percent, $N_e = 100$ Percent.

A



Typical Response Characteristics for a Step Input, With
 zero m of 3.0, of ± 20 Percent, $N_e = 100$ Percent.

B

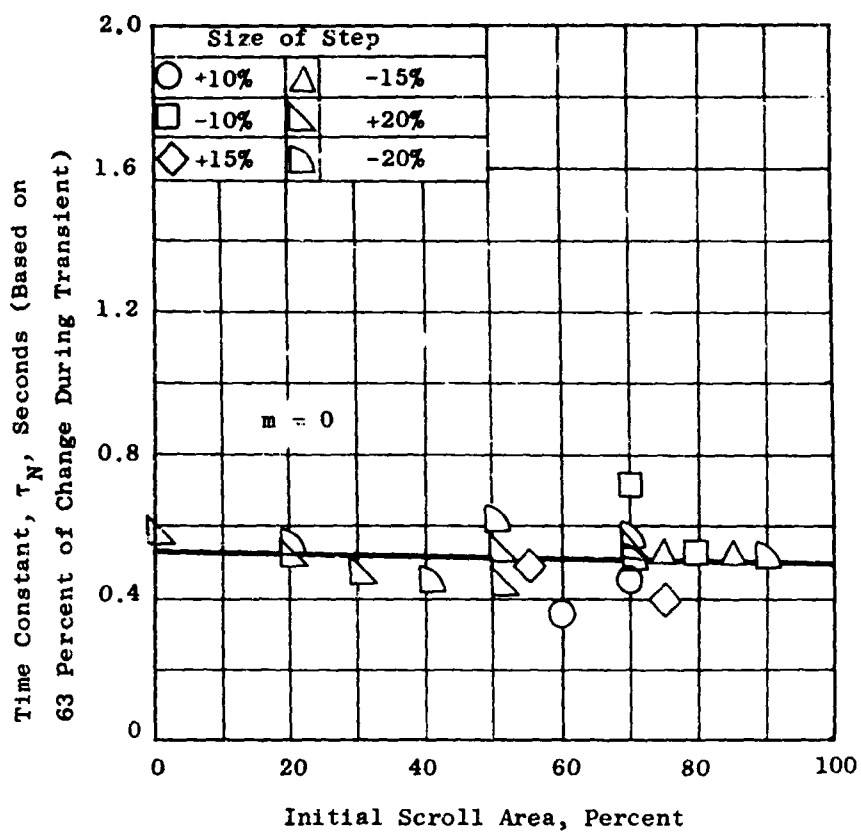


Figure 215. Fan Time Constants During Step Inputs Based on 63 Percent of Change During Transient, $N_e = 95$ Percent.

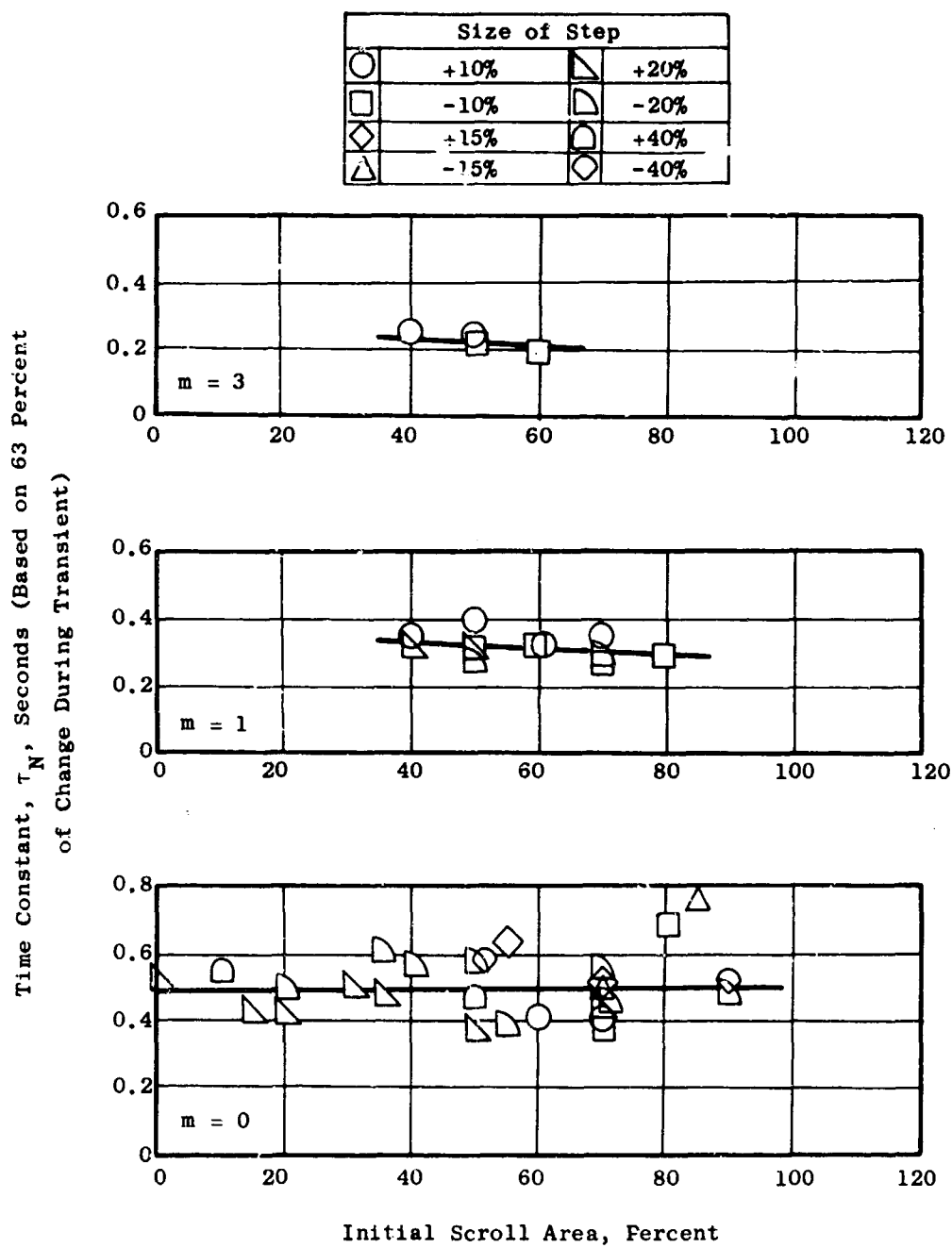


Figure 216. Fan Time Constants During Step Inputs Based on 63 Percent of Change During Transient, $N_e = 100$ Percent.

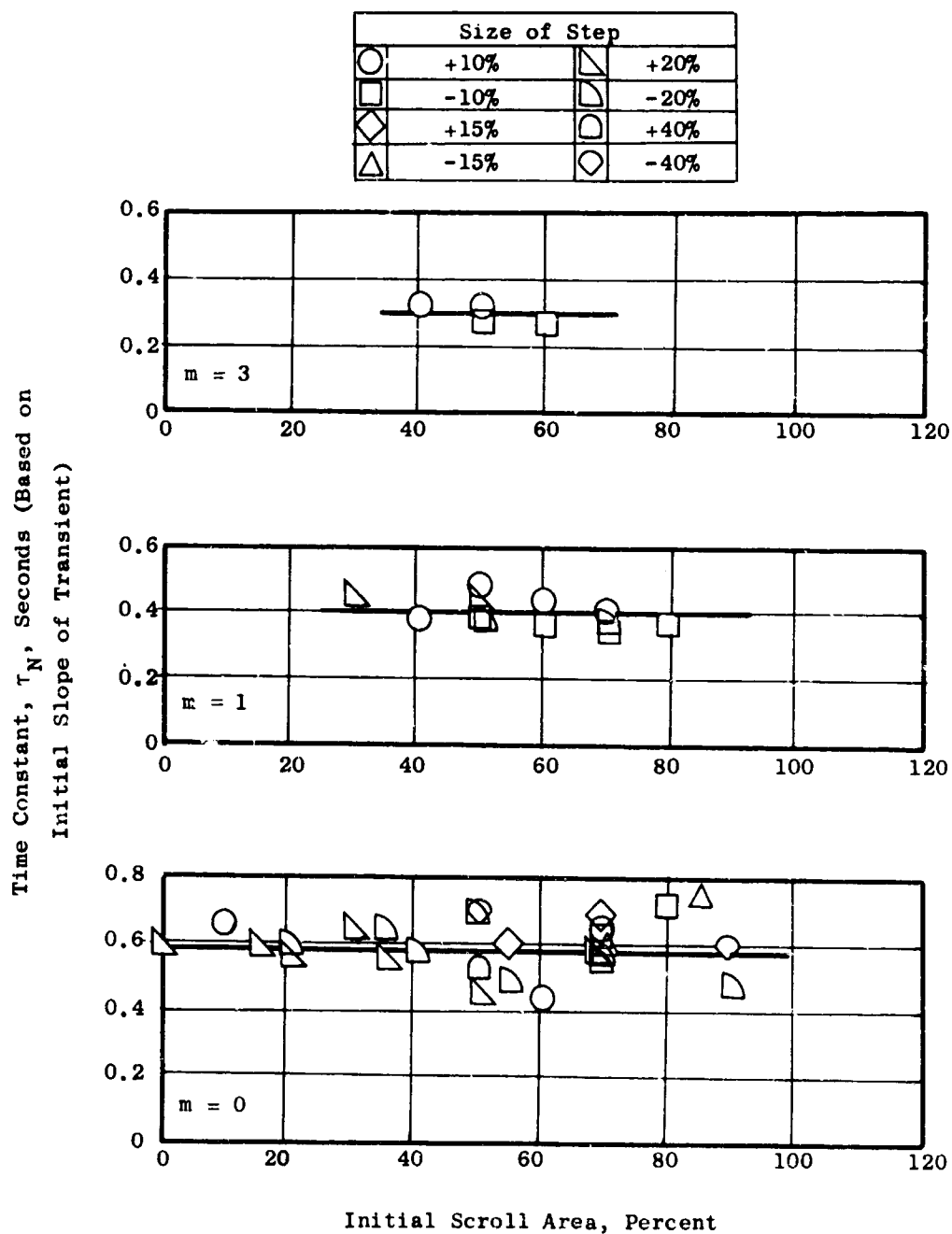


Figure 217. Fan Time Constants During Step Inputs Based on Initial Slope of Transient, $N_e = 100$ Percent.

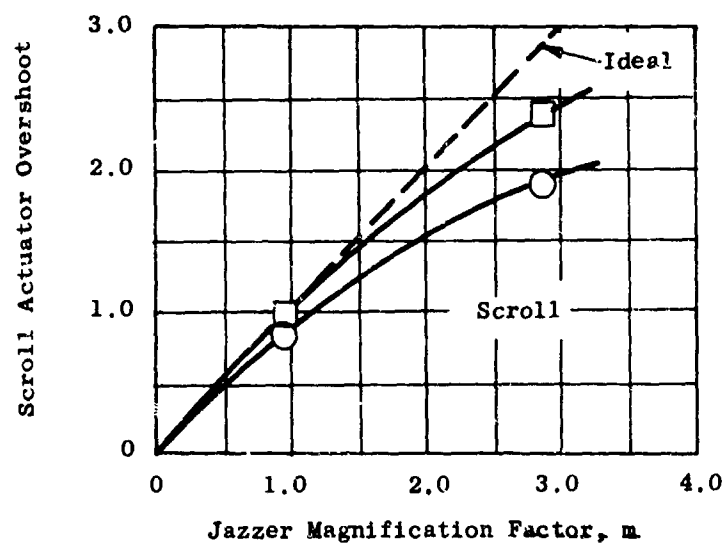
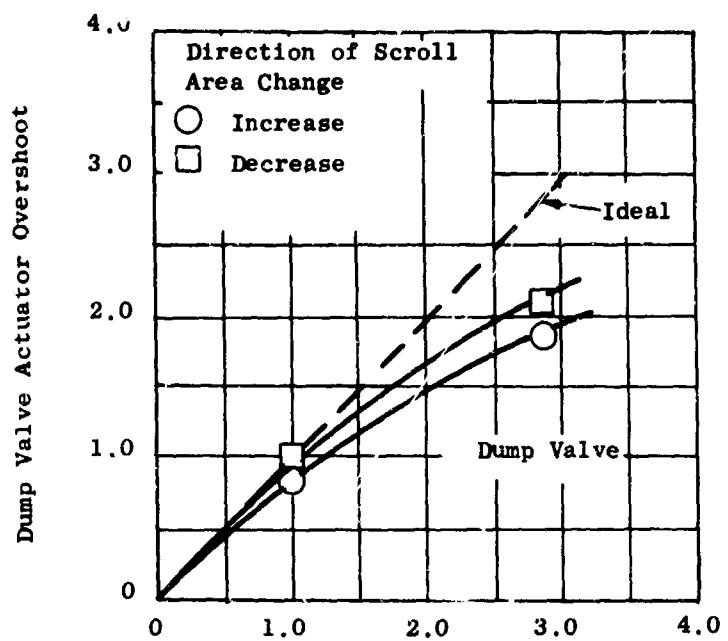


Figure 218. Effects of Jazzer Setting on Actuator Overshoot Levels, $\delta_s = 50 \pm 10$ Percent.

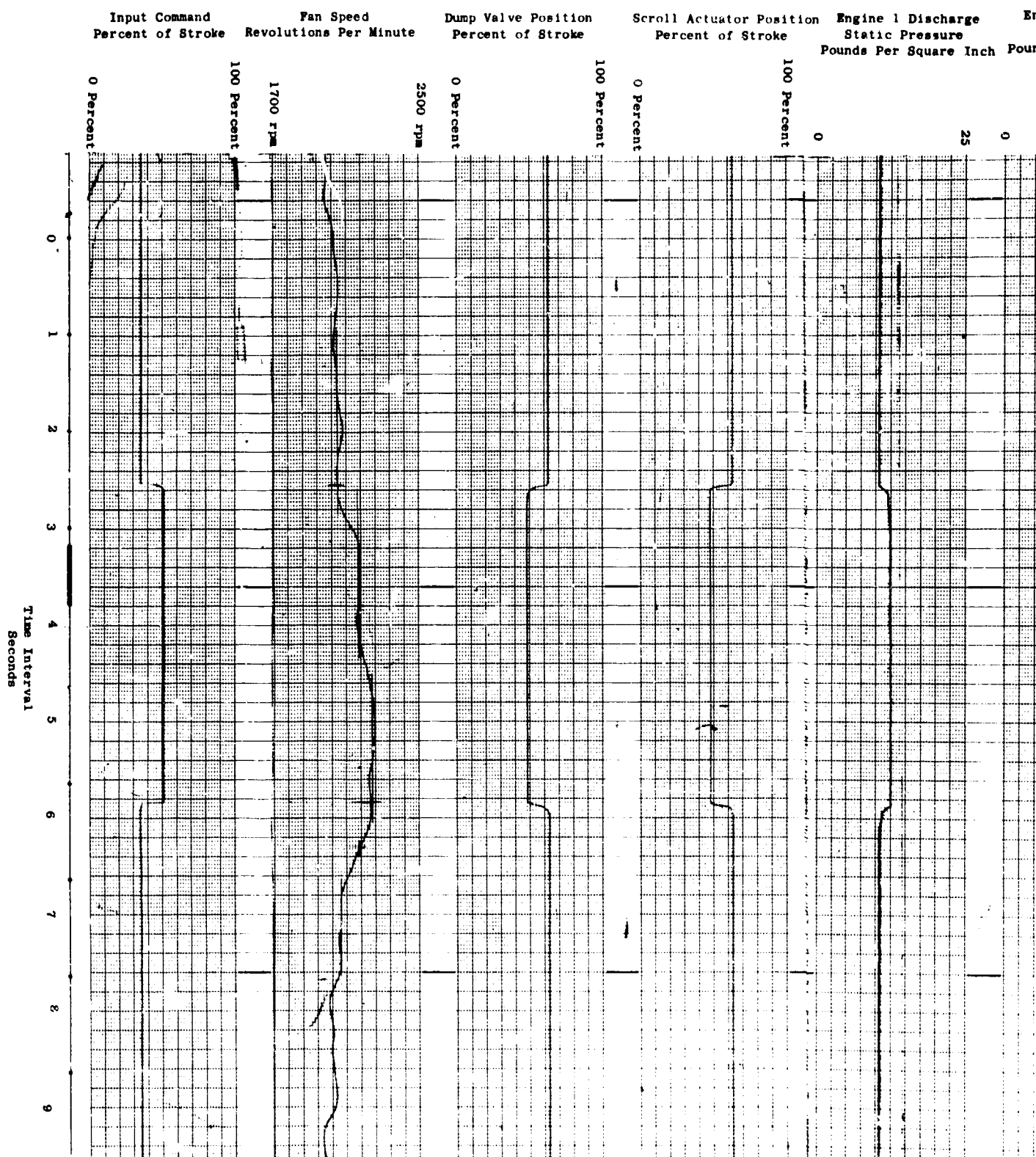
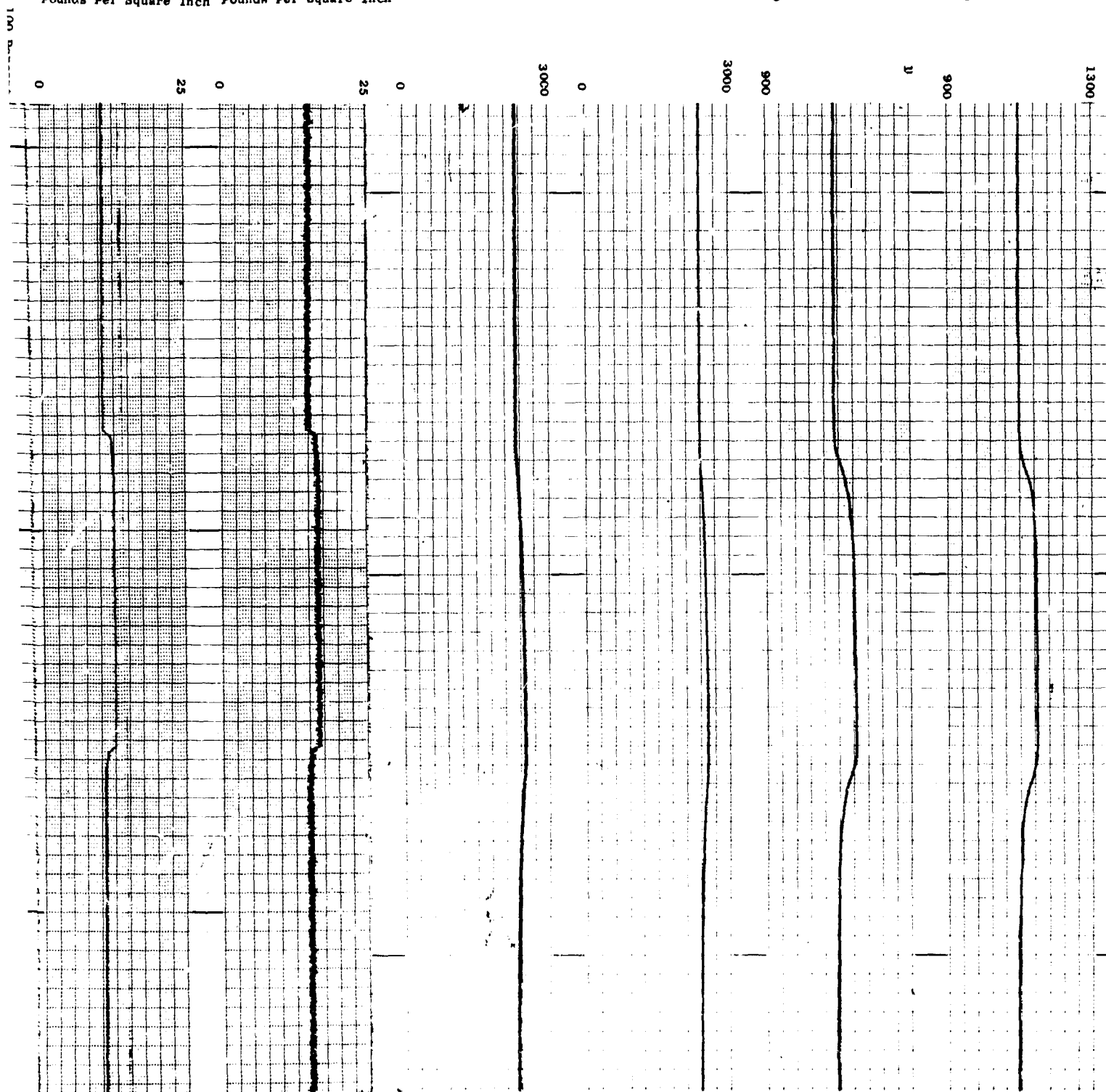


Figure 219. Typical Response Characteristics for a Step Input of 15 Percent Using Area for Height Control, $N_e = 100$ Percent.

Engine Discharge Static Pressure Pounds Per Square Inch	Engine 1 Discharge Total Pressure Pounds Per Square Inch	Engine 2 Fuel Flow Pounds Per Hour	Engine 1 Fuel Flow Pounds Per Hour	Engine 2 Exhaust Gas Temperature Degrees Fahrenheit	Engine 1 Exhaust Gas Temperature Degrees Fahrenheit
---	--	---------------------------------------	---------------------------------------	---	---



18

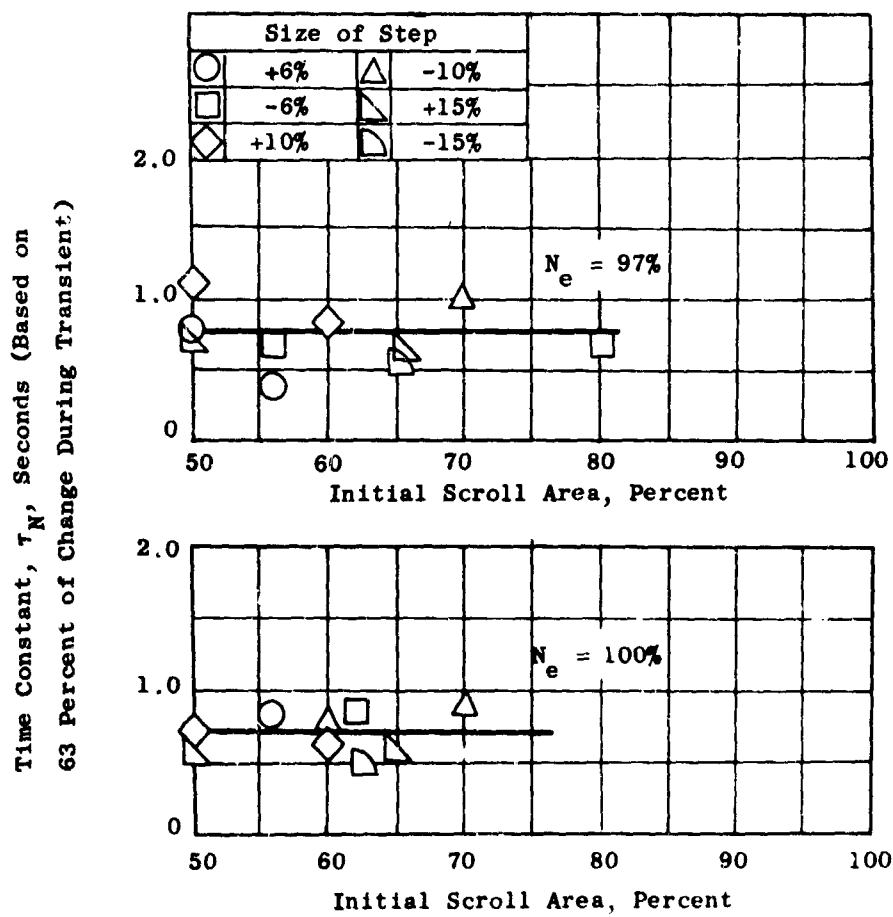


Figure 220. Fan Time Constants During Step Inputs Using Fan Area for Height Control.

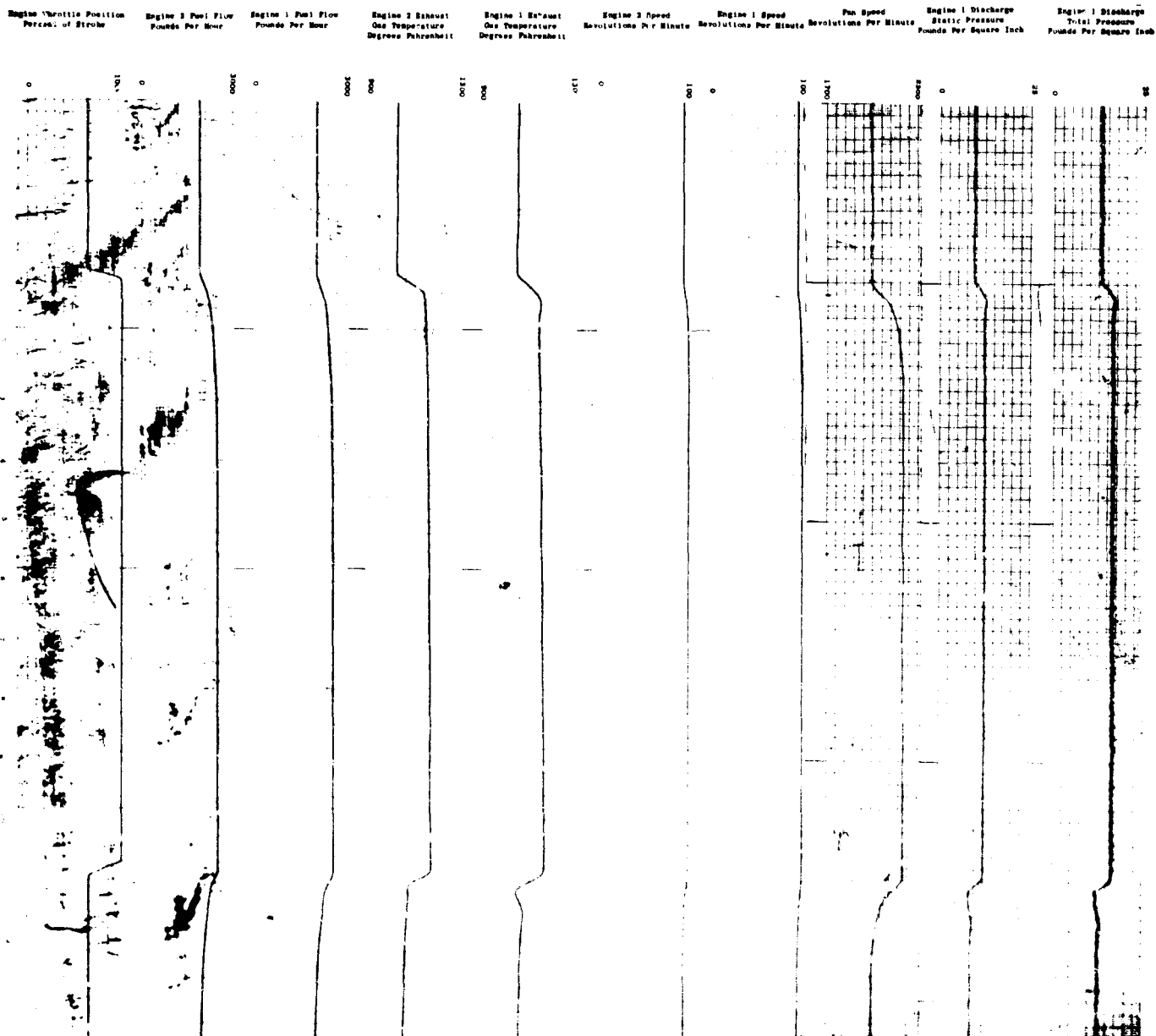


Figure 221. Typical Response Characteristics for a Step Input of Engine Throttle.

Time Constant, τ_N , Seconds (Based
on 63 Percent of Change)

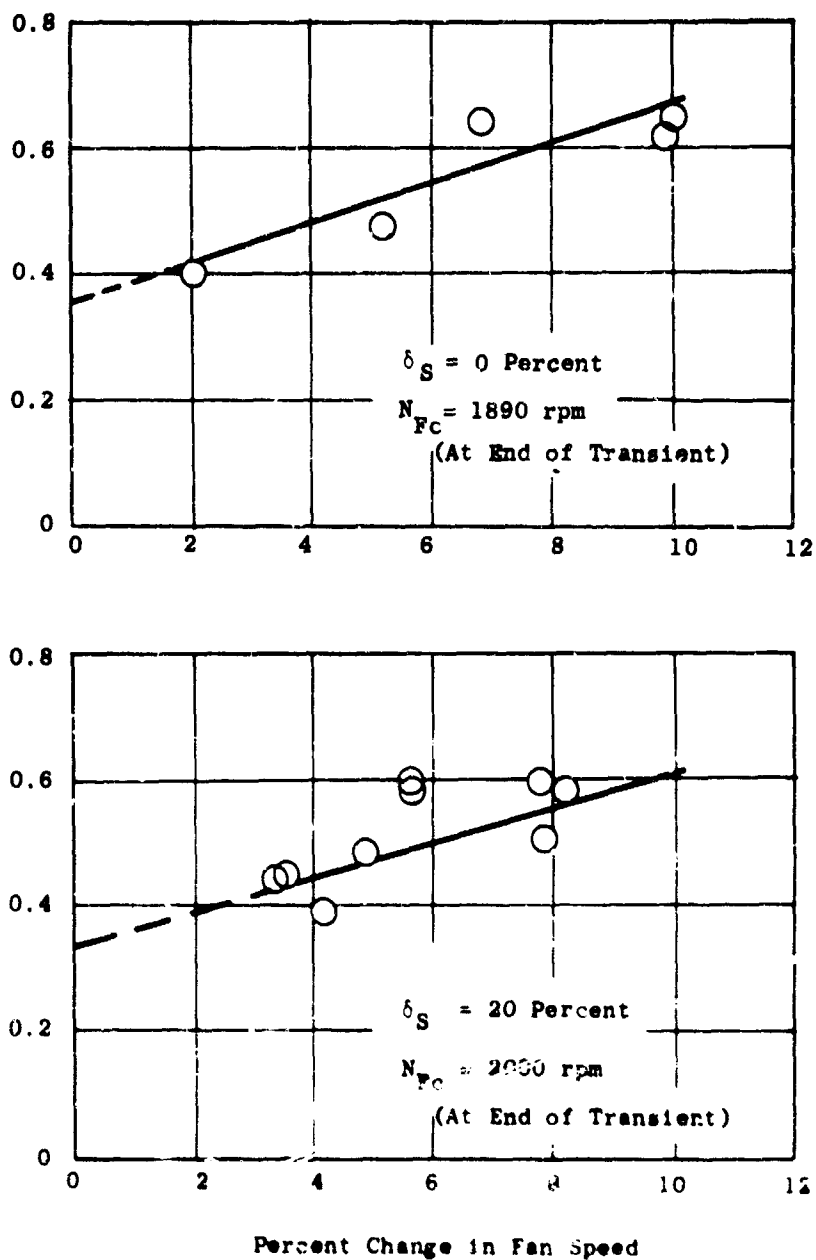
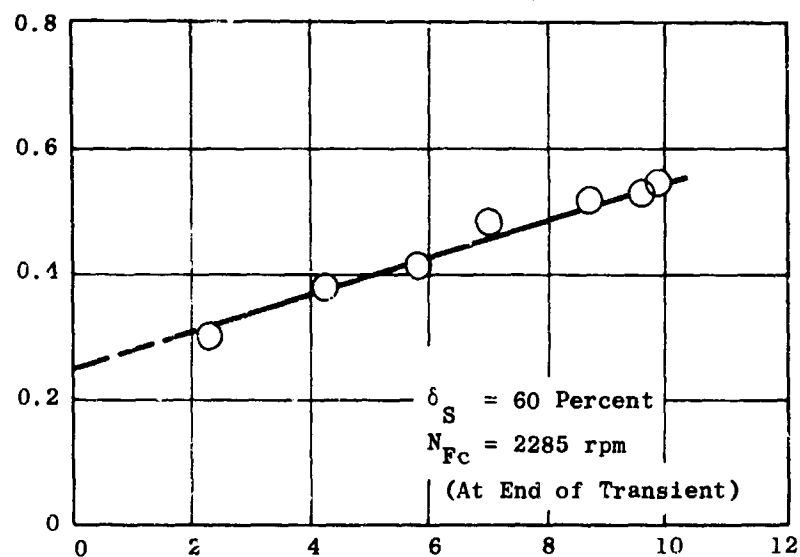
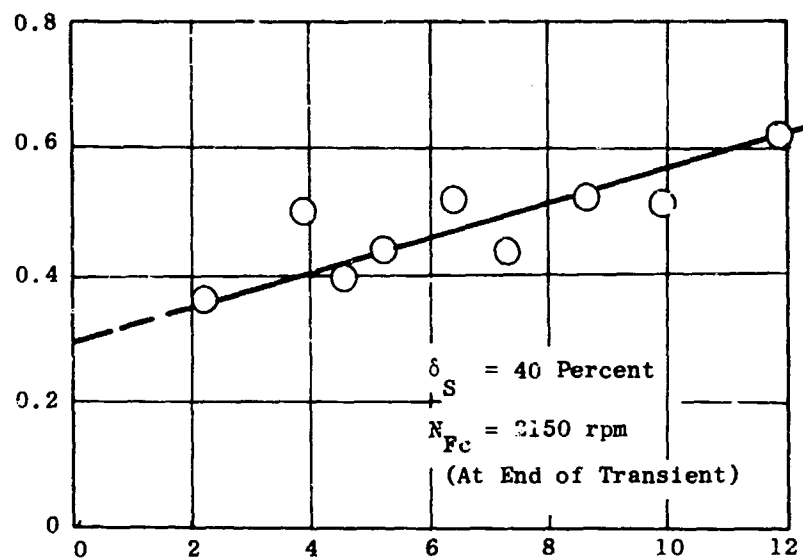


Figure 222. Variation of Fan Speed Time Constant With Size of Speed Change Using Engines for Altitude Control, $\delta_S = 0$ Percent and $\delta_S = 20$ Percent.

Time Constant, τ_N , Seconds (Based
on 63 Percent of Change)



Percent Change in Fan Speed

Figure 223. Variation of Fan Speed Time Constant With Size of Speed Change Using Engines for Altitude Control, $\delta_S = 40$ Percent and $\delta_S = 60$ Percent

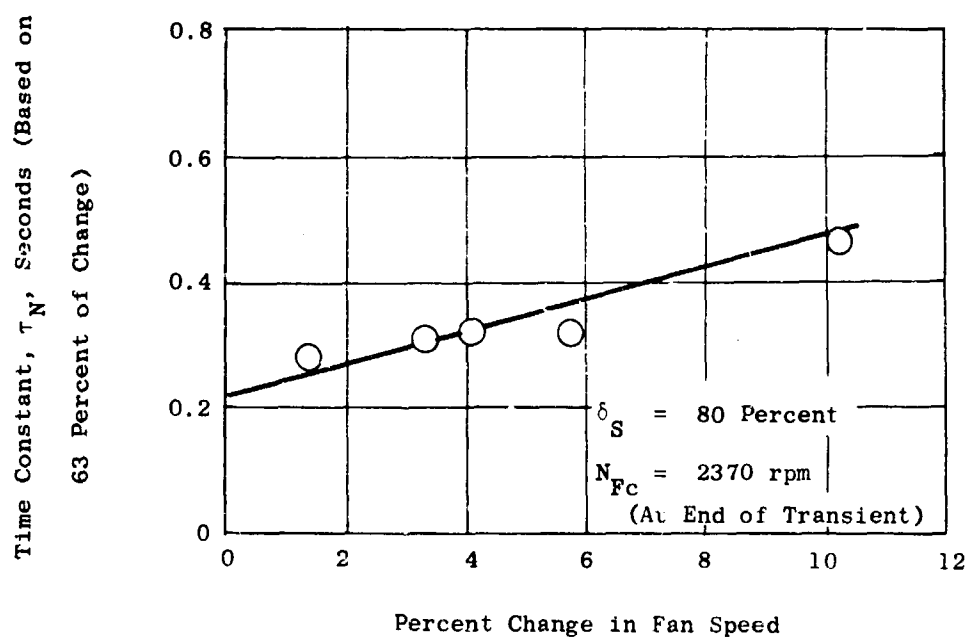


Figure 224. Variation of Fan Speed Time Constant With Size of Speed Change Using Engines for Altitude Control, $\delta_S = 80$ Percent.

Ambient Temperature = 73°F

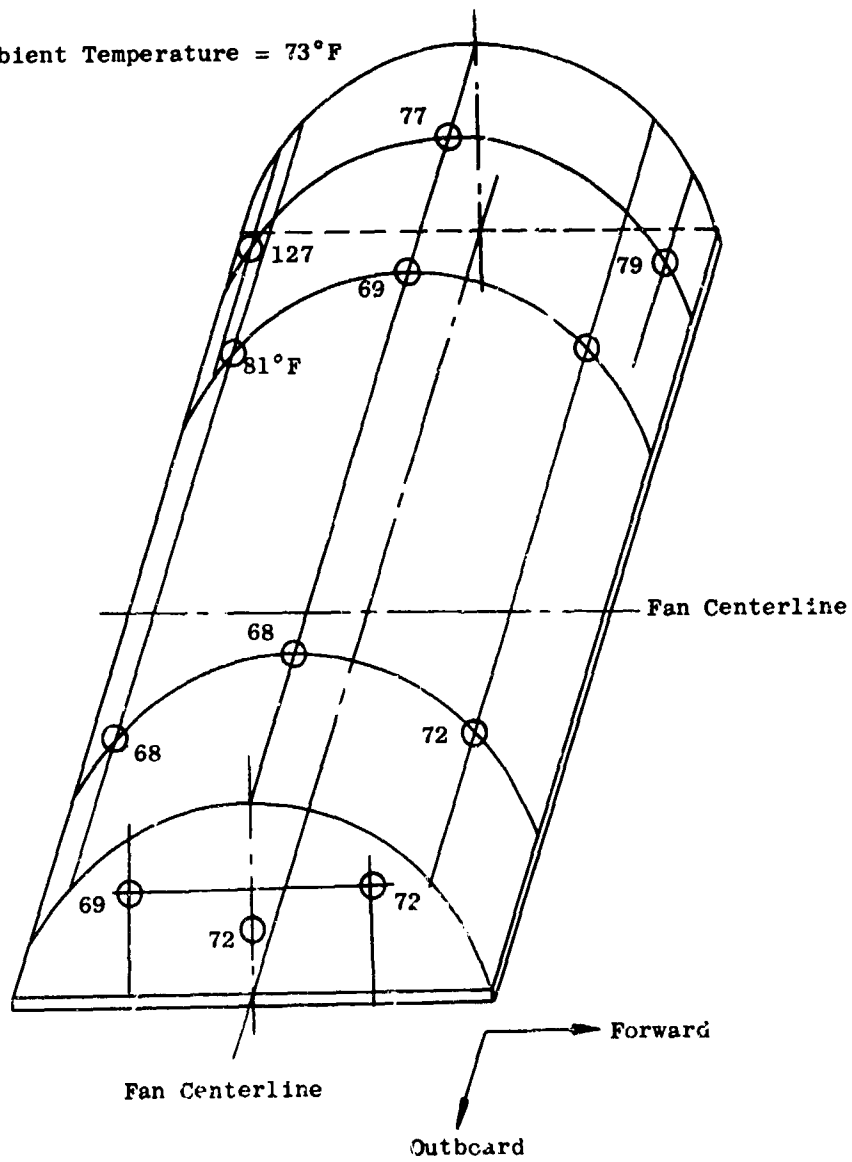


Figure 225. Typical Fan Inlet Screen Temperature Distribution.

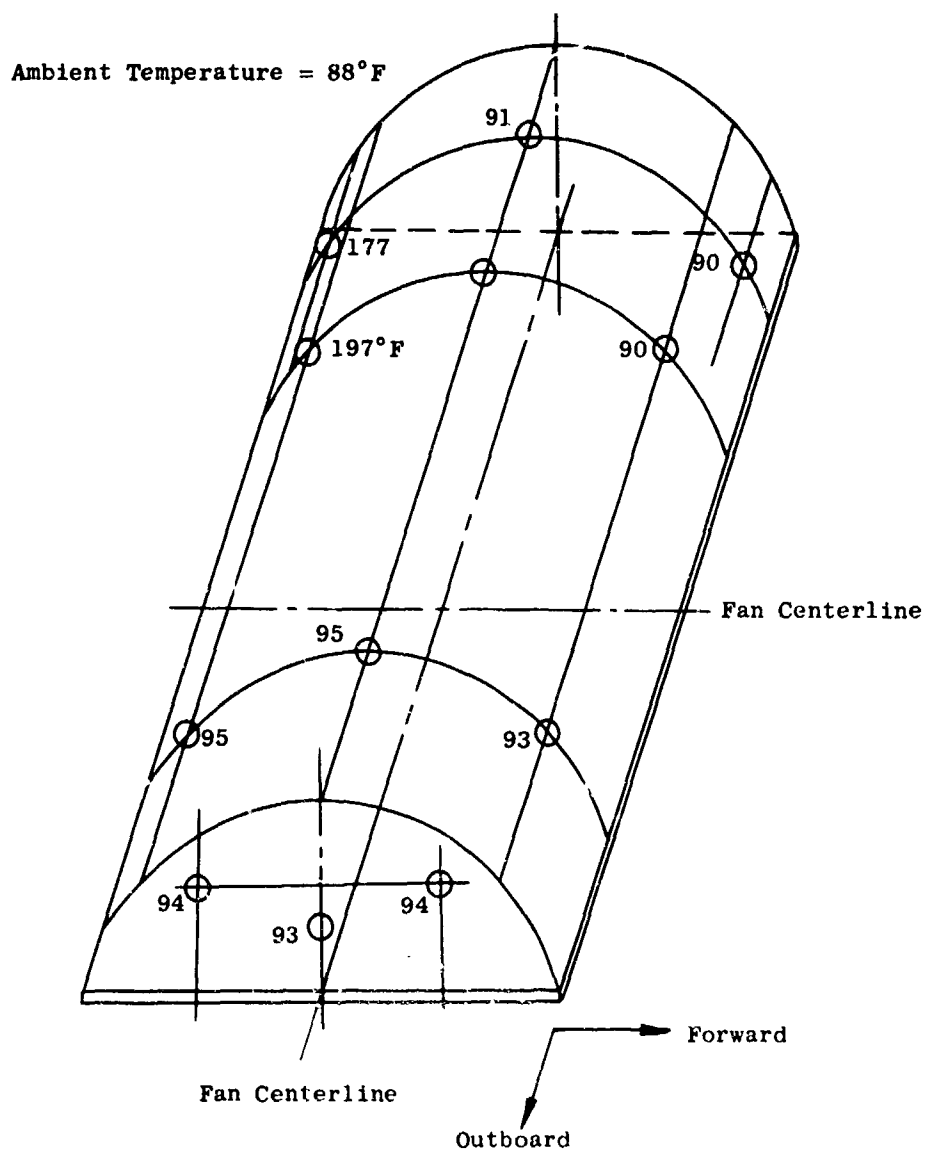


Figure 226. Fan Inlet Screen Temperature Distribution With High Reingestion Region.

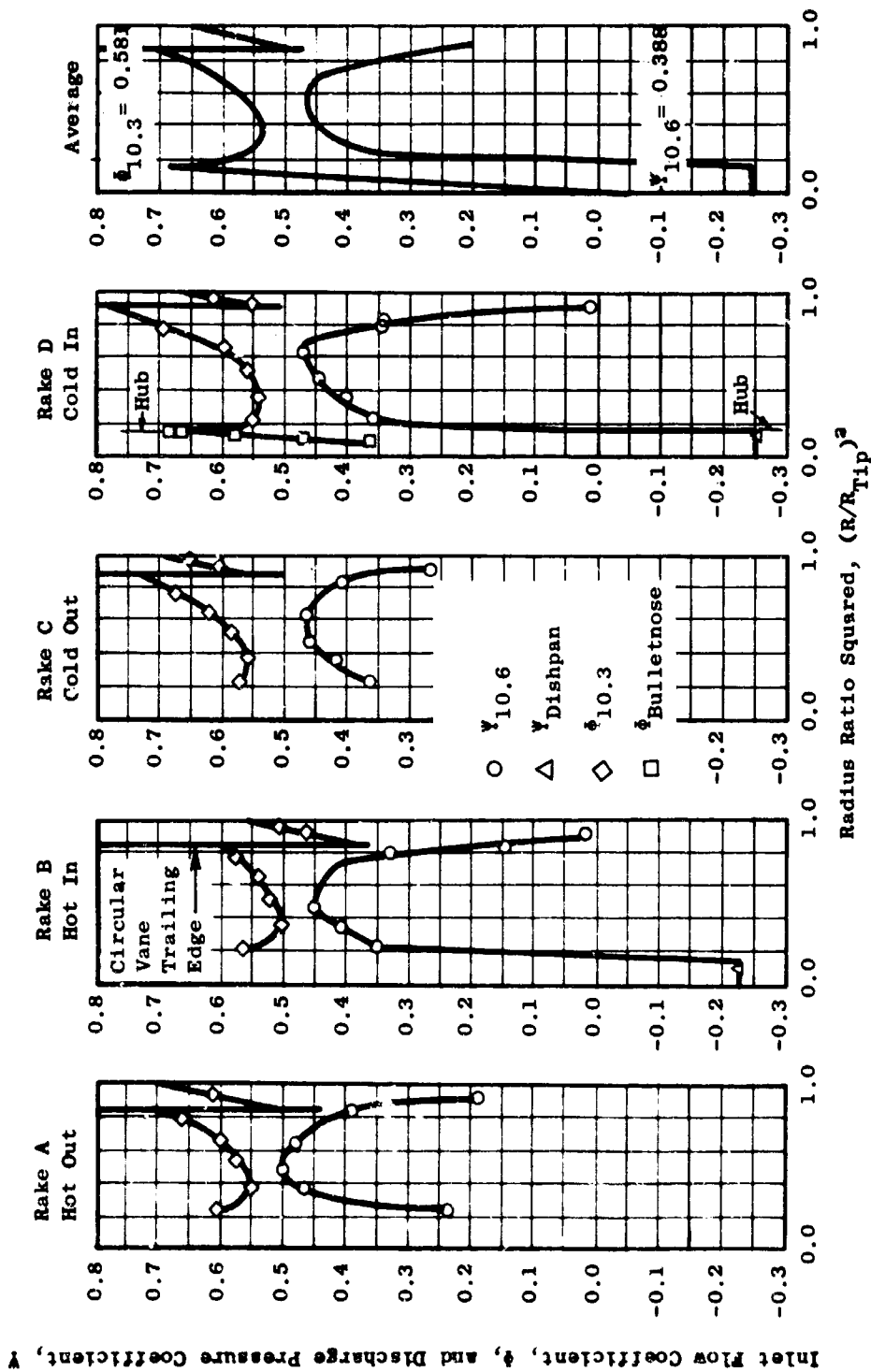


Figure 227. Fan Flow Coefficient and Pressure Coefficient Characteristics, Run 7, Stator Stiffener Rings Out, $\delta_s = 100$ Percent.

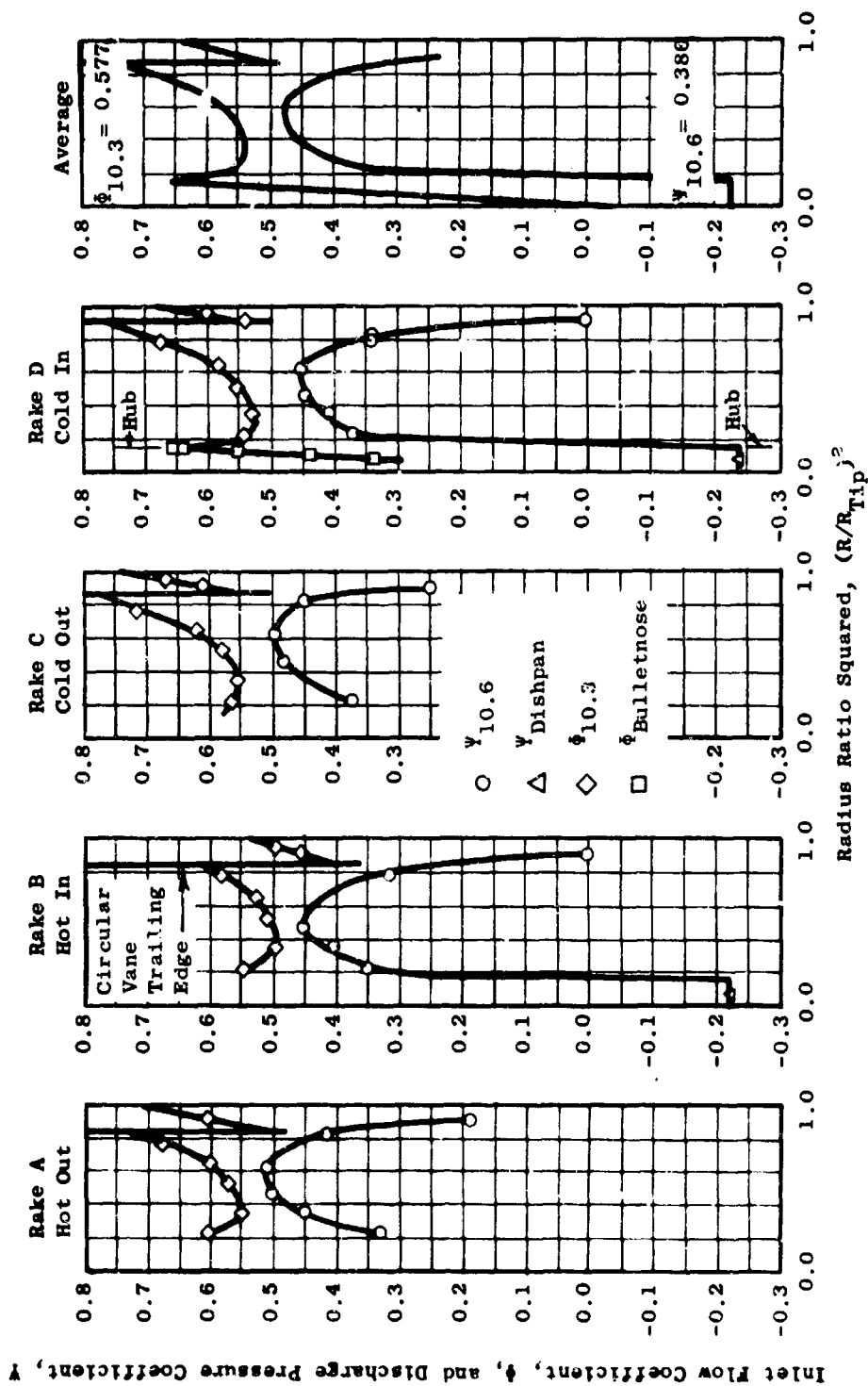


Figure 228. Fan Flow Coefficient and Pressure Coefficient Characteristics, Run 9, Stator Stiffener Rings In, $\delta_g = 100$ Percent.

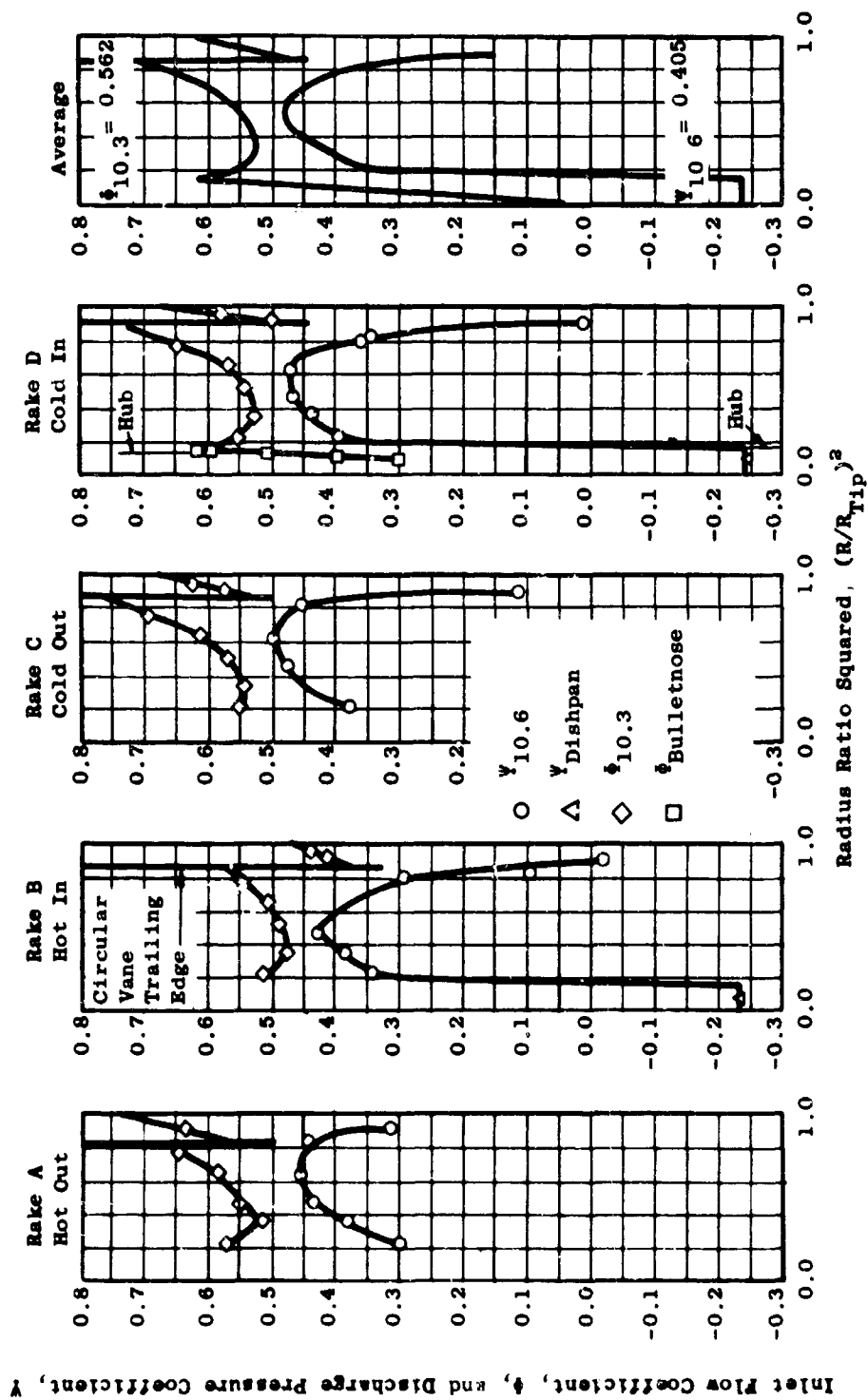


Figure 229. Fan Flow Coefficient and Pressure Coefficient Characteristics, Run 11, Stator Stiffener Rings In, $\delta_s = 0$ Percent.

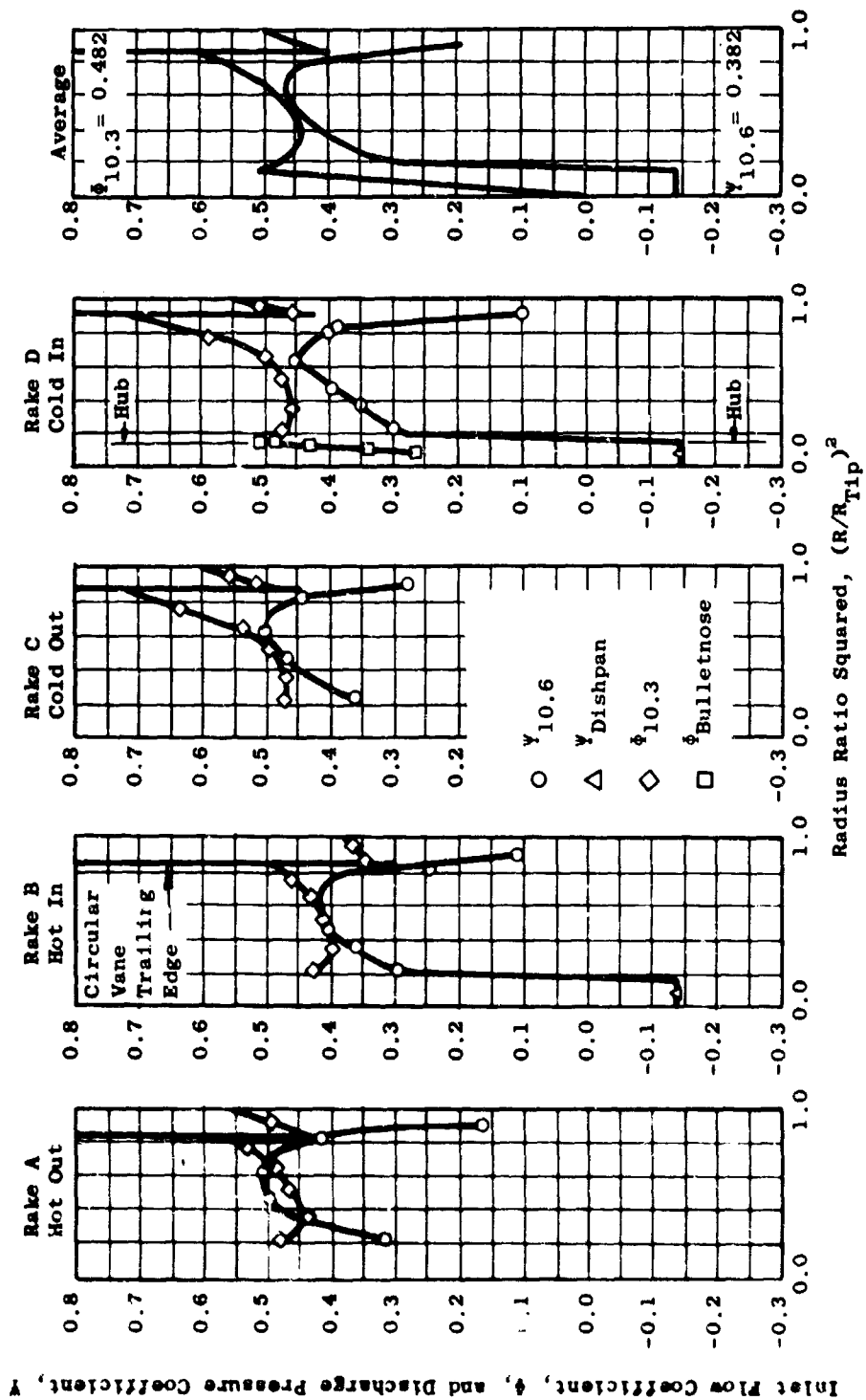


Figure 230. Fan Flow Coefficient and Pressure Coefficient Characteristics, Run 12, $\beta_V = 37$ Degrees, $\delta_S = 76$ Percent.

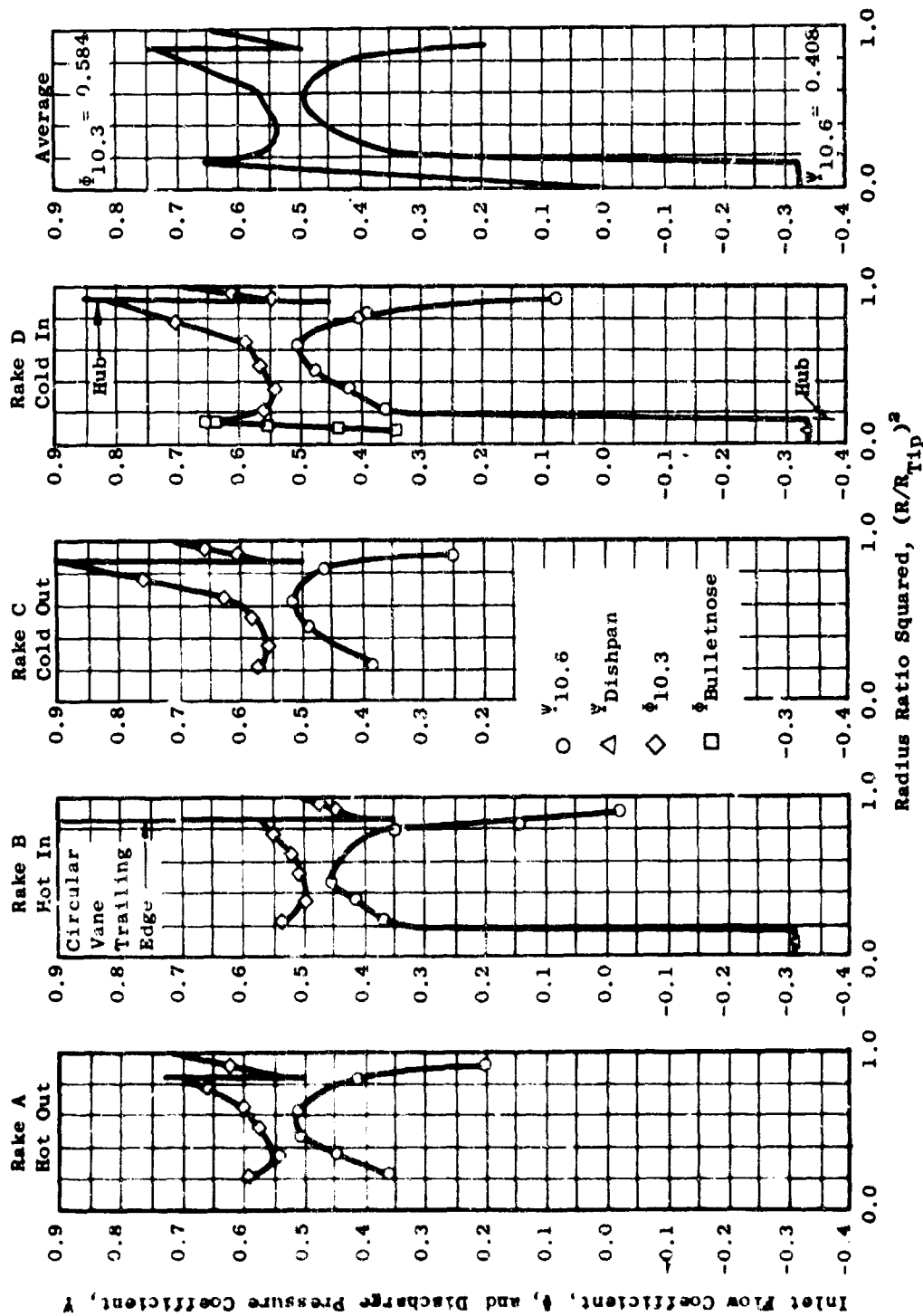


Figure 231. Pan Flow Coefficient and Discharge Pressure Coefficient Characteristics, Run 17, Slip Ring Cavity Covered, $\delta_g = 80$ Percent.

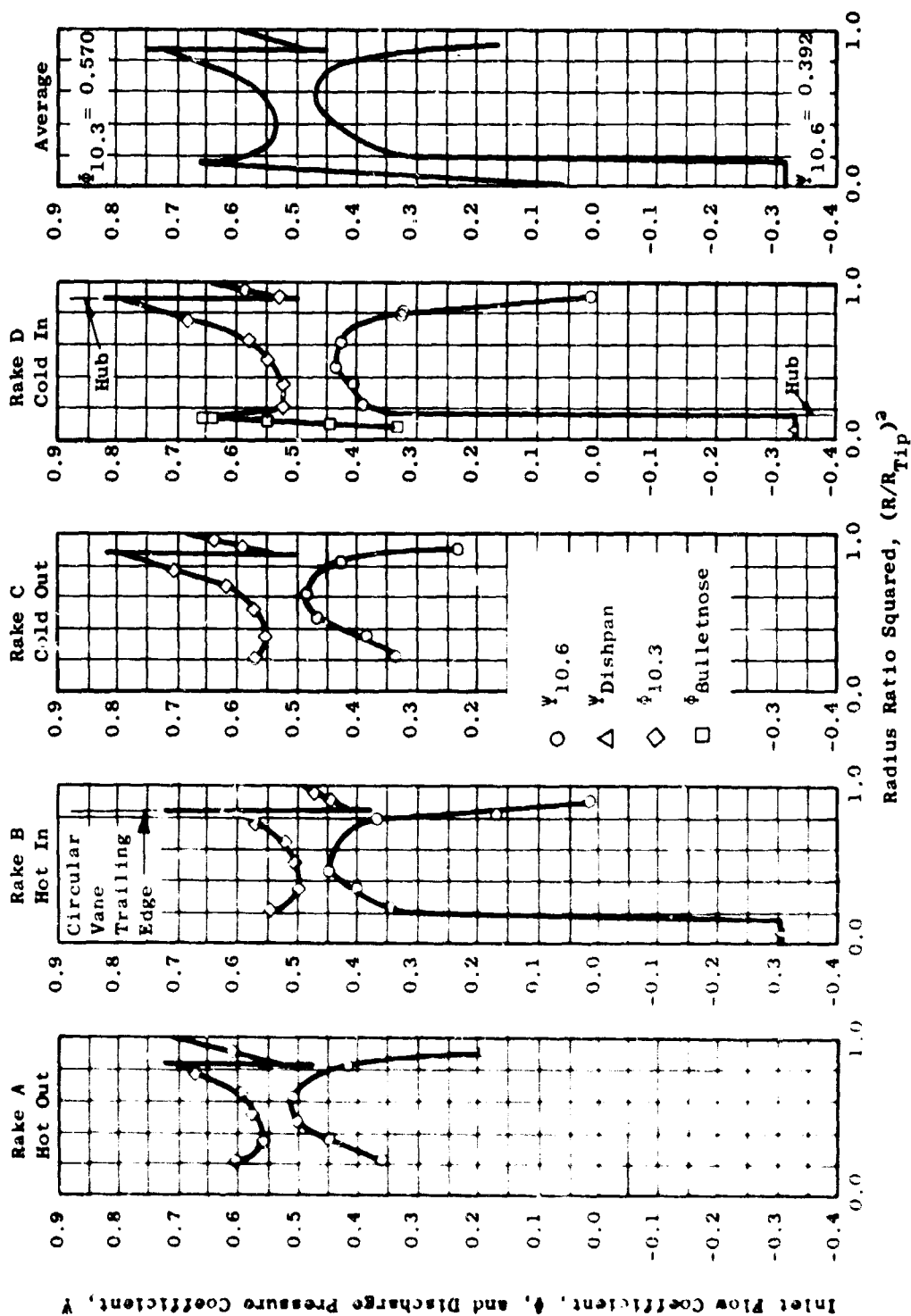


Figure 232. Fan Flow Coefficient and Pressure Coefficient Characteristics, Run 18, 3 to 6 O'Clock Inlet Vane Quadrant Raised, $\delta_s = 80$ Percent.

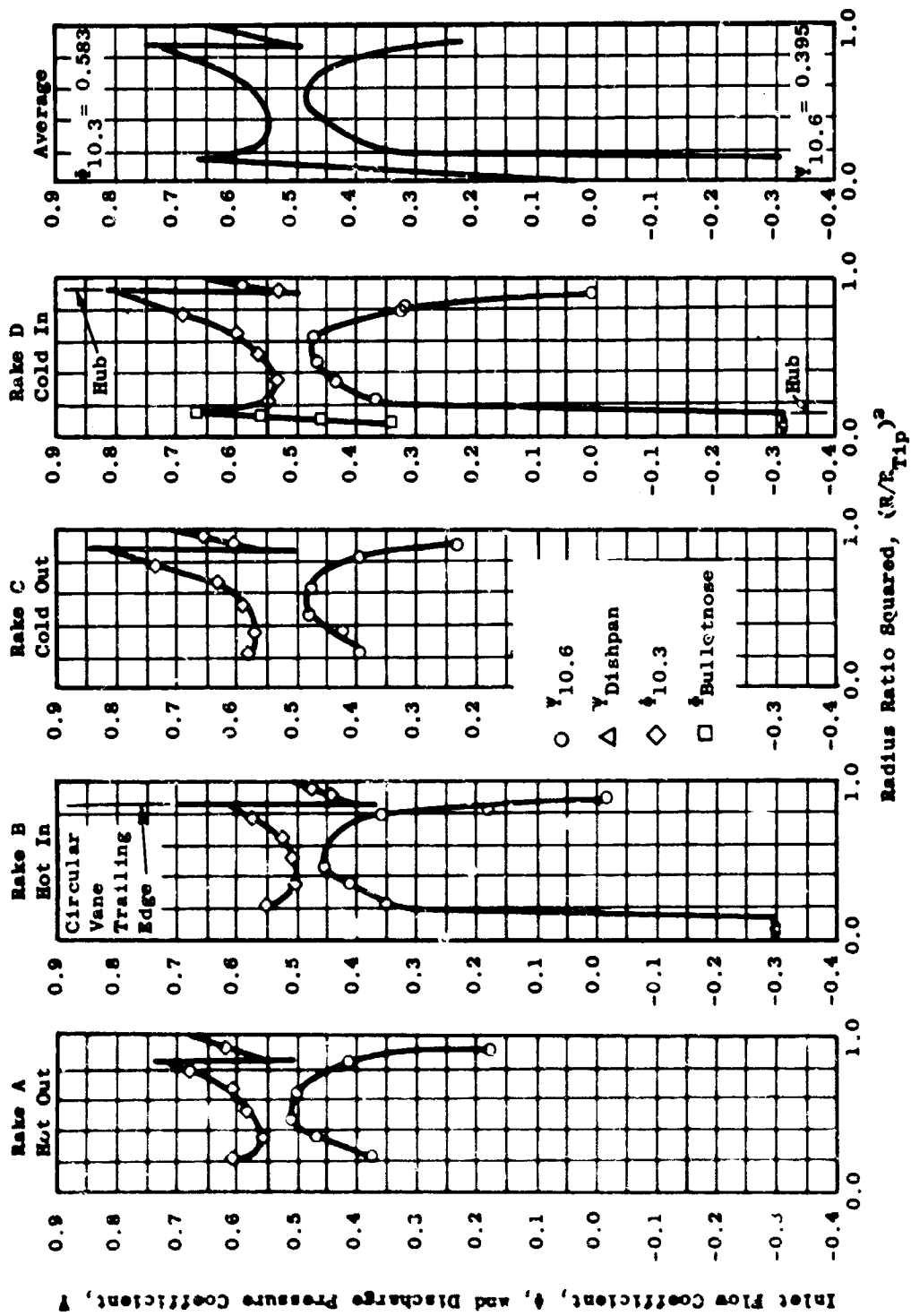


Figure 233. Fan Flow Coefficient and Pressure Coefficient Characteristics, Run 18, Exit Louvers Removed, $\delta_g = 80$ Percent.

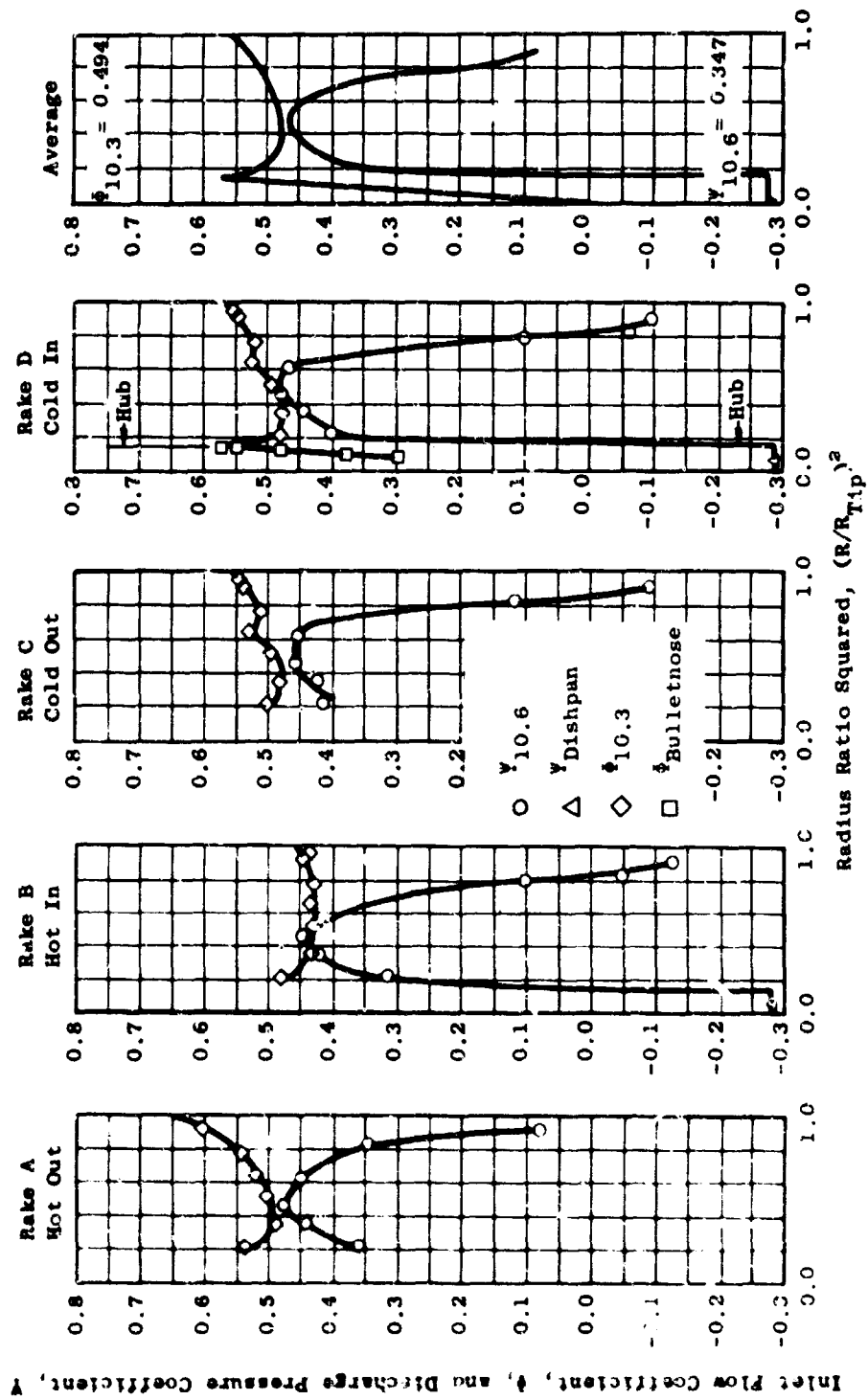


Figure 234. Fan Flow Coefficient and Pressure Coefficient Characteristics, Run 18, Inlet Vane Out, $\xi_g = 80$ Percent.

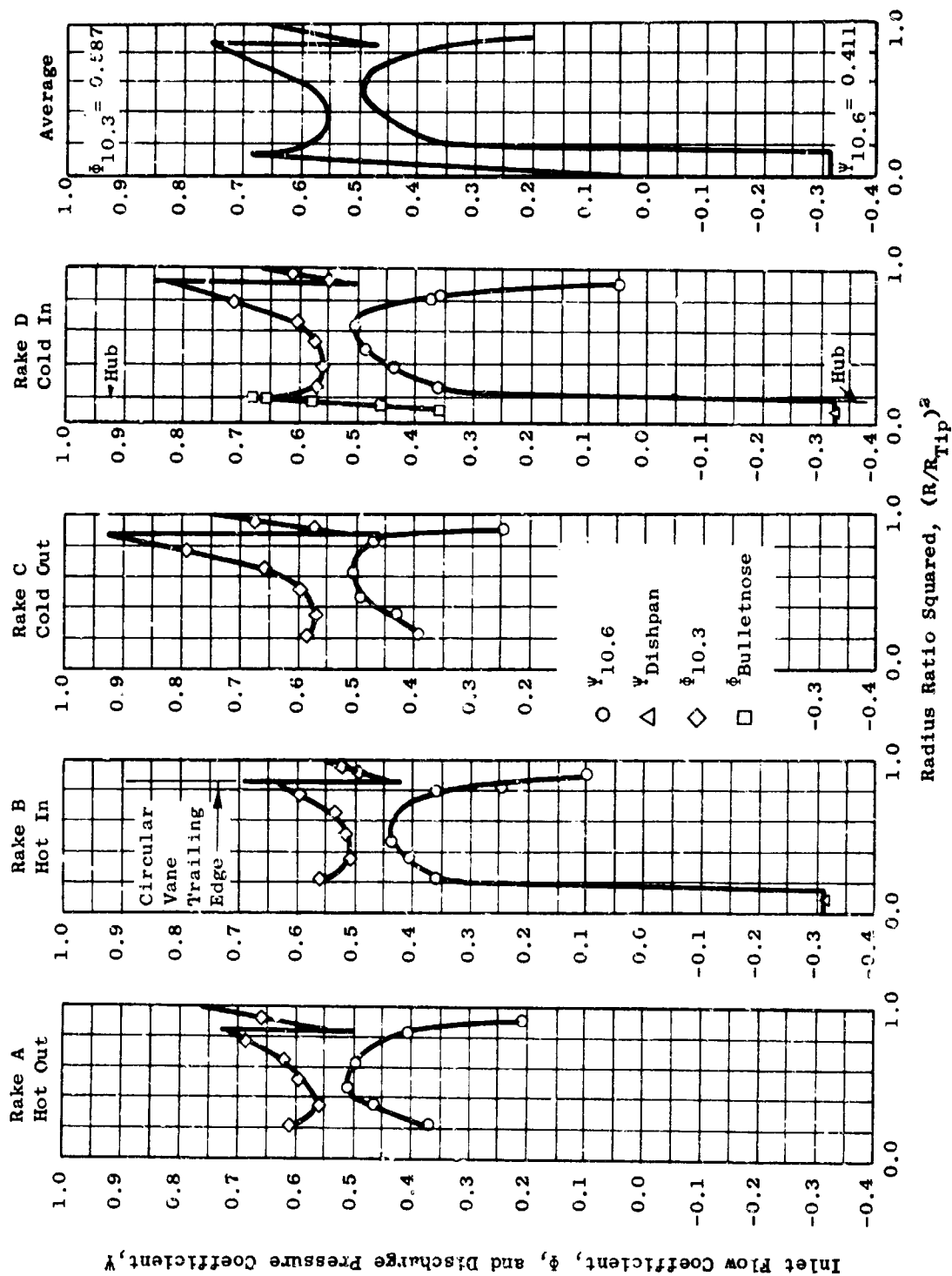


Figure 235. Fan Flow Coefficient and Pressure Coefficient Characteristics, Run 19, Improved Forward Air Seal, $\delta_s = 80$ Percent.

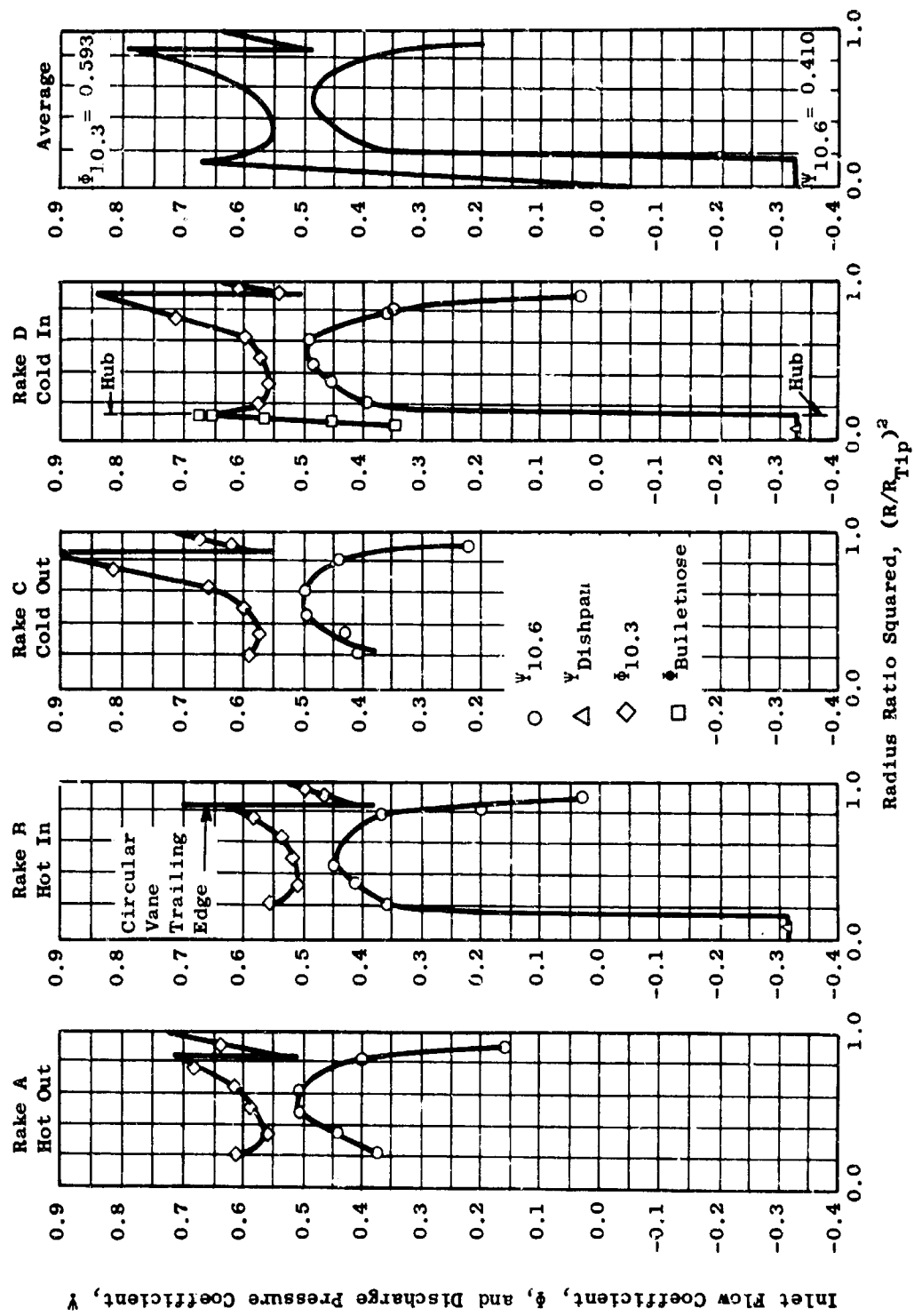


Figure 236. Fan Flow Coefficient and Pressure Coefficient Characteristics, Run 19, Stator Stiffener Rings Out, $\delta_s = 80$ Percent.

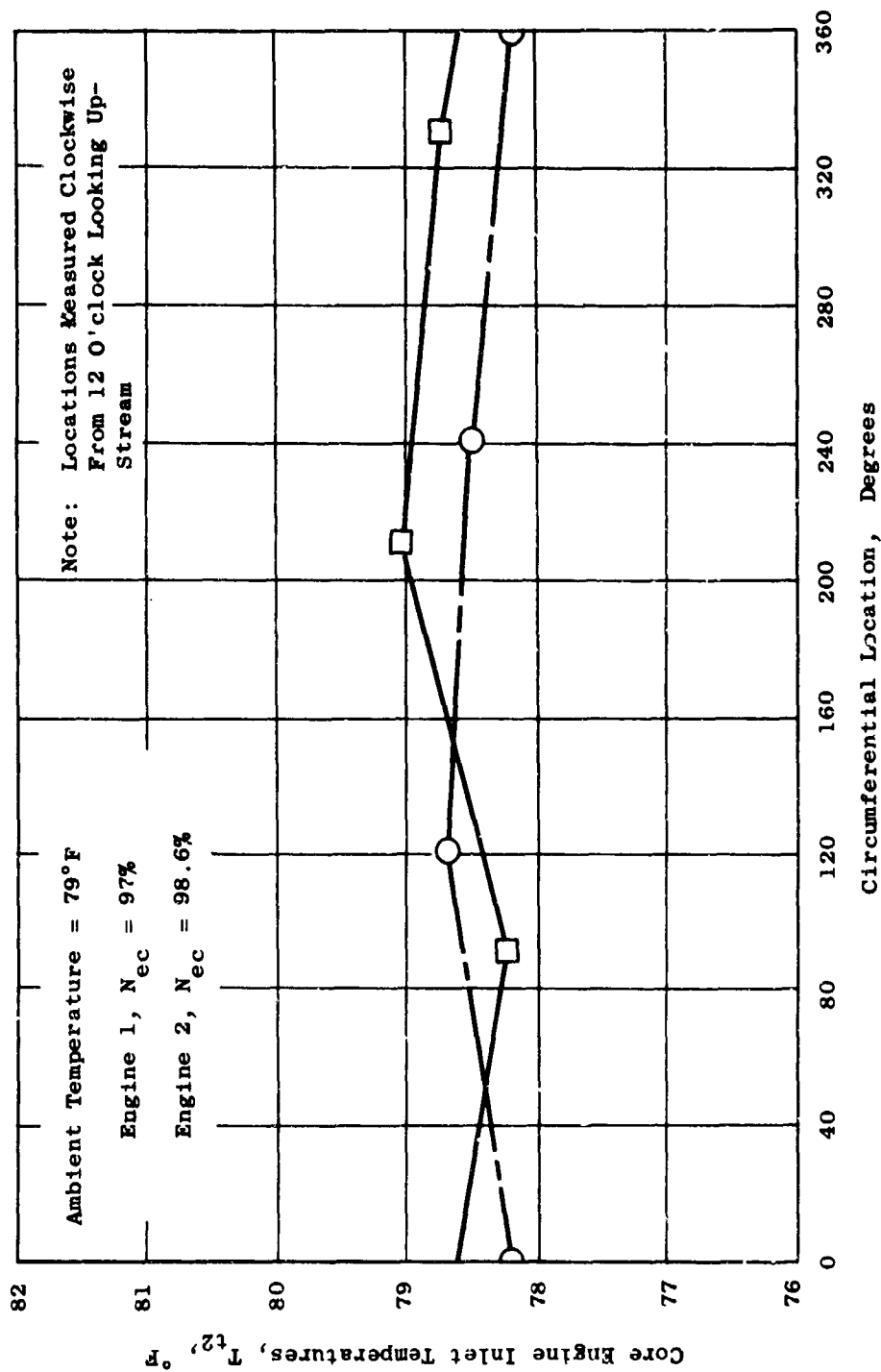


Figure 237. Typical Core Engine Inlet Temperature Distribution.

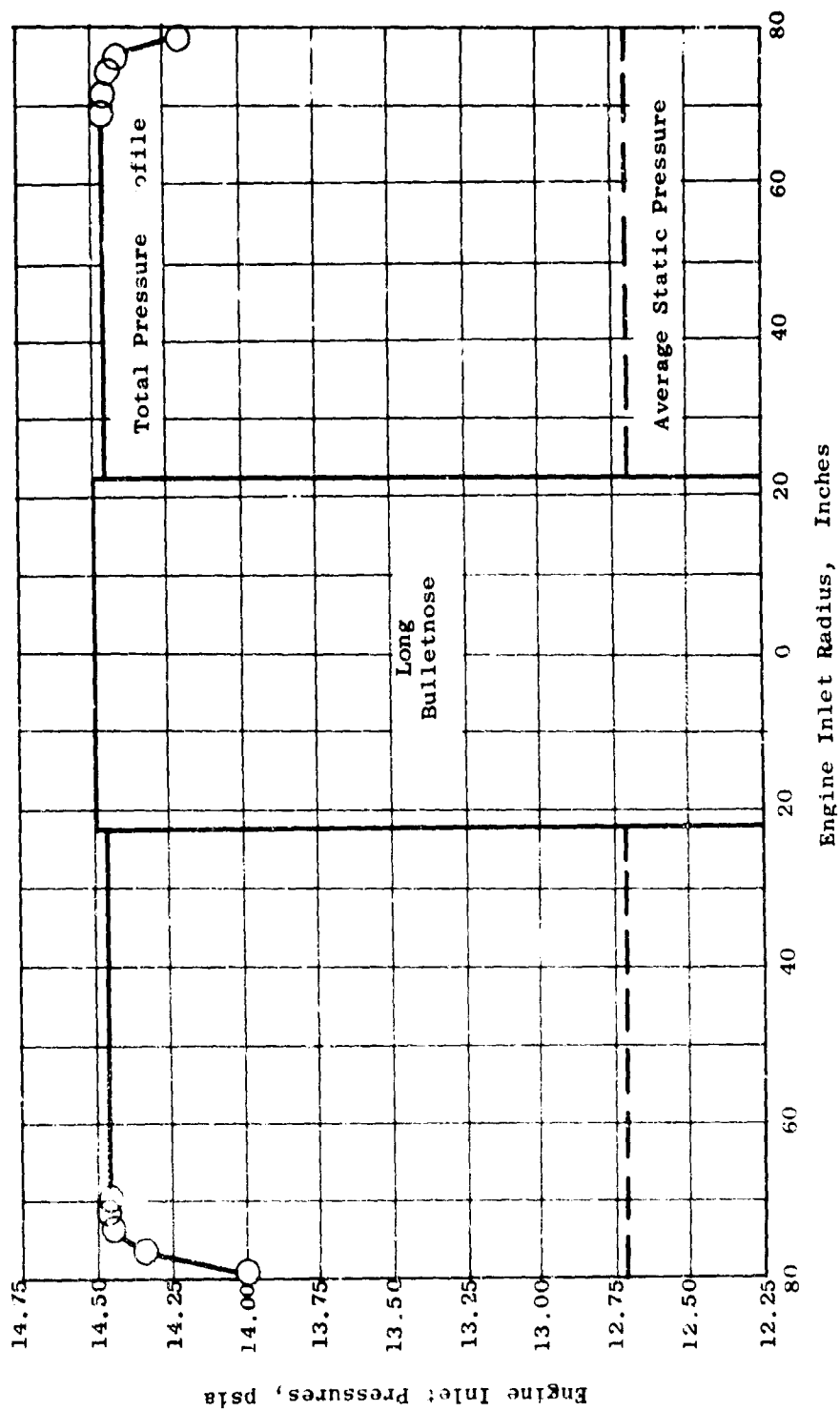


Figure 238. Typical Engine 2 Inlet Pressure Profile, $P_a = 14.467$ psia, $N_{ec2} = 99.2$ Percent.

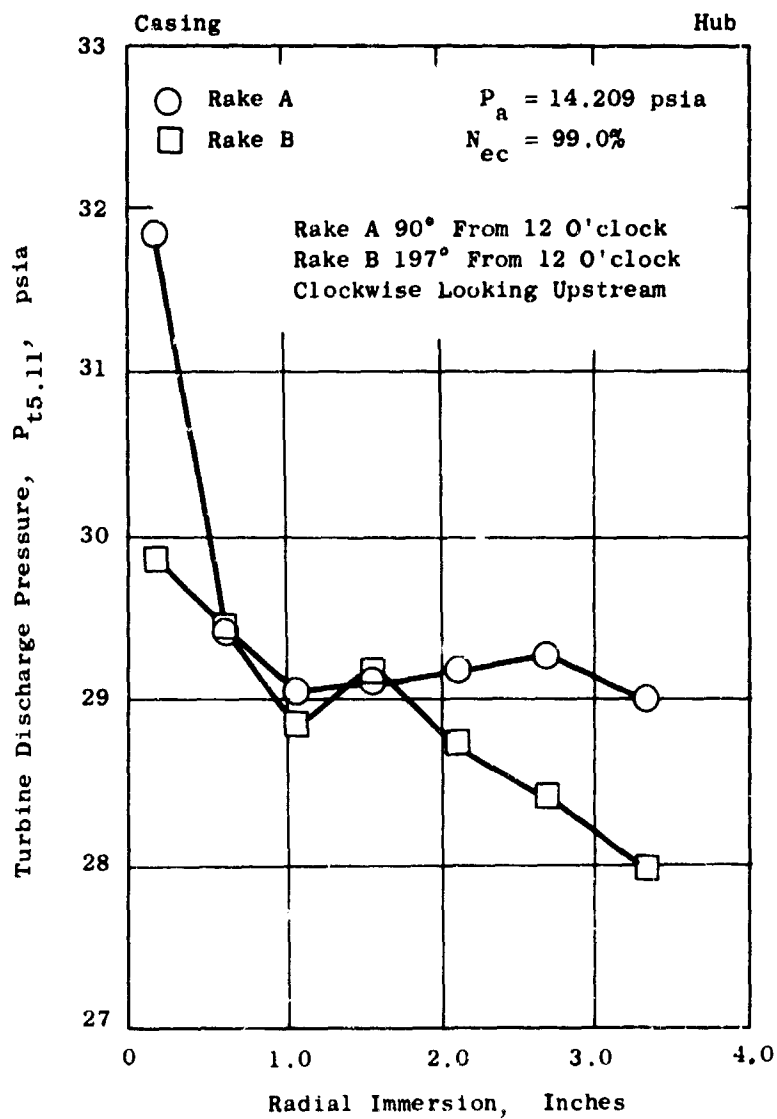


Figure 239. Typical Engine 1 Turbine Discharge Pressure Profile.

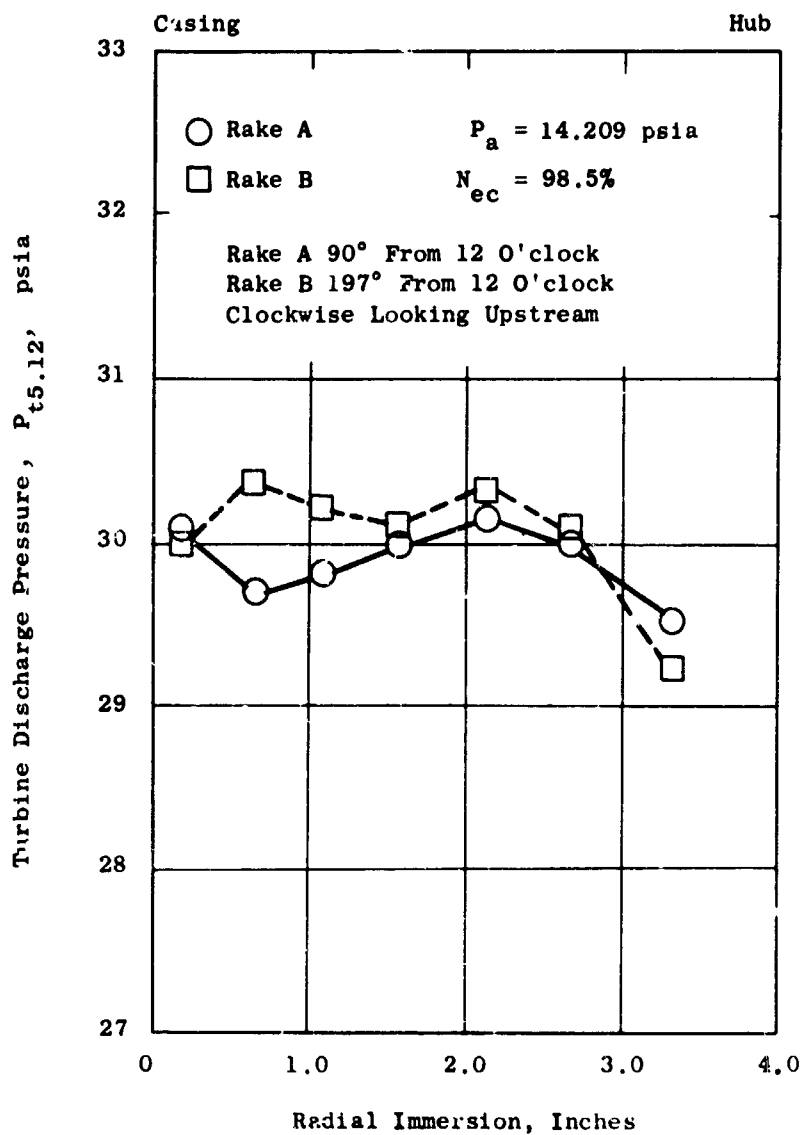


Figure 240. Typical Engine 2 Turbine Discharge Pressure Profile.

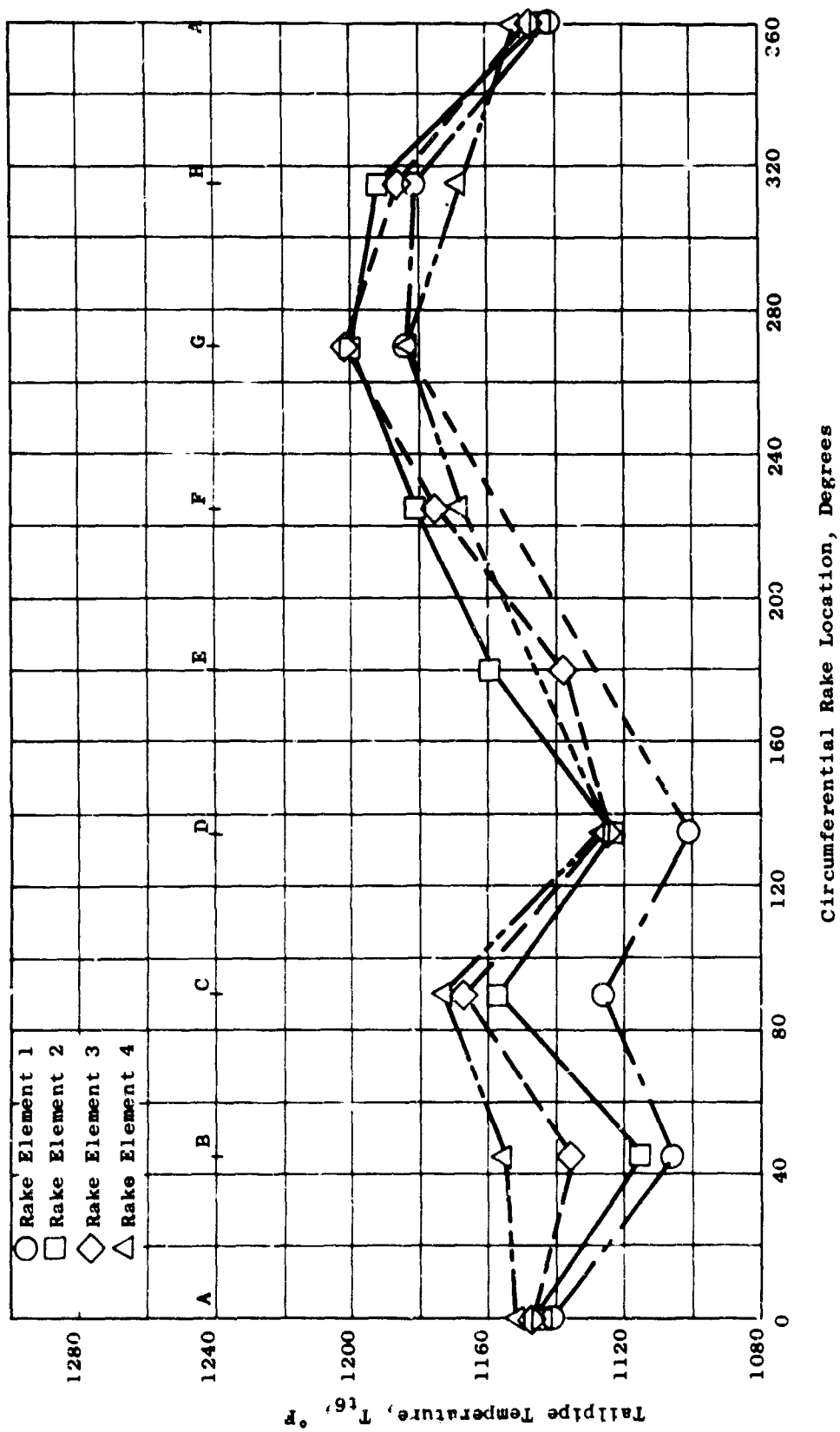


Figure 241. Tailpipe Temperature Profile of Engine 1, YJ85-GE-5, S/N 230105, $N_e = 97.5$ Per-cent, $A_8 = 117.8$ Square Inches.

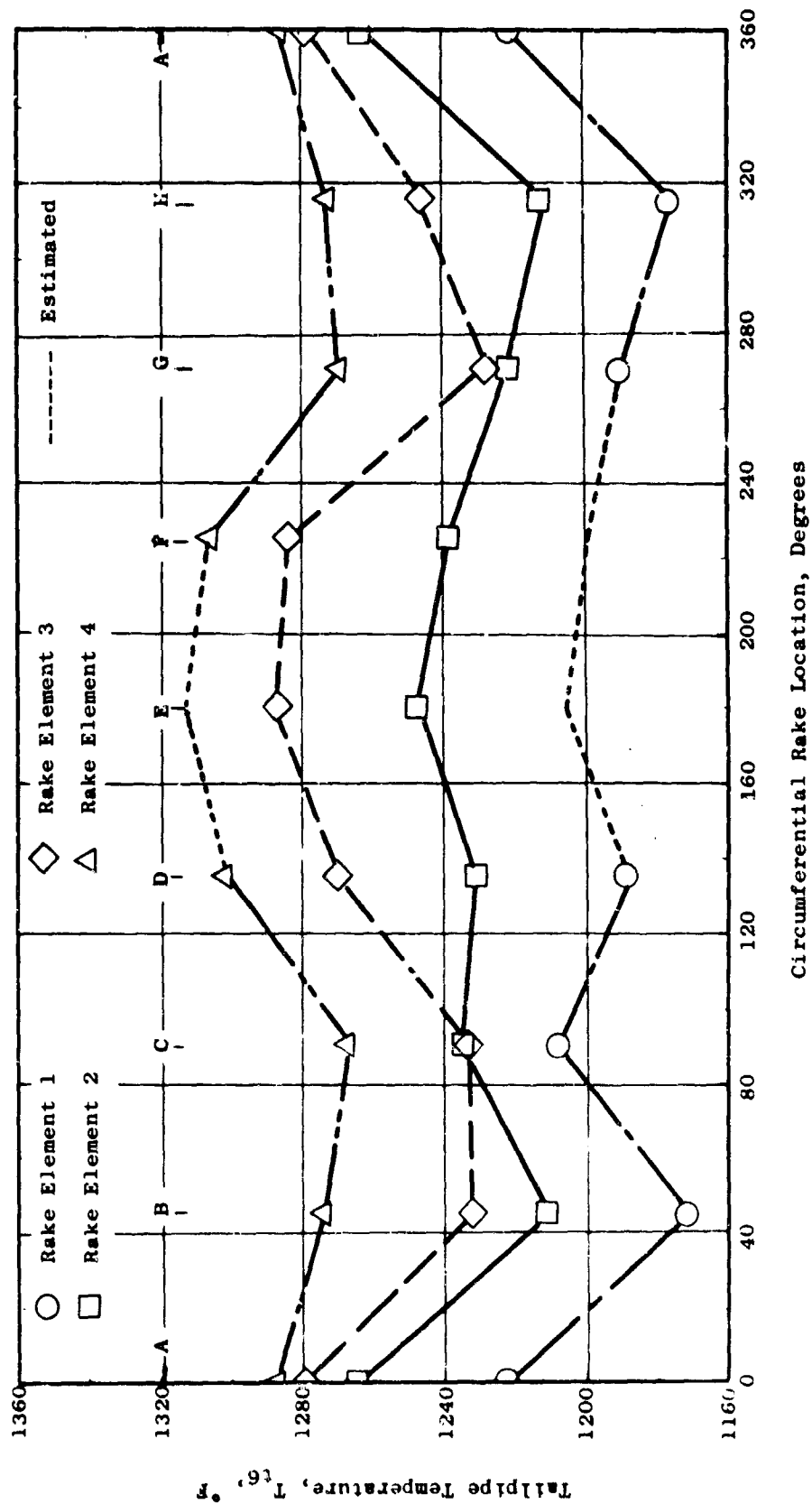


Figure 242. Tailpipe Temperature Profile of Engine 2, J85-GE-5, S/N 231233, $N_e = 100.4$ Percent, $A_8 = 111.8$ Square Inches.

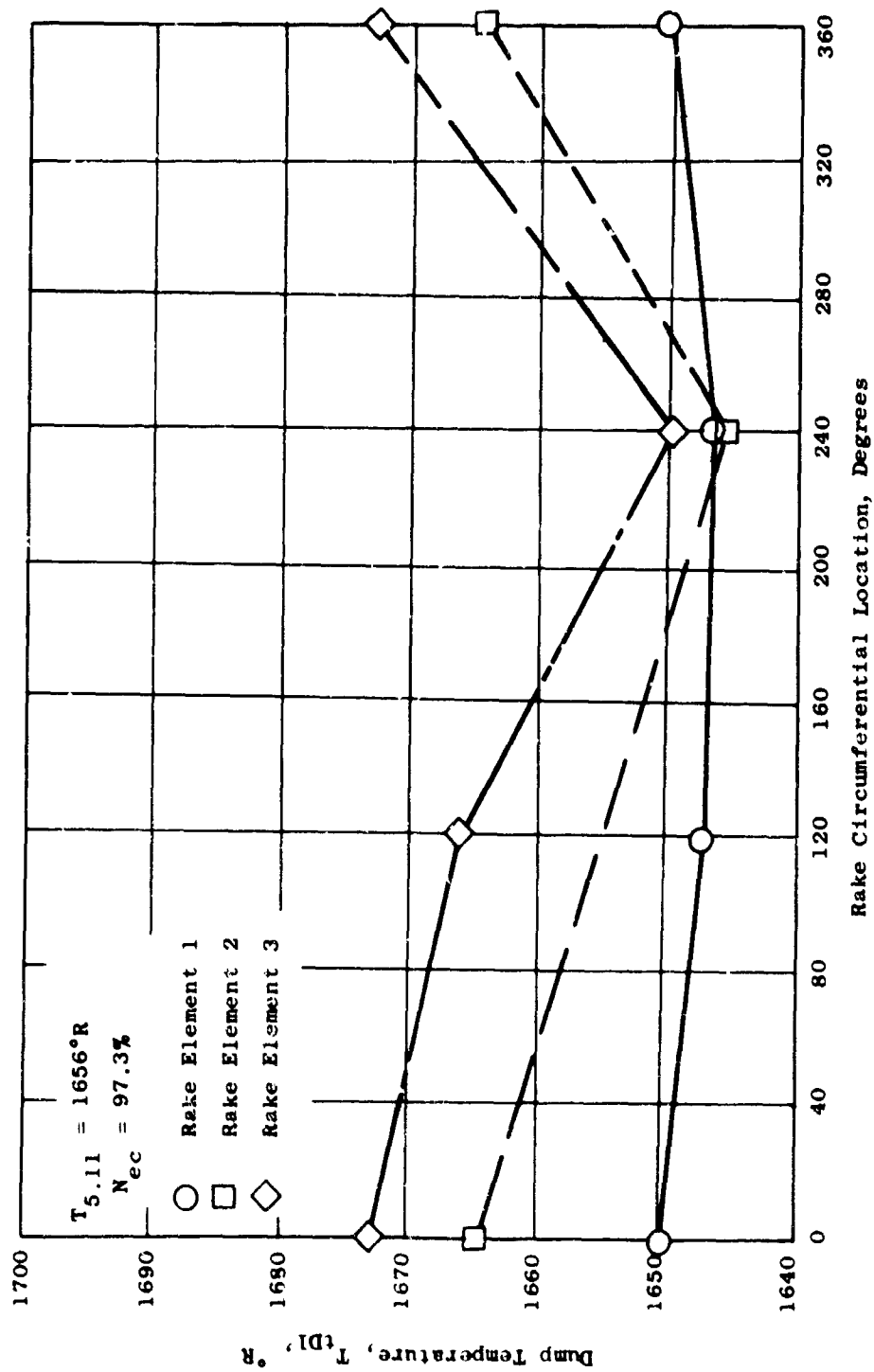


Figure 243. Temperature Distribution Measured in Dump System Supplied by Engine 1.

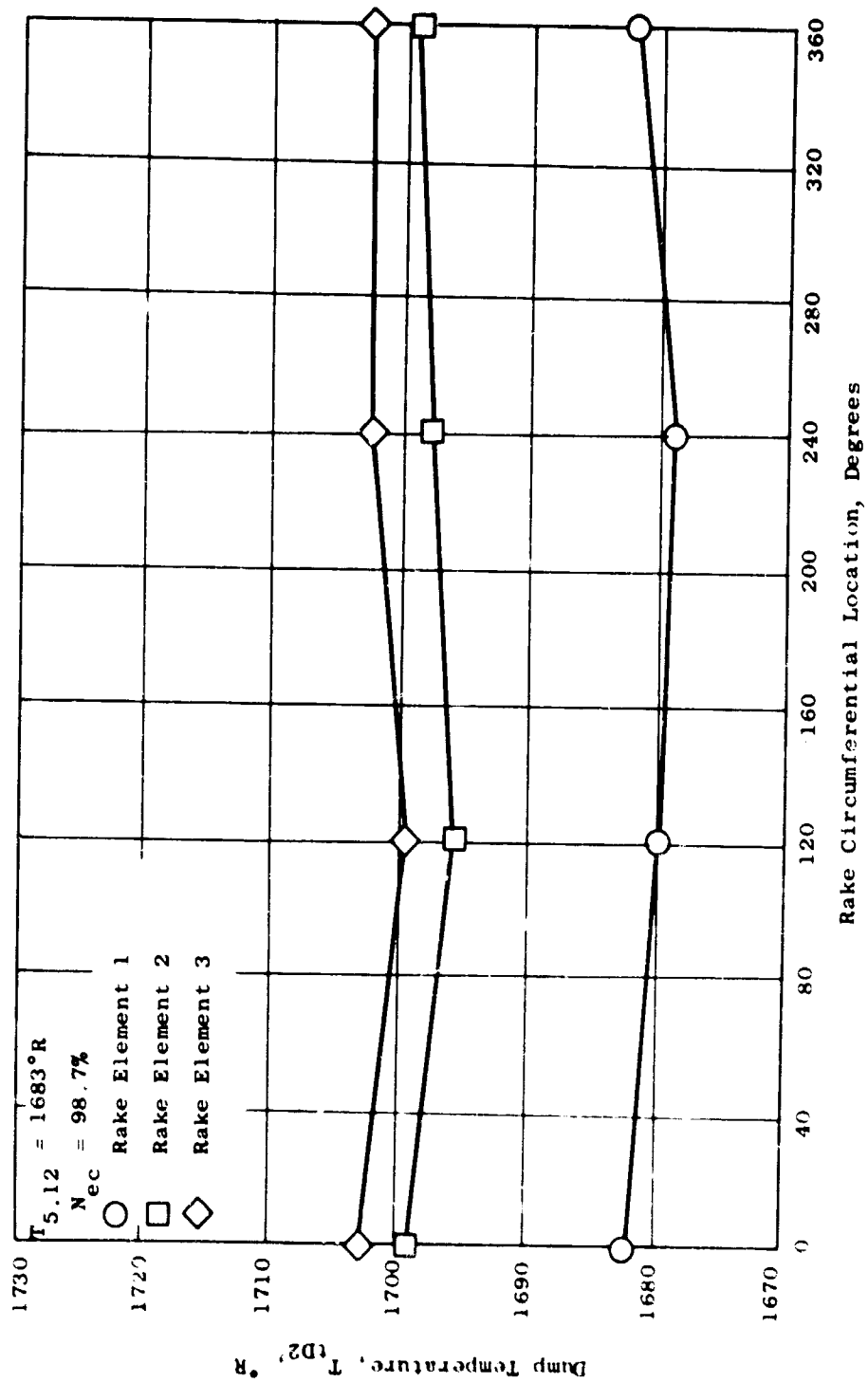


Figure 244. Temperature Distribution Measured in Dump System Supplied by Engine 2.

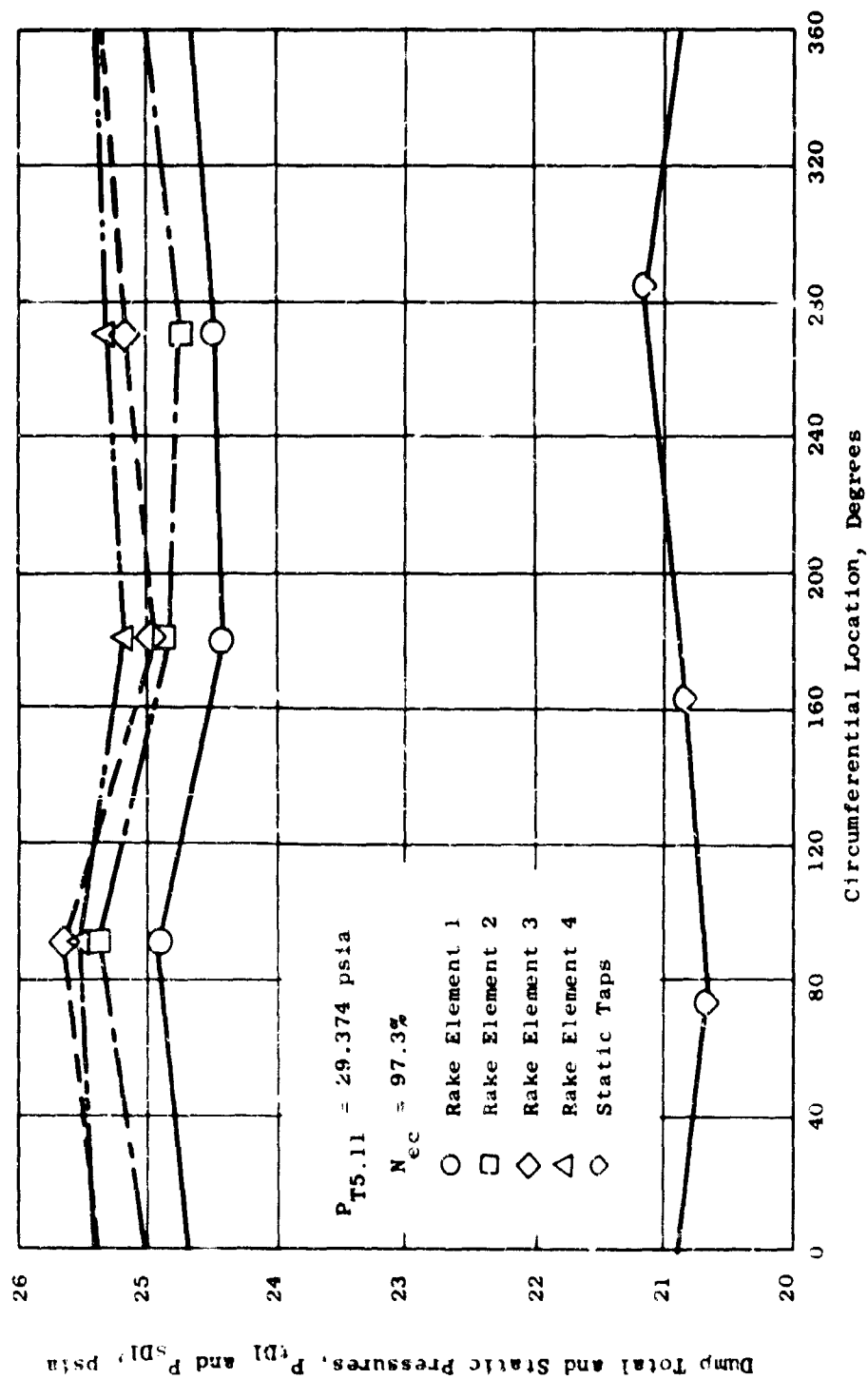


Figure 245. Pressure Distribution Measured in Dump System Supplied by Engine 1.

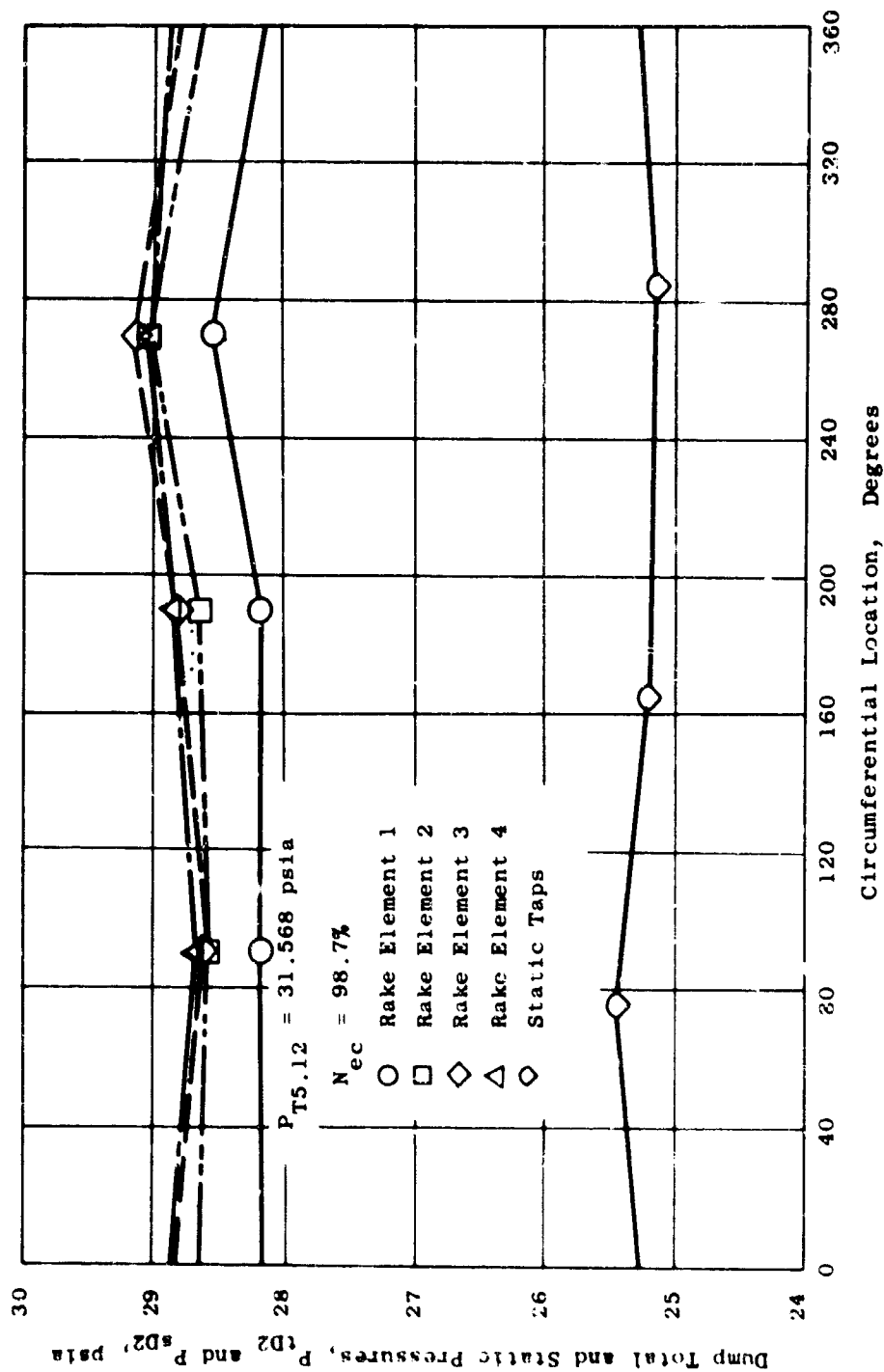


Figure 246. Pressure Distribution Measured in Dump System Supplied by Engine 2.

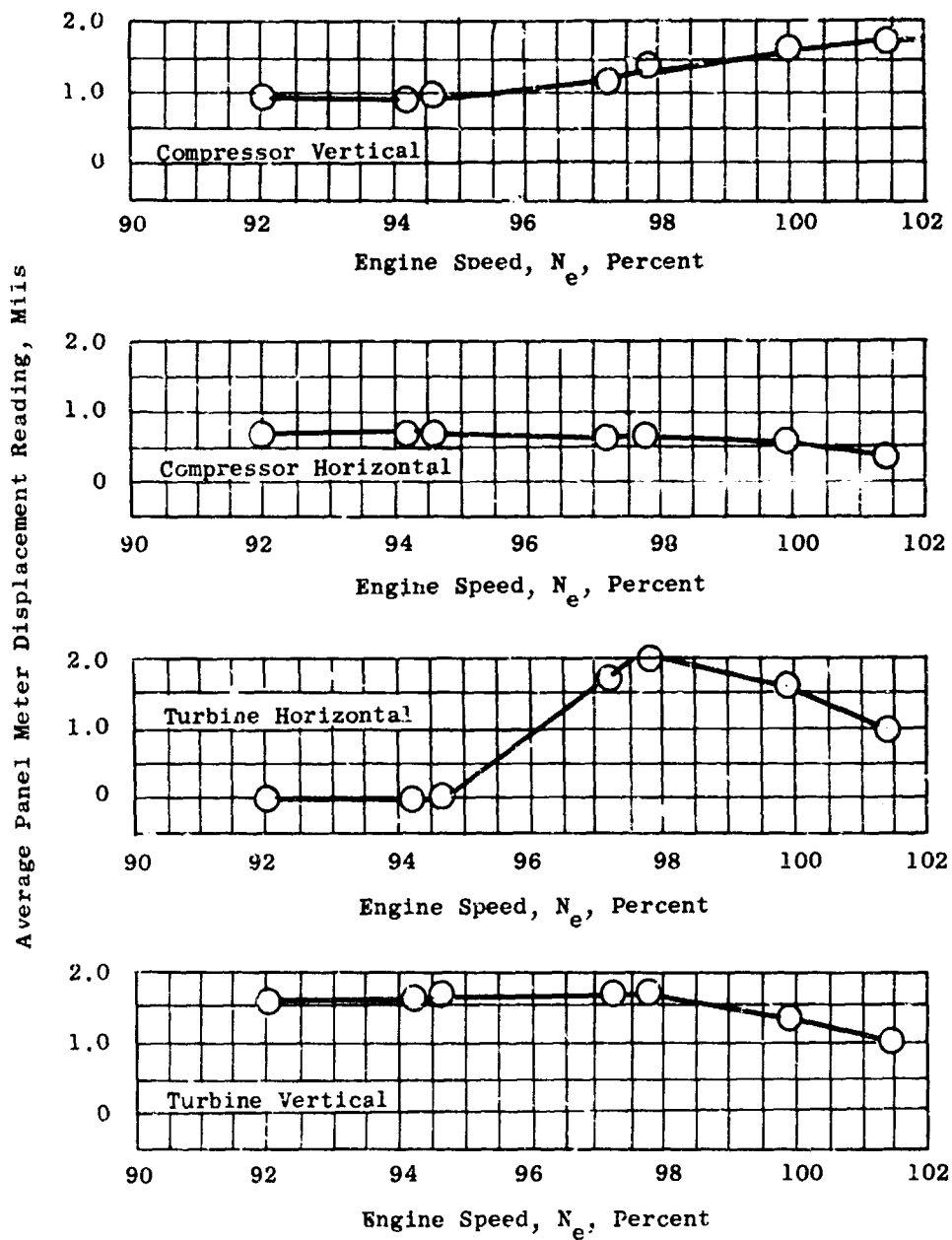


Figure 247. Observed Vibration Characteristics of Engine 1.

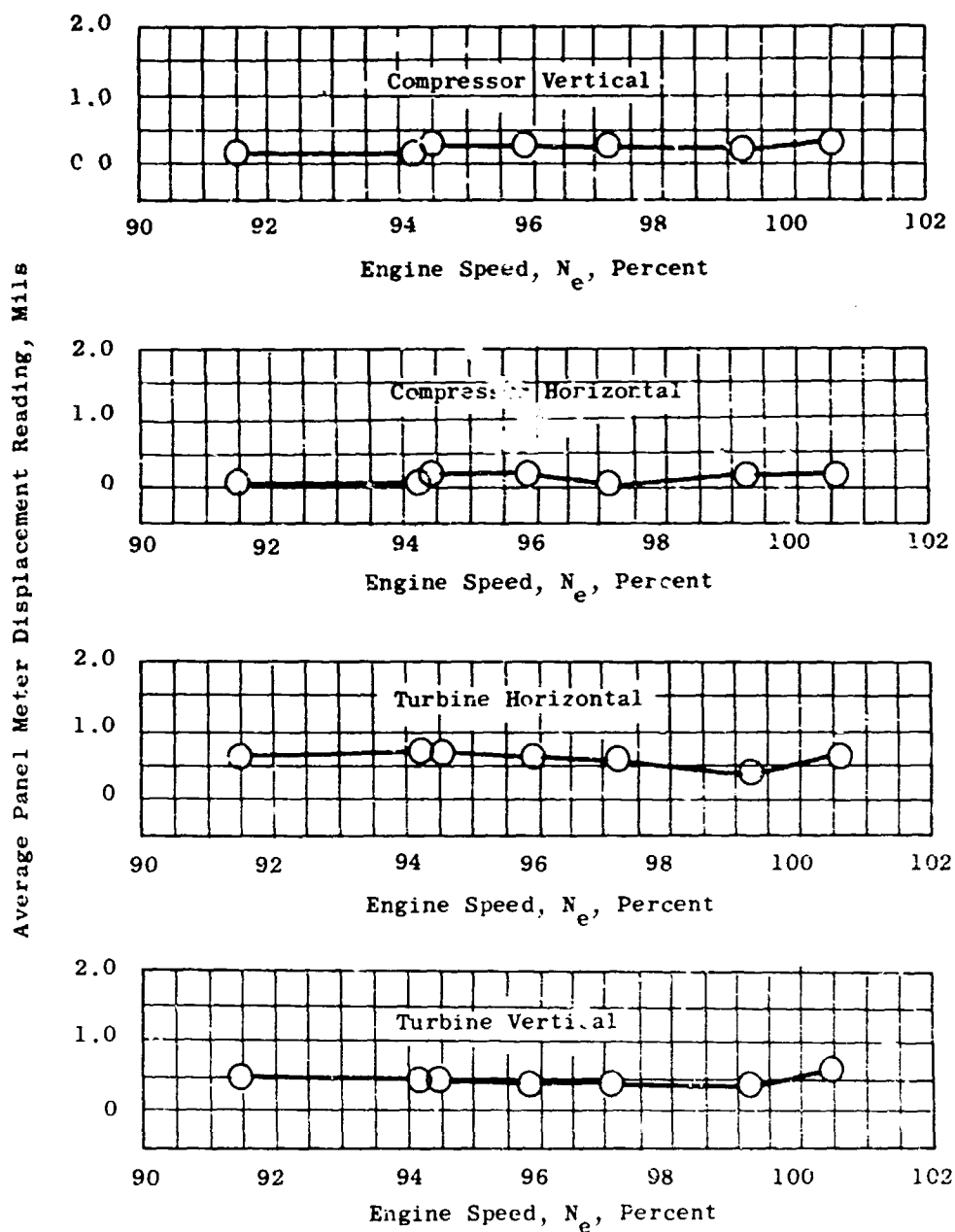


Figure 248. Observed Vibration Characteristics of Engine 2.

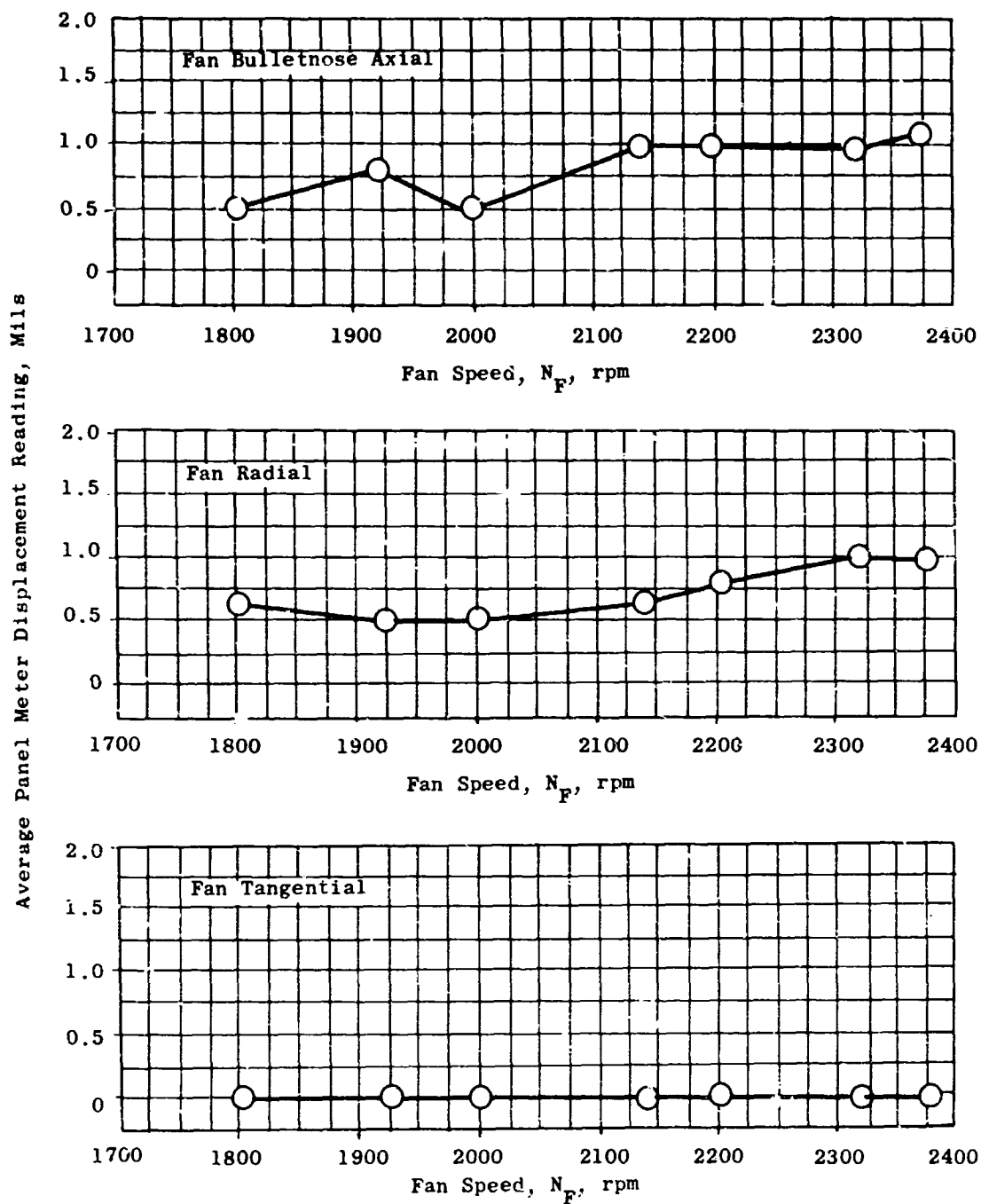


Figure 249. Observed Fan Vibration Characteristics.

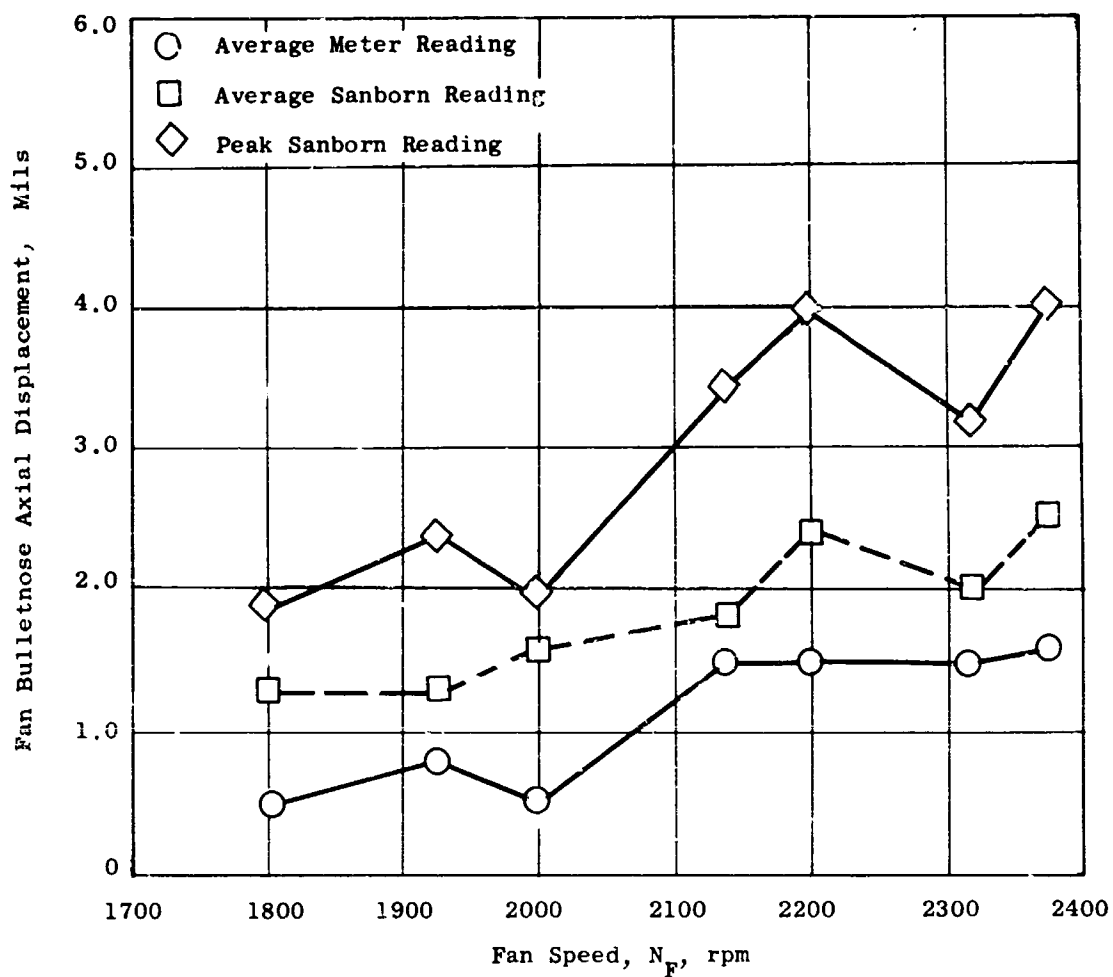


Figure 250. Comparison of Fan Bullethead Axial Vibration Measurements.

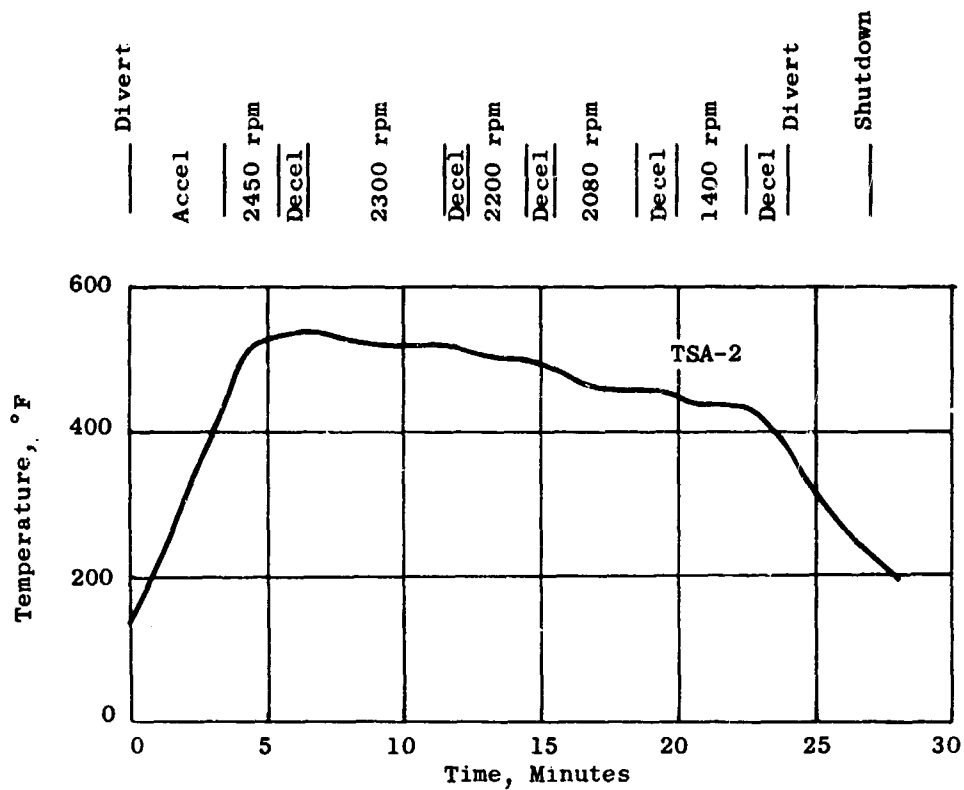


Figure 251. Scroll Actuation Slide Bracket Temperature.

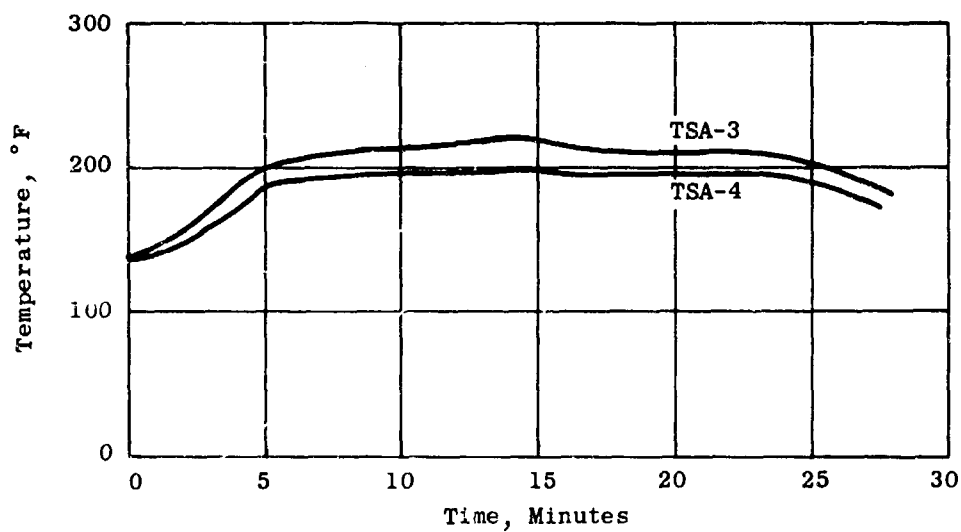


Figure 252. Scroll Actuator Body Temperature.

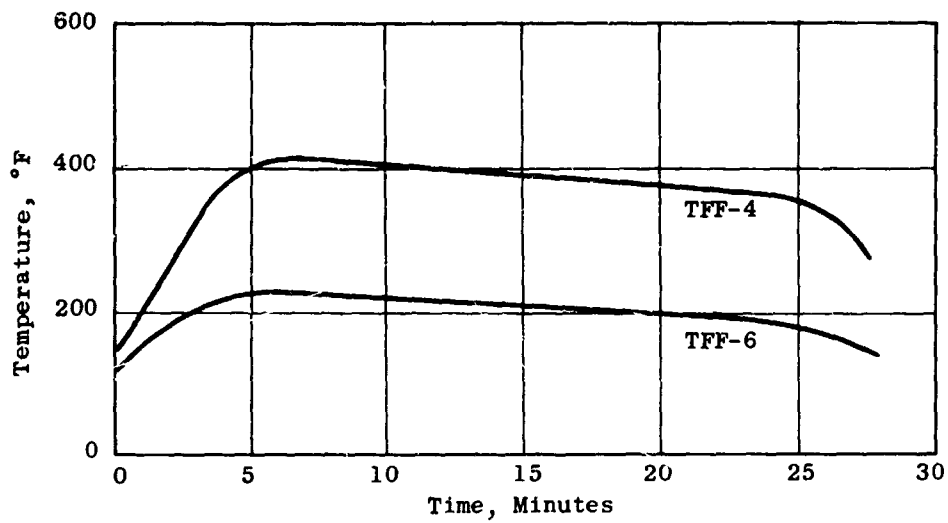


Figure 253. Front Frame Flange Temperature.

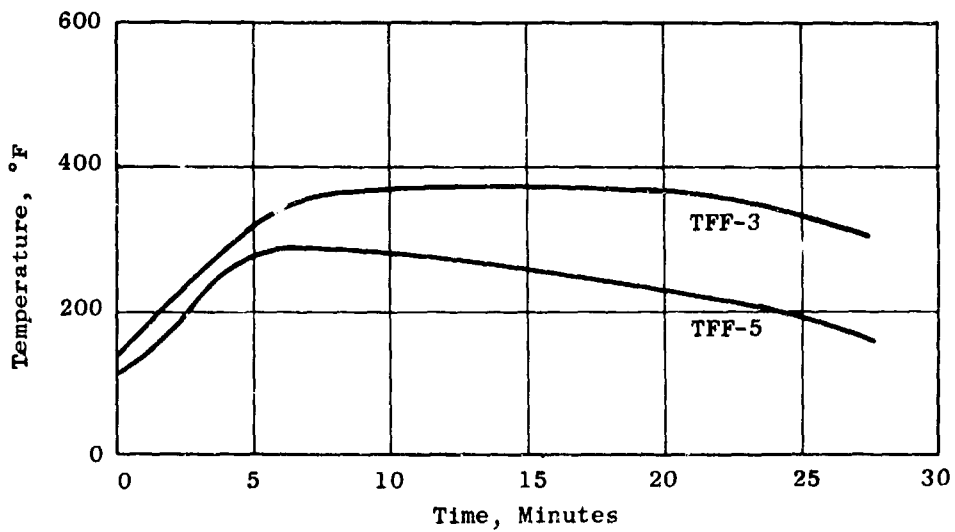


Figure 254. Front Frame Tube Temperatures.

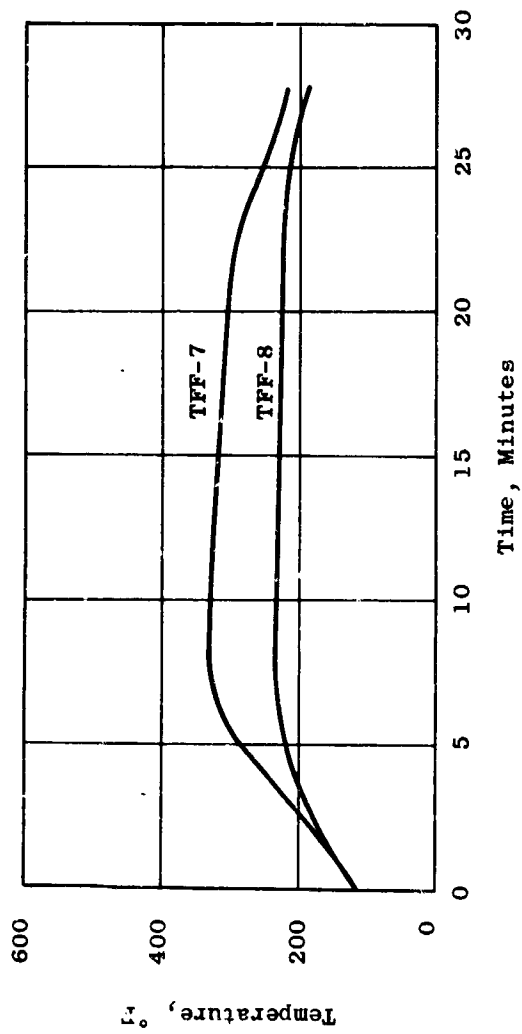


Figure 255. LF2 Front Frame Strut Temperature, Run 7.

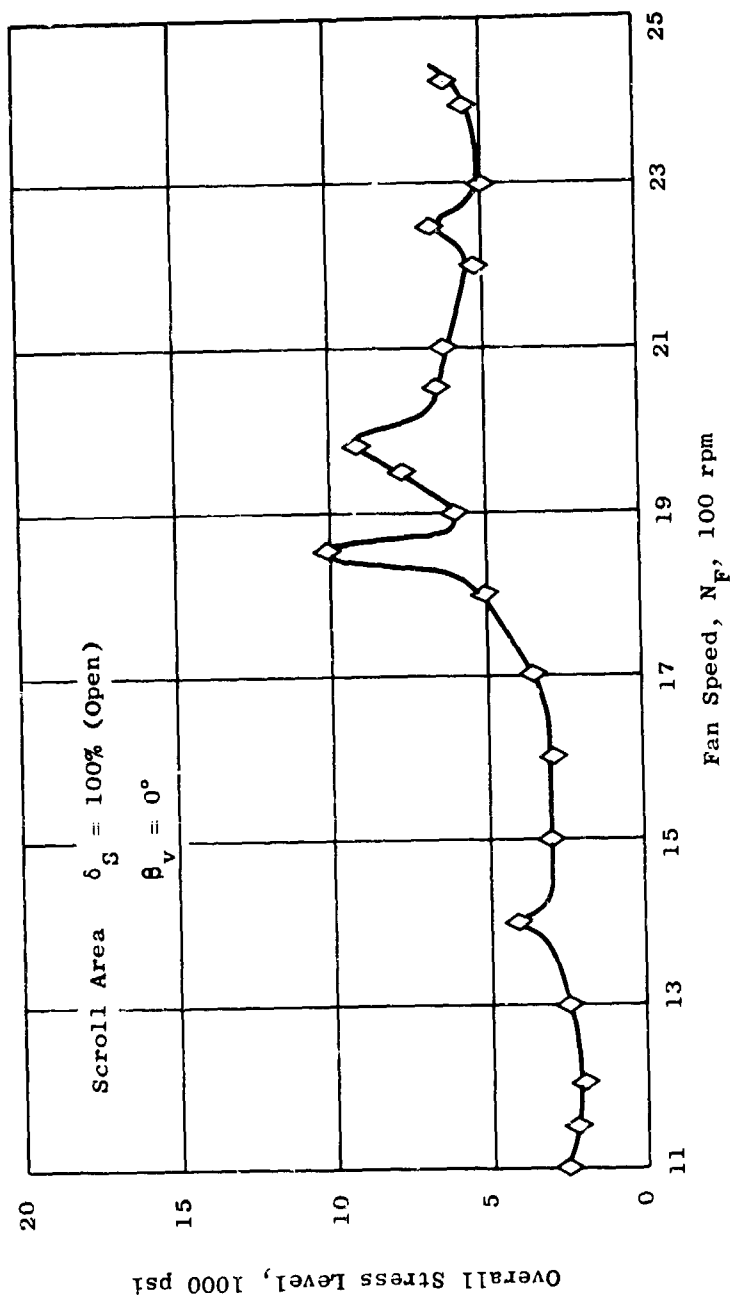


Figure 256. Overall Blade Stress Level Versus Fan Speed for Blade Gage 1,
 $\delta_S = 100$ Percent.

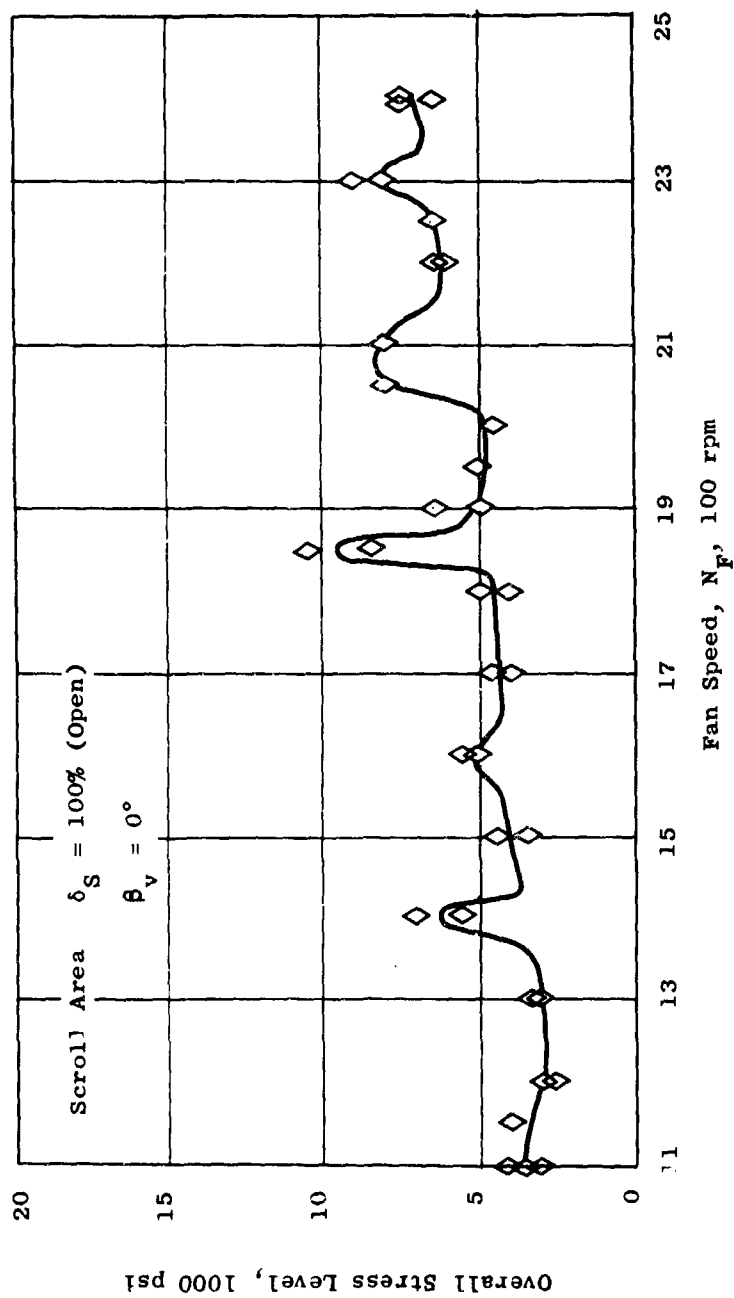


Figure 57. Overall Blade Stress Level Versus Fan Speed for Blade Gage 3, $\delta_S = 100$ Percent.

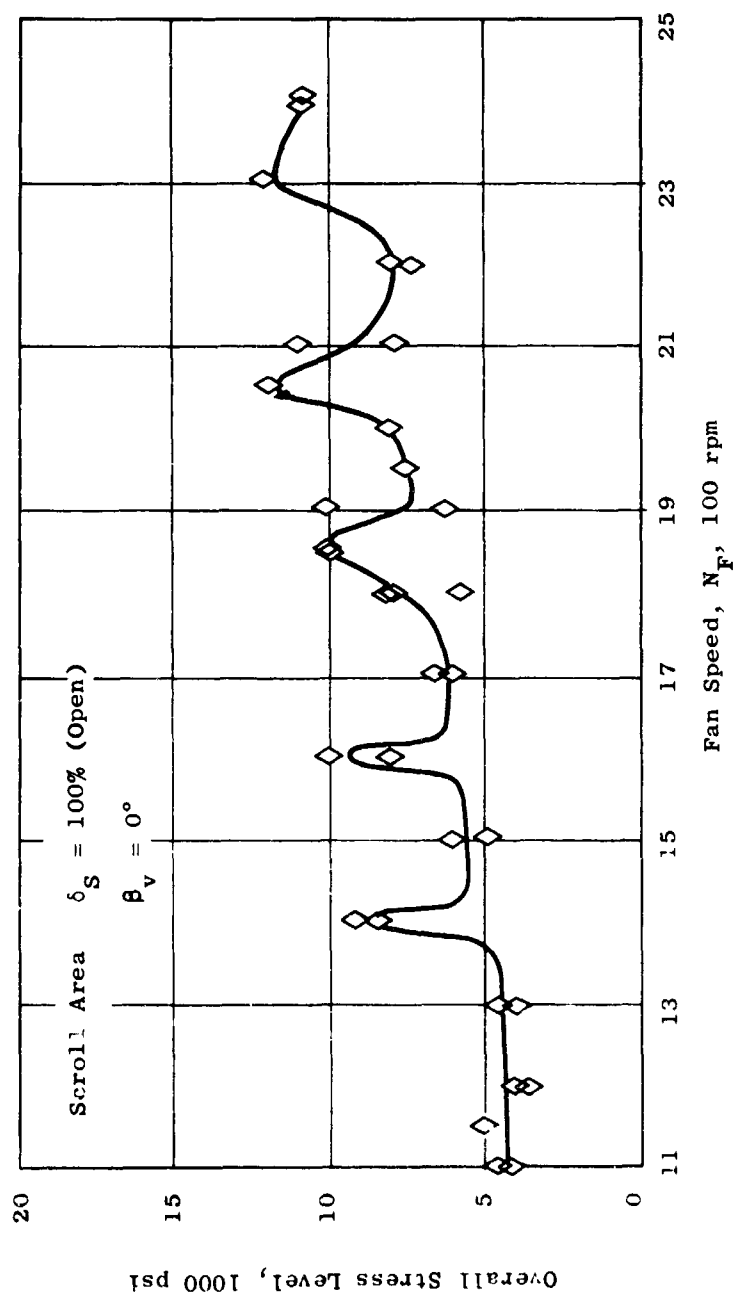


Figure 258. Overall Blade Stress Level Versus Fan Speed for Blade Gage 4,
 $\delta_S = 100$ Percent.

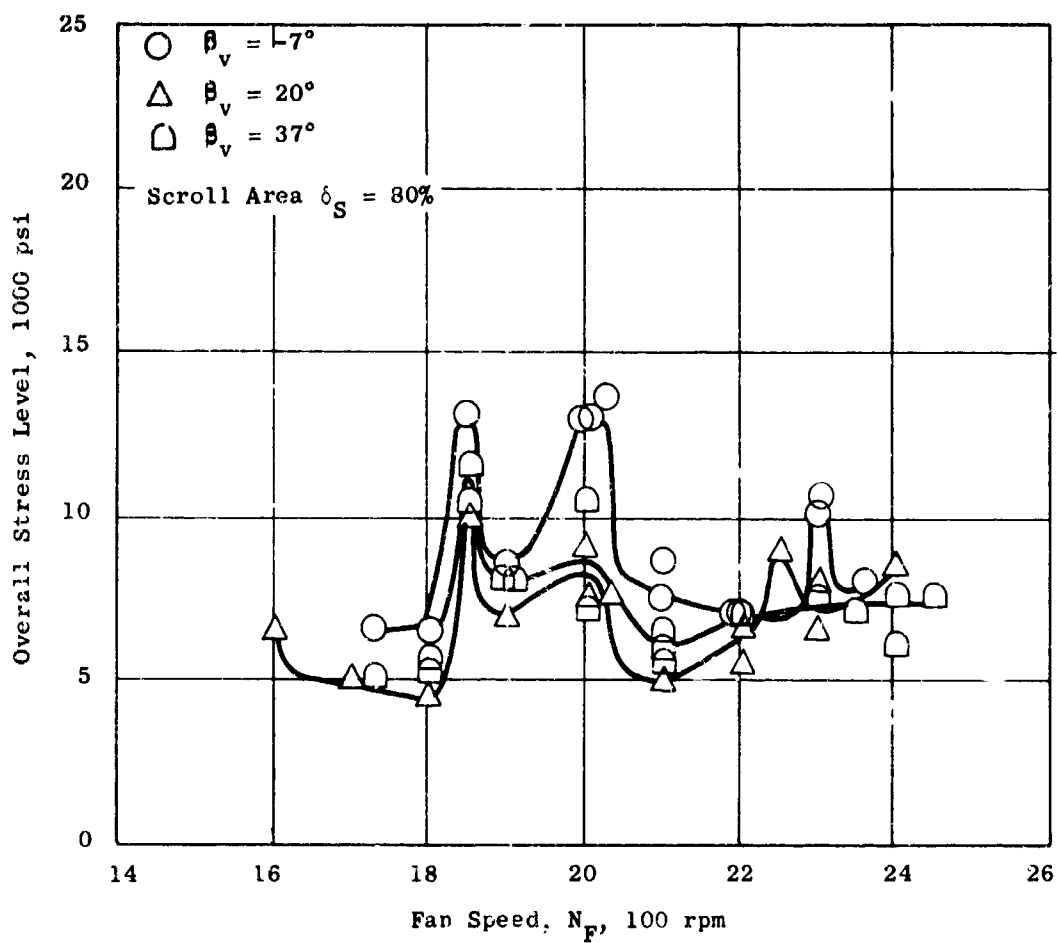


Figure 259. Overall Blade Stress Level Versus Fan Speed for Blade Gage 4, $\delta_S = 80$ Percent.

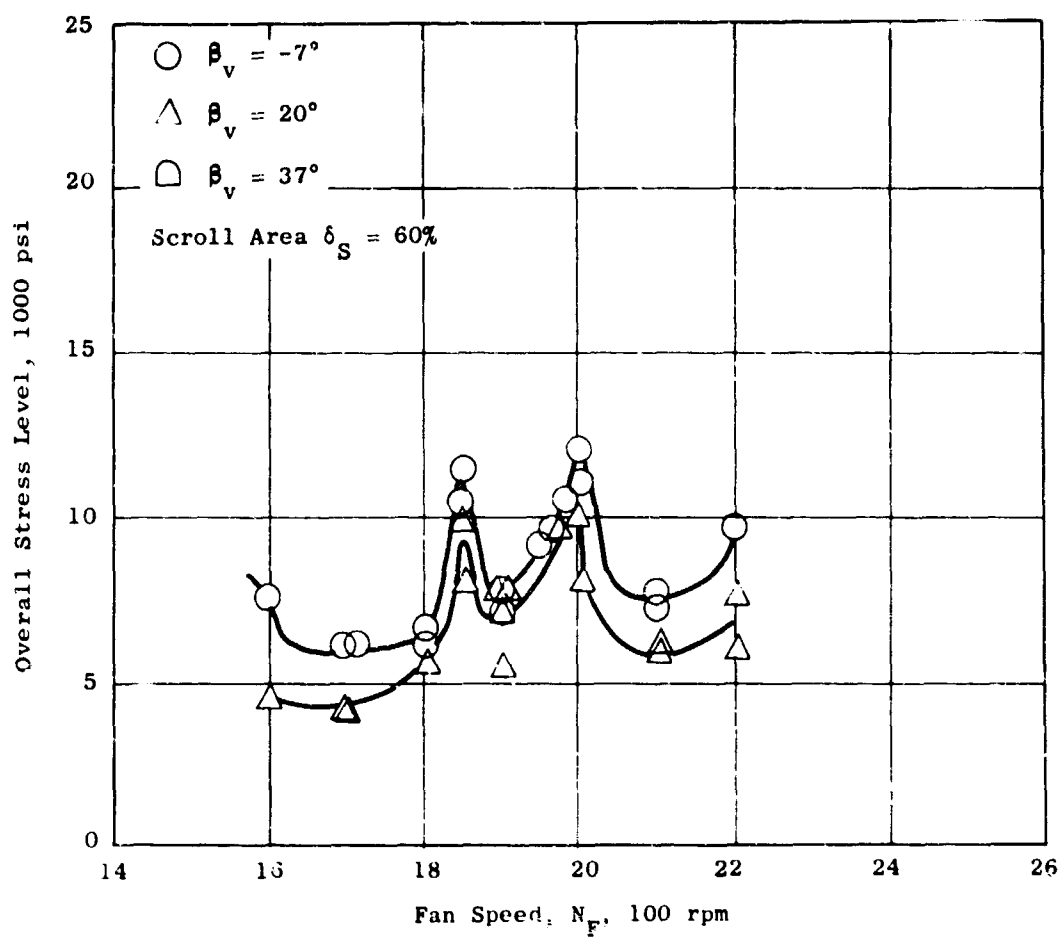


Figure 260. Overall Blade Stress Level Versus Fan Speed for Blade Gage 4, $\delta_S = 60$ Percent.

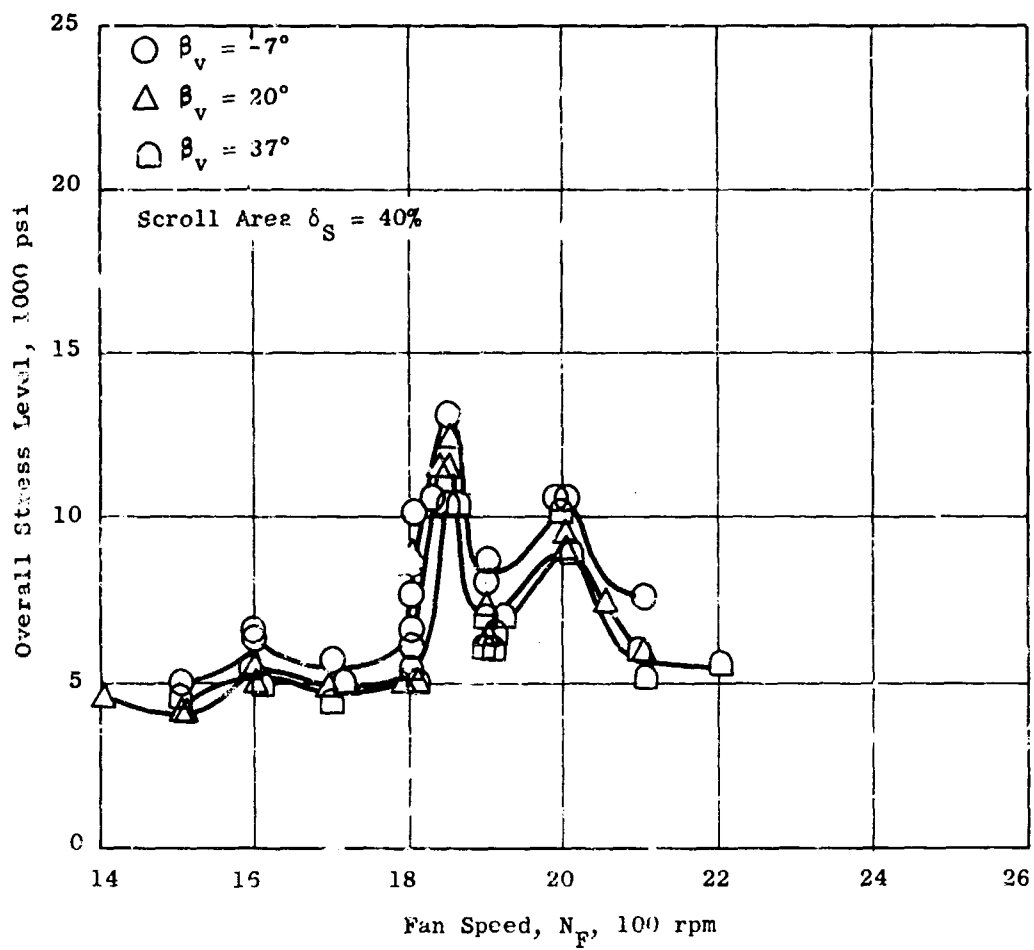


Figure 261. Overall Blade Stress Level Versus Fan Speed for Blade Gage 4, $\delta_s = 40$ Percent.

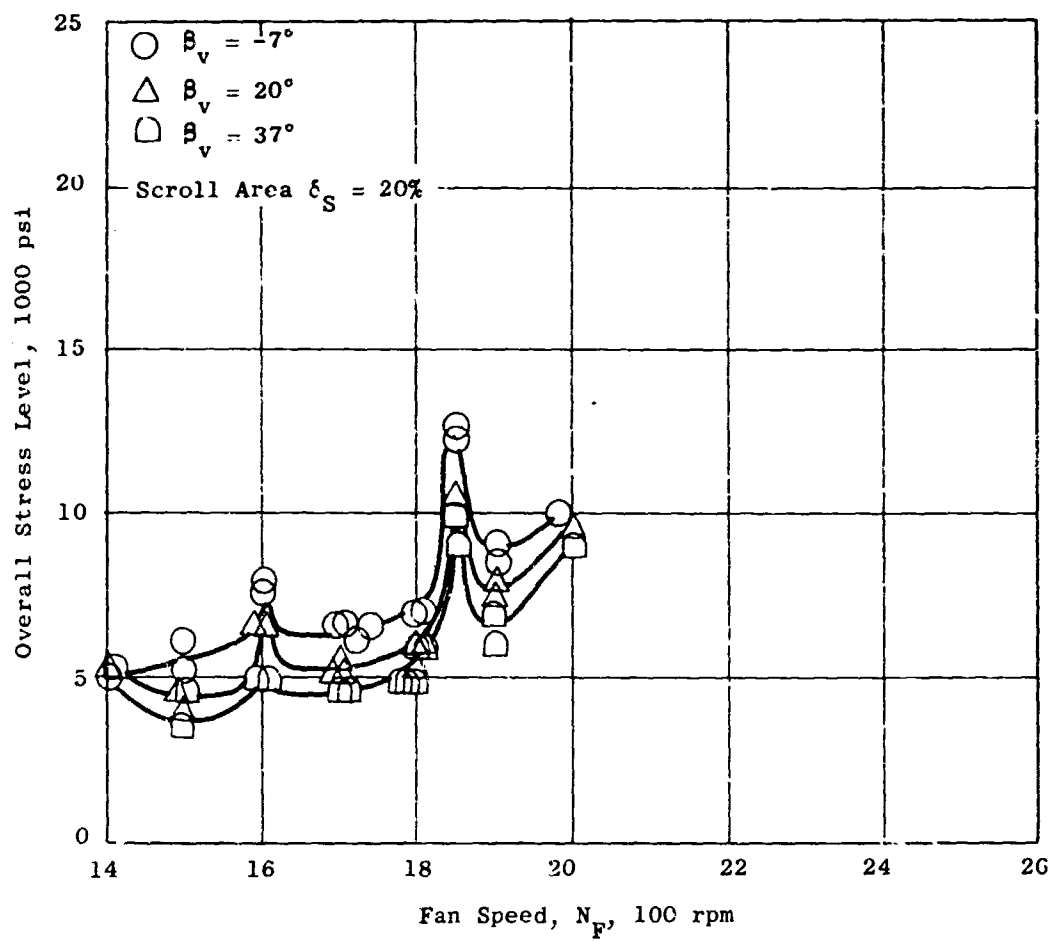


Figure 262. Overall Blade Stress Level Versus Fan Speed for Blade Gage 4, $\delta_S = 20$ Percent.

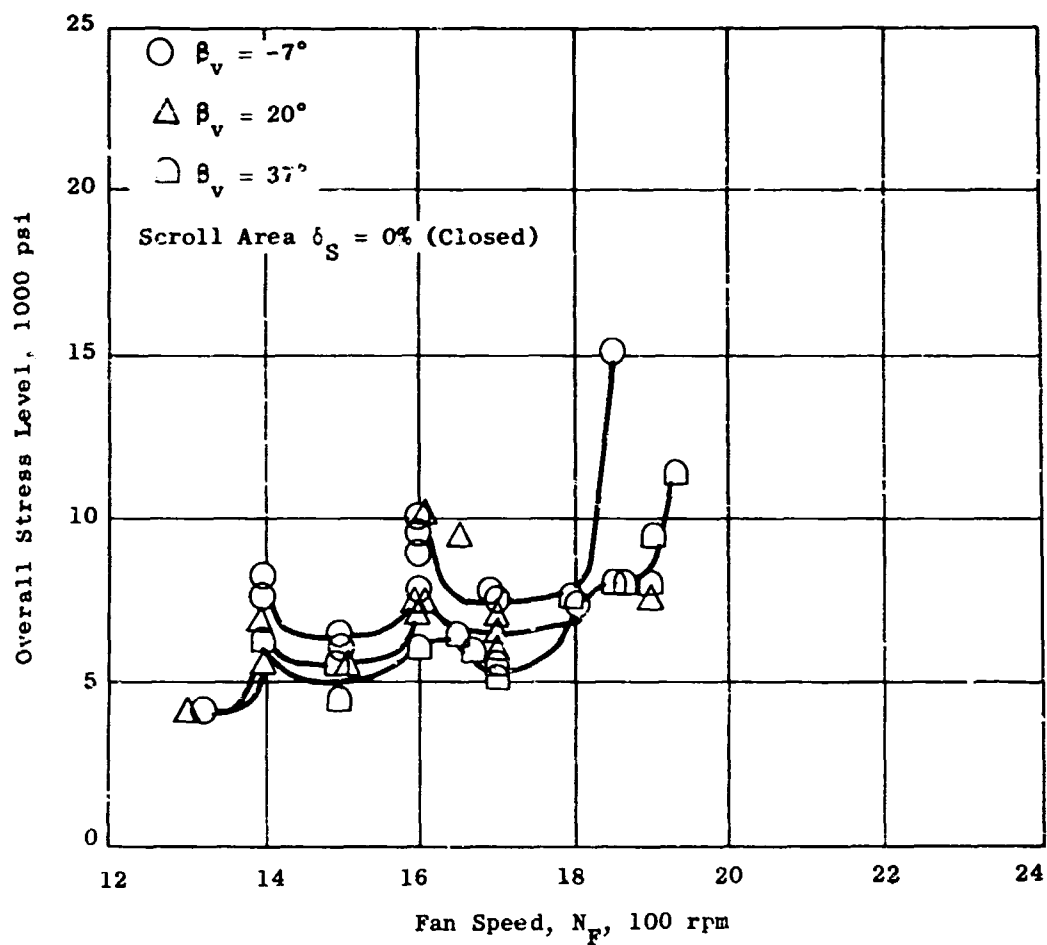


Figure 263. Overall Blade Stress Level Versus Fan Speed for Blade Gage 4, $\delta_s = 0$ Percent.

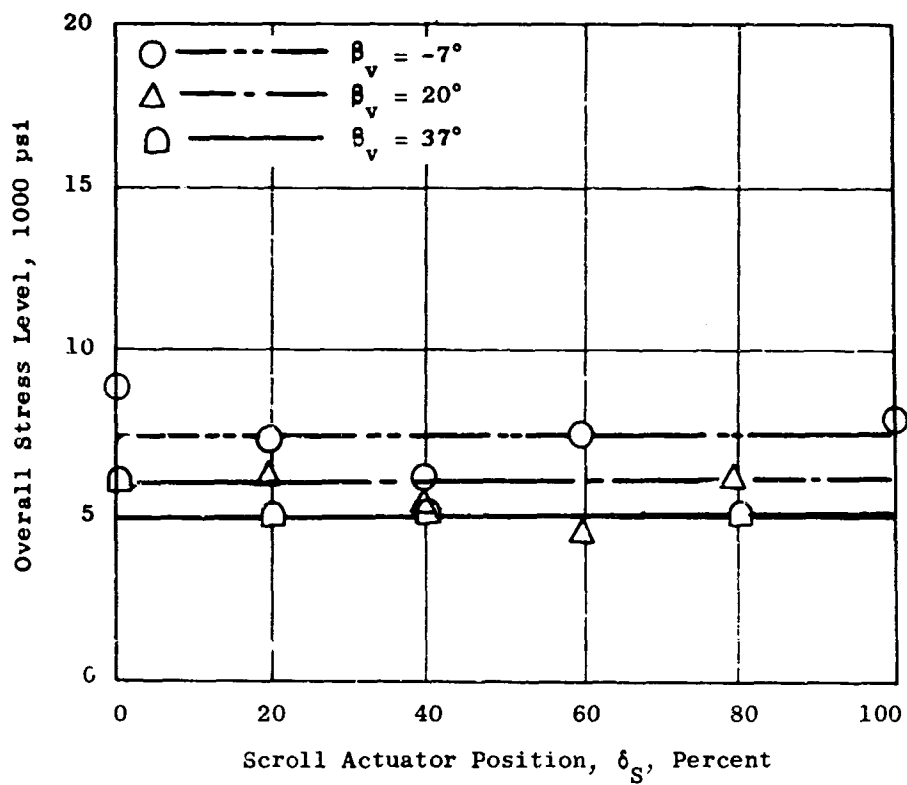


Figure 264. Peak Blade Stress at 1610 rpm Versus Scroll Actuator Position for Blade Gage 4. Blade First Flexural Frequency With 12-Per-Revolution Excitation.

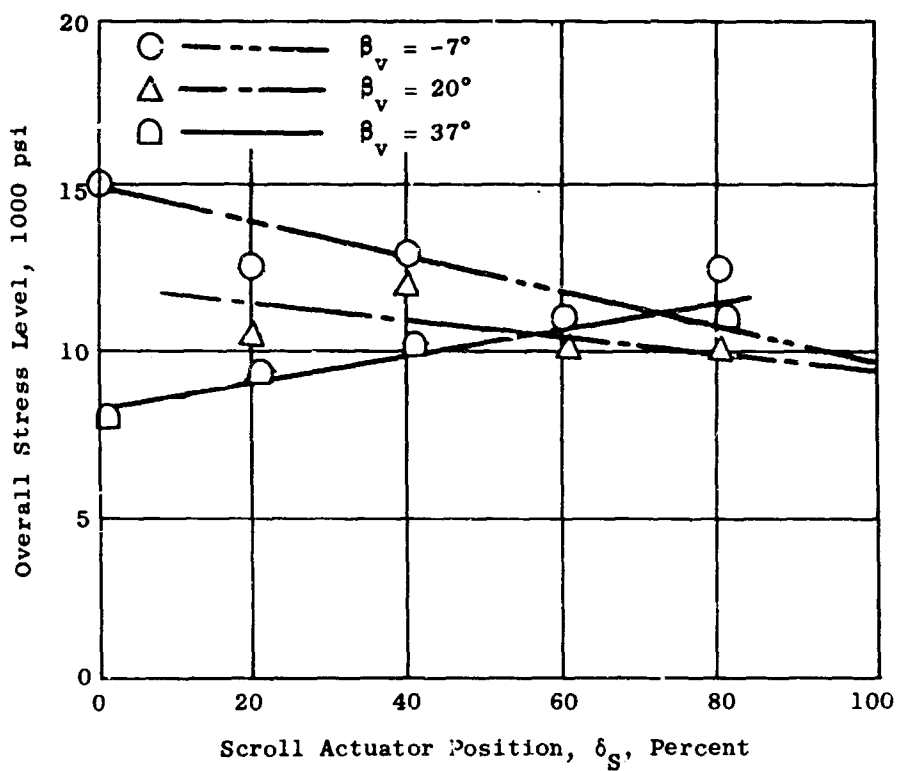


Figure 265. Peak Blade Stress at 1850 rpm Versus Scroll Actuator Position for Blade Gage 4. Blade Second Flexural Frequency With 16-Per-Revolution Excitation.

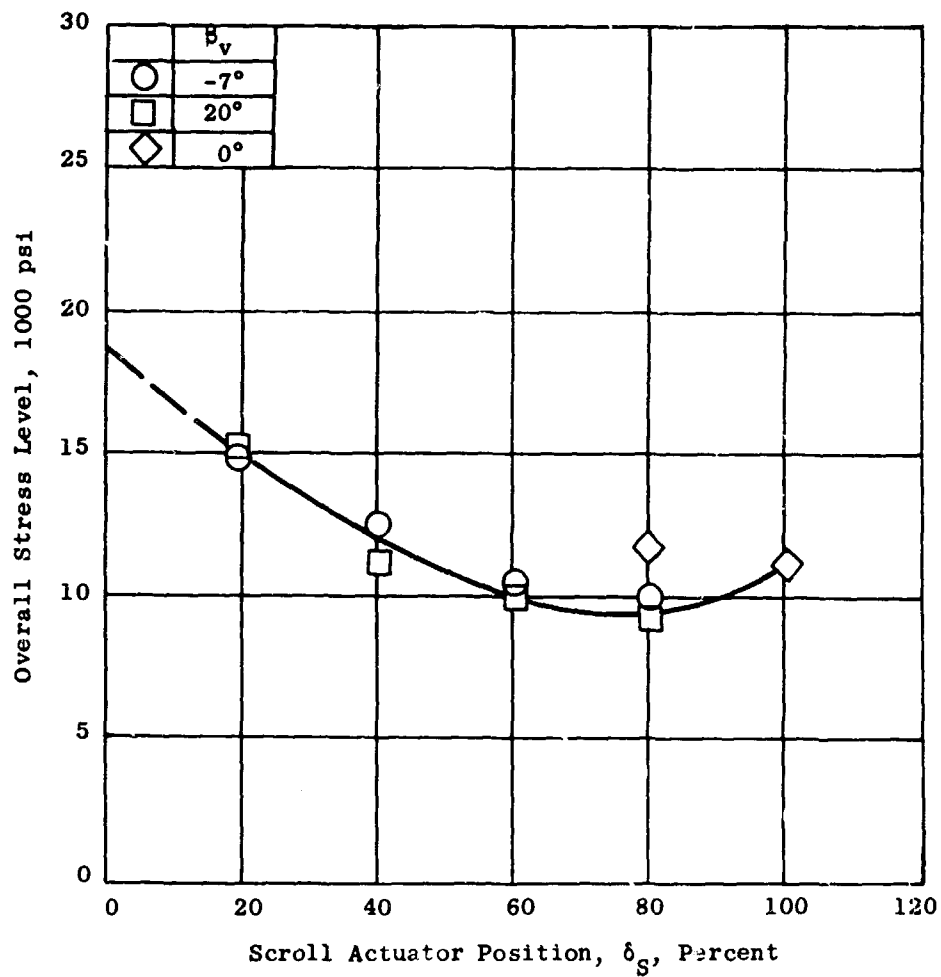


Figure 266. Peak Blade Stress at 1960 rpm Versus Scroll Actuator Position for Blade Gage 1. Wheel 39 Mode Critical Speed.

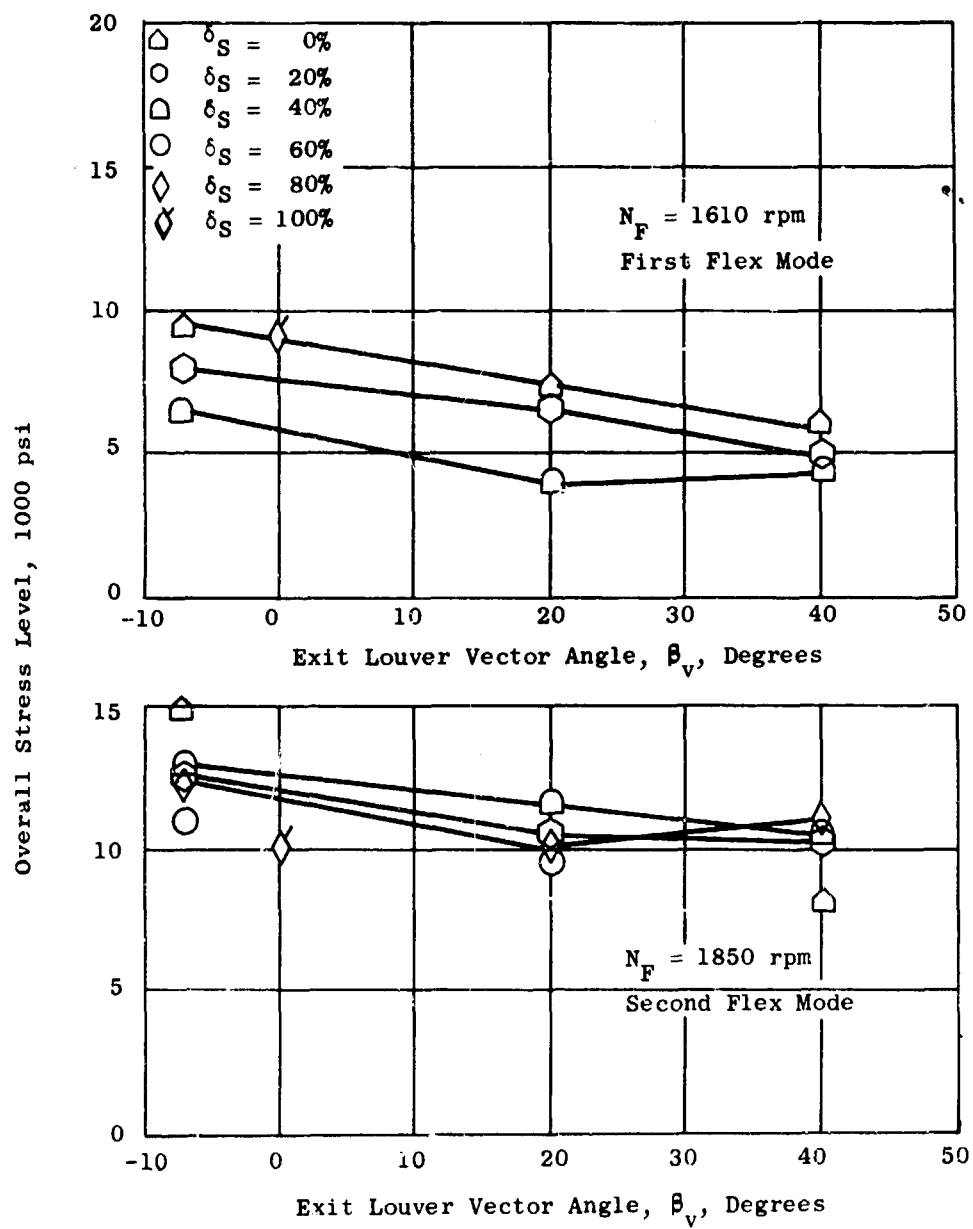


Figure 267. Peak Blade Stress Level in First Flexural and Second Flexural Modes Versus Exit Louver Vector Angle for Blade Gage 4.

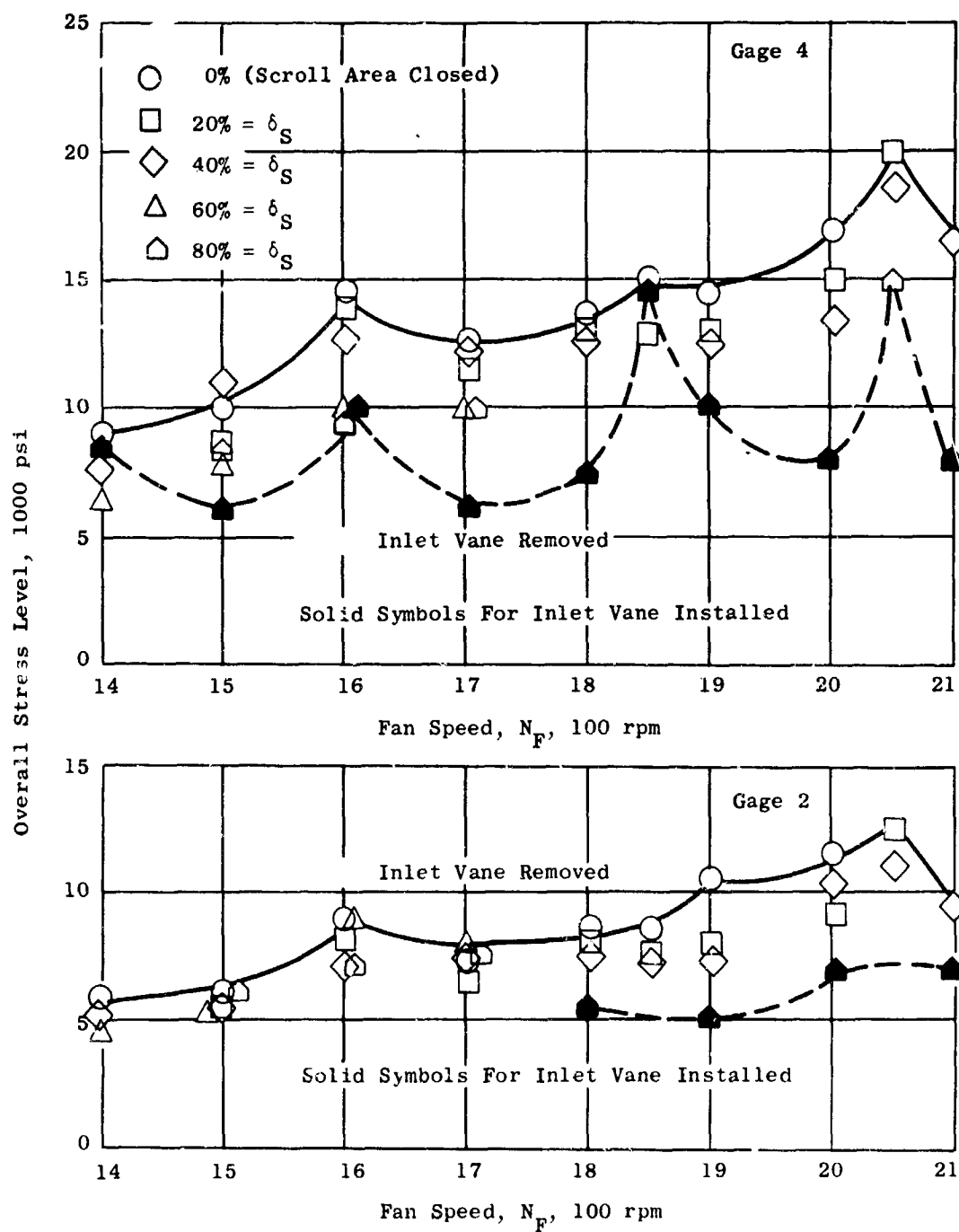


Figure 268. Overall Blade Stress Level Versus Fan Speed to Show Effect of Removing the Inlet Vane.

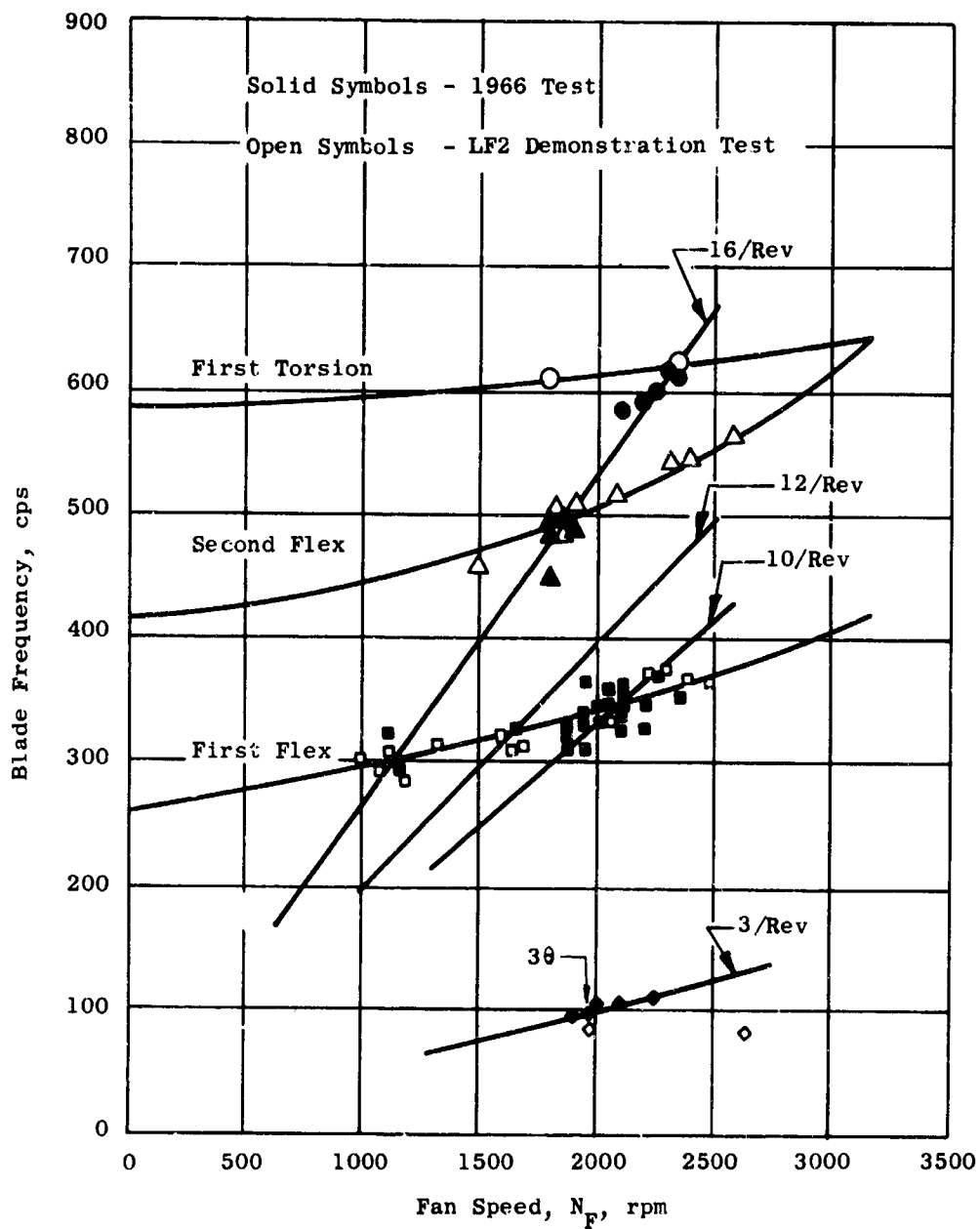


Figure 269. Campbell Diagram of LF2 Blade.

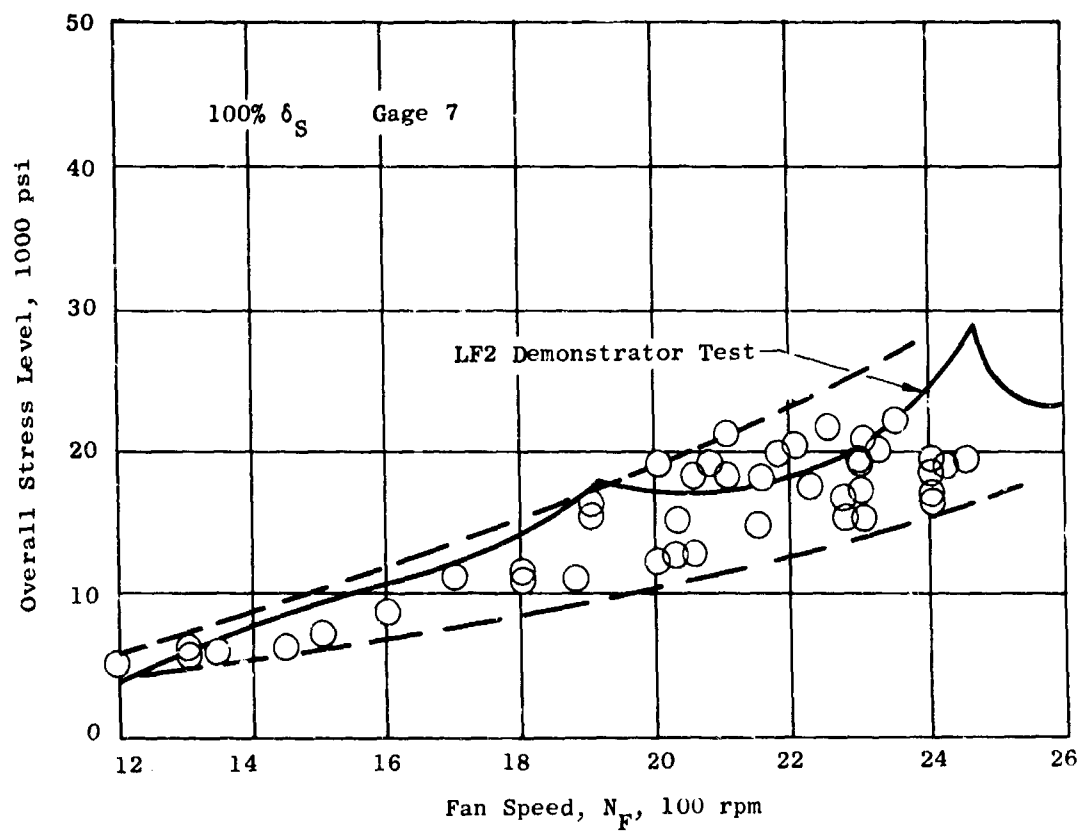


Figure 270. Turbine Bucket Overall Stress Level Versus Fan Speed From Run 7 LF2/VAS Test and From LF2 Demonstrator Test.

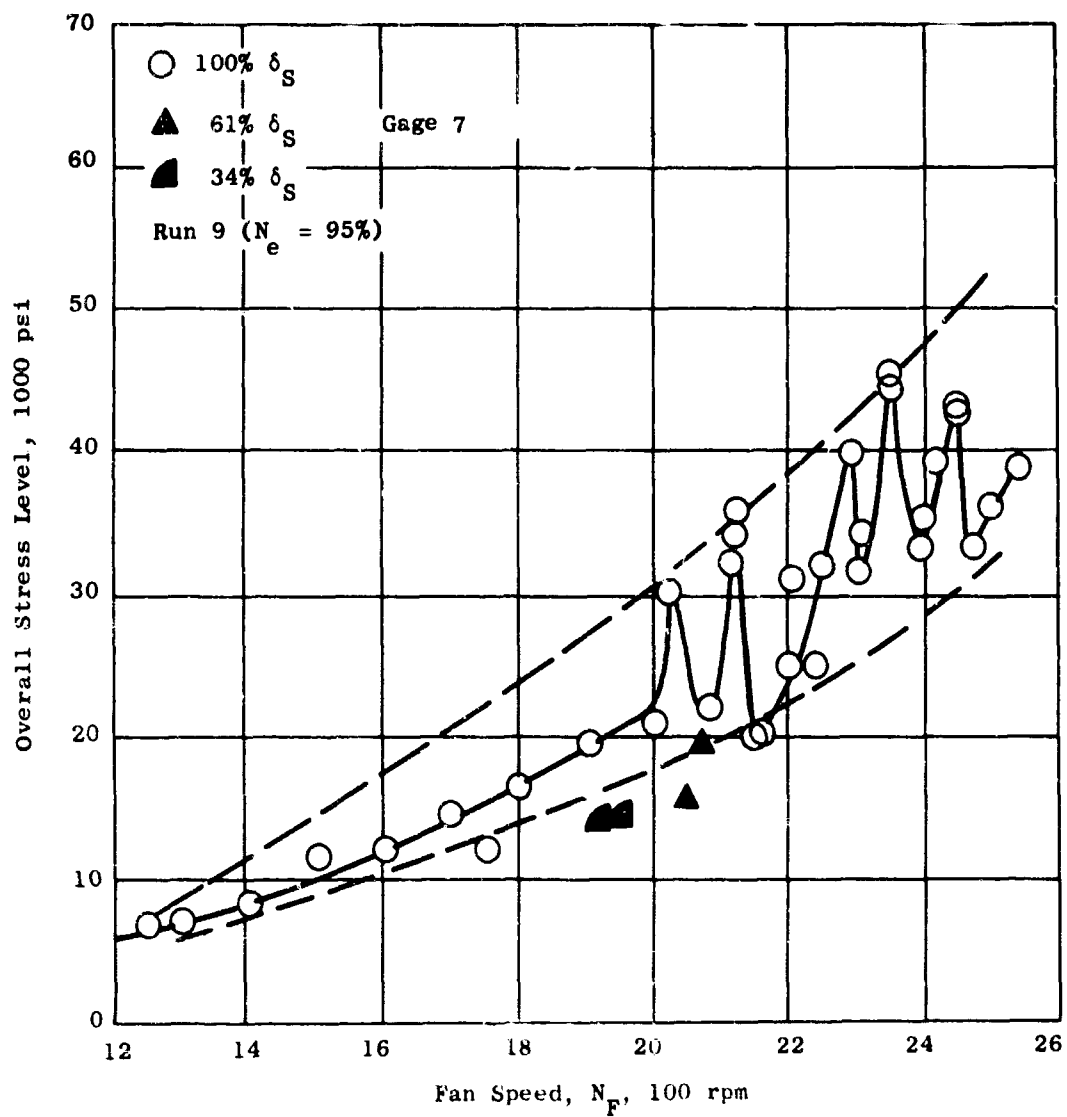


Figure 271. Turbine Bucket Overall Stress Level Versus Fan Speed for 100-Percent Open Scroll Area and for Reduced Scroll Area at 95-Percent Engine Speed.

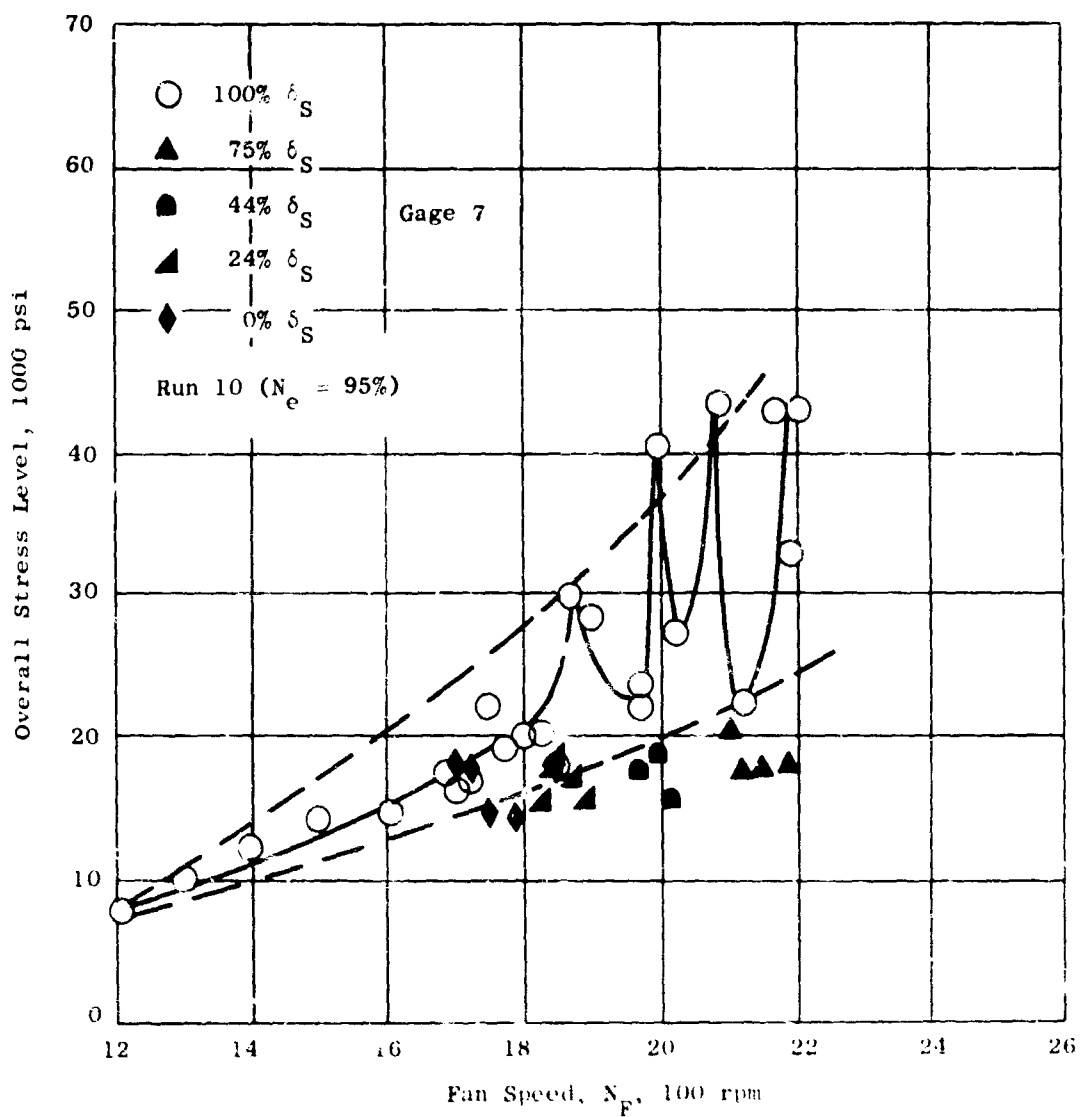


Figure 272. Turbine Bucket Overall Stress Level Versus Fan Speed at 100-Percent Open Scroll Area and at Reduced Scroll Areas for 95-Percent Engine Speed.

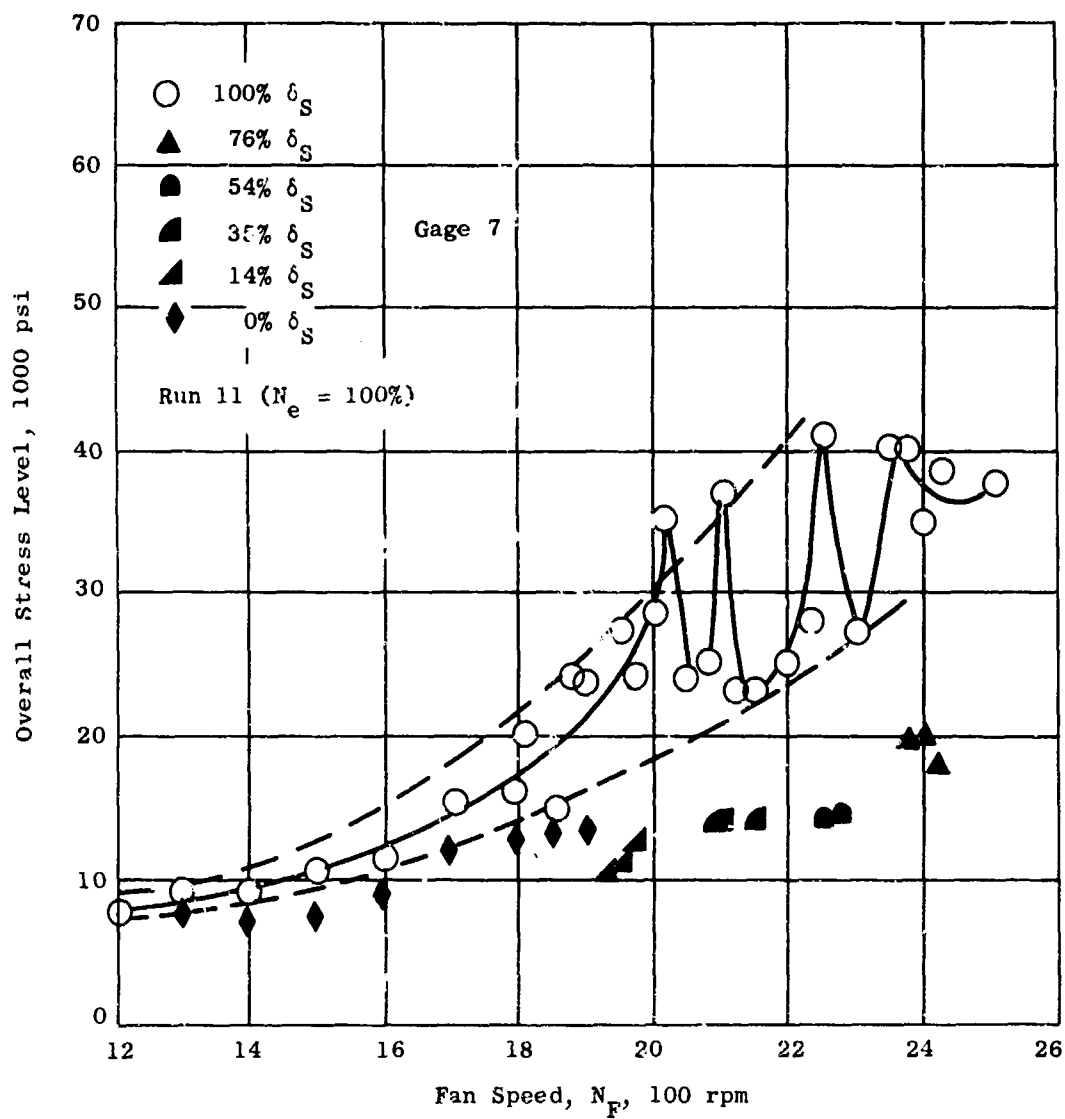


Figure 273. Turbine Bucket Overall Stress Level Versus Fan Speed for 100-Percent Open and 0-Percent Open Scroll Areas With Intermediate Areas for 100-Percent Engine Speed.

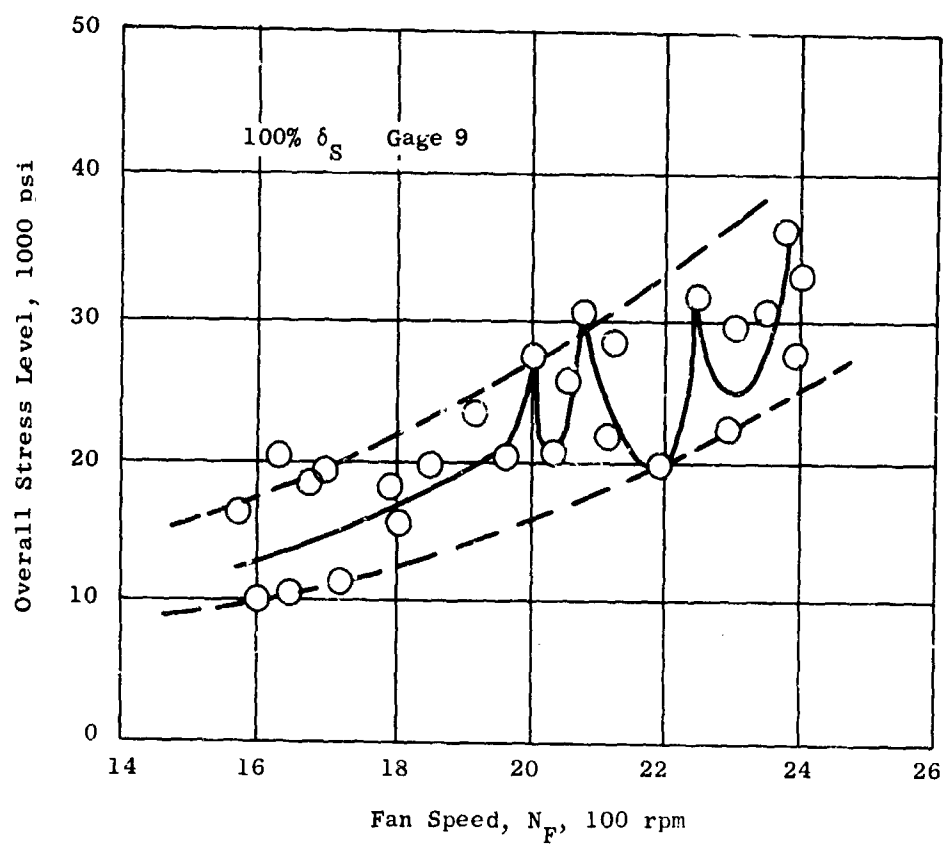


Figure 274. Turbine Bucket Overall Stress Level Versus Fan Speed for 100-Percent Open Scroll Area.

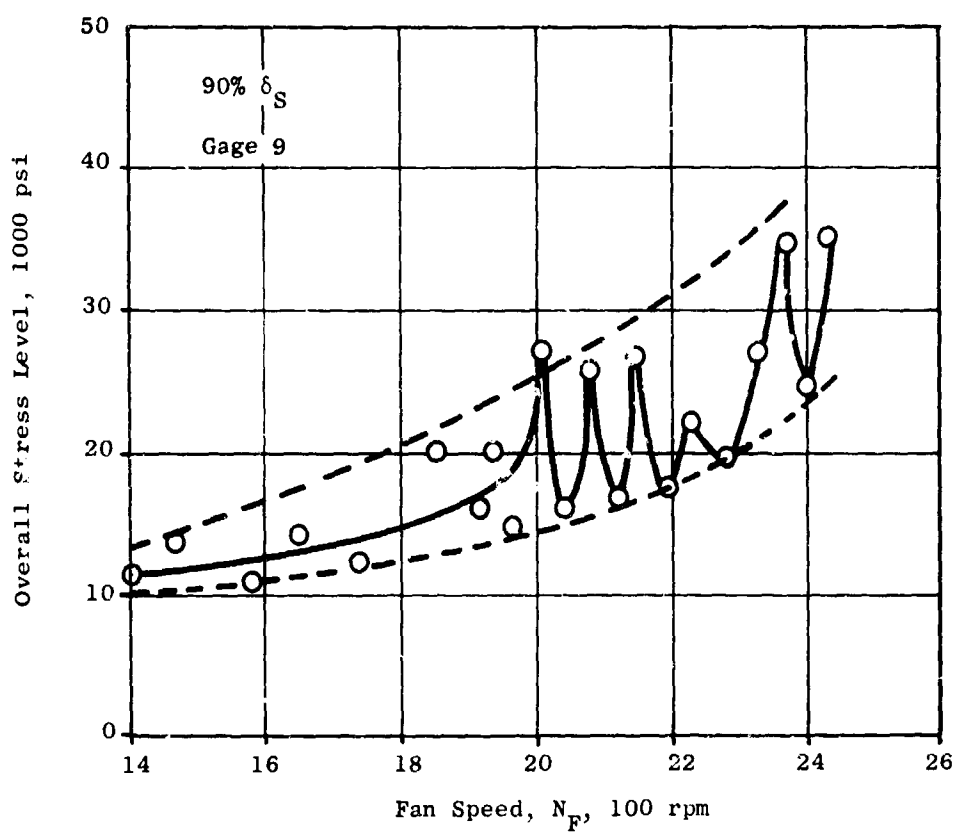


Figure 275. Turbine Bucket Overall Stress Level Versus Fan Speed for 90-Percent Open Scroll Area.

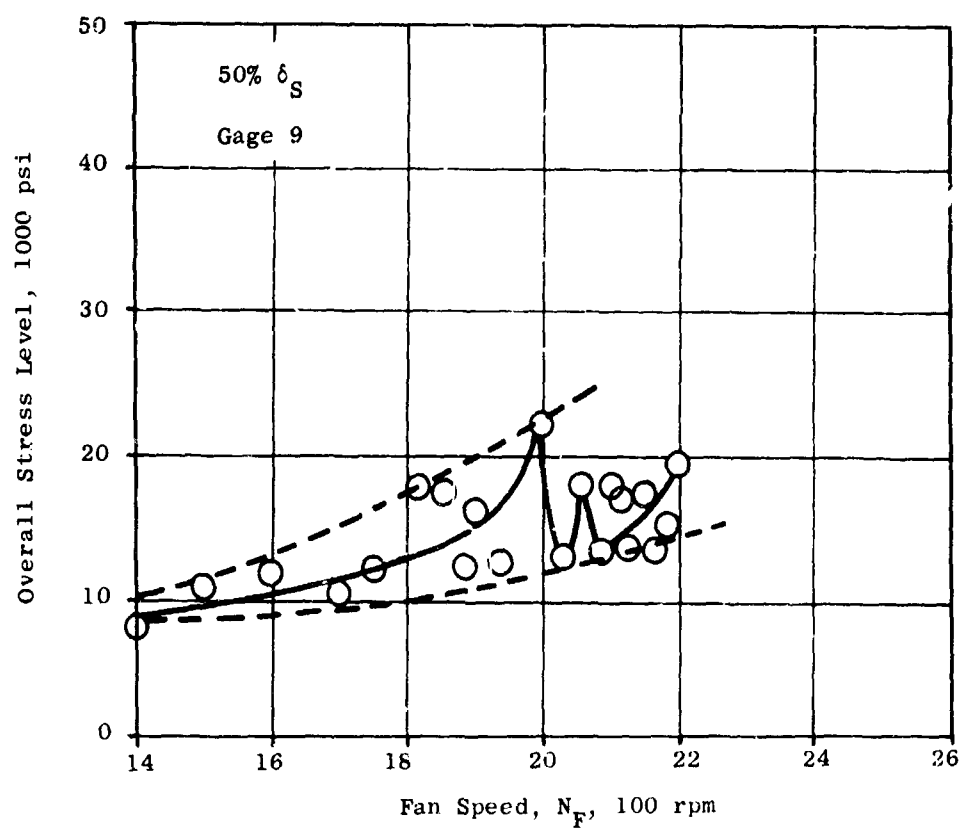


Figure 276. Turbine Bucket Overall Stress Level Versus Fan Speed for 50-Percent Open Scroll Area.

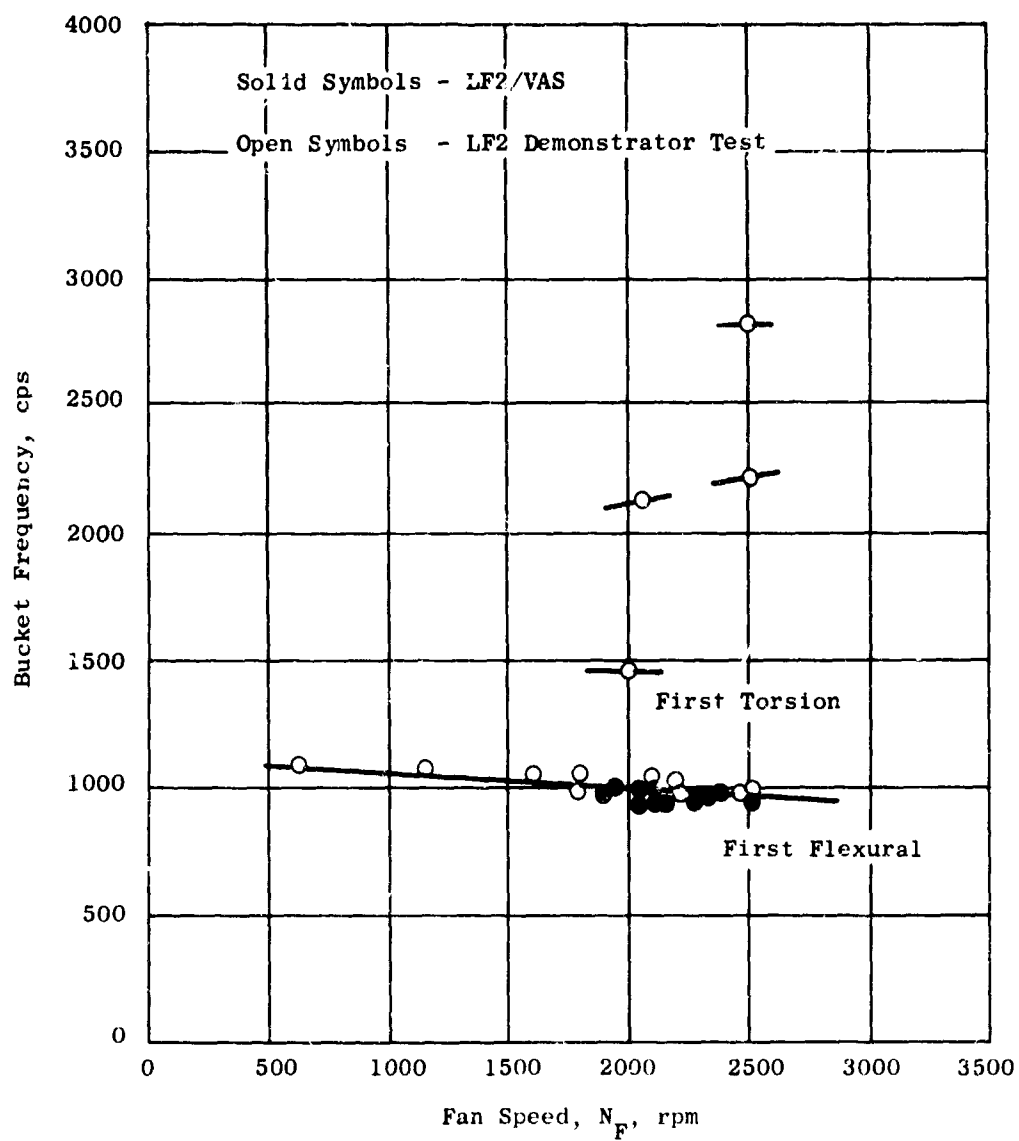


Figure 277. Turbine Bucket Predominant Vibratory Frequency Versus Fan Speed.

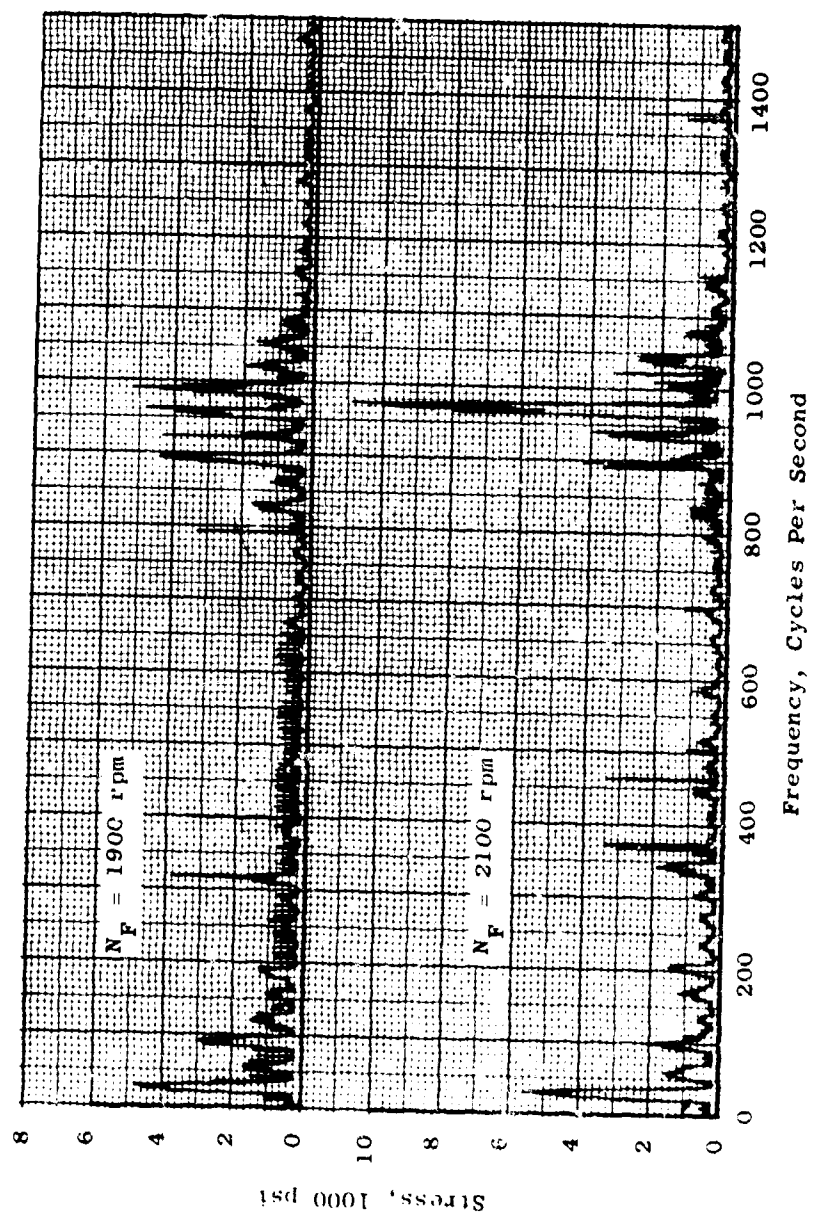


Figure 278. Turbine Bucket Gage 7 Spectrum Analysis, 1900 and 2100 rpm.

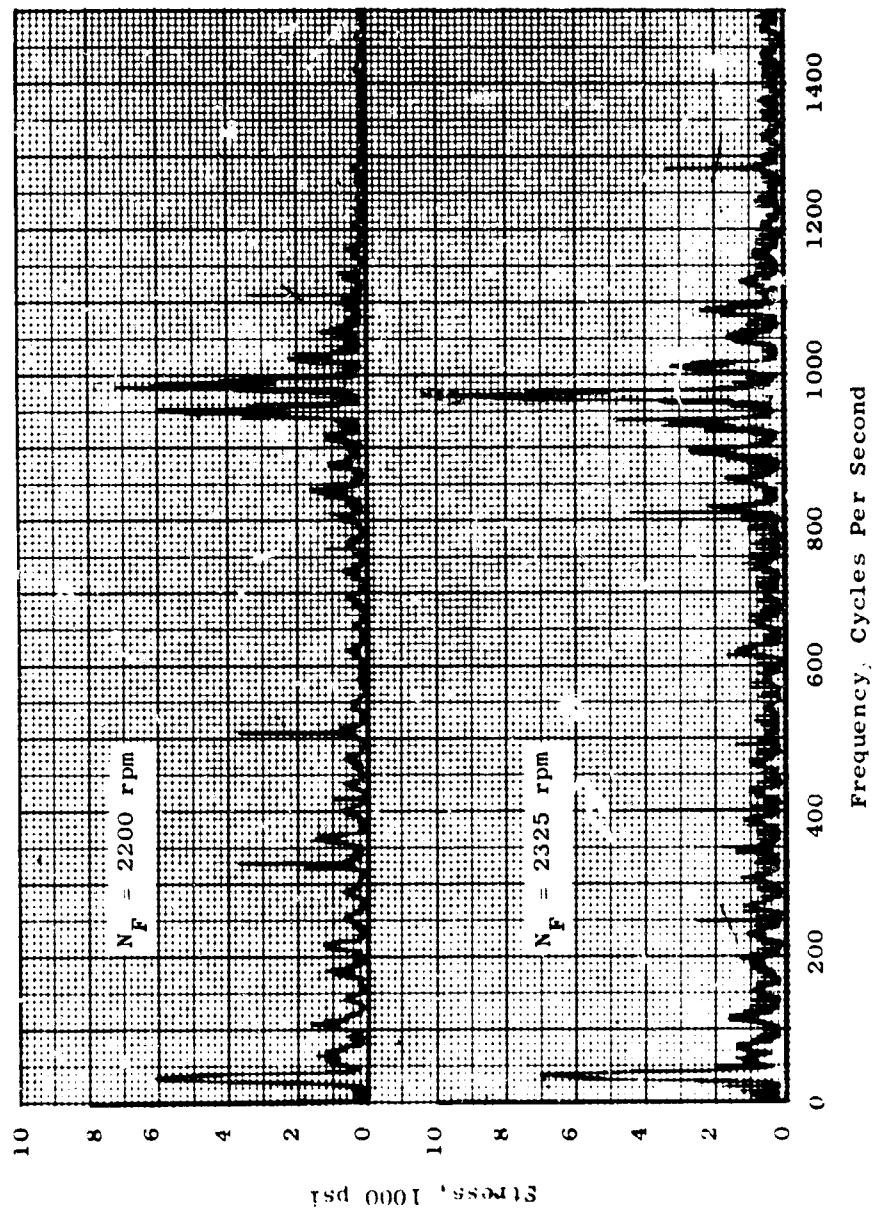


Figure 279. Turbine Bucket Gage 7 Spectrum Analysis, 2200 and 2325 rpm.

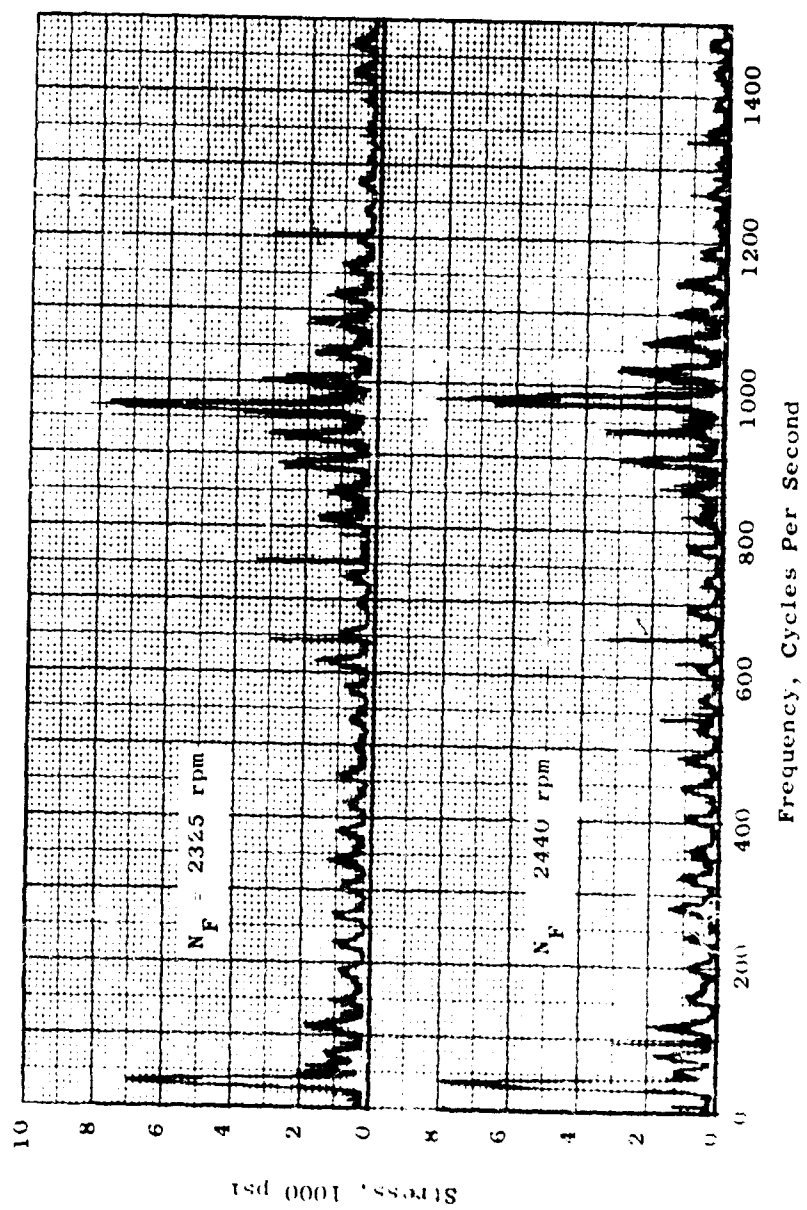


Figure 280. Turbine Bucket Gage 7 Spectrum Analysis, 2325 and 2440 rpm.

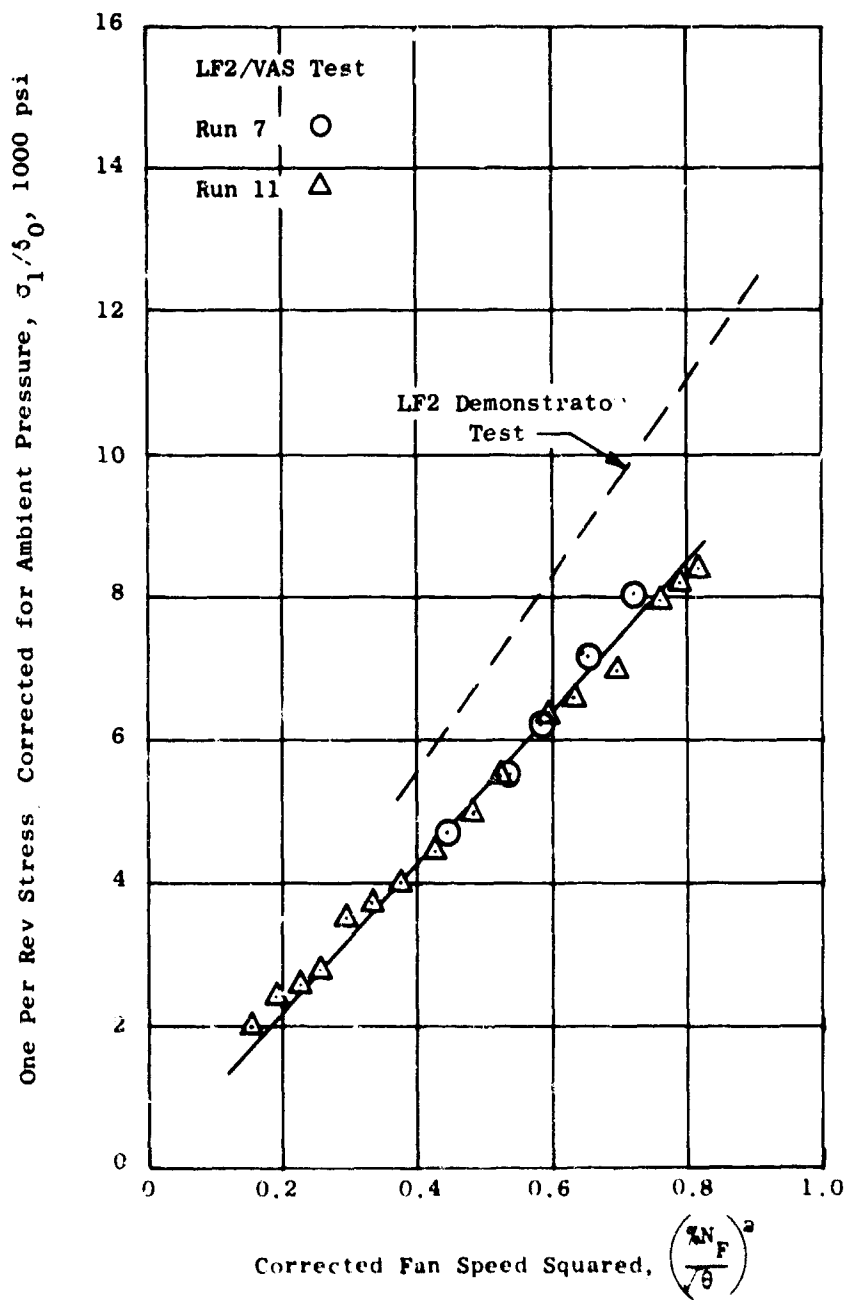


Figure 281. Turbine Bucket One-Per-Revolution Stress Levels, Gage 7.

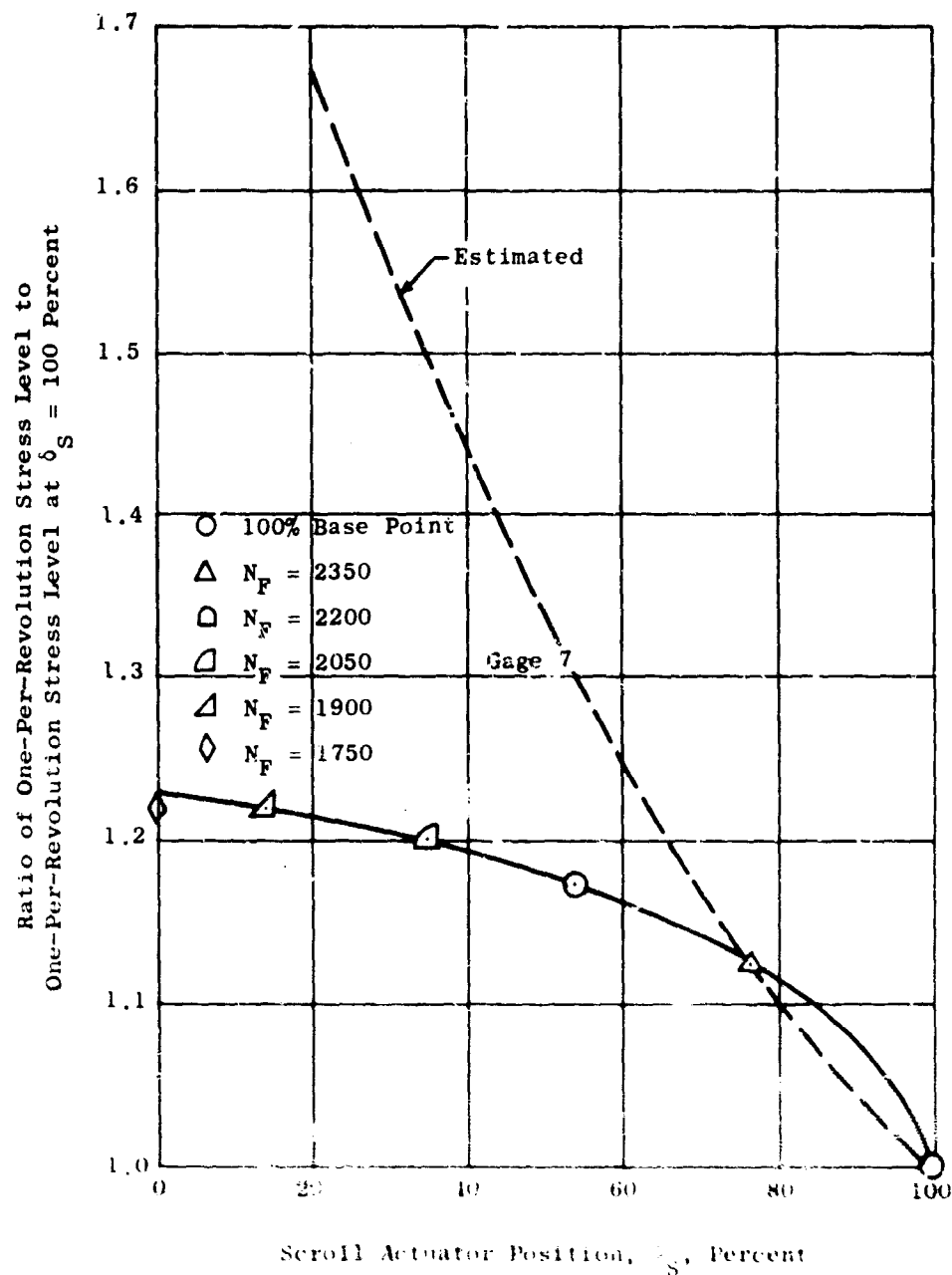


Figure 282. Ratio of Turbine Bucket One-Per-Revolution Stress Component at Reduced Scroll Areas to the One-Per-Revolution Stress Level at 100-Percent Open Area.

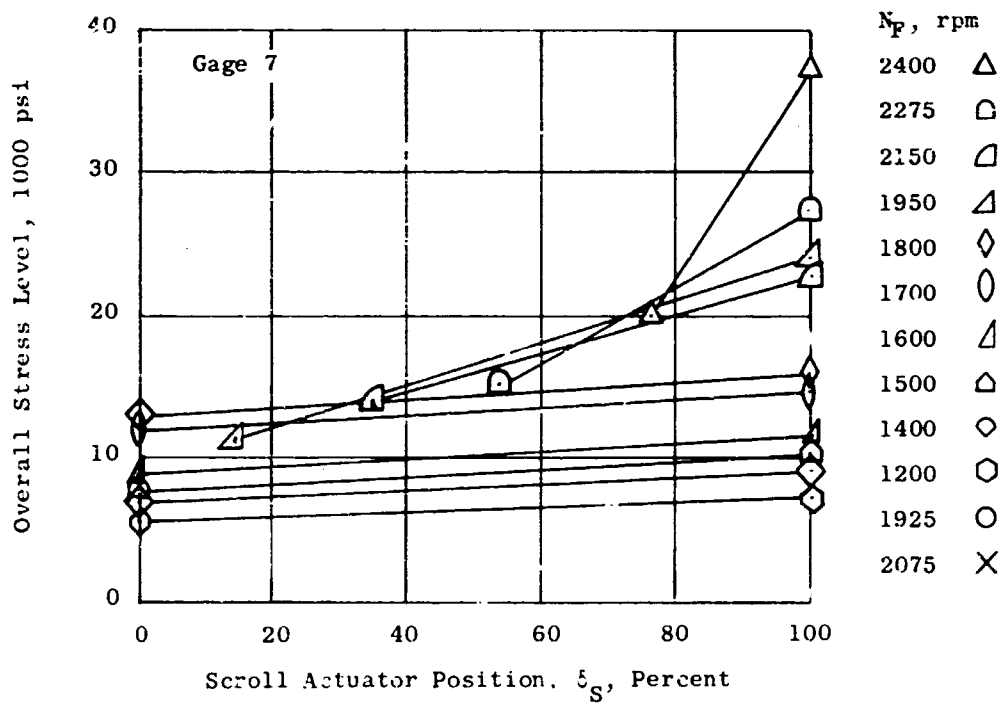
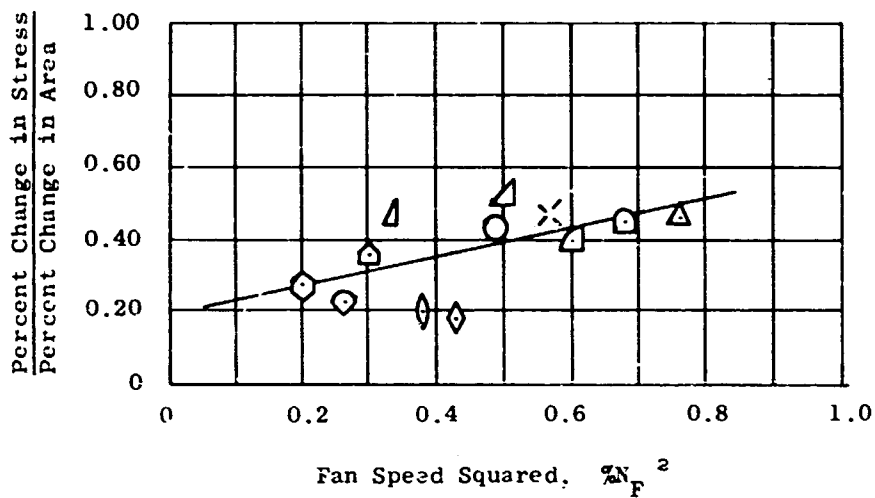
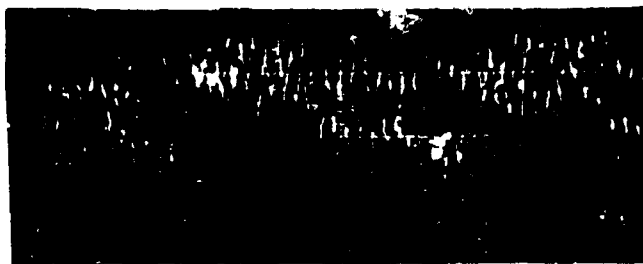


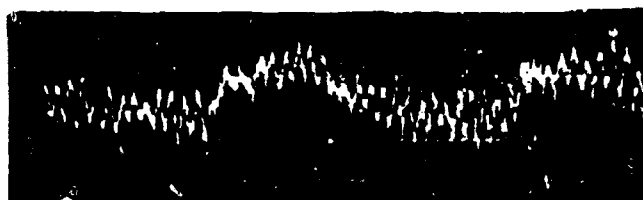
Figure 283. Turbine Bucket Overall Stress Level Versus Scroll Actuator Position and Ratio of Percent Change in Stress to Percent Change in Scroll Area Versus Fan Speed Squared.

$N_F = 2490 \text{ rpm}$



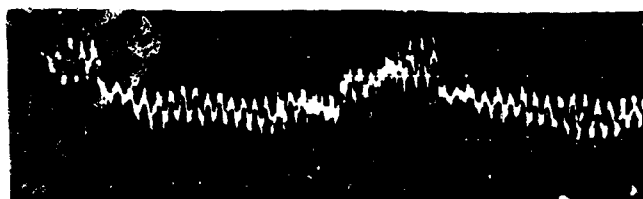
$\delta_S = 100\%$

$N_F = 2370 \text{ rpm}$



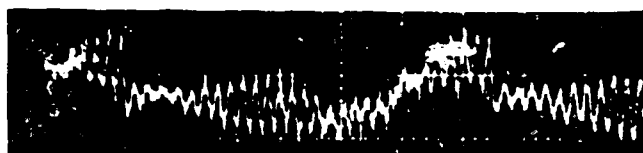
$\delta_S = 76\%$

$N_F = 2110 \text{ rpm}$



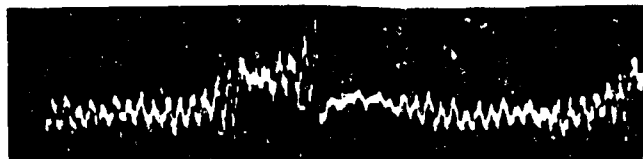
$\delta_S = 35\%$

$N_F = 1935 \text{ rpm}$



$\delta_S = 14\%$

$N_F = 1830 \text{ rpm}$



$\delta_S = 0\%$

Figure 284. Effect of Scroll Area on Turbine Bucket Stress Wave Form, Gage 7.

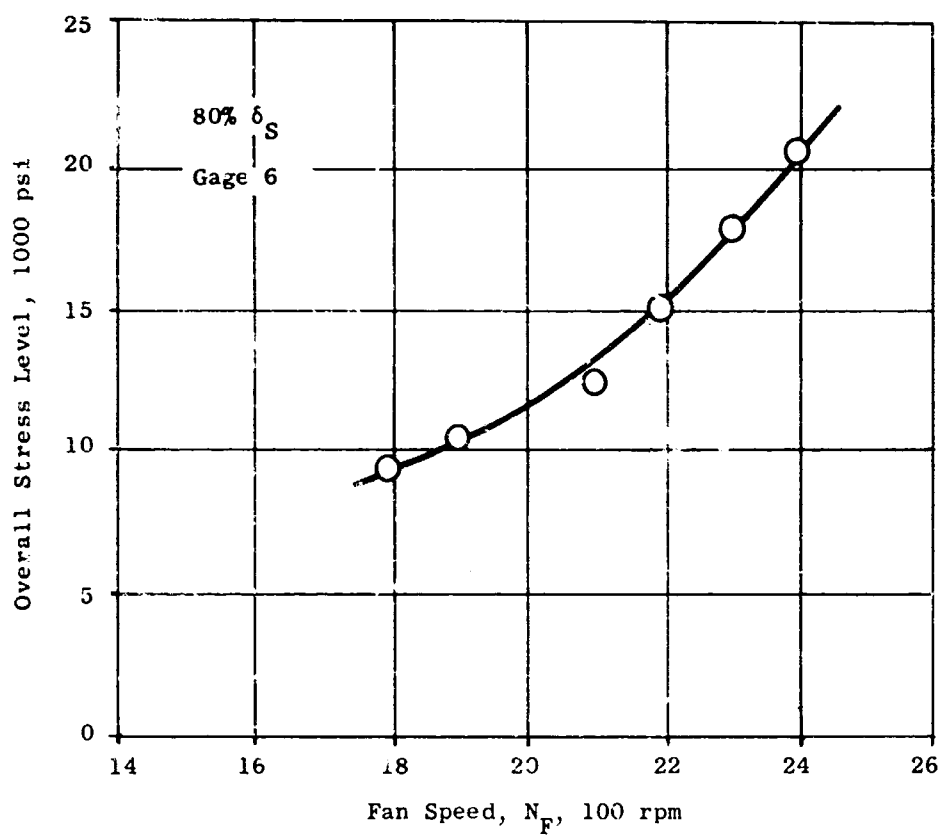


Figure 285. Torque Band Overall Stress Level Versus Fan Speed for 80-Percent Open Scroll Area.

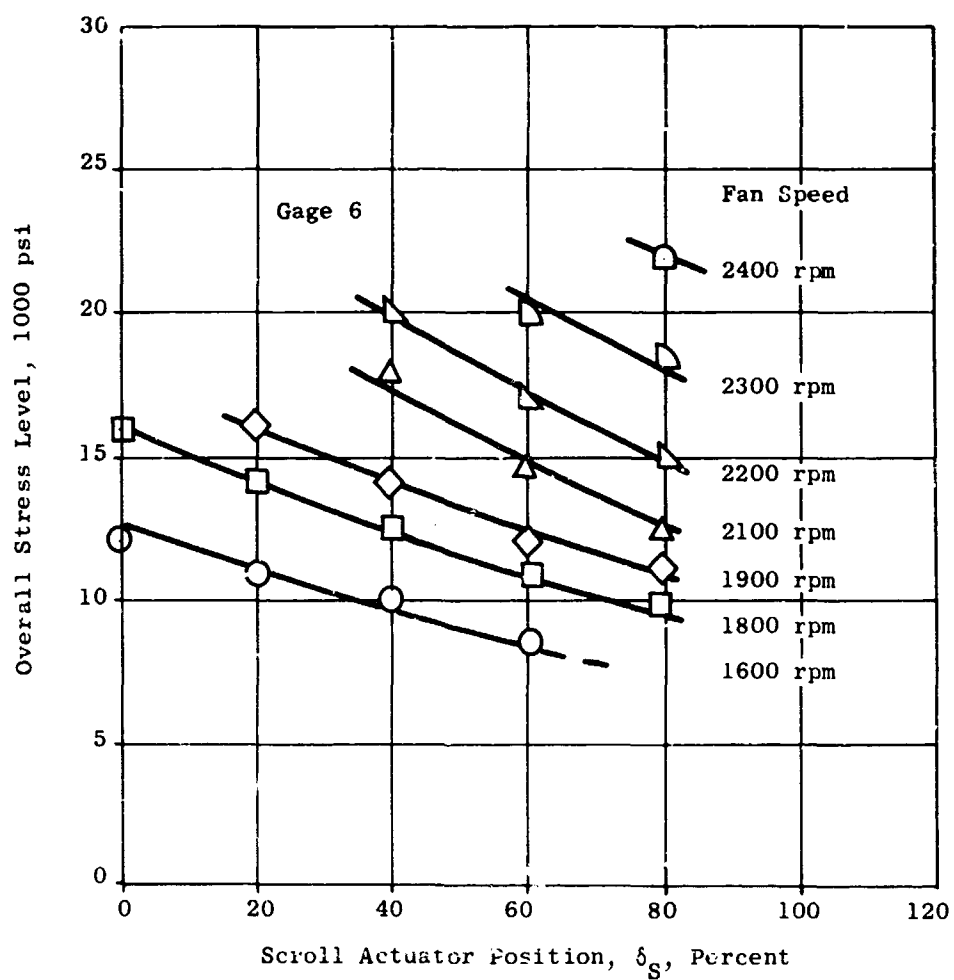


Figure 286. Torque Band Overall Stress Level Versus Scroll Actuator Position for Constant Fan Speed.

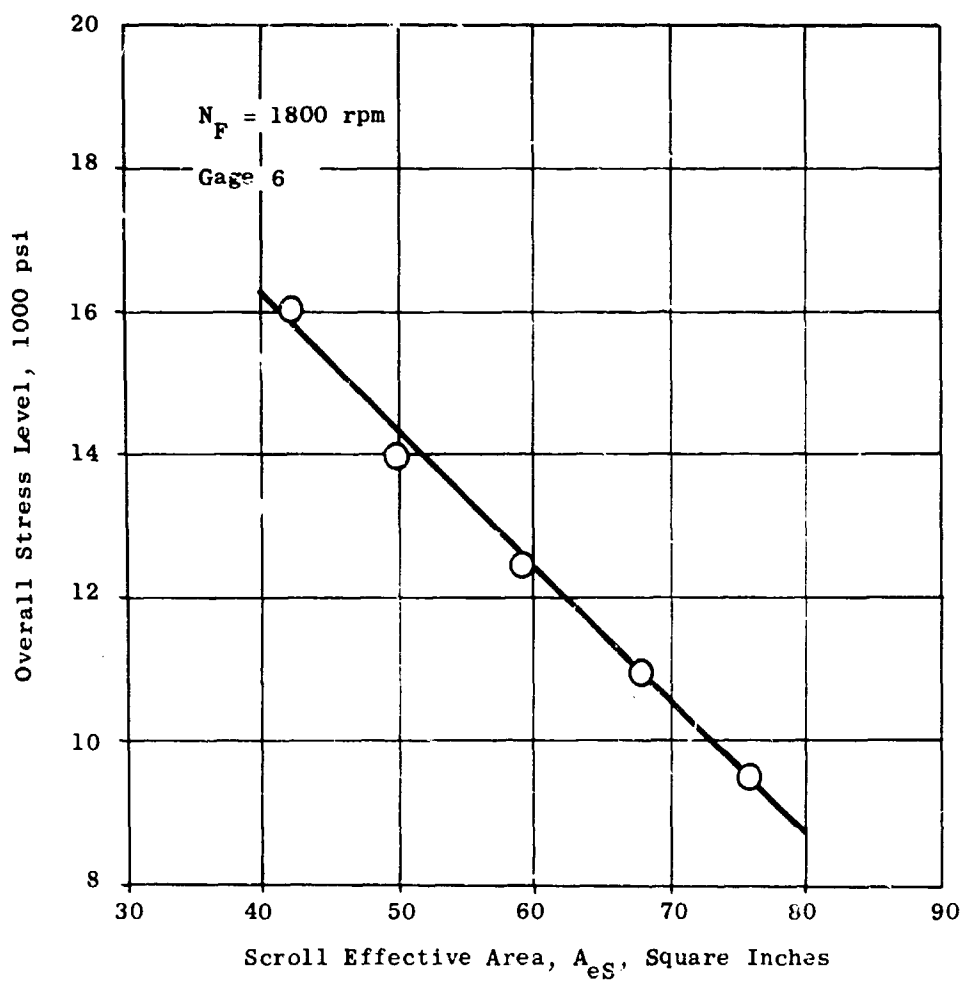


Figure 287. Torque Band Overall Stress Level Versus Scroll Effective Area.

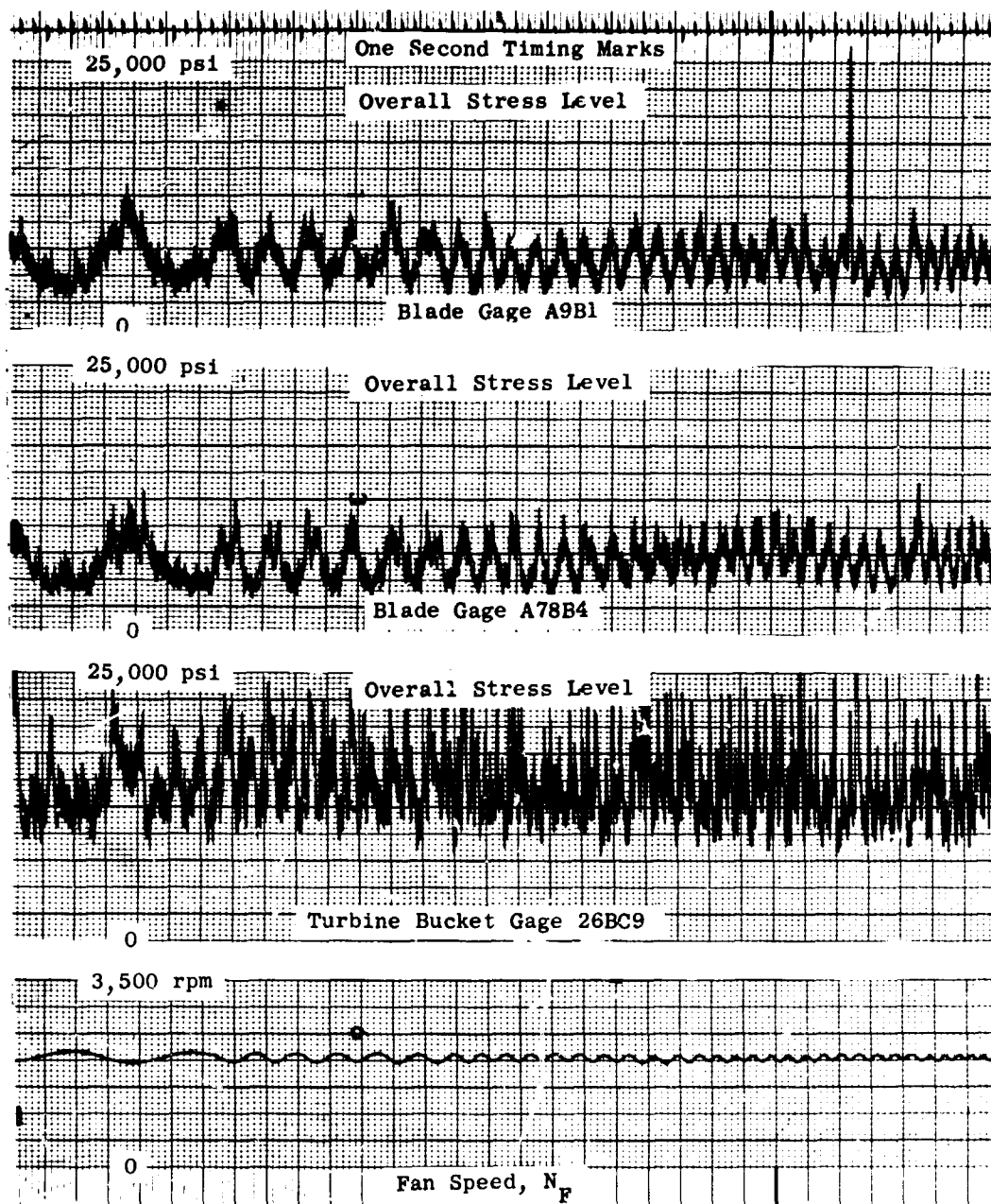


Figure 288. Rotor Stress Transient Response, Scroll Actuator Sine Wave Input, $\delta_S = 50 \pm 20$ Percent.

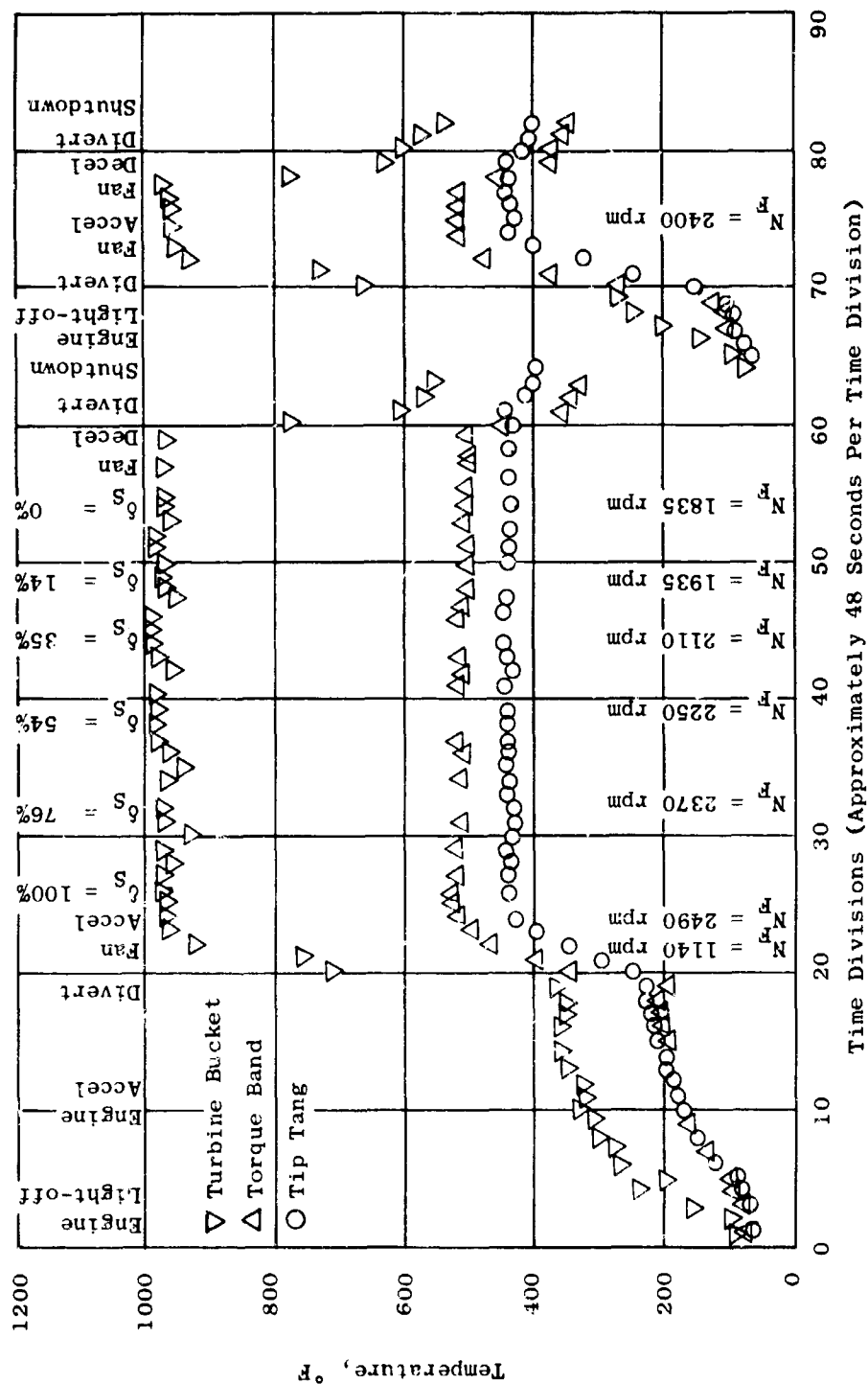


Figure 289. Time History of Rotor Component Temperatures.

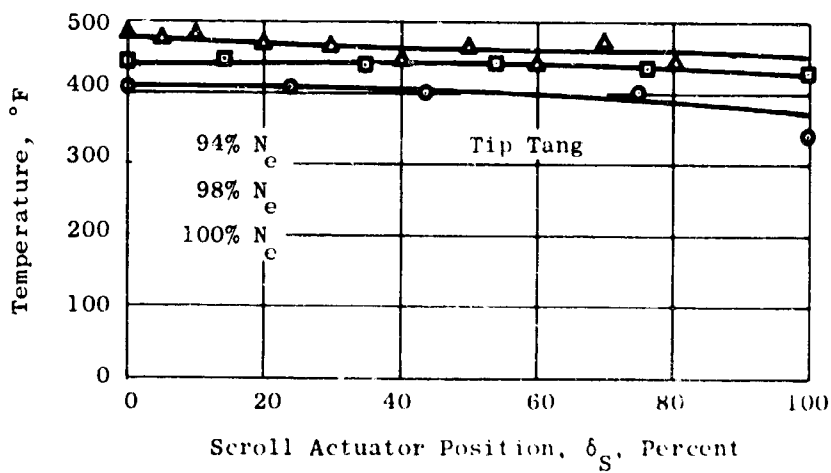
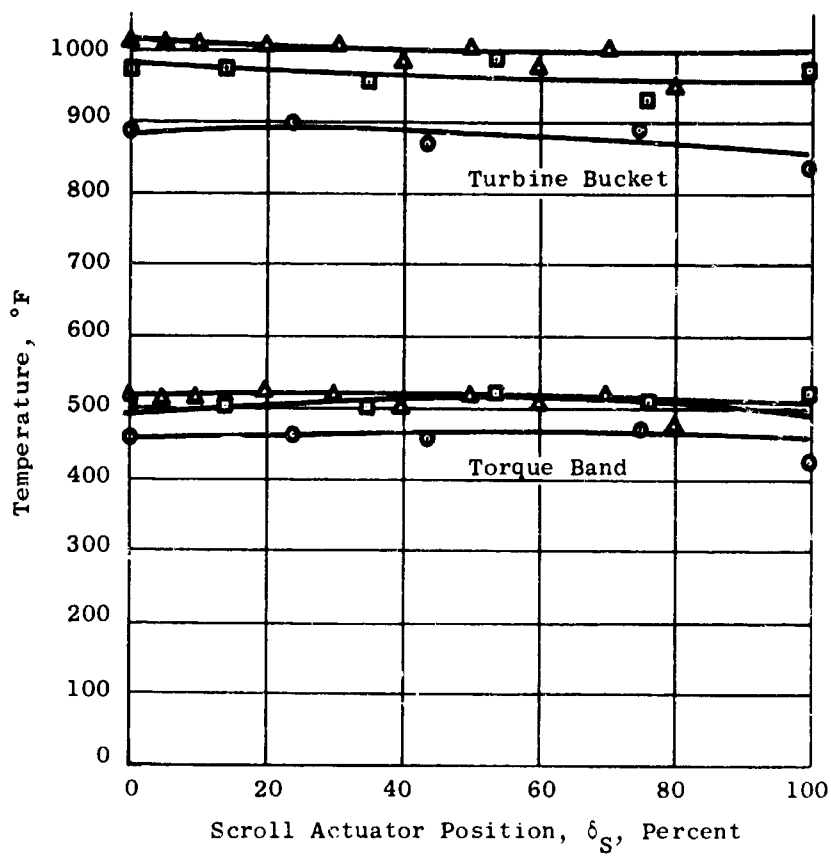


Figure 290. Rotor Component Temperatures Versus Scroll Actuator Position for Constant Engine Power.

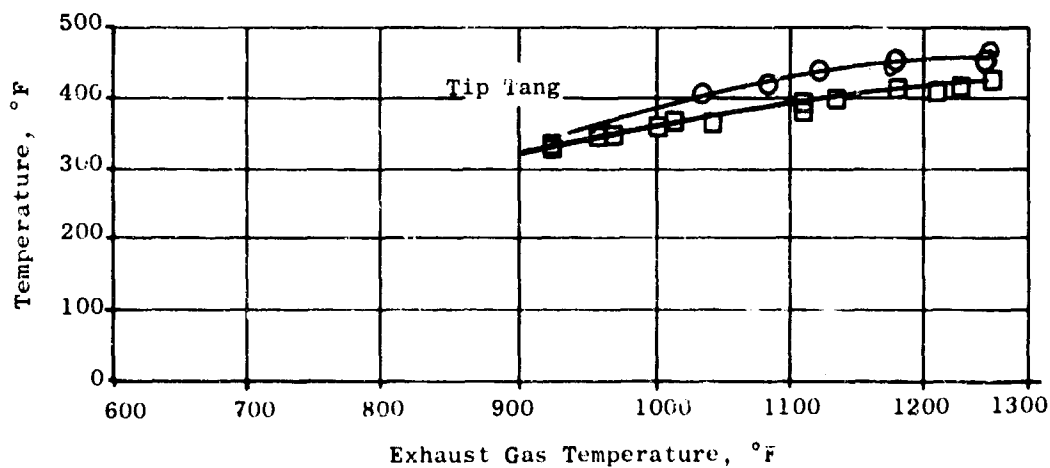
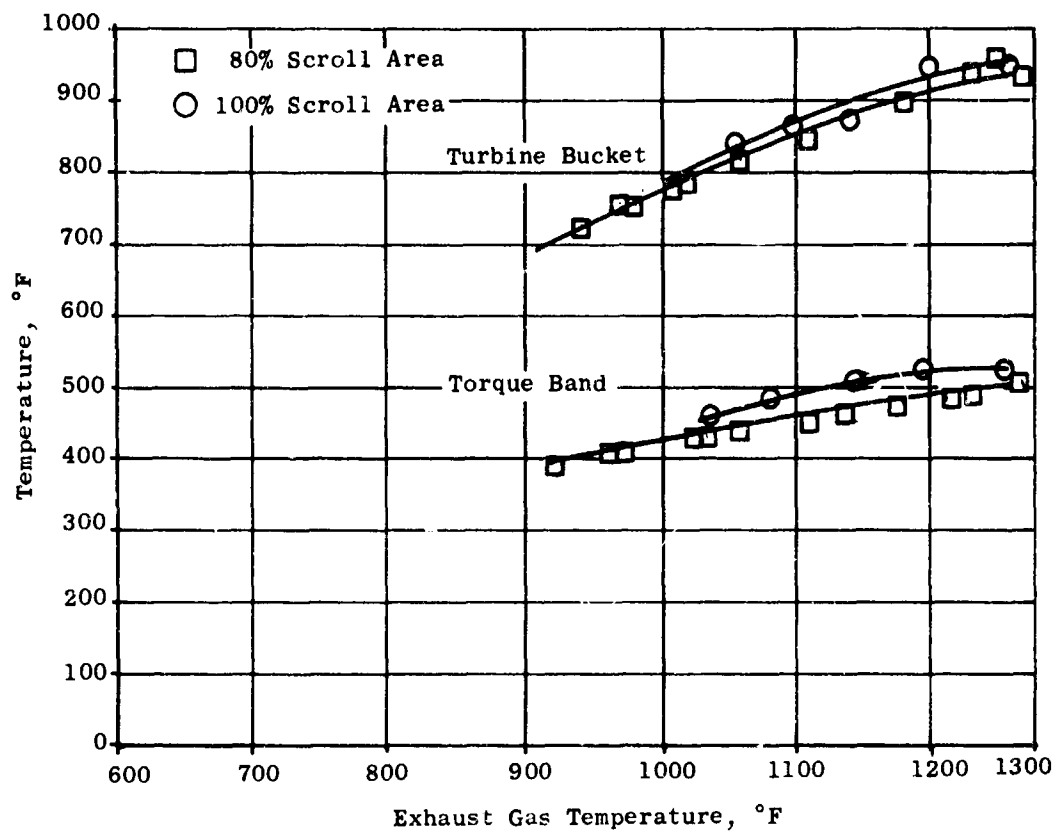


Figure 291. Rotor Component Temperature Versus Core Engine Exhaust Gas Temperature.

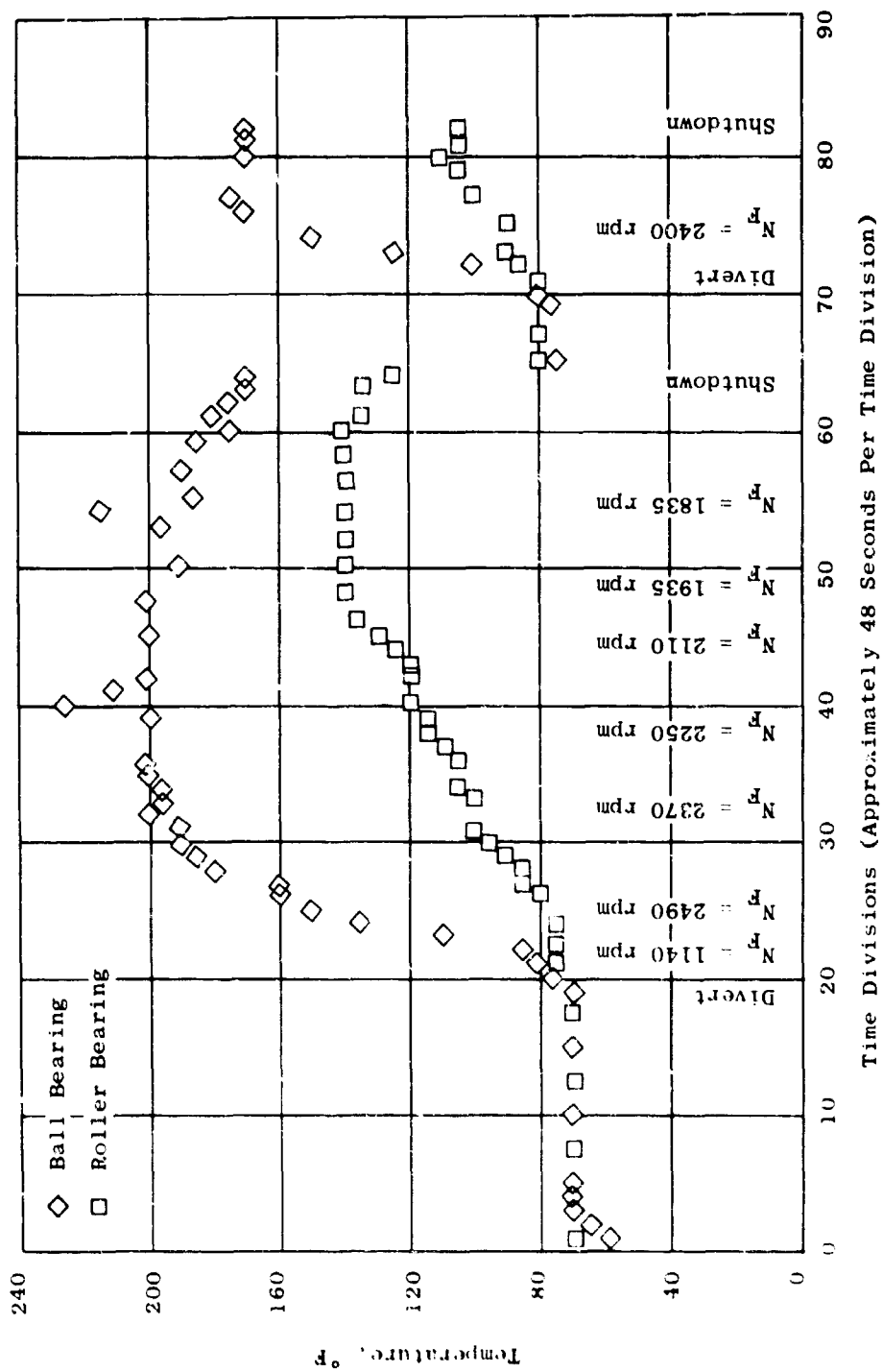


Figure 292. Time History of Bearing Temperatures.

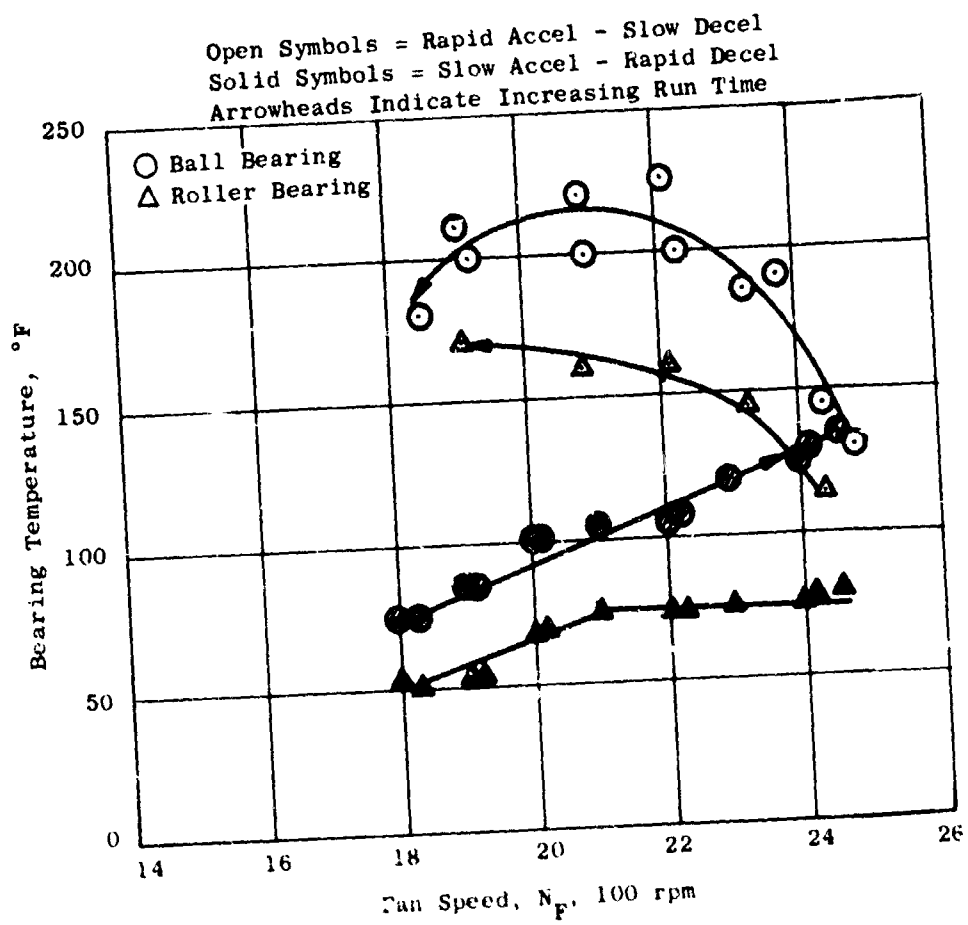
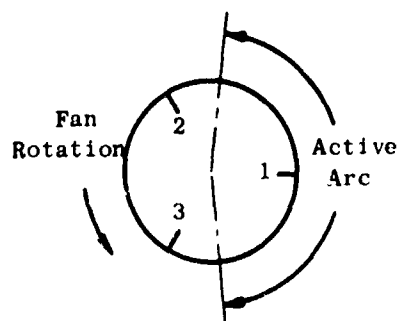


Figure 293. Ball Bearing and Roller Bearing Temperature Versus Fan Speed.



- Turbine Total
- ▤ Tang
- ◇ Bucket
- Tunnel 1
- △ Tunnel 2
- ▥ Tunnel 3

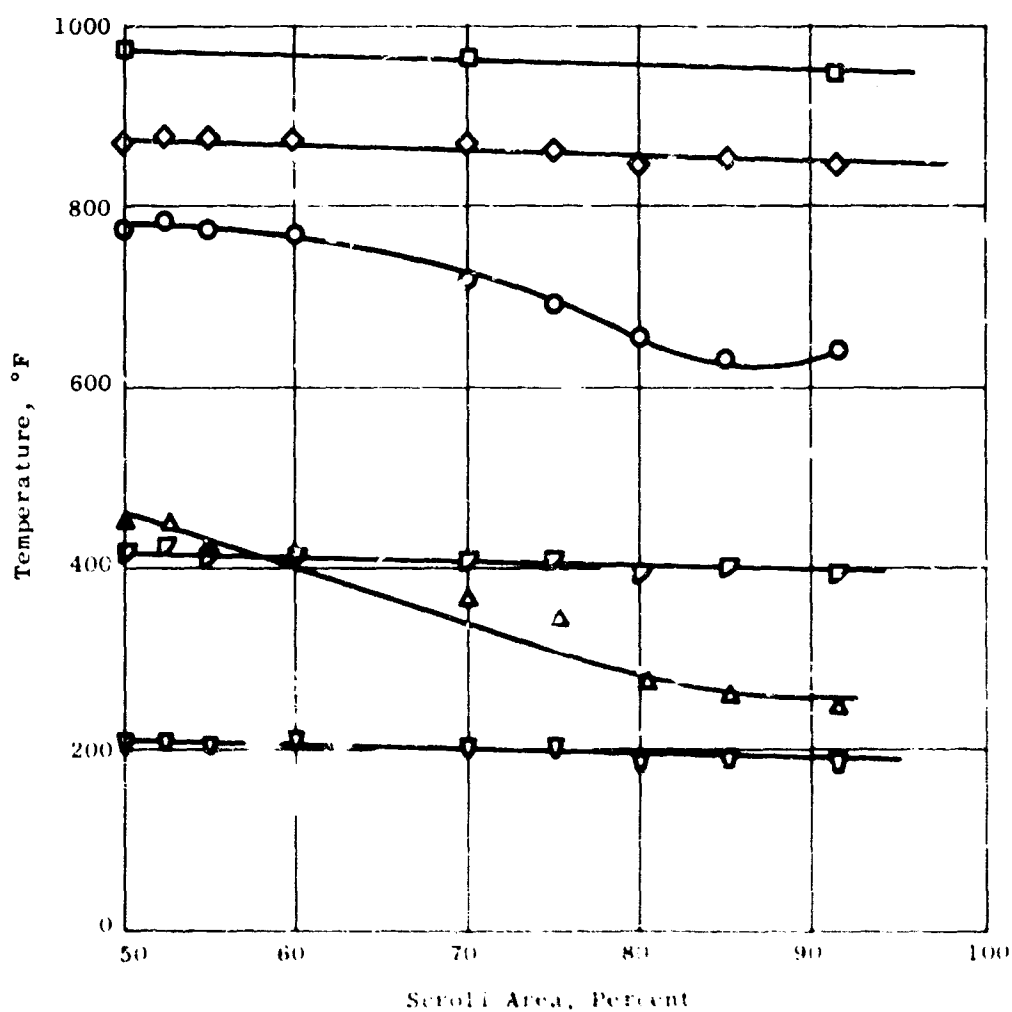


Figure 294. Effect of Scroll Area Variation on Tunnel Gas Temperature.

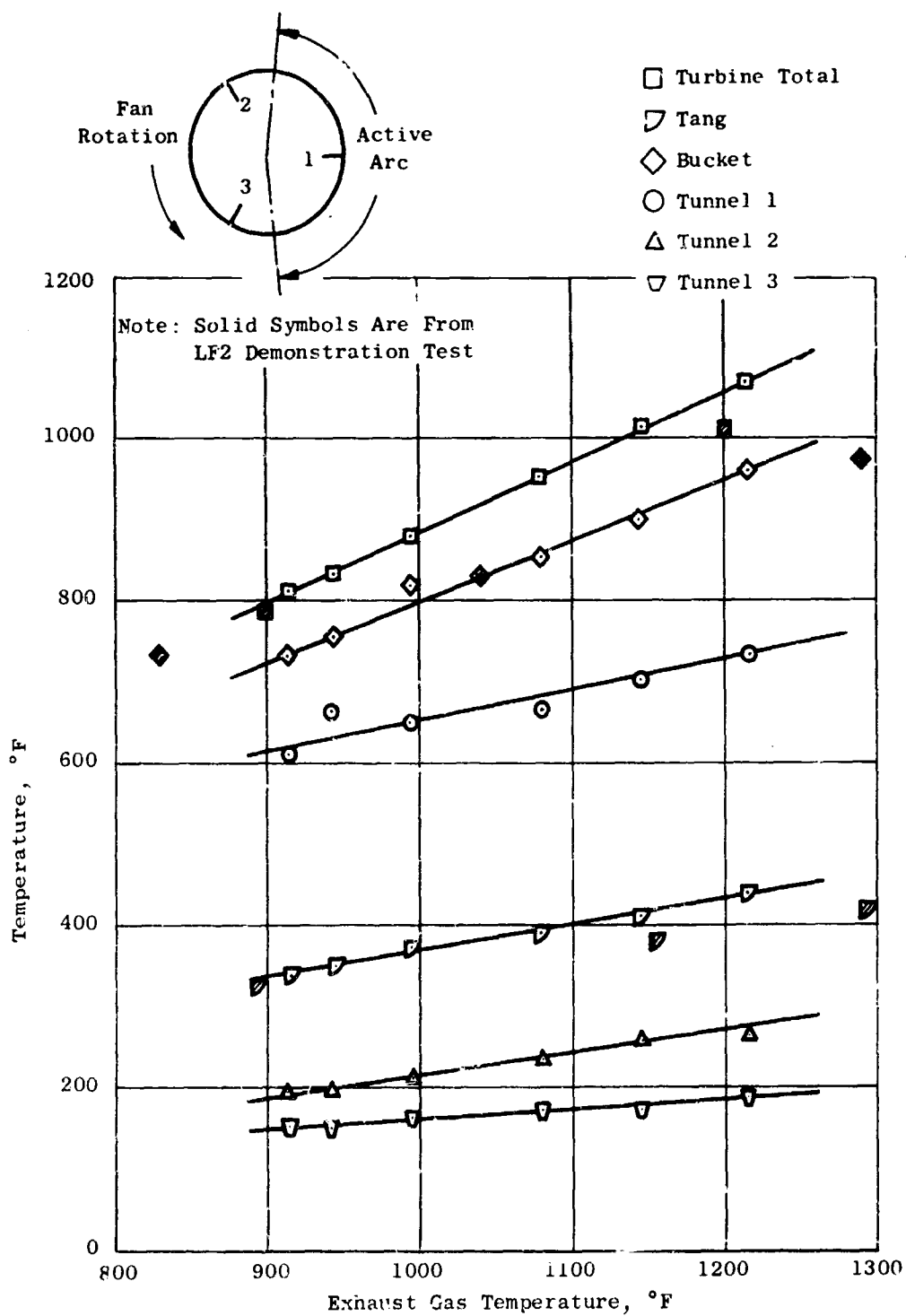
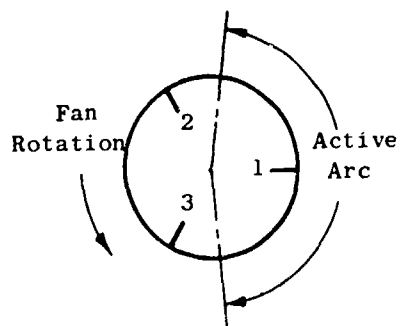


Figure 295. Effect of Exhaust Gas Temperatures on Tunnel Gas Temperature.



- Run 16, Scroll Area = 50%
- Run 16, Scroll Area = 91.5%

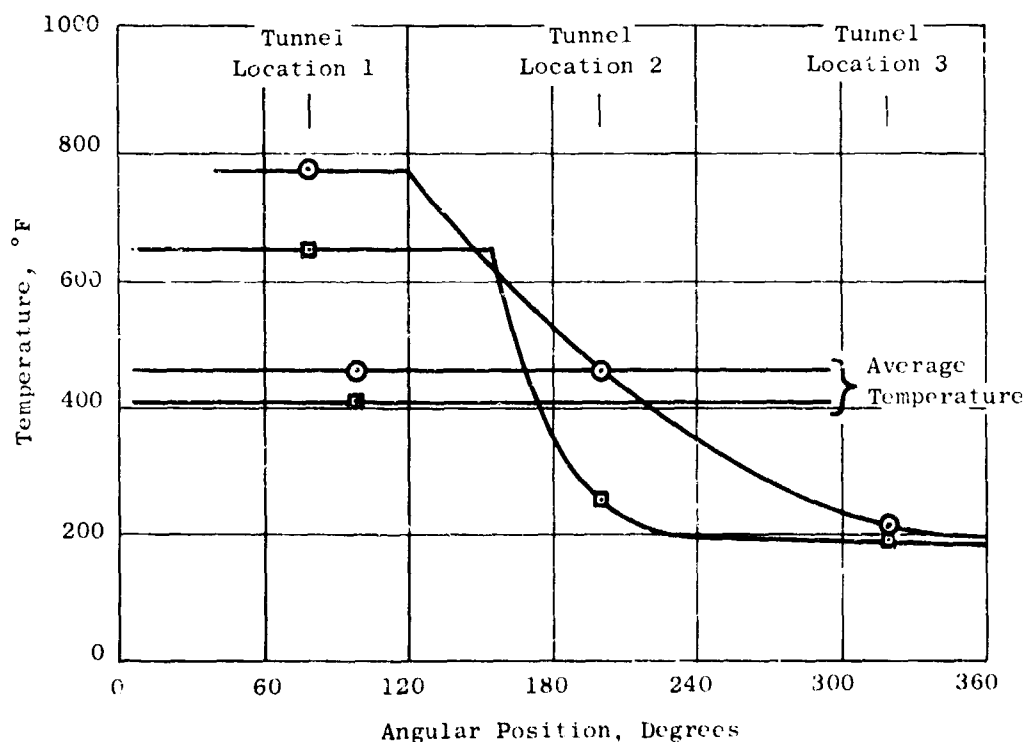


Figure 296. Circumferential Distribution of Tunnel Gas Temperature for Two Scroll Area Settings.

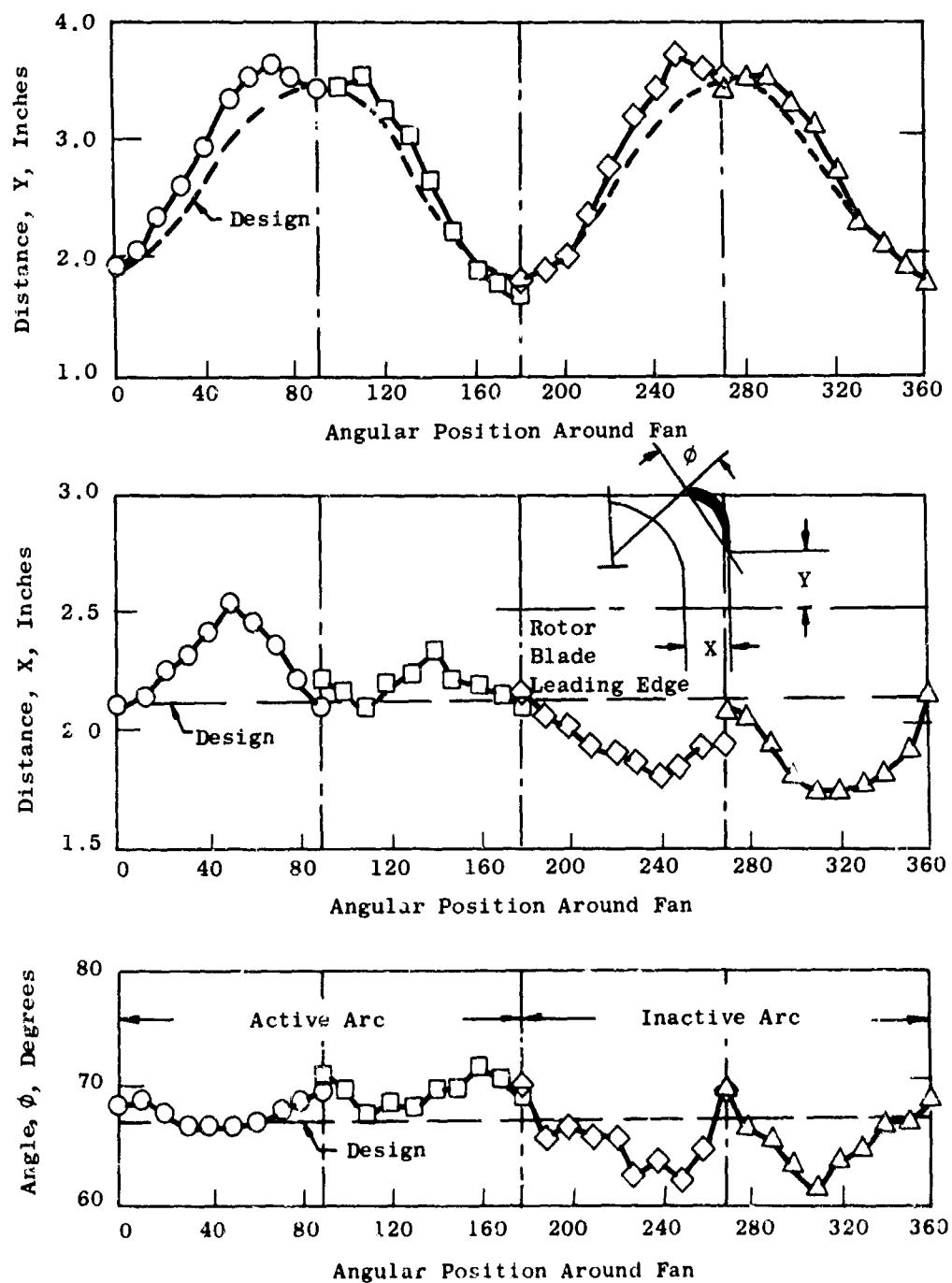


Figure 297. Fan Circular Vane Orientation.

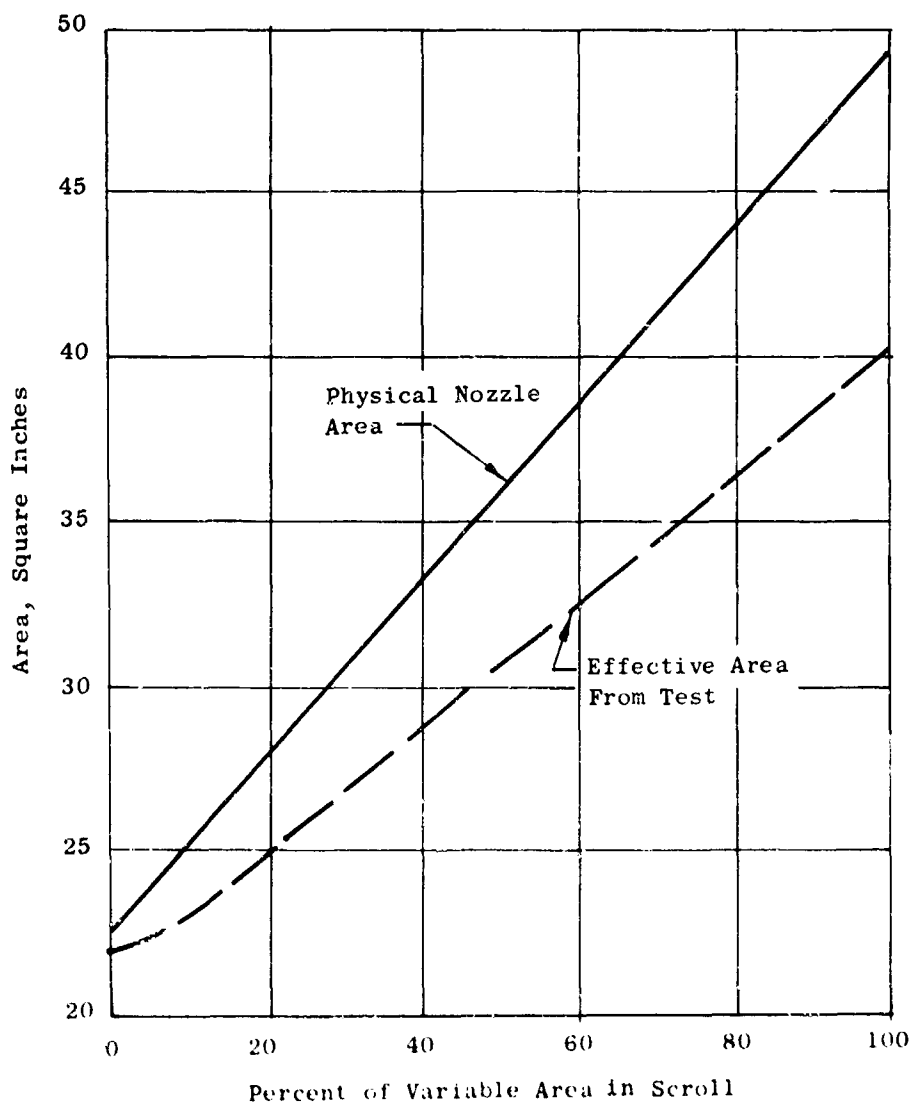


Figure 298. Comparison of Fan Turbine Nozzle Effective and Physical Areas for Scroll 1.

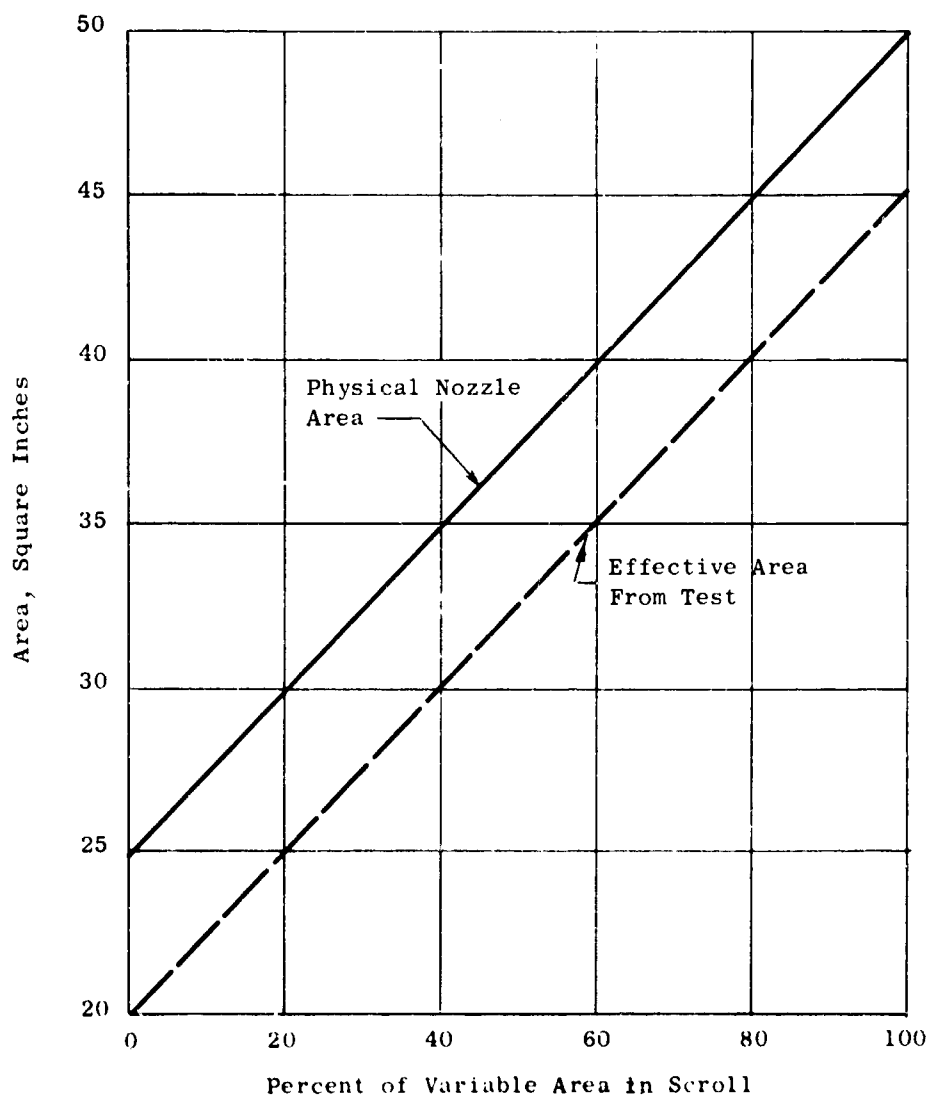


Figure 299. Comparison of Fan Turbine Nozzle Effective and Physical Areas for Scroll 2.

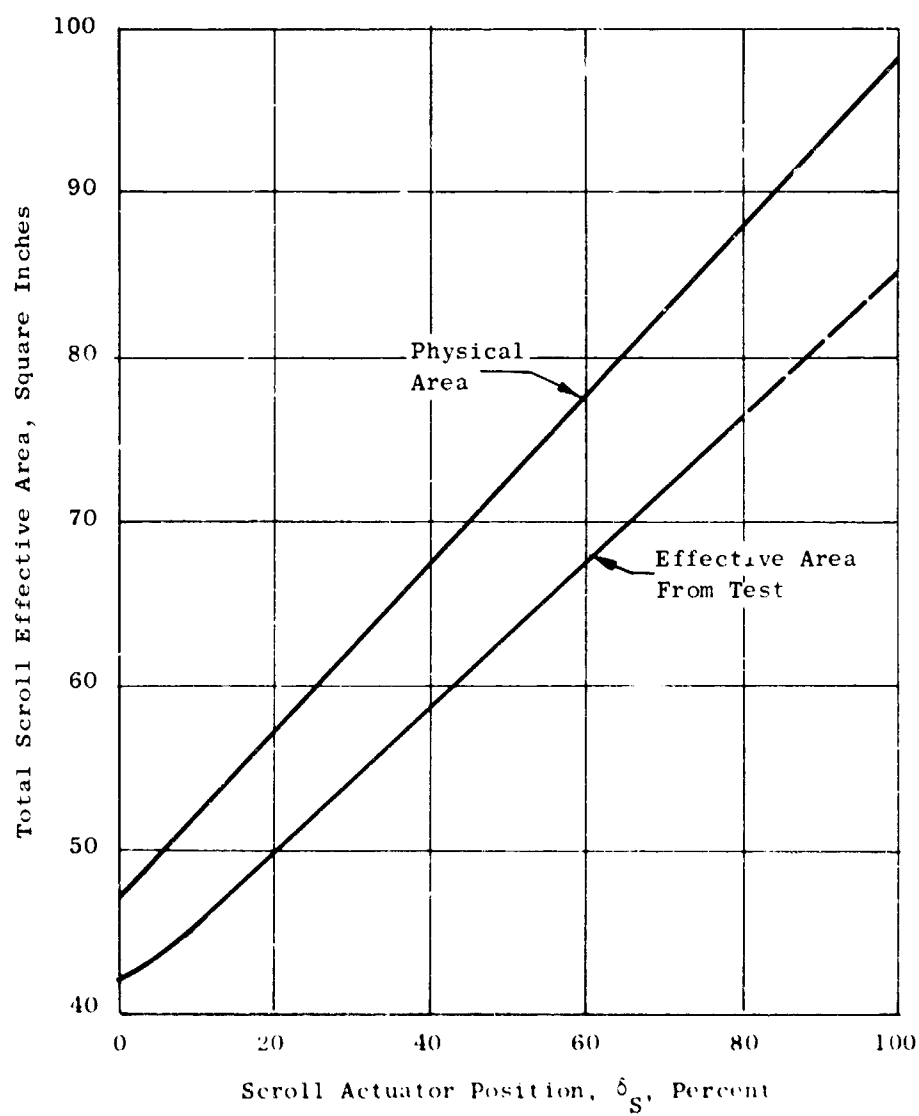


Figure 300. Variation of Fan Scroll Total Effective and Physical Area With Actuator Stroke.

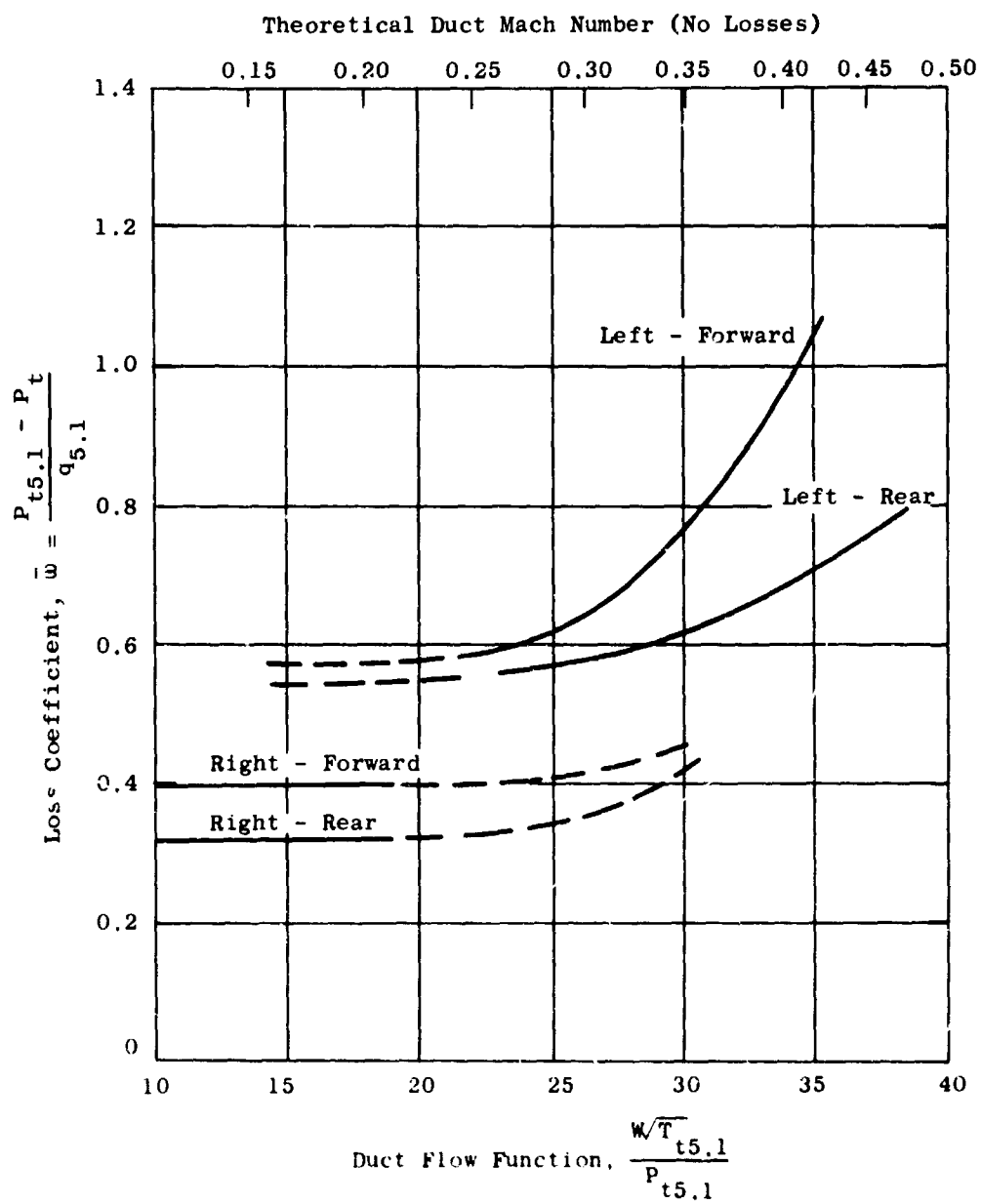


Figure 301. Ducting System Losses Versus Flow Function.

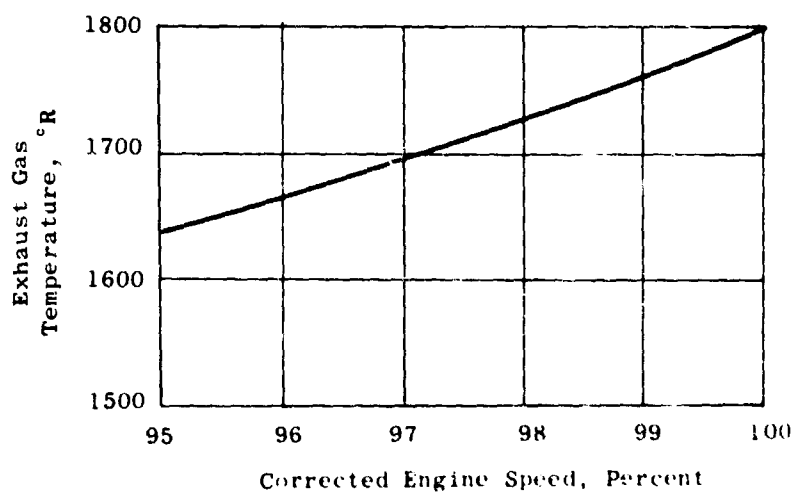
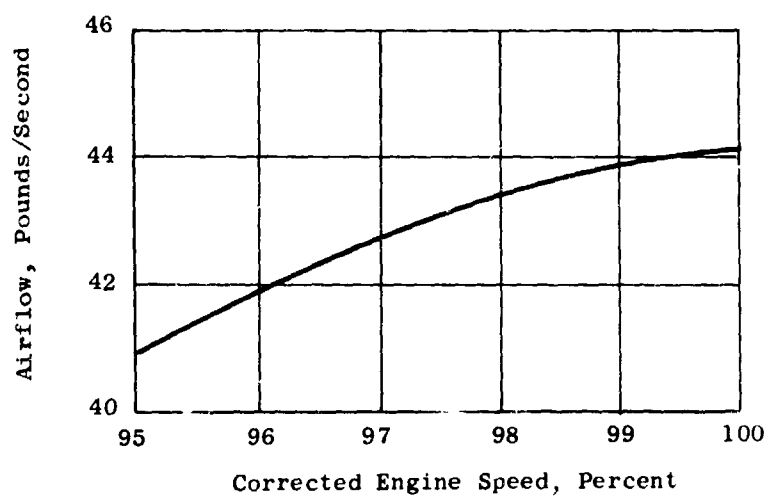


Figure 302. Typical J85/J4 Performance, Airflow and Exhaust Gas Temperature.

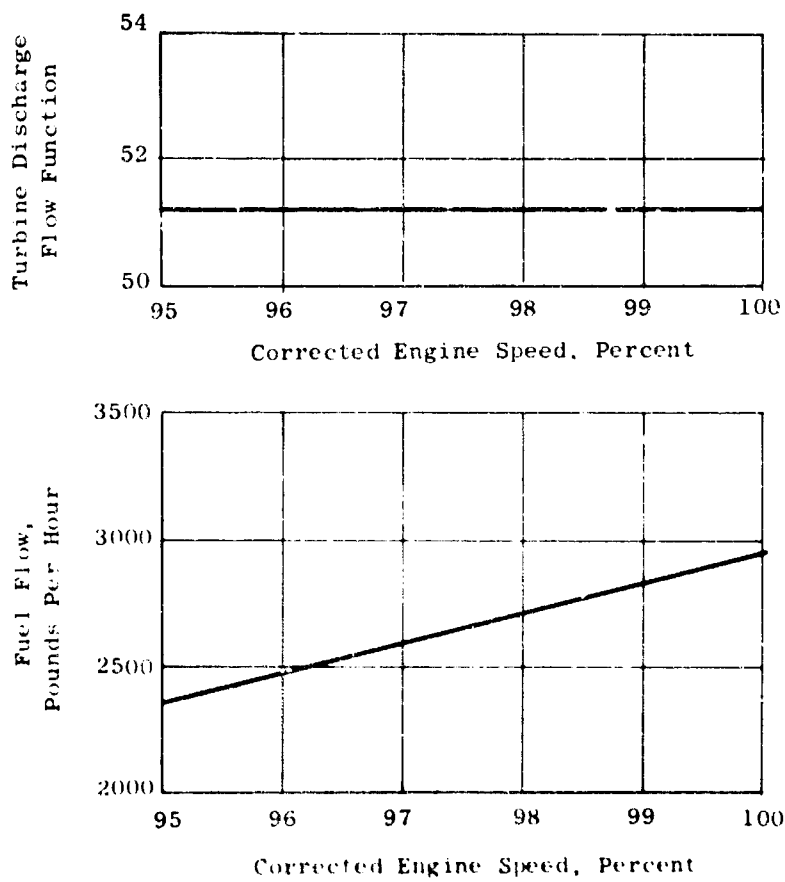


Figure 303. Typical J85 J4 Performance, Fuel Flow and Flow Function.

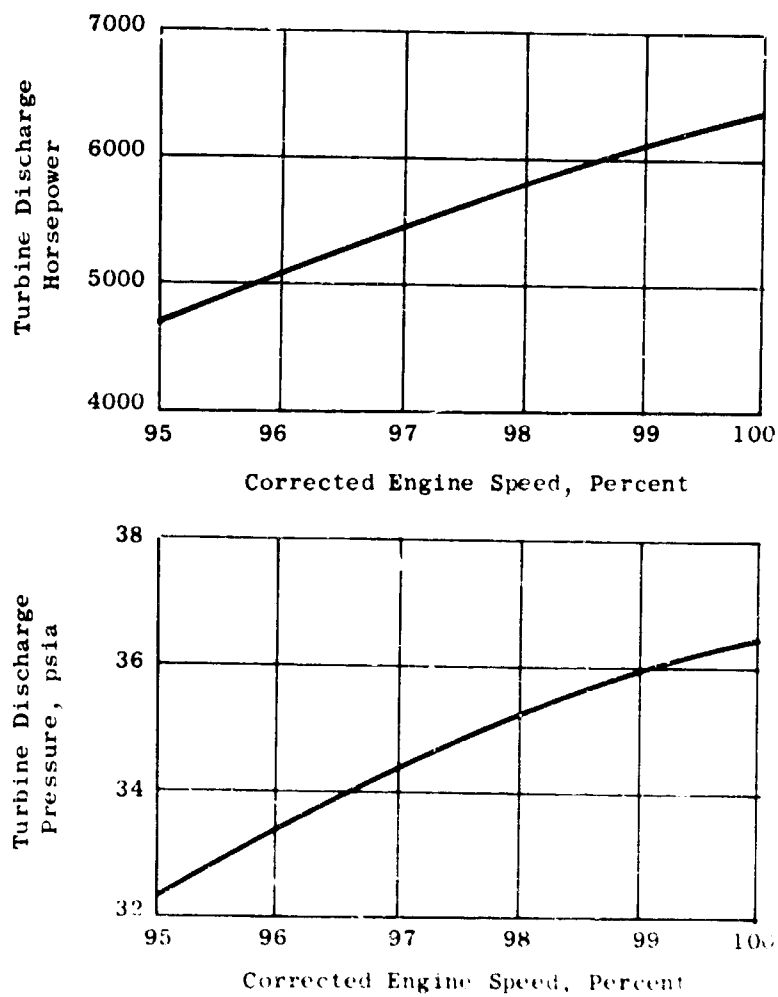


Figure 304. Typical J85 J4 Performance, Turbine Discharge Pressure and Horsepower.

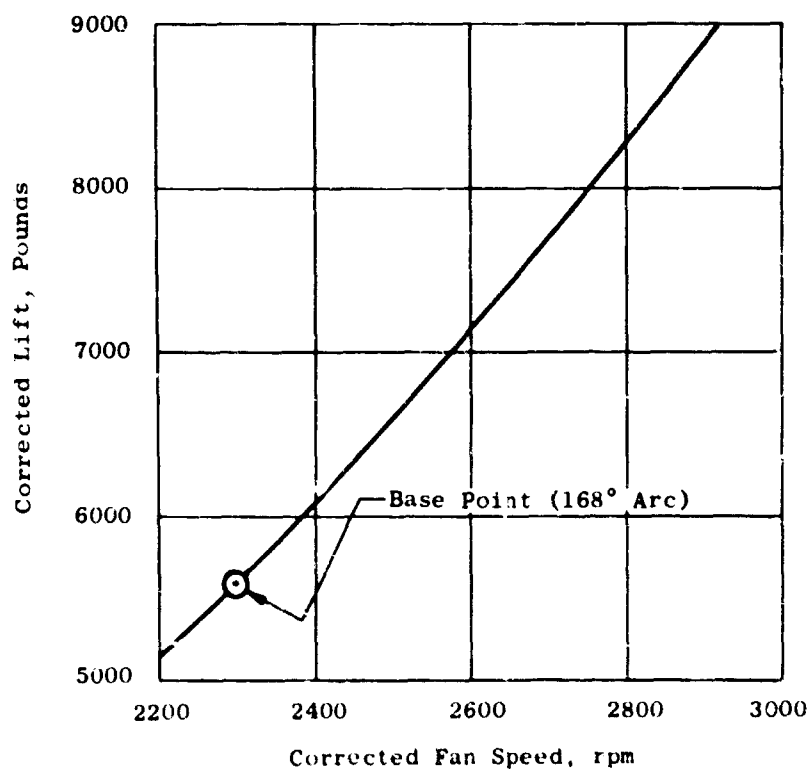


Figure 305. Variation of Lift With Fan Speed Used in Analysis, Scroll Arc Constant at 168 Degrees.

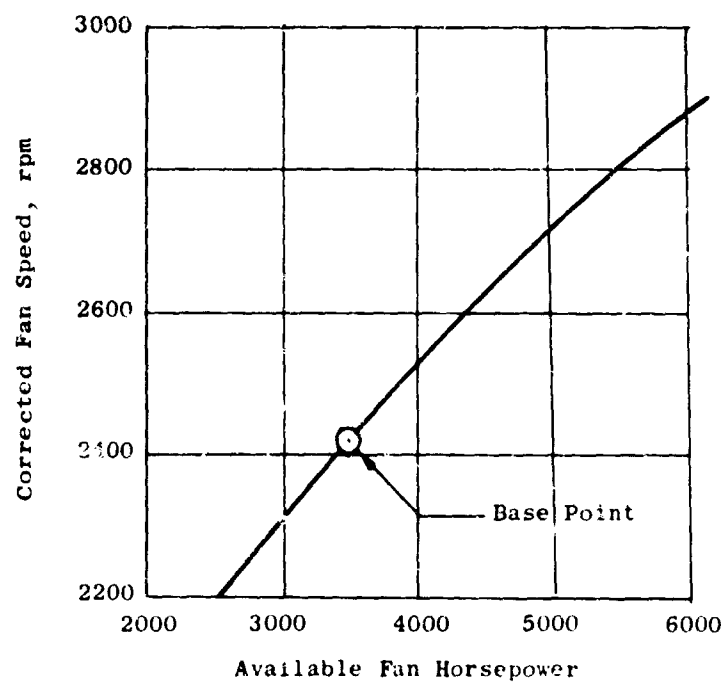


Figure 306. Variation of Fan Speed With Available Horsepower Used in Analysis.

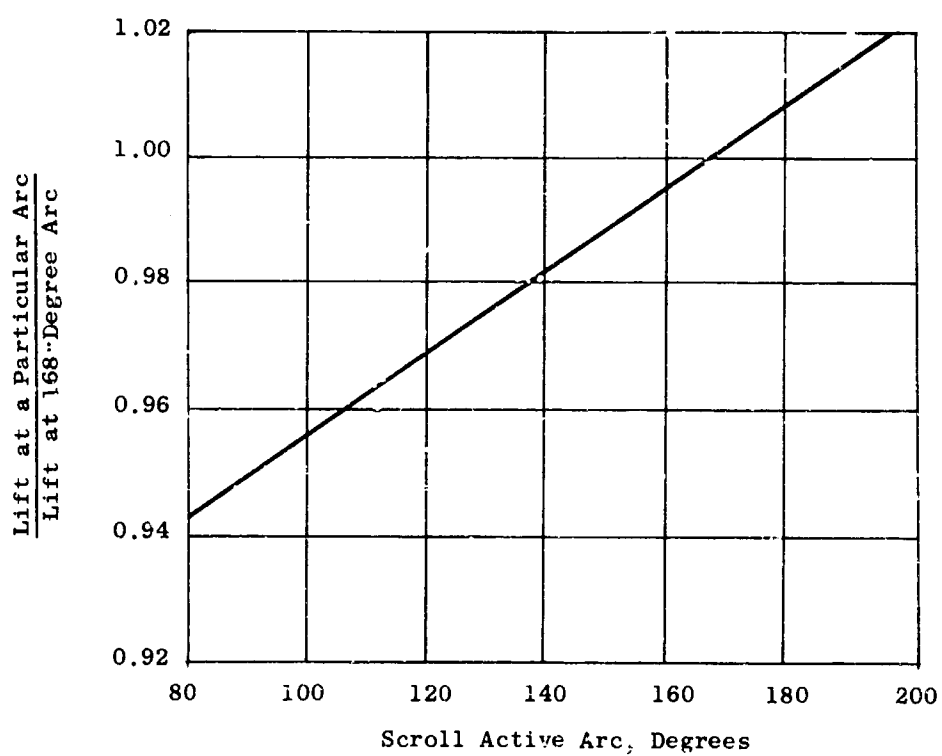


Figure 307. Estimated Variation of Fan Lift With Admission Arc at a Constant Fan Speed.

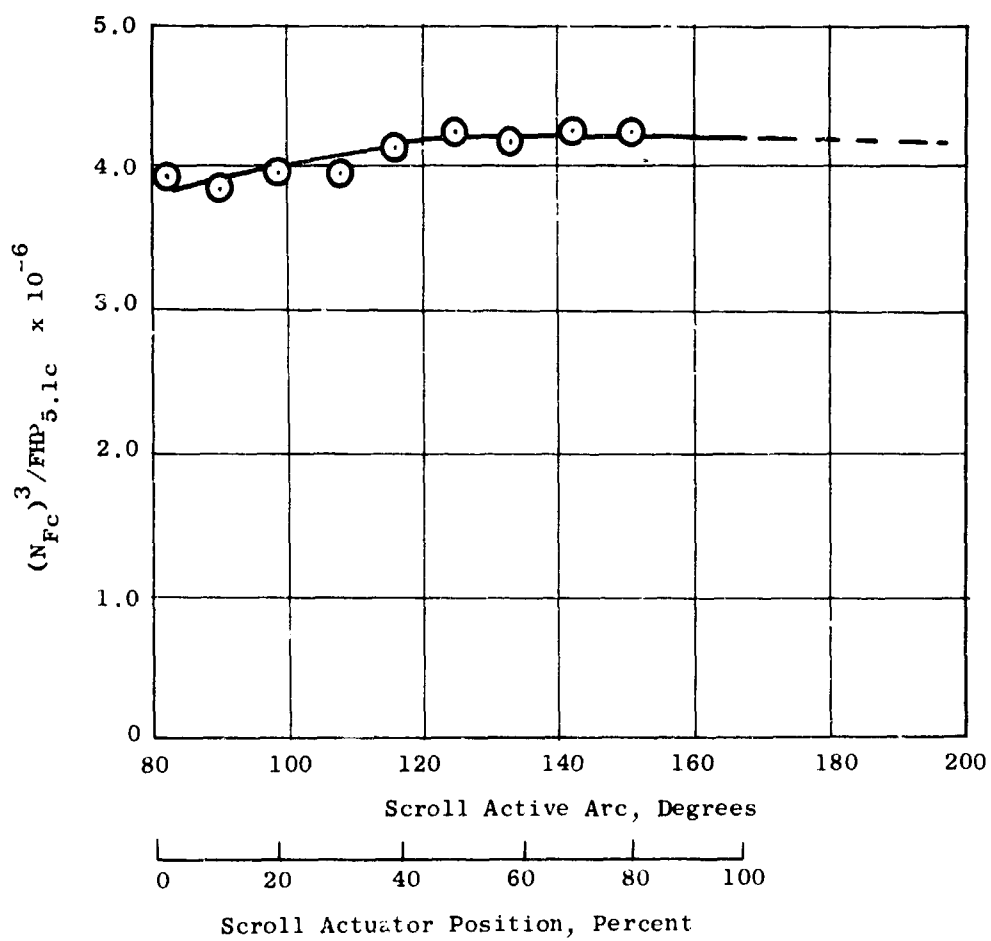


Figure 308. Effects of Scroll Arc on Fan Horsepower Absorption Characteristics.

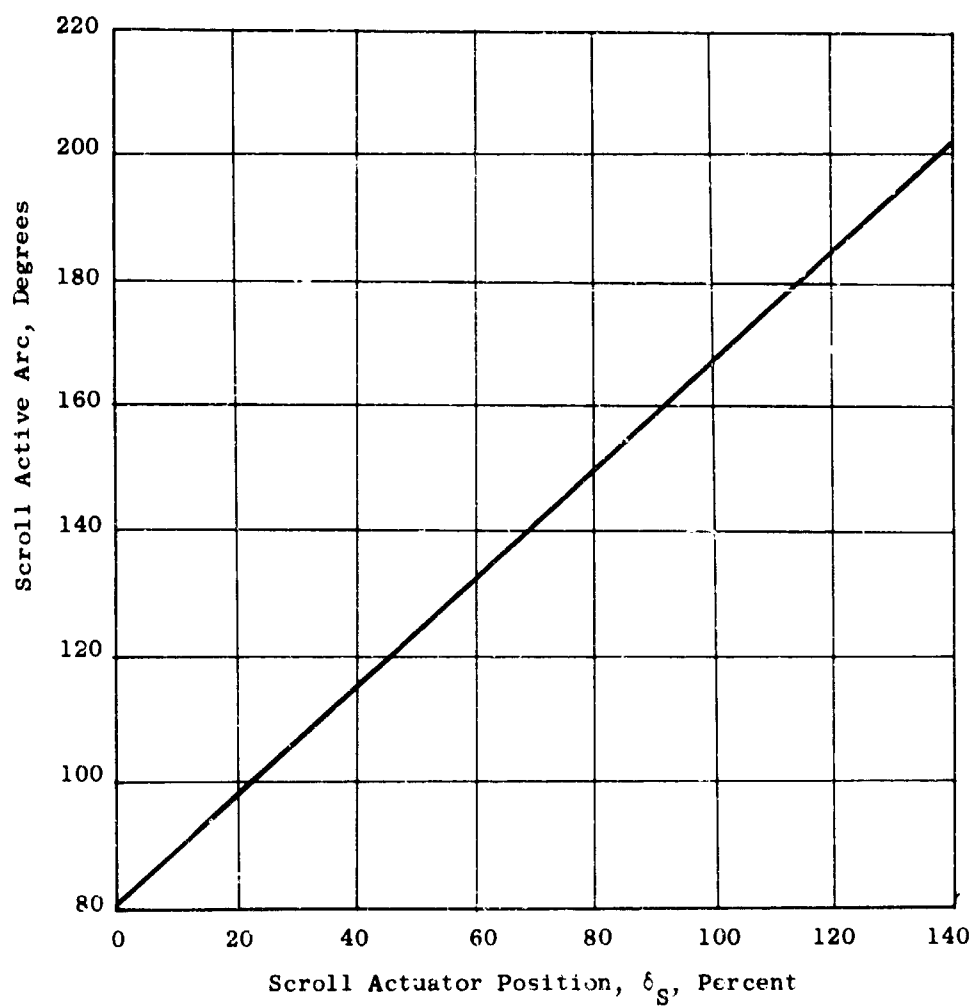


Figure 309. Comparison of Scroll Actuator Position and Scroll Arc Size.

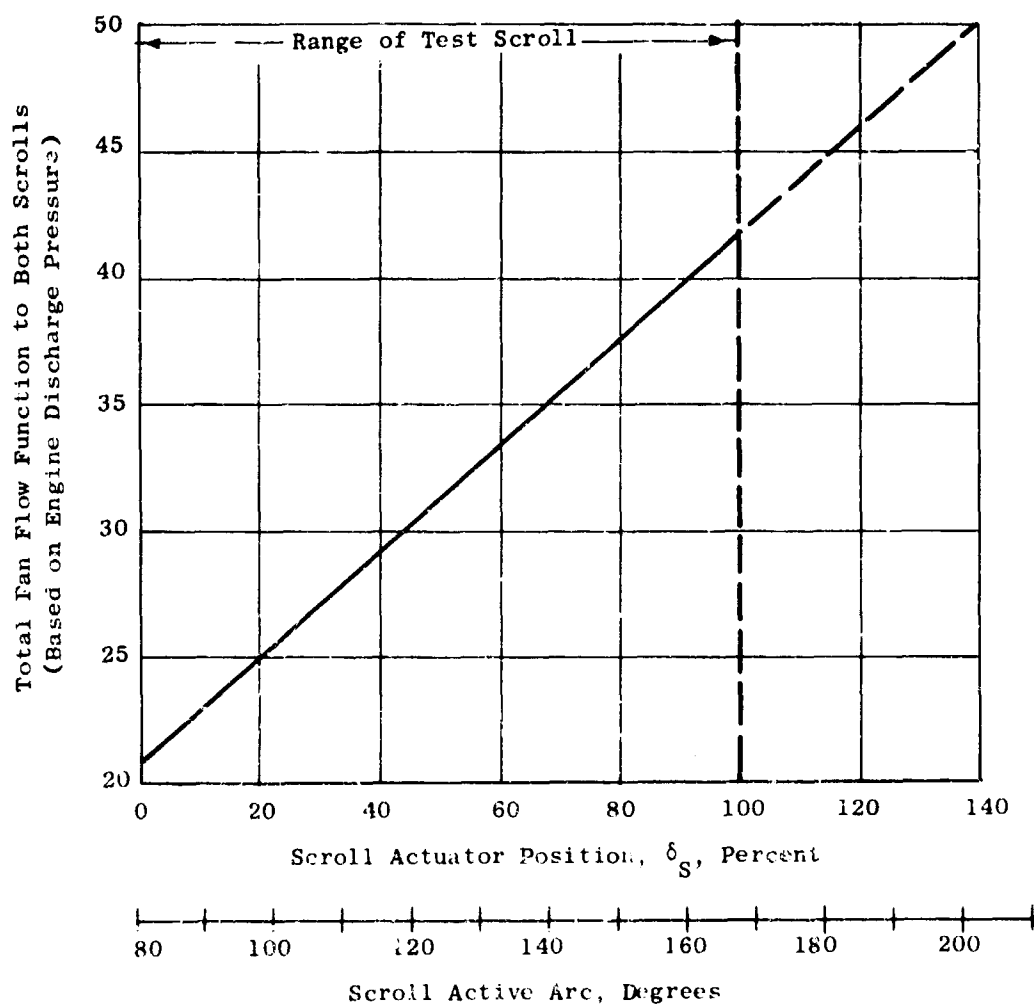


Figure 310. Fan Scroll Flow Function as a Function of Scroll Arc and Actuator Position.

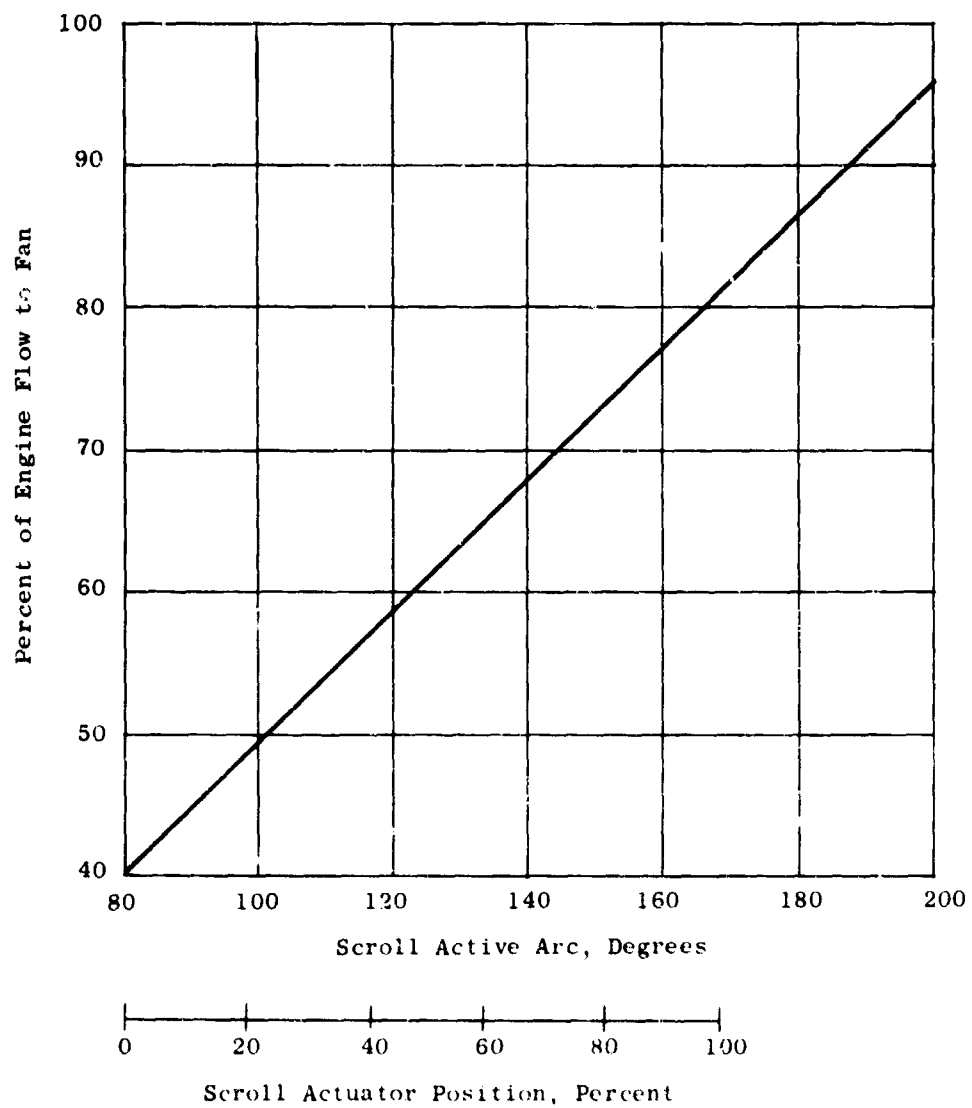


Figure 311. Percentage of J85/J4 Engine Flow Supplied to Fan as a Function of Scroll Arc and Actuator Position.

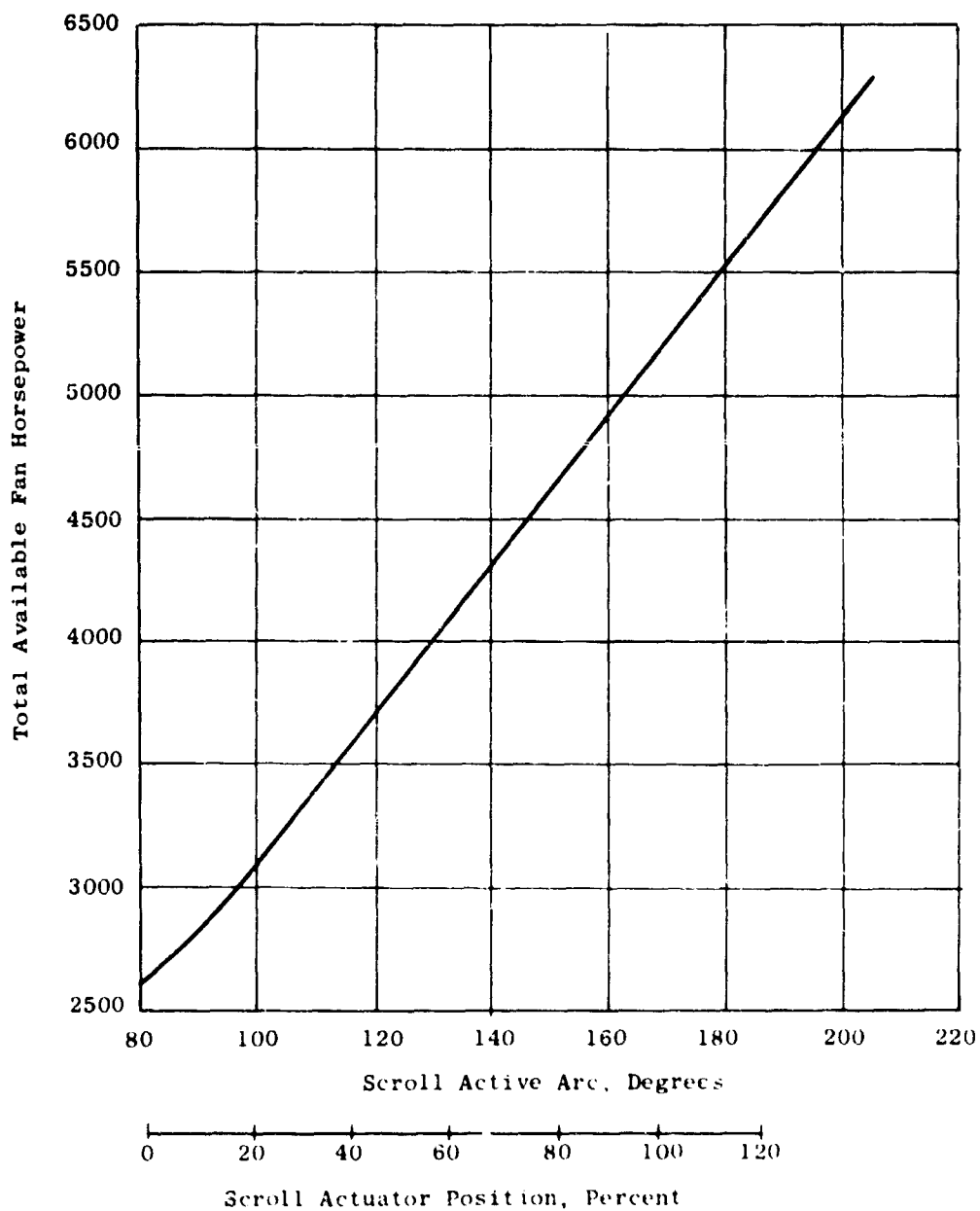


Figure 312. Estimated Available Gas Horsepower to Fan as a Function of Active Arc Size.

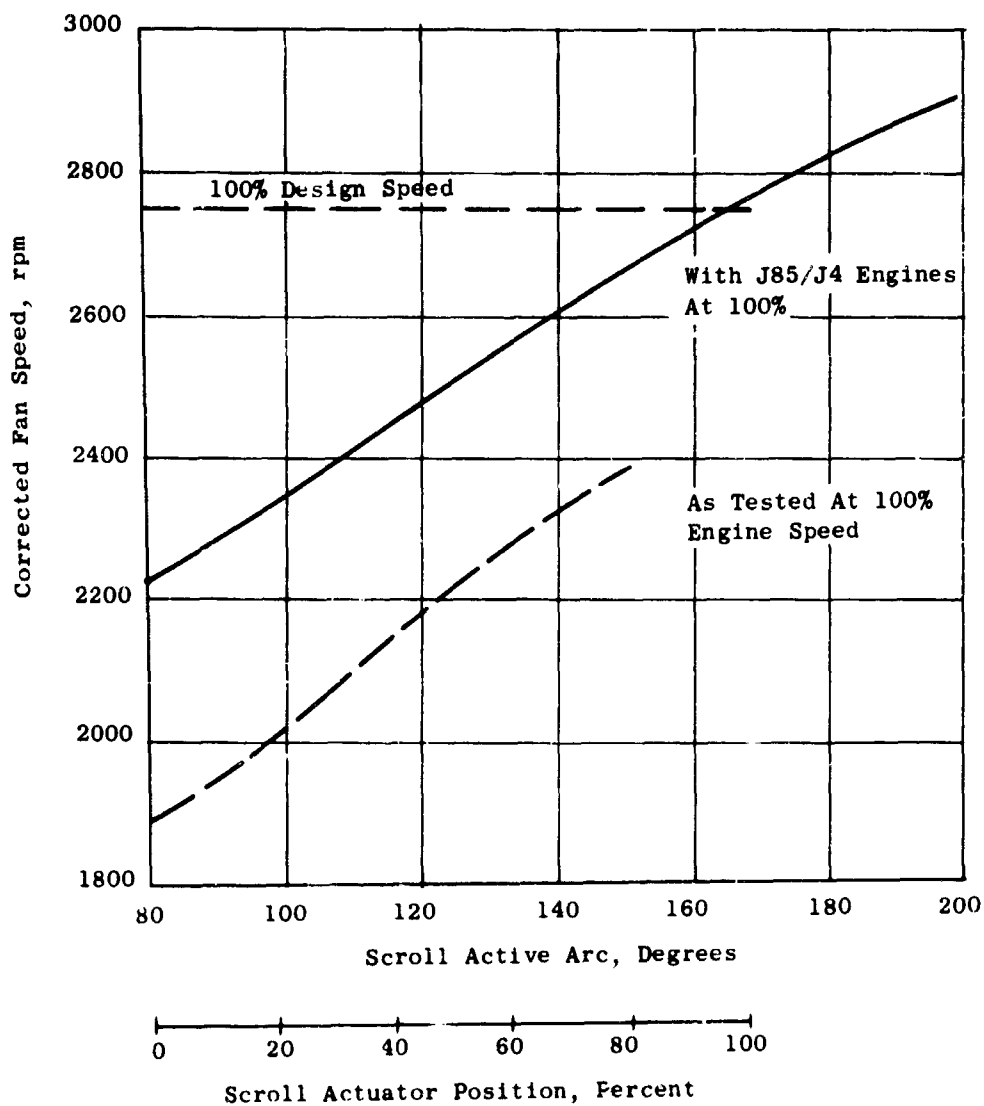


Figure 313. Estimated Fan Speed Variation With Scroll Arc or Actuator Position for the Fan Driven by J85/J4 Engines.

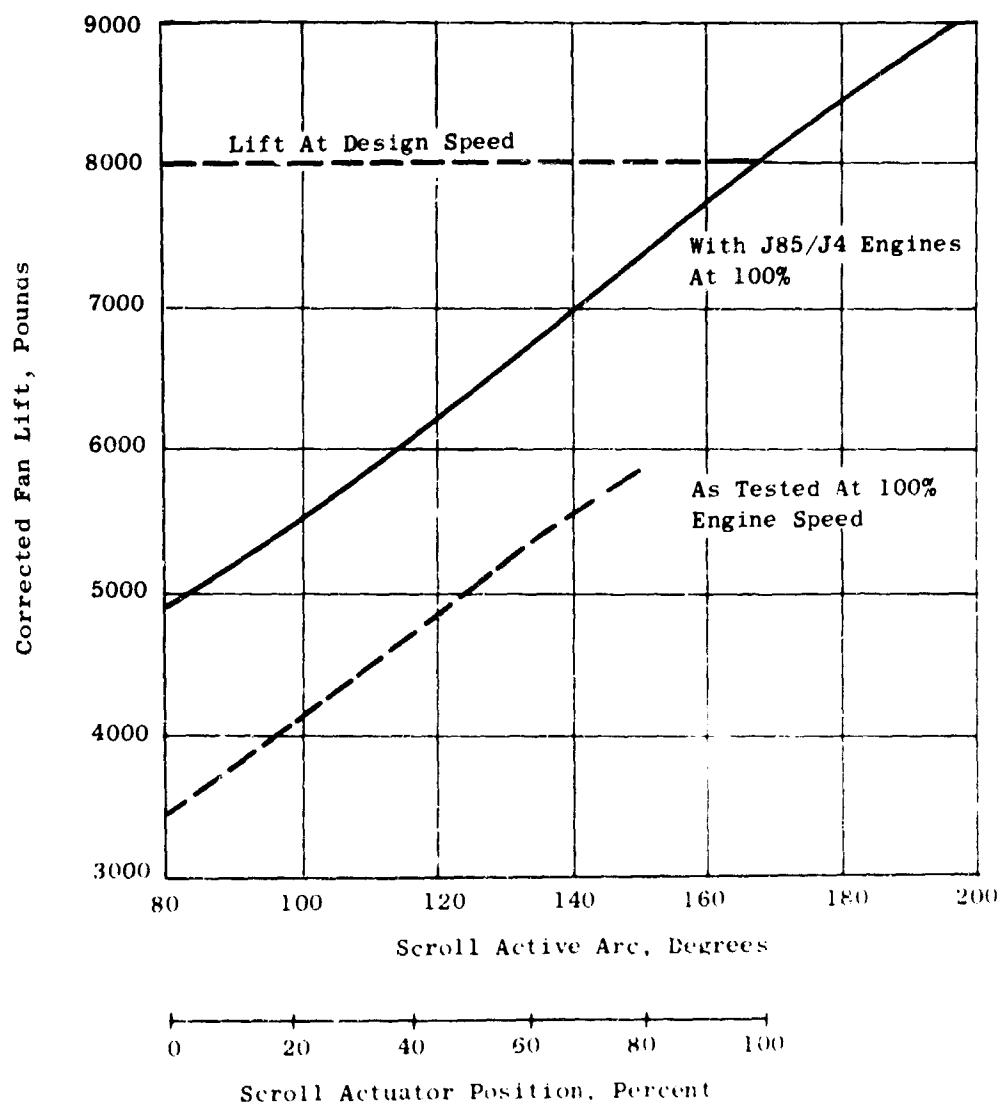


Figure 314. Estimated Fan Lift Variation With Scroll Arc or Actuator Position for the Fan Driven by J85/J4 Engines.

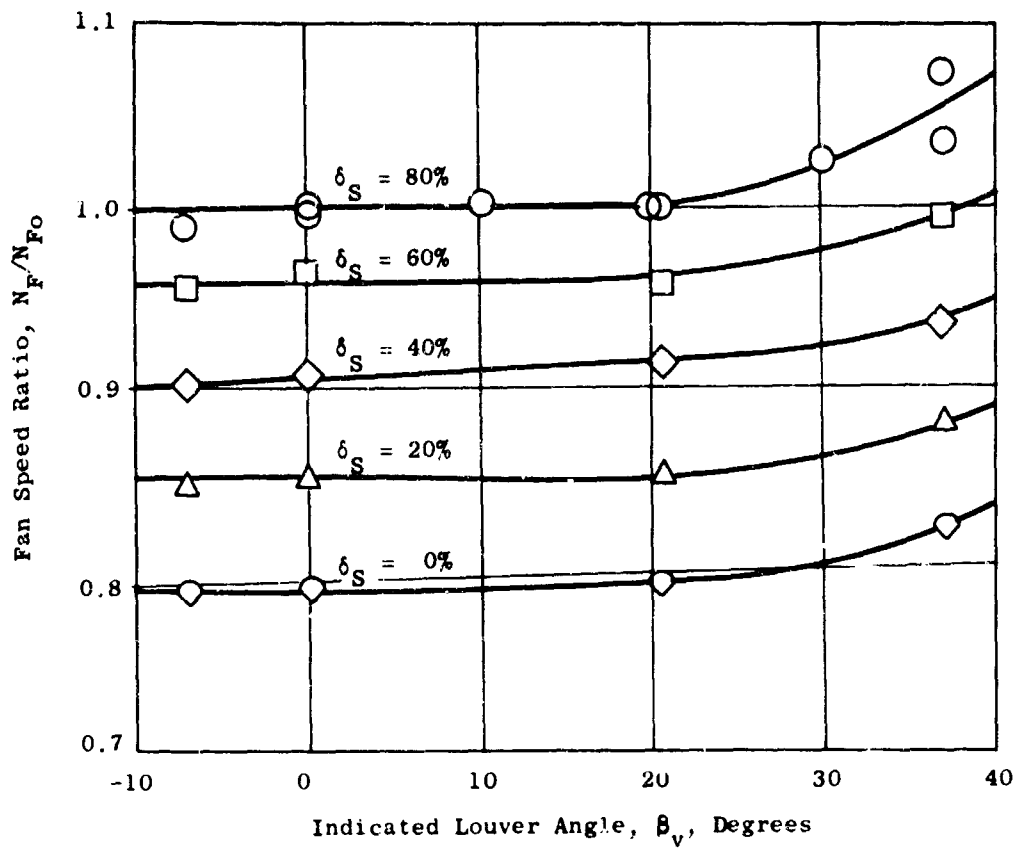


Figure 315. Fan Speed Versus Indicated Louver Angle and Scroll Actuator Position at Constant Core Engine Horsepower.

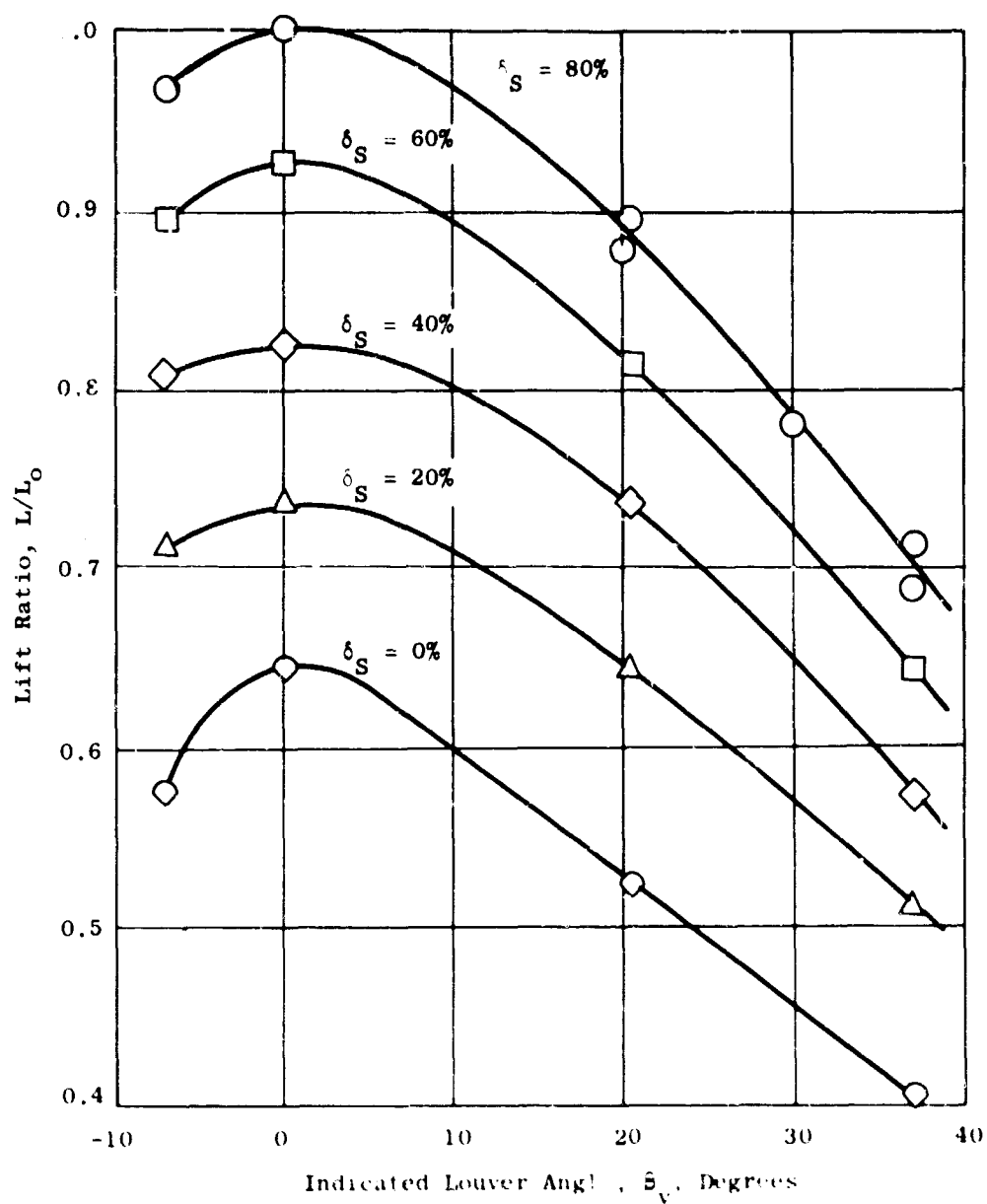


Figure 316. Lift Variation With Louver Angle and Scroll Actuator Position for Constant Core Engine Horsepower.

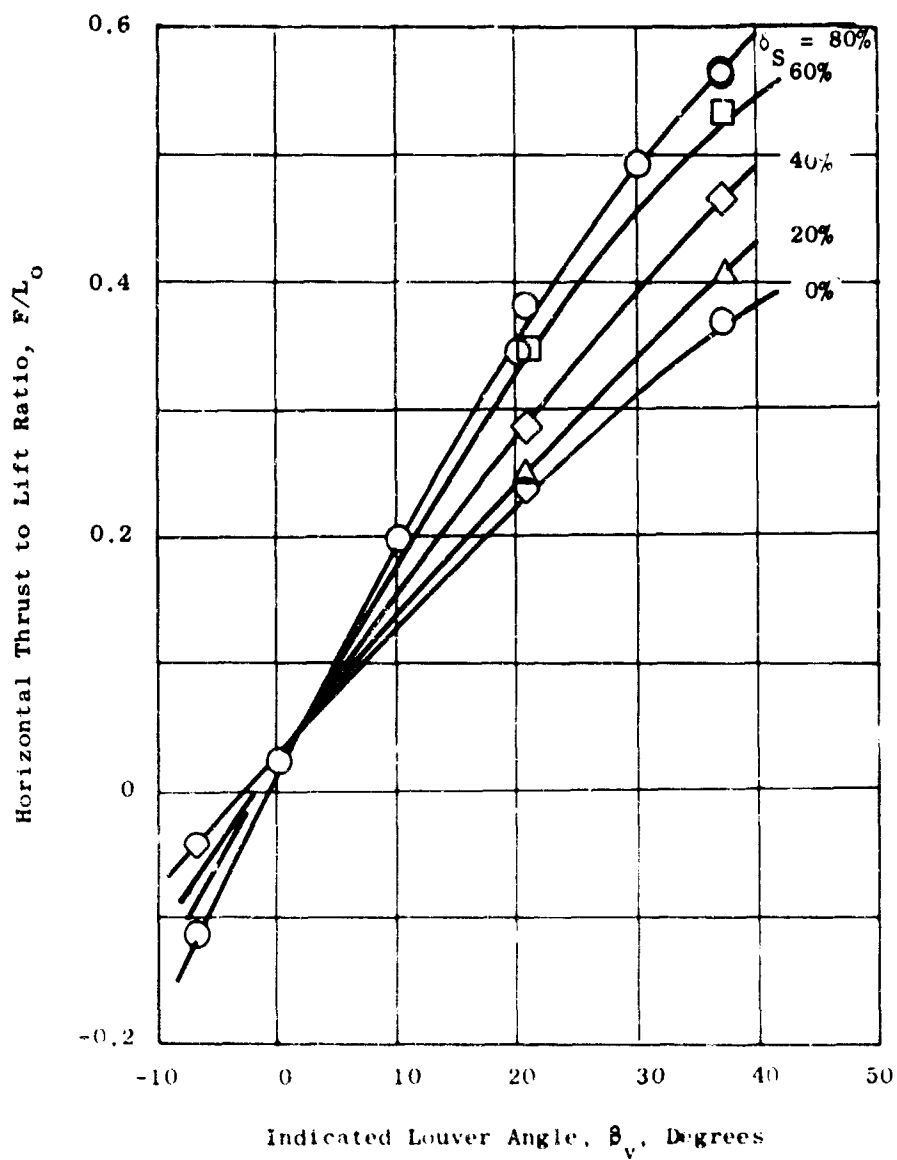


Figure 317. Horizontal Thrust Variation With Louver Angle and Scroll Actuator Position for Constant Core Engine Horsepower.

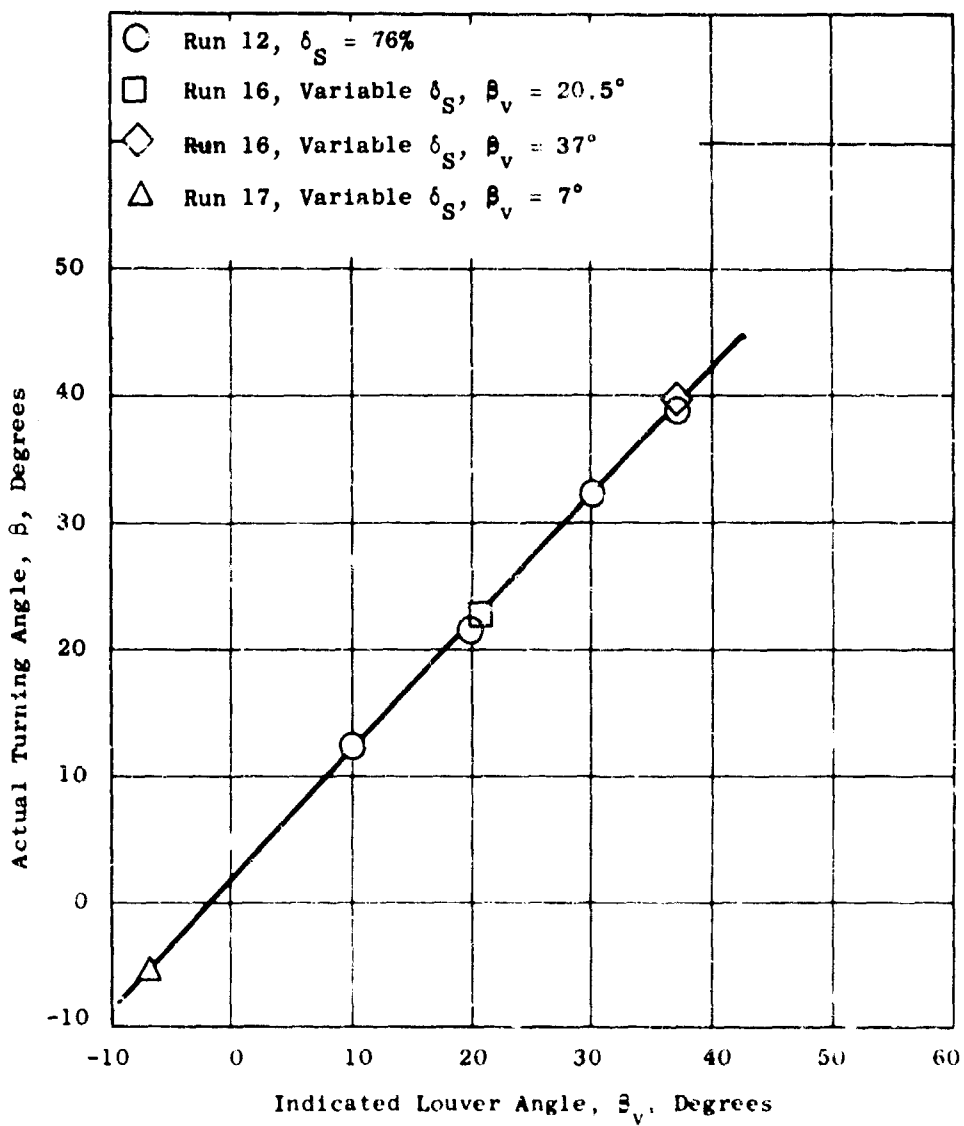


Figure 318. Actual Turning Angle Versus Indicated Louver Angle.

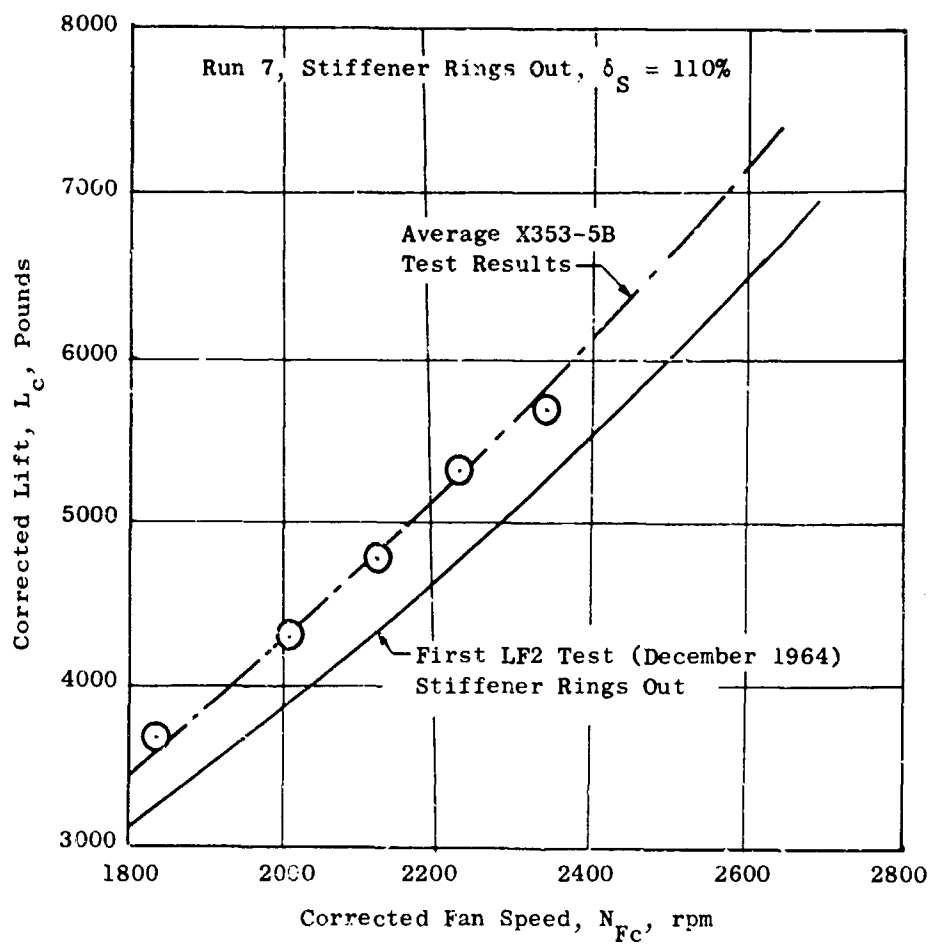


Figure 319. Comparison of X353-5B and LF2 Fan Test Results.

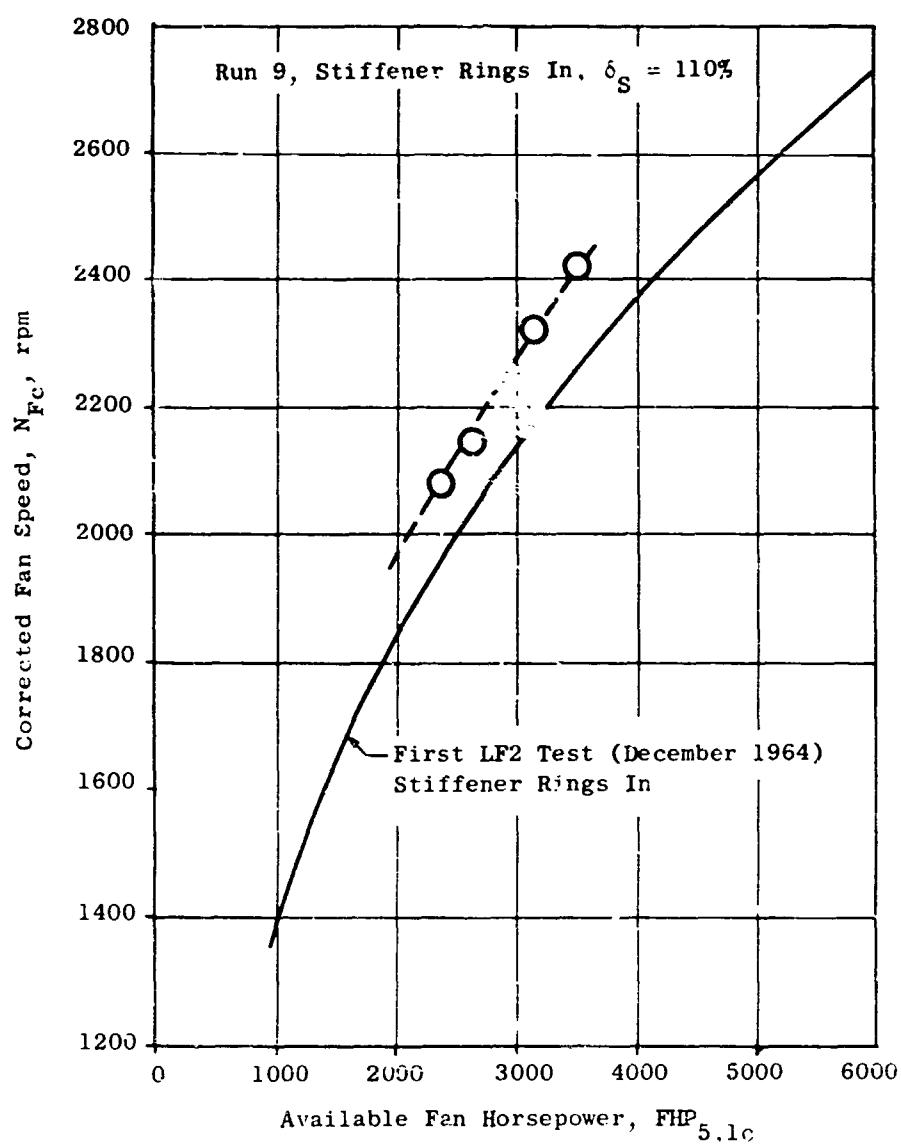


Figure 320. Comparison of Fan Speed Versus Available Fan Horsepower With Characteristic From First LF2 Test Configuration.

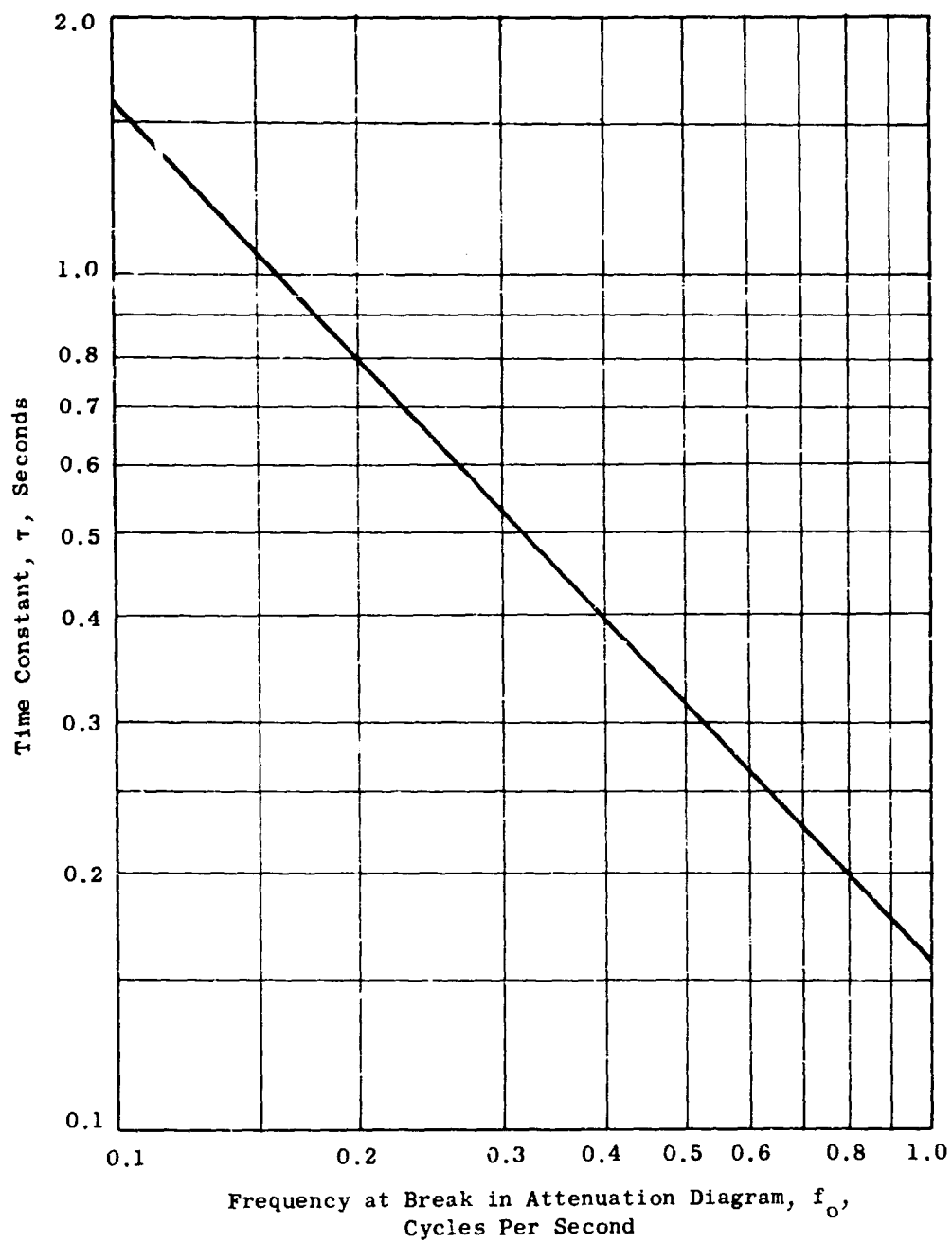


Figure 321. Frequency to Time Constant Conversion Chart.

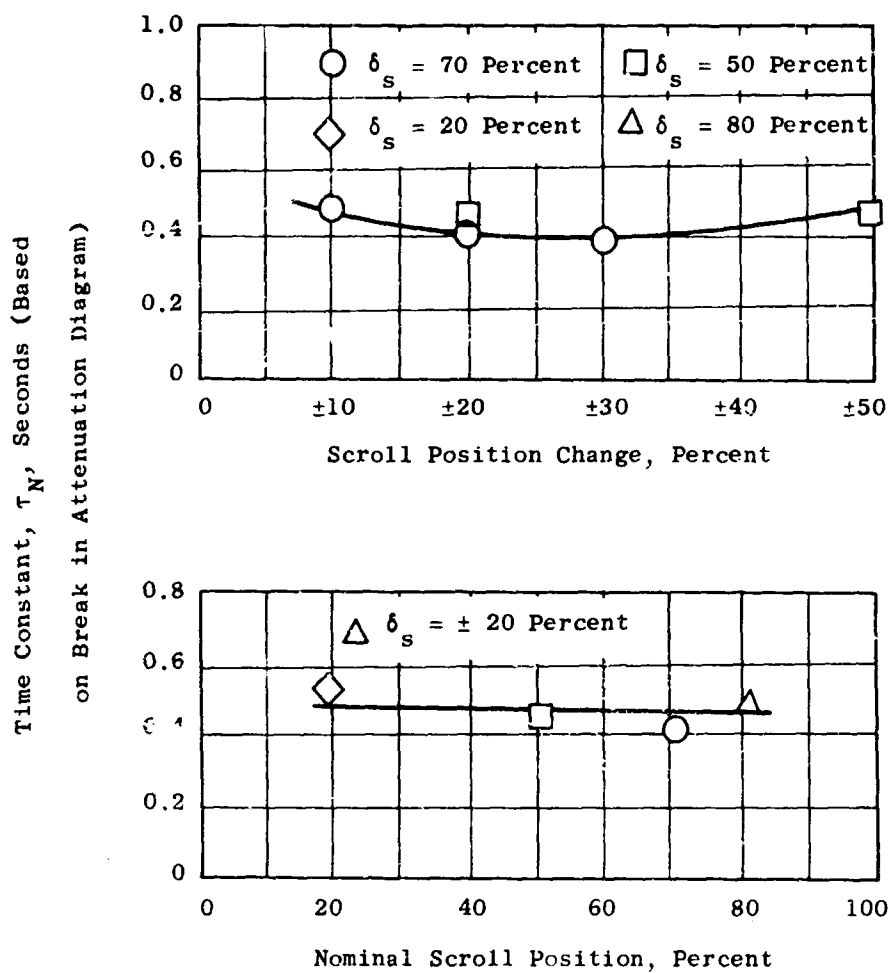


Figure 322. Effects of Scroll Position and Size of Scroll Position Change on Fan Time Constant, $N_e = 95$ Percent.

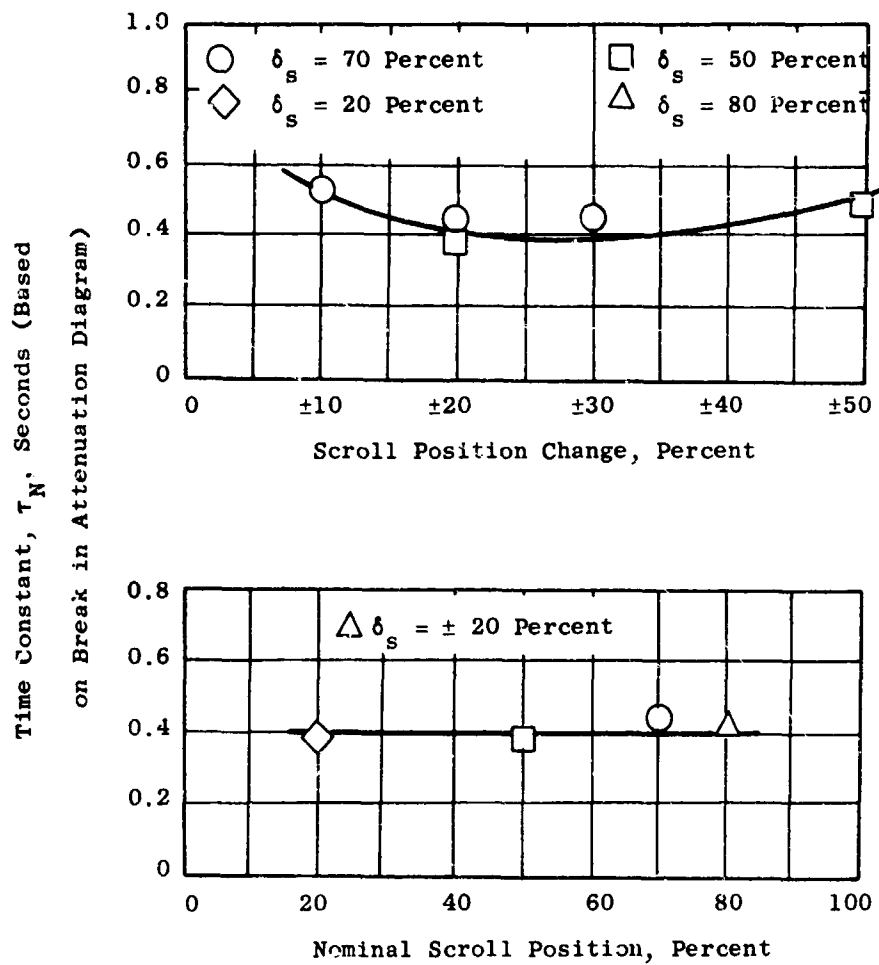


Figure 323. Effects of Scroll Position and Size of Scroll Position Change on Fan Time Constants, $N_e = 100$ Percent.

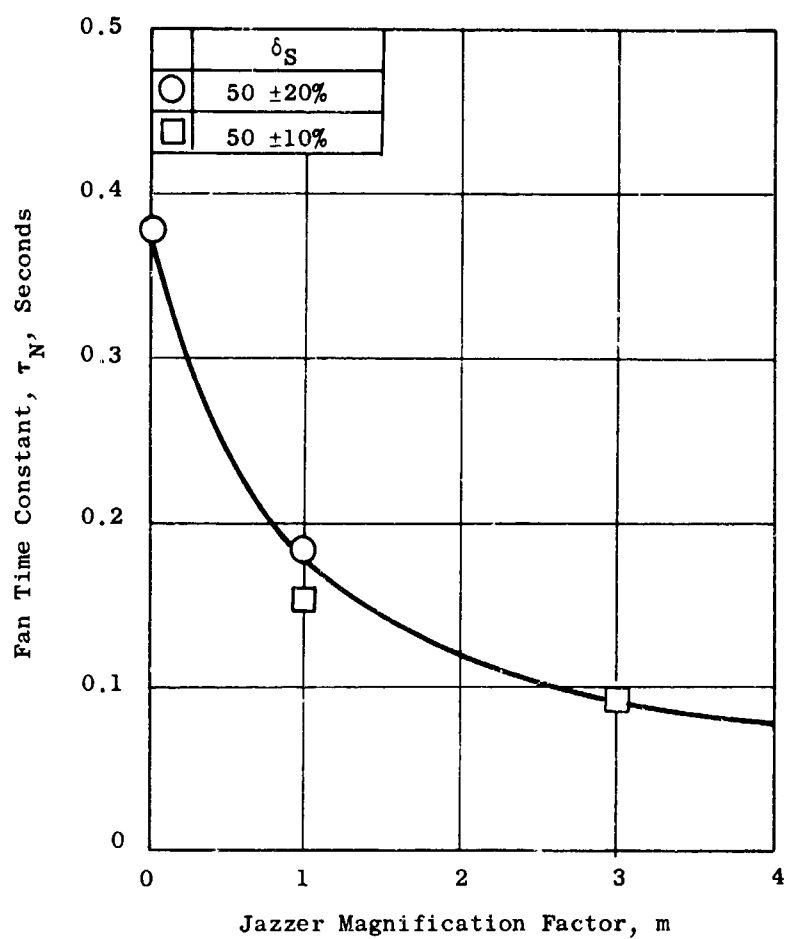


Figure 324. Effects of Jazzer on Fan Time Constants With Steady State Sinusoidal Inputs, $N_e = 100$ Percent.

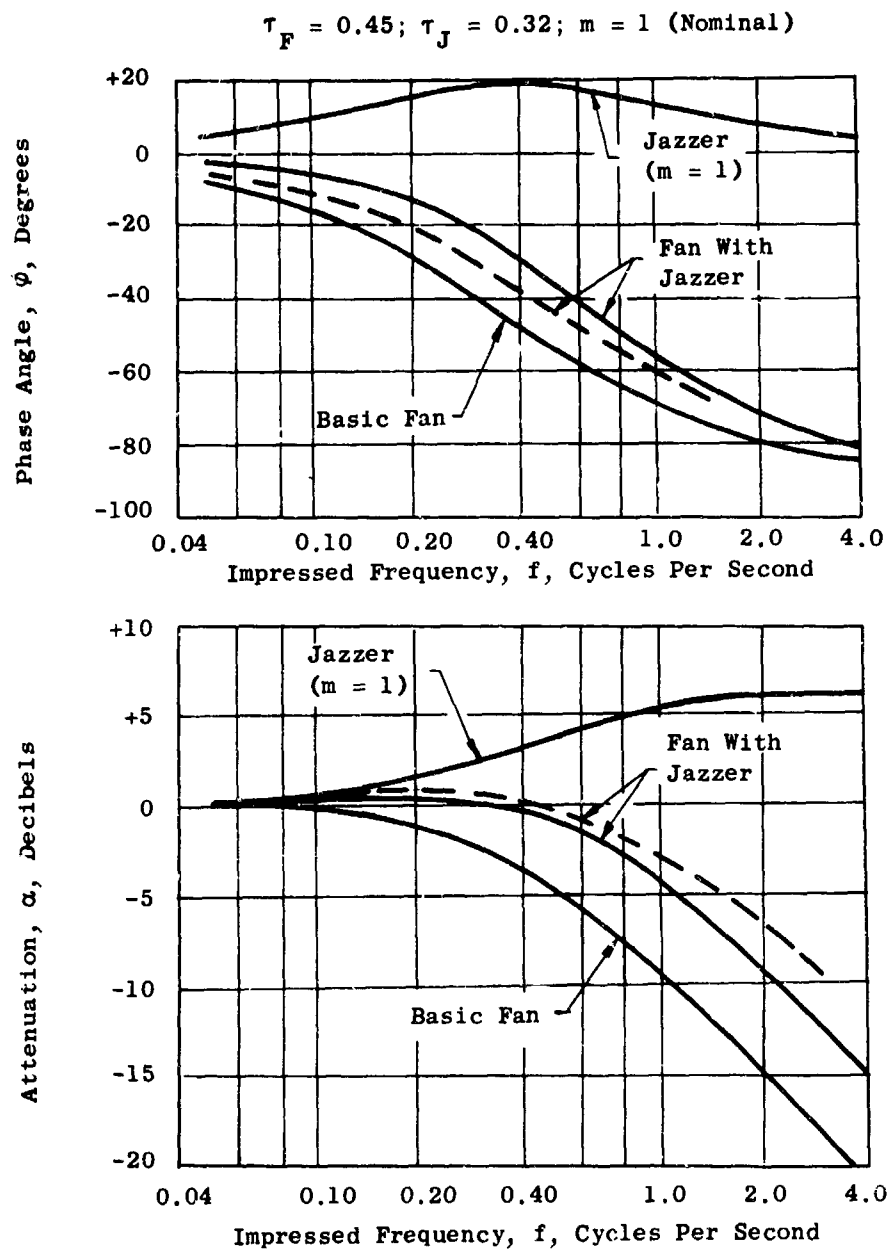


Figure 325. Theoretical Response Characteristics of a Fan With a Jazzer Magnification Factor of 1.0.

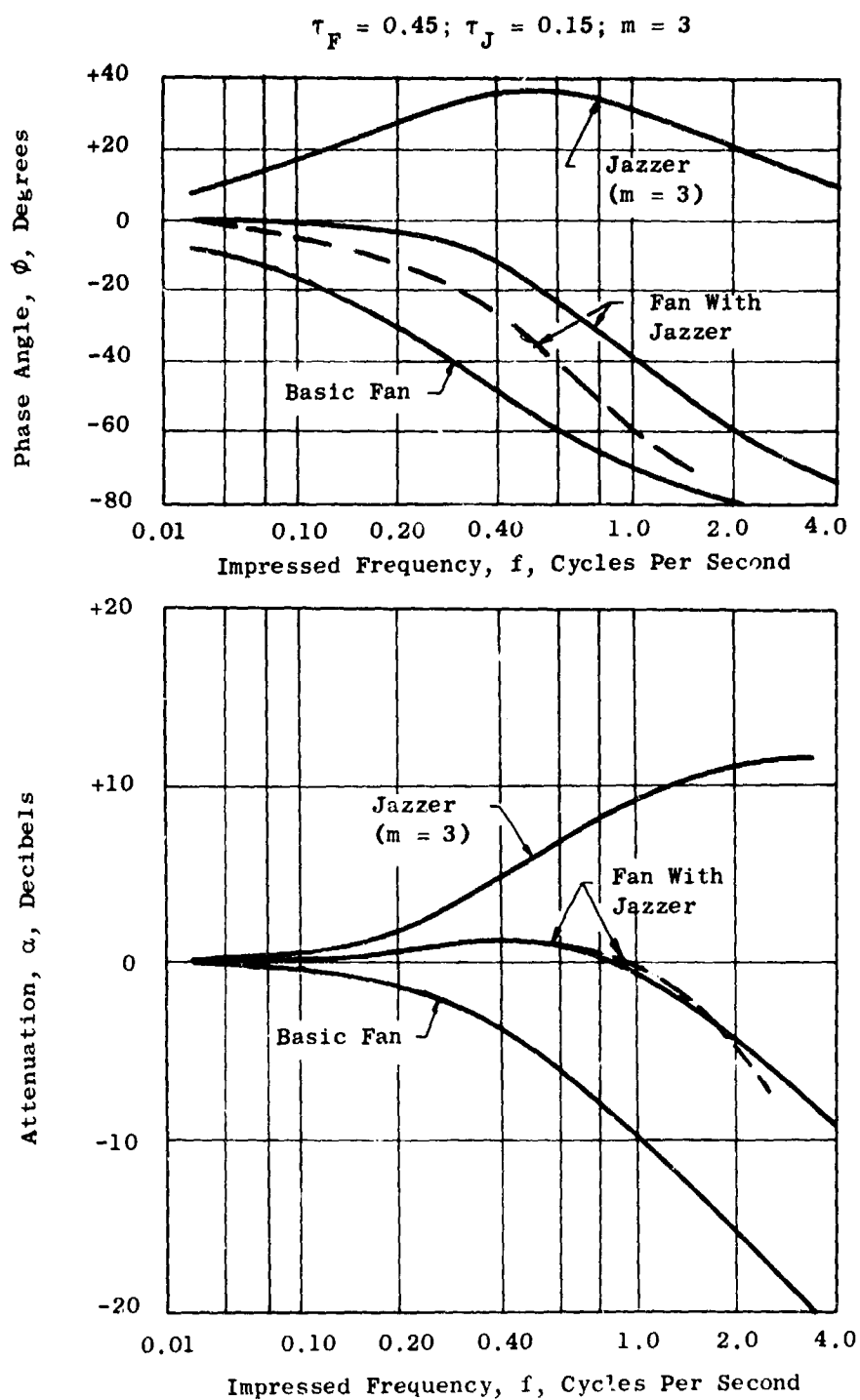


Figure 326. Theoretical Response Characteristics of a Fan With a Jazzer Magnification Factor of 3.0.

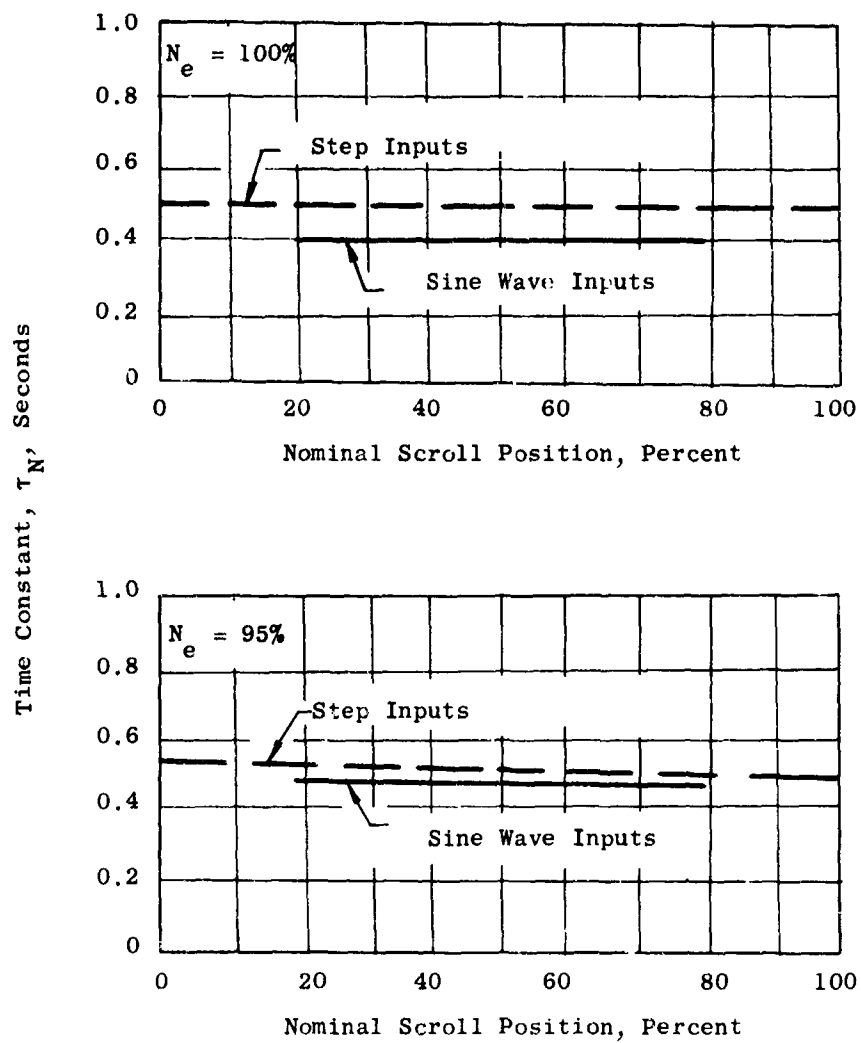


Figure 327. Comparison of Time Constants Measured for Sine Wave and Step Input Types of Commands.

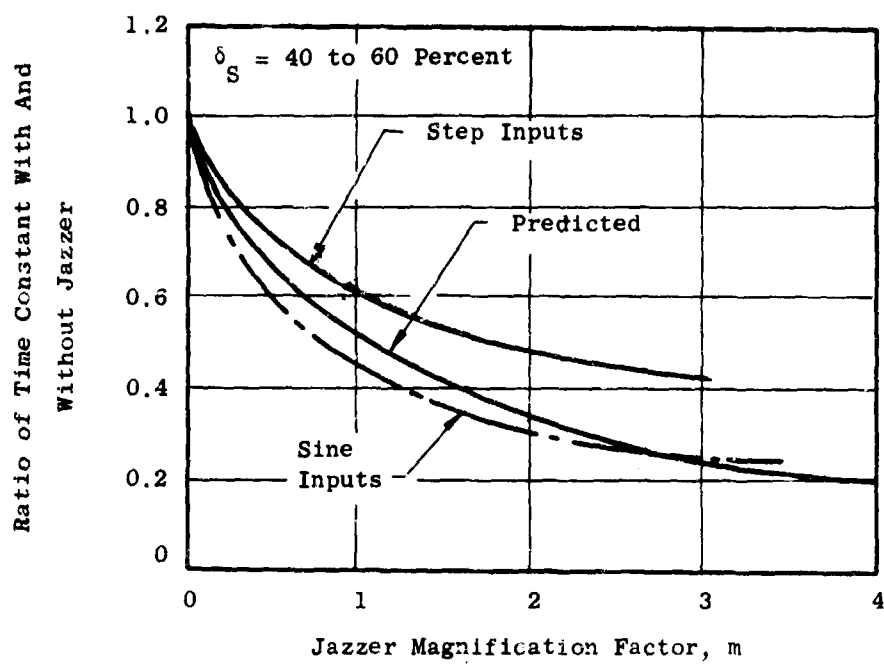


Figure 328. Effects of Jazzer on Fan Time Constant.

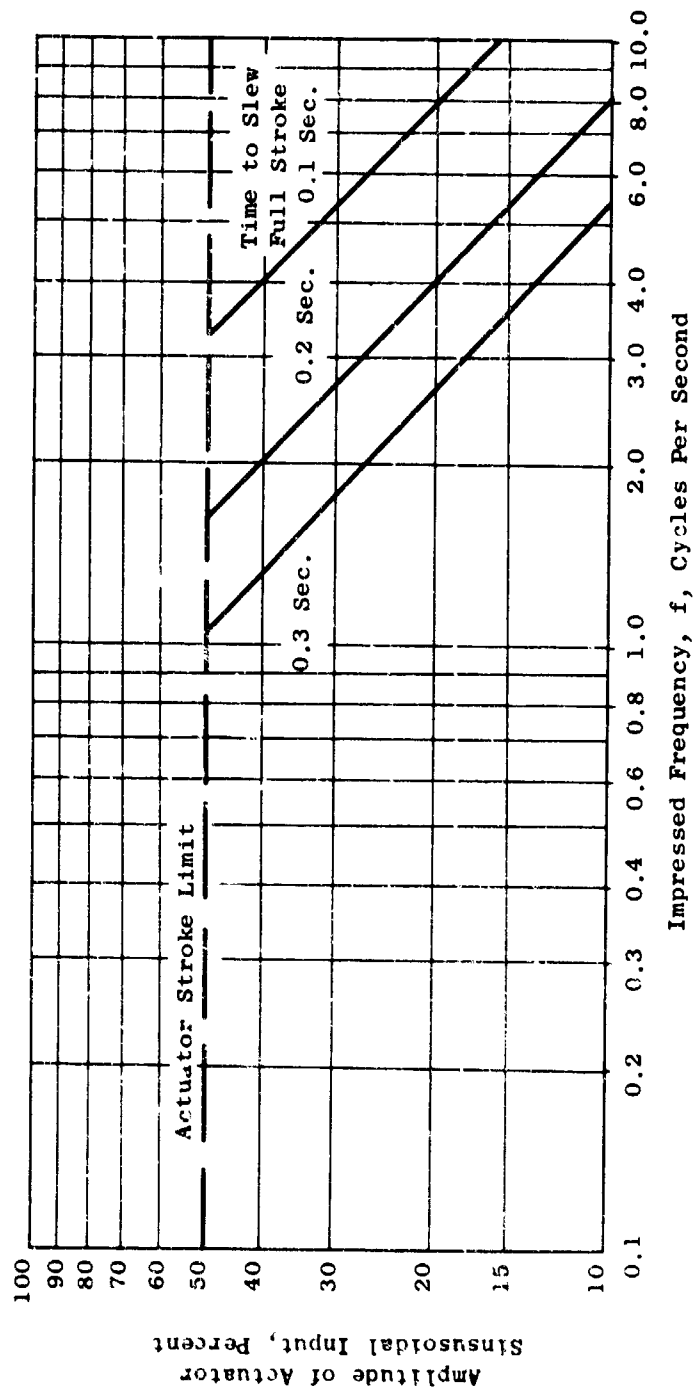


Figure 329. Limits of Amplitude and Frequency for Sinusoidal Inputs as Established by Actuator Slew Rates.

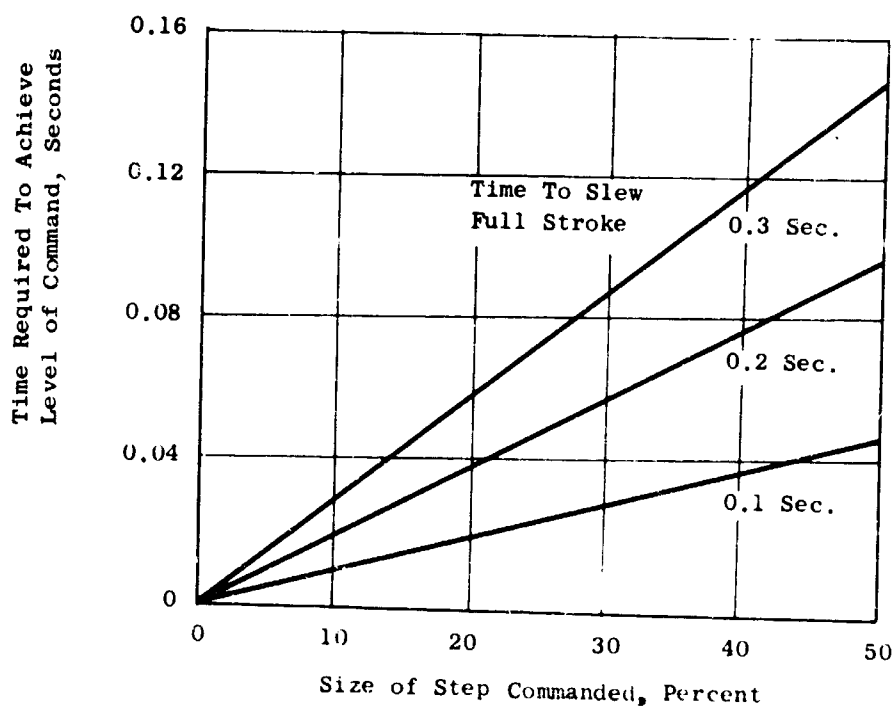


Figure 330. Effects of Actuator Slew Rate on Time Required to Achieve Command Level During Step Inputs.

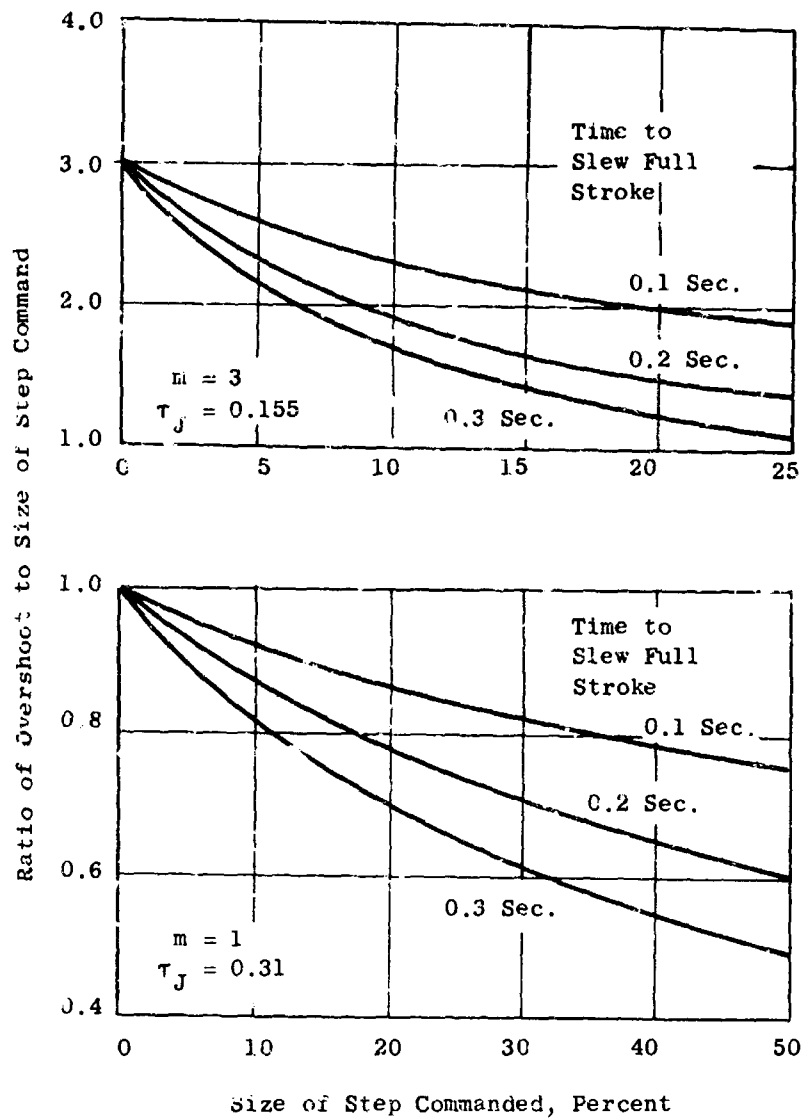


Figure 331. Effects of Actuator Slew Rate and Size of Step Command on Actuator Overshoot With Jazzer.

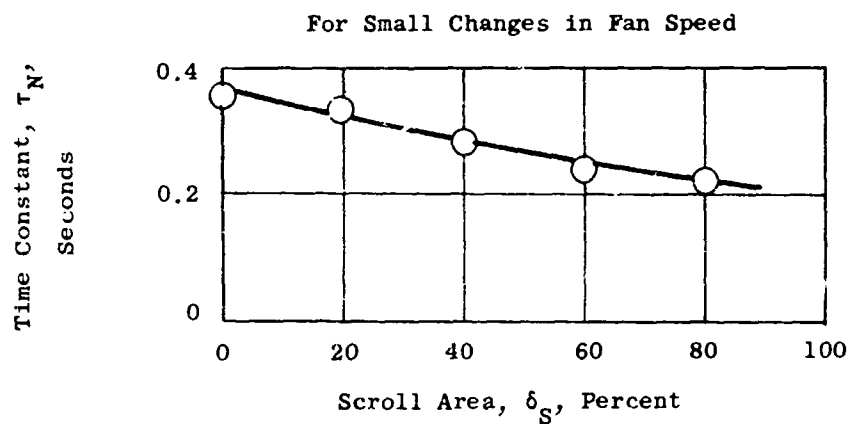
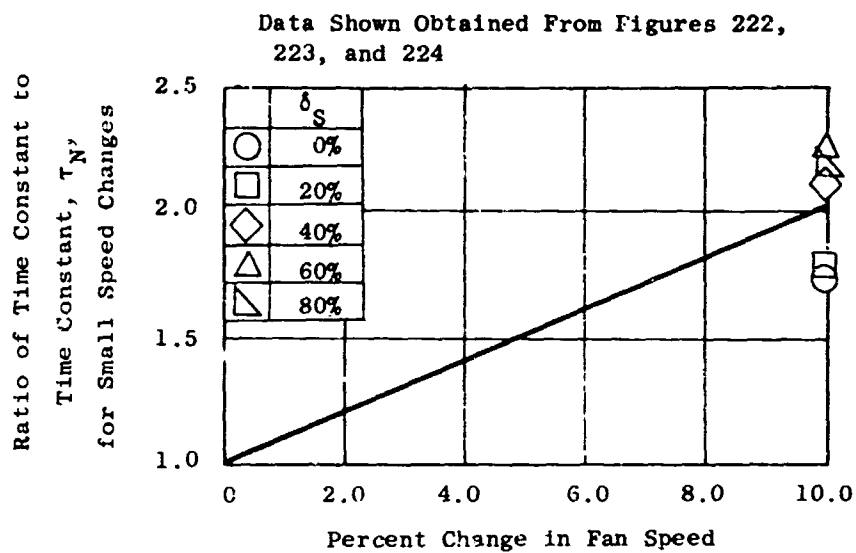


Figure 332. Effects of Scroll Area Setting and Size of Fan Speed Changes on Time Constant When Using Engines for Altitude Control.

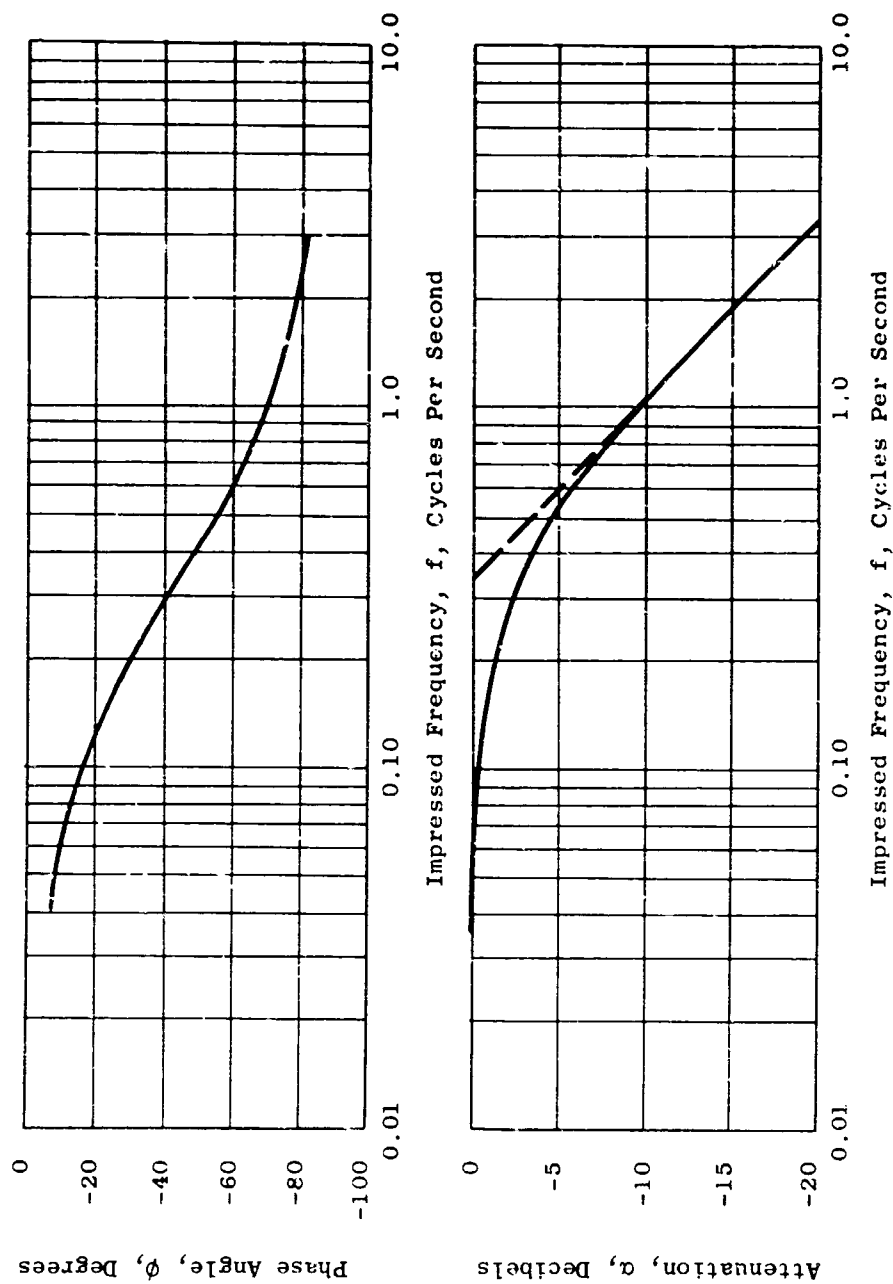


Figure 333. Steady State Frequency Response Characteristics of the Vertical Lift System Based on a Time Constant of 0.47 Second.

$N_{Fc} = 2220 \text{ rpm}$ $\delta_S = 50 \pm 20 \text{ Percent}$
 $\tau_J = 0.31$ $m = 1 \text{ (Nominal)}$

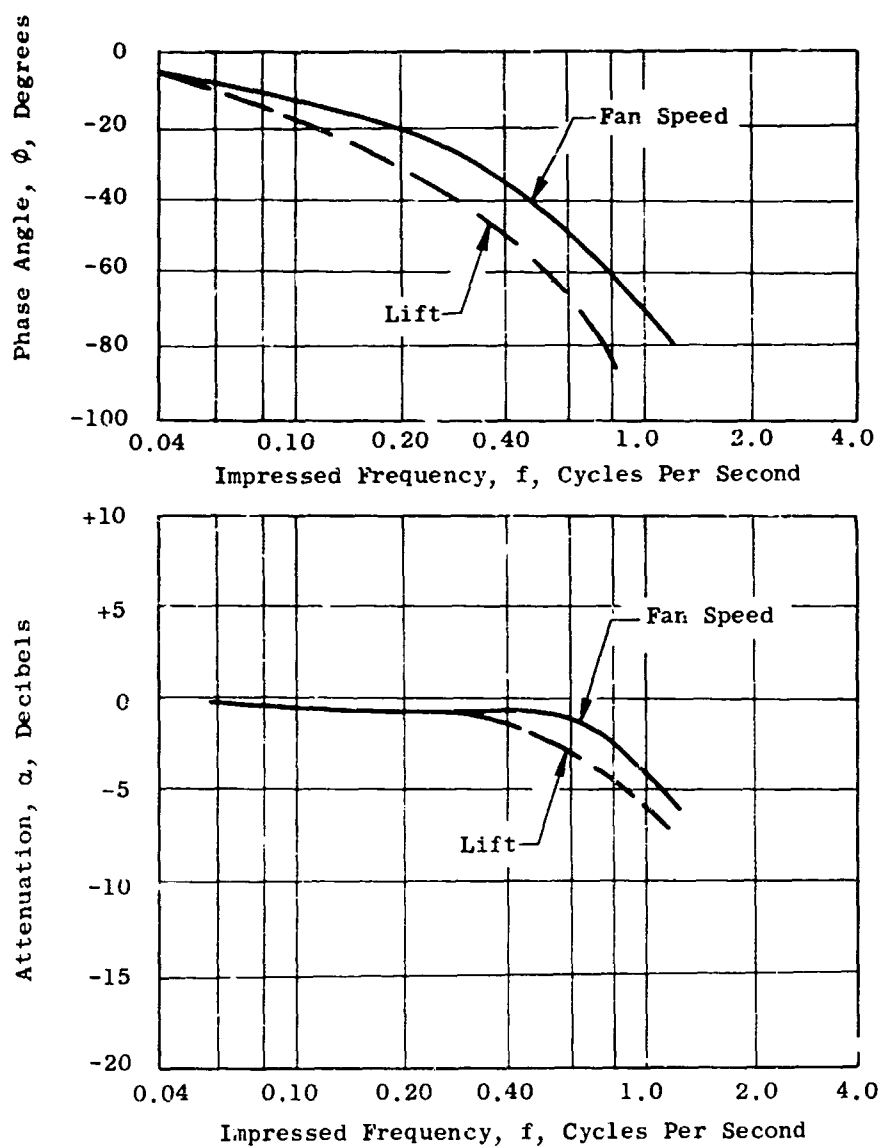


Figure 334. Comparison of Fan Response Based on Fan Speed and Corrected Lift Data, $\tau_J = 0.31$, $m = 1.0$, $\delta_S = 50 \pm 20 \text{ Percent}$.

$N_{Fc} = 2220 \text{ rpm}$

$\delta_S = 50 \pm 10 \text{ Percent}$

$\tau_J = 0.31$

$m = 1 \text{ (Nominal)}$

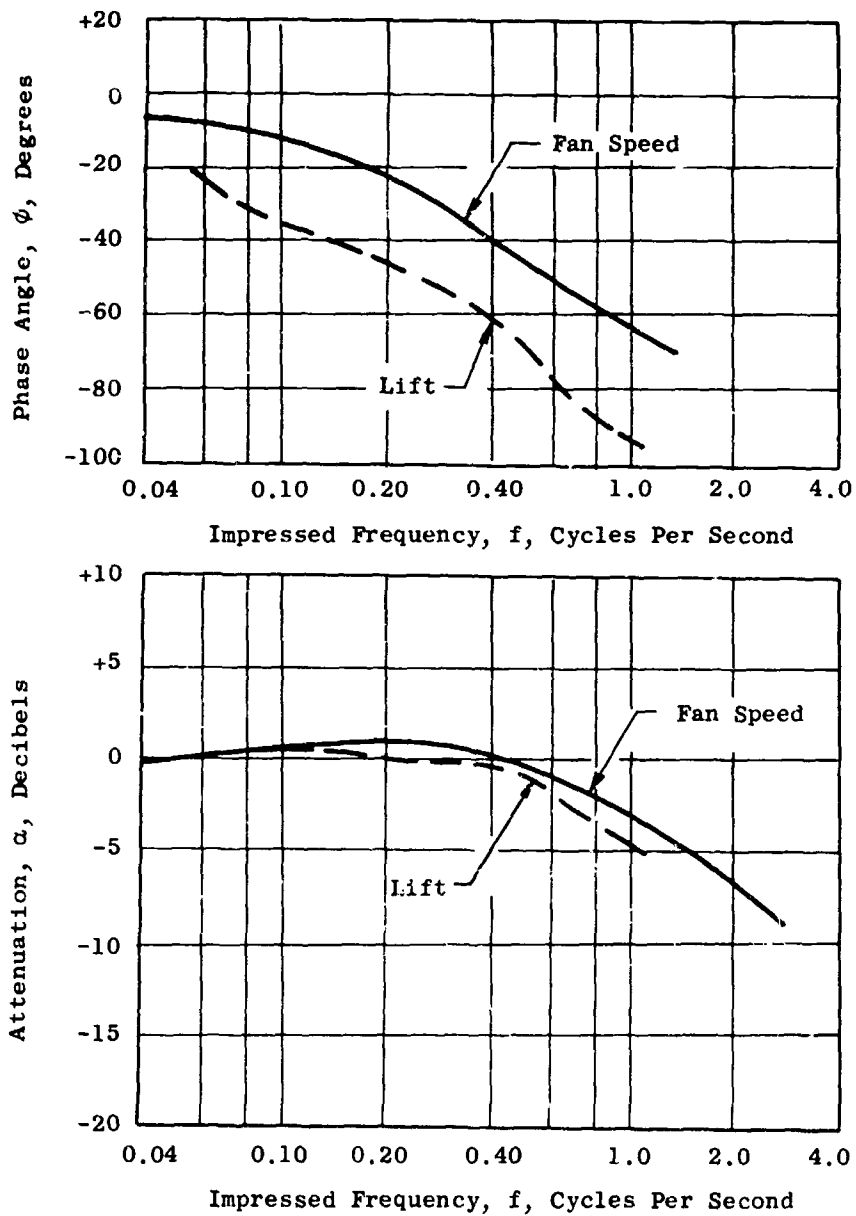


Figure 335. Comparison of Fan Response Based on Fan Speed and Corrected Lift Data, $\tau_J = 0.31$, $m = 1.0$, $\delta_S = 50 \pm 10 \text{ Percent}$.

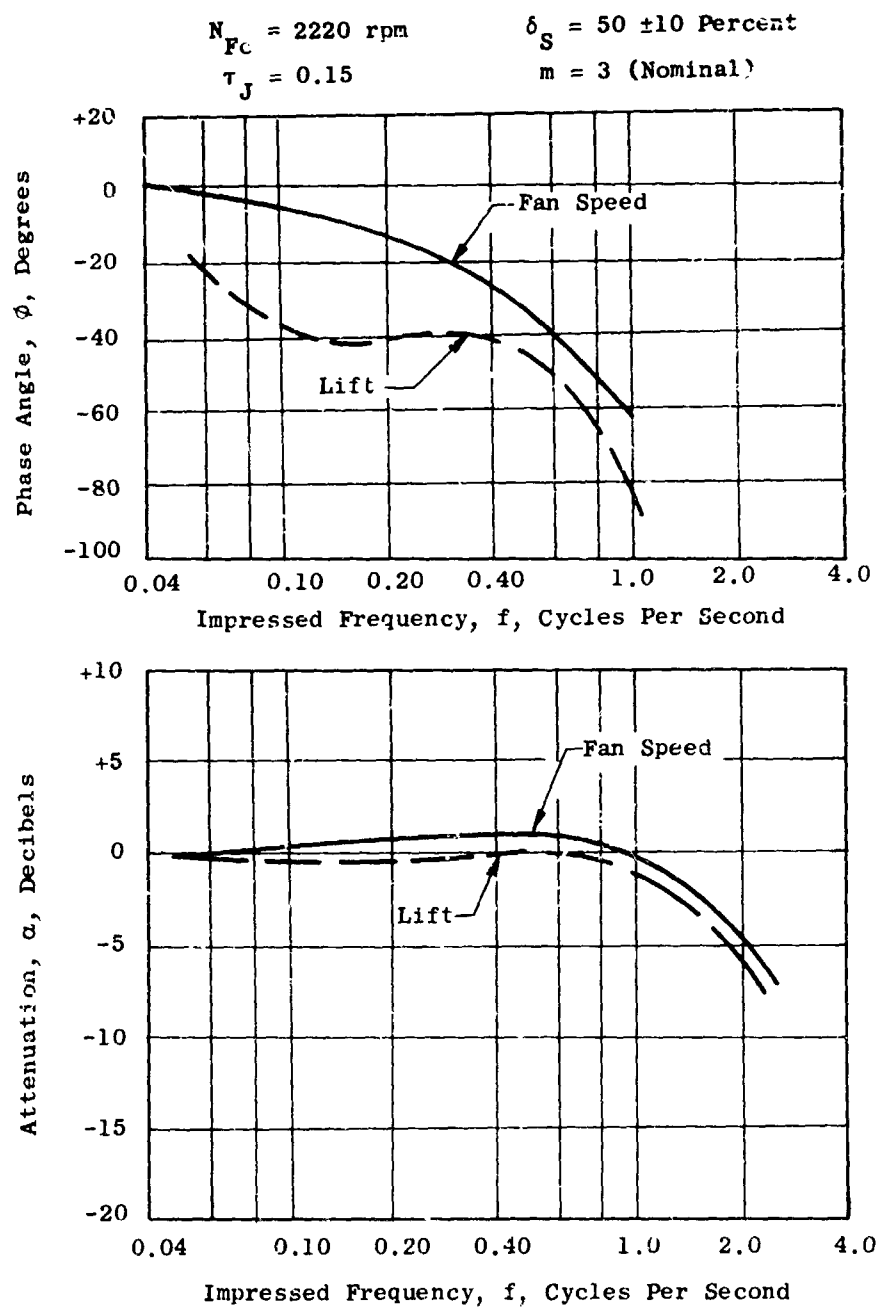


Figure 336. Comparison of Fan Response Based on Fan Speed and Corrected Lift Data, $\tau_J = 0.15$, $m = 3.0$, $\delta_S = 50 \pm 10 \text{ Percent}$.

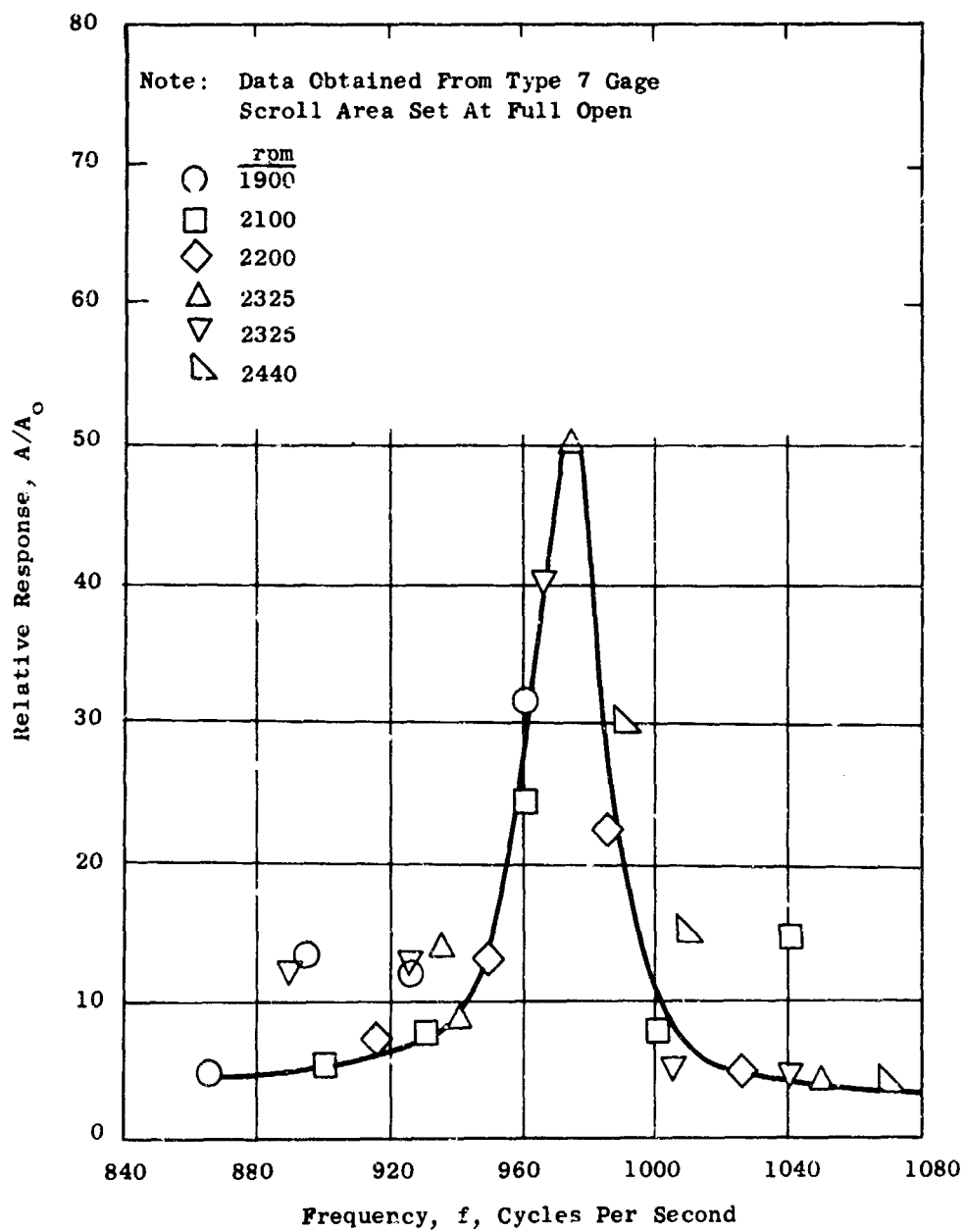


Figure 337. Frequency Response Characteristics of the LF2 Turbine Bucket.

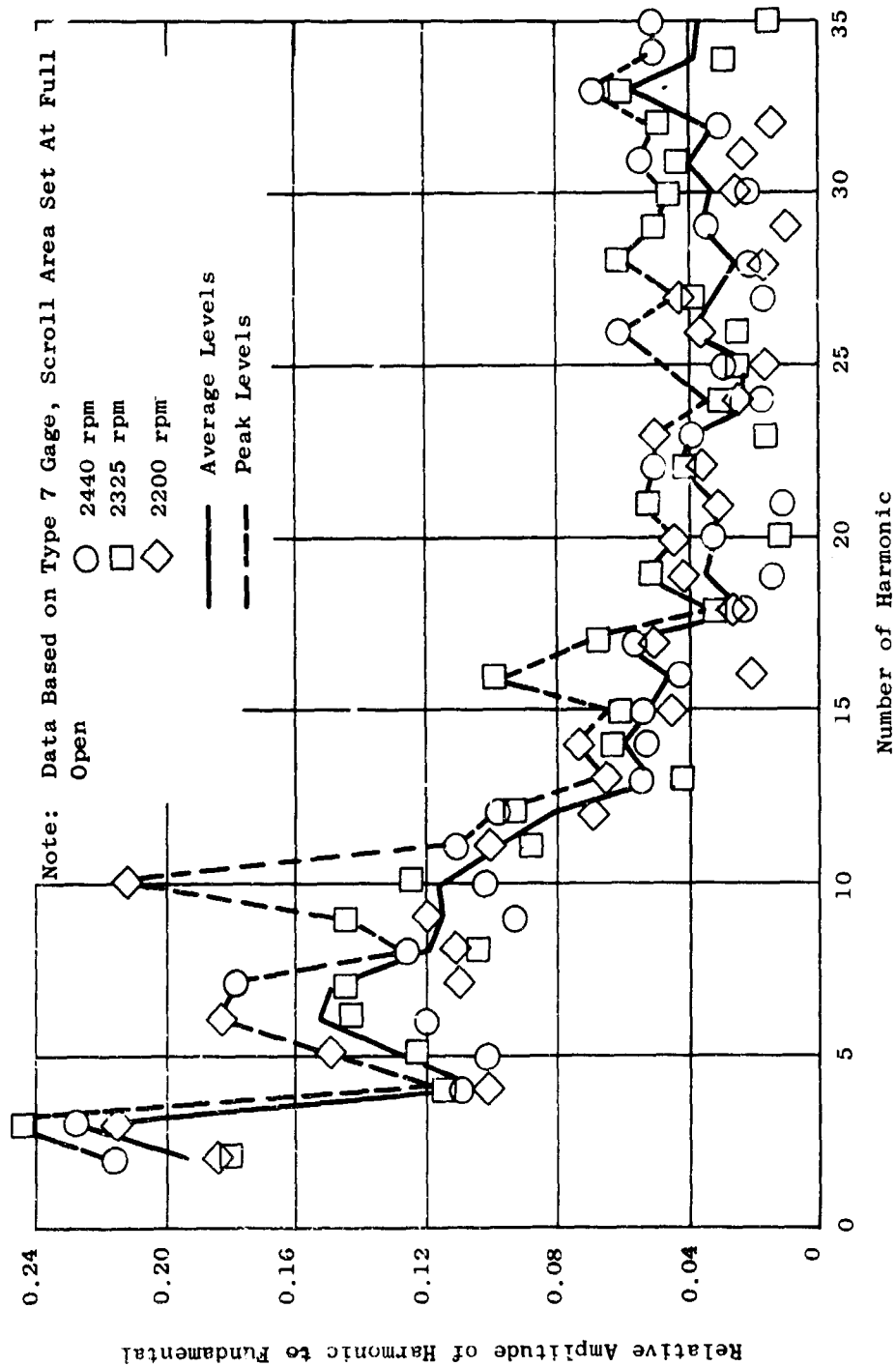


Figure 338. Harmonic Breakdown of Exciting Forces in the LF2/VAS System at Full Open Scroll Conditions.

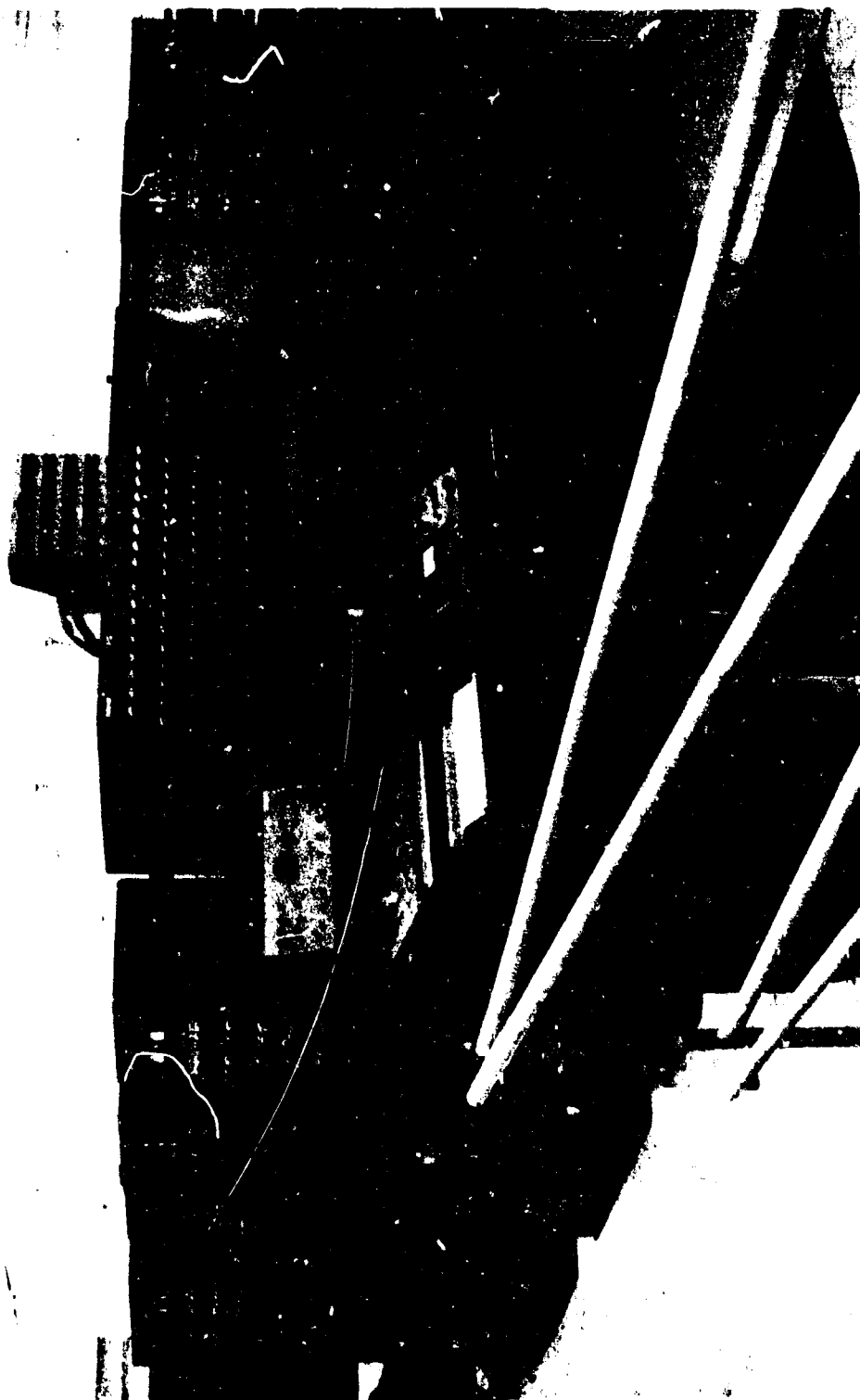


Figure 339 General Electric Evendale Analog Computer Laboratory.

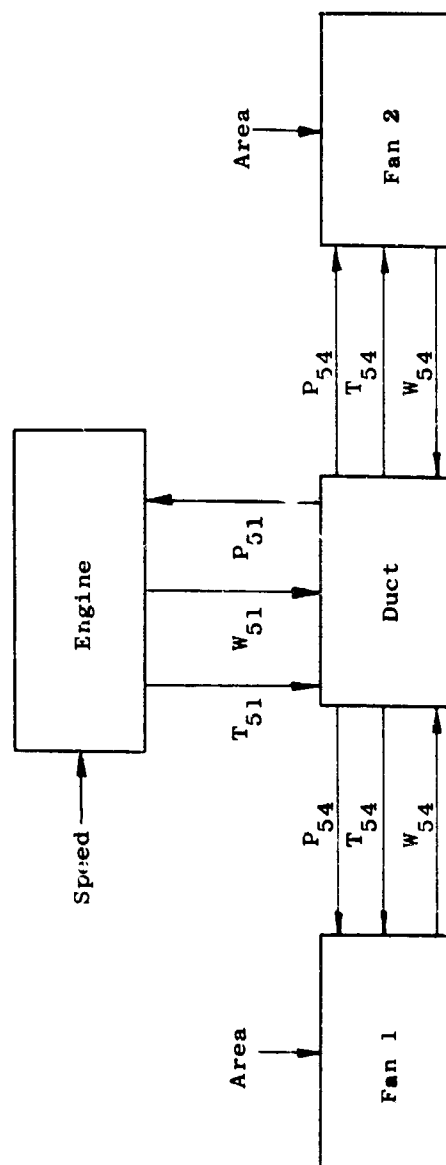


Figure 340. System Analog Block Diagram.

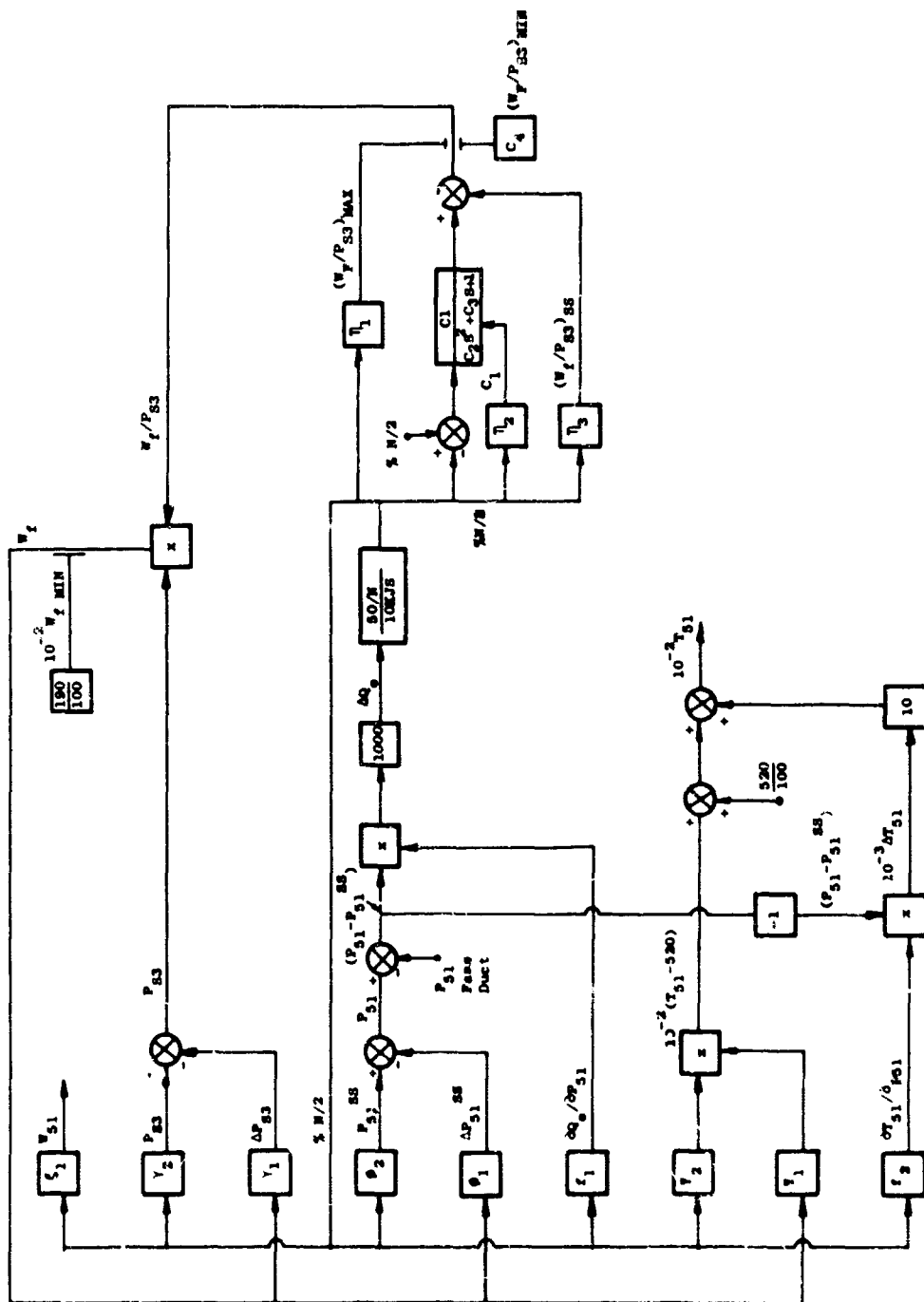


Figure 341. Engine Analog Block Diagram.



507

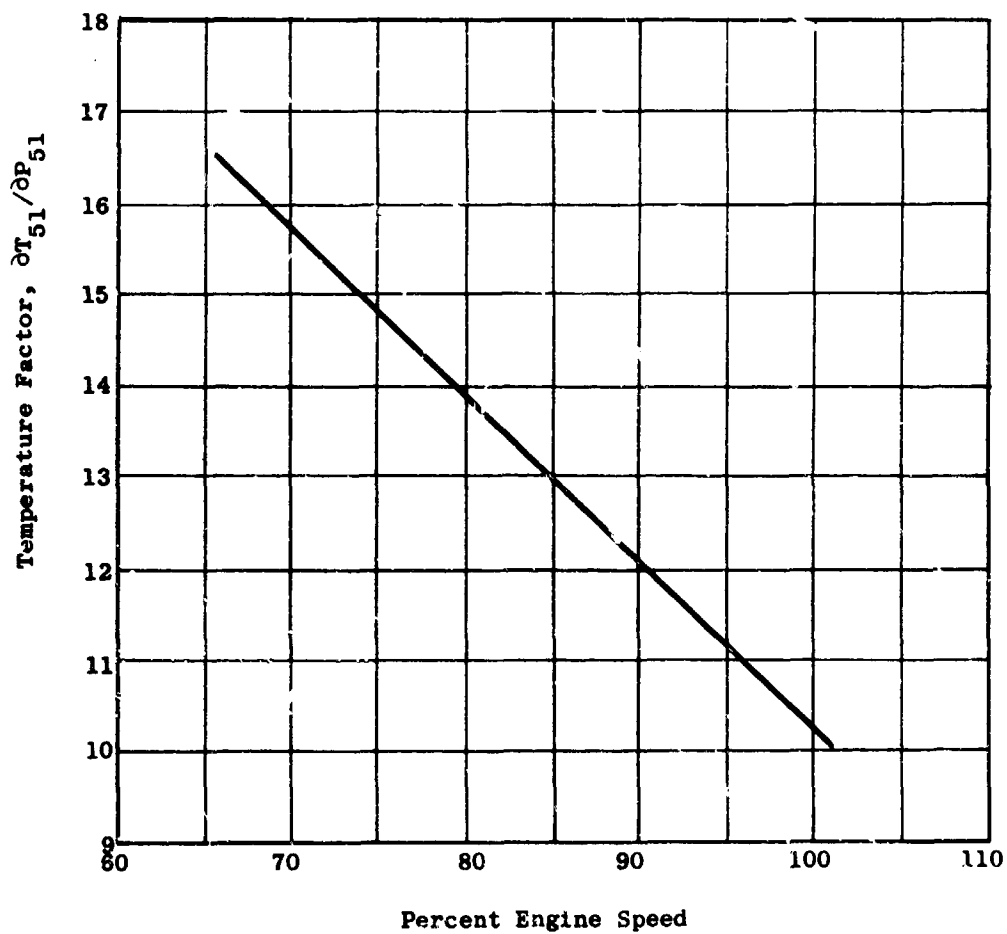


Figure 343. J85/J4 Gas Generator Temperature Factor ($\partial T_{51} / \partial P_{51}$) Versus Engine Speed.

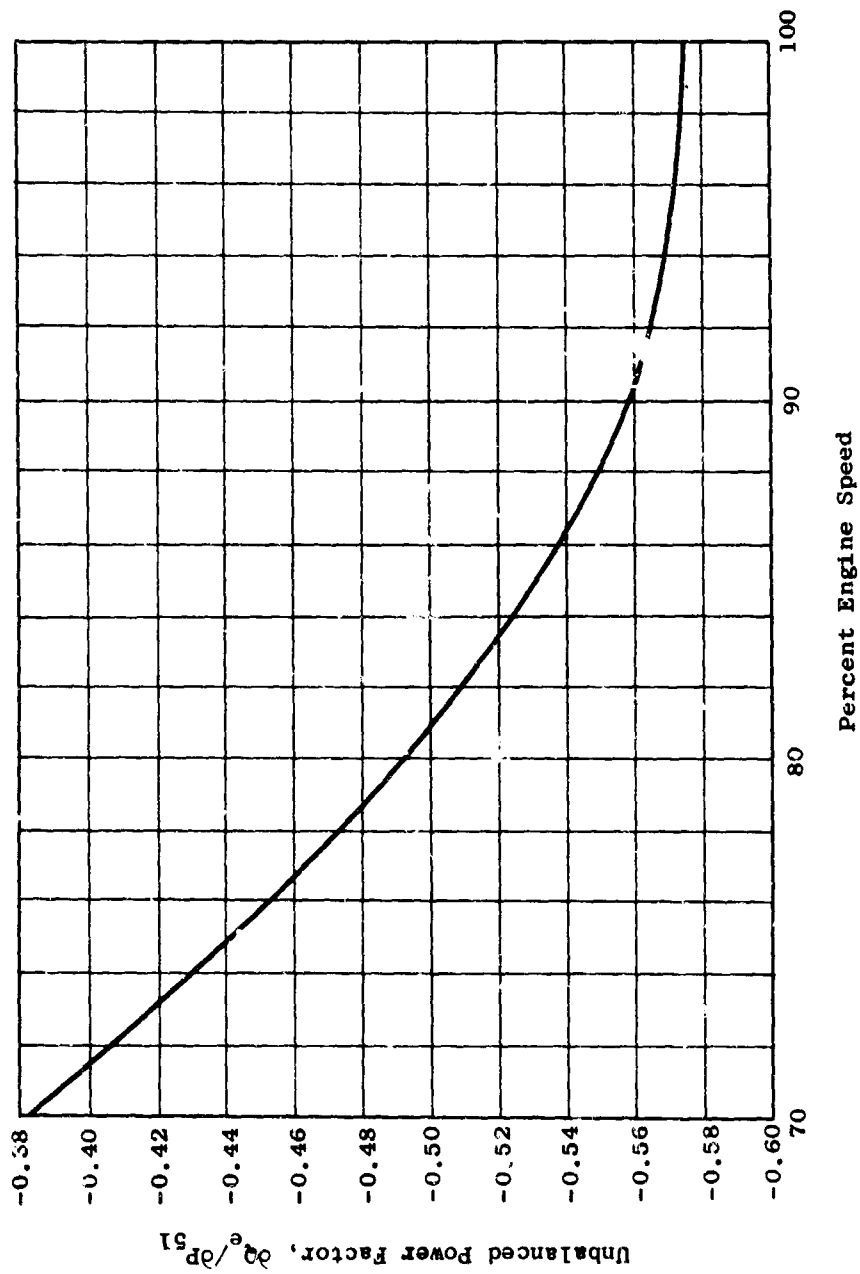


Figure 344. J85/J4 Gas Generator Unbalanced Power Factor ($\partial Q_e / \partial P_{51}$) Versus Engine Speed.

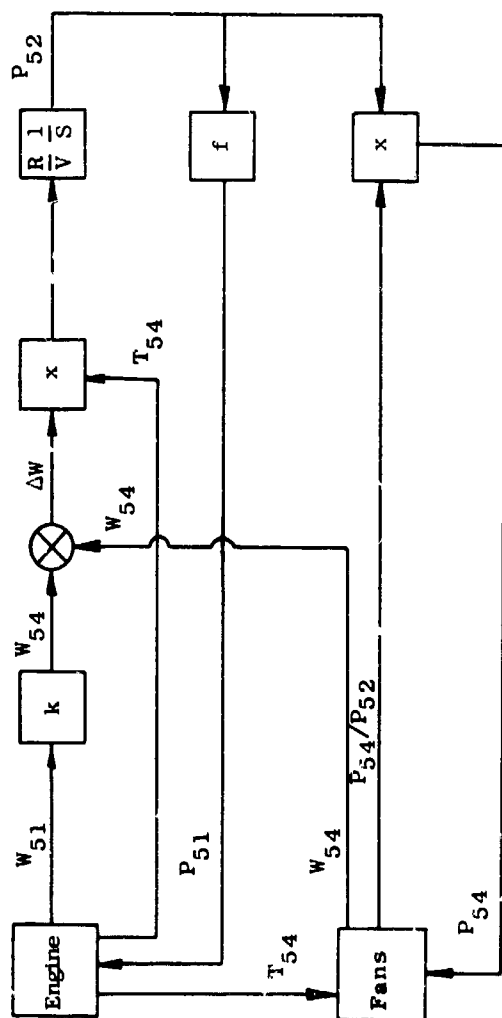


Figure 345. Duct Analog Block Diagram.

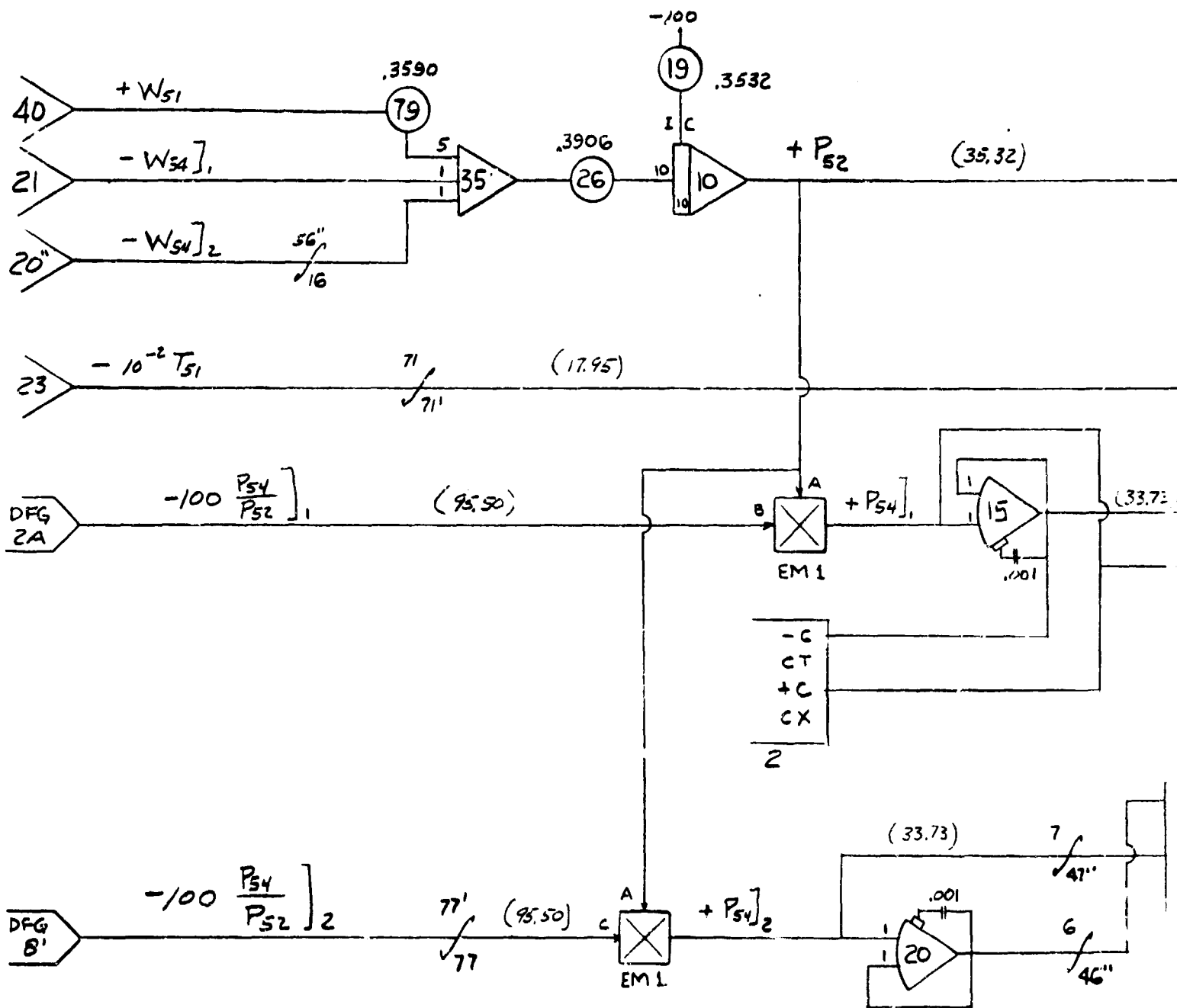


Figure 346. Duct Analog Wiring Diagram.

A

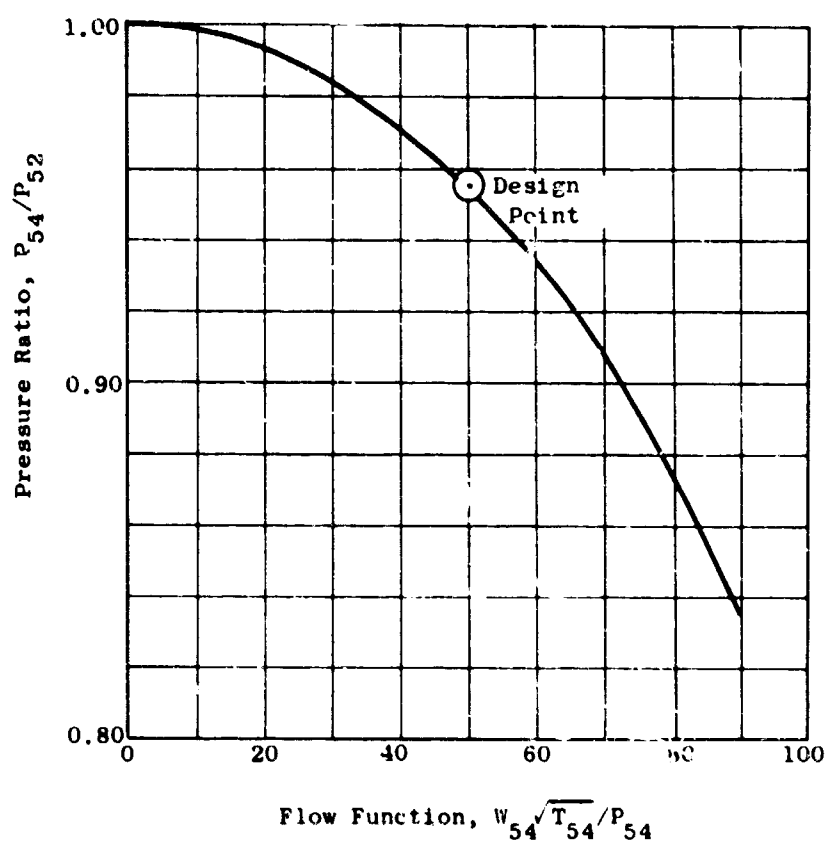
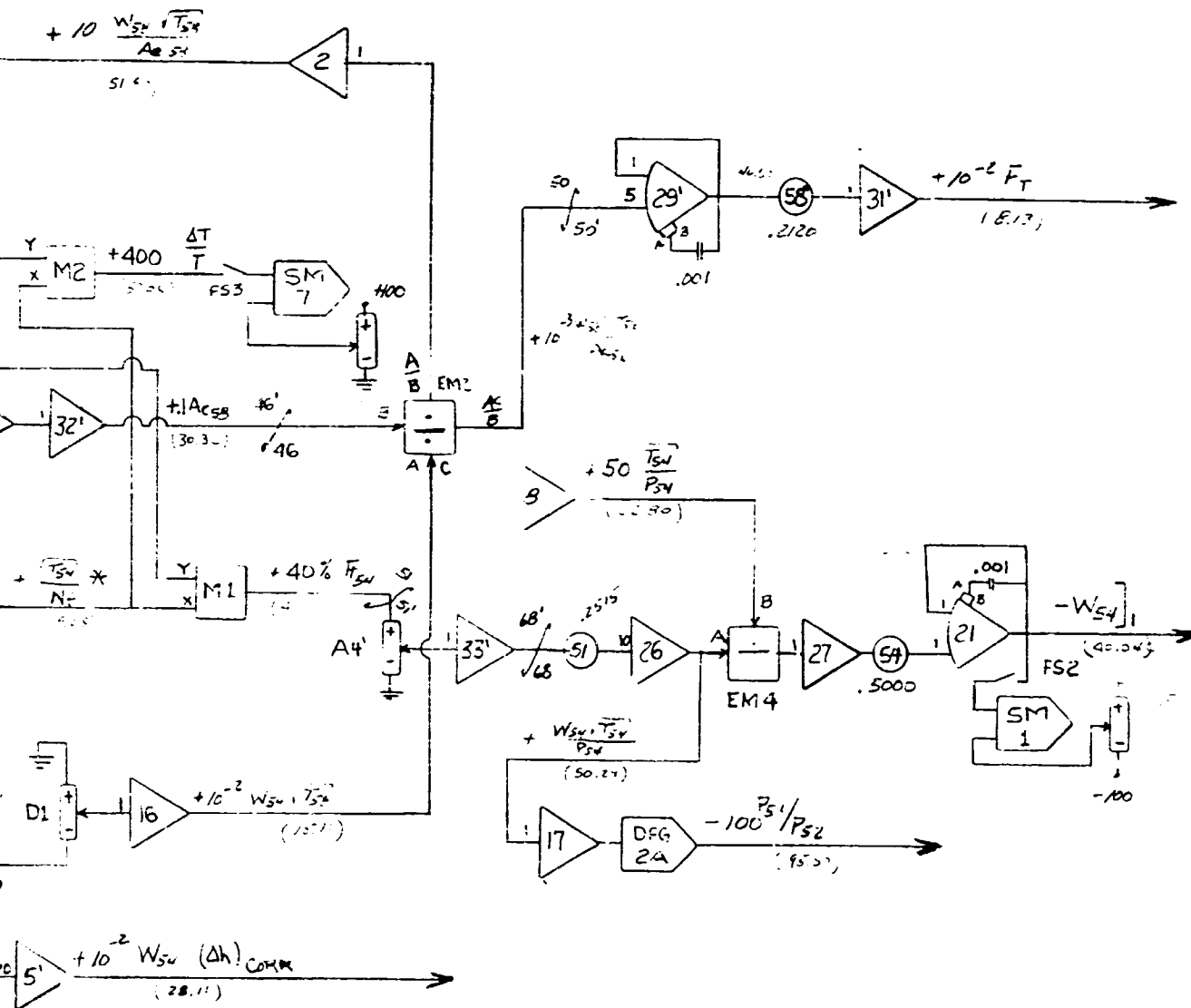


Figure 347. LF2 Lift Fan Scroll Total Pressure Loss Versus Scroll Flow Function.







$$A = .2774 \times .988 \times K$$

$$C_p \text{ loss}$$

B

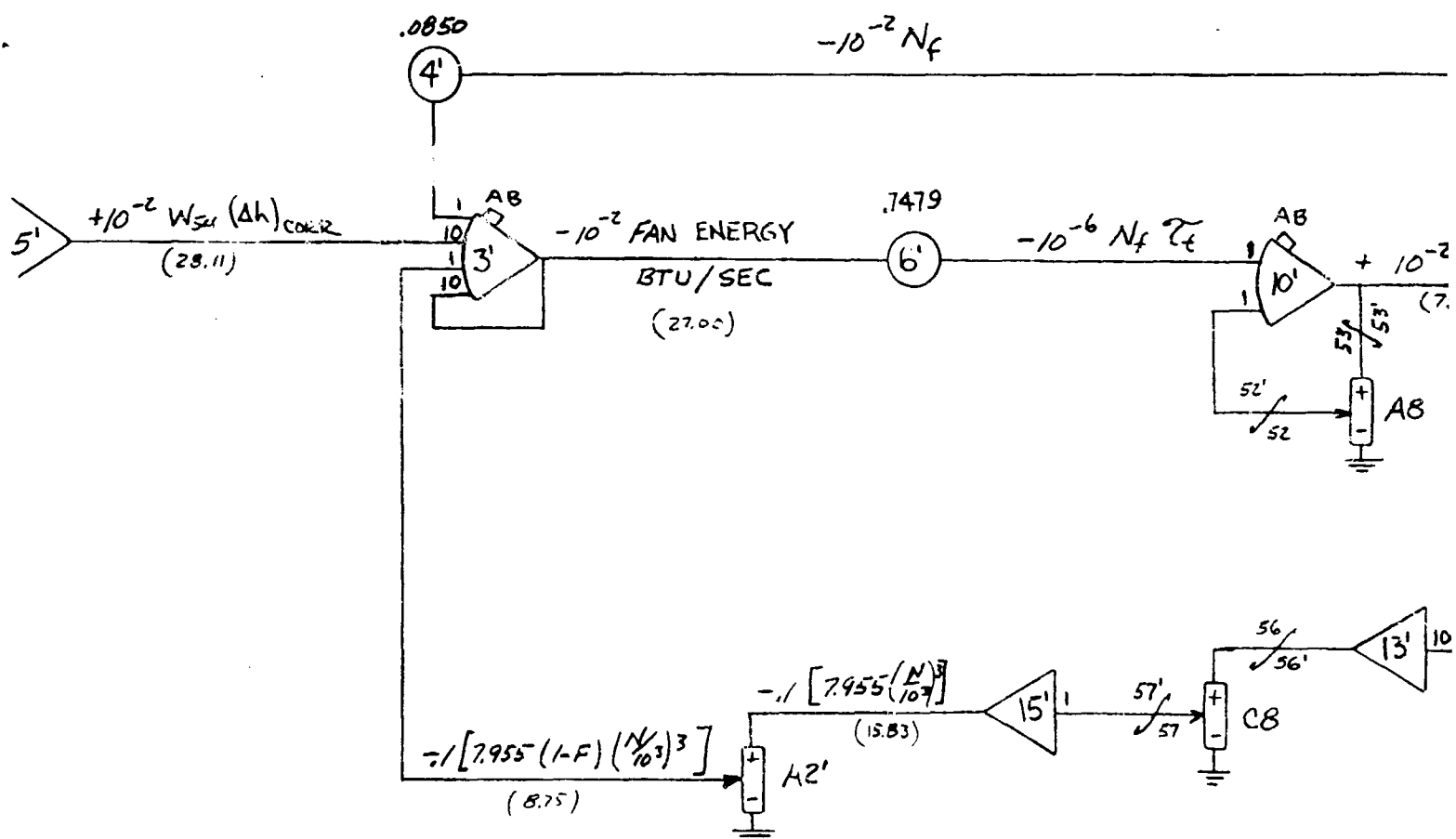
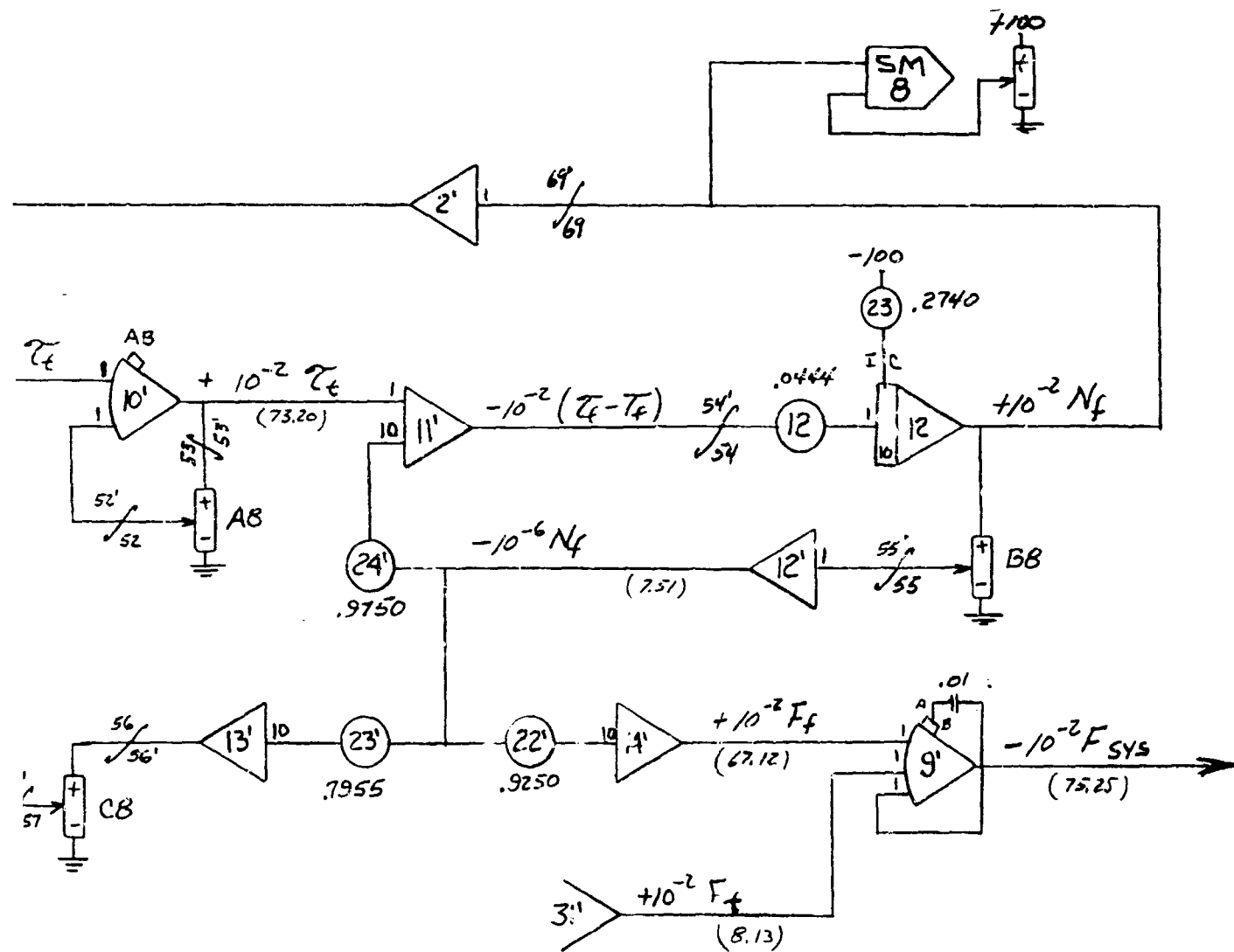


Figure 350. Fan Number 1 Analog Wiring Diagram - Sheet 2.



B

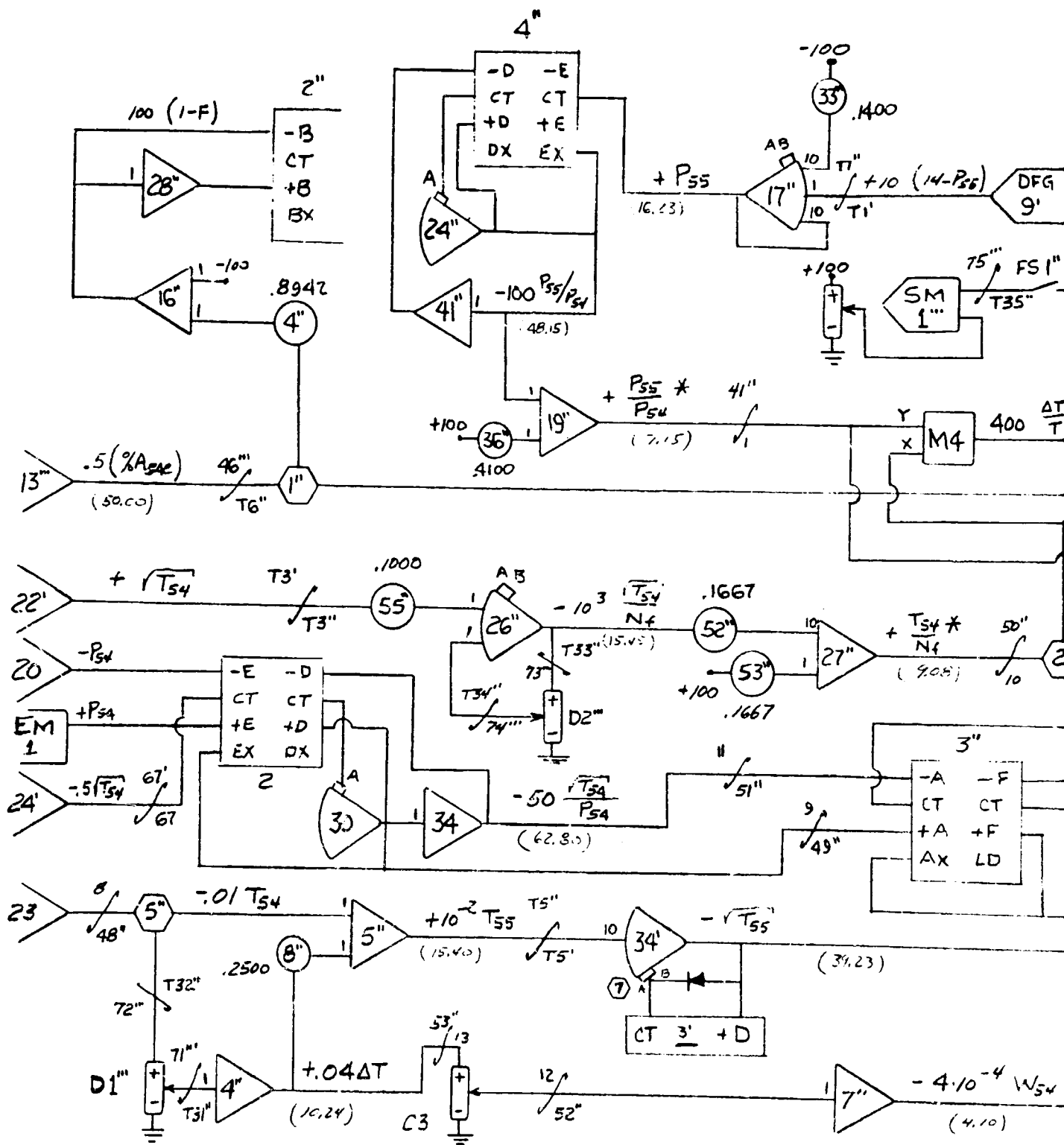
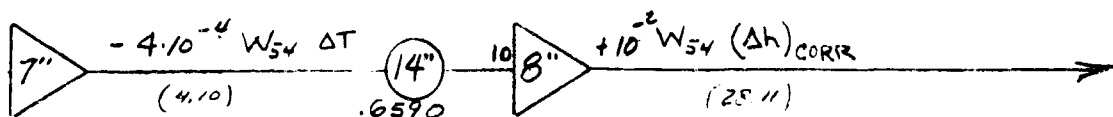
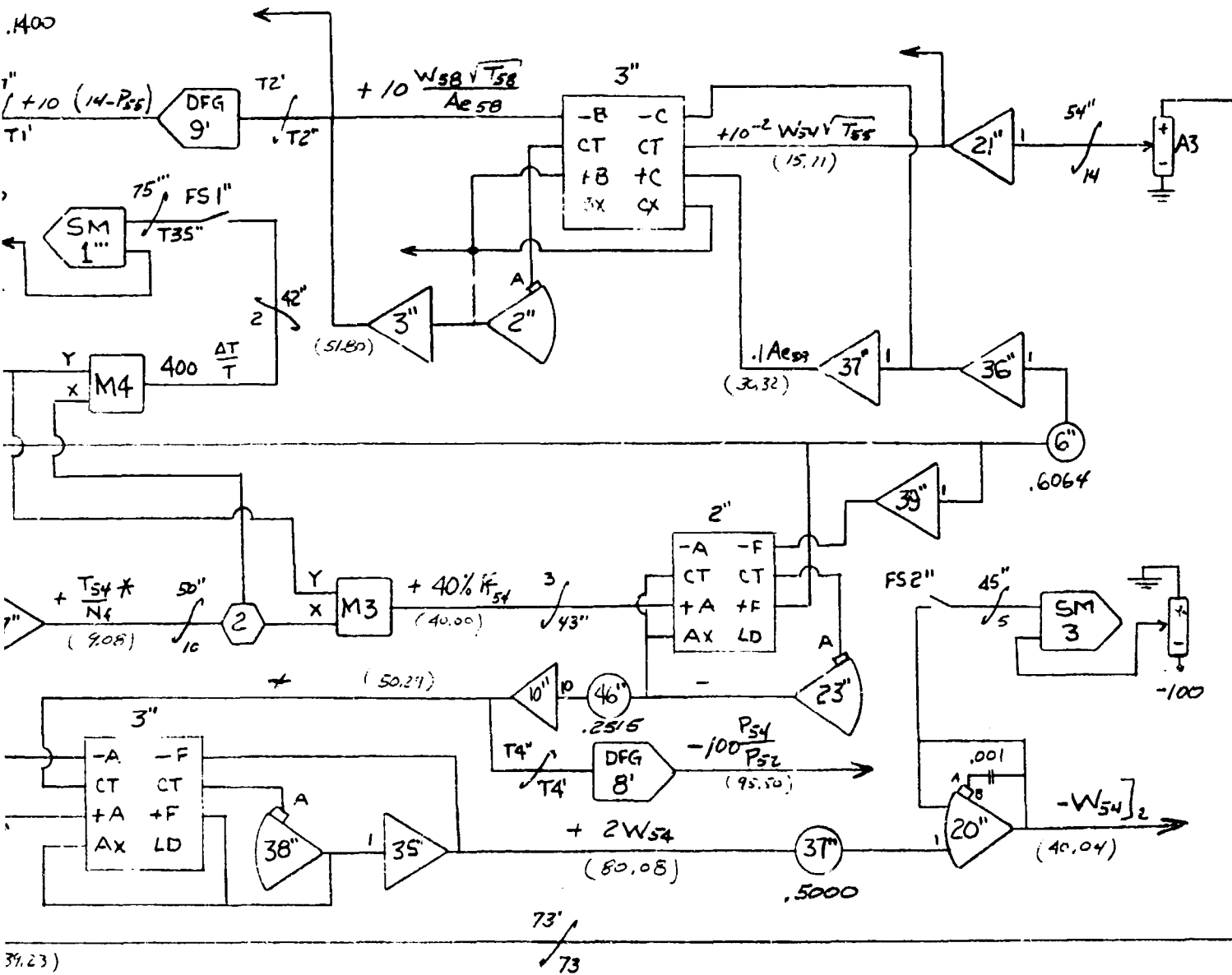


Figure 351. Fan Number 2 Analog Wiring Diagram - Sheet 1.



B

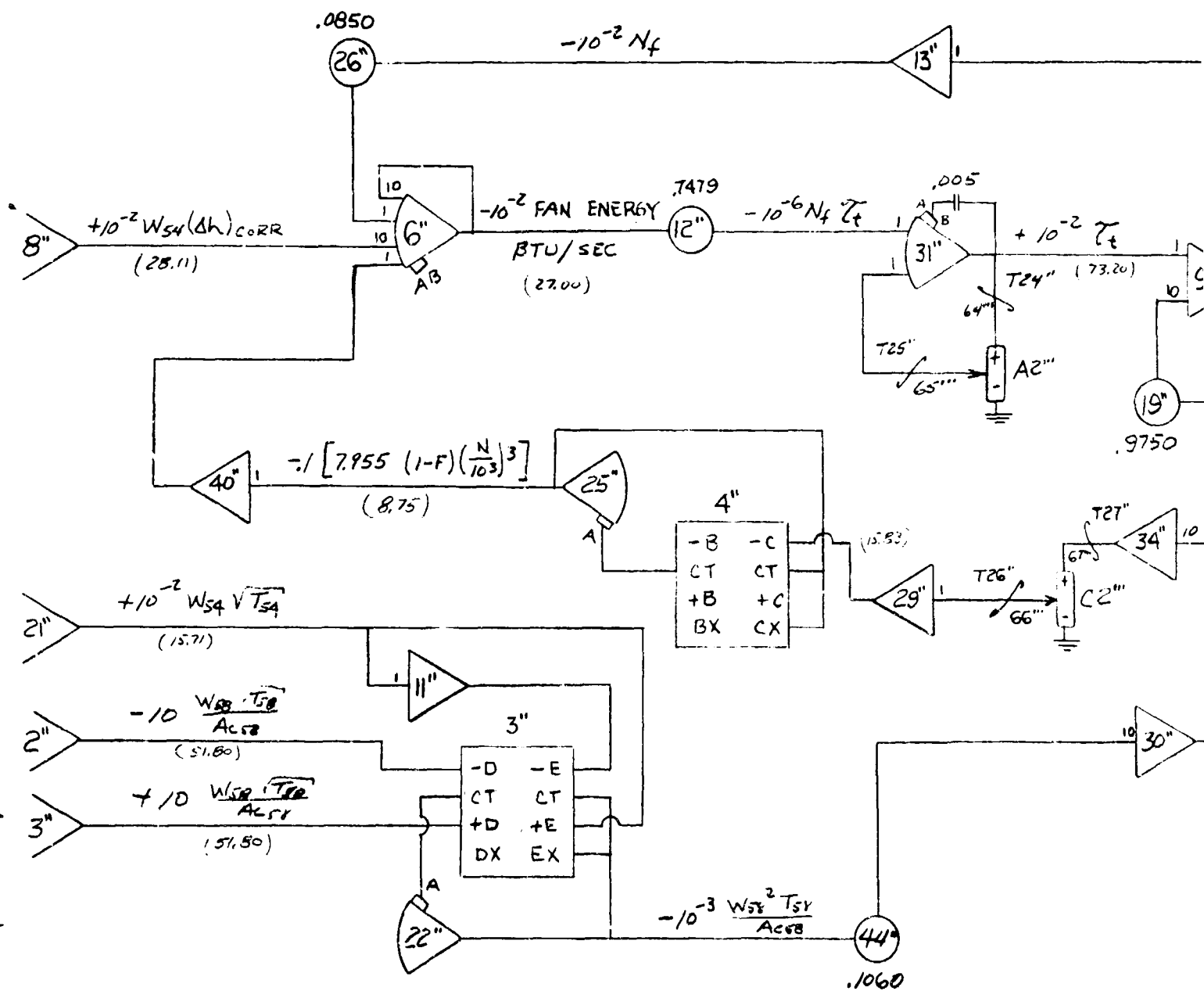
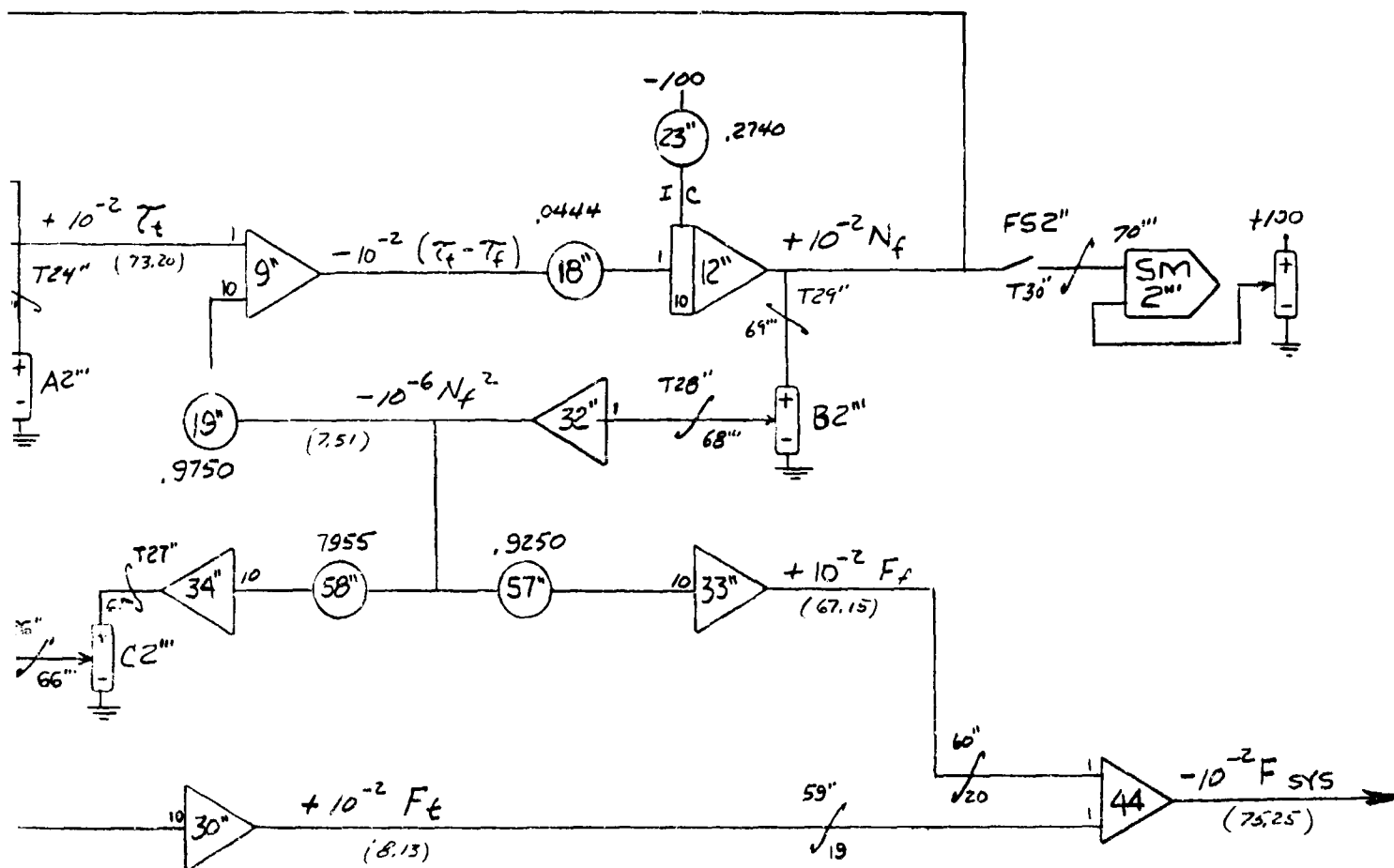
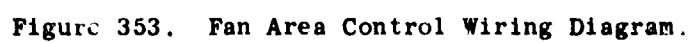


Figure 352. Fan Number 2 Analog Wiring Diagram - Sheet 2.



B



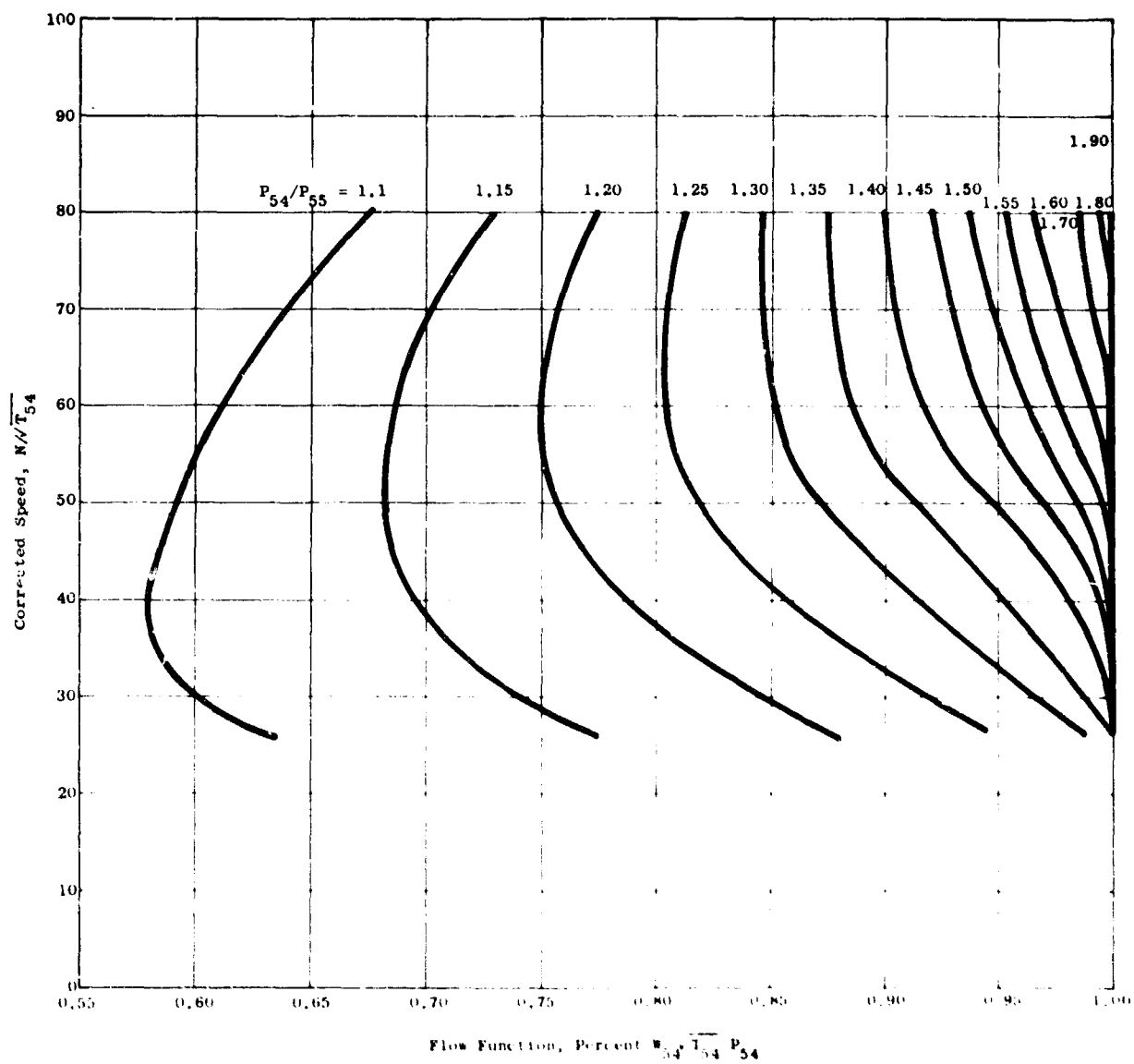


Figure 354. Tip Turbine Map - Flow Function Versus Corrected Speed and Turbine Pressure Ratio.

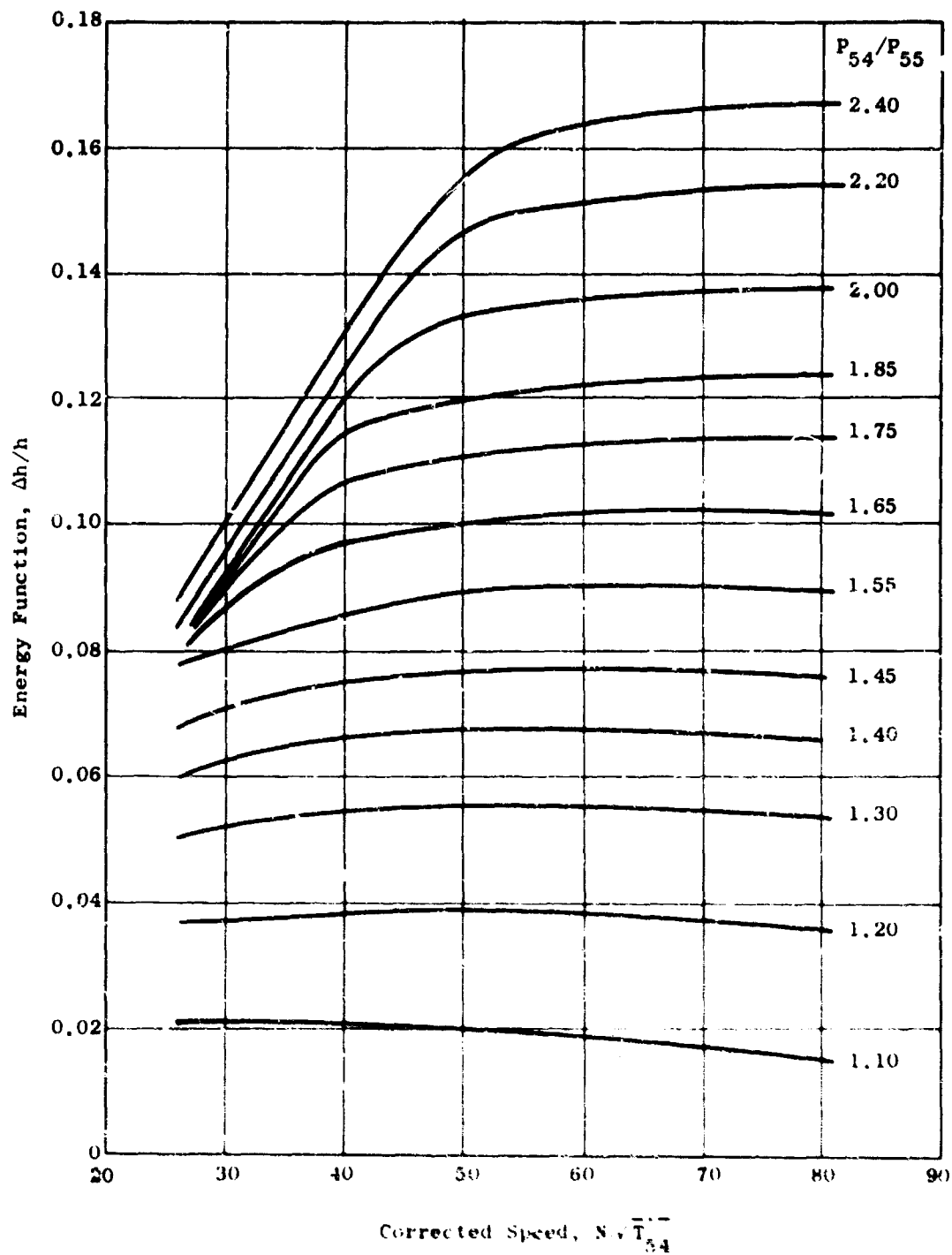


Figure 355 LF2 Tip Turbine Map - Energy Function Versus Corrected Speed and Turbine Pressure Ratio.

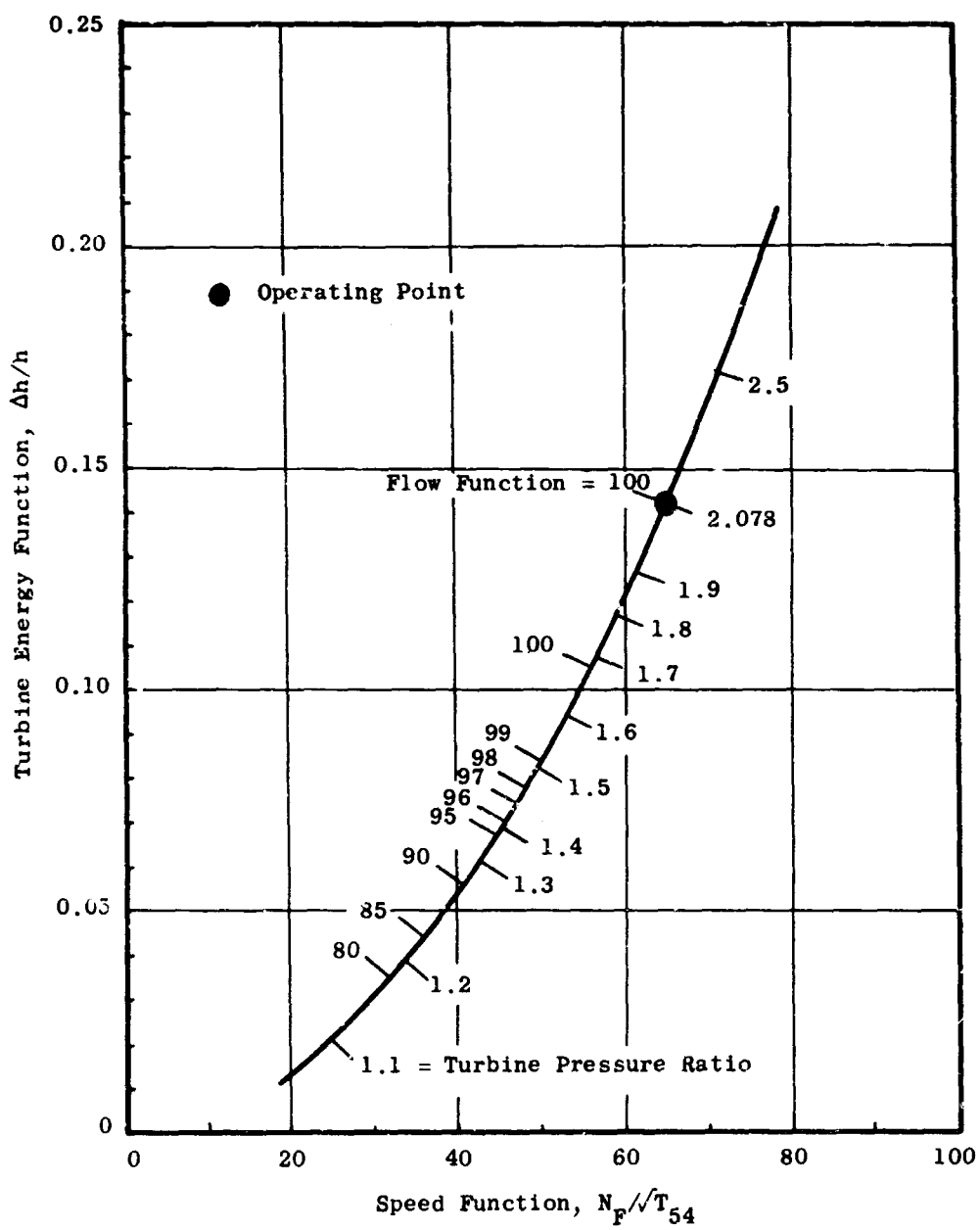


Figure 356. Tip Turbine Map Operating Line.

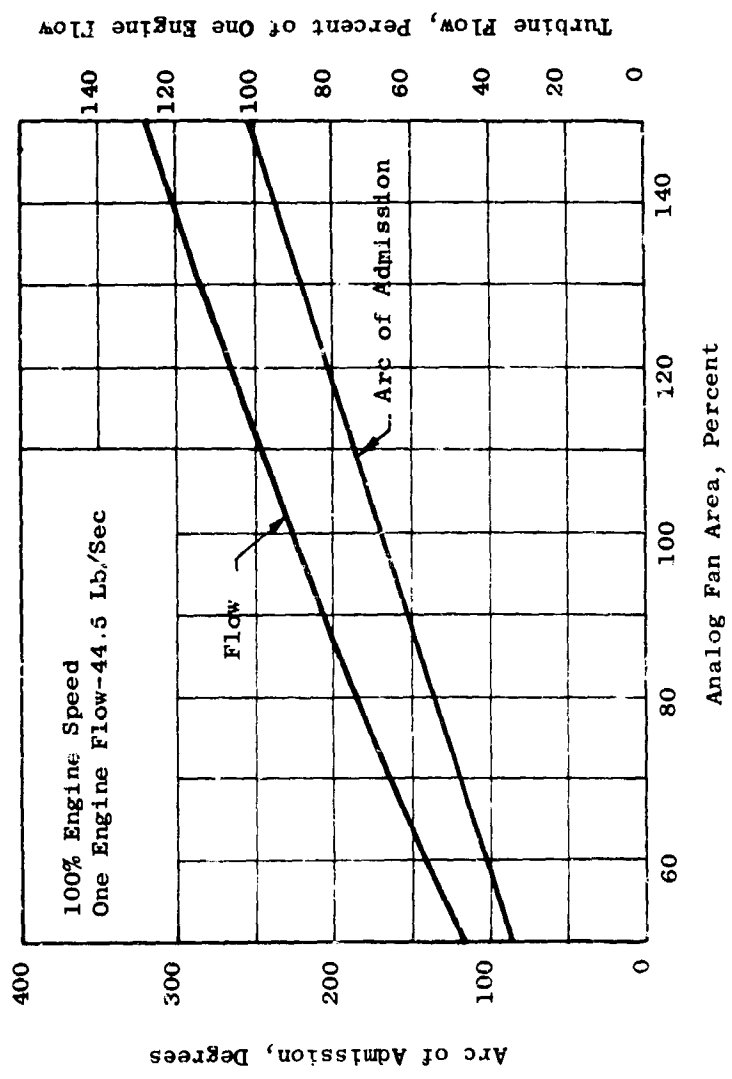


Figure 357. Tip Turbine Arc of Admission and Flow Related to Analog Fan Area.

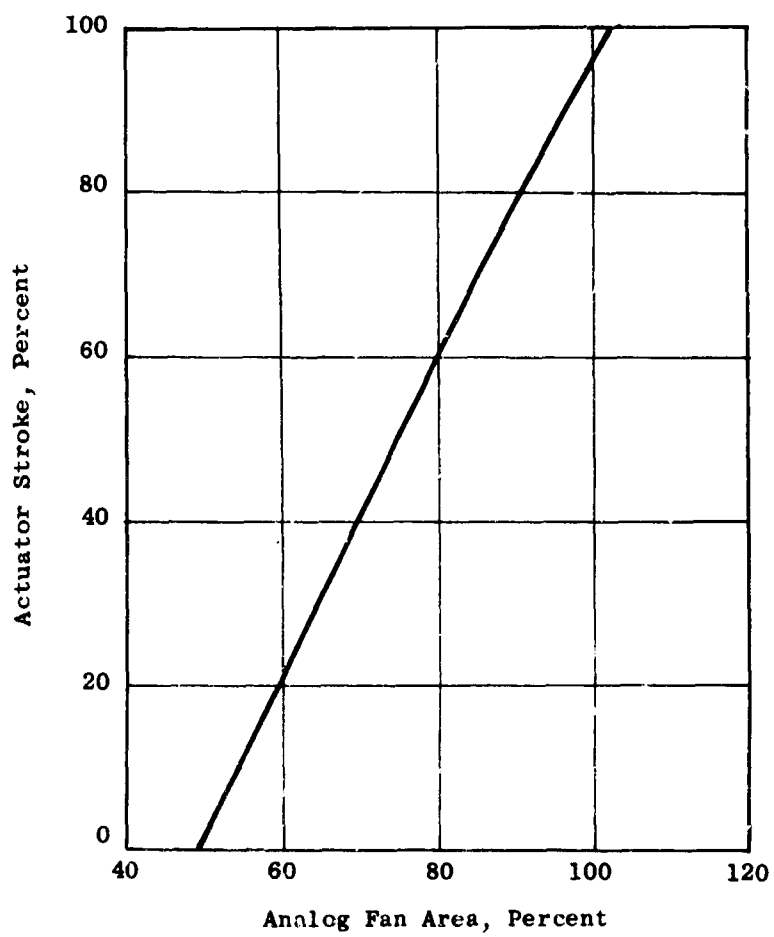


Figure 358. Test Hardware Actuator Stroke Related to Analog Fan Area.

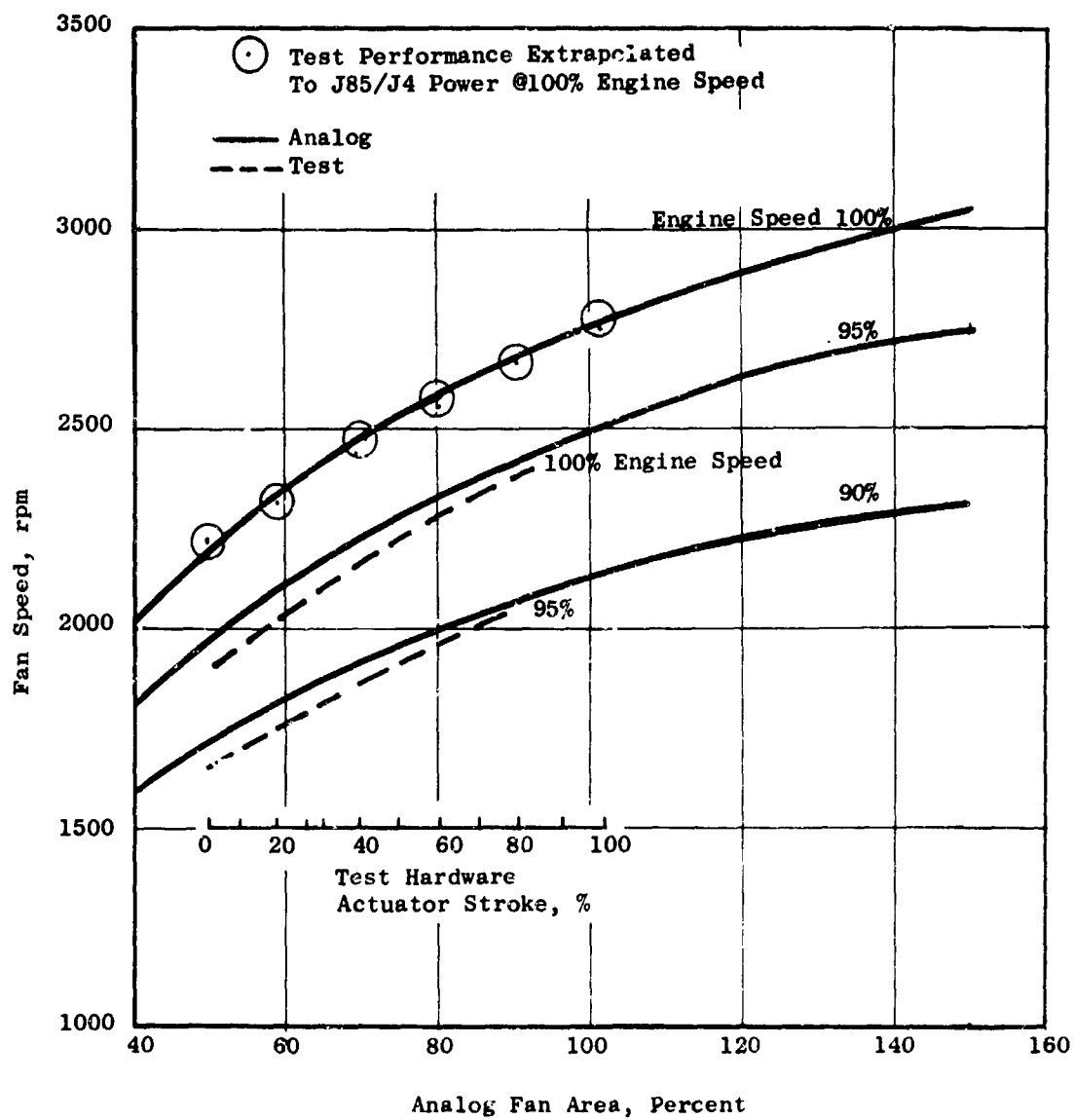


Figure 359. Fan Steady-State Speed Versus Analog Fan Area.

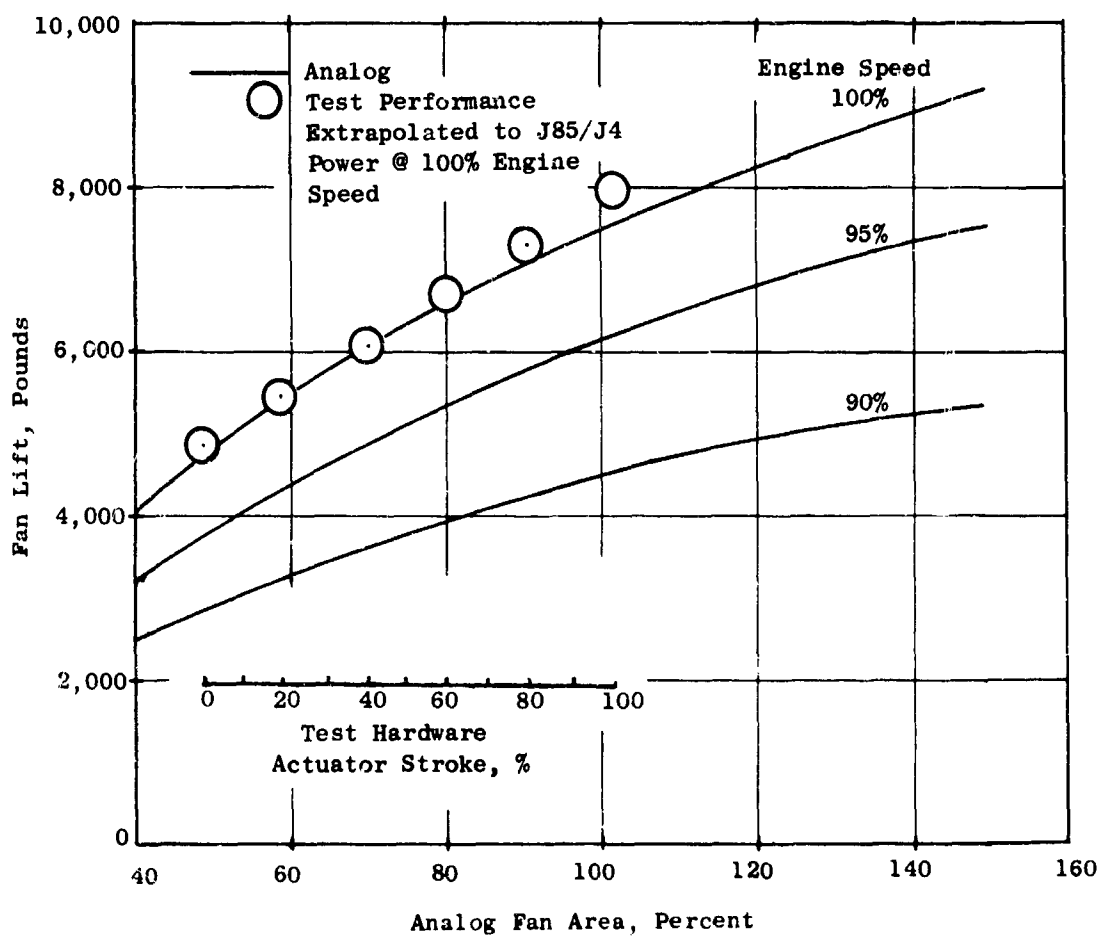


Figure 360. Fan Steady-State Lift Versus Analog Fan Area.

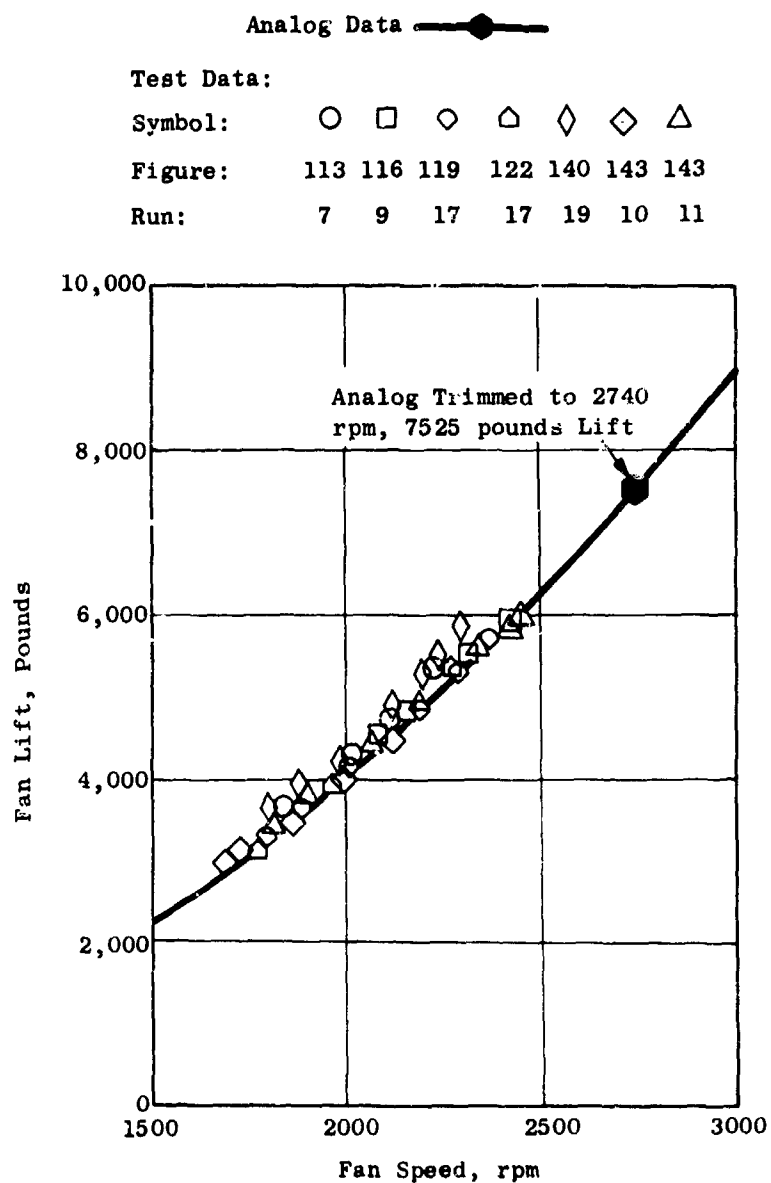


Figure 361. Fan Steady-State Lift Versus Speed.

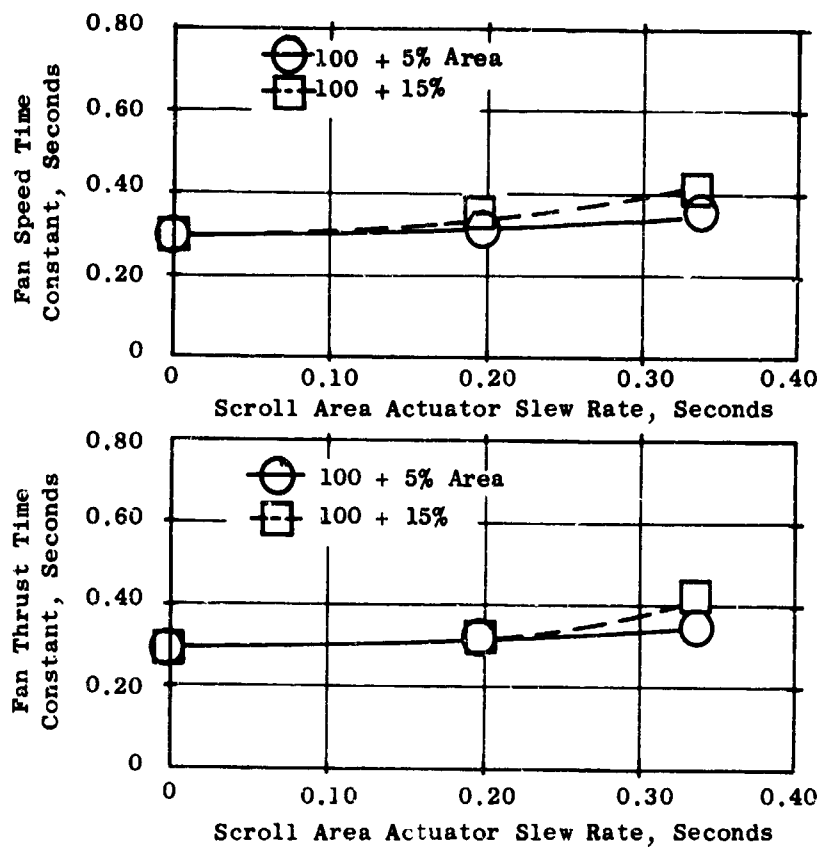


Figure 362. Analog Results - Effect of Actuator Slew Rate on Fan Time Constants for Step Changes in Fan Area.

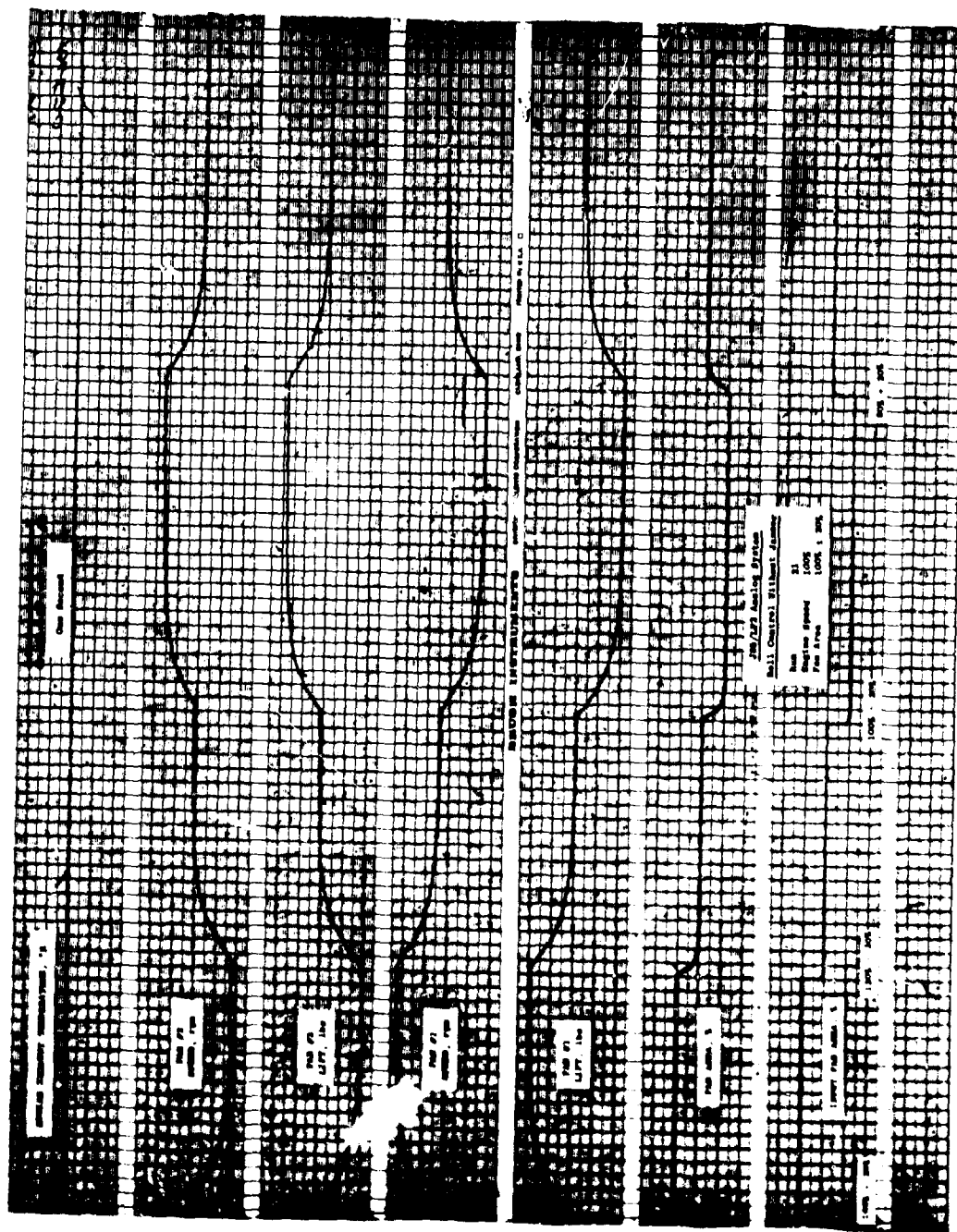


Figure 363. Typical Analog Recorder Trace of Fan Response to a Step Change in Fan Area Without a Jazzer.

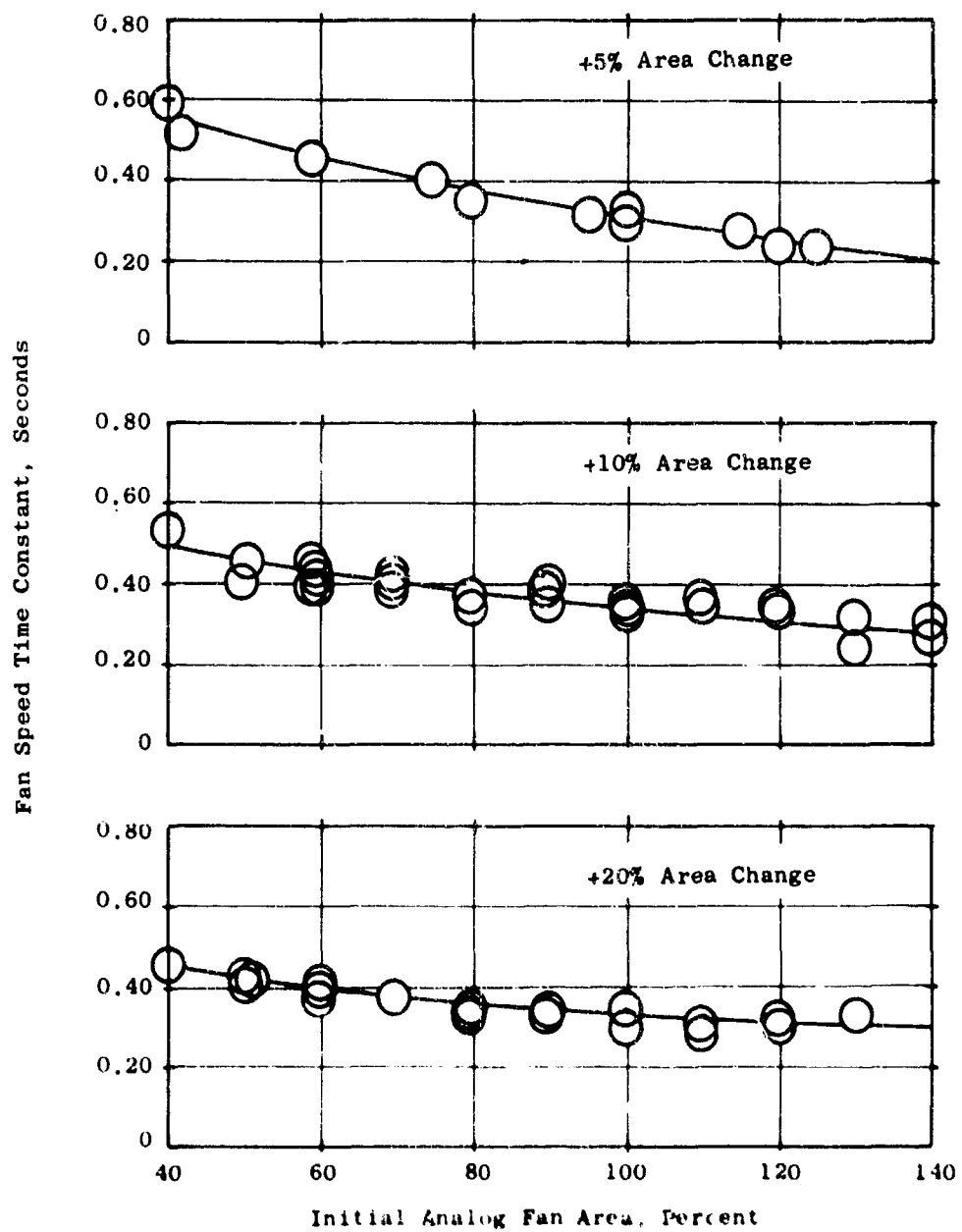


Figure 364. Analog Results - Fan Speed Time Constants for Positive Step Changes in Fan Area Without a Jazzer.

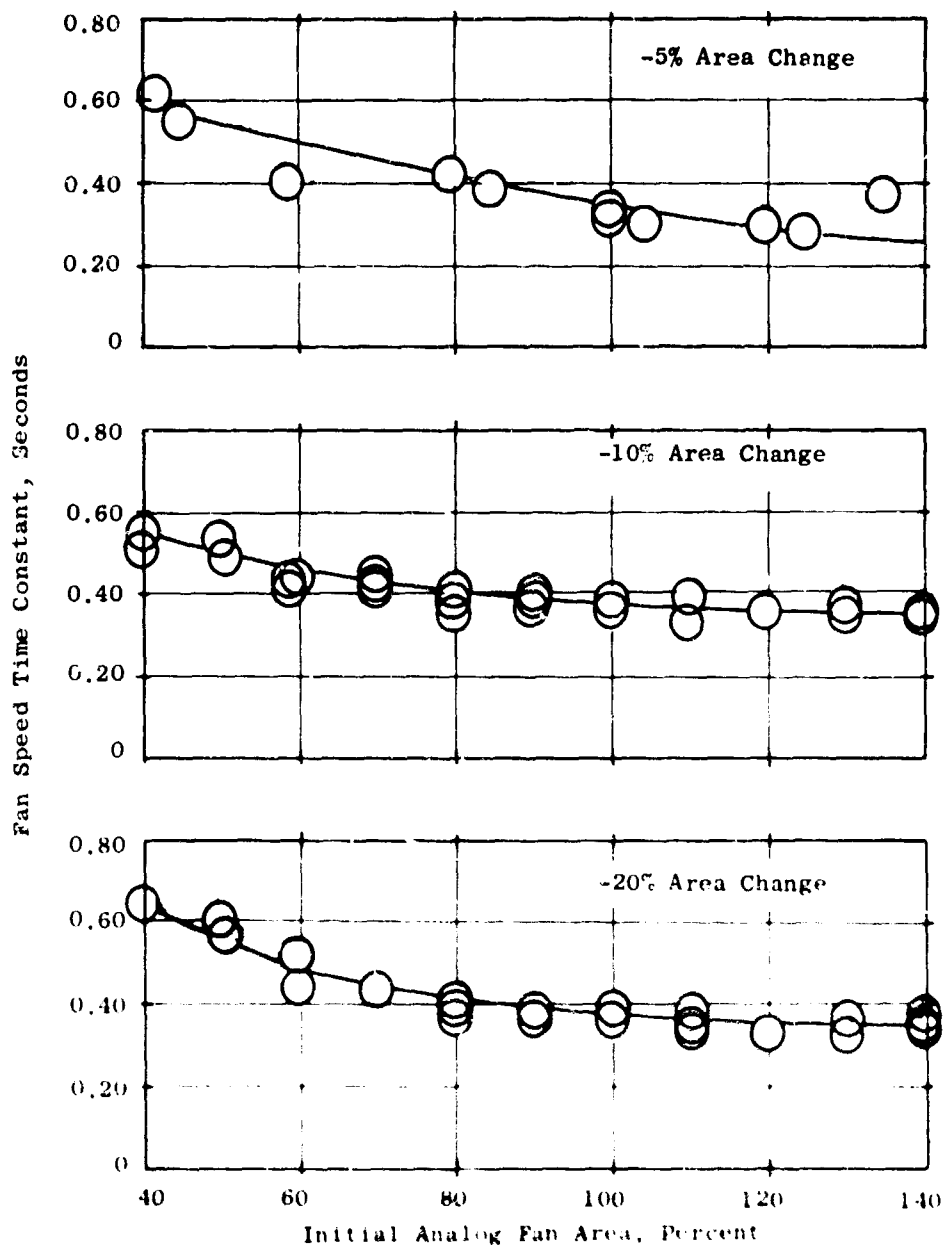


Figure 365. Analog Results - Fan Speed Time Constants for Negative Step Changes in Fan Area Without Jazzer

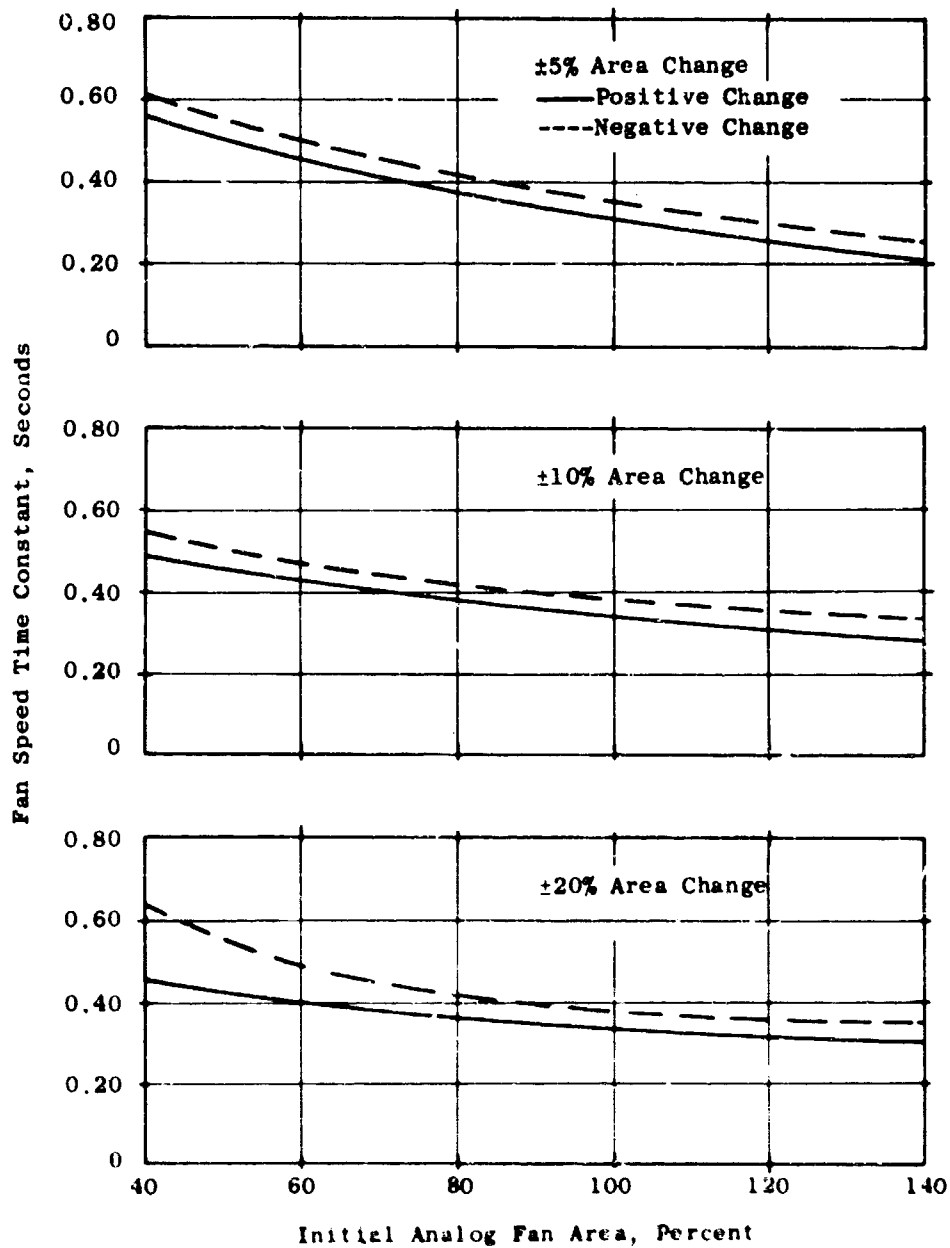


Figure 366. Analog Results - Summary of Fan Speed Time Constants for Step Changes in Fan Area Without a Jazzer.

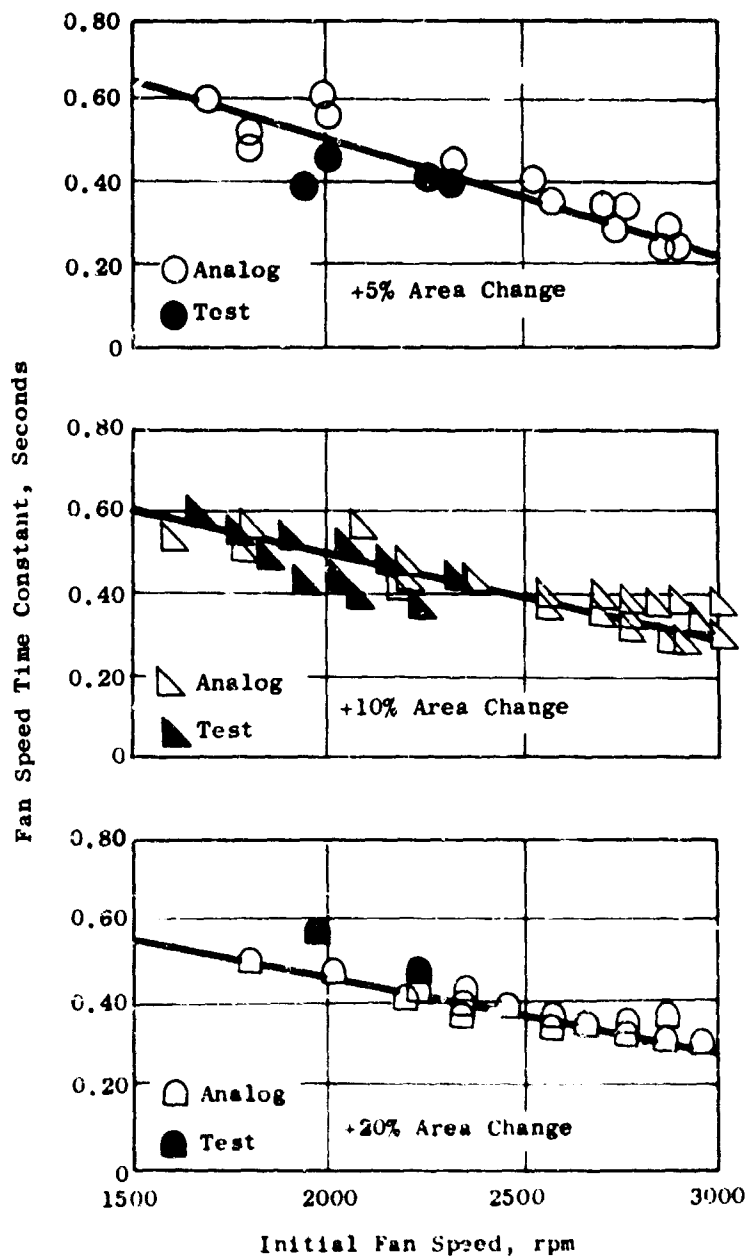


Figure 367. Comparison of Analog and Hardware Test Results - Fan Speed Time Constants for Positive Step Changes in Fan Area Without a Jazzer.

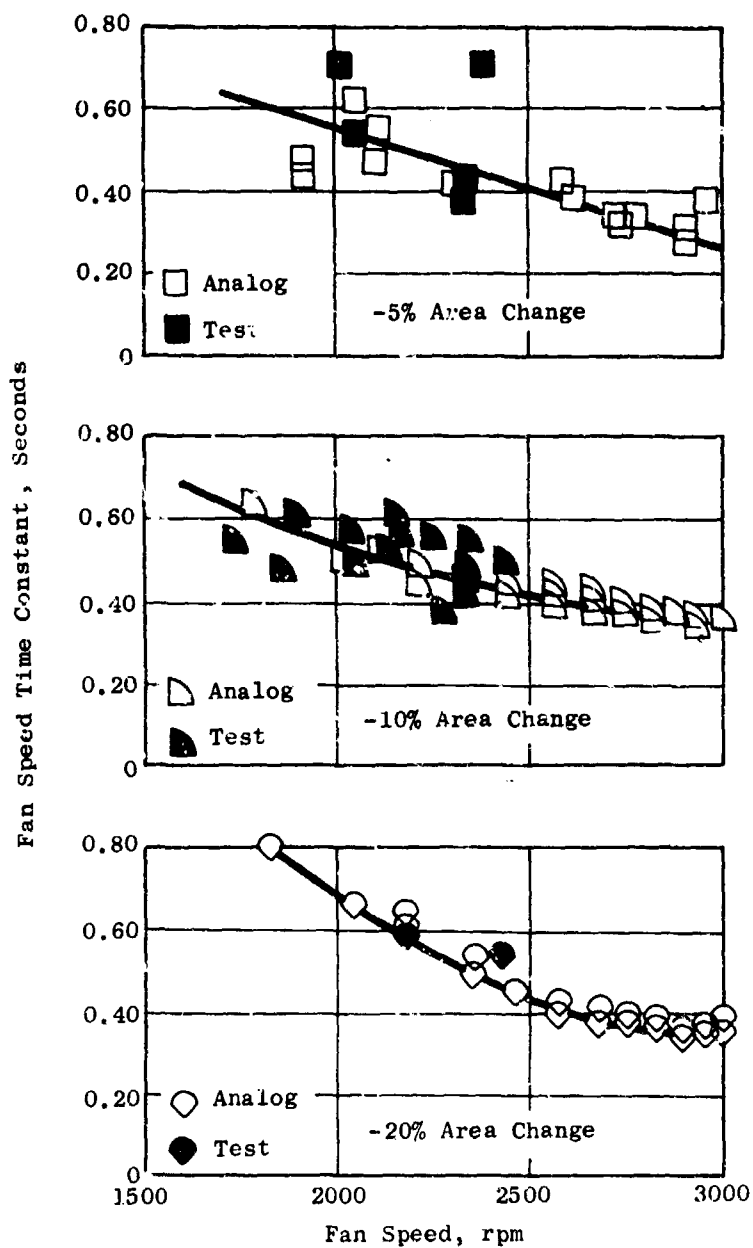


Figure 368. Comparison of Analog and Hardware Test Results for Fan Speed Time Constants for Negative Step Changes in Fan Area Without a Jazzer.

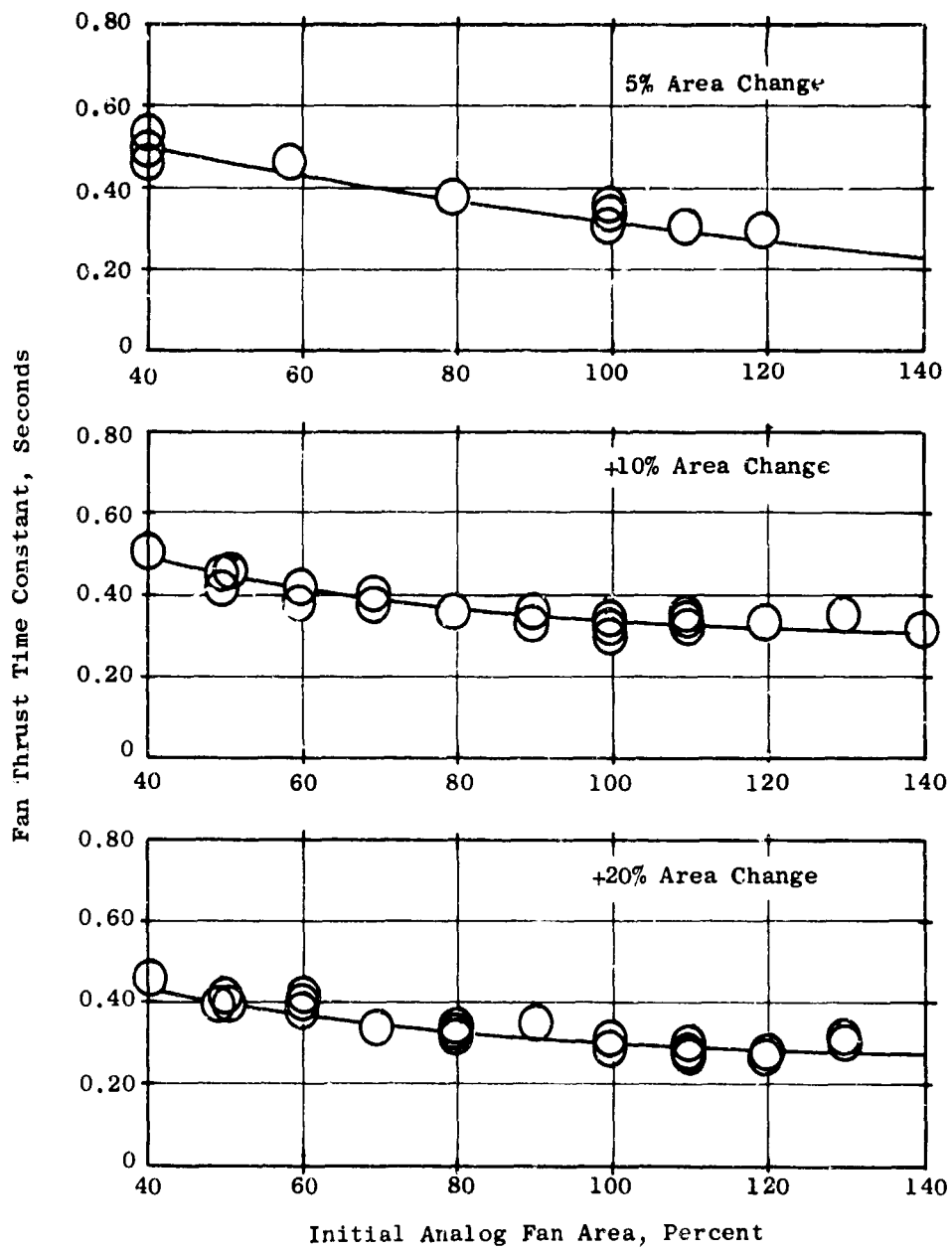


Figure 369. Analog Results - Fan Thrust Time Constants for Positive Step Changes in Fan Area Without a Jazzer.

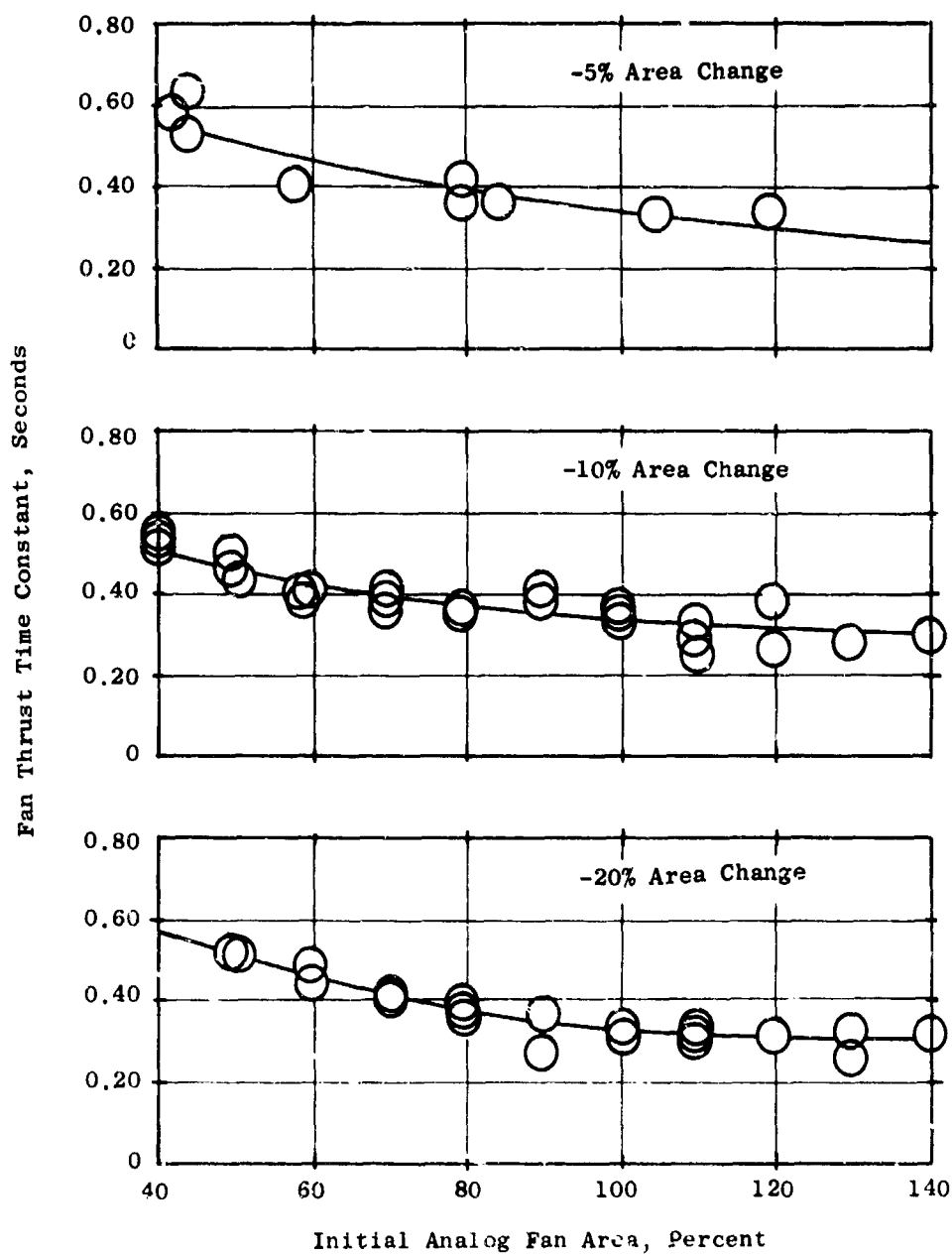


Figure 370. Analog Results - Fan Thrust Time Constants for Negative Step Changes in Fan Area Without a Jazzer.

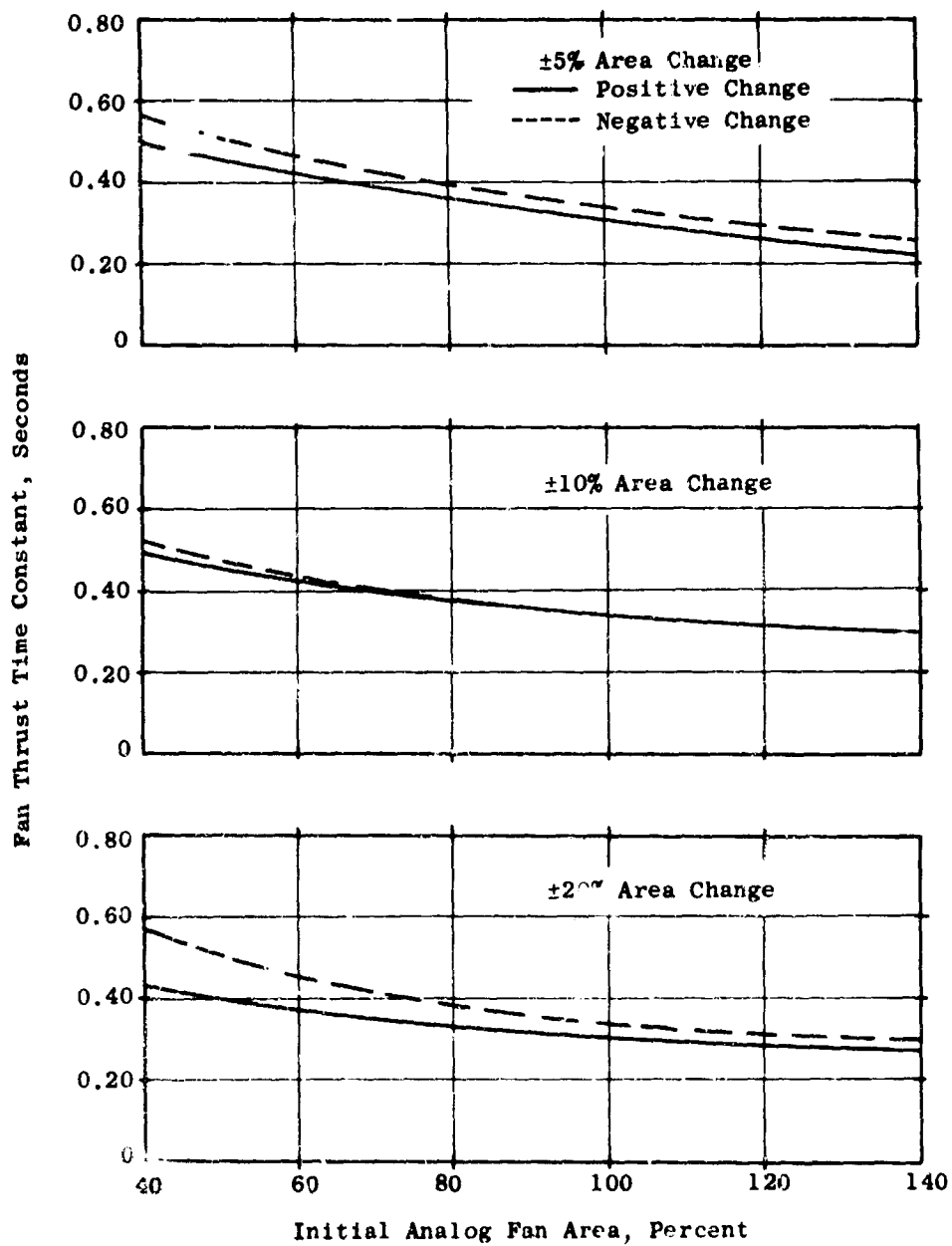


Figure 371. Analog Results - Summary of Fan Thrust Time Constants for Step Changes in Fan Area Without a Jazzer.

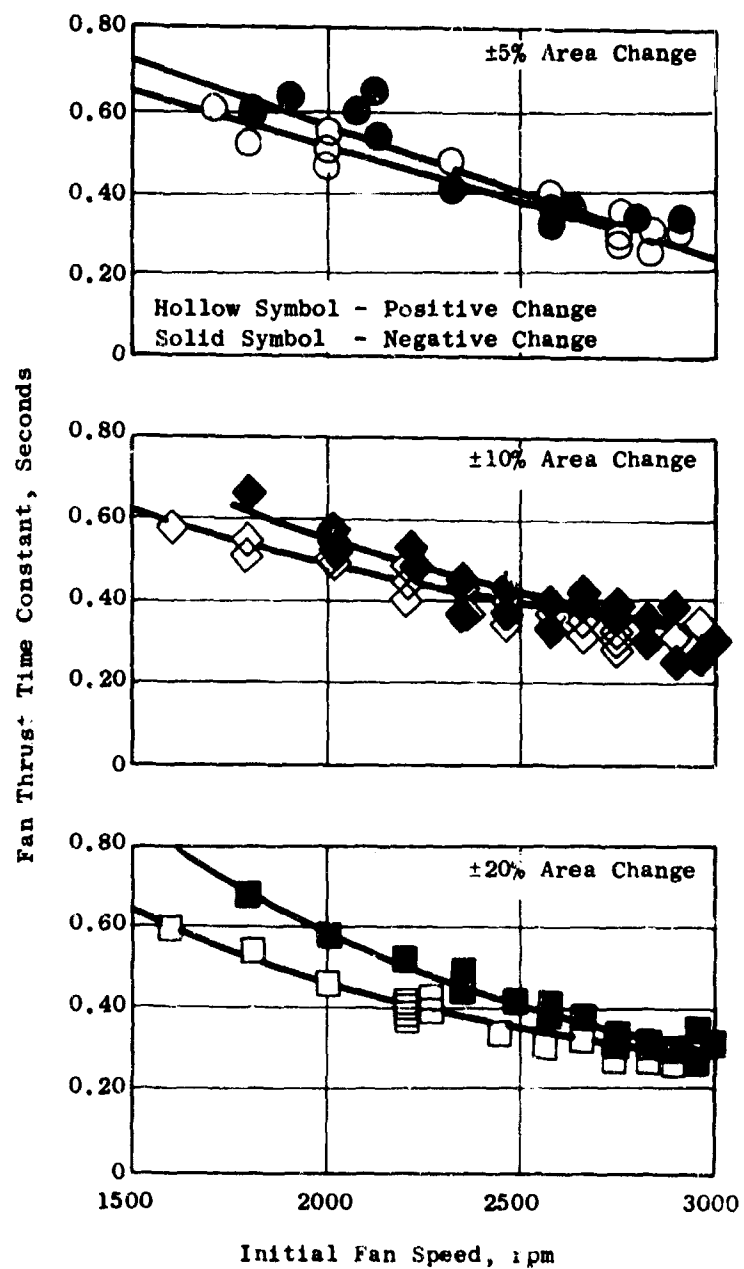


Figure 372. Analog Results - Fan Thrust Time Constants Versus Initial Speed for Step Changes in Fan Area Without a Jazzer.

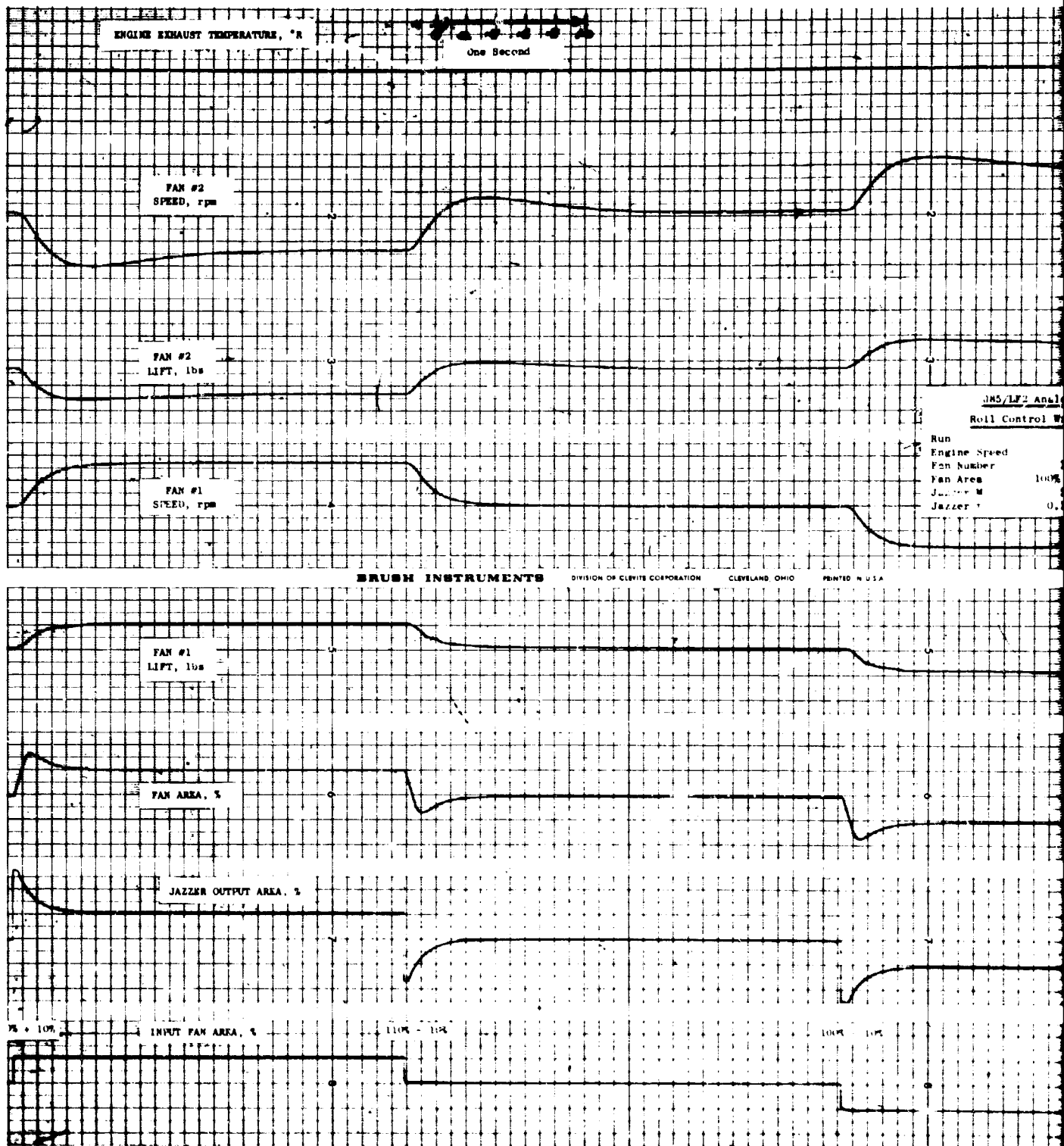
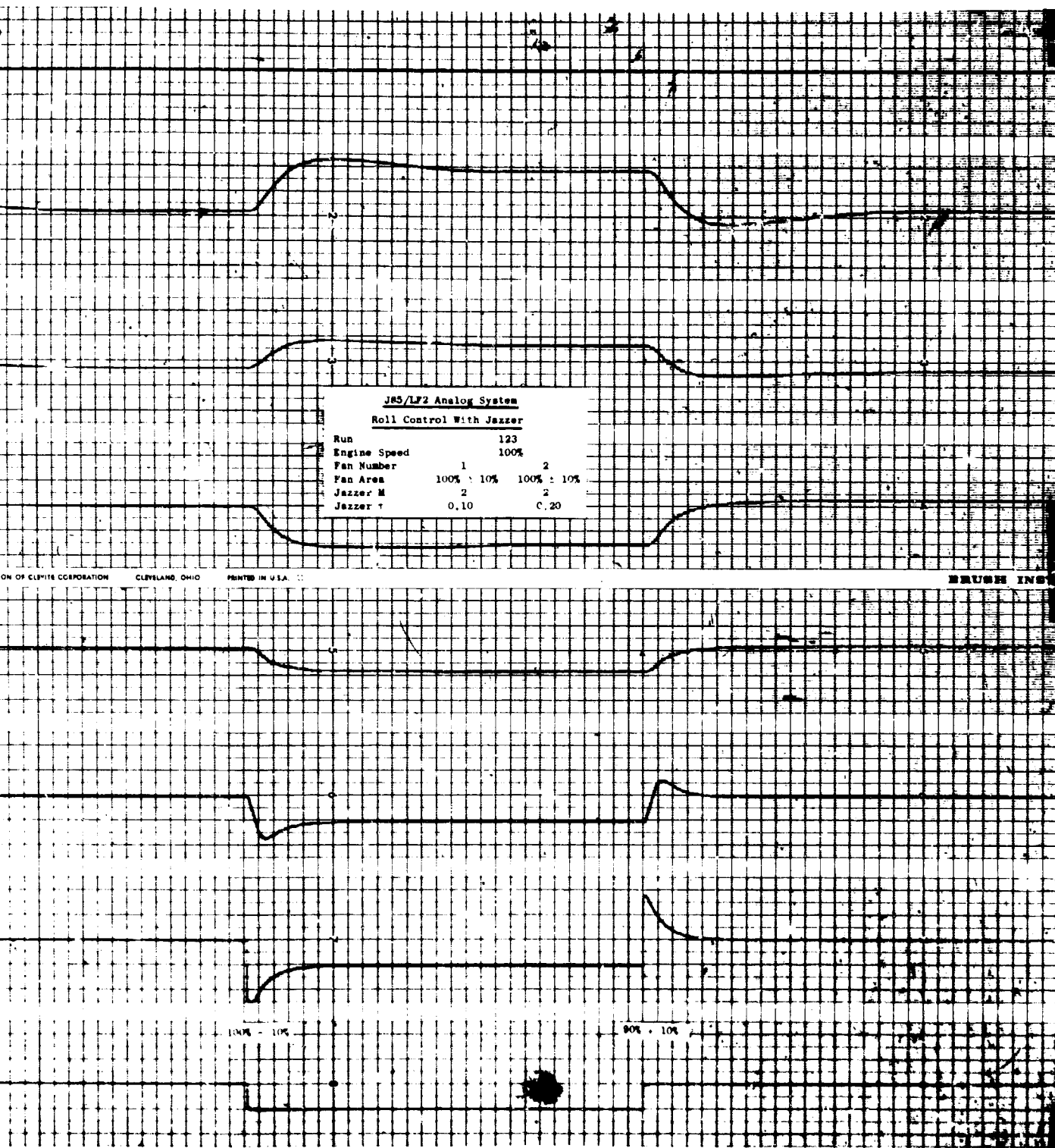


Figure 373. Typical Analog Recorder Trace of Fan Response to a Step Change in Fan Area With a Jazzer.



Fan Response
With a Jazzer.

B

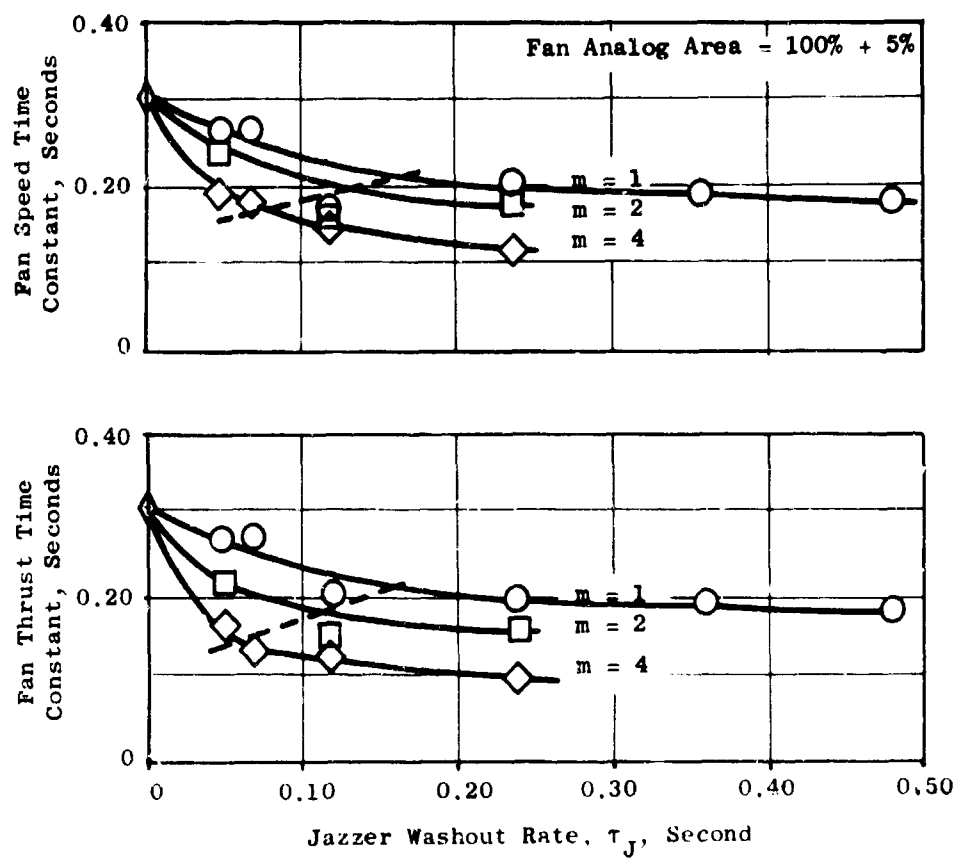


Figure 374. Analog Results - Fan Time Constants for a 5 Percent Step Change in Fan Area With a Jazzer.

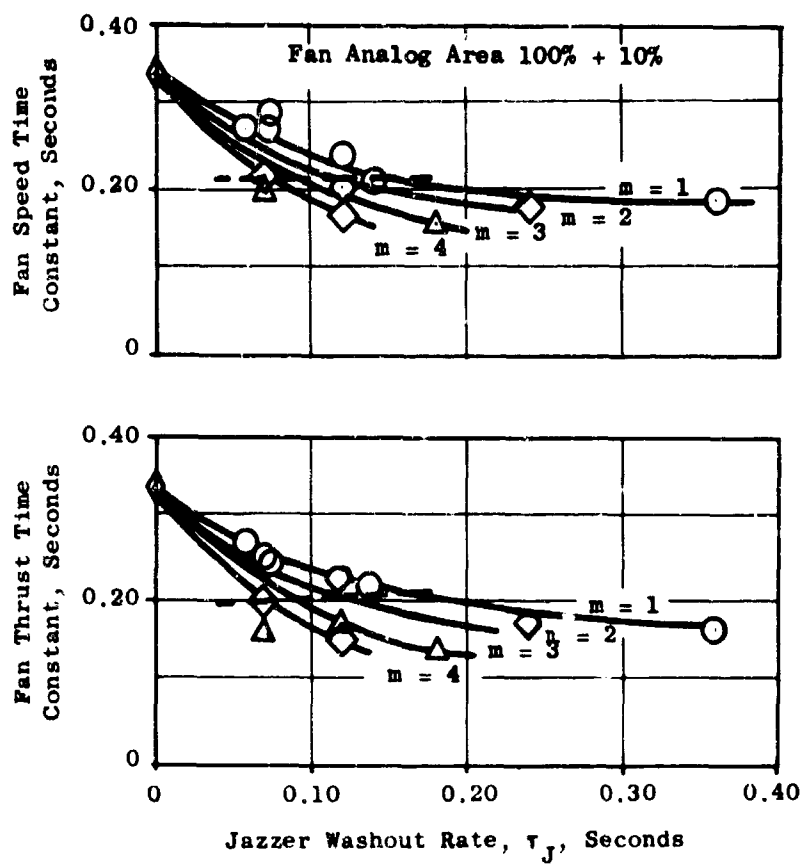


Figure 375. Analog Results - Fan Time Constants for a 10 Percent Step Change in Fan Area With a Jazzer.

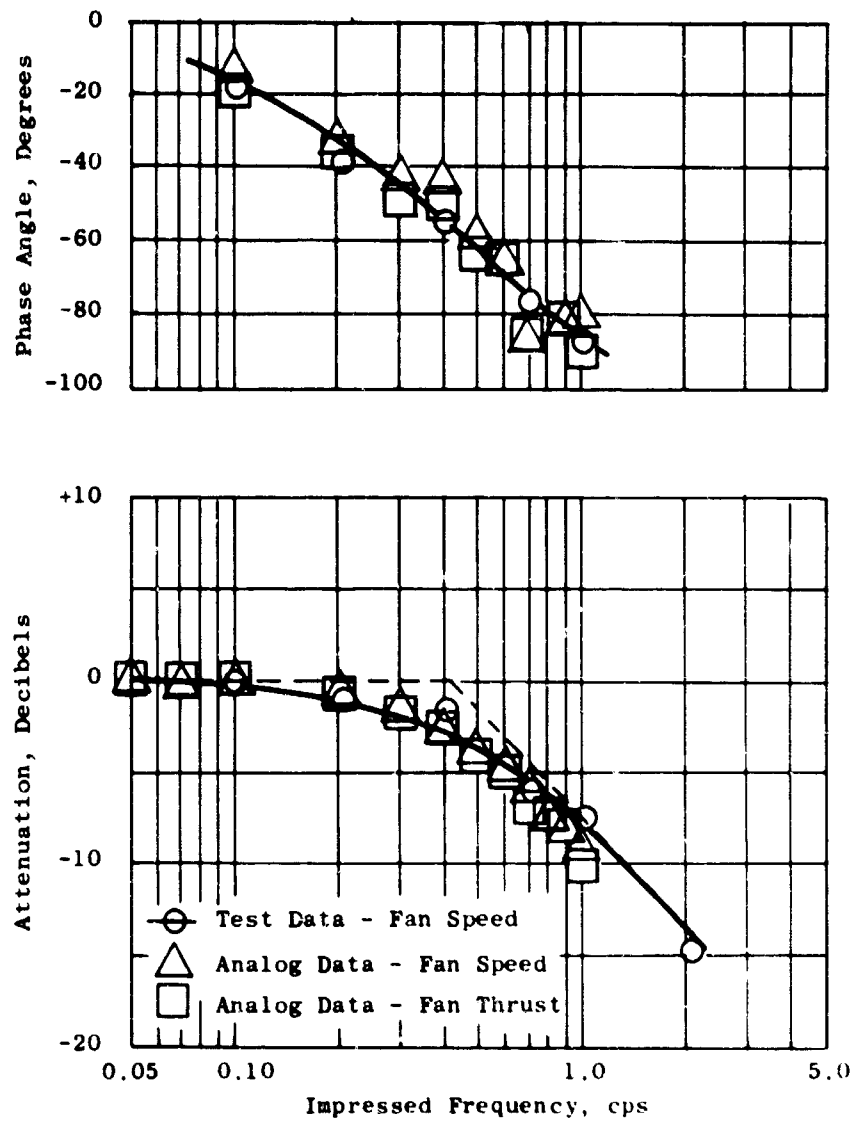


Figure 376. Steady-State Frequency Response - Comparison of Analog and Test Results for test Actuator Stroke of 50 ± 20 Percent Without a Jazzer.

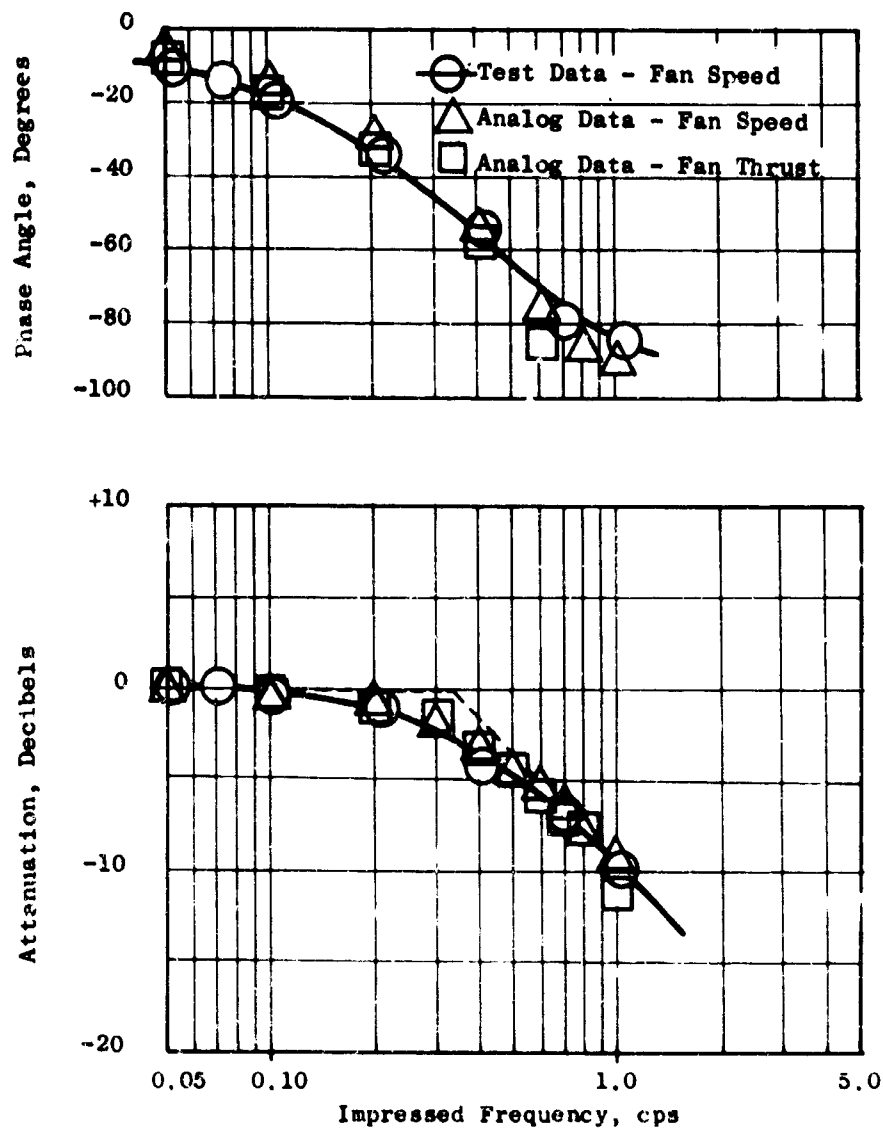


Figure 377. Steady-State Frequency Response - Comparison of Analog and Test Results for Test Actuator Stroke of 50 ± 50 Percent Without a Jazzer.

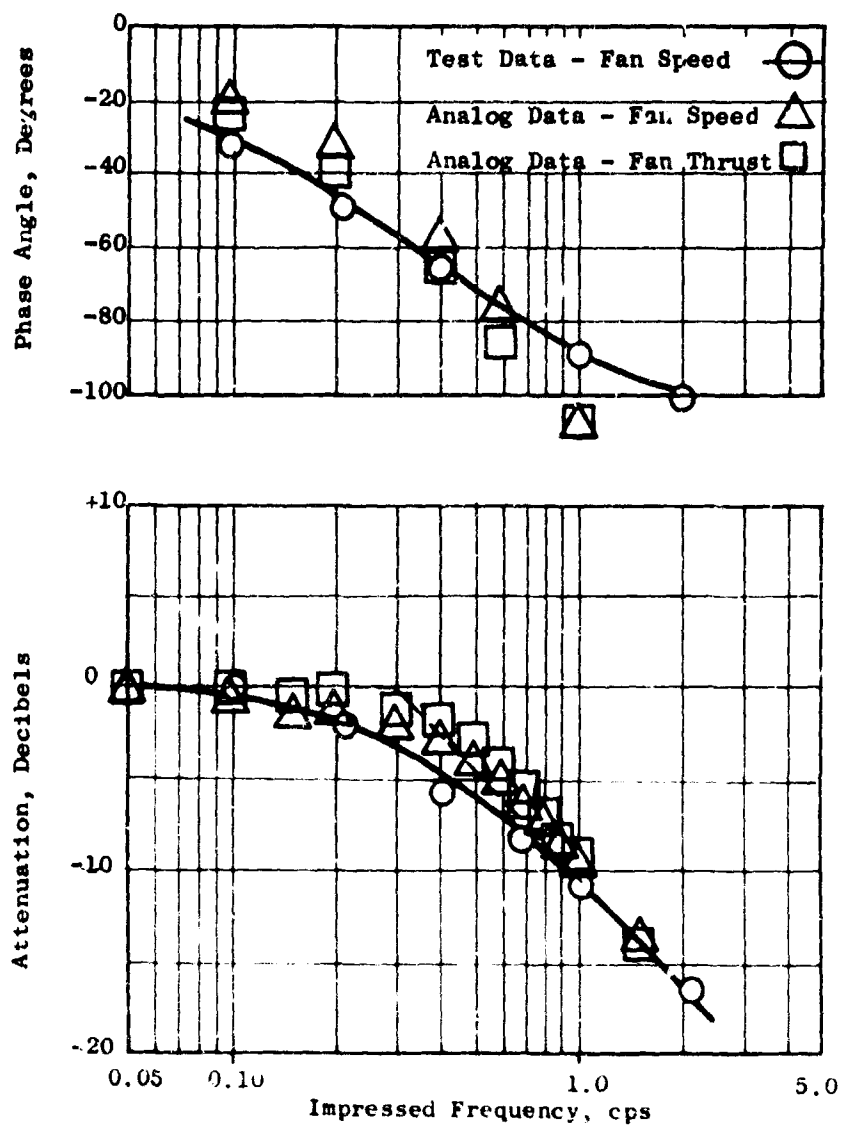


Figure 378. Steady-State Frequency Response - Comparison of Analog and Test Results for Test Actuator Stroke of 70 ± 10 Percent Without a Jazzer.

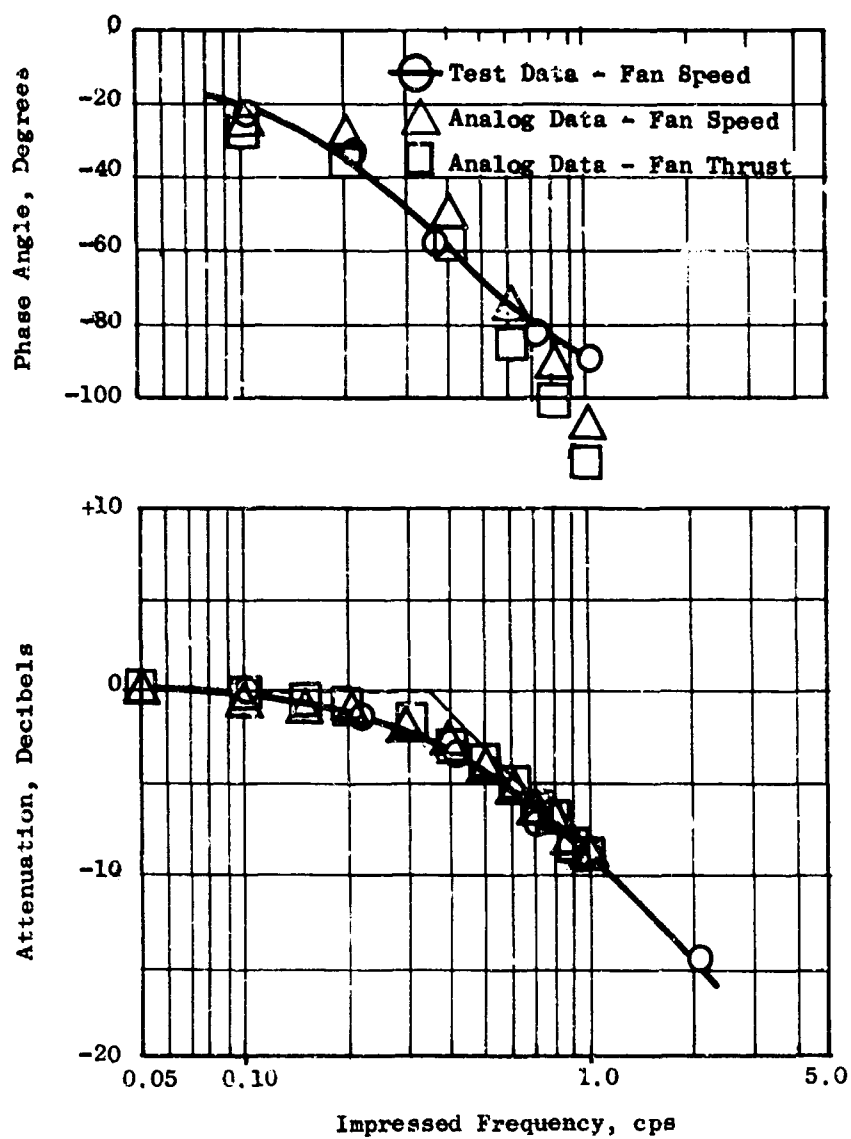


Figure 379. Steady-State Frequency Response - Comparison of Analog and Test Results for Test Actuator Stroke of 70 ± 20 Percent Without a Jazzer.

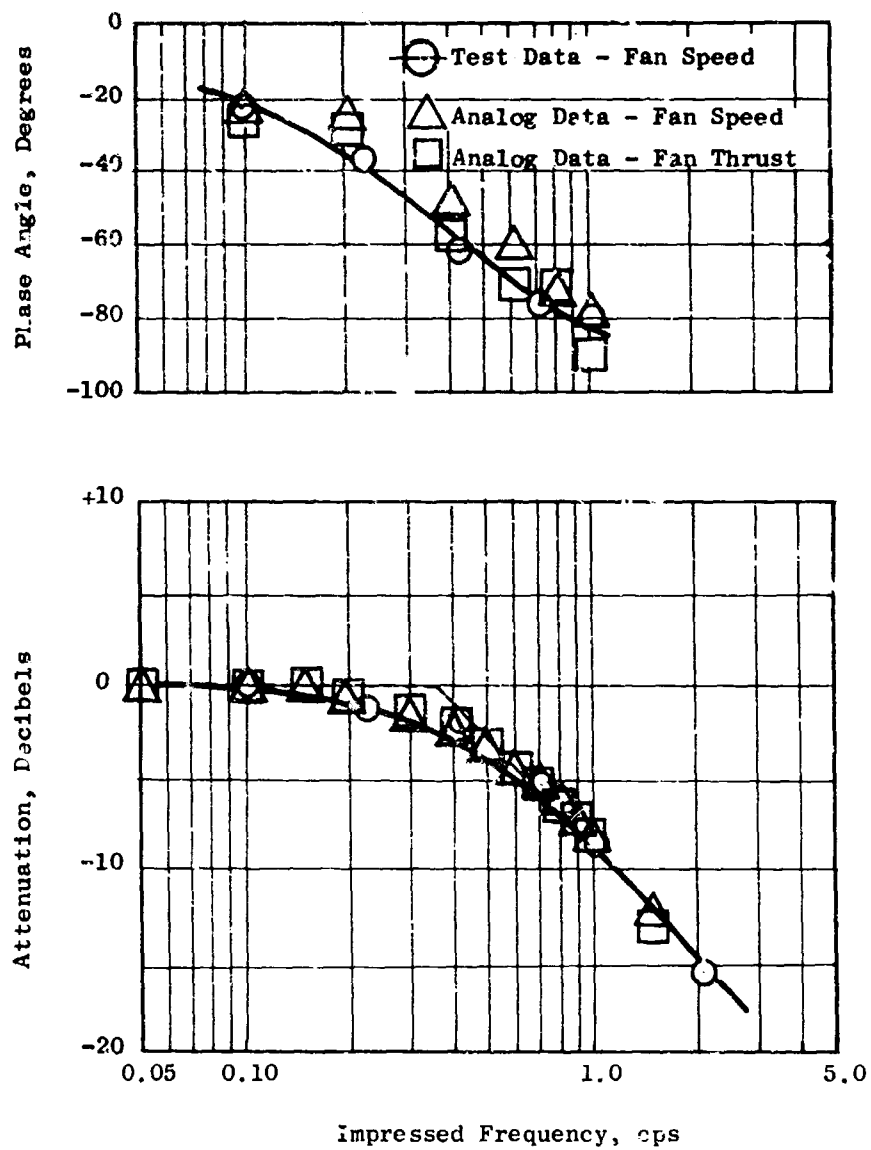


Figure 380. Steady-State Frequency Response -- Comparison of Analog and Test Results for Test Actuator Stroke of 70 ± 30 Percent Without a Jazzer.

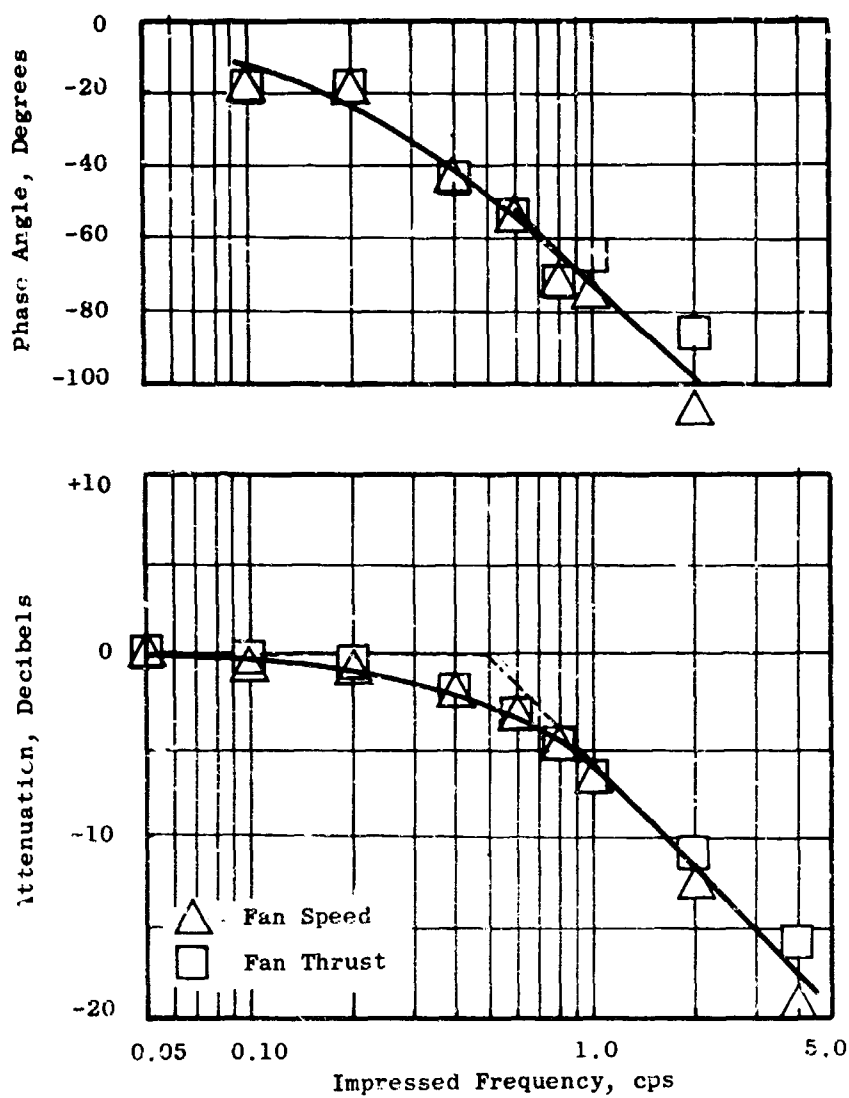


Figure 381. Steady-State Frequency Response - Analog Results for 100 \pm 5 Percent Area Without a Jazzer.

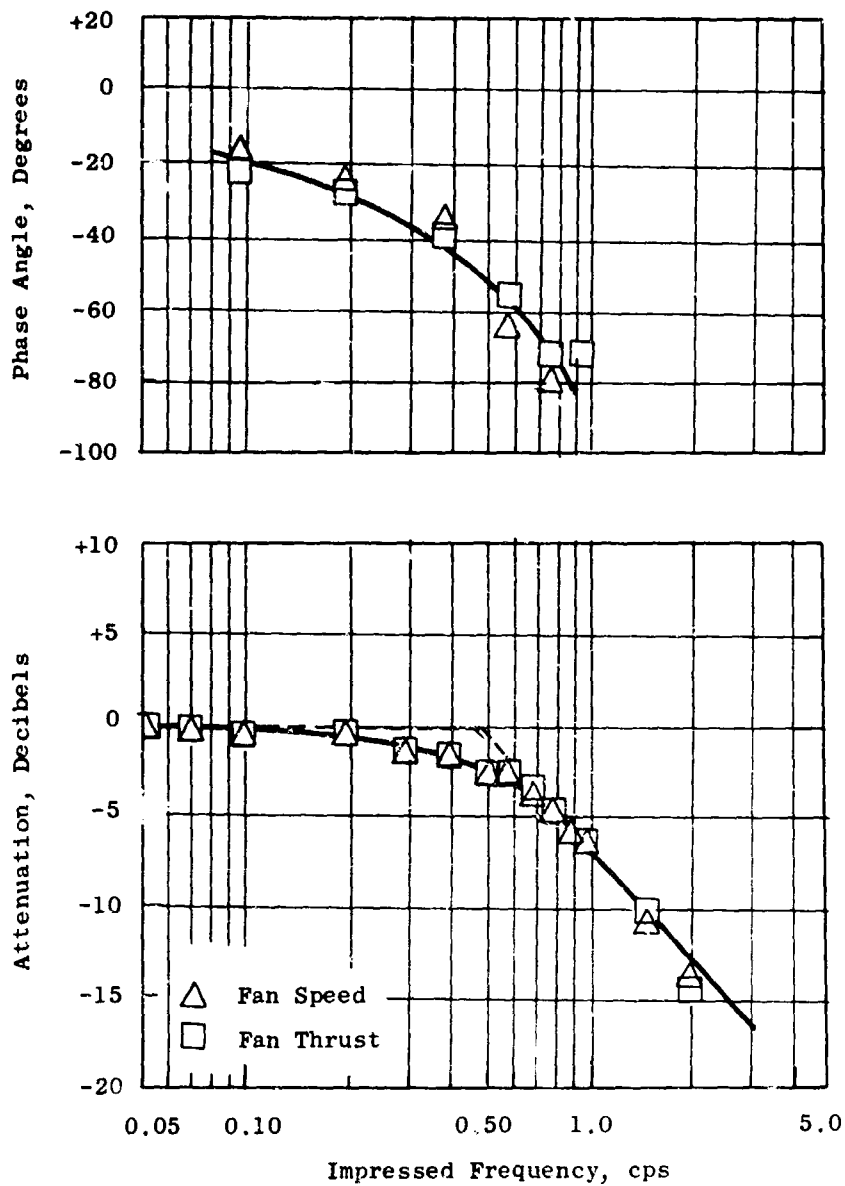


Figure 382. Steady-State Frequency Response - Analog Results for 100 \pm 10 Percent Area Without a Jazzer.

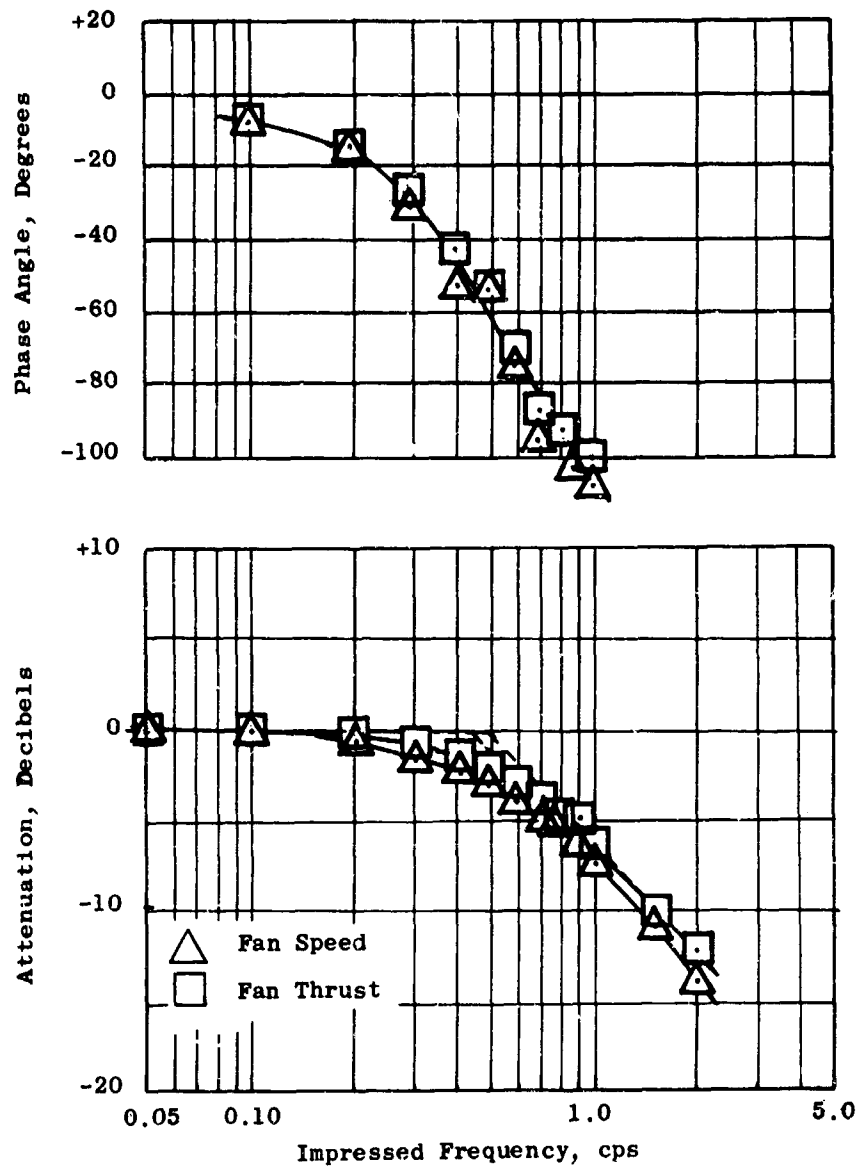


Figure 383. Steady-State Frequency Response - Analog Results for 100 \pm 20 Percent Area Without a Jazzer.

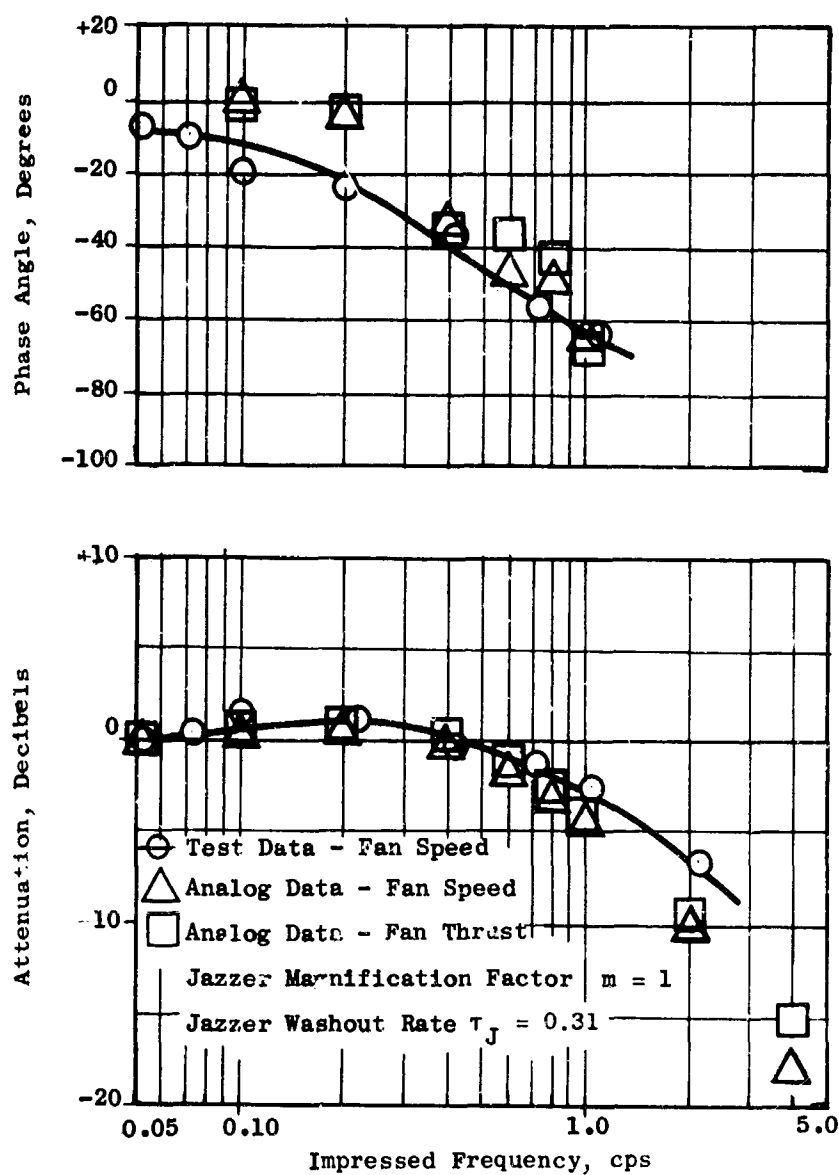


Figure 384. Steady-State Frequency Response - Comparison of Analog and Test Results for Fan Test Actuator Stroke 50 ± 10 Percent With Jazzer Magnification Factor of 1.

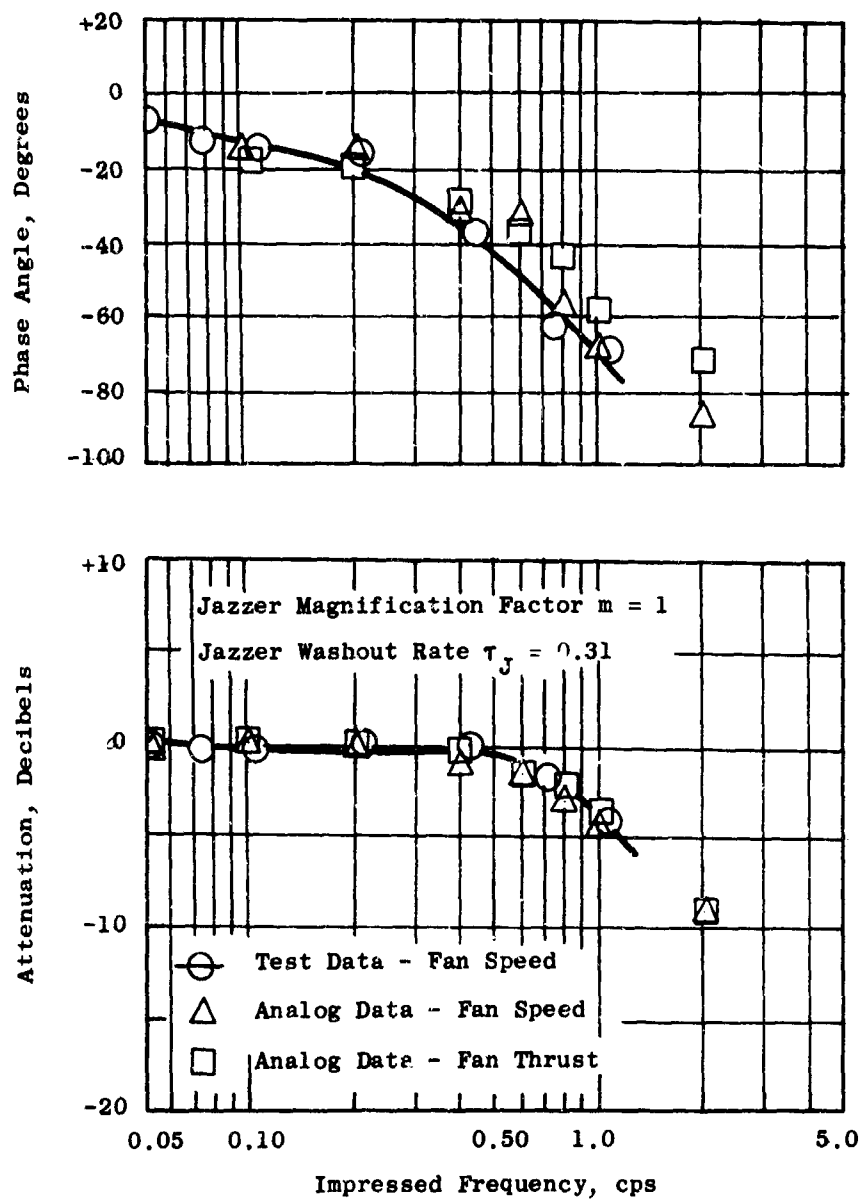


Figure 385. Steady-State Frequency Response - Comparison of Analog and Test Results for an Actuator Stroke of 50 ± 20 Percent With a Jazzter Magnification Factor of 1.

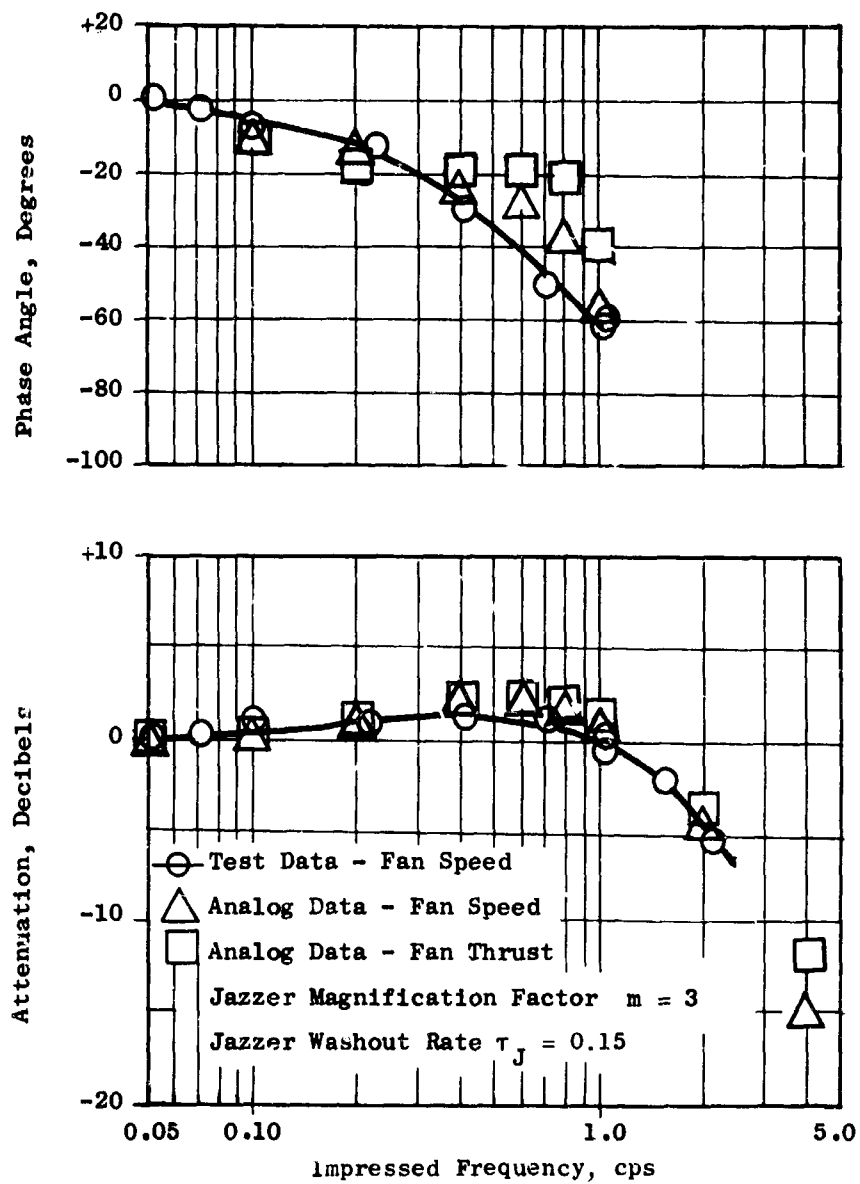


Figure 386. Steady-State Frequency Response - Comparison of Analog and Test Results for Test Actuator Stroke 50 ± 10 Percent With Jazzier Magnification Factor of 3.

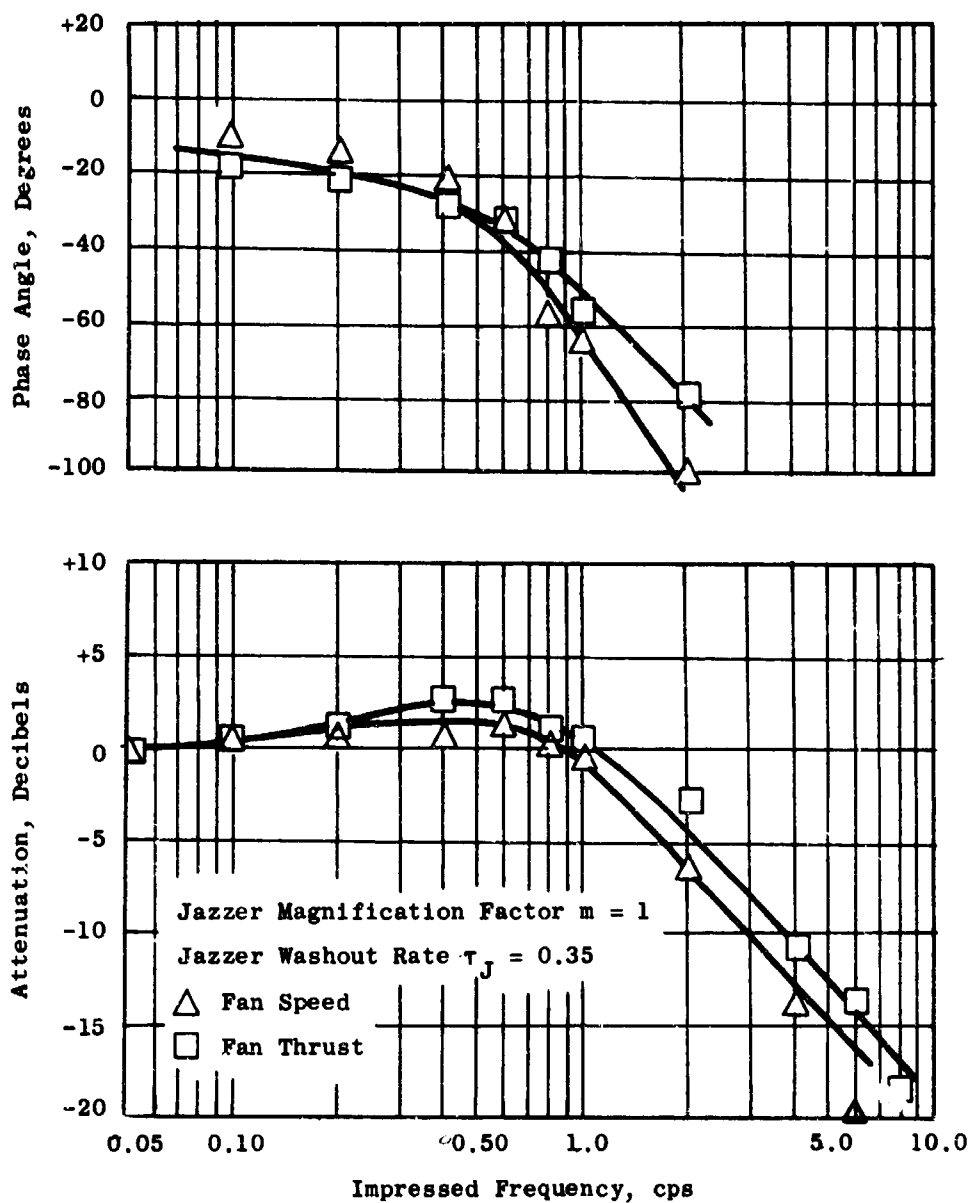


Figure 387. Steady-State Frequency Response - Analog Results for 100 \pm 5 Percent Area With a Jazzer Magnification Factor of 1.

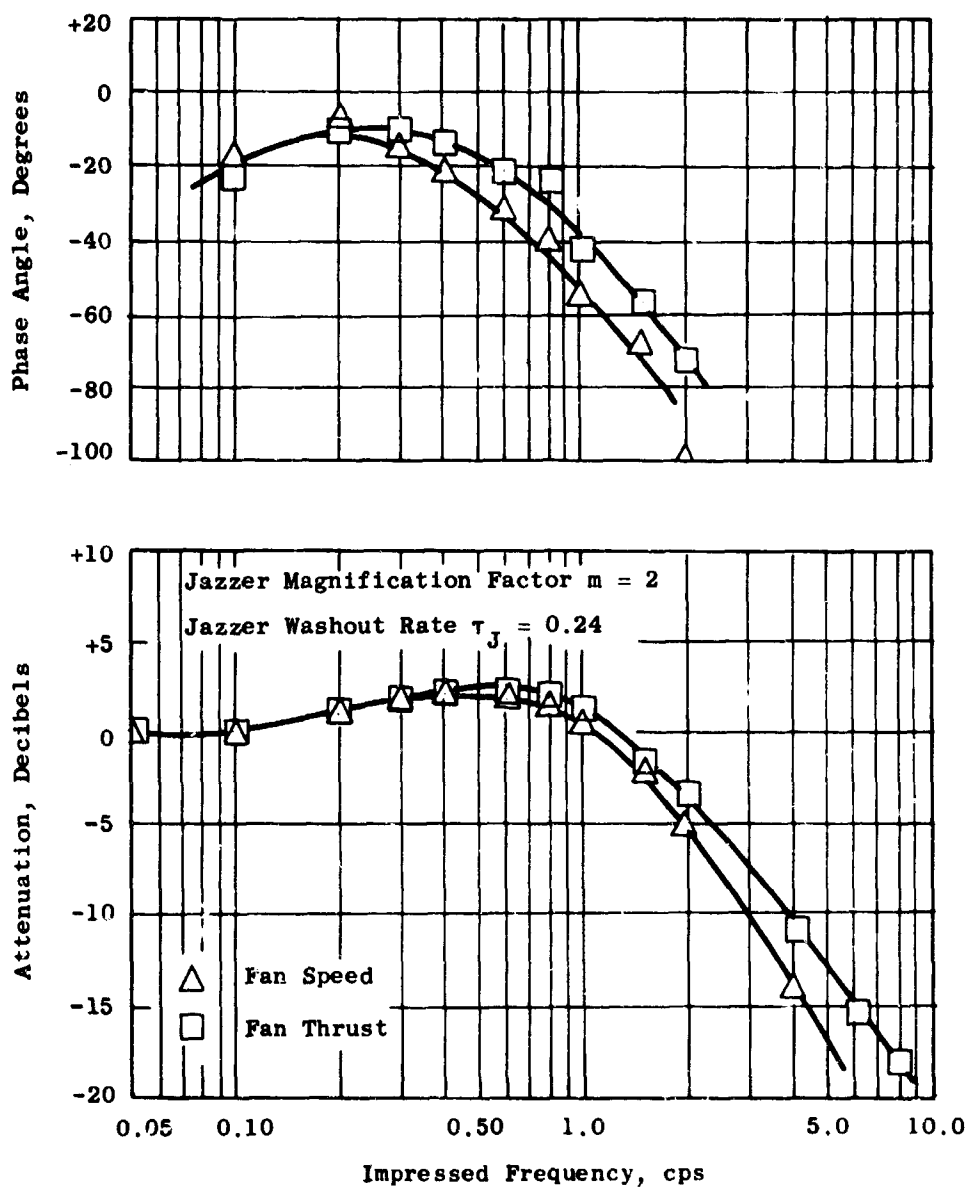


Figure 388. Steady-State Frequency Response - Analog Results for 100 \pm 5 Percent Area With a Jazzer Magnification Factor of 2.

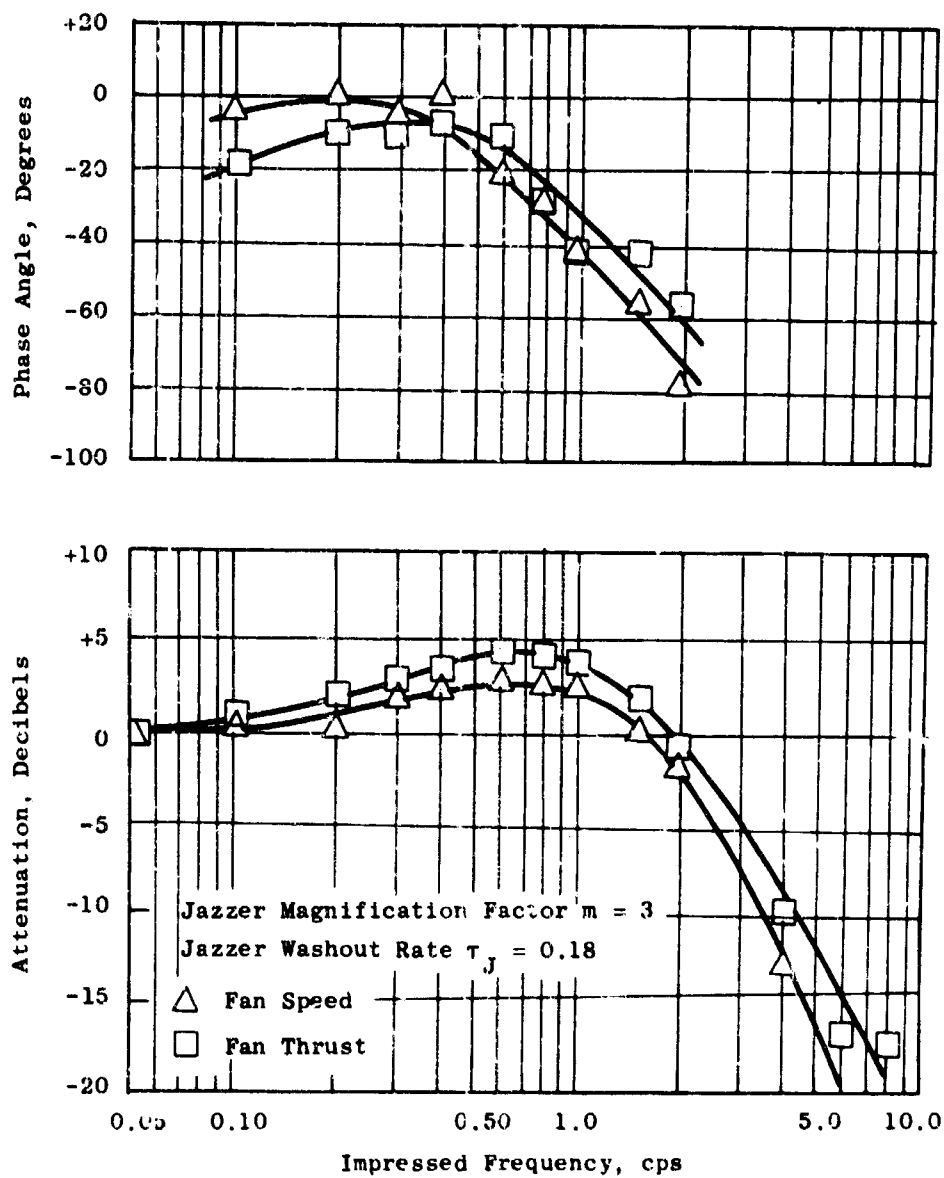


Figure 339. Steady-State Frequency Response - Analog Results for 100 \pm 50 Percent Area With a Jazzer Magnification Factor of 3.

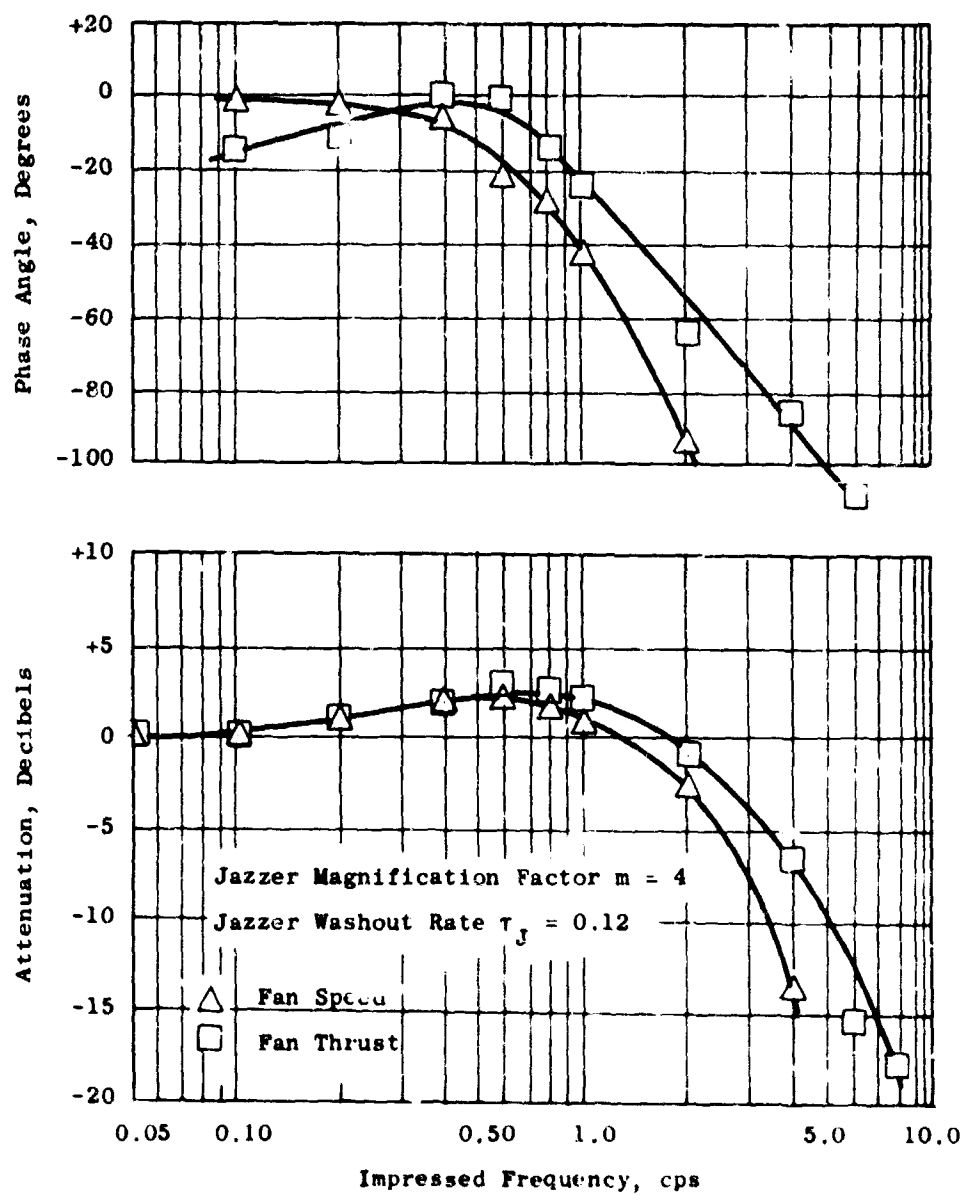


Figure 390. Steady-State Frequency Response - Analog Results for 100 \pm 5 Percent Area With a Jazzer Magnification Factor of 4.

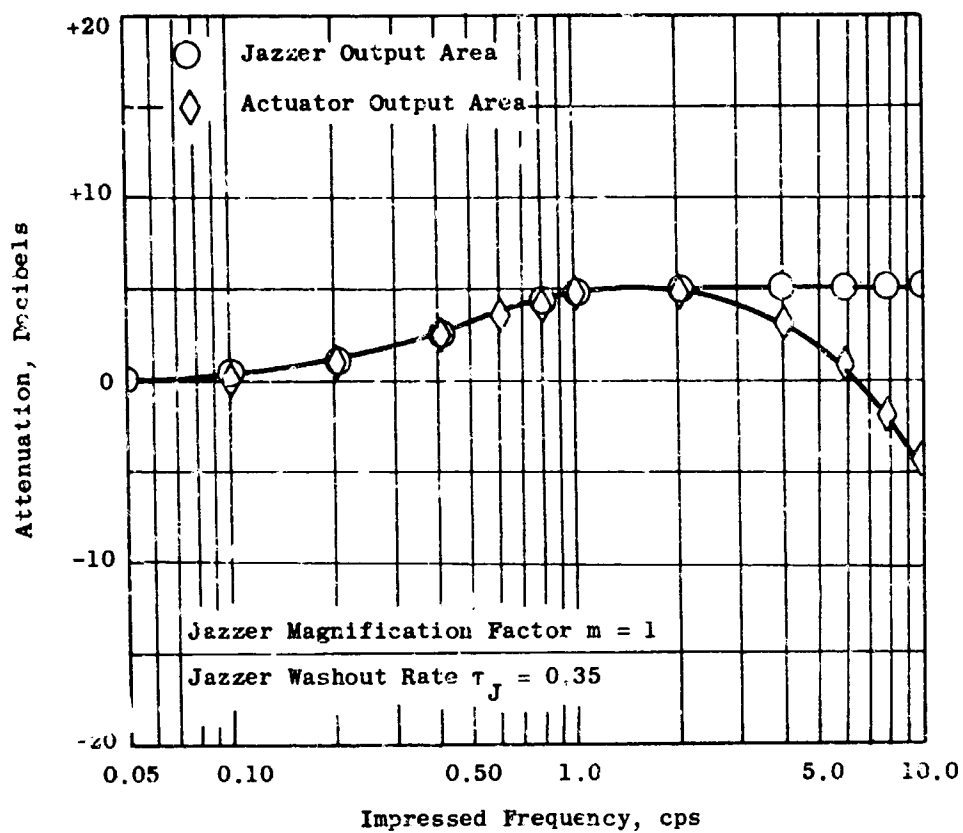


Figure 391. Steady-State Frequency Response - Analog Fan Area Response for 100 ± 5 Percent Area With a Jazzer Magnification Factor of 1.

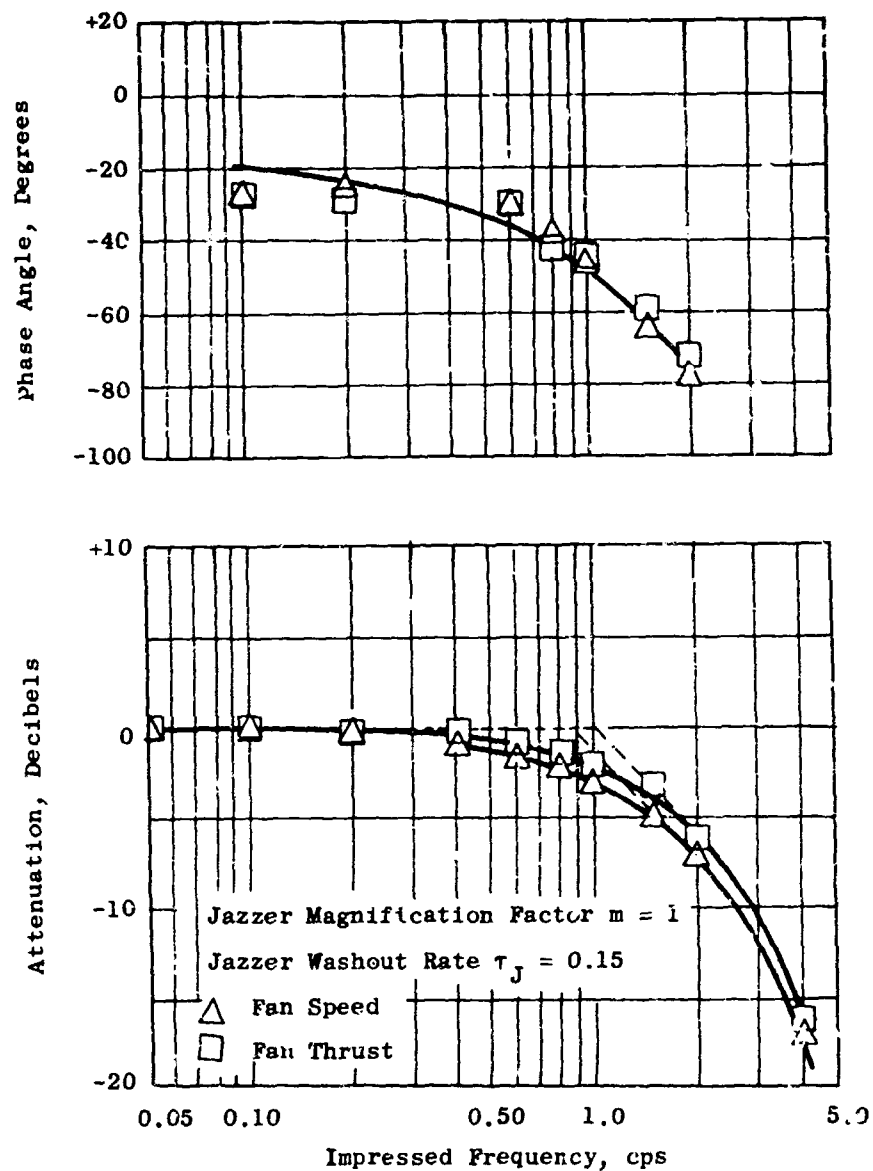


Figure 392. Steady-State Frequency Response - Analog Results for 100 \pm 10 Percent Area With a Jazzer Magnification Factor of 1.

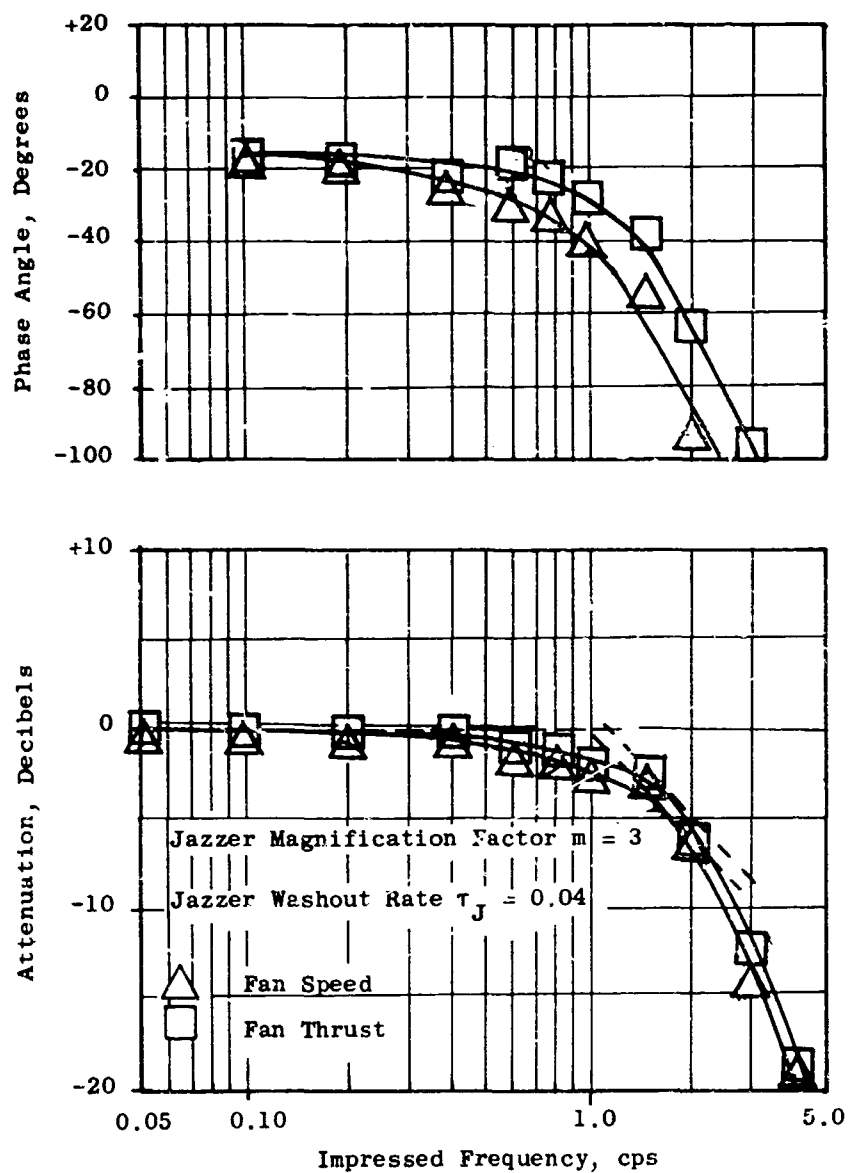


Figure 393. Steady-State Frequency Response - Analog Results for 100 \pm 10 Percent Area With a Jazzer Magnification Factor of 3.

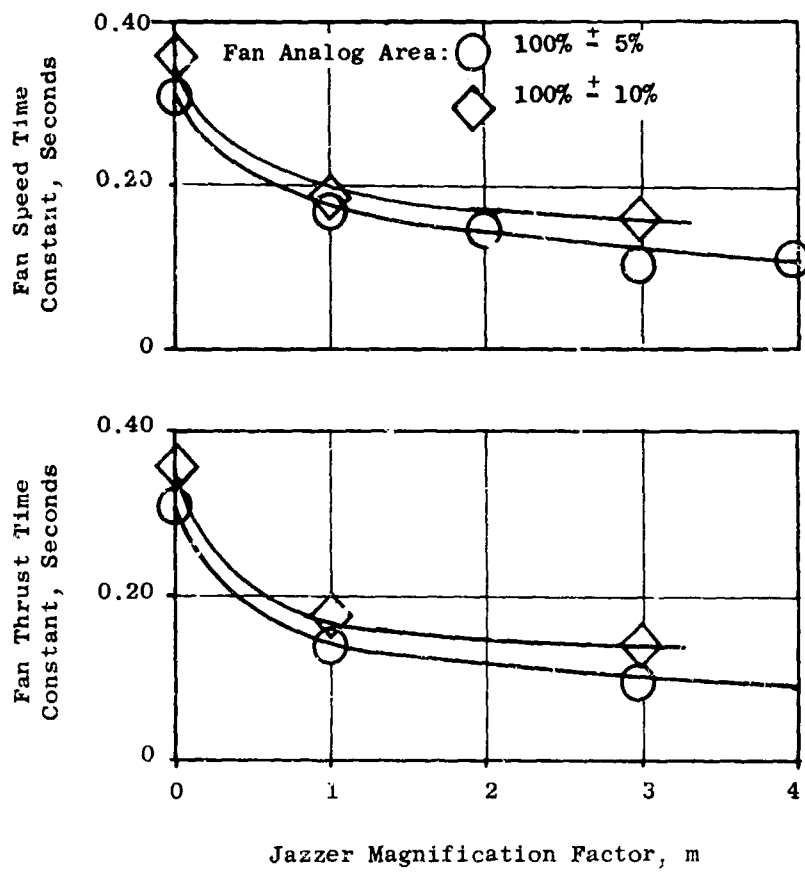


Figure 394. Analog Results - Summary of Fan Time Constants for Steady-State Frequency Response With a Jazzer.

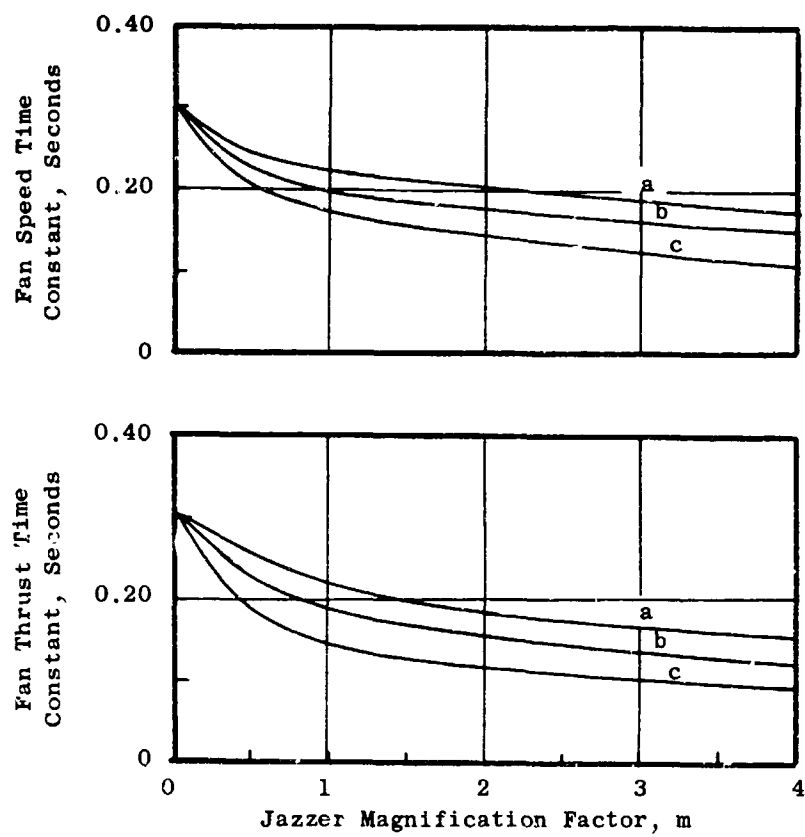


Figure 395. Analog Results - Summary of Effects of Jazzer on Fan Response for Roll Control.



Figure 396. Typical Analog Recorder Trace of Fan and Engine Response to Step Changes in Fan Area Using Fans for Height Control.

J85/LF2 Analog System
Fans For Height Control

Run	406
Engine Speed	100%
Fan Area	100% ± 3%
Jazzer M	1.0
Jazzer r	0.30

CLEVELAND, OHIO PRINTED IN U.S.A.

BRUSH INSTRUMENTS

100% ± 3%

103% ± 3%

B

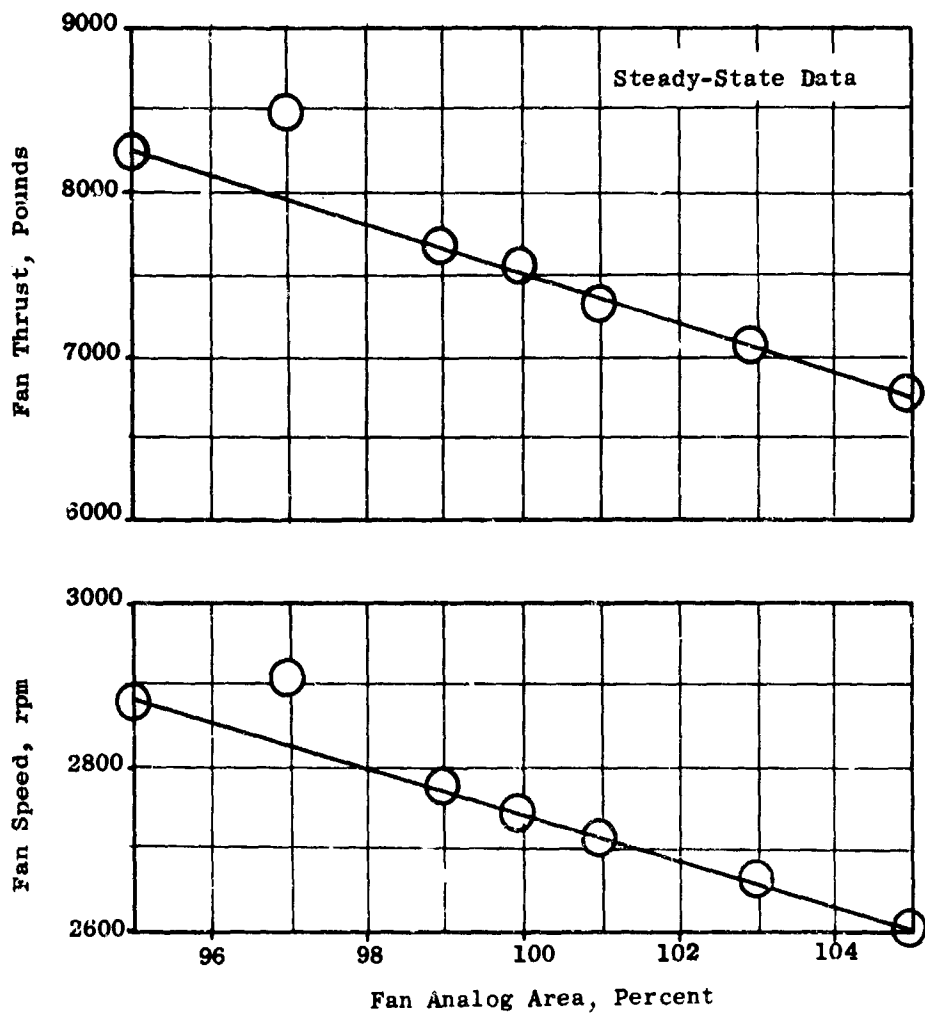


Figure 397. Analog Results - Fan Speed and Thrust Versus Fan Analog Area, Using Fans for Height Control.

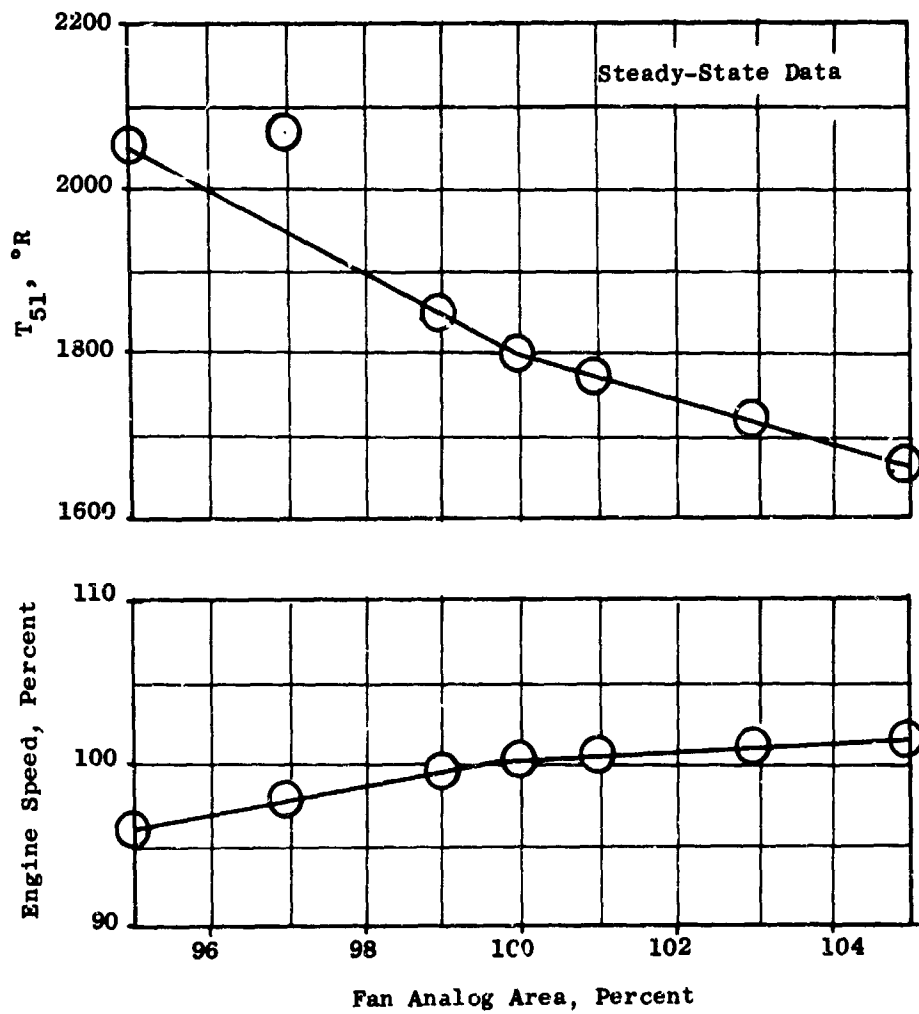


Figure 398. Analog Results - Engine Speed and Exhaust Temperature Versus Fan Analog Area, Using Fans for Height Control.

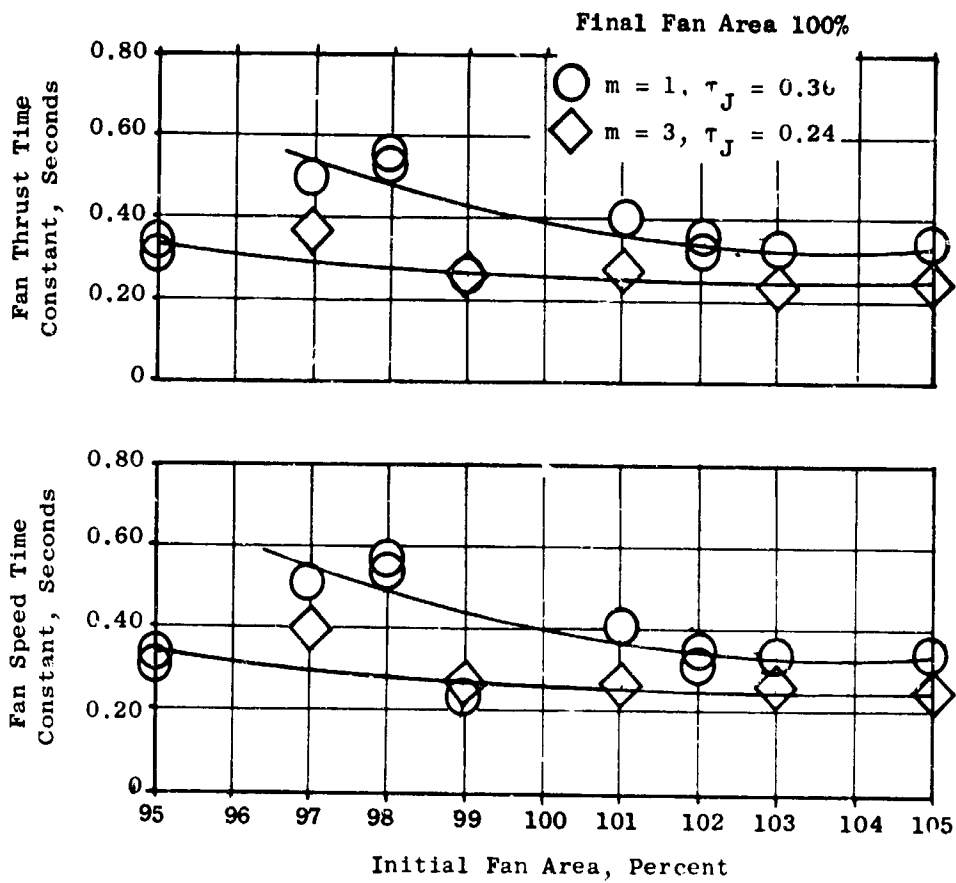


Figure 399. Analog Results - Fan Speed and Thrust Time Constants for Step Changes in Fan Area From the Design Point, Using Fans for Height Control.

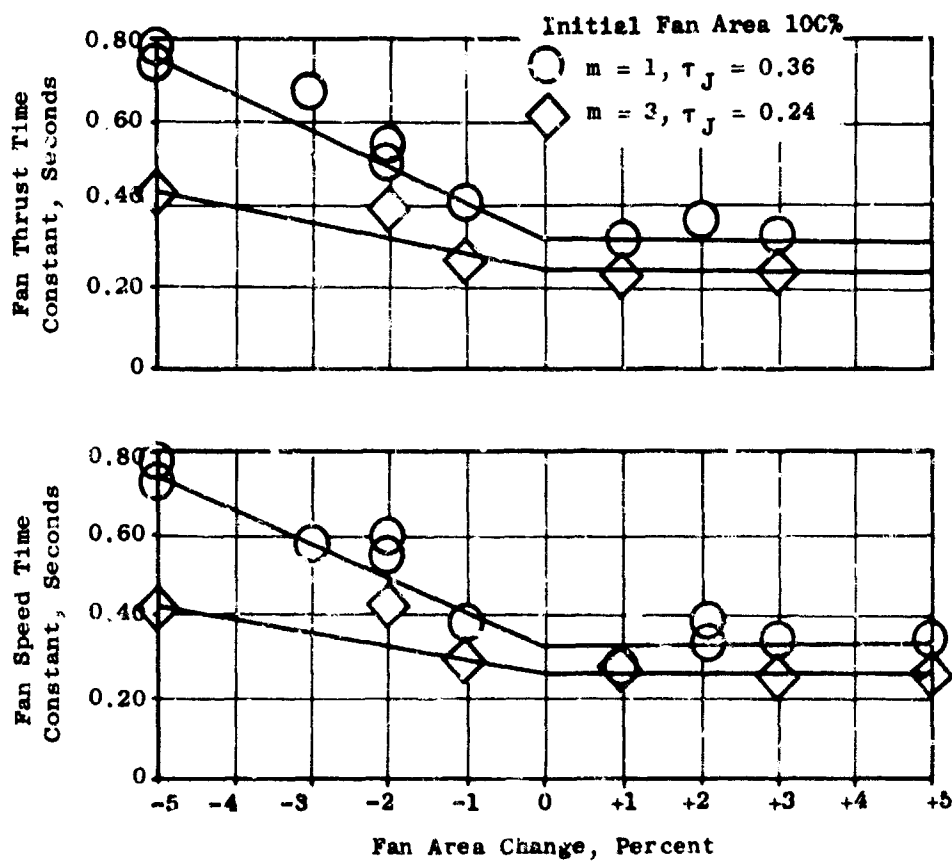


Figure 400. Analog Results - Fan Speed and Thrust Time Constants for Step Changes in Fan Area to the Design Point, Using Fans for Height Control.

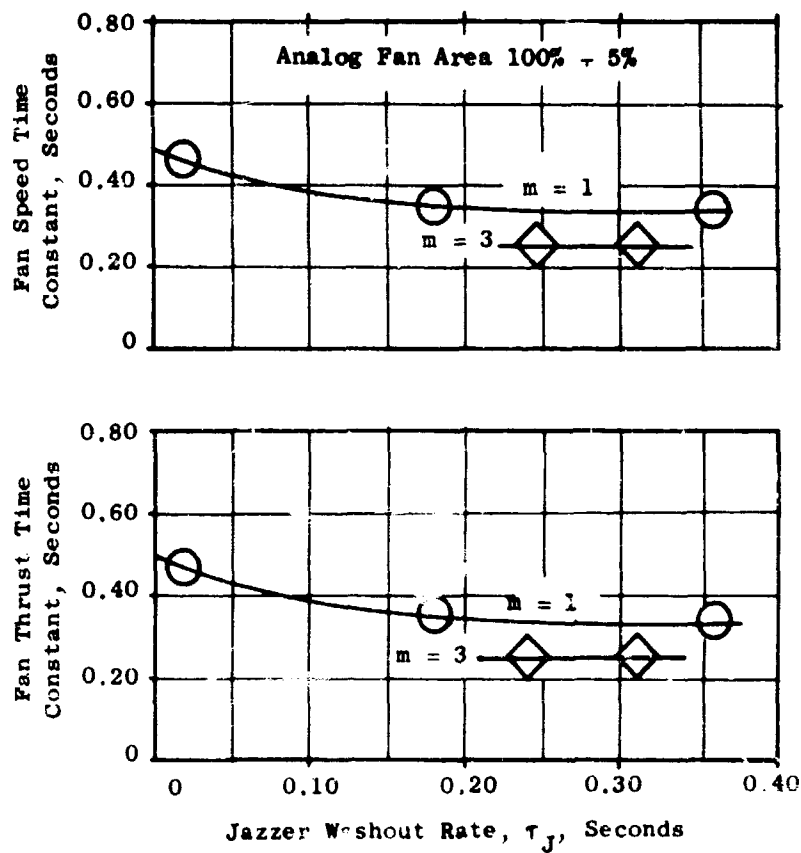


Figure 401. Analog Results - Effects of Jazzer Washout Rate on Fan Time Constants for Step Changes in Fan Area Using Fans for Height Control.

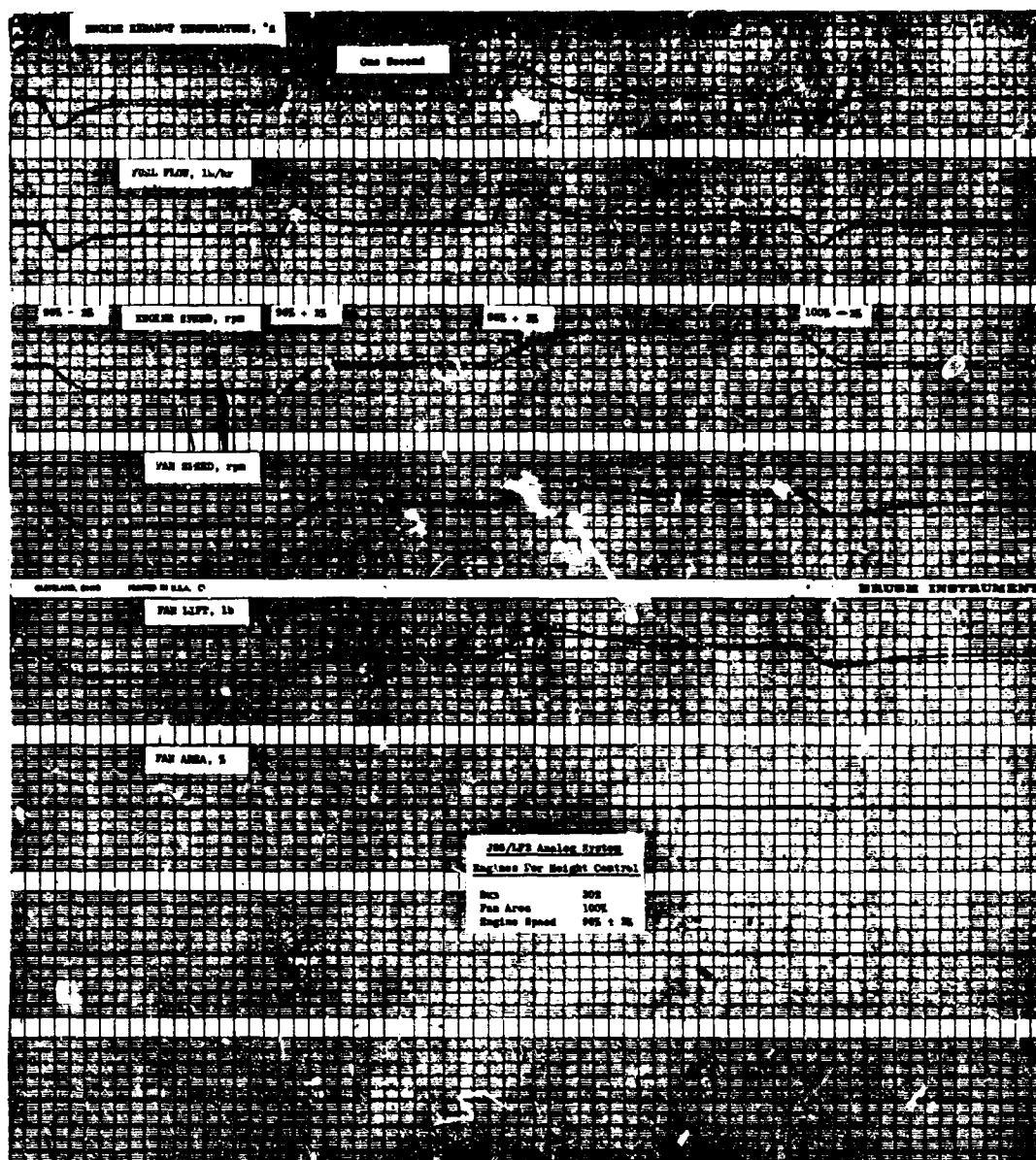


Figure 402. Typical Analog Recorder Trace of Fan and Engine Response to Step Changes in Engine Speed Using Engines for Height Control.

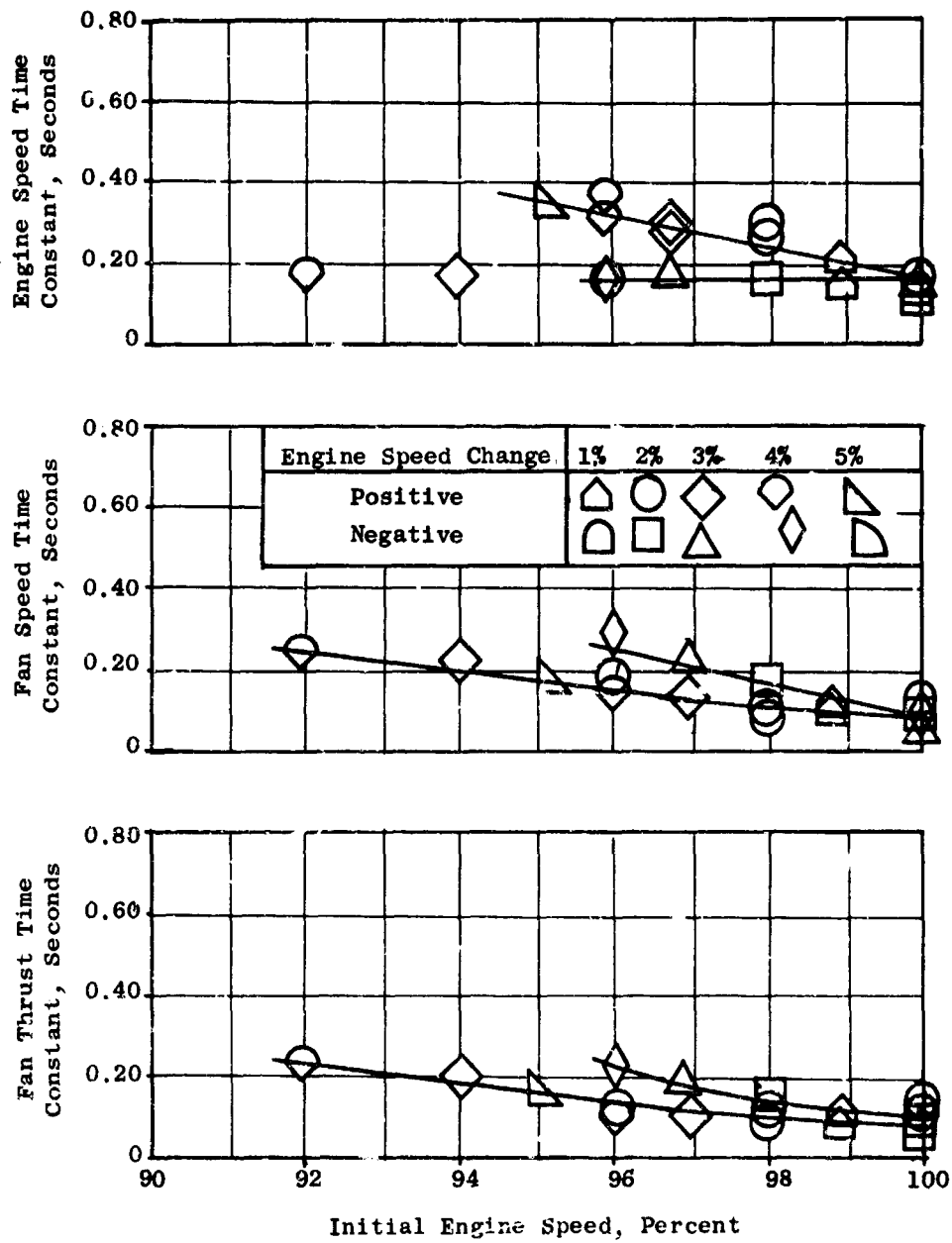


Figure 403. Analog Results - Engine and Fan Time Constants for Step Changes in Engine Speed, Using Engines for Height Control.

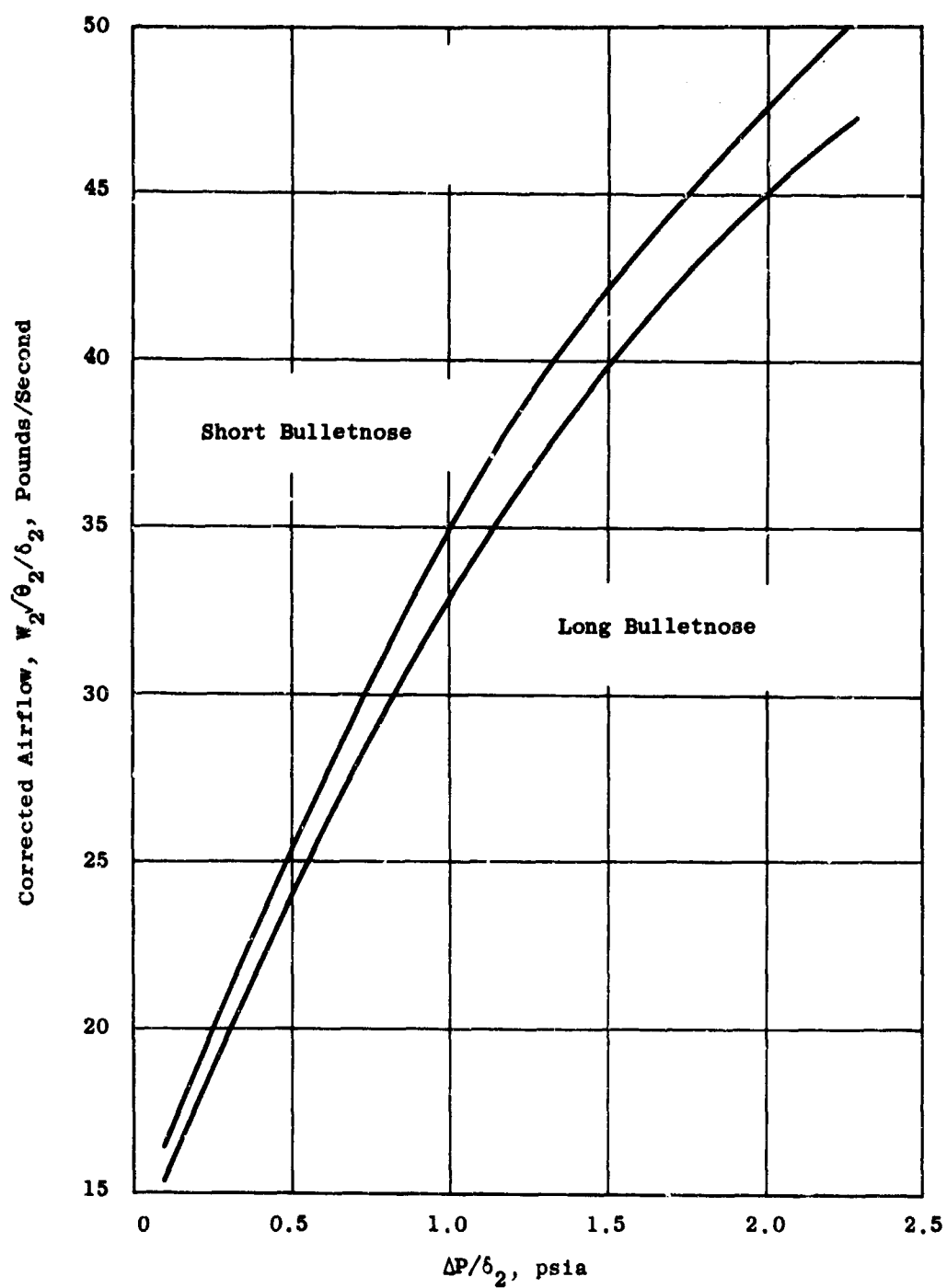


Figure 404. Engine 2 Airflow Calibration.

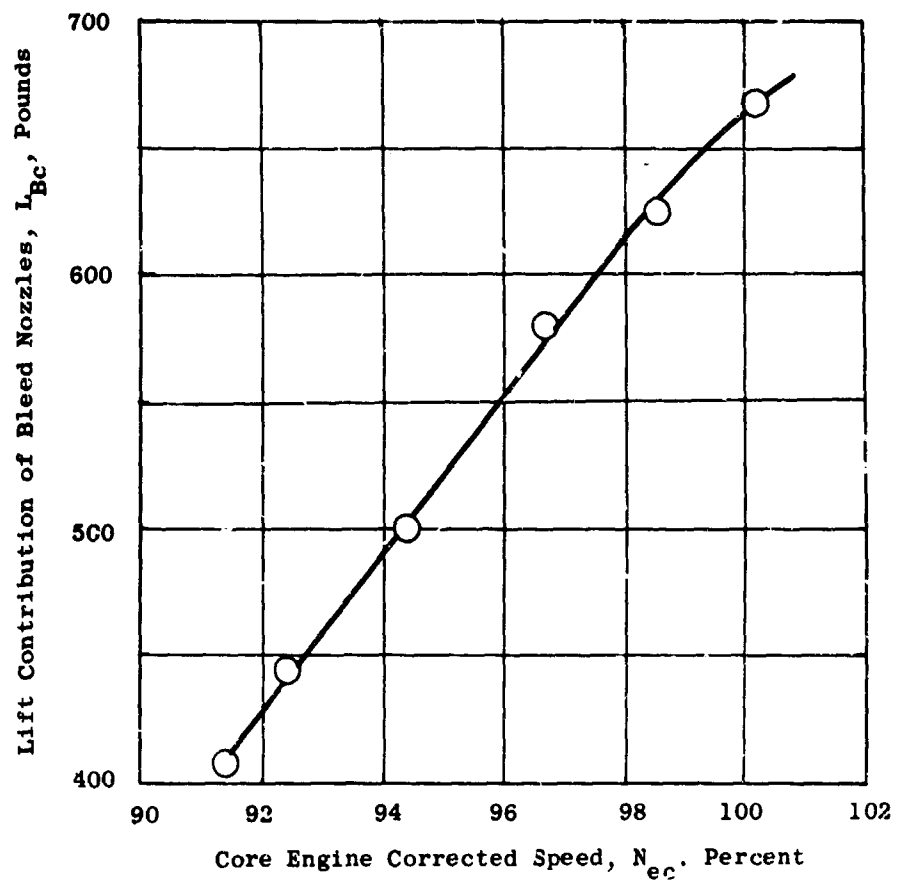


Figure 405. Lift Contribution of Bleed Nozzles Versus Core Engine Speed, Run 17, $\delta_s = 80$ Percent.

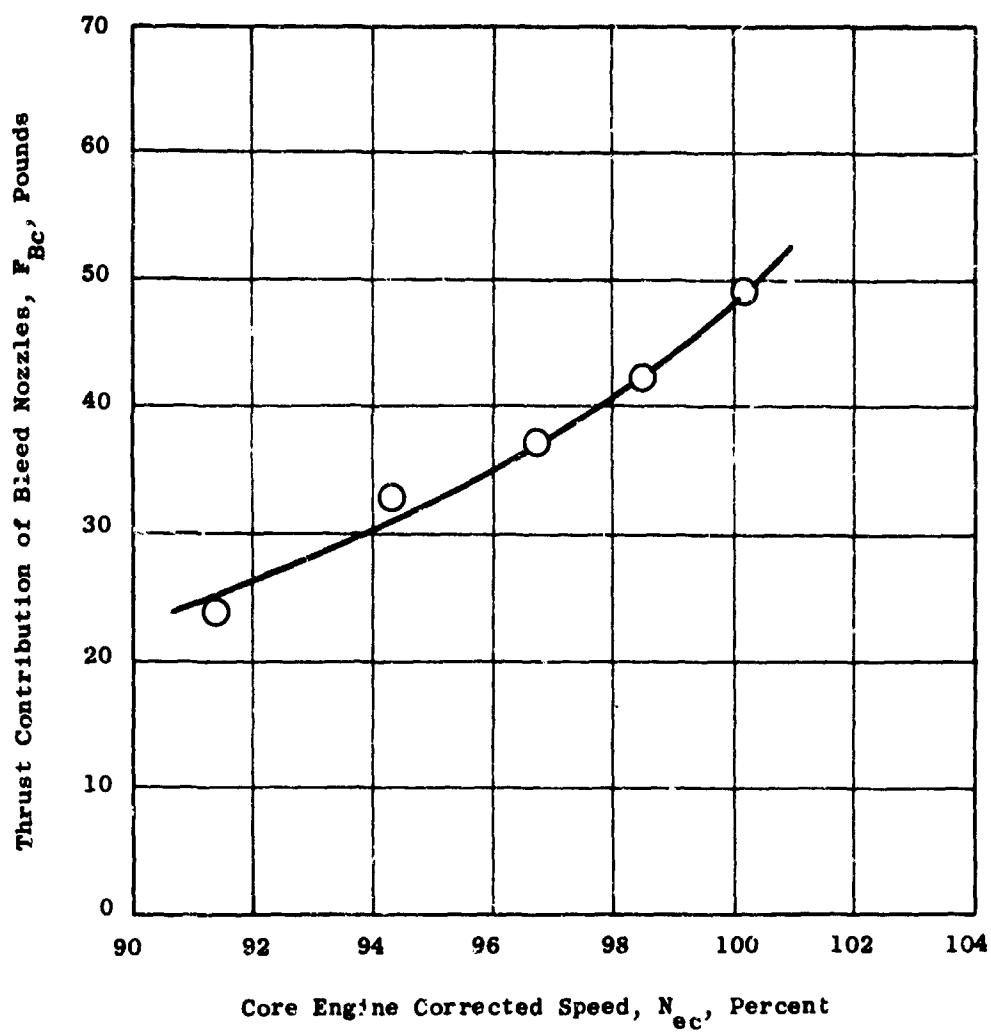


Figure 406. Bleed Nozzle Thrust Contribution Versus Core Engine Speed, Run 17, $\delta_s = 80$ Percent.

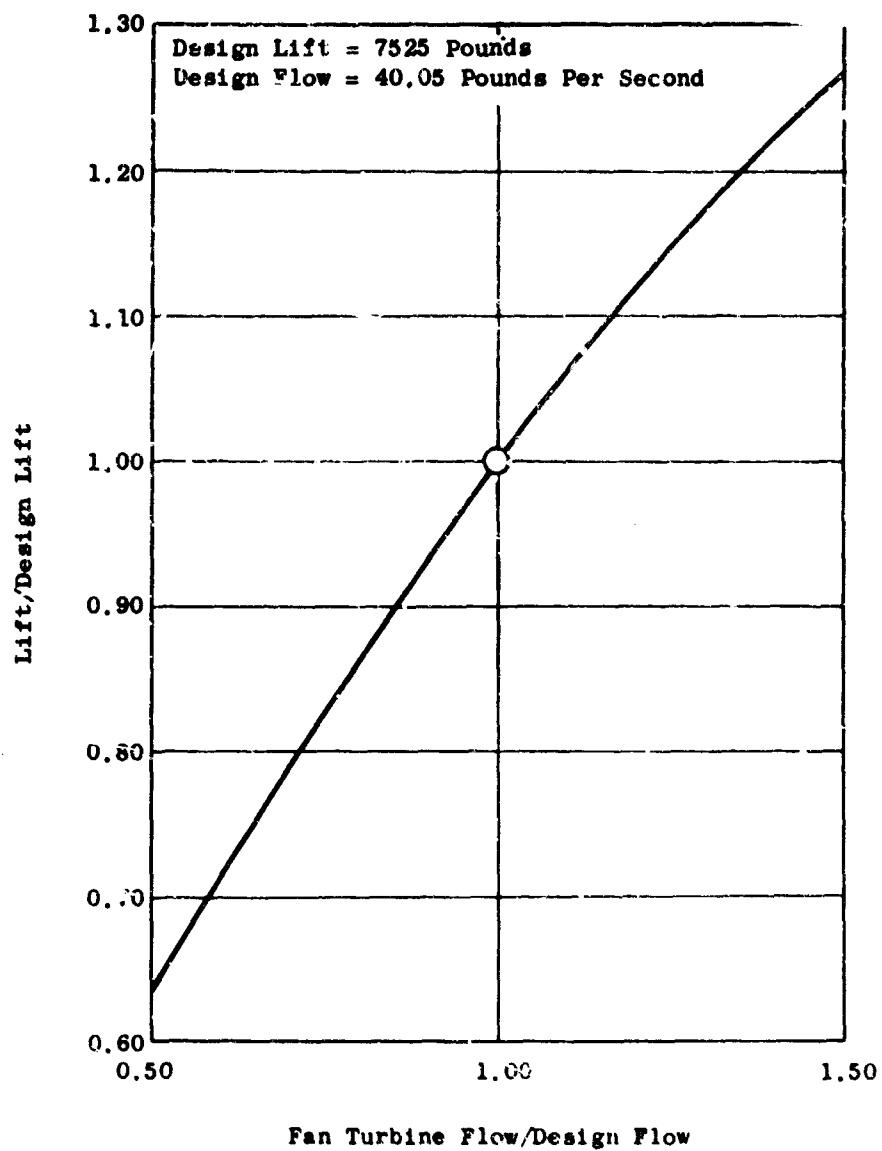


Figure 407. J85/LF2 Lift Versus Flow.

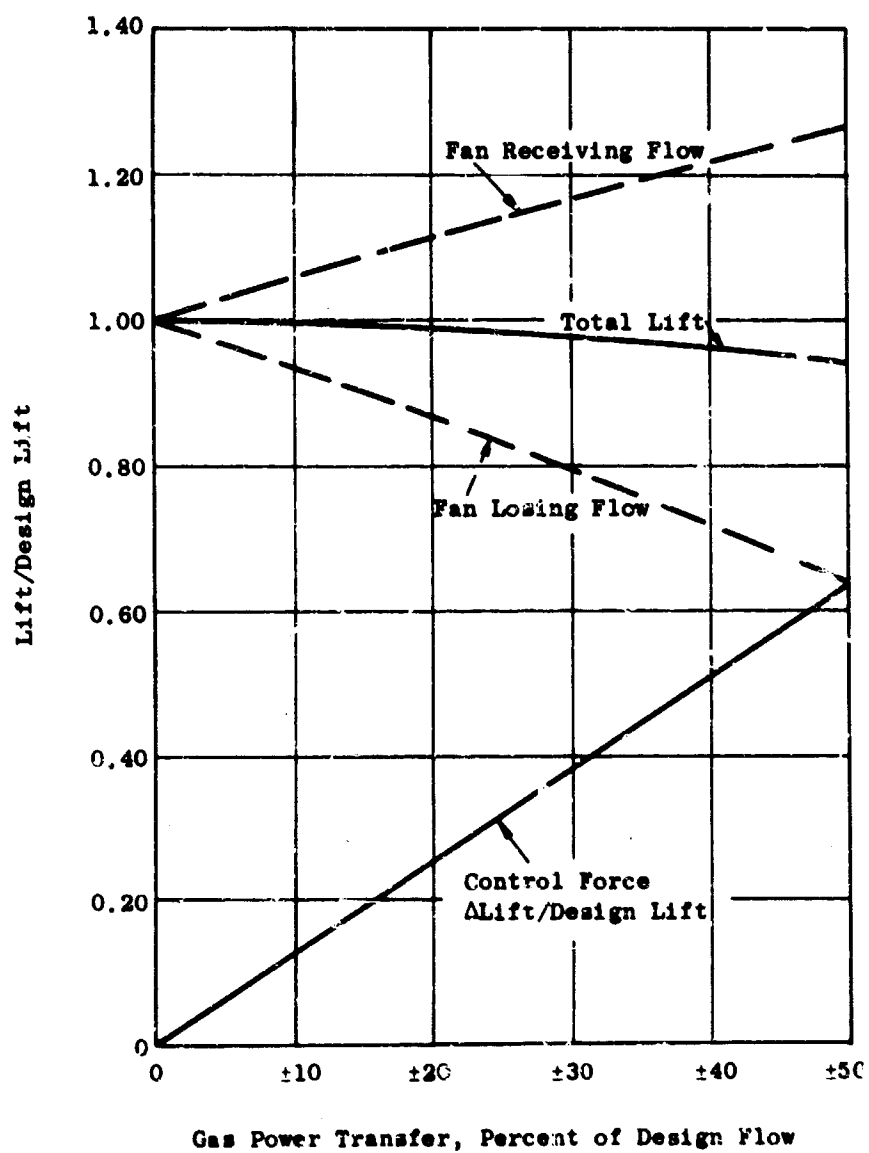


Figure 408. J85/LF2 Gas Power Transfer Performance.

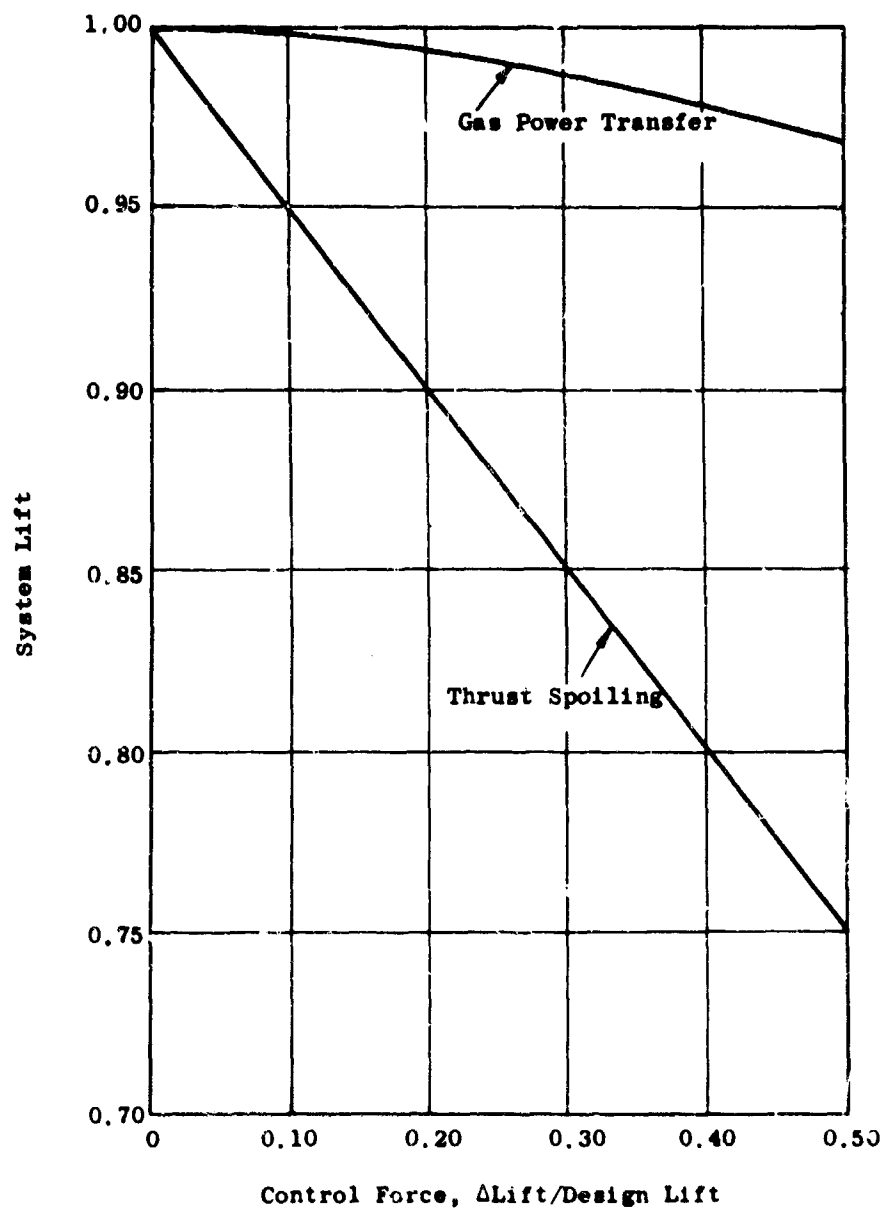


Figure 409. Comparison of Gas Power Transfer and Thrust Spoiling - Lift Loss Versus Desired Control Force.

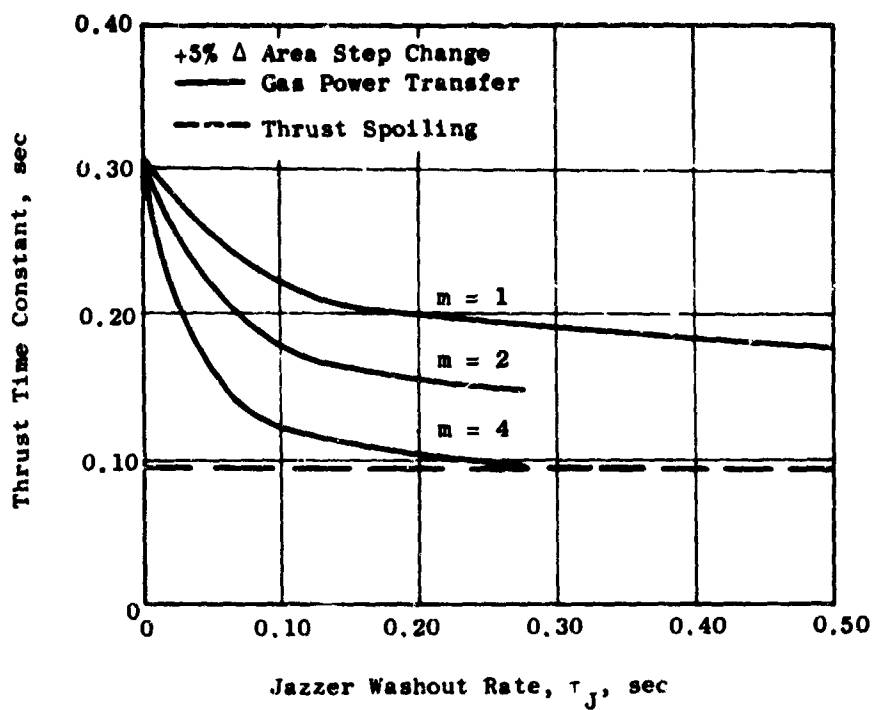


Figure 410. Comparison of Dynamic Response for Gas Power Transfer and Thrust Spoiling.

Unclassified

Security Classification

DOCUMENT CONTROL DATA - R&D		
(Security classification of title, body of abstract and indexing annotation must be entered when the overall report is classified)		
1. ORIGINATING ACTIVITY (Corporate author) Flight Propulsion Division General Electric Company Cincinnati, Ohio 45215		2a. REPORT SECURITY CLASSIFICATION Unclassified
		2b. GROUP
3. REPORT TITLE Investigations of a Variable Area Scroll for Power Transfer in Tip Turbine Lift Fan Systems		
4. DESCRIPTIVE NOTES (Type of report and inclusive dates) Final Report, June 1964 to December 1966		
5. AUTHOR(S) (Last name, first name, initial) Smith, Eugene G.		
6. REPORT DATE November 1967	7a. TOTAL NO. OF PAGES 624	7b. NO. OF REFS 9
8a. CONTRACT OR GRANT NO. DA 44-177-AMC-220(T)	7c. ORIGINATOR'S REPORT NUMBER(S) USAAVLABS Technical Report 67-26	
8b. PROJECT NO. 1F131201D161		
8c.	8d. OTHER REPORT NO(S) (Any other numbers that may be assigned this report) General Electric Company Report R67FPD218	
8d.		
10. AVAILABILITY/LIMITATION NOTICES This document has been approved for public release and sale; its distribution is unlimited.		
11. SUPPLEMENTARY NOTES		12. SPONSORING MILITARY ACTIVITY US Army Aviation Materiel Laboratories Port Eustis, Virginia
13. ABSTRACT <p>Demonstration tests and analog simulations were performed for the variable area scroll power transfer applicable for thrust control of tip turbine driven lift fans. The tip turbine driven lift fan used the lightweight LP2 rotor.</p> <p>Control response rates of 0.31 second for roll control and 0.10 second for height control were demonstrated. The jizzer, an anticipatory device, improved the response to about one-half the original level. Aerodynamic performance of the system met or exceeded objective level.</p>		

DD FORM 1473

Unclassified

Security Classification

Unclassified
Security Classification

14. KEY WORDS	LINK A		LINK B		LINK C	
	ROLE	WT	ROLE	WT	ROLE	WT
Tip Turbine Driven Lift Fan Variable Area Scroll Control Using Power Transfer Roll Control Response Height Control Response Analog Simulation Aerodynamic Performance of Lift Fans Jazzer Demonstration Tests						

INSTRUCTIONS

1. ORIGINATING ACTIVITY: Enter the name and address of the contractor, subcontractor, grantee, Department of Defense activity or other organization (corporate author) issuing the report.

2a. REPORT SECURITY CLASSIFICATION: Enter the overall security classification of the report. Indicate whether "Restricted Data" is included. Marking is to be in accordance with appropriate security regulations.

2b. GROUP: Automatic downgrading is specified in DoD Directive 5200.10 and Armed Forces Industrial Manual. Enter the group number. Also, when applicable, show that optional markings have been used for Group 3 and Group 4 as authorized.

3. REPORT TITLE: Enter the complete report title in all capital letters. Titles in all cases should be unclassified. If a meaningful title cannot be selected without classification, show title classification in all capitals in parenthesis immediately following the title.

4. DESCRIPTIVE NOTES: If appropriate, enter the type of report, e.g., interim, progress, summary, annual, or final. Give the inclusive dates when a specific reporting period is covered.

5. AUTHOR(S): Enter the name(s) of author(s) as shown on or in the report. Enter last name, first name, middle initial. If military, show rank and branch of service. The name of the principal author is an absolute minimum requirement.

6. REPORT DATE: Enter the date of the report as day, month, year, or month, year. If more than one date appears on the report, use date of publication.

7a. TOTAL NUMBER OF PAGES: The total page count should follow normal pagination procedures, i.e., enter the number of pages containing information.

7b. NUMBER OF REFERENCES: Enter the total number of references cited in the report.

8a. CONTRACT OR GRANT NUMBER: If appropriate, enter the applicable number of the contract or grant under which the report was written.

8b, 8c, & 8d. PROJECT NUMBER: Enter the appropriate military department identification, such as project number, subproject number, system numbers, task number, etc.

9a. ORIGINATOR'S REPORT NUMBER(S): Enter the official report number by which the document will be identified and controlled by the originating activity. This number must be unique to this report.

9b. OTHER REPORT NUMBER(S): If the report has been assigned any other report numbers (either by the originator or by the sponsor), also enter this number(s).

10. AVAILABILITY/LIMITATION NOTICES: Enter any limitations on further dissemination of the report, other than those imposed by security classification, using standard statements such as:

- (1) "Qualified requesters may obtain copies of this report from DDC."
- (2) "Foreign announcement and dissemination of this report by DDC is not authorized."
- (3) "U. S. Government agencies may obtain copies of this report directly from DDC. Other qualified DDC users shall request through _____."
- (4) "U. S. military agencies may obtain copies of this report directly from DDC. Other qualified users shall request through _____."
- (5) "All distribution of this report is controlled. Qualified DDC users shall request through _____."

If the report has been furnished to the Office of Technical Services, Department of Commerce, for sale to the public, indicate this fact and enter the price, if known.

11. SUPPLEMENTARY NOTES: Use for additional explanatory notes.

12. SPONSORING MILITARY ACTIVITY: Enter the name of the departmental project office or laboratory sponsoring (paying for) the research and development. Include address.

13. ABSTRACT: Enter an abstract giving a brief and factual summary of the document indicative of the report, even though it may also appear elsewhere in the body of the technical report. If additional space is required, a continuation sheet shall be attached.

It is highly desirable that the abstract of classified reports be unclassified. Each paragraph of the abstract shall end with an indication of the military security classification of the information in the paragraph, represented as (TS), (S), (C), or (U).

There is no limitation on the length of the abstract. However, the suggested length is from 150 to 225 words.

14. KEY WORDS: Key words are technically meaningful terms or short phrases that characterize a report and may be used as index entries for cataloging the report. Key words must be selected so that no security classification is required. Identifiers, such as equipment model designation, trade name, military project code name, geographic location, may be used as key words but will be followed by an indication of technical context. The assignment of links, rules, and weights is optional.

Unclassified
Security Classification

10013